

Durham E-Theses

Monogenetic basaltic edifices: their architecture, volcanology and importance in hydrocarbon basins

REYNOLDS, PETER, WILLIAM

How to cite:

REYNOLDS, PETER, WILLIAM (2015) *Monogenetic basaltic edifices: their architecture, volcanology and importance in hydrocarbon basins*, Durham theses, Durham University. Available at Durham E-Theses
Online: <http://etheses.dur.ac.uk/11369/>

Use policy

The full-text may be used and/or reproduced, and given to third parties in any format or medium, without prior permission or charge, for personal research or study, educational, or not-for-profit purposes provided that:

- a full bibliographic reference is made to the original source
- a [link](#) is made to the metadata record in Durham E-Theses
- the full-text is not changed in any way

The full-text must not be sold in any format or medium without the formal permission of the copyright holders.

Please consult the [full Durham E-Theses policy](#) for further details.

Academic Support Office, Durham University, University Office, Old Elvet, Durham DH1 3HP
e-mail: e-theses.admin@dur.ac.uk Tel: +44 0191 334 6107
<http://etheses.dur.ac.uk>

Monogenetic basaltic edifices: their architecture, volcanology and importance in hydrocarbon basins

Peter William Reynolds

A thesis submitted for the degree of
Doctor of Philosophy

**Department of Earth Sciences
Durham University**

2015

Monogenetic basaltic edifices: their architecture, volcanology and importance in hydrocarbon basins

Peter W. Reynolds

Abstract

Flood basalt provinces host significant hydrocarbon reserves. The provinces are produced during fissure eruptions which construct volcanic edifices atop an erupting dyke. The edifices are important components of volcanic-affected hydrocarbon basins; they provide insights into the underlying structural and magmatic plumbing systems, as well as acting as fluid migration pathways after burial. Furthermore, the edifices host a wealth of volcanological evidence that can be used to derive information relating to eruption dynamics such as eruption column height, mass flux and duration; as well as providing insights into the effects of eruptions on the environment. However, the location of the fissures in many hydrocarbon basins is poorly constrained. Furthermore, few studies have characterised the internal architecture of the edifices produced during fissure eruptions. This thesis uses field, seismic and well data to characterise the architecture of monogenetic basaltic edifices and understand their temporal and spatial evolution.

Field studies along a dissected Holocene fissure, Northeast Iceland, reveal that a scoria-agglutinate cone, spatter ramparts and a scoria rampart were constructed during Hawaiian-style lava fountaining. These edifices are analogous to those formed in the 1783 Laki eruption. Data gathered in this study can be used to recognise fissure-derived edifices in other volcanic provinces. I then contrast these dyke-fed edifices with rootless cones; a morphologically similar volcanic edifice produced during explosive interaction between inflating pāhoehoe lava and unconsolidated sediment. This thesis reveals that rootless cones can be distinguished from dyke-fed edifices on the basis of their juvenile clast morphology and clast density. This allows us to better recognise dyke-proximal locations. Lastly, I use exceptional quality 3D seismic and well data to show how a series of submarine monogenetic volcanoes evolved; progressing from a maar-forming stage, to a pillow volcano and tuff-cone-building stage as the confining pressure decreased above the growing edifices. These insights allow us to distinguish volcanic edifices from similar non-volcanic edifices in other seismic data sets, and also indicates that our understanding of submarine volcanism has previously been biased towards recognition of constructional features.

Copyright © by Peter W Reynolds

The copyright of this thesis rests with the author. No quotation from it should be published without prior written consent and information derived from it should be acknowledged.

Acknowledgements

With thanks to:

Uncle Hess
Rich Brown
Nick Schofield
Simon Holford
Thor Thordarson
Ed Llewellyn
Kevin Fielding
Davie Brown
Brian Bell
Douglas Halliday
Colin MacPherson
Claire Horwell
Paula Elliott
Karen Atkinson
April Furnal
Ian Chaplin
Dave Stevenson
Mat Hepburn
Cat Hirst
Sam Clark
Bob Jamieson
Alex Peace
Clayton Grove
Tim Watton
Heather Rawcliffe
Kirsty Wright
Tim Dempster
Gia Pendred
Nick Crabtree
Alwyn Ross
Dougal Jerram
Sverre Planke
John Millett

and especially

Charlotte Simmons

and

Susan Reynolds

Table of Contents

| | |
|--|-----|
| Abstract | i |
| Acknowledgements | iii |
| Chapter 1: Introduction | 1 |
| 1.1 Flood basalt volcanism and hydrocarbon exploration | 1 |
| 1.2 The importance of fissure volcanism | 2 |
| 1.3 The importance of volcanic edifices | 2 |
| 1.4 The problem: identifying volcanic edifices and constraining their architecture | 3 |
| 1.4.1 Identifying volcanic edifices in remote datasets | 3 |
| 1.4.2 Characterising the architecture of volcanic edifices in the field | 5 |
| 1.5 Aims | 6 |
| 1.6 Thesis Outline | 7 |
| 1.7 References | 8 |
| Chapter 2: Background Information | 12 |
| 2.1 Introduction | 12 |
| 2.2 The North Atlantic Igneous Province | 12 |
| 2.2.1 The Faroe Shetland Basin | 13 |
| 2.3 The eruption of basaltic magma | 16 |
| 2.3.1 Feeder dykes for monogenetic eruptions | 17 |
| 2.3.2 Eruption styles | 19 |
| 2.3.2.1 Physical processes governing eruption style | 20 |
| 2.3.2.2 Hydromagmatic eruptions | 20 |
| 2.3.2.3 Magmatic volatile-driven eruptions | 21 |
| 2.3.2.3.1 Fissure eruptions | 22 |
| 2.3.3 Pyroclast accumulation and lava fountains | 23 |
| 2.4. Basaltic lavas | 24 |
| 2.4.1 Definition of terms | 24 |
| 2.4.2 Emplacement | 27 |
| 2.4.2.1 Inflation of pāhoehoe lavas | 29 |
| 2.4.3 Types of pāhoehoe lavas | 30 |
| 2.4.4 Physical features of lava flow fields | 33 |
| 2.4.4.1 Rootless eruptions | 34 |
| 2.4.5 Internal features of lava flows | 35 |

| | |
|---|-----------|
| 2.4.5.1 Crustal structure | 35 |
| 2.4.5.2 Cooling joints | 36 |
| 2.5 Volcanic edifices | 38 |
| 2.5.1 Monogenetic volcanoes | 38 |
| 2.5.1.1 Spatter cones and ramparts | 42 |
| 2.5.1.2 Scoria cones | 42 |
| 2.5.1.3 Shield volcanoes | 44 |
| 2.5.1.4 Agglutinate cones | 45 |
| 2.5.1.5 Tuff cones | 46 |
| 2.5.1.6 Tuff rings | 47 |
| 2.5.1.7 Maars | 47 |
| 2.5.2 Polygenetic volcanoes | 48 |
| 2.5.2.1 Seamounts | 49 |
| 2.6 The identification and importance of volcanic features in hydrocarbon basins | 50 |
| 2.6.1 Lavas | 50 |
| 2.6.1.1 Basaltic lavas in seismic data | 51 |
| 2.6.1.2 Basaltic lavas in well data | 51 |
| 2.6.2 Volcanic edifices | 52 |
| 2.6.2.1 Volcanic edifices in seismic data | 52 |
| 2.6.2.1.1 Monogenetic volcanoes | 52 |
| 2.6.2.1.2 Polygenetic volcanoes | 53 |
| 2.6.2.1.3 Seamounts | 54 |
| 2.6.2.2 Volcanic edifices in well data | 57 |
| 2.7 Non-volcanic edifices found in hydrocarbon basins | 57 |
| 2.7.1 Mud volcanoes | 58 |
| 2.7.2 Hydrothermal vents | 62 |
| 2.7.3 Comparison between types of sedimentary edifices | 64 |
| 2.8 Summary | 65 |
| 2.9 References | 65 |
| Chapter 3: The Evolution of the 6–8 kyr R-K Basaltic Fissure Eruption, Northeast Iceland | 79 |
| 3.1 Introduction | 79 |
| 3.2 Geological setting | 80 |

| | |
|--|-----|
| 3.3 Methods | 87 |
| 3.4 Pyroclastic lithofacies | 89 |
| 3.4.1 Lithofacies descriptions | 100 |
| 3.4.2 Distribution of the pyroclastic lithofacies | 108 |
| 3.4.3 Temporal variations in pyroclast welding intensity, bedding and contacts | 109 |
| 3.4.4 Variations in componentry | 109 |
| 3.5 Lava flow field architecture | 112 |
| 3.6 Sedimentary lithofacies | 132 |
| 3.7 Architecture of the pyroclastic deposits | 136 |
| 3.7.1 The R-K feeder dykes | 145 |
| 3.7.2 Rootless cones | 148 |
| 3.7.3 Scoria ramparts | 151 |
| 3.7.4 Sheet-like fall deposits | 157 |
| 3.7.5 Scoria-agglutinate cone | 158 |
| 3.7.6 The spatter ramparts | 162 |
| 3.8 Evolution of the fissure | 173 |
| 3.9 Discussion | 176 |
| 3.9.1 Feeder dyke and conduit morphology | 176 |
| 3.9.2 Rootless eruption mechanisms | 177 |
| 3.9.3 Scoria ramparts | 177 |
| 3.9.4 Scoria-agglutinate cone | 178 |
| 3.9.5 Spatter ramparts | 179 |
| 3.9.6 Comparison with high-volume fissure eruptions | 180 |
| 3.10 Summary | 184 |
| 3.11 References | 184 |
| Chapter 4: Rootless Cone Processes Informed from Dissected Vent and Tephra Deposits | 191 |
| 4.1 Introduction | 191 |
| 4.2 Geological setting of the Columbia River Basalt Province | 193 |
| 4.3 Method | 195 |
| 4.4 Ice Harbor rootless cone field | 196 |
| 4.4.1 Volcanic ash substrate | 196 |
| 4.4.2 Ice Harbor lava flows | 197 |
| 4.4.3 Rootless cone conduits | 197 |

| | |
|---|-----|
| 4.4.4 Rootless cone tephra deposits | 200 |
| 4.4.4.1 Juvenile pyroclast types | 200 |
| 4.4.4.2 Pyroclastic lithofacies | 205 |
| 4.4.4.3 Lava-silicic volcanic ash interaction textures in tephra deposits | 211 |
| 4.5 Emplacement of the Ice Harbor rootless cones | 213 |
| 4.6 Comparison with other rootless cones | 216 |
| 4.7 Conclusions | 220 |
| 4.8 References | 220 |
| Chapter 5: The Construction of Submarine Volcanoes: Insights from 3D | 224 |
| Seismic Data | |
| 5.1 Introduction | 224 |
| 5.1.1 Aims | 225 |
| 5.2 Geological setting | 225 |
| 5.3 Dataset and methodology | 227 |
| 5.3.1 Seismic and well data | 224 |
| 5.3.2 Composition of the edifices | 235 |
| 5.3.3 Calculating edifice dimensions | 235 |
| 5.3.4 Seismic facies analysis | 237 |
| 5.4 Edifice characteristics | 240 |
| 5.4.1 Pit craters | 240 |
| 5.4.2 Cone-shaped edifices | 240 |
| 5.4.2.1 Pointed edifices | 240 |
| 5.4.2.2 Flat-topped edifices | 240 |
| 5.4.2.3 Cratered edifices | 241 |
| 5.4.3 Edifice distribution | 243 |
| 5.5 Discussion | 247 |
| 5.5.1 Physical volcanology of the edifices | 248 |
| 5.5.2 Temporal and spatial evolution of the Bass Basin volcanic field | 249 |
| 5.5.3 Comparison with other volcanoes in seismic data | 252 |
| 5.5.4 Implications for the identification of submarine volcanoes | 253 |
| 5.5.5 Edifice Preservation | 253 |
| 5.5.6 Limitations of the study | 254 |
| 5.6 Conclusion | 254 |
| 5.7 References | 254 |

| | |
|--|-----|
| Chapter 6: Discussion | 261 |
| 6.1 Introduction | 261 |
| 6.2 Fissure-eruption derived volcanoes | 261 |
| 6.3 Rootless cones | 263 |
| 6.4 Monogenetic edifices in seismic data | 265 |
| 6.5 References | 266 |
| Chapter 7: Summary | 270 |
| 7.1 Summary and conclusions | 270 |
| Chapter 8: Future Work | 272 |
| 8.1 Directions for future work | 272 |
| 8.2 References | 273 |
| Appendix 1: Support Material for Chapter 3 | 275 |
| Appendix 2: Support Material for Chapter 4 | 381 |
| Appendix 3: Support Material for Chapter 5 | 422 |
| Appendix 4: Material Published in Support of the Thesis | 425 |

List of Figures

| | | |
|-------------|--|----|
| Figure 1.1. | Map showing the distribution of Large Igneous Provinces and basins that are the sites of current hydrocarbon exploration. Modified from Coffin and Eldholm (1992), Coffin and Eldholm (1994), Courtillot et al. (1999), Sheth (1999), Jerram and Widdowson (2005), Ross et al. (2005), Rohrman (2007), Bryan and Ernst (2008) and Wright (2013). | 1 |
| Figure 1.2. | Seismic section from offshore Norway illustrating the sub-basalt imaging problem – notice that the stratigraphy is obscured beneath the basalt cover. Taken from Jerram (2002). | 5 |
| Figure 2.1. | Location, structure and volcanic features of the Faroe-Shetland Basin. Modified from Stoker et al. (1993), Ritchie et al. (1996, 1999), Sørensen (2003), Ellis et al (2009), Moy and Imber (2009) and Wright (2013). | 16 |
| Figure 2.2. | Factors controlling lava fountain structure. Modified from Head and Wilson (1989). | 24 |
| Figure 2.3. | Schematic diagram illustrating the difference between lava flows, lobes and flow fields. The lava lobe shown is 300 cm wide. Individual lava flows are shaded. The lava flow field ranges in size from tens to hundreds of kilometres. Photograph from Swanson (1974). Diagram modified from Self et al. (1998). | 26 |
| Figure 2.4. | Tabular classic (A) and Compound braided flow facies (B) found within flood basalt provinces. Modified from Jerram (2002). | 27 |
| Figure 2.5. | Cross section of an ‘a’ā lava. The flow has a massive core with irregular vesicles and an upper and lower crust composed of clinker. | 28 |
| Figure 2.6. | Schematic diagram illustrating how pāhoehoe lava transitions to ‘a’ā as a function of strain rate and viscosity. Modified from Peterson and Tilling (1980). | 29 |
| Figure 2.7. | Photographs showing (A) P-type, (B) S-type, (C) silvery (D) blue glassy and (E) shelly pāhoehoe. Photograph C is from Leverington (2002) and D is from Wilch (2011). The ruler in A is | 32 |

| | | |
|--------------|--|----|
| | 10 cm long and the scale card in E is 10 cm long. | |
| Figure 2.8. | Photographs showing spiny (A), rubbly (B), entrail (C) and clastogenic (D) pāhoehoe. Photograph C from Pendred (2011). | 33 |
| Figure 2.9. | Schematic cross section through P-type pāhoehoe. The lobe has a tripartite structure defined by variations in vesicularity, crystallinity and jointing. The basal crust is 20–100 mm thick regardless of lobe thickness and is hypohyaline – hypocrystalline. Cooling joints are sparse. The core of the flow is non-vesicular and holocrystalline. Columnar jointing may penetrate the core. Vesicle cylinders (VCs) and vesicle sheets (VSs) are found. The upper crust comprises 40–60% of the lobe thickness. It is vesicular and hypohyaline – hypocrystalline. It may contain prismatic or irregular joints and numerous horizontal vesicle zones (VZs). Modified from Self et al. (1998). | 36 |
| Figure 2.10. | Jointing styles in lavas. (A) The colonnade of a lava flow with regular, columnar jointing. These joints form due to thermal contraction during cooling. (B) The entablature of a lava flow with characteristic wavy-shaped joints. These joints form due to percolation of water through the cooling lava. (C) A tiered lava flow, displaying both an entablature and colonnade. This style of jointing develops due to intermittent flooding and dry periods. | 37 |
| Figure 2.11. | Schematic cross section of the Rothenburg scoria cone. Taken from Houghton and Schmincke (1989). | 44 |
| Figure 2.12. | Profiles of shield volcanoes in Iceland. The dark column represents the feeder dyke. Taken from Rossi (1996). | 45 |
| Figure 2.13. | Schematic cross section of an agglutinate cone. Modified from Brown et al. (2014). | 46 |
| Figure 2.14. | Schematic cross section of a tuff cone. (1) Explosion breccia, (2) thinly bedded deposits (3) thickly bedded, massive deposits. Adapted from Wohletz and Sheridan (1983). | 46 |
| Figure 2.15. | Schematic cross section of a tuff ring. (1) Explosion breccia, (2) thinly bedded deposits. Adapted from Wohletz and Sheridan (1983). | 47 |

| | | |
|--------------|---|----|
| Figure 2.16. | Schematic cross section of a maar and underlying diatreme. UD=Upper diatreme; LD=Lower Diatreme, RZ=root zone. Taken from White and Ross (2011). | 48 |
| Figure 2.17. | Schematic cross section of a polygenetic seamount. The seamount is ≥ 5 km in diameter and several hundred metres in height. Modified from Schnur (2007). | 50 |
| Figure 2.18. | A comparison of the volcanoes currently recognised in seismic data. (A) Shield volcano, taken from Magee et al. (2013). (B) Maar crater, described by Wall et al. (2010). (C) Seismic line from Jólnir (left) and Stóra-Hraun (right) in the vicinity of Surtsey. Modified from Thors and Jakousson (1982). (D) Seamount in the Faroe-Shetland Basin, modified from Bell and Butcher (2002). (E) Kora andesitic stratovolcano, offshore New Zealand, modified from Bergman et al. (1991). | 55 |
| Figure 2.19. | Schematic cross section of a mud volcano. The vertical scale varies from hundreds to thousands of metres. Modified from Evans et al. (2007). | 61 |
| Figure 2.20. | Seismic cross section of Lich mud volcano. Modified from Kopf (2002). | 61 |
| Figure 2.21. | Schematic cross section of a hydrothermal vent. Vent formation is linked to the heating of pore fluids adjacent to the sill. Modified from Jamtveit et al. (2004). | 63 |
| Figure 2.22. | Seismic cross section of an eye-type hydrothermal vent. Modified from Svensen et al. (2003). | 64 |
| Figure 3.1 | Location of the Sveinar graben in the Holocene rift zone of Northern Iceland. Inset map shows the location of the study area outlined in red and the Tjörnes Fracture Zone (TFZ). Adapted from Gudmundsson et al. (2008). | 82 |
| Figure 3.2 | Regional geology map of the Rauduborgir-Kvensödul fissure. See Figure 3.1 for location. Lavas produced during the eruption pond in the Sveinar graben towards the south. | 83 |
| Figure 3.3 | Geological map of the study area. See Figure 3.2 for location. | 84 |
| Figure 3.4 | Map of faults in the study area. The faults are coloured to indicate | 85 |

| | | |
|------------|---|----|
| | formation prior to, during, or post eruption. Black outline indicates the limit of the R-K stratigraphy. See text for details. See Figure 3.2 for location. | |
| Figure 3.5 | Google Earth image showing the change in strike of the R-K fissure as it is captured by the Sveinar graben. Pyroclastic edifices are shown; not all edifices are numbered for clarity. Note the large (3.5 km) gap between edifices 29 and 30, perhaps resulting from post-eruption erosion. Edifice 35 is located at the end of this section of the fissure. | 86 |
| Figure 3.6 | Pyroclast types identified in the study area. (A) Spindle-shaped and (B) ragged clast typical of Hawaiian and Strombolian activity. (C) Clast with a brittle rind (outlined) extruding melt from its interiors (arrowed). (D) Fluid clasts that agglutinate, produced from the inner part of the lava fountain or a low fountain. (E) Fluid clasts that coalesce, produced from the inner lava fountain or a low fountain. (F) Cored bombs produced by the recycling of clasts within an edifice. They have a core of cognate lithic clasts and a 10 mm thick coating of lava. (G) An armoured clast with an accidental or cognate lithic core and a partial coating of lava. (H) Scoria lapilli produced from a rootless lava fountain. Notice the furrows in the crust, similar to those in breadcrust bombs. | 90 |
| Figure 3.7 | Pyroclastic lithofacies observed in the study area. (A) Non-welded scoria lapilli. Inter-clast cavities are visible (outlined). Note the absence of clast flattening. (UTM 557085/7264940). (B) Incipiently welded scoria. Inter-clast cavities are visible (outlined) and clasts are sintered at contacts. Minor clast flattening is observed. (UTM 557442/7264902). (C) Moderately welded scoria. Clast outlines are visible (dashed outline) and some inter-clast cavities (circled) remains. Sub-horizontal clast flattening is parallel to the dashed lines. (UTM 557356/7265748). (D) Densely welded scoria. Flattened clasts (dashed outline) are visible. Small (<1 cm diameter) inter-clast cavities remain. (UTM 563879/7301531). (E) Incipiently welded spatter. Resinous clast rinds are visible (arrowed). (UTM 557433/7264891). (F) | 91 |

| | | |
|-------------|--|----|
| | <p>Moderately welded spatter. Vesicular cores of clasts remain (dashed outline) and define the bedding. (UTM 557442/7264902). (G) Densely welded spatter. Thin relict vesicular cores (dashed outline) are visible between densely welded zones. The ghost clasts dip $\sim 10^\circ$. (UTM 557356/7265748). (H) Massive scoria lapilli and bombs. The clasts are incipiently welded. Armoured clasts with an accidental lithic core are common in these deposits. (UTM: 557790/7264865).</p> | |
| Figure 3.8 | <p>Thin section images of pyroclastic lithofacies (plane polarised light). (A) Non-welded scoria lapilli. Note the sphericity of the vesicles compared to the other lithofacies. (B) Incipiently welded scoria. The dashed line indicates an inferred contact between welded clasts. (C) Moderately welded scoria. Domains of less vesicular scoria (dashed outline) are inferred to represent welded clasts. (D) Densely welded scoria. The lithofacies appears texturally similar to clast-supported moderately welded scoria lapilli and bombs (mwSc). (E) Incipiently welded spatter. The dashed line indicates a clast rind folded into the clast core. (F) Moderately welded spatter. Note the increasing crystal content relative to (D) and (E). (G) Densely welded spatter. Note the laminated appearance of the groundmass. The crystal-rich groundmass contains a band of vesicles and is interpreted as the relict core of a spatter bomb. (H) Massive scoria lapilli and bombs. Note the thick bubble septae relative to A and B.</p> | 93 |
| Figure 3.9 | <p>Density histograms for the pyroclastic lithofacies. (A) Scoria lapilli. (B) Incipiently welded scoria. (C) Moderately welded scoria. (D) Densely welded scoria. (E) Incipiently welded spatter. (F) Moderately welded spatter. (G) Densely welded spatter. (H) Graph showing that clast aspect ratio increases with density for the pyroclastic lithofacies (average of 50; see Table. 3.2).</p> | 95 |
| Figure 3.10 | <p>Stratigraphic logs showing variations in grain size (black line) and clast aspect ratio (red line); each the average of 10 measurements. Abbreviations for lithofacies are given in Table 3.1. Note the restriction of the lithic clasts to within the crater.</p> | 96 |

| | | |
|-------------|---|-----|
| Figure 3.11 | Stratigraphic logs showing variations in grain size (black line) and clast aspect ratio (red line); each the average of 10 measurements. Abbreviations for lithofacies are given in Table 3.1. Note the restriction of the lithic clasts to within the crater. | 97 |
| Figure 3.12 | Dispersal and welding characteristics of the tephra and lavas. (A) Graph to show the relationship between distance from the fissure (m) and pyroclast size (mm). Pyroclasts decrease in size with distance. (B) Graph to show the relationship between distance from the fissure (m) and pyroclast lithofacies thickness (m). Deposits thin with distance. (C) Graph to show the relationship between distance from the fissure (m) and aspect ratio. Clast aspect ratio (i.e. welding intensity) decreases with distance. For descriptions of lithofacies see Tables 3.1 and 3.2. | 111 |
| Figure 3.13 | Lavas observed in the study area. (A) Hummocky lava (Hu) with little erosional dissection. Tumuli and squeeze outs (arrowed) create the hummocky topography. The contact with pre-existing topography is marked by the dashed line. (UTM 556219/7266138). (B) Lava-like agglutinate. Tension gashes (dashed outline) are sub-parallel to the basal contact (UTM 557447/7264902). (C) Clastogenic pāhoehoe (Cl). Gas blisters (outlined) are common. Ghost clasts are identified by intensely deformed non- and incipiently vesicular patches (dashed outline). (UTM 556985/7264113). (D) Crust of spiny pāhoehoe (dashed outline). The crust dips 30° toward the viewer. Spines on the surface of the crust are oriented parallel to the solid white lines. Hammer for scale. (UTM 557457/7265092). (E) Hyaloclastite. The pillow lava (dashed outline) occurs in a matrix of palagonitised pillow fragments. (UTM 558272/7263904). (F) Shelly pāhoehoe. The crusts and internal cavity is visible. The resinous interior surface is thought to be caused by draining of lava from the lobe (UTM 557463/7264067). | 113 |
| Figure 3.14 | Thin section images of lavas (plane polarised light). (A) Shelly pāhoehoe. Note the large vesicles. (B) Clastogenic pāhoehoe. (C) Lava-like agglutinate. (D) Hyaloclastite. The thin section is taken | 114 |

| | | |
|-------------|--|-----|
| | from the palagonite matrix. Vesicles are labelled v; sideromelane fragments are labelled s and palagonite is labelled p. | |
| Figure 3.15 | Density histograms for lava lithofacies with a pyroclastic origin. (A) Lava-like agglutinate. (B) Clastogenic lava. | 115 |
| Figure 3.16 | Features of the columnar-jointed pāhoehoe. (A) Alternating beds of sheet-like columnar-jointed pahoehoe (Cp) and clast-supported weakly agglutinated scoria lapilli and bombs (waSc) (UTM 557469/7264936). (B) Hummocky morphology flow (sensu Self et al. 1998); Cr: crust, Co: core, Ca: cavity. The hammer (circled) is 30 cm long. (UTM 557145/7265409). (C) Megavesicle in the flow core. Graticules on the scale card are 10 cm. (UTM 557772/7265756). (D) Platy fabric observed towards the base of the flow. The scale on the ruler is mm. (UTM 557772/7265756). (E) Vesicle cylinder in the core of a flow. Graticules on the scale card are 1 cm. (UTM 557544/72651054). | 119 |
| Figure 3.17 | Features of the clastogenic lava. (A) Photograph showing the internal texture of the clastogenic flows, with highly deformed ghost clasts and a suture between lobes towards the base. Hammer for scale. (B) Clastogenic lava with a break out of shelly lava. The shelly lava has been subsequently covered by later clastogenic breakouts. Hammer for scale. (UTM 556985/7264113). (UTM 557465/7266307). (C) Clastogenic lava that has been flooded with water during cooling. The lava has a distinctive entablature comprised of two dominant sets of joints, in which the subsidiary set radiate from the master set. (UTM 556935/7263621). | 122 |
| Figure 3.18 | Hummocky lava features. (A) A tumulus, with the upper crust partially eroded and the core exposed. Hammer for scale. (UTM 556481/7266232). (B) A lava channel on the surface of the flow field. The channel has resinous walls with vertical striations caused by the draining of lava within the channel. Direction of flow is inferred from the slope (toward viewer). The channel is ~3 m wide. (UTM 547155/7208827). (C) An elongate squeeze out at the margin of the flow field. The squeeze out is composed of numerous crusts that dip radially from the centre of the structure. | 124 |

| | | |
|-------------|---|-----|
| | Hammer for scale. (UTM 556215/7266339). (D) Photograph of the inside of a lava tube. Backpack for scale. (UTM 557462/7265995). | |
| Figure 3.19 | Features of the lava-like agglutinate (l-l Agg). (A) Tension gashes at the top of unit 5 in log 81. Graticules on the scale card are 1 cm, the arrow indicates up. (UTM 557442/7264902). (B) Intrusion of lava-like agglutinate (l-l Agg) into overlying clast-supported weakly agglutinated scoria lapilli and bombs (waSc). Dashed line indicates contact. (UTM 557442/7264902). (C) Ghost clasts (outlined) in lava-like agglutinate (l-l Agg), overprinted by a spherical vesicle (arrowed). These spherical vesicles suggest post depositional vesiculation of the lava. (UTM 557772/7265756). (D) Equant ghost clast (outlined) interpreted to represent a lava crust lithic. Compare this ghost clast with those in C and clast-supported moderately welded spatter bombs (mwSp; Figure 3.7). (UTM 557772/7265756). (E) Cored bomb with a rind of vesicular juvenile magma. The core is composed of dense agglutinate. (UTM 557442/7264902). | 126 |
| Figure 3.20 | Figure 3.20. Features of the hyaloclastite. (A) Photograph showing the stratigraphic relationship of hyaloclastite and pillow lavas (Hy) with clastogenic pāhoehoe (Cl) and fSxb (UTM 557949/7263864). (B) Vertical section through the pillow-dominated and fragmental hyaloclastite. This section is also represented in log 7; Figure 3.10 (UTM 557908/7263830). (C) Detail of a pillow lava. The chilled rinds have spalled or been abraded from the majority of the pillow. The aligned vesicles occur in a zone 5 cm wide. The core has large, irregular vesicles (UTM 558272/7263904). | 129 |
| Figure 3.21 | Panoramic photos of the western wall of the graben formed by faults F9 and F12. The photos show that the area is dominantly composed of clastogenic lavas underlain by lobate beds of clast-supported weakly agglutinated scoria lapilli and bombs (waSc) <0.5 m in thickness. 3 m wide flows of shelly pāhoehoe are also observed. Hyaloclastite thickens towards the southwest (Figure | 130 |

| | | |
|-------------|---|-----|
| | 3.3) and is inferred to be underlain by fSxb, as observed on the east of the graben (Figure 3.22). (A: UTM557585/7264214; B: UTM557595/7264181; C: UTM557601/7264125; D: UTM557616/7264059; E: UTM557649/726; F: UTM 557656/7263914). | |
| Figure 3.22 | Panoramic photos of the eastern wall of the graben formed by faults F9 and F12. The photos show that the area is composed of clastogenic and hummocky lavas underlain by lobate beds of clast-supported weakly agglutinated scoria lapilli and bombs (waSc) <0.5 m in thickness. The contacts between the hummocky and clastogenic lavas are unclear. Numerous lobes 1–5 m thick are observed within the clastogenic lavas. Hyaloclastite thickens towards the southwest (Figure 3.3) and is underlain by fSxb. Note the absence of Clast-supported weakly agglutinated scoria lapilli and bombs (waSc) at the base of the stratigraphy in (A), suggesting either that this section of the fissure was dominated by effusive activity, or that the pyroclasts coalesced to form lava which subsequently interacted with surface water (forming hyaloclastite). (A: UTM 557934/7263920; B: UTM 558083/7264079; C: UTM 557849/7264219). | 131 |
| Figure 3.23 | Photograph showing shelly pāhoehoe at the opening of a horseshoe-shaped scoria cone (UTM 557647/7265074). | 132 |
| Figure 3.24 | Sedimentary lithofacies observed in the study area. (A) Fine, diffusely bedded volcanoclastic pebbly sandstone (pebbles are outlined). See log 16 for stratigraphic position. (UTM 557437/7263977). (B) Inverse-graded cobble breccia. See log 16 for stratigraphic position. (UTM 557437/7263977). (C) Fine, cross bedded volcanoclastic sandstone with gravel, pebbles and cobbles. See log 81 for stratigraphic position. (UTM 557495/7265751). (D) Fine, hummocky cross-stratified pebbly sandstone. Sub-horizontal diffuse beds ~10 cm thick are marked by dashed lines. See log 81 for stratigraphic position. (UTM 557442/7264902). See Tables 3.1 and 3.2 for lithofacies descriptions. | 133 |

| | | |
|-------------|---|-----|
| Figure 3.25 | <p>Photographs of the canyon walls. (A) Cross section of a scoria-agglutinate cone (location 289; edifice 26) and scoria rampart (location 280). Crater 2 of an overlapping edifice is also shown. (UTM 557542/7264269). (B) Photograph of the canyon wall north of image A. The R-K volcanic sequence is composed of sheet-like fall deposits, scoria ramparts and lava flows of columnar-jointed pāhoehoe (Cp) and clastogenic pāhoehoe (Cl). Numerous faults are visible with throws of ~1 m. The northwestern bounding fault of the Sveinar graben is ~20 m left of the image. (UTM 557617/7265642). (C) Photograph of the western canyon wall. A scoria rampart (Location 477) is observed and has anticlinal bedding at its base. Clastogenic lavas onlap the rampart towards the southeast. Contacts beneath the rampart within crystalline and clastic successions are gradational and beds may pinch-out laterally. The graben bounding fault (F33) is visible toward the southeast. The northwest graben fault is not visible from this location. (UTM 557356/7265748). (D) Photograph of the western canyon wall. The volcanoclastic sandstone with planar bedding (vSpb) is observed at the base of the R-K volcanic sequence. Faults are numbered according to Figure 3.4. (UTM 557617/7265642).</p> | 137 |
| Figure 3.26 | <p>Location and orientation of faults associated with edifice 26 and the scoria rampart (location 280). Faults are labelled according to Figure 3.4 and are indicated by the dashed line. Arrows indicate the direction of downthrown. The contact between the underlying stratigraphy and the R-K stratigraphy is indicated. (A) F10 is exploited by the R-K feeder dyke. Throw is observed to be ~3 m southeast. (UTM 557542/7264269). (B) Numerous faults in the scoria rampart (location 280). Note the throw in the upper pyroclastic units (stippled lines). (UTM 557465/7264189). Images C–F show deformed blocks of clast-supported densely welded spatter bombs (dwSp) located at the top of normal faults (UTM 564033/7302375). Ghost clasts indicate the original depositional fabric, whilst tension gashes that intersect the bedding suggest</p> | 138 |

| | | |
|-------------|---|-----|
| | ductile deformation in a viscous deposit. Movement was not along the depositional planes, nor confined to the margins of the clast-supported densely welded spatter bombs (dwSp). Ghost clasts are downthrown towards the west (indicated by the dashed line) and suggest extensional deformation. The ruler in C is 70 cm. The block in E is 20 mm wide. Similar features are observed in the clast-supported densely welded spatter bombs (dwSp) at the top of F2. Deformation is interpreted to be the result of syn-eruptive faulting. (G) Map showing location of the faults. | |
| Figure 3.27 | Location and orientation of selected faults (dashed lines). Faults are labelled according to Figure 3.4. Arrows indicate direction of downthrown. The contact between the underlying stratigraphy and the R-K stratigraphy is indicated. (A) F6 forms the margin of an inlet and offsets the upper clastogenic pāhoehoe (Cl). (UTM 557601/7265530). (B) Syn-eruptive slip along F17 is inferred to have resulted in the ductile deformation of the upper agglutinated pyroclastic units resulting in a break in slope at the surface. (UTM 557772/7265756). (C) Fault 21 forms an inlet on the river and forms a gully. There is no topographic expression of the fault in the uppermost lavas. (UTM 557772/7265756). (D) Faults 19 and 20. Columnar-jointed pāhoehoe (Cp) occurs within the graben formed by these faults. (UTM 557601/7265530). (E) Map showing location of the faults. | 140 |
| Figure 3.28 | Location and orientation of the Sveinar graben bounding faults and stereonet data. Faults are labelled according to Figure 3.4 and are indicated by the dashed line. Arrows indicate direction of downthrown. The contact between the underlying stratigraphy and the R-K stratigraphy is indicated. (A) Segmented graben bounding faults (F31–33) east of the river. (UTM 557432/7264244). (B) Graben bounding fault west of the river. The lava-like agglutinate (l-l Agg) terminates against the footwall of the graben. The contact between the lava-like agglutinate (l-l Agg) and clastogenic pāhoehoe (Cl) is shown as a stippled line. Note the absence of faulting in the hummocky pāhoehoe (Hu), | 141 |

| | | |
|-------------|---|-----|
| | <p>indicating that the fault existed prior to the eruption. (UTM 563879/7301531). (C) Google Earth image showing F33 (arrowed) faulting the uppermost clastogenic lavas, indicating that the fault had several stages of growth. The fault is concealed further north by scoria (dashed outline). (D) F9 forming the margin of an inlet. The clastogenic pāhoehoe (Cp) is offset by the fault. (UTM 557617/7265642). (E) Pole to plane plot showing the orientation of faults XA, F0,1,4–6,9,13,17, 19–21, 31–33 and 38. (F) Google Earth image showing that F33 (the eastern Sveinar graben bounding fault) does not have a scarp east of the river. This suggests that either: the fault is segmented and slip did not occur on this section of the fault; and/or the eruption continued after faulting. (G) Map showing location of the faults.</p> | |
| Figure 3.29 | Google Earth image showing the extent and bedding of the pyroclastic constructs. See text for details. | 143 |
| Figure 3.30 | <p>Figure 3.30 (overleaf). Architectural features of the dyke. (A) Thin section image of the dyke (plane polarised light). The sample is taken 30 cm from the country rock contact. (B) View toward the conduit from the west of the canyon. The underlying plagioclase porphyritic lava flows are the source of the lithic clasts in log 29 (Figure 3.12). Note the scalloped contacts between the dyke and country rock and the numerous intrusions into the overlying pyroclasts. (UTM 557617/7265642). (C) Plot of depth from the top of the canyon vs. conduit radius. The flaring hinge is located at a depth of 40 m at the base of the porphyritic lavas. (D) An effusive dyke on the west of the canyon feeding overlying lava-like agglutinate (l-l Agg). Dashed lines indicate cooling joint orientations. See Figure 3.25 for location. (UTM 557460/7264234). (E) A section of the dyke adjacent to the river on the west of the canyon. Dashed lines indicate cooling joint orientations. The solid line indicates the contact with the country rock. Bag (circled) is ~0.5 m. See Figure 3.25 for location. (UTM 557510/7264268). (F) Multiple chilled margins at the dyke/country rock contact. The scale card is 10 cm long. Dashed</p> | 147 |

| | | |
|-------------|--|-----|
| | lines indicate laminations spaced ~ 2 cm. See (D) for location. (UTM 557510/7264268). (G) Arrested dyke intruding into overlying pyroclastics west of the river. See Figure 3.25 for location. Lithofacies codes are as Figs. 3.8 and 3.13. (UTM 557519/7264280). | |
| Figure 3.31 | Comparison between rootless vents at Hjalparfoss (UTM 402187/7098548) and those along the R-K fissure (UTM 557772/7265756). Images A and C show the vents and the host lavas flows along the R-K fissure and at Hjalparfoss respectively, images B and D show the contact between the columnar jointed pāhoehoe (Cp) lava and massive scoria lapilli and bombs (mSc). Notice the colonnade (CN) and entablature (EN) of the lava flows with cooling joints that radiate from the hummocky, bowl-shaped upper contact. The ruler in B and D is 25 cm. | 150 |
| Figure 3.32 | Photograph (A) and a reconstruction of the geometry of the pyroclastic constructs immediately after the eruption (B). Truncated beds are visible in the NW margin of the scoria rampart (location 280) and in the crater of cone 26. Field observations suggest ~10 m of stratigraphy is has been eroded from the cone and the rampart. (A: UTM 557542/7264269). | 155 |
| Figure 3.33 | Google Earth image showing the inferred location of paleo-channels, contemporary channels and the outcrops of sedimentary lithofacies. | 156 |
| Figure 3.34 | Scoria ramparts adjacent to the Laki fissure. (A) Google earth image showing that the ramparts are linear and crescent-shaped, elongated parallel to the fissure. They occur on the outer margin of the cones. (B) Photo of scoria ramparts, showing that they are asymmetric and larger than the adjacent cones. The ramparts decrease in thickness towards and with distance from the fissure. Photo: Nick Crabtree. | 157 |
| Figure 3.35 | Photographs showing the architecture of edifice 26. (A) The rosette structure is located above the feeder dyke. The cooling joints at the top of the rosette are more closely spaced and shorter than those at the base, implying that the rosette cooled from the | 161 |

| | | |
|-------------|---|-----|
| | <p>top downwards. (UTM 557498/7264870). (B) A lobate lense of clast-supported weakly agglutinated scoria lapilli and bombs (waSc) within the lava-like agglutinate (l-l Agg). The lava-like agglutinate (l-l Agg) has distinct contacts with the clast-supported weakly agglutinated scoria lapilli and bombs (waSc) and is interpreted to be part of a lava sill/dyke network. (UTM 557447/7264902). (C) View of the northern crater rim showing the outwardly dipping units of lava-like agglutinate (l-l Agg) which merge further west. Inverse-graded cobble breccia (cPi) and fine, diffusely bedded volcanoclastic pebbly sandstone (fSdb) are visible inside the crater. (UTM 557438/7264880). (D) Photo of the outwardly dipping lithofacies on the crater rim. (UTM 557447/7264902).</p> | |
| Figure 3.36 | <p>Orientation and onlap relationships of the spatter ramparts. (A) Google Earth image showing that some spatter ramparts are oriented perpendicular to the strike of the fissure. (B) Google Earth image of eroded spatter ramparts that are oriented parallel to the strike of the fissure. (C) Photograph of the spatter ramparts shown in B. (D) Google Earth image of scoria cone 22 overprinting adjacent spatter ramparts. The onlapping relationship of the edifices cannot be used to constrain the direction in which the fissure propagated.</p> | 165 |
| Figure 3.37 | <p>Figure 3.37. Google earth image (A), geological map (B) of the spatter ramparts west of the river. See Figure 3.3 for location.</p> | 166 |
| Figure 3.38 | <p>Features and measurements associated with location Y29. (A) Scoured agglutinate slab with adjacent sections missing, exposing underlying rubbly agglutinate. The slab has detached from the upper section (arrowed) where the dip of the outcrop changes. The tape measure (arrowed) is 1 m long. (UTM 564346/7301822). (B) Close up of the scours overprinted by tension gashes (outlined), indicating deformation of the agglutinate after the external surface was scoured. Graticules on the scale card are 1 cm. (UTM 564346/7301822). (C) Stereonet plot to show orientation of bedding (black) and scours (purple) on</p> | 167 |

| | | |
|-------------|--|-----|
| | <p>the southwest face of location Y29. The scour plunges are not parallel to the bedding dip direction suggesting that sliding from the outer face occurred in numerous directions with a component of lateral movement. (D) Cross sectional view of the snout of an agglutinate bed. The tension gashes (dashed lines) on the crust (Cr) are perpendicular to the scours (sub vertical striations) and give the snout a rugose texture. The core of the bed (Co) is also exposed (see Figure 3.39 for details). The tape measure is 1 m long. (UTM 564346/7301822). (E) A rugose textured surface, showing irregular protrusions separated by tension gashes. The ruler is 10 cm long. (UTM 557584/72664247). (F) Graph showing that tension gashes are most abundant towards the snout of the agglutinate sheets, where 0 = the snout tip. (G) Graph showing that crenulation width tends to decrease with distance from the snout of agglutinate beds, where 0 = the snout tip. Graphs F and G suggest that strain is greatest towards the snout of the beds.</p> | |
| Figure 3.39 | <p>Stratigraphic log showing the internal componentry of location Y29. The outcrop is composed of numerous discordant slabs of agglutinate. The upper unit of agglutinate is shown in Figure 3.38D. See Figure 3.37 for the location.</p> | 169 |
| Figure 3.40 | <p>Photographs and measurements associated with location Y28. (UTM 564390/7301820). (A) Cross section of the agglutinate, with clast-supported incipiently welded spatter bombs (waSp) beneath. The agglutinate becomes more vesicular with height and has a 70 mm thick platy crust. Tension gashes occur at the base (arrowed) and in the incipiently vesicular agglutinate in the upper 0.5 m. The tape measure is 50 cm long. (B) Log showing the internal stratigraphy of A. Clast aspect ratio is shown in red, juvenile clast size in black. (C) Details of the ghost clasts (solid lines). Graticules on the scale card are 1 cm. (D) Stereonet to show the orientation of the crust (great circles) tension gashes (black) and ghost clasts (purple). The tension gashes are approximately perpendicular to the outer crust. (E) Photo of the upper crust showing the jigsaw-fit plates. The tape measure is 25</p> | 170 |

| | | |
|-------------|--|-----|
| | cm long. | |
| Figure 3.41 | <p>Schematic diagram to show the development of Location Y29. Images A and B show the accumulation and coalescence of constituent spatter bombs during Hawaiian-style activity. Images C–E show the evolution of the south face, whilst images F–H show the evolution of the north face of the rampart. (C) Agglutinate slides down the rampart, scouring the underlying face. The material that causes the scouring is not observed. (D) Continued lava fountaining deposits spatter bombs atop the scoured surface. (E) The spatter bombs coalesce forming a slab of agglutinate, on which a crust develops. This crust is deformed by tension gashes (found dominantly towards the snout of the slab) during clastogenic flow. This slab has scours on its outer surface, suggesting repeating episodes of deposition and flow (not shown). The absence of material at the toe of the slab may suggest collapse of the slab in stages. (F) On the northern slope scouring occurs due to sliding of material down the outer rampart face. (G) The scours are preserved as the rampart cools and a brittle crust develops. (H) Fractures form at the change in dip amplitude and sections of the outer crust collapse due to gravitational instability.</p> | 171 |
| Figure 3.42 | <p>Interpretive picture to show the development of location Y28. (A) High rate accumulation of spatter bombs during lava fountaining. Welding intensity is greatest beneath the dashed line. (B) Agglutination and coalescence of pyroclasts. Ghost clasts remain in the upper part of the deposit. (C) Bubbles migrate upwards in the deposit and a crust forms. (D) Gravitational spreading is initiated along the basal lubricating layer. The crust is fractured into numerous plates. Note that stages A and B are contemporaneous: welding and coalescence occurring during deposition.</p> | 172 |
| Figure 3.43 | <p>Schematic diagram to show the development of the R-K fissure. (A) Phase 0: The Sveinar graben pre-dates the fissure. Drainage patterns are controlled by pre-existing faults. (B) Phase I: The dyke fed numerous en-echelon fissure segments that propagated</p> | 175 |

| | | |
|------------|---|-----|
| | north-south. (C) Phase II: Lava flows buried scoria ramparts. The fissure began to evolve to numerous point sources due to thermal instabilities. (D) Phase III: Low fountains ≤ 100 m in height constructed edifice 26 (location 289). (E) Phase IV: In the north of the study area, hummocky lava was emplaced. (F) Phase V: Pyroclastic constructs were deformed by slip along faults. Post-eruption faulting associated with the Sveinar graben continued. Diagram not to scale. | |
| Figure 4.1 | Generalised structure of a rootless cone. The cones form on active lava flows. The conduits in the host lava flow are irregular funnels that widen upwards. The upper parts of the conduits are filled with tephra. Cooling joints in the host lava flow radiate from the conduit. Cone forming deposits are composed of lapilli- to bomb-sized material that is often reversely graded and formed by fallout. Platform and sheet deposits are formed by fallout and deposition from pyroclastic density currents. Adapted from Hamilton et al. (2010a). | 193 |
| Figure 4.2 | Location of the study area. (A) The CRFBP in the NW USA, adapted from Brown et al. (2014). (B) Map of the area showing the Ice Harbor fissure as described by Swanson et al. (1975) and the field area on the banks of the Snake River. (C) Sites of the tephra and conduit deposits described in this study. | 195 |
| Figure 4.3 | Field photographs and schematic diagrams showing the varying geometries of rootless conduits. (A) Field sketch showing the upper part of a funnel-shaped conduit at location 6 (UTM Nad83 zone 11T, 359 987 E/5 126 647 N). View to the southwest. (B) Field photograph of massive spatter (mSp) within the conduit in a, composed of spatter bombs, silicic volcanic ash and hypocrySTALLINE lapilli. (C) Irregular lower part of a conduit in the lava flow at location 22 (UTM Nad83 zone 11T, 359 724 E/5 128 162 N) with cooling joints (white) radiating from the conduit/lava core contact (outlined). The ruler is 1 m. Inset D shows a close up of the conduit inner wall with embedded juvenile and lava crust lithic clasts. The ruler is 25 cm. Image E shows a cross section | 199 |

| | | |
|------------|---|-----|
| | through the conduit wall, with hypohyaline lapilli embedded into the surface. (F) Interpretive sketch of E. (G) Plan view of a section of conduit wall, approximately 100 mm across, showing clasts that are inferred to have become embedded in the conduit wall during explosions (dashed outlines). | |
| Figure 4.4 | Clast types recognised in this study. (A) Folded spatter bomb with embedded lapilli (dashed outline). Graticules on the scale card are 1 cm (UTM Nad83 zone 11T, 359 942 E/5 126 519 N). (B) Ventricular clast (outlined). The clast has an amoeboid shape with a hypohyaline rind approx. 10 mm thick that grades inwards into the core. Vesicles up to 8 cm in diameter (dashed outline) have angular shapes and give clasts their characteristic ventricular morphology (UTM Nad83 zone 11T, 359 942 E/5 126 519 N). (C) Globular bomb (outlined). The bombs have a sub-spherical shape and a black hypohyaline rind ~1 cm thick that becomes more orange in colour toward the core. Sub angular, dull black coloured basaltic lapilli (arrowed) are contained within the cores of the bombs. Cooling joints (dashed lines) penetrate from the clast margin up to 10 mm towards the core (UTM Nad83 zone 11T, 359 942 E/5 126 519 N). (D) Armoured bomb (solid outline) with 1 cm thick dense rind and vesicular core (dashed outline) (UTM Nad83 zone 11T, 360 015 E/5 126 664 N). (E) Sideromelane clast (arrowed) formed by fragmentation in a brittle state (arrowed). (F) Sideromelane clast (arrowed) formed by ductile disruption of molten lava. | 202 |
| Figure 4.5 | Lithofacies found in the study area. (A) mL A with ventricular bomb (outlined) enclosing laminated silicic volcanic ash. Graticules on the scale card are 1 cm (UTM Nad83 zone 11T, 359 881 E/5 126 506 N) (B) lensLA with hypocrySTALLINE lapilli-rich lenses. Dashed white outlines indicate lenses (UTM Nad83 zone 11T, 359 868 E/5 126 485 N) (C) lensLA with silicic ash-rich lenses. White outlines indicate lenses (UTM Nad83 zone 11T, 359 868 E/5 126 485 N) (D) xsLA, white outlines indicate beds. The ruler is 25 cm long (UTM Nad83 zone 11T, 359 868 E/5 126 | 206 |

| | | |
|------------|--|-----|
| | 485 N) (E) //bSp, showing bedded spatter bombs. The ruler is 50 cm (UTM Nad 83 zone 11T, 359 942 E/5 126 519 N). | |
| Figure 4.6 | Lithofacies logs of tephra deposits south of the river. Clast size is shown on the top axis with divisions at 32, 64, 128 and 256 mm (Location 9 uses 32, 64, 128, 256 and >1000 mm divisions). Silicic volcanic ash abundance (black squares; %) is shown across the bottom axis in 25% graticules. Logs are shown at relative altitudes. For locations of the sections see Fig. 4.2. | 209 |
| Figure 4.7 | Photographs and interpretive pictures of Location 9 (UTM Nad 83 zone 11T, 359 942 E/5 126 519 N). a, b Outcrop of platform-forming admixed tephra and silicic volcanic ash. c,d Outcrop of cone-forming tephra composed of lithofacies //bSp. | 210 |
| Figure 4.8 | Peperite-like textures produced by the interaction of juvenile clasts and silicic volcanic ash. (A) Fluidal peperite with elongate and globular clasts in lithofacies //bSp (UTM Nad 83 zone 11T, 359 942 E/5 126 519 N). (B) Blocky peperite with jigsaw-fit fractures (circled). Graticules are 1 cm (UTM Nad 83 zone 11T, 360 014 E/5 126 649 N). Thin section C and interpretive sketch D shows section of mingled spatter and silicic volcanic ash. The spatter clasts exhibit elongate and globular morphologies. The silicic ash is thermally altered and contains vesicles. Vesicles within the spatter clasts enclose silicic volcanic ash. Section of a ventricular bomb E and interpretive sketch F are also shown. The hypohyaline rind is spalling from the core and has encapsulated a domain of silicic volcanic ash. Fluidal basalt clasts are found within the silicic ash domain (arrowed) indicating that the core of the bomb was molten when the sediment was encapsulated. | 212 |
| Figure 4.9 | Inferred eruption chronology for the cones. (A) Lava flow traverses wet ground and subsides heterogeneously into the underlying silicic volcanic ash. (B) Initial mingling of lava with the silicic ash results in the formation of globular and ventricular juveniles and peperite-like textures. (C) Interaction between molten lava and water saturated silicic volcanic ash results in explosive brecciation of the host lava flow and fragmentation of | 215 |

| | | |
|-------------|---|-----|
| | <p>the globular and ventricular juveniles into lapilli and ash sized clasts. Episodic eruptions and dilute PDC's deposit poorly sorted juveniles and clasts sourced from the host lava flow, forming sheet and platform deposits (lithofacies m/nLA(f), lensLA, xsLA). Minor clast recycling may occur, producing armoured bombs. Substrate pore water is gradually depleted beneath the lava flow. (D) Decreasing water availability results in less efficient fragmentation and lava fountains are generated. These fountains produce lithofacies //bSp that builds a cone. Lapilli are also impacted into the cooling conduit walls. (E) With time water availability decreases and eruptions cease. The lava flow may continue to inflate and deform the conduit. Post-eruption cooling of the lava promotes the formation of cooling joints that radiate from the conduit.</p> | |
| Figure 4.10 | <p>Photographs of Leitin and Búrfell rootless cones in southern Iceland (UTM Nad 83, zone 27, 500 000 E/7 097 014 N; 402 187 E/7 098 548 N respectively). (A) Overlapping cone stratigraphies composed of crudely bedded spatter and scoria bombs and lapilli and clastogenic lava. The sequence is ~6 m thick. (B) Bomb-sized clast of sediment (outlined) within a sequence of scoria and spatter. The ruler is 40 cm long. (C) Sediment-rich pyroclastic density current deposit at the base of the cone forming stratigraphy. The reddish colour is given by the agglutinated sediment (inferred to be a lacustrine siltstone), not oxidation of the pyroclasts. The scale card is 120 mm long. (D) Bomb-sized, ventricular-type pyroclast (outlined) within the bedded spatter and scoria. The ruler is ~25 cm long. (E) Initial cone-forming fall deposit, composed of scoria lapilli. Beds often form inversely-graded couplets. The bed indicated is ~6 cm thick. Beds thickness and clast size increases up-section. (F) Cross section of the conduit wall, with lapilli sized pyroclasts agglutinated to the outer wall. Cooling joints (dashed lines) radiate from the contact and are perpendicular to the conduit contact. The arrow points towards the core of the lava flow. The</p> | 217 |

| | | |
|-------------|--|-----|
| | ruler is 30 cm long. (G) A lava flow affected by rootless cone formation. The lava flow can be divided into a colonnade (CN) and an entablature (EN), and has an irregular upper contact that forms the rootless conduit. The lava is ~10 m thick. | |
| Figure 5.1. | Location of the study area. The Bass Basin is shown in green, the red outline delimits the Labatt survey and the yellow delimits Yolla survey. Bass-1, King-1, Yolla-1 and Cormorant-1 wells are also shown. A 2D seismic line (A–A'; Fig. 5.2) between the surveys is shown. A simplified stratigraphy of the Bass Basin is also shown. Modified from Boral Energy Resources Ltd. (1998). | 226 |
| Figure 5.2. | Seismic line A–A' and interpretation intersecting the Cormorant-1, Bass-1 and Yolla-1 wells. Correlated horizons are also shown. | 229 |
| Figure 5.3. | Well logs for King-1, Cormorant-1, Bass-1 and Yolla-1. Seismic horizons are also shown: LMM=Lower Mid Miocene, TV=Top Volcanic, BV=Base Volcanic, OH=Oligocene, Demons Bluff=DB, EVCM=Eastern View Coal Measures, LV=Lower Volcanic, TA=Top Aroo and BA=Base Aroo. Adapted from Trigg et al. (2003). | 230 |
| Figure 5.4. | Time (A) and amplitude (B) maps of the TV horizon in the Labatt survey. The edifices (dashed outline) are numbered in B. See Fig. 5.5 for cross section. | 232 |
| Figure 5.5. | Seismic line B–B' and interpretation in the Labatt survey. See Fig. 5.4 for location. | 228 |
| Figure 5.6. | Time (A) and amplitude (B) maps of the TV horizon in the Yolla survey. The edifices (dashed outline) are numbered in B. See Fig. 5.7 for cross section. | 233 |
| Figure 5.7. | Seismic line C–C' and interpretation in the Yolla survey. See Fig. 5.6 for location. | 234 |
| Figure 5.8. | Seismic line X–Y showing that the basal diameter of the edifices (A–B) is calculated from the change in seismic facies and amplitude of the edifice. See Fig. 5.4 for location. | 236 |
| Figure 5.9. | Seismic sections showing the seismic facies of the pit craters (A), pointed (B), flat-topped (C) and cratered (D) edifices. The | 242 |

| | | |
|--------------|--|-----|
| | location of the sections is shown in the time map of the Labatt survey (E). | |
| Figure 5.10. | Features associated with the pointed edifices. Seismic line (A). Horizons V1 and V2 are shown in B and C respectively. See Fig. 5.9 for location. (B) Concentric faulting (dashed lines) in horizon V1 around the underlying conduit. (C) Concentric faulting (dashed lines) in horizon V2 around the underlying conduit. (D) Time slice at 0.63 s TWTT beneath the edifice showing an onion-ring structure. | 243 |
| Figure 5.11. | Seismic line (A) and interpretation (B) showing that the edifices in linear clusters young towards the south. | 245 |
| Figure 5.12. | Seismic section (A) and time map (B) of a flat-topped edifice fed by a sill/dyke system. See Fig. 5.4 for location. | 246 |
| Figure 5.13. | Amplitude map of the LV horizon. Inset B shows a RGB decomposition image of the lava flows. | 247 |
| Figure 5.14. | Schematic diagram to show the evolution of a submarine monogenetic volcano. (A) Submarine maar-diatreme complexes form during Taalian-style activity. Syn- and post-eruptional sediments fill the Continued activity results in the submarine effusion of lavas, building pillow volcanoes. These are represented by the pointed edifices. (C) Tuff cones, represented by the flat-topped and cratered edifices, are formed during Surtseyan activity. Ponding of lavas within the crater resulted in the formation of flat-topped volcanoes. These edifices may have been emergent. Image (D) shows the location of diagrams A–C. | 251 |
| Figure A.1. | Seismic section (A) and interpretations (B and C) of the cone-shaped edifice observed on the 2D seismic line between the Yolla and Labatt surveys. The edifice has identical internal facies to the edifices observed in the Labatt and Yolla surveys, although its morphology is somewhat different. Well data from King-1 indicates that the edifice is composed of volcanic rock. LMM=Lower Mid Miocene, TV= Top Volcanic. | 422 |
| Figure A2. | Amplitude map of the Lower Volcanic Horizon in the Labatt survey. | 423 |

List of Tables

| | | |
|-----------|--|-----|
| Table 2.1 | Summary of volcanic edifice morphology. Data from Waters and Fisher (1971); Wood (1980); Head et al. (1981); Wilson and Head (1981); Thors and Jakousson (1982); Wohletz and Sheridan (1983); Gatliff et al. (1984); Ross (1986); Rossi (1996); Vespermann and Schmincke (2000); White and Ross (2011); Grosse et al. (2009); Mitchell et al. (2012) and (Brown et al., 2014). | 40 |
| Table 2.2 | Table 2.2. Summary of volcanic edifice architecture (*water depth to summit). Data from Macdonald (1972); Wohletz (1983); Lorenz (1986); Rossi (1996); Riedel et al. (2003); Grosse et al. (2009); White and Ross (2011); Mitchell et al. (2012); Magee et al. (2013) and Brown et al. (2014). | 41 |
| Table 2.3 | Summary of the seismic characteristics of volcanic edifices in seismic section. Data from Thors and Jakousson (1982); Bergman et al. (1991); Bell and Butcher (2002); Thomson (2005); Wall et al. (2010) and Magee et al. (2013). | 56 |
| Table 2.4 | Summary of the morphology of sedimentary edifices. Data from Kopf et al. (1998); Yusifov and Rabinowitz (2004); Davies and Stewart (2005); Planke et al. (2005); MØller Hansen (2006); Svensen et al. (2006); Svensen et al. (2007); Huuse et al. (2010); Grove (2013). | 58 |
| Table 2.5 | Summary of the seismic characteristics of sediment type vents in seismic section. Data from Kopf et al. (1998); Davies and Stewart (2005) Stewart and Davies (2006); Evans et al. (2007) and Roberts (2011). | 59 |
| Table 3.1 | Terminology and definitions. | 88 |
| Table 3.2 | Summary descriptions of pyroclastic lithofacies. | 98 |
| Table 3.3 | Summary of the texture, distribution and petrography of the pyroclastic lithofacies | 99 |
| Table 3.4 | Summary table of lavas and dyke (* sample depth 80 m beneath paleo-surface) | 116 |

| | | |
|--------------|--|-----|
| Table 3.5 | Summary of sedimentary lithofacies. All lithofacies are interpreted as fluvial deposits, possibly related to glacial floods. | 134 |
| Table 3.6 | Summary features of pyroclastic deposits. *shortest axis | 144 |
| Table 4.1 | Summary descriptions of pyroclast types. | 204 |
| Table 4.2 | Summary descriptions of cone-forming and conduit deposits. | 208 |
| Table 4.3 | Comparison of rootless and littoral cone structures using data from Simpson and McPhie (2001); Mattox and Mangan (1997); Moore and Ault (1965); Fisher (1968); Hamilton et al. (2010a); Melchior Larsen et al. (2006); Jurado-Chichay et al. (1996); and this study. | 219 |
| Table 5.1 | Summary characteristics and interpretation of seismic facies. | 235 |
| Table A1.1 | Orientations of faults | 275 |
| Table A1.2 | Point count data for lithofacies. | 276 |
| Table A1.3 | Measurements of platy zone in columnar basalt, log 14, unit 4 | 276 |
| Table A1.4 | Measurements of platy zone in columnar basalt, Log 30, unit 1. | 276 |
| Table A1.5 | Measurements of platy zone in columnar basalt, Log 12, unit 11. | 277 |
| Table A1.6 | Density measurements for waSp. | 278 |
| Table A1.7 | Density measurements for mwSp. | 280 |
| Table A1.8 | Density measurements for l-l Agg. | 282 |
| Table A1.9 | Density measurements for dwSp. | 286 |
| Table A1.10 | Density measurements for ScL. | 287 |
| Table A1.11 | Density measurements for waSc. | 289 |
| Table A.1.12 | Density measurements for mwSc. | 292 |
| Table A1.13 | Density measurements for Cl. | 293 |
| Table A1.14 | Density measurements for dwSc. | 295 |
| Table A1.15 | Bedding measurements for edifices. | 296 |
| Table A1.16 | Dispersal characteristics for the tephra. | 298 |
| Table A1.17 | Bedding measurements in scoria rampart. | 301 |
| Table A1.18 | Stratigraphic log measurements from 2012. | 303 |
| Table A1.19 | Stratigraphic log measurements from 2013. | 335 |
| Table A1.20 | Measurements of lithic clasts. | 338 |
| Table A1.21 | Measurements of scours at location y29. | 366 |

| | | |
|-------------|---|-----|
| Table A1.22 | Measurements of tension gashes at location y26. | 367 |
| Table A1.23 | Measurements of scours at location Y29. | 368 |
| Table A1.24 | Measurements of tension gashes at location y26. | 368 |
| Table A1.25 | Measurements of tension gashes at location y28. | 370 |
| Table A1.26 | Measurements of tension gashes at location y28. | 371 |
| Table A1.27 | Measurements of tension gashes at location y29. | 372 |
| Table A1.28 | Measurements of tension gash distribution at Location Y29. | 372 |
| Table A1.29 | Measurements of tension gash lengths at location y29. | 373 |
| Table A1.30 | Measurements of tension gashes at location y29. | 374 |
| Table A1.31 | Measurements of tension gashes at location y27. | 375 |
| Table A1.32 | Measurements of tension gashes at location y29. | 376 |
| Table A1.33 | Measurements if tension gashes at location y35. | 377 |
| Table A1.34 | Measurements of tension gashes at location y37. | 377 |
| Table A1.35 | Measurements of tension gashes at location y37. | 378 |
| Table A1.36 | Measurements of tension gashes at Location Y42. | 379 |
| Table A2.1 | Measurements of the lapilli impacted into the conduit walls. | 381 |
| Table A2.2 | Measurements of juvenile clast sizes and lithofacies type. | 395 |
| Table A2.3 | Summary of unit thickness, average maximum clast size and Silicic volcanic ash abundance. | 400 |
| Table A2.4 | Spacing of cooling joints in host lava flows. | 401 |
| Table A2.5 | Juvenile abundance calculated using IJ. | 402 |
| Table A2.6 | Point count measurements of pyroclasts. Glass content corrected for vesicles and Silicic volcanic ash. Point counts conducted at 20X mag. | 403 |
| Table A2.7 | Image analysis measurements of sideromelane ash. | 406 |
| Table A2.8 | UTM coordinates of study locations. | 408 |
| Table A2.9 | Sorting of Silicic volcanic ash calculated by sieving. | 408 |
| Table A2.10 | Measurements of largest clasts in lithofacies mSp. | 409 |
| Table A2.11 | Density measurements for the Ice Harbor lava core. Weight is in g, density in kg m^{-3} , vesicularity in %. | 410 |
| Table A2.12 | Density measurements for the spatter bombs. Weight is in g, density in kg m^{-3} , vesicularity in %. | 412 |
| Table A2.13 | Density measurements for the armoured bombs. Weight is in g, | 414 |

| | | |
|-------------|--|-----|
| | density in kg m ⁻³ , vesicularity in %. | |
| Table A2.14 | Density measurements for the hypocrystalline lapilli. Weight is in g, density in kg m ⁻³ , vesicularity in %. | 417 |
| Table A2.15 | Measurements of ventricular and globular bomb fragments in lithofacies lensLA, mSp and mLA. | 419 |
| Table A3.1 | Summary of measurements for vents described in this study. Vents 1–28 are found within the Labatt survey, 29 – 34 are within the Yolla survey. | 424 |

Chapter 1: Introduction

1.1 Flood basalt volcanism and hydrocarbon exploration

Flood basalt volcanism has produced the largest and most extensive lava flow fields in Earth's history, covering areas 10^6 km^2 in size (Jerram and Stollhofen 2002; Bryan and Ernst 2008; Bryan et al. 2010). The products of this volcanism provide information on the timing of major mantle melting events and may be linked to mass extinctions (e.g. Thordarson et al. 1996; Wignall 2001; Jerram 2002; Thordarson et al. 2009). Since flood basalt emplacement is associated with continental breakup (Courtilot et al. 1999), many flood basalt provinces are located in oceanic basins. These basins are frontier regions for hydrocarbon exploration (Fig. 1.1). The Faroe Shetland Basin (FSB) in the North Atlantic Igneous Province (NAIP) is one such basin and provides the motivation for this research.

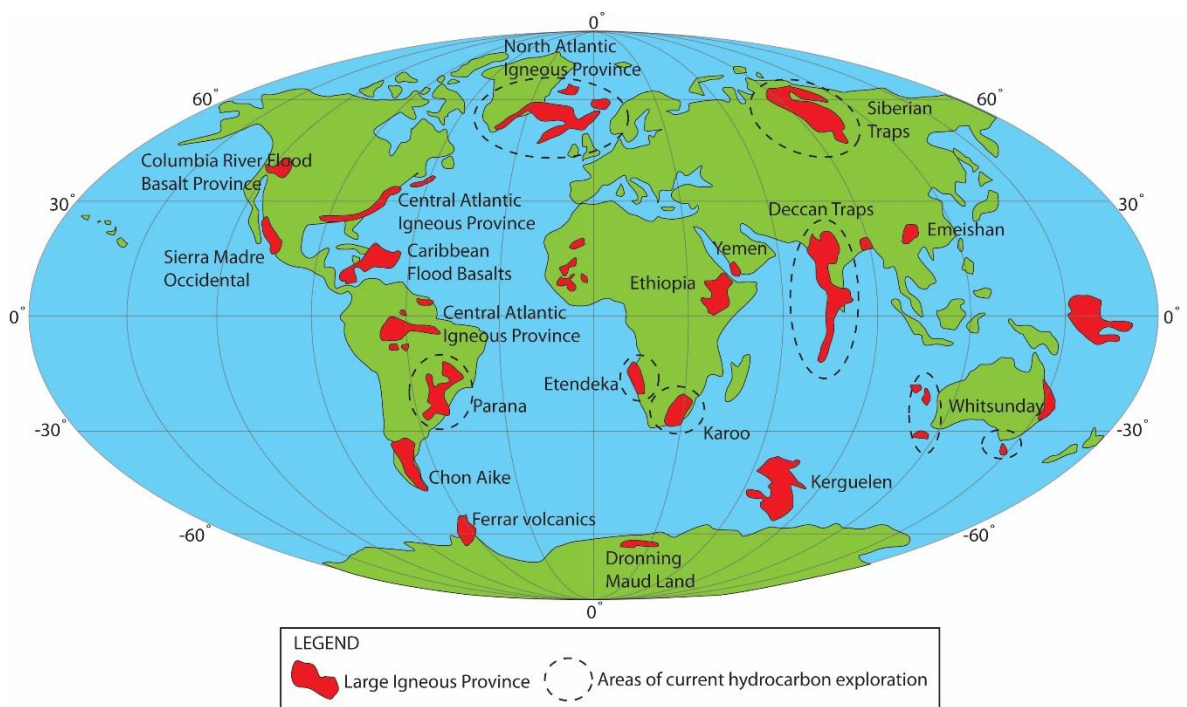


Figure 1.1. Map showing the distribution of Large Igneous Provinces and basins that are the sites of current hydrocarbon exploration. Modified from Coffin and Eldholm (1992), Coffin and Eldholm (1994), Courtilot et al. (1999), Sheth (1999), Jerram and Widdowson (2005), Ross et al. (2005), Rohrman (2007), Bryan and Ernst (2008) and Wright (2013).

1.2 The importance of fissure volcanism

Flood basalts are inferred to have been erupted from fissures (e.g. Swanson et al. 1975; Reidel and Tolan 1992; Thordarson and Self 1998; Kent et al. 1998; Hooper 2000; Walker 2000; Bondre et al. 2004a; Passey and Bell 2007; White et al. 2009; Brown et al. 2014). Fissure eruptions are monogenetic events that are the starting point for most continental basaltic eruptions (Valentine and Gregg 2008). They are linear vents that produce lavas and a variety of pyroclastic edifices; most of which are magmatic (e.g. Swanson et al. 1975; Fedotov et al. 1980; Karhunen 1988; Carracedo et al. 1992; Thordarson and Self 1993; Walker 1993; Valentine and Cortés 2013; Brown et al. 2014). Magmatic edifices include agglutinate cones, spatter ramparts and Earth's most abundant volcanic landform: the scoria cone (Riedel et al. 2003). Despite the abundance of these magmatic edifices, they have remained elusive in many, if not all volcanic-affected hydrocarbon basins.

1.3 The importance of volcanic edifices

The location and development of monogenetic volcanic edifices has important implications for hydrocarbon basin architecture. Edifices partly determine lava flow field morphology as lava production is commonly focused from particular edifices (e.g. Karhunen 1988; Valentine and Cortés 2013). The lava flow field then determines the development of overlying sedimentary systems, which are potential hydrocarbon reservoirs (e.g. Schofield and Jolley 2013). Volcanic edifices also indicate underlying dyke and sill systems (e.g. Bell and Butcher 2002) which can compartmentalise and metamorphose underlying reservoirs, reducing their porosity (e.g. Girard et al. 1989; Doyle 2001; McKinley et al. 2001; Rateau et al. 2013; Grove 2014). Alternatively, underlying dykes and sills may focus fluid flow (e.g. Rateau et al. 2013). Thus, edifices and their plumbing systems can act as fluid migration pathways long after burial (e.g. Holford et al. 2012). The pyroclasts of which edifices are composed may also act as fluid reservoirs, similar to the vesicular flow tops of lava flows (e.g. Cukur et al. 2010; Burns et al. 2014; Holford and Schofield in review). Volcanic edifices can also be used to identify structural trends (e.g. Connor and Conway 2000) concealed by poor imaging in underlying stratigraphy (e.g. Jerram 2002). Moreover, edifice location helps predict lateral thickness variations in extrusive units that are below the resolution of seismic data.

Volcanic edifices also provide a host of volcanological information that can be used for hazard assessment (e.g. Cronin and Neall 2001; Riedel et al. 2003; Houghton et al.

2006) and for determining the effects of eruptions on the environment (e.g. Thordarson et al. 1996; Brown et al. 2014). The architecture of an edifice (i.e. its geometry and component pyroclasts) record temporal and spatial variations in depositional mechanisms (e.g. Sohn 1996). For instance, pyroclasts record the efficiency of magma fragmentation and explosion frequency (Valentine and Gregg 2008) and can be used to determine edifice construction timescales (e.g. Brown et al. 2014). Pyroclasts also retain fluid-dynamic and rheological information that is specific to the vent-proximal environment (e.g. Sumner 1998; Sumner et al. 2005). Paleo-environmental conditions (e.g. abundant surface water) can also be inferred from edifice architecture, since distinctive edifices (e.g. tuff cones or scoria cones) form in different hydrological regimes (e.g. Wohletz and Sheridan 1983; Sheridan and Wohletz 1983).

Furthermore, volcanoes provide insights into the underlying geology and feeder system. Clasts from the underlying stratigraphy are excavated during edifice construction (e.g. Valentine and Groves 1996; Németh and White 2003; Carrasco-Núñez et al. 2007; Valentine 2012) and eruption style is affected by dyke host-rock lithology (e.g. Sohn 1996). Pressure conditions and magma flux variations in the conduit are also recorded (Riggs and Duffield 2008; Valentine and Cortés 2013), as is information on crystallization and fluid dynamic processes in the ascending magma (Genareau et al. 2010).

1.4 The problem: identifying volcanic edifices and constraining their architecture

1.4.1 Identifying volcanic edifices in remote datasets

Seismic and well data are the most commonly used remote datasets during hydrocarbon exploration. There are several factors which make volcanic edifices difficult to locate in these datasets. Firstly, seismic data in volcanic-affected basins is often of poor quality beneath the uppermost basalt horizon. This is because the high density, internal structure and lithological heterogeneity of volcanic rocks causes scattering, attenuation and absorption of seismic waves (the "sub basalt imaging problem"; Fig. 1.2; see Jerram and Robbe 2001; Maresh et al. 2006; Shaw et al. 2008; Davison et al. 2010). Furthermore, fragmental volcanic rocks (e.g. pyroclasts) have a lower velocity than the surrounding lavas (e.g. Planke and Eldholm 1994; Nelson et al. 2009; Wright 2013). This produces an impedance contrast and causes a further loss of seismic energy, making edifices difficult to distinguish against background "noise" (Maresh and White 2005; Maresh et al. 2006; Shaw et al. 2008; Wright 2013). Additionally, some volcanic edifices (e.g. spatter

ramparts) are unresolvable due to their height and basal diameter being below the vertical resolution and line spacing of the seismic survey (e.g. Magee et al. 2013). Even if edifices are within the vertical resolution of the data, edifices may become buried by lavas from the same eruption (e.g. Keszthelyi et al. 2004).

When edifices have been identified, poor imaging has concealed their internal architecture (e.g. Thomson 2005). Alternatively, their architecture appears similar to that of sedimentary edifices and they have been misidentified until being drilled (e.g. Davies et al. 2002; Grove 2013). The inaccuracies associated with converting Two-Way-Time to absolute height also makes it difficult to make accurate measurements of edifice morphology, thus making them difficult to distinguish from other types of edifice (see Chapter 2, Section 2.6.2). Since few volcanic edifices have been positively identified, the seismic facies which typify vent-proximal areas are poorly constrained, unlike those of lava flow fields (e.g. Planke et al. 2000; Wright 2013).

Edifice-building sequences (e.g. pyroclastic rocks) have also yet to be recognised from well data, including information gathered by wireline log, core, formation micro-imaging (FMI) and formation micro-scanner (FMS) tools. Edifice building sequences can be quickly reworked (e.g. Manville et al. 2009 and references there-in), making it difficult to ascertain whether encountered sequences are in-situ. Secondly, due to the fragmental nature of the rocks and rapid transition of basaltic glass to clays (Pettijohn et al. 1987) it is difficult to determine primary textural characteristics in these sequences (e.g. Cummings and Blevin 2003; Clark 2014). Therefore pyroclastic successions are not recognised, and fragmental volcanic rocks are commonly described as “volcaniclastic”, with little indication of their origin (Planke et al. 2000; Bell and Butcher 2002; Wright 2013).

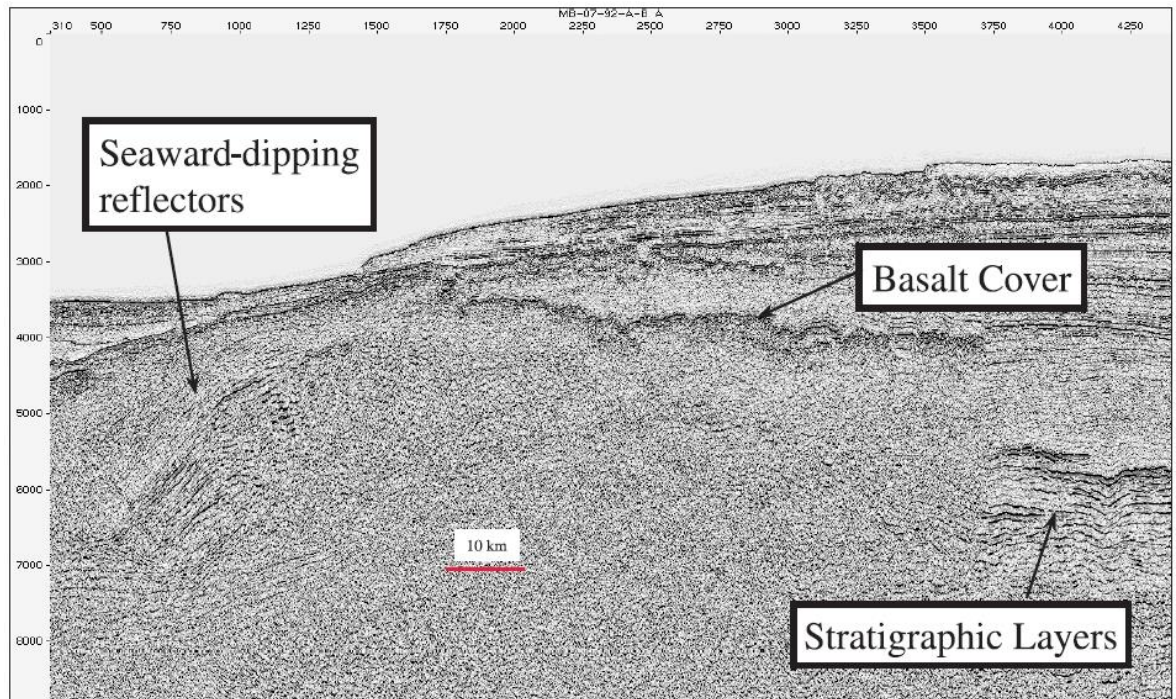


Figure 1.2. Seismic section from offshore Norway illustrating the sub-basalt imaging problem – notice that the stratigraphy is obscured beneath the basalt cover. Taken from Jerram (2002).

1.4.2 Characterising the architecture of volcanic edifices in the field

Monogenetic and small scale volcanic edifices have not traditionally been a research focus for volcanologists. Furthermore, there are a range of problems specific to these edifices that have made their internal architecture difficult to constrain. Although we can observe edifice construction (e.g. Moore and Ault 1965; Moore et al. 1966; Moore et al. 1980; Moore 1985; Wolfe et al. 1988), how the eruption processes are recorded is poorly known as the early products are buried by later products. Volcanic edifices also have a variable chance of preservation depending on background sedimentation rates (Manville et al. 2009). They may be eroded, such that the only record of their presence is the depocentre created by the vents themselves (Manville et al. 2009). Moreover, many edifices are degraded without exposure of their internal architecture (e.g. Wood 1980; Hooper and Sheridan 1998; Martin and Németh 2006).

In addition, edifices in flood basalt provinces are elusive; pyroclastic material may account for <0.001% of the volume of extruded material (Ross et al. 2005). Subsequent rifting and eruptions may occur along trends of earlier fissures, destroying evidence of the vent region (Hooper 2000; White et al. 2009). Our only examples of flood basalt edifices

come from the Columbia River Flood Basalt Province (e.g. Swanson et al. 1975; Reidel and Tolan 1992; Brown et al. 2014), which may not be typical of other flood basalt provinces (Bondre et al. 2004b).

There are also inherent difficulties in distinguishing between different types of volcanic edifices. For instance, several types produce pyroclastic density currents (PDCs), including tuff rings, tuff cones and rootless cones (e.g. Sohn and Chough 1989; Chough and Sohn 1990; Fagents et al. 2002; Sohn and Park 2005; Fagents and Thordarson 2007; Hamilton et al. 2010; White and Ross 2011). Since edifice architecture is determined by depositional method (e.g. Sohn 1996), these edifices share internal characteristics. Furthermore, since characterisation of an edifice is strongly based on their crater/basal diameter ratio (e.g. White and Ross 2011) eroded structures only providing internal exposure are difficult to identify. Identification becomes particularly problematic with edifices that are poorly described internally, e.g. spatter cones/ramparts, scoria cones and rootless cones. Correct identification is particularly important for rootless cones, since these structures are not dyke fed and can occur at significant distances away from the vent.

1.5 Aims

The aim of this thesis is to characterise the spatial and temporal development of monogenetic basaltic edifices using field, seismic and well data. Specifically, the thesis will:

- document the architecture, componentry and shallow level feeder system of basaltic fissure-derived edifices. This will help us to understand how edifice architecture varies as a result of variations in lava fountaining and associated clastogenic flow processes, as well as providing insights into the development of their feeder system. The outcomes of the study will aid recognition of fissure-derived edifices in field and well data sets, such as those affected by flood basalt volcanism (e.g. the FSB).
- document the architecture and componentry of rootless cones and their host lava flows. This will provide insights into the processes associated with their construction and help to distinguish between rootless cones and dyke-fed edifices. It will therefore allow accurate recognition of dyke-proximal settings in other volcanic provinces.
- use exceptionally high resolution 3D seismic data to analyse and characterise the architecture (e.g. seismic facies) and temporal development of submarine monogenetic basaltic edifices. This will allow us to distinguish between volcanic and similar non-

volcanic edifices (e.g. hydrothermal vents) in other seismic data sets, and provide insights into the 3D evolution of a submarine monogenetic volcanic field.

1.6 Thesis Outline

Chapter 1: An introduction to hydrocarbon exploration in volcanic-affected basins, the importance of volcanic edifices, problems associated with them and thesis aims.

Chapter 2: This chapter reviews: (1) the sub-aerial eruption and emplacement of basaltic lavas and edifices; (2) the architecture of the basaltic pyroclastic deposits as derived from field studies and from seismic datasets; (3) the criteria for distinguishing between volcanic and sedimentary edifices in seismic data.

Chapter 3: This chapter provides a detailed chronology of how volcanic edifices were constructed during a Holocene fissure eruption in NE Iceland. The internal architecture of edifices such as these is rarely exposed, and the chapter provides an unrivalled opportunity to link the deposits of low volume eruptions with those of high volume eruptions.

Chapter 4: This chapter uses field data from a newly-discovered rootless cone field in the Columbia River Flood Basalt Province to document and interpret the architecture and rootless cones. It also provides criteria to distinguish rootless cones and tephra from dyke-fed cones and tephra.

Chapter 5: This chapter uses 3D seismic data to document and interpret the architecture of submarine volcanic edifices offshore Australia. Currently, this chapter provides the only description of the development of a monogenetic volcanic field in seismic data.

Chapter 6: A discussion of the results of this study in the context of flood basalt emplacement and hydrocarbon exploration.

Chapter 7: A summary of the conclusions of the thesis.

Chapter 8: This chapter provides directions for future research.

1.7 References

- Bell B, Butcher H (2002) On the emplacement of sill complexes: evidence from the Faroe-Shetland Basin. Geological Society, London, Special Publications 197(1):307-329
- Bondre N, Duraiswami R, Dole G (2004a) Morphology and emplacement of flows from the Deccan Volcanic Province, India. *B Volcanol* 66(1):29-45
- Bondre N, Duraiswami R, Dole G (2004b) A brief comparison of lava flows from the Deccan Volcanic Province and the Columbia-Oregon Plateau Flood Basalts: Implications for models of flood basalt emplacement. *Journal of Earth System Science* 113(4):809-817
- Brown RJ, Blake S, Thordarson T, Self S (2014) Pyroclastic edifices record vigorous lava fountains during the emplacement of a flood basalt flow field, Roza Member, Columbia River Basalt Province, USA. *Geol Soc Am Bull* 126:875-891
- Bryan SE, Ernst RE (2008) Revised definition of large igneous provinces (LIPs). *Earth-Science Reviews* 86(1):175-202
- Bryan SE, Peate IU, Peate DW, Self S, Jerram DA, Mawby MR, Marsh JS, Miller JA (2010) The largest volcanic eruptions on Earth. *Earth-Science Reviews* 102(3-4):207-229
- Burns E, Williams C, Ingebritsen S, Voss C, Spane F, DeAngelo J (2014) Understanding heat and groundwater flow through continental flood basalt provinces: insights gained from alternative models of permeability/depth relationships for the Columbia Plateau, USA. *Geofluids*
- Carracedo JC, Rodriguez Badiola E, Soler V (1992) The 1730–1736 eruption of Lanzarote, Canary Islands: a long, high-magnitude basaltic fissure eruption. *J Volcanol Geoth Res* 53(1-4):239-250
- Carrasco-Núñez G, Ort MH, Romero C (2007) Evolution and hydrological conditions of a maar volcano (Atexcac crater, Eastern Mexico). *J Volcanol Geoth Res* 159(1):179-197
- Chough S, Sohn Y (1990) Depositional mechanics and sequences of base surges, Songaksan tuff ring, Cheju Island, Korea. *Sedimentology* 37(6):1115-1135
- Clark SJ (2014) Constraining diagenetic timings, processes and reservoir quality in igneous-affected basins. PhD Thesis, Durham University, Department of Earth Sciences.
- Coffin MF, Eldholm O (1992) Volcanism and continental break-up: a global compilation of large igneous provinces. Geological Society, London, Special Publications 68(1):17-30
- Coffin MF, Eldholm O (1994) Large igneous provinces: crustal structure, dimensions, and external consequences. *Reviews of Geophysics* 32(1):1-36
- Connor CB, Conway MF (2000) Basaltic volcanic fields. In: Sigurdsson H (ed) *Encyclopedia of Volcanoes*. Academic Press, San Diego, pp 331-343
- Courtillot V, Jaupart C, Manighetti I, Tapponnier P, Besse J (1999) On causal links between flood basalts and continental breakup. *Earth and Planetary Science Letters* 166(3):177-195
- Cronin SJ, Neall VE (2001) Holocene volcanic geology, volcanic hazard, and risk on Taveuni, Fiji. *New Zealand Journal of Geology and Geophysics* 44(3):417-437
- Cukur D, Horozal S, Kim DC, Lee GH, Han HC, Kang MH (2010) The distribution and characteristics of the igneous complexes in the northern East China Sea Shelf Basin and their implications for hydrocarbon potential. *Marine Geophysical Researches* 31(4):299-313
- Cummings AM, Blevin J (2003) Nature and distribution of igneous rocks. In: Blevin, J. (compiler), *Petroleum Geology of the Bass Basin - Interpretation Report, an Output of the Western Tasmanian Regional Minerals Program*. Geoscience Australia, Record 2003/19
- Davies R, Bell BR, Cartwright JA, Shoulders S (2002) Three-dimensional seismic imaging of Paleogene dike-fed submarine volcanoes from the northeast Atlantic margin. *Geology* 30(3):223-226
- Davison I, Stasiuk S, Nuttall P, Keane P (2010) Sub-basalt hydrocarbon prospectivity in the Rockall, Faroe–Shetland and Møre basins, NE Atlantic. Geological Society, London, Petroleum Geology Conference series 7:1025-1032
- Doyle MG (2001) Volcanic influences on hydrothermal and diagenetic alteration: evidence from Highway-Reward, Mount Windsor Subprovince, Australia. *Economic Geology* 96(5):1133-1148
- Fagents SA, Lanagan P, Greeley R (2002) Rootless cones on Mars: a consequence of lava-ground ice interaction. Geological Society, London, Special Publications 202(1):295-317

- Fagents SA, Thordarson T (2007) Rootless cones in Iceland and on Mars. In: Chapman M, Skilling IP (eds) *The Geology of Mars: Evidence from Earth-Based Analogues*. Cambridge University Press, pp 151–177
- Fedotov S, Chirkov A, Gusev N, Kovalev G, Slezin Y (1980) The large fissure eruption in the region of Plosky Tolbachik volcano in Kamchatka, 1975–1976. *B Volcanol* 43(1):47–60
- Genareau K, Valentine G, Moore G, Hervig R (2010) Mechanisms for transition in eruptive style at a monogenetic scoria cone revealed by microtextural analyses (Lathrop Wells volcano, Nevada, U.S.A.). *B Volcanol* 72(5):593–607
- Girard J-P, Deynoux M, Nahon D (1989) Diagenesis of the Upper Proterozoic siliciclastic sediments of the Taoudeni Basin (West Africa) and relation to diabase emplacement. *Journal of Sedimentary Research* 59(2)
- Grove C (2013) Submarine hydrothermal vent complexes in the Paleocene of the Faroe-Shetland Basin: Insights from three-dimensional seismic and petrographical data. *Geology* 41(1):71–74
- Grove C (2014) Direct and Indirect Effects of Flood Basalt Volcanism on Reservoir Quality Sandstone. PhD Thesis, Durham University, Department of Earth Sciences.
- Hamilton CW, Thordarson T, Fagents SA (2010) Explosive lava–water interactions I: architecture and emplacement chronology of volcanic rootless cone groups in the 1783–1784 Laki lava flow, Iceland. *B Volcanol* 72(4):449–467
- Holford S, Schofield N, MacDonald J, Duddy I, Green P (2012) Seismic analysis of igneous systems in sedimentary basins and their impacts on hydrocarbon prospectivity: examples from the Southern Australian margin. *Australian Petroleum Production and Exploration Association Journal* 52:229–252
- Holford S, Schofield N (in review) Three-dimensional seismic analysis for non-magmatic reactivation of buried volcanic complexes in sedimentary basins.
- Hooper DM, Sheridan MF (1998) Computer-simulation models of scoria cone degradation. *J Volcanol Geoth Res* 83(3):241–267
- Hooper PR (2000) Flood Basalt Provinces. In: Sigurdsson H (ed) *Encyclopedia of Volcanoes*.
- Houghton BF, Bonadonna C, Gregg CE, Johnston DM, Cousins WJ, Cole JW, Del Carlo P (2006) Proximal tephra hazards: Recent eruption studies applied to volcanic risk in the Auckland volcanic field, New Zealand. *J Volcanol Geoth Res* 155(1–2):138–149
- Jerram DA, Robbe O (2001) Building a 3-D model of a flood basalt: an example from the Etendeka, NW Namibia. *Visual Geosciences* 6(1):1–8
- Jerram DA (2002) Volcanology and facies architecture of flood basalts. *Geological Society of America Special Papers* 362:119–132
- Jerram DA, Stollhofen H (2002) Lava–sediment interaction in desert settings; are all peperite-like textures the result of magma–water interaction? *J Volcanol Geoth Res* 114(1–2):231–249
- Jerram DA, Widdowson M (2005) The anatomy of Continental Flood Basalt Provinces: geological constraints on the processes and products of flood volcanism. *Lithos* 79(3–4):385–405
- Karhunen R (1988) Eruption mechanism and rheomorphism during the basaltic fissure eruption in Biskupsfell, Kverkfjöll, North-central Iceland, Lic. Phil. thesis, University of Iceland, Department of Geology and Mineralogy.
- Kent RW, Thomson BA, Skelhorn RR, Kerr AC, Norry MJ, Walsh JN (1998) Emplacement of Hebridean Tertiary flood basalts: evidence from an inflated pahoehoe lava flow on Mull, Scotland. *J Geol Soc London* 155(4):599–607
- Keszthelyi L, Thordarson T, McEwen A, Haack H, Guilbaud MN, Self S, Rossi MJ (2004) Icelandic analogs to Martian flood lavas. *Geochemistry, Geophysics, Geosystems* 5(11)
- Magee C, Hunt-Stewart E, Jackson CAL (2013) Volcano growth mechanisms and the role of sub-volcanic intrusions: Insights from 2D seismic reflection data. *Earth and Planetary Science Letters* 373(0):41–53
- Manville V, Németh K, Kano K (2009) Source to sink: a review of three decades of progress in the understanding of volcanoclastic processes, deposits, and hazards. *Sedimentary Geology* 220(3):136–161
- Maresh J, White RS (2005) Seeing through a glass, darkly: strategies for imaging through basalt. *First Break* 23(5)
- Maresh J, White RS, Hobbs RW, Smallwood JR (2006) Seismic attenuation of Atlantic margin basalts: Observations and modeling. *Geophysics* 71(6):B211–B221

- Martin U, Németh K (2006) How Strombolian is a “Strombolian” scoria cone? Some irregularities in scoria cone architecture from the Transmexican Volcanic Belt, near Volcán Ceboruco, (Mexico) and Al Haruj (Libya). *J Volcanol Geoth Res* 155(1–2):104-118
- Mckinley JM, Worden RH, Ruffell AH (2001) Contact diagenesis: the effect of an intrusion on reservoir quality in the Triassic Sherwood Sandstone Group, Northern Ireland. *Journal of Sedimentary Research* 71(3):484-495
- Moore JG, Ault WU (1965) Historic littoral cones in Hawaii. *Pacific science* XIX(3-11)
- Moore JG, Nakamura K, Alcaraz A (1966) The 1965 Eruption of Taal Volcano. *Science* 151(3713):955-960
- Moore JG (1985) Structure and eruptive mechanisms at Surtsey Volcano, Iceland. *Geol Mag* 122(06):649-661
- Moore RB, Helz RT, Dzurisin D, Eaton GP, Koyanagi RY, Lipman PW, Lockwood JP, Puniwai GS (1980) The 1977 eruption of Kilauea volcano, Hawaii. *J Volcanol Geoth Res* 7(3):189-210
- Nelson CE, Jerram DA, Hobbs RW (2009) Flood basalt facies from borehole data: implications for prospectivity and volcanology in volcanic rifted margins. *Petroleum Geoscience* 15(4):313-324
- Németh K, White JDL (2003) Reconstructing eruption processes of a Miocene monogenetic volcanic field from vent remnants: Waipiata Volcanic Field, South Island, New Zealand. *J Volcanol Geoth Res* 124(1–2):1-21
- Passey SR, Bell BR (2007) Morphologies and emplacement mechanisms of the lava flows of the Faroe Islands Basalt Group, Faroe Islands, NE Atlantic Ocean. *B Volcanol* 70(2):139-156
- Pettijohn J, Potter P, Siever R (1987) Sand and sandstone. Published by Springer.
- Planke S, Eldholm O (1994) Seismic response and construction of seaward dipping wedges of flood basalts: Vøring volcanic margin. *Journal of Geophysical Research: Solid Earth* (1978–2012) 99(B5):9263-9278
- Planke S, Symonds PA, Alvestad E, Skogseid J (2000) Seismic volcanostratigraphy of large-volume basaltic extrusive complexes on rifted margins. *J. Geophys. Res.* 105(B8):19335-19351
- Rateau R, Schofield N, Smith M (2013) The potential role of igneous intrusions on hydrocarbon migration, West of Shetland. *Petroleum Geoscience* 19(3):259-272
- Reidel SP, Tolan TL (1992) Eruption and emplacement of flood basalt: An example from the large-volume Teepee Butte Member, Columbia River Basalt Group. *Geol Soc Am Bull* 104(12):1650-1671
- Riedel C, Ernst GGJ, Riley M (2003) Controls on the growth and geometry of pyroclastic constructs. *J Volcanol Geoth Res* 127(1–2):121-152
- Riggs NR, Duffield WA (2008) Record of complex scoria cone eruptive activity at Red Mountain, Arizona, USA, and implications for monogenetic mafic volcanoes. *J Volcanol Geoth Res* 178(4):763-776
- Rohrman M (2007) Prospectivity of volcanic basins: Trap delineation and acreage de-risking. *AAPG bulletin* 91(6):915-939
- Ross P-S, Ukstins Peate I, McClintock M, Xu Y, Skilling I, White J, Houghton B (2005) Mafic volcanoclastic deposits in flood basalt provinces: a review. *J Volcanol Geoth Res* 145(3):281-314
- Schofield N, Jolley DW (2013) Development of intra-basaltic lava-field drainage systems within the Faroe–Shetland Basin. *Petroleum Geoscience* 19(3):273-288
- Shaw F, Worthington M, White R, Andersen M, Petersen U (2008) Seismic attenuation in Faroe Islands basalts. *Geophysical Prospecting* 56(1):5-20
- Sheridan MF, Wohletz KH (1983) Hydrovolcanism: Basic considerations and review. *J Volcanol Geoth Res* 17(1–4):1-29
- Sheth H (1999) Flood basalts and large igneous provinces from deep mantle plumes: fact, fiction, and fallacy. *Tectonophysics* 311(1):1-29
- Sohn YK, Chough SK (1989) Depositional processes of the Suwolbong tuff ring, Cheju Island (Korea). *Sedimentology* 36(5):837-855
- Sohn YK (1996) Hydrovolcanic processes forming basaltic tuff rings and cones on Cheju Island, Korea. *Geol Soc Am Bull* 108(10):1199-1211
- Sohn YK, Park KH (2005) Composite tuff ring/cone complexes in Jeju Island, Korea: possible consequences of substrate collapse and vent migration. *J Volcanol Geoth Res* 141(1–2):157-175
- Sumner JM (1998) Formation of clastogenic lava flows during fissure eruption and scoria cone collapse: the 1986 eruption of Izu-Oshima Volcano, eastern Japan. *B Volcanol* 60(3):195-212

- Sumner JM, Blake S, Matela RJ, Wolff JA (2005) Spatter. *J Volcanol Geoth Res* 142(1-2):49-65
- Swanson DA, Wright TL, Helz RT (1975) Linear vent systems and estimated rates of magma production and eruption for the Yakima Basalt on the Columbia Plateau. *American Journal of Science* 275(8):877-905
- Thomson K (2005) Extrusive and intrusive magmatism in the North Rockall Trough. Geological Society, London, Petroleum Geology Conference series 6:1621-1630
- Thordarson T, Self S (1993) The Laki (Skaftár Fires) and Grímsvötn eruptions in 1783–1785. *B Volcanol* 55(4):233-263
- Thordarson T, Self S, Oskarsson N, Hulsebosch T (1996) Sulfur, chlorine, and fluorine degassing and atmospheric loading by the 1783–1784 AD Laki (Skaftár Fires) eruption in Iceland. *B Volcanol* 58(2-3):205-225
- Thordarson T, Self S (1998) The Roza Member, Columbia River Basalt Group: A gigantic pahoehoe lava flow field formed by endogenous processes? *J. Geophys. Res.* 103(B11):27411-27445
- Thordarson T, Rampino M, Keszthelyi LP, Self S (2009) Effects of megascale eruptions on Earth and Mars. *Geological Society of America Special Papers* 453:37-53
- Valentine G, Cortés J (2013) Time and space variations in magmatic and phreatomagmatic eruptive processes at Easy Chair (Lunar Crater Volcanic Field, Nevada, USA). *B Volcanol* 75(9):1-13
- Valentine GA, Groves KR (1996) Entrainment of Country Rock during Basaltic Eruptions of the Lucero Volcanic Field, New Mexico. *The Journal of Geology* 104(1):71-90
- Valentine GA, Gregg TKP (2008) Continental basaltic volcanoes — Processes and problems. *J Volcanol Geoth Res* 177(4):857-873
- Valentine GA (2012) Shallow plumbing systems for small-volume basaltic volcanoes, 2: Evidence from crustal xenoliths at scoria cones and maars. *J Volcanol Geoth Res* 223–224(0):47-63
- Walker GPL (1993) Basaltic-volcano systems. Geological Society, London, Special Publications 76(1):3-38
- Walker GPL (2000) Basaltic volcanoes and volcanic systems. In: Sigurdsson H (ed) *Encyclopedia of volcanoes*. Academic Press, San Diego, pp 283-289
- White J, Bryan S, Ross P, Self S, Thordarson T (2009) Physical volcanology of continental large igneous provinces: update and review. *Studies in Volcanology: The Legacy of George Walker*. Special Publications of IAVCEI 2:291-321
- White JDL, Ross PS (2011) Maar-diatreme volcanoes: A review. *J Volcanol Geoth Res* 201(1–4):1-29
- Wignall P (2001) Large igneous provinces and mass extinctions. *Earth-Science Reviews* 53(1):1-33
- Wohletz KH, Sheridan MF (1983) Hydrovolcanic explosions; II, Evolution of basaltic tuff rings and tuff cones. *American Journal of Science* 283(5):385-413
- Wolfe WE, Neal AC, Banks GN, Toni DJ (1988) The Puu Oo Eruption of Kilauea Volcano, Hawaii: Episodes 1 Through 20, January 3, 1983, Through June 8, 1984. U.S Geological Survey Professional Paper 1463
- Wood CA (1980) Morphometric evolution of cinder cones. *J Volcanol Geoth Res* 7(3–4):387-413
- Wright K (2013) Seismic Stratigraphy and Geomorphology of Palaeocene Volcanic Rocks, Faroe-Shetland Basin. PhD Thesis, Durham University, Department of Earth Sciences.

Chapter 2: Background Information

2.1 Introduction

This chapter first provides an outline of the Faroe-Shetland Basin (FSB) and the North Atlantic Igneous Province (NAIP) within which it is situated, since exploration within the FSB is the motivation for this research. I then review our understanding of basaltic volcanism, with a focus on monogenetic volcanism. This focus is driven by the occurrence of monogenetic eruptions in all volcanic regions, including those such as the FSB affected by flood basalt volcanism (e.g. Walker 1993; Brown et al. 2009). I also focus on eruptions driven by magmatic volatiles, since these eruptions have traditionally received less attention in the literature, despite their common occurrence. I begin with a discussion of the eruption of basaltic magma; focusing initially on how basaltic magma is transported to the surface in dykes. I then describe the physical processes governing the possible styles of eruption. Following this I summarise the literature describing lava fountains and related pyroclast accumulation processes.

In the proceeding section, I summarise the literature for basaltic lavas, since lavas are a significant component of volcanic-affected basins. This section is divided to describe the key terms of lava flows and flow fields, how lava is emplaced and the different types of lava that are found. I also detail the internal features of pāhoehoe lavas. Following this, I describe the numerous types of volcanic edifices produced during basaltic volcanism.

The chapter then describes the difficulties associated with recognising the aforementioned lavas and volcanoes in volcanic-affected hydrocarbon basins. I also provide a summary of non-volcanic edifices in seismic data, since there are superficial similarities between these features and volcanoes which can make them difficult to distinguish.

2.2 The North Atlantic Igneous Province

The NAIP encompasses Western Greenland, the Faroe Islands and the British Tertiary Igneous Province (BTIP; see Fig. 1.1, Chapter 1). The minimum areal extent of the province is $1.3 \times 10^6 \text{ km}^2$ (Eldholm and Grue 1994; Coffin and Eldholm 1994). The province was constructed as a result of seafloor spreading in the Late Paleocene – Early Eocene. The onset of volcanism is also explained by plume (Naylor et al. 1997) and non-plume hypotheses (Hansen et al. 2009). The province is characterised by predominantly subaerial lava flows, intrusions and volcanic centres. The earliest volcanism is recorded at

63 Ma (Naylor et al. 1997). Initial volcanic activity was characterised by interactions with water forming hyaloclastites, construction of shield volcanoes, emplacement of ponded lava flows. Minor acidic volcanism occurred at this time (Jerram and Widdowson 2005). The ensuing main volcanic phase was characterised by the emplacement of laterally extensive flood basalt plateaus (Jerram and Widdowson 2005). Later eruptions were dominated by more silicic magmas due to melting of continental crust or sediments (Ross et al. 2005; Jerram and Widdowson 2005; Bryan and Ernst 2008). Volcanism ceased once seafloor spreading had become established, and crustal subsidence dominated from the Paleocene onwards (Skogseid et al. 2000; Ceramicola et al. 2005; Praeg et al. 2005). The presence of numerous volcanic disconformities within the sequence suggests that there was significant lateral and temporal variation in volcanic style and eruption rate (Jerram and Widdowson 2005).

2.2.1 The Faroe Shetland Basin

The FSB is located between the Shetland and Faroe Islands (Fig. 2.1). The basin is a 260 km wide, 460 km long series of sub-rift basins that formed as a result of compression and rifting. Compression was initiated in the Early Palaeozoic by NE trending Caledonian Orogeny thrust belts (McKerrow et al. 2000; Ritchie et al. 2011). Subsequent rifting in the Permo-Triassic resulted in the formation of asymmetric half-graben basins in a semi-arid environment, and by the early Jurassic marine conditions had developed (Moy and Imber 2009 and references there-in). Elsewhere in NW Europe there is evidence for late Jurassic rifting (Doré et al. 1999), but the absence of north-south trending rifts in the FSB suggests this did not occur here (Moy and Imber 2009). Subsequent Cretaceous rifting led to the formation of NW-SE trending sub-basins (Roberts et al. 1999; Soper and Woodcock 2003; Ritchie et al. 2011). These sub-basins are separated along several transfer zones by structural highs associated with changes in crustal structure (Dean et al. 1999; Moy and Imber 2009; Wright 2013; Fletcher et al. 2013; Clark 2014).

The FSB is dominated by interbedded igneous and sedimentary rocks of Cretaceous and Palaeocene age. Most sediments were sourced from the Scotland-Shetland platform towards the east (Ritchie and Hitchen 1996; Ritchie et al. 1999; Sørensen 2003; Wright 2013), although their distribution and provenance was partially controlled by the structural lineaments and lava flow field morphology (Jolley and Morton 2007; Ellis et al. 2009; Moy and Imber 2009). The Colsay Member is the main target hydrocarbon reservoir (Schofield and Jolley 2013) whilst source rocks within the basin are dominantly the

Kimmeridgian mudstones (Holmes et al. 1999). Hiatuses during the main phase of volcanic activity are represented by the Sneiss and Prestfjall Formations, which are composed of volcanoclastic and siliciclastic rocks of fluvial and lacustrine association (Passey and Bell 2007).

The flood basalts of the FSB cover an area of 40 000 km² and act as seals to fluids in parts of the FSB (Naylor et al. 1997). The lavas were emplaced 57 Ma ago and are thought to have been erupted over 2.6 Ma (Passey and Jolley 2008). They form a 6.6 km thick succession, divided into the Beinisdvörð (BF), Malinstindur (MF) and Enni (EF) Formations. These formations are underlain at the base by the Lopra Formation, a sequence of volcanoclastic rocks and sills (Ellis et al. 2002).

The BF is dominated by thick, laterally extensive aphyric sheet lobes that reach 3300 m in thickness (Passey and Bell 2007). These flows record the onset of flood basalt volcanism (Passey and Bell 2007; Wright 2013). The MF is composed of compound, subaerial lavas of olivine phyric, aphyric and plagioclase-phyric basalts (Passey and Bell 2007). The Enni Formation is composed of interbedded simple and compound flows (Passey and Bell 2007). The BF and EF are inferred to have been emplaced from fissures due to their sheet morphology (Passey and Bell 2007). The source fissures for the EF lavas may be located offshore (Schofield and Jolley 2013). In contrast, the compound flows of the EF are inferred to have been emplaced from low shields (Passey and Bell 2007 and references there-in). Conflicting evidence from seismic data and lava flow morphology suggests that the MF were sourced from fissures and/or shield volcanoes (Passey and Bell 2007; Schofield and Jolley 2013). The source fissure for the BF lavas is thought to be represented by a 1 km long NW-SE trending row of tuff-agglomerate deposits on the Faroe Islands (Larsen et al. 1999). Eruption of the lavas resulted in the formation of the Faroe-Shetland Escarpment. This escarpment is a curved structure across the basin, interpreted as a lava-fed delta system composed of steep, prograding foresets of hyaloclastite (Wright et al. 2012; Wright 2013). The escarpments' progradational structure suggests retreat of the shoreline as volcanism overwhelms the submarine basin.

Intrusive complexes are composed of dolerite sills and dykes which intrude preferentially into upper Cretaceous shales and the lower part of the Palaeocene, and which extend laterally beyond the flood basalt cover (Rateau et al. 2013). These complexes were intruded between 53 and 55 Ma (Ritchie and Hitchen 1996; Schofield and Jolley 2013).

Partially-eroded igneous centres are also recognised from seismic reflection data, gravity and magnetic surveys (Gatliff et al. 1984; Jolley and Bell 2002). These include the

Erlend complex and Brendans dome (Gatliff et al. 1984; Ritchie and Hitchen 1996). Whilst these structures provide seismic evidence of lava extrusion (Gatliff et al. 1984), most of the centres are identified solely by geophysical methods (e.g. the Westray volcanic centre, see Ritchie and Hitchen 1996). Therefore their link with the overlying extrusive units is uncertain. Fissures are recognised from seismic data in the Flett Basin (see Section 2.6.2.1.1), although their relationship to the surrounding lava flows is uncertain (Thomson 2007).

In summary, the source vents for the flood basalts that dominate the FSB are likely to be large complexes (such as Brendans Dome) and dyke-fed fissures, such as those identified onshore and offshore (e.g. Larsen et al. 1999; Thomson 2007; Schofield and Jolley 2013). However, these fissure vents are poorly described, and the architecture of the edifices along them is poorly constrained in both seismic and well data. The relationship (if any) between the fissures, their abundance and central complexes is also unknown. Given the conflicting evidence for the source of the MF lavas, the reliability of lava flow morphology (i.e. tabular or compound) as an indicator of source type is unknown.

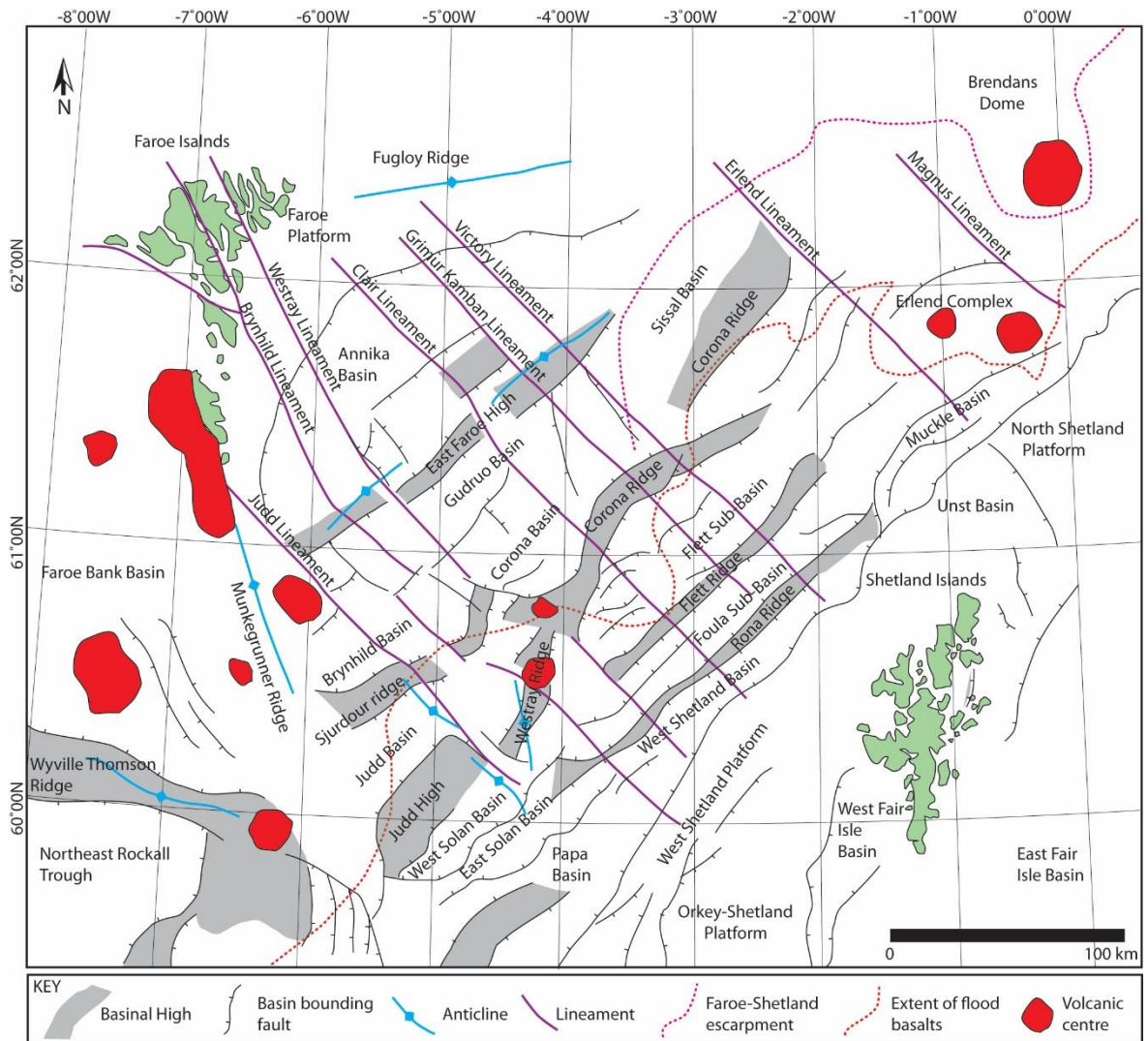


Figure 2.1. Location, structure and volcanic features of the Faroe-Shetland Basin. Modified from Stoker et al. (1993), Ritchie et al. (1996, 1999), Sørensen (2003), Ellis et al (2009), Moy and Imber (2009) and Wright (2013).

2.3 The eruption of basaltic magma

The products of basaltic eruptions are intimately linked to the eruption styles that produced them. Therefore, we need to understand the physical processes that govern these eruption styles. Furthermore, since the movement of magma in the shallow subsurface drives all basaltic eruptions, it is important to understand their feeder systems. This section first outlines the feeder dykes for magmatic, volatile-driven monogenetic basaltic eruptions. I then outline the range of basaltic eruption styles common at monogenetic volcanic centres. There is a particular focus on eruptions driven purely by magmatic volatiles (“dry” eruptions; see Chapter 1). I then outline pyroclast accumulation processes

(e.g. welding) and lava fountains, common during dry eruptions. These processes play an important part in governing the architecture of volcanic edifices during Hawaiian and Strombolian-style eruptions.

2.3.1 Feeder dykes for monogenetic eruptions

Feeder dykes bring magma to the surface, whilst non-feeder dykes do not (Geshi et al. 2010). Feeder dykes link to the paleo-surface and often have a flaring geometry (Keating et al. 2008; Geshi et al. 2010; Geshi and Oikawa 2014). Non-feeder dykes are observed to terminate 15–45 m beneath the surface (Geshi et al. 2010). In reality, it is unknown if many dykes are feeders or not, given that their uppermost portion is rarely observed.

The geometry of feeder dykes partially determines the style of eruption and hence the architecture of the deposits (see section 2.5). Eruption style is altered through a combination of shallow degassing and groundmass crystallisation in the feeder (hence increasing fragmentation, see section 2.3.2.1 and Valentine and Gregg 2008) and/or changes in volumetric flux (see section 2.3.2.1). At depth these dykes are decimetres to metres wide (Valentine and Krogh 2006; Valentine et al. 2006; Valentine and Keating 2007; Valentine 2012). The duration and type of discharge from the fissure is influenced by country rock lithology and irregularities in the fissure geometry (Wylie et al. 1999). The length of the dyke also affects eruption style, since longer dykes allow greater gas segregation, causing unstable variations in flow regime (Pioli et al. 2008). With time, fissure eruptions localise to form conduits due to thermal instabilities and convective processes within the magma (Bruce and Huppert 1989; Genareau et al. 2010; Valentine 2012), and due to wall rock widening (Valentine and Groves 1996; Keating et al. 2008; Valentine 2012). Localisation has been observed in historical eruptions (e.g. Richter 1970; Sumner 1998). This localisation increases the pressure and velocity of rising magma (Valentine and Groves 1996), resulting in increased volumetric flux (Wadge 1981).

Although there are numerous studies of the conduits for phreatomagmatic eruptions (Lorenz 1986; e.g. Németh et al. 2001), there are much fewer for studies of the shallow conduits of “dry” basaltic eruptions. This is because the dykes are commonly eroded to such a depth that it is impossible to determine their link (if any) to the paleosurface (e.g. Geiki 1897; Walker 1995). Alternatively, the erupted products bury the dykes (e.g. Doubik and Hill 1999). In these cases, indirect measurements (e.g. xenolith abundances in the pyroclastic stratigraphy) are used to infer shallow sub-surface conduit processes. Studies that use indirect measurements have concluded that feeder dykes flare upwards, most

prominently within the upper 50–200 m of stratigraphy (Valentine and Groves 1996; Doubik and Hill 1999; Valentine 2012).

Direct observations of feeder dykes in the shallow sub-surface (e.g. Keating et al. 2008; Geshi et al. 2010; Galindo and Gudmundsson 2012; Friese et al. 2013; Geshi and Oikawa 2014) support the conclusions of Valentine and Groves (1996); Doubik and Hill (1999) and Valentine (2012), showing that feeder dykes widen in the upper 200 m of stratigraphy. In addition to dyke material, the flared region may be filled with scoria, variably welded spatter, and basaltic and host rock breccias (Keating et al. 2008; Lefebvre et al. 2012; Valentine 2012). However, dyke widening is greater than predicted by numerical models by a factor of 10 at <50 m depth. Host rock heterogeneities and dyke splaying account for the greater widening. Furthermore, outcrops represent a final snapshot of conduit morphology and not a single, steady emplacement event as predicted by models (Keating et al. 2008).

Conduit widening processes are summarised by Keating et al. (2008) and Valentine and Groves (1996) and include: (1) thermal erosion resulting in host rock volume loss – particularly at greater depths where lithostatic pressure is too great for mechanical erosion to occur. (Bruce and Huppert 1989; Keating et al. 2008); (2) mechanical erosion – increasing with decreasing confining pressure and partly dependent on regional and local host rock heterogeneities (Delaney and Pollard 1981; Keating et al. 2008); (3) erosion from particle collisions (Macedonio et al. 1994); (4) conduit collapse due to variations in magmatic pressure as a result of conduit processes e.g. variations in magma pressure, shock/rarefaction waves (Wilson and Head 1981; Macedonio et al. 1994); (5) hydromagmatic processes involving the interaction of magma with groundwater or saturated sediments (Delaney and Pollard 1981; Lorenz 1986; White 1991); (6) magma viscosity variations induced by cooling of magma at dyke margins, leading to flow localization (Wylie et al. 1999); (7) inclusion of wall rock blocks where offshoot dykes re-join the master (Keating et al. 2008); (8) pore pressure build-up (Delaney and Pollard 1981).

Geshi and Oikawa (2014) concluded that feeder dyke morphology is related to eruptive style. Coherent dykes are inferred to represent effusive end-members, whilst dykes that fragment at depths of 20–150 m are inferred to represent highly explosive end members. Moderately explosive feeders have a morphology transitional between the two and the magma fragments at depths of <20 m. Feeder dykes can develop an irregular morphology as they intrude into overlying edifices (Hintz and Valentine 2012; Friese et al.

2013). Furthermore, dyke morphology and orientation is variably affected by regional stress orientation. Dykes intruded into relay structures between rifts change orientation relative to the regional stress, developing an arcuate shape over their length (Friese et al. 2013). In contrast, some dykes are unaffected by regional stress orientation (Hintz and Valentine 2012). Feeder dykes also trigger slip on pre-existing faults (Gudmundsson et al. 2008; Galindo and Gudmundsson 2012) and are accommodated by a combination of elastic and inelastic deformation of host rock (Valentine and Krogh 2006). Studies have also shown that magma frozen in the dyke may become more vesicular in shallow regions (Hintz and Valentine 2012; Galindo and Gudmundsson 2012). The vesicles are attributed to magmatic pulses caused by pressure fluctuations in the magma column (Hintz and Valentine 2012; Galindo and Gudmundsson 2012); inferred to be a common process in dyke emplacement (Hintz and Valentine 2012). However, this is not common to all examples (Lefebvre et al. 2012; Friese et al. 2013).

Despite a number of studies describing feeder dykes in the shallow sub-surface, whether feeder dyke geometry is diagnostic of all eruption styles is uncertain. For instance, although Geshi and Oikawa (2014) describe effusive feeder dykes, the morphology of dykes for Hawaiian or Strombolian style eruptions is unreported. Valentine and Gregg (2008) also outline problems related to the dyke-conduit transition; including how to predict the rate and location of the transition and whether the flared shape of conduits is a general feature across volcanic fields.

2.3.2 Eruption styles

Monogenetic basaltic volcanism is typified by a range of eruption styles. These styles are evidenced at historic eruptions (e.g. Krauskopf 1948; Thorarinsson 1966; Moore et al. 1966; Richter 1970; Thordarson and Self 1993) or have been inferred from deposit characteristics (e.g. Houghton and Schmincke 1989; Valentine and Gregg 2008; Carracedo Sánchez et al. 2012; Brown et al. 2014). Eruption styles are generally classified according to the degree of fragmentation (i.e. pyroclast size) and dispersal of the deposits (see Walker 1973). The broadest classification scheme is determined by the presence of magma–water interaction. Dry eruptions include weak ash emissions, Hawaiian, Strombolian and Violent Strombolian eruptions. Wet eruptions include Surtseyan and Taalian styles. Many studies document transitions between styles (e.g. Ross 1986; Houghton and Schmincke 1989; Valentine et al. 2005; Genareau et al. 2010; Németh et al. 2011; Otterloo et al. 2013).

2.3.2.1 Physical processes governing eruption style

In eruptions driven by magmatic volatiles, eruption style is determined by volumetric flux and pyroclast size. The effect of flux on eruption style is discussed in depth by Jaupart and Vergnolle (1988); Jaupart and Vergnolle (1989); Parfitt and Wilson (1995); Vergnolle and Mangan (2000) and Parfitt (2004). These authors have proposed two models. The Rise Speed Dependant (RSD) model suggests homogeneous, single fluid-phase flow of magma and gas within the conduit. Eruption style is governed by the speed at which the magma rises relative to the bubbles within it. When the magma rises quickly relative to the bubbles, the magma and bubbles are erupted together and behave as a single fluid phase. This results in a Hawaiian eruption. As magma rise speed (i.e. mass flux) decreases, bubbles may coalesce within the magma column. Bubble coalescence results in the formation of large gas slugs, producing Strombolian eruptions. This model is compatible with features observed during Hawaiian eruptions (Parfitt 2004).

In contrast, the Collapsing Foam (CF) model suggests that eruptions are the result of two-phase flow of magma and gas (Vergnolle and Jaupart 1986; Jaupart and Vergnolle 1988; Jaupart and Vergnolle 1989; Parfitt 2004). In this model, Hawaiian eruptions result from annular flow, whilst Strombolian eruptions result from slug flow. These varying flow regimes are the result of instantaneous foam collapse (for Hawaiian eruptions) and partial foam collapse (for Strombolian eruptions) deep in the magma storage system. The degree of collapse is related to the viscosity of the liquid, and thus Strombolian eruptions are more common in more viscous magmas. However, the CF model cannot explain many of the features observed during the 1983–1986 Pu’u ‘O’o eruption (see Parfitt 2004).

Pyroclast size determines the amount of heat transferred to the eruption column. Greater heat transfer results in higher columns, capable of dispersing tephra more widely. Clasts >64 mm are inefficient at transferring heat to the gas phase and prevent the formation of a buoyant eruption column (Woods and Bursik 1991). These clasts are typical of Strombolian and Hawaiian eruptions. Current estimates suggest that 50% of the erupted clasts must be >64 mm to prevent clast-gas heat transfer, although this fraction is poorly constrained (Valentine and Gregg 2008). Clast size can be decreased by increasing magma viscosity via crystallisation or rapid water quenching (e.g. Wohletz 1983; Genareau et al. 2010).

2.3.2.2 Hydromagmatic eruptions

Eruption styles resulting from magma-water interaction include Surtseyan (e.g. Thorarinsson 1966; Wohletz and Sheridan 1983; White and Houghton 2000) and Taalian (e.g. Moore et al. 1966; Kokelaar 1986). The water in these eruptions may be encountered in the subsurface (e.g. in aquifers; see Sohn 1996) or above ground (e.g. Thorarinsson 1966; Kokelaar and Durant 1983; Moore 1985). Surtseyan eruptions occur at submarine and emergent volcanoes. They produce pyroclastic density currents, tephra jets and eruption columns that reach several kilometres height (Kokelaar 1986; White and Houghton 2000). The deposits are characterised by vesiculated tuffs with abundant accretionary lapilli and lithic clasts (White and Houghton 2000). Surtseyan eruptions form steep-sided tuff cones (Sohn and Chough 1992; Sohn 1996; Cole et al. 2001). Taalian eruptions may initiate on land (Moore et al. 1966; Kokelaar 1986), although similar diatreme-forming eruptions occur in submarine settings (Lefebvre and Kurszlaukis 2008; Pittari et al. 2008; Suiting and Schmincke 2009). These eruptions produce dilute pyroclastic density currents (Kokelaar 1986), and generate eruption columns that reach heights of 15–20 km (White and Houghton 2000). Deposits from these eruptions are dominated by non-juvenile material of ash–block size. The eruptions produce craters at the site of eruption and may also form small cones and diatremes.

2.3.2.3 Magmatic volatile-driven eruptions

These eruption styles include Hawaiian, Strombolian, Violent Strombolian and weak ash emission (see Vergnolle and Mangan 2000; Parfitt 2004; Valentine and Gregg 2008). The deposits of eruptions can be classified according to their grain size, sorting, welding intensity and bedding. Since weak ash emissions do not build proximal edifices due to their low volume flux and negligible gas thrust they are not discussed (see Patrick et al. 2007; Valentine and Gregg 2008).

Hawaiian eruptions are typified by sustained fountains commonly <500 m in height that are composed of clots of lava (Vergnolle and Mangan 2000). Clasts are poorly coupled in momentum and thermal energy with the erupting gas. Thus Hawaiian eruptions have eruption columns <2 km in height (Valentine and Gregg 2008). Given the large clast size and relatively high mass flux, proximal deposits are often densely to partially welded (Valentine and Gregg 2008). However, pulsing in the fountain can result in beds of moderate or weak welding (Head and Wilson 1989; Valentine and Gregg 2008). Proximal deposits also include massive to inversely graded beds of partially welded coarse lapilli

and bombs in beds that are lenticular to continuous in geometry (Valentine and Gregg 2008). Cooler clasts from the outer part of the fountain are often stripped by the wind and fallout several kilometres downwind (Parfitt 1998).

Strombolian eruptions are characterised by intermittent, low fountains caused by the bursting of gas pockets rising through a slow moving magma column (Parfitt 2004; Valentine and Gregg 2008). These bursts produce lapilli and bombs that build a scoria cone through repeated episodes of grain avalanching (McGetchin et al. 1974; Chouet et al. 1974). In proximal regions Strombolian eruptions produce inversely graded to massive beds of coarse lapilli, bombs and blocks (Valentine and Gregg 2008). The beds are usually lenticular with local zones of dense welding close to the vent (Valentine and Gregg 2008). The deposits have a restricted dispersal past the base of the cone.

Violent Strombolian eruptions are characterised by sustained eruption columns <10 km in height (Arrighi et al. 2001; Valentine and Gregg 2008). These eruptions are typified by multiple eruption column events (Valentine and Gregg 2008). Their proximal deposits include massive and graded beds with internal stratification. These beds are composed of coarse ash and lapilli sized juvenile clasts with rare blocks and bombs. The beds are mainly planar, with local lenticular zones and cross bedded ash-rich horizons. Defining features of the deposits of these eruptions are the absence of welding (since clasts cool within the tall eruption column) and fall deposits that mantle underlying units with limited components of grain avalanching (Valentine and Gregg 2008).

2.3.2.3.1 Fissure eruptions

Basaltic fissures are found in all tectonic environments and are particularly common in extensional settings (e.g. Iceland). They are also found in association with central volcanoes (Walker 1995). Many fissure eruptions are Hawaiian in style (e.g. Swanson et al. 1979; Wolfe et al. 1988; Thordarson and Self 1993). However, fissures may also exhibit sub-Plinian behaviour (e.g. Walker et al. 1984; Thordarson and Self 1993; Sumner 1998; Sable et al. 2006; Brown et al. 2014). They produce a spectrum of pyroclastic edifices (see Section 2.5) and lavas (see Section 2.4).

Historic eruptions are characterised by low, linear fountains in their initial stages (e.g. Thorarinsson et al. 1973; Swanson et al. 1979; Wolfe et al. 1988). Early pyroclastic constructs and deposits are commonly rafted away from the vent (Parcheta et al. 2012), or become buried by subsequent deposits (e.g. Wolfe et al. 1988). Brief phreatomagmatic

episodes may occur throughout the eruption (Thordarson and Self 1993; Valentine and Cortés 2013). The fountain quickly localises to numerous point sources due to thermal instabilities along the fissure (Bruce and Huppert 1989; Keating et al. 2008). Localisation may result in an increase in fountains reaching 100–500 m in height (e.g. Heliker and Mattox 2003; Stovall et al. 2011; Parcheta et al. 2012). They may also become more sustained (e.g. Sumner 1998; Valentine et al. 2005) or intermittent with time (e.g. Thordarson and Self 1993; Németh et al. 2011). The final stages of eruptions may be characterised by rapid surges in eruption rate and abrupt cessation of fountaining (e.g. Stovall et al. 2011), or prolonged effusion events (Vergnolle and Mangan 2000).

Fissures are the source of some or all flood basalts in the Columbia River Flood Basalt Province (CRFBP), NAIP and Deccan Volcanic Province (DVP). Lava flows in the CRFBP can be linked petrologically to linear dyke swarms (e.g. Swanson et al. 1975). Rows of pyroclastic edifices occur along the strike of these dykes (Swanson et al. 1975; Reidel and Tolan 1992; Brown et al. 2014). The Hebridean lavas of northwest Scotland are flat lying, suggesting they were erupted over a large area (Walker 1995). Dykes associated with these lavas are widely scattered, contradictory to a point source (Walker 1995). An absence of pyroclastic deposits is also thought to be evidence of fissure fed flood basalts in eastern Iceland (Walker 1958; Gibson et al. 1966). Linear dyke swarms in the DVP are suggestive of a fissure source (Sheth 2006).

Whether lava flow morphology can be used accurately to infer the source (i.e. central volcano or fissure) is uncertain; both compound and simple flows are known to originate from fissures (Sheth 2006). Furthermore, as fissures are often found in close association with central volcanoes (Hjartardóttir et al. 2012; Óskarsson and Riishuus 2013) it is uncertain in the NAIP where fissure-fed lavas end and lavas erupted from central volcanoes begin (Walker 1995). Whether the dykes exposed in the NAIP represent feeder-dykes is uncertain; it is often impossible to determine the link between a dyke and erupted products (see Section 4.2.1).

2.3.3 Pyroclast accumulation and lava fountains

Welding, agglutination and coalescence are common processes during lava fountaining due to interactions between molten pyroclasts (see Cas and Wright 1987; Branney and Kokelaar 1992; Wolff and Sumner 2000; Sumner et al. 2005). These processes depend on clast accumulation rate and local temperature and are ultimately determined by the lava fountain structure. Welding is a compactional process and describes

the sticking together of clasts in a hot deposit due to overburden pressure. Numerical modelling has shown that welding can occur up to several kilometres from the vent given the right combination of exit velocity, ejection angle, and clast size, density and shape (Capaccioni and Cuccoli 2005). Carey et al. (2008) state that welding may be a “regional” process (i.e. present over tens of metres) or a “local” process, where discrete welding halos are created around larger clasts. However, the importance of regional versus local welding in monogenetic eruptions is not recorded. Agglutination describes the flattening of clasts as they impact on an accumulation surface (Sumner et al. 2005). Agglutination is promoted by the splashing of pyroclasts commonly ≥ 10 cm diameter, falling at terminal speed and with viscosities $< 10^5$ Pa s (Sumner et al. 2005). These conditions are easily met by clasts in the inner part of the lava fountain. However, the effects of shear and compaction on deposit texture have not been investigated. Coalescence describes the complete agglutination of fluidal clasts, forming a homogeneous liquid in which clast outlines are obliterated (Sumner et al. 2005). It is by rapid coalescence that clastogenic lavas are formed.

The lava fountain structure governs the architecture of pyroclastic deposits and clastogenic lavas. Fountain structure is primarily determined by magma gas content and volume flux (Fig. 2.2; Head and Wilson 1989). Gas content determines the height and collimation (i.e. spread from vertical) of the fountain. Non-collimated fountains with high volume fluxes (e.g. many Hawaiian eruptions) produce large pyroclasts that do not cool rapidly (e.g. spatter bombs). Most fall back into the vent and agglutinate and/or coalesce. Conversely, widely spread or high fountains produce abundant rapidly cooled clasts that are less likely to weld and agglutinate (e.g. scoria lapilli). Volume flux primarily controls clast size, which in turn controls local clast temperature. Fountain structure is also affected by local wind variations, as wind can strip clasts from the outer, cooler part of the fountain.

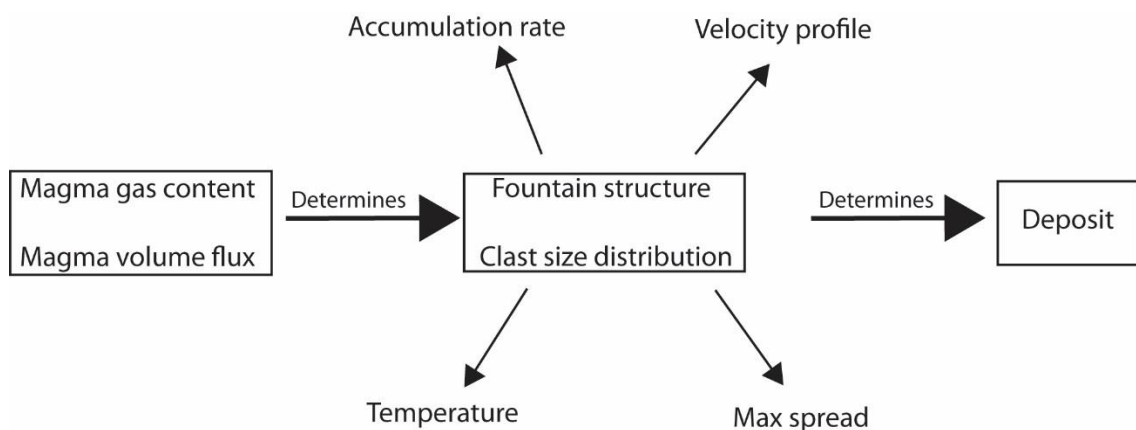


Figure 2.2 (overleaf). Factors controlling lava fountain structure. Modified from Head and Wilson (1989).

2.4. Basaltic lavas

Lava flows are ubiquitously encountered in hydrocarbon basins affected by basaltic volcanism (e.g. Gatliff et al. 1984; Maresh et al. 2006; Jerram et al. 2009; Davison et al. 2010; Holford et al. 2012). Lava flow fields can cover areas up to $3 \times 10^5 \text{ km}^2$ (Hooper 2000) and reach thicknesses of 2 km (Bondre et al. 2004b). They account for >99% of the erupted products in flood basalt provinces (Ross et al. 2005).

2.4.1 Definition of terms

The smallest individual package of a lava flow is a lava lobe (Self et al. 1998). Pāhoehoe lobes are initially 20–50 cm thick, 20–300 cm wide and 0.5–5 m long (Fig. 2.3; Self et al. 1998). The lobes can coalesce forming large sheets with steep monoclinical margins and distinctive flat tops up to thousands of metres wide (Hon et al. 1994). Sheet flows form on slopes $<2^\circ$ (Hon et al. 1994). Numerous lava lobes are the constituent parts of a lava flow, the product of a single outpouring of lava (Self et al. 1998). Long-lived eruptions may produce a number of lava flows constructing a lava flow field (Self et al. 1998). Thus a lava flow field is the largest descriptive unit of a single or numerous eruptions. Lava flows may also be described as either compound or simple flows. The terms were first used by Walker (1971) to differentiate between numerous flows of the same size (compound flows) and large sheet flows (simple flows). Jerram (2002) used similar descriptive terms for tabular classic (i.e. simple) and compound braided facies (i.e. compound) lava flows in flood basalt provinces (Fig. 2.4). Effusion rate is defined as the rate at which lava is erupted from a dyke (Harris et al. 2007). Effusion rate controls surface morphology, heat loss (and thus crystallisation) and pressure conditions within an inflating lava flow (Harris et al. 2007). Flow rate is defined as the volumetric discharge at the vent and is intimately linked to subsurface magma transport system (Rowland and Walker 1990).

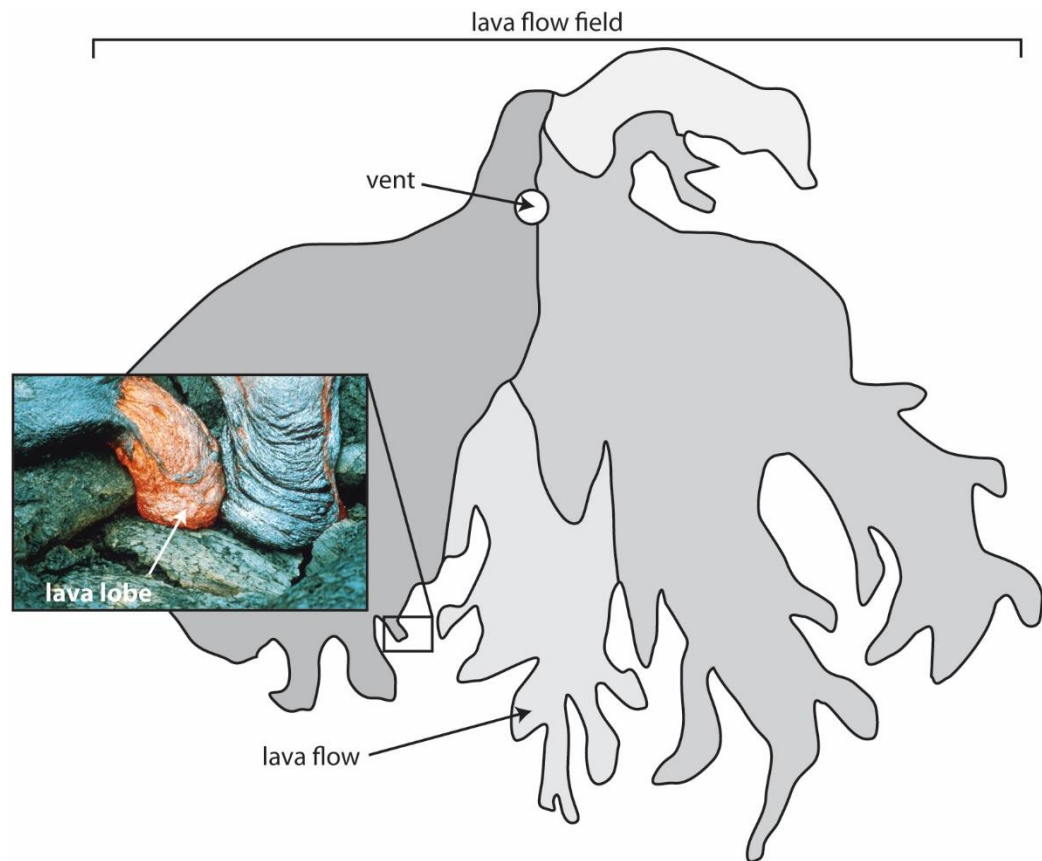


Figure 2.3. Schematic diagram illustrating the difference between lava flows, lobes and flow fields. The lava lobe shown is 300 cm wide. Individual lava flows are shaded. The lava flow field ranges in size from tens to hundreds of kilometres. Photograph from Swanson (1974). Diagram modified from Self et al. (1998).

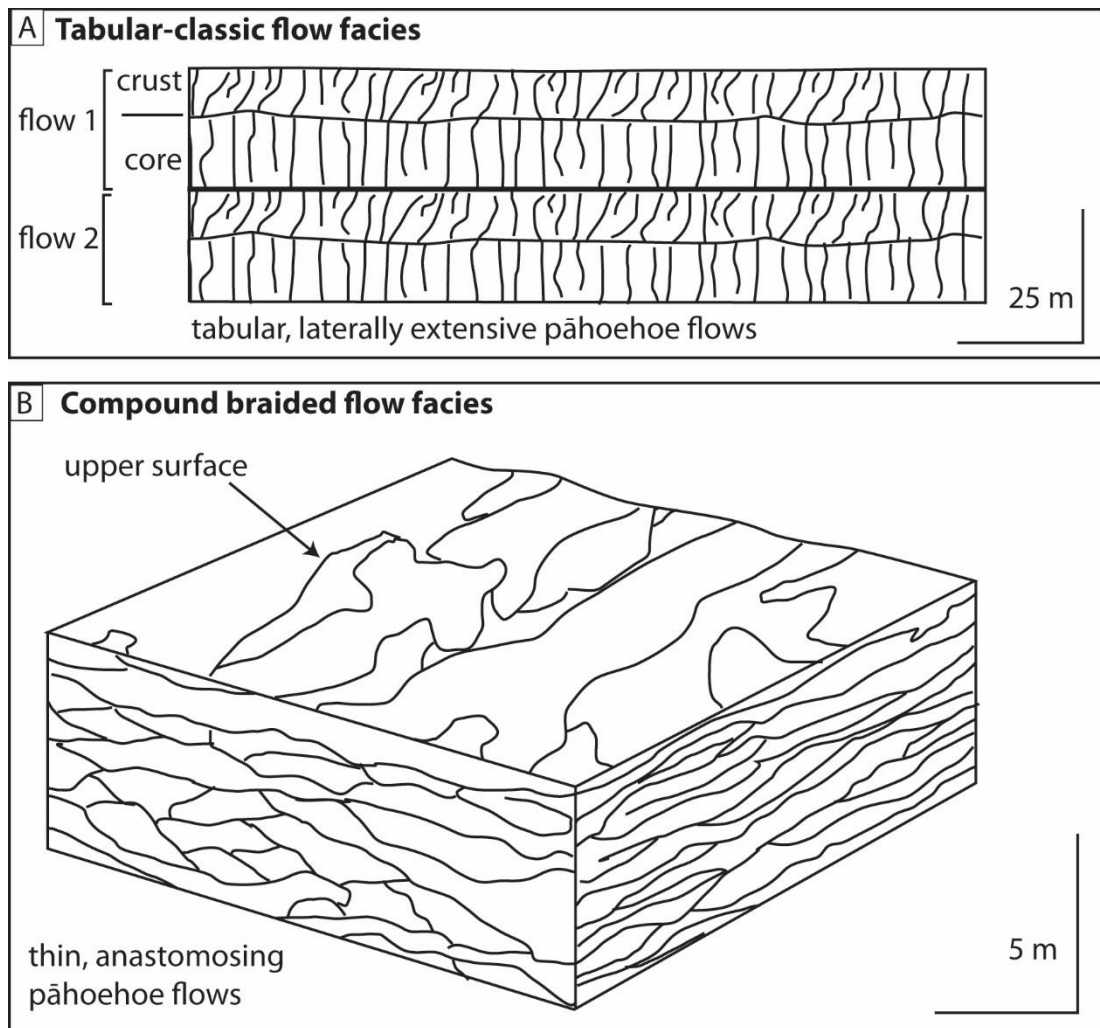


Figure 2.4. Tabular classic (A) and Compound braided flow facies (B) found within flood basalt provinces. Modified from Jerram (2002).

2.4.2 Emplacement

Two basaltic lava types are recognised: ‘ā‘ā and pāhoehoe (Macdonald 1953; Self et al. 1998). ‘Ā‘ā lavas (Fig. 2.5) are emplaced during eruptions with effusion rates $>5\text{--}10\text{ m}^3\text{ s}^{-1}$. They have clinkery basal and upper breccias that grade in to massive cores with irregular vesicles (Macdonald 1953). Near to the vent the flows move in a fashion similar to a caterpillar track (Rowland and Walker 1990). ‘Ā‘ā tends to travel within open channels 0.1–2.5 km wide (Rowland and Walker 1990). The flows grow exogenously, i.e. without inflating (see section below). During flow the lava core is continually overturned, promoting heat loss and rapid groundmass crystallisation (Booth and Self 1973; Crisp and Baloga 1994; Harris and Rowland 2001). Rapid crystallisation is critical for ‘ā‘ā lavas to form (Cashman et al. 1999; Soule and Cashman 2005).

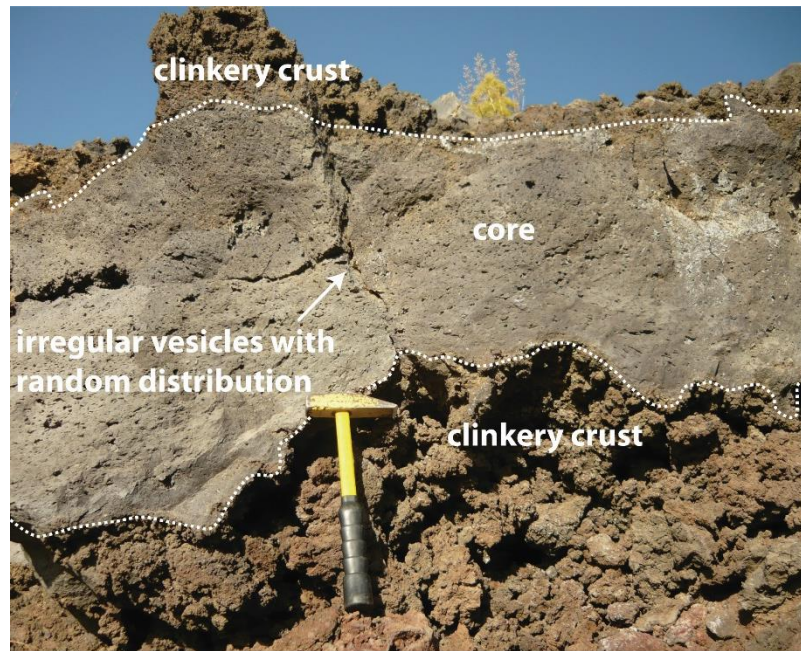


Figure 2.5. Cross section of an 'a'ā lava. The flow has a massive core with irregular vesicles and an upper and lower crust composed of clinker.

In contrast, pāhoehoe lavas have smooth, billowy and ropey upper surfaces that act to insulate the flow as it moves (Hon et al. 1994; Keszthelyi and Denlinger 1996; Keszthelyi and Self 1998). Pāhoehoe is emplaced during low effusion rates of $<5\text{--}10\text{ m}^3\text{ s}^{-1}$ (Rowland and Walker 1990). Flows typically move very slowly (Self et al. 1998) although rapid advancement is also documented (Solana et al. 2004). Pāhoehoe advances by budding and inflation and can be emplaced by tube and channel systems (e.g. Pinkerton and Wilson 1994; Dragoni et al. 1995; Calvari and Pinkerton 1998; Calvari and Pinkerton 1999; Cashman et al. 2006; Valerio et al. 2008). Pāhoehoe can also be produced by pyroclast coalescence and effusion (e.g. Cas and Wright 1987; Head and Wilson 1989; Wolff and Sumner 2000; Harris et al. 2007).

Lavas may transition from pāhoehoe to 'a'ā during flow. The transition between pāhoehoe and 'a'ā is dependent on an increase in viscosity and/or shear strain (Fig. 2.6; Peterson and Tilling 1980). Increases in viscosity are promoted by rapid cooling of the lava during flow (e.g. by channelisation on steep slopes, promoting turnover of the flow core; see Gregg and Fink 2000). Increased slope angle also increases strain rate within flows (Hon et al. 2003). Viscosity also changes as the lava degasses during flow and fountaining episodes. Degassing promotes crystallisation (Lipman et al. 1985), forming vesicles which affect the rate of heat loss from the lava flow surface (Keszthelyi 1994). In addition, the

lava eruption temperature affects the time crystallisation occurs, thus affecting viscosity. For a review of the transition, see Cashman et al. (1999).

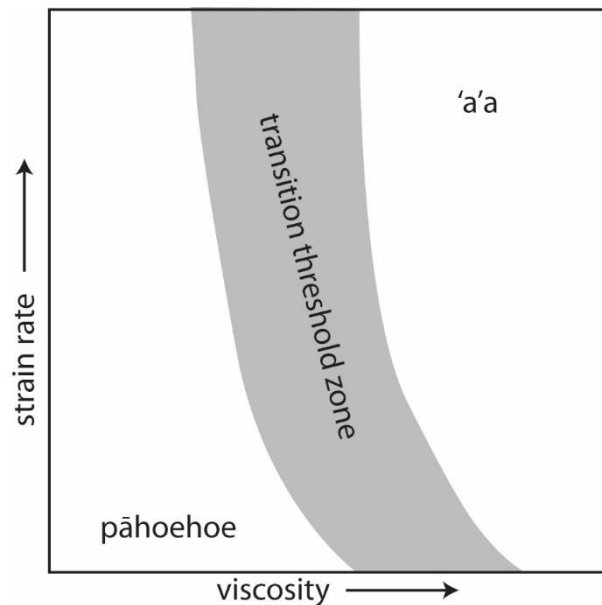


Figure 2.6. Schematic diagram illustrating how pāhoehoe lava transitions to 'a'a as a function of strain rate and viscosity. Modified from Peterson and Tilling (1980).

2.4.2.1 Inflation of pāhoehoe lavas

Inflation is the injection of lava beneath a cooled, solidified crust, causing thickening of the lava flow. As the lava flow thickens, new crustal material is accreted to the base of the upper crust and the flow propagates by budding of new lobes. Internally the flow develops a characteristic tripartite structure. The pioneering work of Hon et al. (1994) allowed quantitative determination of the time required to emplace an inflated pāhoehoe flow using the equation:

$$t = 164.8C^2$$

where t = time in hours

and C = crustal thickness in metres

Externally the flow field may develop tumuli and squeeze-outs. Recognising inflation in contemporary Hawaiian flows revolutionised understanding of flood basalt emplacement (e.g. Self et al. 1998; Thordarson and Self 1998). However, whether inflation

occurs via a series of lava pulses as opposed to by sustained lava input is debated (Anderson et al. 1999).

2.4.3 Types of pāhoehoe lavas

Pāhoehoe lavas are the most common type of basaltic lavas on Earth (Self et al. 1998). They are found in subaerial and submarine settings and dominate in flood basalt provinces (e.g. Walker 1971; Self et al. 1998; Thordarson and Self 1998; Jerram 2002; Bondre et al. 2004a; Bondre et al. 2004b; Waichel et al. 2006; Passey and Bell 2007; Duraiswami et al. 2008). Pāhoehoe lava types include: P-type (e.g. Wilmoth and Walker 1993; Self et al. 1998); S-type (e.g. Walker 1989); blue glassy (e.g. Self et al. 1998; Oze and Winter 2005); silvery (e.g. Self et al. 1998); shelly (e.g. Swanson 1973); spiny/toothpaste (e.g. Rowland and Walker 1987); slabby (e.g. Guilbaud et al. 2005); rubbly (e.g. Duraiswami et al. 2008); entrail (e.g. Kilburn 2000) and clastogenic (e.g. Cas and Wright 1987). These distinctions are based on surface texture/colour and internal characteristics (Figs. 2.7 and 2.8).

P-type pāhoehoe has pipe vesicles at the base of the lava flow (Wilmoth and Walker 1993; Self et al. 1998). These vesicles indicate emplacement on slopes $<4^\circ$ (Kent et al. 1998; Walker et al. 1999; Passey and Bell 2007). However, their formation mechanism is debated (Philpotts and Lewis 1987). These flows decrease in vesicularity toward their core. P-type lava flows are inflated (Self et al. 1998; Thordarson and Self 1998). S-type or spongy pāhoehoe has the opposite vesicle structure to P-type; with vesicles increasing in size and abundance towards the core of the flow. These flows are common in medial and distal areas (Walker 1989). The abundance or significance of S-type flows is otherwise unknown.

The surface colour of silvery pāhoehoe is the result of the trapping of a thin layer of air under a <1 mm thick glass layer (Self et al. 1998). S-type pāhoehoe commonly has a silvery colour, although silvery pāhoehoe may also have pipe vesicles (Self et al. 1998). In contrast, blue glassy pāhoehoe owes its surface colour to its longer residence time within the lava supply network, lower temperature than silvery pāhoehoe (Self et al. 1998) and the concentration of iron and magnesium at the surface (Oze and Winter 2005). Their colour may also result from gases being forced back into solution due to increased pressure during inflation (Hon et al. 1994). This lava indicates inflation occurred for at least two weeks prior to emplacement of the blue glassy flow (Self et al. 1998).

Shelly pāhoehoe can be divided into two types: sheet flood and amoeboid (Swanson 1973). However, inter gradation between types is common. Local relief at the source vent

and emplacement rate is thought to control morphology, with the sheet flood variety occurring where relief is <1 m and during faster emplacement (Swanson 1973). Both types are considered reliable indicators of proximity to the source vent; shelly pāhoehoe evolves rapidly into other lava types and has been used as an indicator of proximity to source in ancient successions (e.g. Swanson 1973; Reidel and Tolan 1992; Brown et al. 2014). (e.g. Swanson et al. 1975; Reidel and Tolan 1992; Self et al. 1998; Guilbaud et al. 2005). However, the maximum distance this lava is emplaced from the vent is unknown. Limiting factors in the lavas advance are described by Swanson (1973) as slopes of $>5^\circ$ and withdrawal of the lava feeding column. Shelly pāhoehoe also forms during lava channel overflows (e.g. Stevenson et al. 2012).

Spiny pāhoehoe is transitional between pāhoehoe and 'a'ā (see section 2.4.2). Its surface is characterised by longitudinal grooves and ridges, parallel to the direction of flow, with spines 1–5 long and 1 cm wide. It typically appears dull due to the abundance of microlites (Rowland and Walker 1987).

Slabby pāhoehoe is relatively rare, recognised only in the Laki flow field and Deccan Volcanic Province (Duraishwami et al. 2003; Guilbaud et al. 2005). It forms due to periods of differential inflation, with high flux rate periods leading to the disruption of the upper crust (Guilbaud et al. 2005). It provides evidence of incipient transformation of pāhoehoe lava to 'a'ā (Duraishwami et al. 2003). If disruption is cyclical, rubbly pāhoehoe may be formed (Duraishwami et al. 2008). Rubbly pāhoehoe is characterised by brecciated flow tops composed of varying sizes of disrupted, highly vesicular pāhoehoe crust (Bondre et al. 2004a). Flows have gently undulating tachylitic flow bases (Duraishwami et al. 2008).

Entrail pāhoehoe is an informal term used to describe the commonly small, compound flows whose lobes resemble intestines (Kilburn 2000). No studies define specific emplacement mechanisms. However, studies of compound flows in the Deccan Volcanic Province suggest they are produced during low effusion rate episodes (Walker 1971).

Lava flows of coalesced pyroclasts are known as clastogenic flows (Cas and Wright 1987). They may have pāhoehoe or 'a'ā type crusts (e.g. Thordarson and Self 1998; Waythomas et al. 2014). This lava is fountain-fed; produced from the agglutination and coalescence of pyroclasts. Fountain-fed lavas may be rootless, lacking a lithological link to the source vent (Cas and Wright 1987). Clastogenic pāhoehoe is exceptionally common although many lava flows retain little evidence of their pyroclastic origin (Thordarson and Self 1998). The importance of inflation during emplacement is unknown. Internally the flows are composed of agglutinated – coalesced agglutinate (e.g. Sumner 1998) and

contain numerous irregular vesicle patches that represent relict pyroclasts known as “ghost” clasts (e.g. Sumner 1998; Brown et al. 2014). The significance of these textures is interpreted in relevance to the accumulation rate of the constituent pyroclasts (Sumner et al. 2005). The effects of shear, compaction and inflation are not described. Furthermore, no studies document lateral and vertical changes in the lavas internal texture. Recent work by Sumner et al. (2005) showed that clastogenic lavas may also result from the collapse of an edifice; thought to be a common process during the construction of basaltic edifices. Clastogenic lavas are also found as ponds within vents (Carracedo Sánchez et al. 2012).

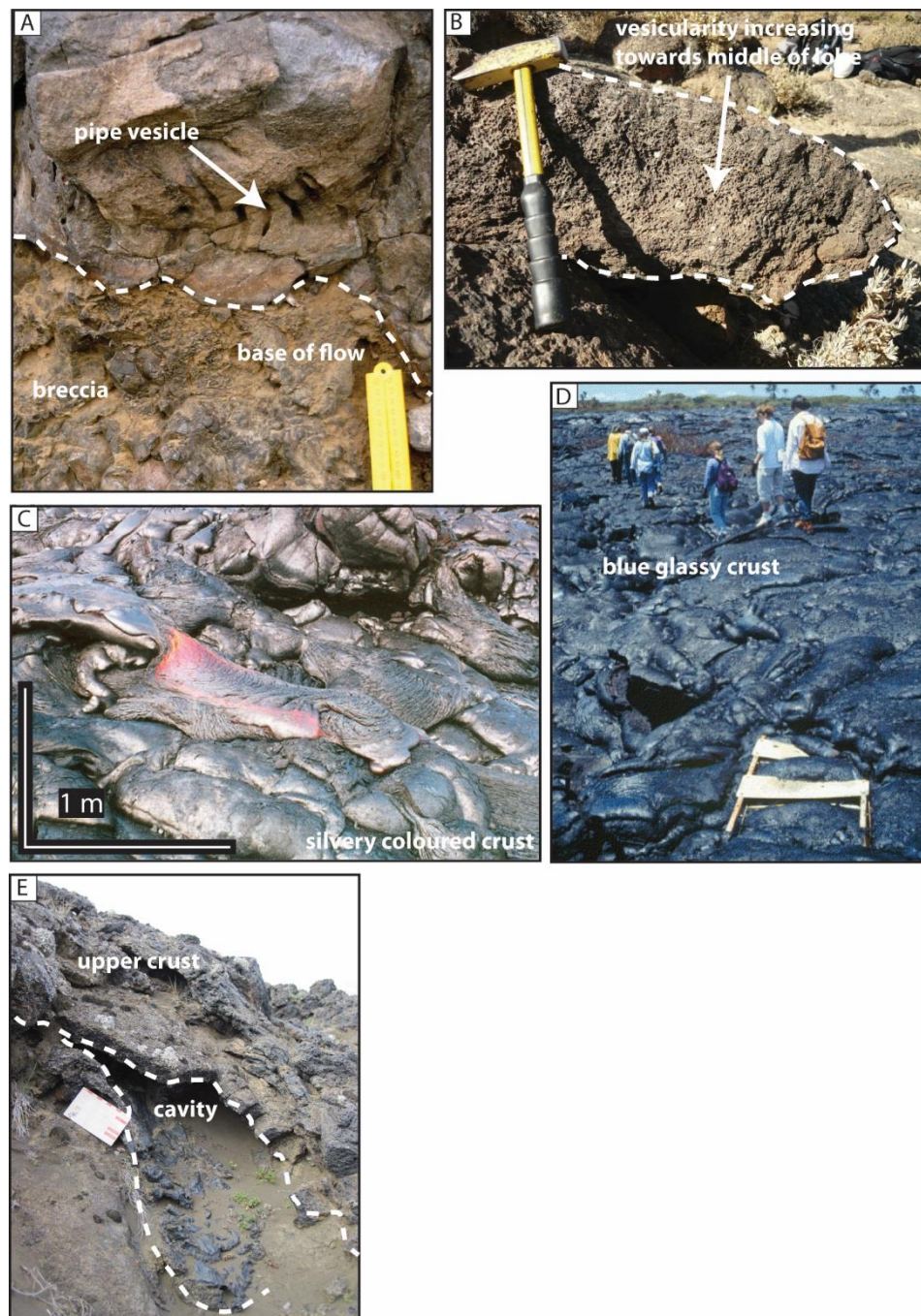


Figure 2.7. (overleaf) Photographs showing (A) P-type, (B) S-type, (C) silvery (D) blue glassy and (E) shelly pāhoehoe. Photograph C is from Leverington (2002) and D is from Wilch (2011). The ruler in A is 10 cm long and the scale card in E is 10 cm long.

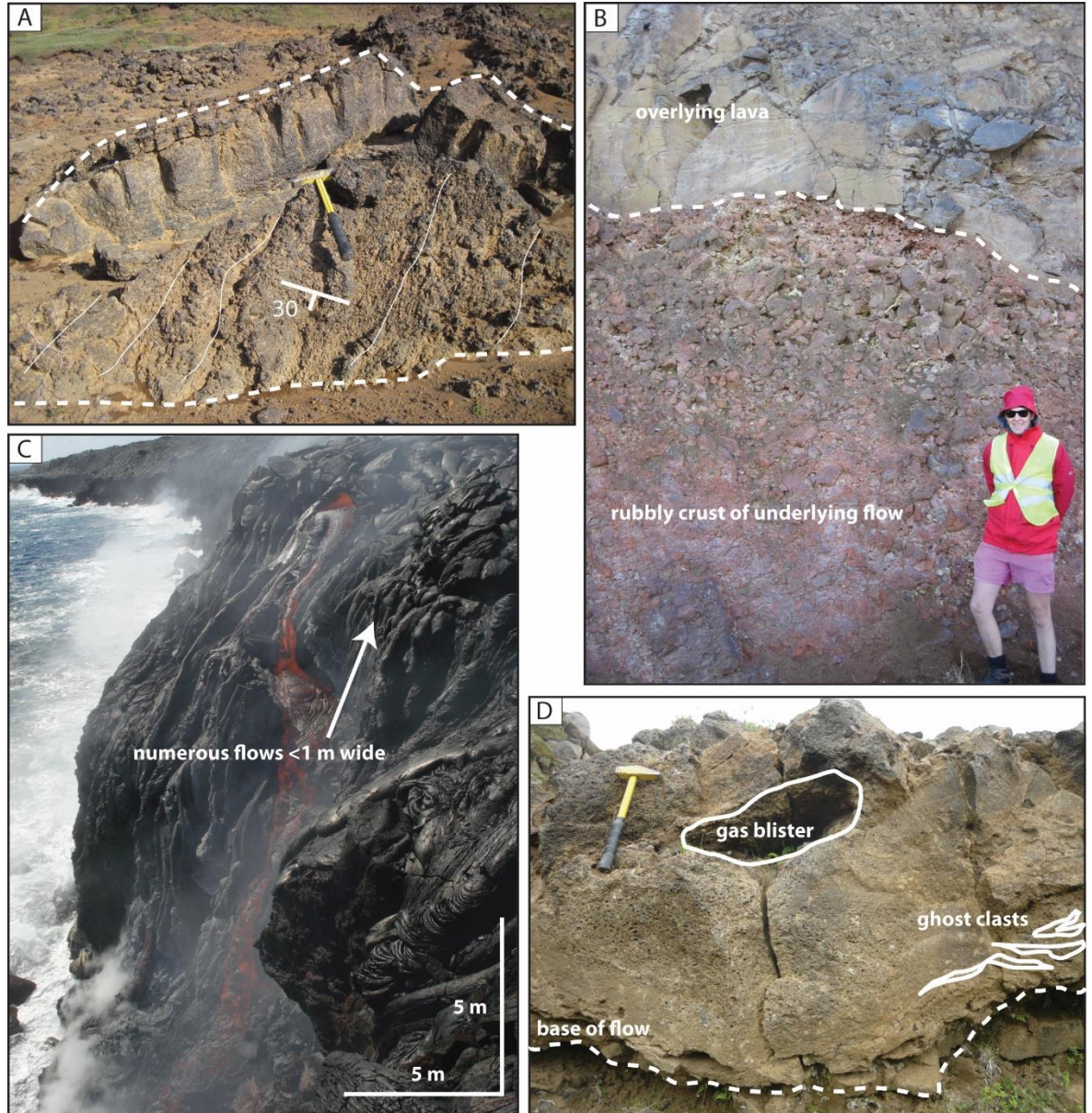


Figure 2.8. Photographs showing spiny (A), rubbly (B), entrail (C) and clastogenic (D) pāhoehoe. Photograph C from Pendred (2011).

2.4.4 Physical features of lava flow fields

Lava flow fields contain a range of large scale features that can be used to determine emplacement conditions (e.g. inflation). Features include tumuli, tubes, channels, squeeze-outs, rafted deposits and lava rise pits. Tumuli form during inflation and are roughly

circular or elongate mounds with axial or star-like clefts in their crust (Walker 1991). They are often found above tubes (Walker 1991). Tubes and channels represent arterial delivery systems to the distal regions of the flow field. Tubes and channels form within both *ʻā* and pāhoehoe lavas at varying effusion rates (e.g. Hon et al. 1994; Calvari and Pinkerton 1998; Calvari and Pinkerton 1999; Solana et al. 2004). Processes leading to their formation are described by Dragoni et al. (1995); Cashman et al. (2006) and Valerio et al. (2008). Squeeze-outs are found where injection of lava beneath the crust is extruded from beneath the solidified crust. They are common in distal regions of the flow field (Sumner 1998). Rafted deposits are fragments of pyroclasts or other lava flows that are carried down flow by the lava (Sumner 1998; Valentine and Gregg 2008; Riggs and Duffield 2008). The deposits may be carried entirely upon the top of the lava flow, or may begin to sink into the flow, depending on the rheology of the lava and deposit (Valentine and Gregg 2008). Lava rise pits result from topography inversion, and are depressions (originally topographic highs) between tumuli or lava rises. When a lava flow propagates into a large body of standing water, hyaloclastite and lava deltas form (see references within Wright 2013; Watton 2013). If a lava flow propagates into a marginal lacustrine or marshy environment, rootless eruptions may occur (e.g. Fagents et al. 2002; Fagents and Thordarson 2007; Hamilton et al. 2010a; Hamilton et al. 2010b).

2.4.4.1 Rootless eruptions

Rootless eruptions occur as a result of explosive interaction between saturated sediments and actively inflating pāhoehoe lava flows. These eruptions build cones on top of the lava flow and excavate a vent in the host lava flow. Similar rootless edifices (known as littoral cones) occur when lava flows enter the sea. Rootless cones vary in size from 2–40 m high and 5–450 m in basal diameter. They resemble small scoria cones, tuff cones or steep-sided spatter cones (Fagents and Thordarson 2007). They are composed of inversely graded beds of lapilli and bombs from fragmented molten lava core, clasts from the lava flow crust and sediment from beneath the lava flow (Hamilton et al. 2010b). Cones may exhibit complex stratigraphic relationships (Fagents and Thordarson 2007; Hamilton et al. 2010b) and occur in clusters that cover areas of up to 150 km² (Hamilton et al. 2010b). However, the stratigraphy, depositional sequence and componentry of these cones are poorly described. Furthermore, how the vents within the host lava flows are created, maintained and subsequently recognised in the field is not described.

2.4.5 Internal features of lava flows

2.4.5.1 Crustal structure

P-type pāhoehoe is comprised of an upper crust, a core and a basal crust (Self et al. 1998). This tripartite structure is defined by variations in vesicularity and indicates that the lava inflated (Fig. 2.9) (Self et al. 1998). The vesicular upper crust comprises 40–60% of the lobe thickness and its groundmass is hypohyaline – hypocrySTALLINE. It may contain prismatic or irregular joints. The crust often has horizontal vesicular zones (VZs) that are centimetres to decimetres thick. Bubbles within the zones increase in size with depth before increasing again at their base. They form due to variations in magma flux and/or pressure during inflation. The core is non-vesicular and holocrystalline. It contains vesicle sheets (VSs) and vesicle cylinders (VCs). Vesicle sheets are 1–5 cm thick and form due to the buoyant uprising of differentiated residuum from the core, which spread on contact with the solidified crust. Vesicle cylinders are similar to vesicle sheets and are formed by the diapiric rise of bubble-rich, low density residuum (Goff 1996). The basal crust can be almost as vesicular as the upper crust, but is only 20–100 mm thick regardless of flow thickness (Self et al. 1998). Its groundmass is hypohyaline – hypocrySTALLINE. The basal crust is sparsely jointed. The vesicularity, crustal structure of other lavas (e.g. shelly and clastogenic pāhoehoe) and the implications for their emplacement mechanisms remains uninvestigated.

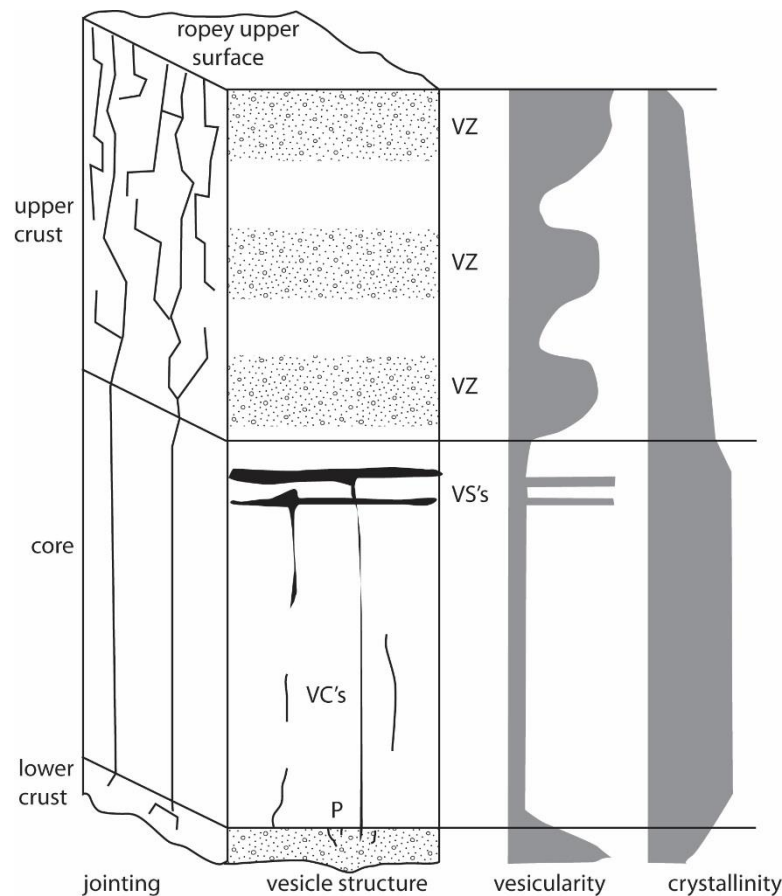


Figure 2.9. Schematic cross section through P-type pāhoehoe. The lobe has a tripartite structure defined by variations in vesicularity, crystallinity and jointing. The basal crust is 20–100 mm thick regardless of lobe thickness and is hypohyaline – hypocrySTALLINE. Cooling joints are sparse. The core of the flow is non-vesicular and holocrystalline. Columnar jointing may penetrate the core. Vesicle cylinders (VCs) and vesicle sheets (VSs) are found. The upper crust comprises 40–60% of the lobe thickness. It is vesicular and hypohyaline – hypocrySTALLINE. It may contain prismatic or irregular joints and numerous horizontal vesicle zones (VZs). Modified from Self et al. (1998).

2.4.5.2 Cooling joints

Both pāhoehoe and a’ā lava flows develop thermal contraction joints as they cool. These joints grow towards the interior of the flow as the crust thickens (Degraff et al. 1989). Many lava flows (eg. in Hawaii) have thin, crudely columnar tops, whilst larger flows (e.g. those within the Columbia River) have spectacular columnar jointing (Fig. 2.10). This jointed zone is defined as the colonnade (Tomkeieff 1940) and occurs in the core of lava flows (Thordarson and Self 1998). James (1920) considered that joint morphology is dependent on viscosity, temperature, rate and regularity of cooling and

homogeneity of the lava. Recent studies of cooling joints have shown that their radius is proportional to the cooling rate of the lava (Ryan and Sammis 1978; Goehring et al. 2006; Goehring and Morris 2008). Welded pyroclastic units can also develop columnar cooling joints (Brown et al. 2014).

The entablature (Fig. 2.10) is found in the upper crust of flows (e.g. Thordarson and Self 1998) and is produced by percolation of extreme rainfall ($>>250$ cm/yr) or flooding by fluvial systems (Long and Wood 1986). Similar pseudopillow fracture systems, formed by lava interaction with an aqueous coolant, indicate both brittle and ductile fracture mechanisms (Forbes et al. 2012). In all cases, percolating water uses master joints as a pathway for penetration into the lava flow (Forbes et al. 2014). Some lava flows have a tiered structure (Fig. 2.10) due to intermittent flooding events and dry periods (Long and Wood 1986).

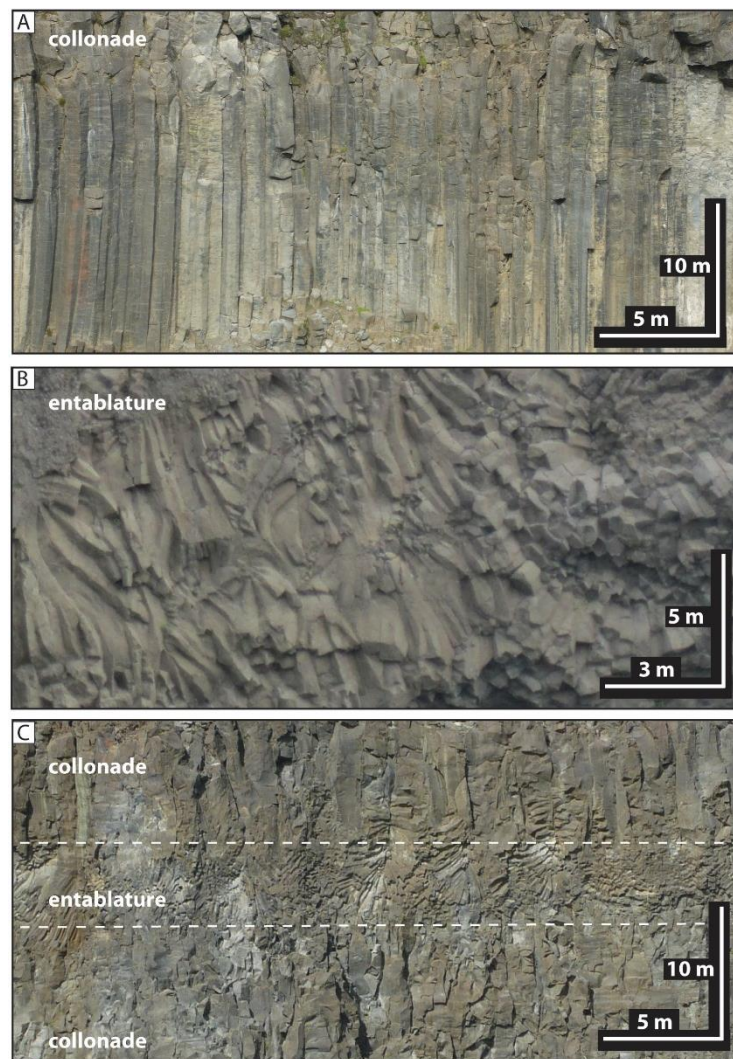


Figure 2.10. Jointing styles in lavas. (A) The colonnade of a lava flow with regular,

columnar jointing. These joints form due to thermal contraction during cooling. (B) The entablature of a lava flow with characteristic wavy-shaped joints. These joints form due to percolation of water through the cooling lava. (C) A tiered lava flow, displaying both an entablature and colonnade. This style of jointing develops due to intermittent flooding and dry periods.

2.5 Volcanic edifices

This section describes volcanic edifices in field datasets. A focus is given to monogenetic volcanic edifices formed during magmatic eruptions (e.g. scoria and spatter cones and spatter ramparts) since these edifices are found on fissures feeding flood basalt provinces and many other basaltic flow fields (e.g. Swanson et al. 1975; Reidel and Tolan 1992; Thordarson and Self 1993; Sumner 1998; Valentine et al. 2005; Riggs and Duffield 2008; Németh et al. 2011). Thus, edifices formed during magmatic volatile driven eruptions are candidates for volcanic edifices in hydrocarbon basins (e.g. the FSB).

These edifices may be monogenetic (i.e. erupt only once; Walker 2000) or polygenetic (i.e. erupt several times), which I describe in turn. I then provide a summary of seamounts, whose origin (i.e. mono or polygenetic) is often unknown.

2.5.1 Monogenetic volcanoes

Monogenetic edifices are 0.25–2.5 km in diameter and <30–450 m in height (Wood 1980; White and Ross 2011). They are common along fissures and may form linear chains along structural features (e.g. faults) or have scattered distributions (Walker 1993; Connor and Conway 2000). They are composed of lava flows and pyroclasts, depending on surface/ground water abundance, lava fountain structure, the underlying substrate and magma rheology/rise speed (Wohletz and Sheridan 1983; Jaupart and Vergnolle 1988; Head and Wilson 1989; Sohn 1996; e.g. Valentine and Gregg 2008). Edifices formed during magmatic eruptions include spatter cones, spatter ramparts, scoria cones, shield volcanoes and agglutinate cones. Edifices formed during magma-water interaction include tuff cones, tuff rings and maars. The amount of water involved in producing phreatomagmatic edifices is poorly constrained (see conflicting hypotheses in Vespermann and Schmincke 2000; White and Ross 2011). These edifices may intersect and merge in a complex fashion (e.g. Thordarson and Self 1993) and may form hybrid edifices (e.g. Verwoerd and Chevalier, 1987). Thus, edifices are part of a continuous spectrum of types.

Monogenetic edifices have a distinctive morphology (Tables 2.1 and 2.2; Vespermann and Schmincke 2000; White and Ross 2011). Field data suggests that the eruptions are fed by sills intruded to depths as shallow as 250 m (Németh and Martin 2007), whilst seismic data from historic eruptions show sills at depths of ~1.5 km feeding eruptions (Chadwick et al. 2006). These sills then feed dykes, which link to diatremes beneath maars and tuff rings. The exact methods by which edifices link to feeder systems in the shallow subsurface have been difficult to constrain (see section 2.3.1).

| Vent type | Basal D (km) | Crater/plateau D (km) | Vertical scale of edifice (km) | Calculated height/basal diameter ratio | Volume (km³) | Height/rim ratio | Flank dip (°) | Example |
|---|--------------|-----------------------|--------------------------------|--|--------------|------------------|----------------------------------|---------------------------------|
| Spatter cone | <0.10 | No data | 0.10–0.30 | No data | No data | No data | Steep, can approach vertical | Kapoho phase of Kilauea, Hawaii |
| Scoria cone | 0.25–2.50 | 0.10–1.00 | 0.04–0.45 | 0.18 | 0.0001–1 | 0.45 | 25–38 | Heimaey, Iceland |
| Shield-like volcano | 1.0–12.00 | 0.10–1.80 | 0.05 –0.50 | No data | 0.4–11 | No data | 0–10 | Rangitoto Island, New Zealand |
| Agglutinate cone | 0.2–0.4 | | 0.01–0.16 | No data | 0.0001–0.01 | No data | 15–19 | Roza cones, Columbia River |
| Tuff cone | 0.50–5 | <0.1 –1 | 0.05–0.30 | 0.06 | 0.0001–1 | 0.5–0.2 | 10–30 | Udo tuff cone, Korea |
| Tuff ring | 1.60 | 0.20–3.00 | <0.05 | 0.03 | 0.0001–1 | 0.13–0.15 | 1–20 | Songaksan, Korea |
| Maar | 1.4 | 0.2–3 | <0.03 | 0.02 | No data | 0.13–0.15 | 1–20 | Ukinrek West, Alaska |
| Polygenetic cone | No data | No data | 0.35–2.25 | No data | 0.50–75 | No data | Variable; 21–34 for simple cones | Mt. Teide, Tenerife |
| Seamount | 0.70–2.30 | No data | 0.09–0.39 | 0.04–0.24 | 0.24–0.39 | No data | <20–30 | MOK seamount, East Pacific Rise |
| Table 2.1. Summary of volcanic edifice morphology. Data from Waters and Fisher (1971); Wood (1980); Head et al. (1981); Wilson and Head (1981); Thors and Jakousson (1982); Wohletz and Sheridan (1983); Gatliff et al. (1984); Ross (1986); Rossi (1996); Vespermann and Schmincke (2000); White and Ross (2011); Grosse et al. (2009); Mitchell et al. (2012) and (Brown et al., 2014). | | | | | | | | |

| Vent type | Plumbing system | External morphology | Formation environment | Components |
|---|-------------------------------|---|---|--|
| Spatter cone/ramparts | Dyke fed | Roughly circular in plan view (cones); linear, paired or singular features (ramparts), pipe like or fissure conduit remains open to several tens of feet below crater | Sub aerial, no magma-water interaction | Spatter and agglutinate |
| Scoria cone | Dyke fed | Small, truncated, cone shaped volcanic hills with bowl shaped craters | Sub aerial, no magma-water interaction | Ash, scoria, spatter and lava |
| Shield-like volcano | Dyke fed | Roughly circular in plan view, crater floors generally above land surface | Sub aerial | Basaltic lava flows; basaltic dredge samples from other similar structures |
| Agglutinate cone | Dyke fed | Roughly circular in plan view, crater floors above land surface | Sub aerial | Agglutinated spatter and scoria |
| Tuff cone | Dyke fed | Roughly circular in plan view crater floors generally above land surface | Subaerial, emergent submarine | Pyroclastic and crystalline basaltic rocks |
| Tuff ring | Underlain by shallow diatreme | Roughly circular in plan view with broad crater that may extend below surface | Sub aerial | Ash, scoria, spatter |
| Maar | Underlain by deep diatreme | Roughly circular in plan view with broad crater cutting 10–500 m into pre-eruption surface and low rim. | Requires enough water to allow explosive fragmentation, with hydrostatic pressure <30 bars. | Ash, abundant country rock |
| Polygenetic cone | Dyke fed | Very variable, from simple cones to massifs | Sub aerial and submarine | Pyroclasts and lava; variable in chemistry and texture |
| Seamount | Dyke fed | Broadly cone shaped, becoming flatter in shallower water, or flat where lava overflows from pond | Submarine, 200–400 m* | Lava, hyaloclastite, volcanoclastics |
| Table 2.2. Summary of volcanic edifice architecture (*water depth to summit). Data from Macdonald (1972); Wohletz (1983); Lorenz (1986); Rossi (1996); Riedel et al. (2003); Grosse et al. (2009); White and Ross (2011); Mitchell et al. (2012); Magee et al. (2013) and Brown et al. (2014). | | | | |

2.5.1.1 Spatter cones and ramparts

Spatter cones and ramparts are steep-sided edifices. Spatter cones range from 10–40 m high and 5–15 m in diameter (Green and Short 1971; Opheim and Gudmundsson 1989; Thordarson and Self 1993; Rymer et al. 1998; Heliker et al. 1998). They are dominantly composed of large, deformed and strongly welded spatter bombs (Riedel et al. 2003; Cimarelli et al. 2013). Variations in their morphology (e.g. crater – cone width) are not well documented. Spatter cones constructed along the Laki fissure are inferred to have been constructed during phases of dominantly effusive activity (Thordarson and Self 1993).

Spatter ramparts consist of variably welded scoria, spatter, rheomorphic spatter and lava (Alparone et al. 2003; Branca et al. 2009; Parcheta et al. 2012). Despite their abundance in many terrestrial volcanic environments and on Mars (e.g. Moore et al. 1980; Cattermole 1986; McNutt et al. 1991; Thordarson and Self 1993; Wilson et al. 1995; Dickson 1997; Alparone et al. 2003; Branca et al. 2009; Mourão et al. 2010; Parcheta et al. 2012), they have received very little attention in the literature. Ramparts form symmetrically or asymmetrically distributed, paired or single features. These are commonly elongated parallel to the strike of the fissure and set-back ≤ 30 m (Parcheta et al. 2012). Each rampart is ≤ 5 m in height, 12–24 m in width and 3–6 m in length (Moore et al. 1980; Dickson 1997; Parcheta et al. 2012). They may form at the site of maximum effusion from the fissure (e.g. Swanson et al. 1979).

A variety of clastogenic flow processes have been observed during their construction. McNutt et al. (1991) observed the partial collapse of an unstable, asymmetric rampart on steep slopes. Heslop et al. (1989) and Andronico et al. (2014) observed lava flows issuing from their base. Ramparts constructed during the 1977 eruption of Kilauea were eroded by lava drainback, suggesting that their outer surfaces remained molten (Moore et al. 1980). However, they also develop a brittle crust whilst they internally remaining molten (Heslop et al. 1989). Descriptions of the agglutinated deposits common in these edifices are found from literature describing scoria cones, lava ponds and cones in flood basalt provinces (e.g. Holm 1987; Sumner 1998; Valentine and Keating 2007; Riggs and Duffield 2008; Carracedo Sánchez et al. 2012; Brown et al. 2014).

2.5.1.2 Scoria cones

Scoria cones (Fig. 2.11) are truncated, cone-shaped volcanic hills with bowl-shaped craters (Macdonald 1972). They are commonly 0.25–5 km in basal diameter and ≤ 0.45 km

in height (Vespermann and Schmincke 2000). Their slopes dip 25–38° and their crater is above the land surface (White and Ross 2011). Scoria cones range in volume from 10^5 – 10^9 m³ and their crater is small in comparison to their basal diameter. Constituent fall deposits are lapilli–bomb size. Lithic clasts are rare. Examples include the Lathrop wells and Rothenberg scoria cones (see Houghton and Schmincke 1989; Valentine et al. 2005; Valentine et al. 2007; Genareau et al. 2010). They are commonly constructed by lava fountains <400 m in height (Head and Wilson 1989).

Wood (1980) and McGetchin et al. (1974) suggested that cone growth occurred via ballistic ejection of pyroclasts and outwards migration of the cone rim. As cone volume increased, a talus slope forms (McGetchin et al. 1974). The lava fountain also affects cone lithofacies architecture (Head and Wilson 1989). Riedel et al. (2003) demonstrated that cone growth dominantly occurred via deposition of lapilli from an eruption jet column.

Breaching and rafting of the cone by lava flows is a relatively common process (e.g. Valentine et al. 2005; Riggs and Duffield 2008; Valentine and Gregg 2008; Németh et al. 2011). Some breached cones may be partially or wholly rebuilt, leading to internal discontinuities within the edifice (e.g. Riggs and Duffield 2008). Lava flow effusion may be initiated by shallow degassing (e.g. Valentine and Keating 2007; Genareau et al. 2010), clastogenic flow (Sumner 1998), variations in magma flux and feeder dyke processes (Valentine and Gregg 2008). Lava may be effused from boccas at the base of cones (Sánchez et al. 2014) or occur as overspills from lakes in the crater (Carracedo Sánchez et al. 2012).

Scoria cone morphology and internal lithofacies architecture is dependent on variations in pyroclast accumulation rate; magma properties; breaching of the cone by lava flows; phreatomagmatic events and variations in conduit geometry. Variations in pyroclast accumulation rate (see section 2.3.3) can result from changes to fountain structure, inclination (e.g. pyroclast ejection angle, wind speed and direction) and intensity, and can result in variations in welding intensity (Wolfe et al. 1988; Head and Wilson 1989; Vespermann and Schmincke 2000). Variations in magma properties include the magma ascent rate, composition and gas content/flux. These may all result in variations in eruption style (see section 2.3.2).

Some cones are built on pre-existing tuff cones e.g. the Rothenburg scoria cone (Houghton and Schmincke 1989). Fluctuations in ground/surface water supply and magma flux can result in episodic phreatomagmatic events (e.g. Németh et al. 2001; Valentine and Cortés 2013). Variations in conduit geometry include widening (see section 2.3.1) and

constriction, which both affect eruption style (e.g. Keating et al. 2008). Constrictions are caused by lava withdrawal, causing partial collapse and blockage of the conduit neck (e.g. Wolfe et al. 1988).

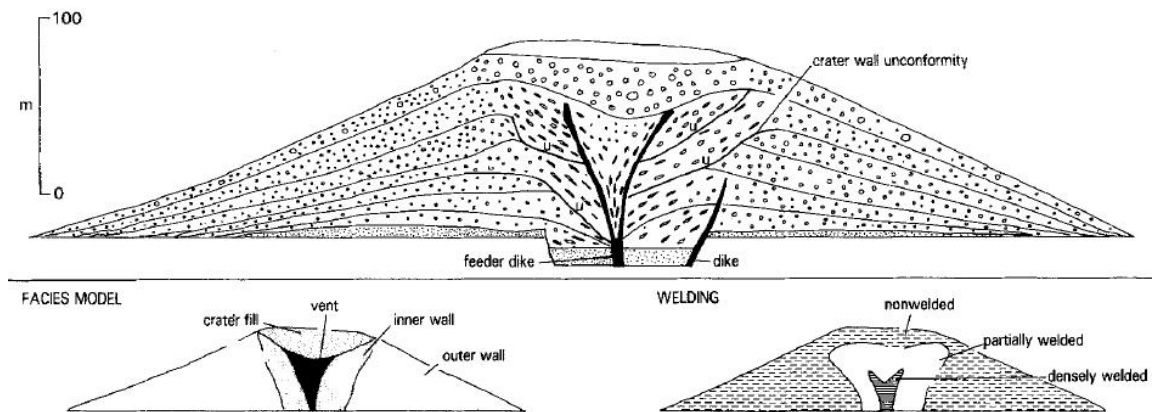


Figure 2.11. Schematic cross section of the Rothenburg scoria cone. Taken from Houghton and Schmincke (1989).

2.5.1.3 Shield volcanoes

Monogenetic shield volcanoes (Fig. 2.12) have basal diameters of 1–12 km and heights of 50–550 m (Rossi 1996). They are dominantly composed of lava flows that build a characteristic summit cone and an extensive lava apron. The cones are flat-topped or slightly convex to concave and convex-concave in cross-section and roughly symmetrical in plan view, with flanks that dip 0–10° (Rossi 1996). Their morphology is dependent on the changes in lava delivery (e.g. tube fed, overspill or rootless) and therefore effusion rate and eruption duration (Rossi 1996). There are few dissected examples of these edifices and the variations in morphology and construction mechanisms are unknown.

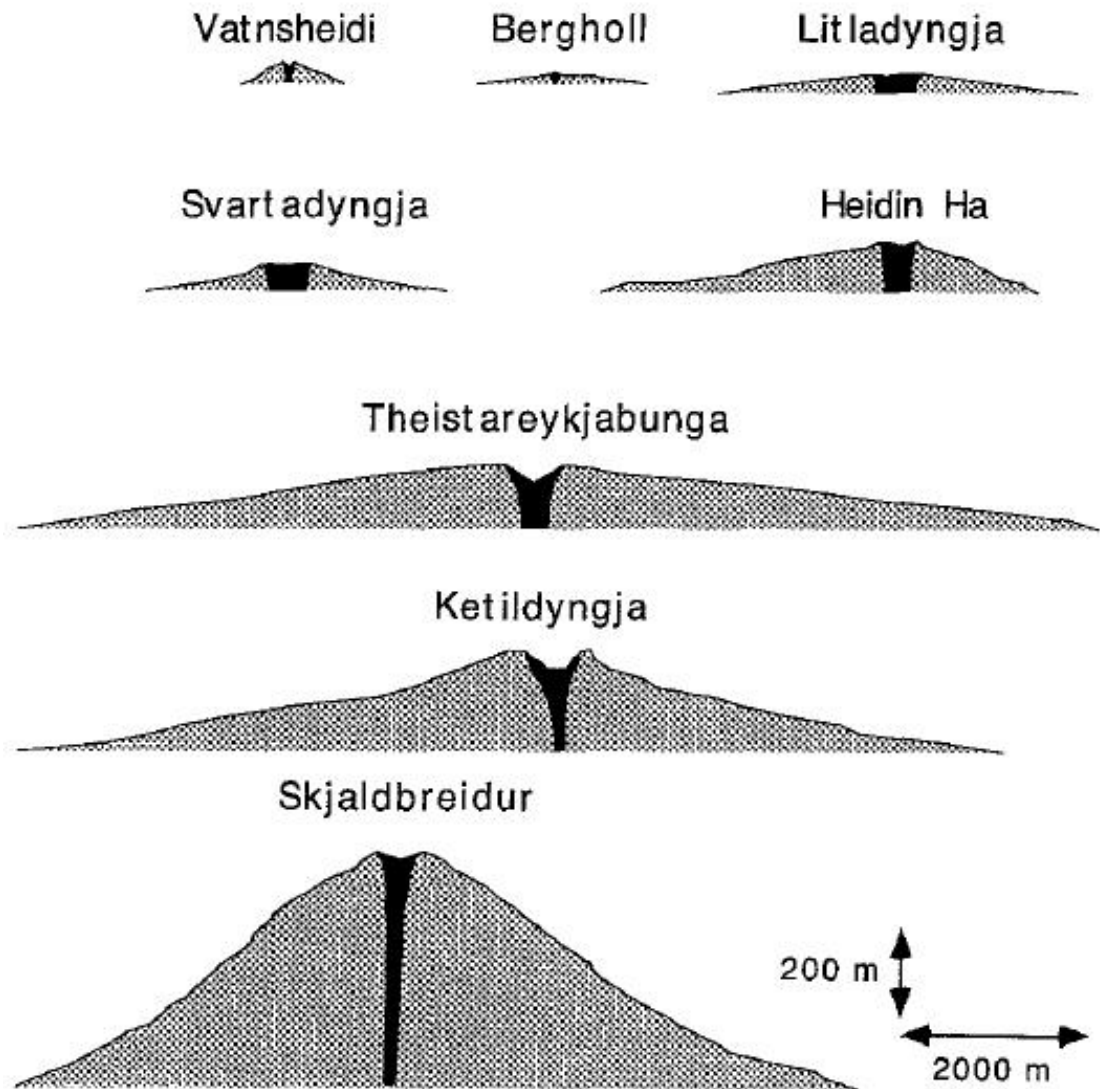


Figure 2.12. Profiles of shield volcanoes in Iceland. The dark column represents the feeder dyke. Taken from Rossi (1996).

2.5.1.4 Agglutinate cones

Agglutinate cones (Fig. 2.13) occur along the Roza fissure in the Columbia River Flood Basalt Province (Brown et al. 2014). The cones have basal diameters of 0.2–0.4 km and are 15–160 m in height. They are dominantly composed of agglutinate and scoria. The mean dip of the cone flanks is 15–19°. Edifices along the fissure are spaced ~1 km apart. The cones are inferred to have been constructed beneath a lava fountain 1 km in height (Brown et al. 2014).

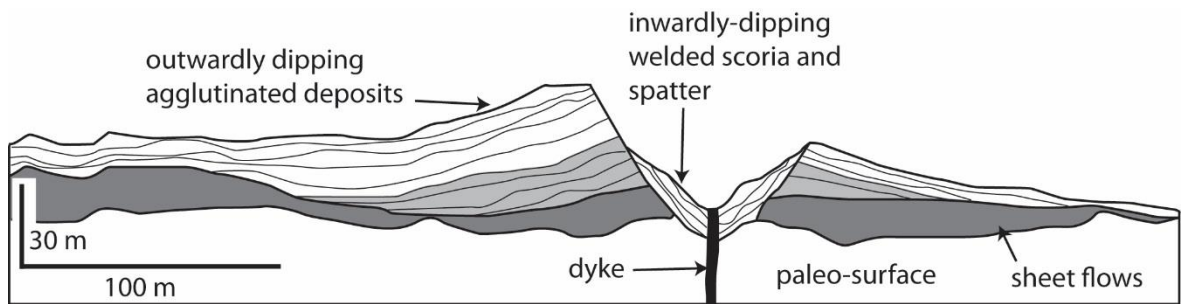


Figure 2.13. Schematic cross section of an agglutinate cone. Modified from Brown et al. (2014).

2.5.1.5 Tuff cones

Tuff cones (Fig. 2.14) are 0.25–5 km in basal diameter and ≤ 0.3 km in height (White and Ross 2011). They are formed during phreatomagmatic eruptions. Their slopes dip 10–30° and their crater floor is above the land surface (Vespermann and Schmincke 2000). The volume of tuff cones ranges from 10^5 – 10^9 m³ and the crater diameter is of medium size in comparison to the basal diameter of the cone (White and Ross 2011). Constituent pyroclasts are deposited by either fall or flow and are dominantly ash–lapilli sized (White and Ross 2011). Tuff cones are composed largely of juvenile clasts with subordinate amounts of accidental lithic clasts (Vespermann and Schmincke 2000). Re-deposition of pyroclasts may occur on steep slopes, resulting in lenticular, massive or chaotic bedded lapilli tuffs (Vespermann and Schmincke 2000). Examples of tuff cones include the Udo tuff cone in Korea and Surtsey, offshore Iceland (Thorarinsson 1966; Sohn and Chough 1993).

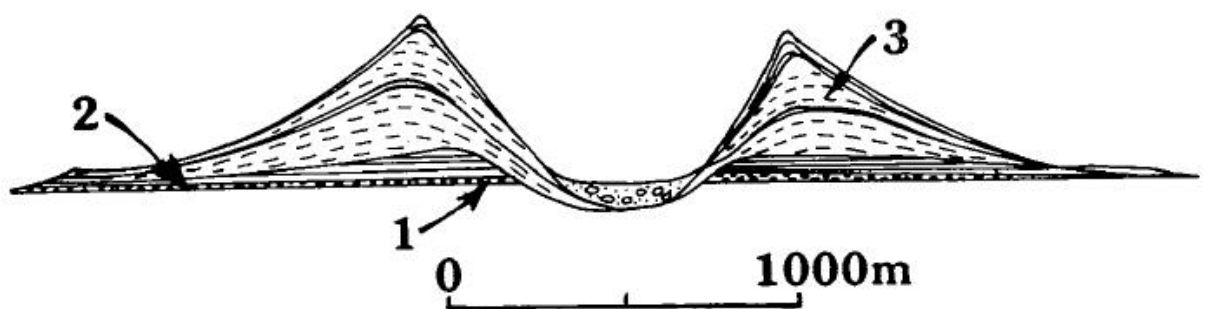


Figure 2.14. Schematic cross section of a tuff cone. (1) Explosion breccia, (2) thinly bedded deposits (3) thickly bedded, massive deposits. Adapted from Wohletz and Sheridan (1983).

2.5.1.6 Tuff rings

Tuff rings (Fig. 2.15) are constructional landforms formed during phreatomagmatic eruptions. They are commonly 0.25–5 km in basal diameter and up to 0.6 km in height. Their slopes dip sub-horizontally to 20° and their craters may extend below the land surface. Their volume ranges from 10^5 – 10^9 m³ (White and Ross 2011). Tuff rings have a large crater in comparison to their basal diameter. Component pyroclasts are deposited dominantly by flow and fall, and constituent pyroclasts are ash–lapilli size (White and Ross 2011). In comparison to tuff cones, flow is the dominant depositional method. They are dominantly composed of juvenile clasts; lithic clasts vary in abundance. Examples include the Suwolbong and Songaksan tuff rings in Korea (Sohn and Chough 1989; Chough and Sohn 1990).

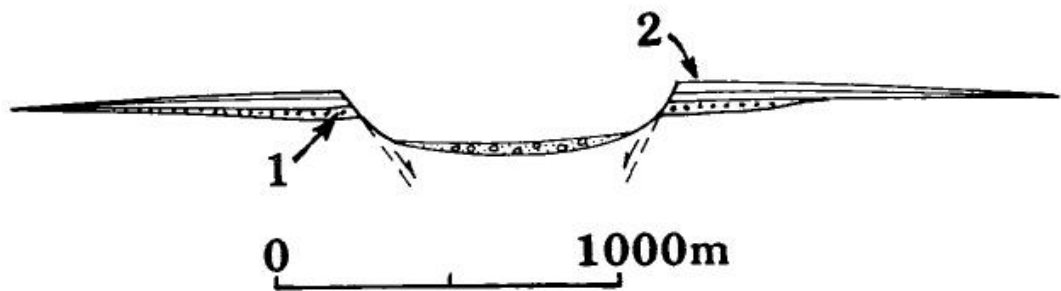


Figure 2.15. Schematic cross section of a tuff ring. (1) Explosion breccia, (2) thinly bedded deposits. Adapted from Wohletz and Sheridan (1983).

2.5.1.7 Maars

Maars (Fig. 2.16) are depressions in the land surface with a low rim of ejecta. Beds within the ejecta rim dip sub-horizontally to 20° and their craters vary from 0.2–3 km in diameter (Head et al. 1981). Individual maars may also overlap; within flood basalt provinces these complexes can be >30 km² in size (e.g. McClintock and White, 2006). Their volume range is unknown. Maars have a large crater in comparison to their basal diameter. Component pyroclasts are deposited dominantly by flow and fall, and constituent pyroclasts are ash–lapilli size (White and Ross 2011). They are composed of juvenile clasts and a high abundance of lithic clasts (White and Ross 2011). Examples include the crater formed during the 1965 eruption of Taal (Moore et al. 1966; White and Ross 2011). In comparison to tuff rings, maar-forming eruptions are triggered at greater depths beneath the surface. Maars are underlain by deep diatremes – a downwards-tapering structure cut

into the substrate (White and Ross 2011). They may reach up to 2500 m in depth and grade downwards into dykes (Vespermann and Schmincke 2000). They form via a combination of phreatomagmatic fragmentation and wall rock collapse (Vespermann and Schmincke 2000). See Lorenz (1975); White (1991); White and Ross (2011); Ross et al. (2013) and Graettinger et al. (2014) for in-depth discussions on their formation.

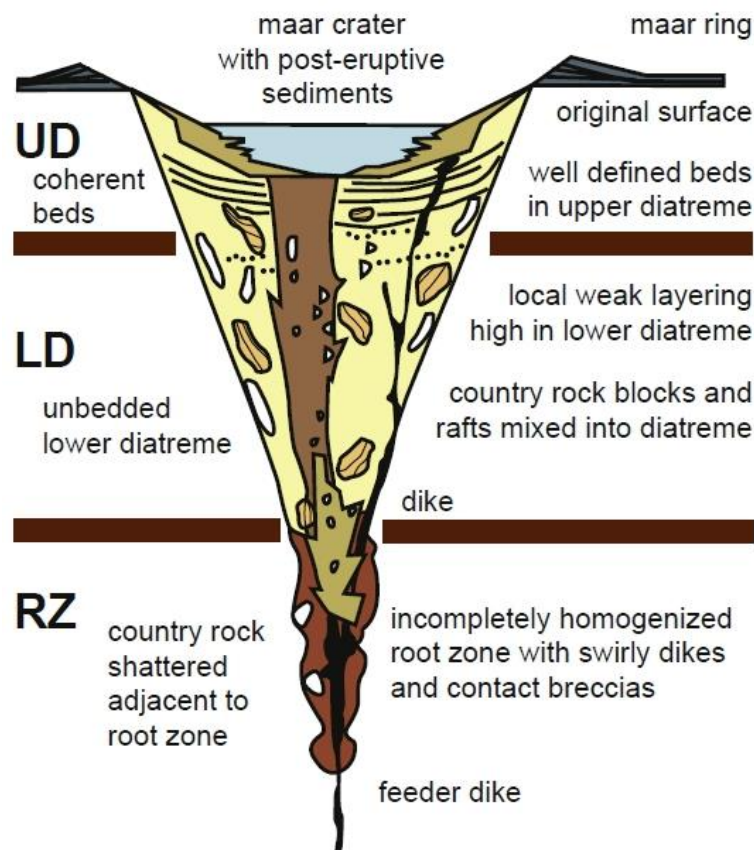


Figure 2.16. Schematic cross section of a maar and underlying diatreme. UD=Upper diatreme; LD=Lower Diatreme, RZ=root zone. Taken from White and Ross (2011).

2.5.2 Polygenetic volcanoes

Polygenetic or composite cones are constructed by numerous eruptions punctuated by periods of dormancy (e.g. Davidson and De Silva 2000). These long lived edifices are composed of a variety of extrusive volcanic rocks (including lavas and pyroclastic rocks of basaltic to dacitic and rhyolitic composition). They are found on convergent and divergent plate margins, as well as at mantle hotspots. These volcanoes may evolve from cones to overlapping massif structures (Grosse et al. 2009) and form linear chains 100's of kilometres in length (e.g. in the Andes). They are rarely >3000 m in height and have volumes of $\leq 200 \text{ km}^3$ (Davidson and De Silva 2000). Parasitic monogenetic volcanoes

form on the flanks of polygenetic edifices. When large scale evacuation of the magma chamber occurs, calderas form (e.g. Branney and Kokelaar 1994). Polygenetic volcanoes may evolve from submarine to sub aerial features, e.g. Mauna Loa, Hawaii. Brendan's Dome and the Darwin, Rockall and Erlend volcanic complexes and are reported as polygenetic centres within the FSB (Gatliff et al. 1984; Ritchie et al. 1997), although the emplacement mechanisms of these centres is not well documented .

2.5.2.1 Seamounts

Seamount is a term given to discrete elevations on the seafloor. They may be volcanic or non-volcanic. Non volcanic seamounts are restricted to forearc systems and are composed of horsts and diapirs of altered serpentinite (Schmidt and Schmincke 2000). Volcanic seamounts (Fig. 2.17) can be monogenetic or polygenetic structures (e.g. Hirano et al. 2008; McKee et al. 2010). These structures are common in all tectonic settings and there are estimated to be over 100,000 seamounts worldwide (Wessel et al. 2010). Due to their remoteness, they are commonly studied using a combination of sonar and seismic data (e.g. Thors and Jakousson 1982; Clague et al. 2000; Das et al. 2007; Mitchell et al. 2012). Bathymetric data and more rarely drill core data indicate that they are predominantly composed of hyaloclastite, pillow lavas and pelagic ooze (Schmidt and Schmincke 2000). Eruptions can build small (<200 m height) conical pillow volcanoes (Batiza and White 2000). In addition, their vents may also be composed of lithic breccias and scoria (Schmidt and Schmincke 2000; Mitchell et al. 2012). Vents formed in shallow waters (≤ 200 m summit depth) produce flat topped tephra cones (Mitchell et al. 2012). This 200 m cut-off from is a result of forced spreading of the eruption column at the air/water interface (Mitchell et al. 2012). Flat-topped seamounts are also formed as a result of continual overflow from long-lived lava ponds (Clague et al. 2000).

Large seamounts reach >100 km in basal diameter (e.g. Hawaii) and submerged structures are 0.05–8 km in height (Wessel et al. 2010). Seamounts align along faults, providing information on the local and regional stress field (Das et al. 2007; Paulsen and Wilson 2010). Different morphological types have been identified including shallow sloped, shield, inverted soup bowl, domed and flat topped types (Simkin 1972; Clague et al. 2000; Das et al. 2007; Mitchell et al. 2012). Some seamounts have pit craters and calderas, evidencing explosive activity (Schmidt and Schmincke 2000). Factors influencing their morphology include water depth (Clague et al. 2000; Mitchell et al. 2012), magma transport route (Mitchell et al. 2012), the effusion rate, eruption duration

and steadiness, the slope on which the edifice forms (Clague et al. 2000), the composition of the magma, conduit geometry, local and regional tectonics setting and the thermo-physical properties of the underlying lithosphere (Das et al. 2007).

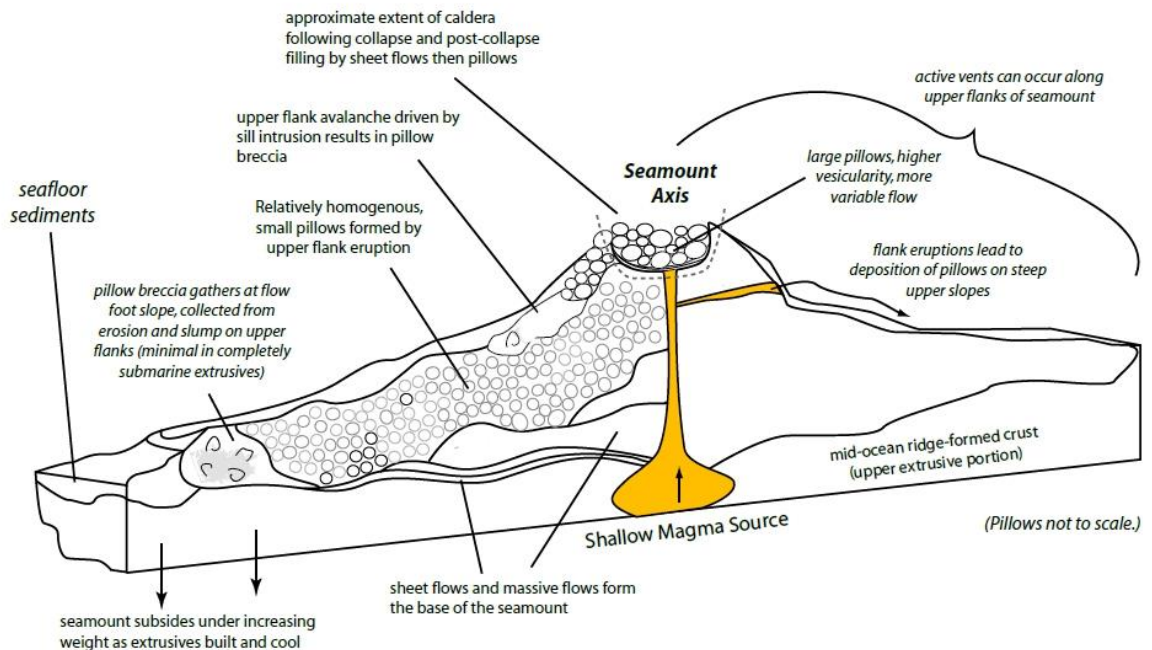


Figure 2.17. Schematic cross section of a polygenetic seamount. The seamount is ≥ 5 km in diameter and several hundred metres in height. Modified from Schnur (2007).

2.6 The identification and importance of volcanic features in hydrocarbon basins

2.6.1 Lavas

Lavas are important components in volcanic-affected hydrocarbon basins. They can decrease the porosity and permeability of underlying reservoir rocks, (Jerram and Stollhofen 2002; Grove 2014). Furthermore, they determine the architecture of overlying sedimentary systems (Schofield and Jolley 2013). The dense cores of lavas also act as seals (e.g. Schutter 2003; Rohrman 2007), whilst their vesicular crusts and cooling joints act as reservoirs and pathways for hydrocarbons (e.g. Burns et al. 2012; Burns et al. 2014). Drilling through lava sequences can also cause significant loss of drilling fluids and mud (e.g. Millett 2015). Lavas also provide indications of relative crustal movement (e.g. Seaward Dipping Reflectors; see Planke and Eldholm 1994) and help locate break-up axes in rift settings. Lavas also provide a range of challenges during seismic imaging (see below).

2.6.1.1 Basaltic lavas in seismic data

Lavas are responsible for the scattering and attenuation of seismic waves (Ogilvie et al. 2001; Jerram 2002; Maresh and White 2005; Maresh et al. 2006; Shaw et al. 2008; Nelson et al. 2009a; Wright 2013). In regions with significant basalt cover, this scattering creates what is known as “the sub-basalt imaging problem”, whereby large sections of stratigraphy underlying the basalt is so poorly imaged that no structure can be determined (e.g. Jerram 2002; White et al. 2003). In addition to the loss of imaging quality, volcanic rocks can also cause distortion of seismic data and result in the formation of multiples, which are repetitions of a seismic wave as it reverberates between the top of the volcanics and the sea bed and within a volcanic body itself (Fliedner and White 2001; Nelson et al. 2009a; Wright 2013). Distorted seismic data appears as pull-ups or push-downs that cause the reflection edifice to appear closer or further from the surface respectively. These are caused by seismic waves entering a low velocity structure that is overlain by high velocity lithologies (pull-up), or vice versa in the case of push-downs (Sheriff and Geldart 1995; Wright 2013).

Planke et al. (2000) and Wright (2013) have distinguished regional scale volcanic features (e.g. lava deltas) in seismic datasets, but as yet seismic facies typical of the vent-proximal regions have not been identified. In addition, the diversity of lavas outlined in section 2.4 has not been distinguished in seismic data. Furthermore, none of the common features of lava flow fields are recognised; features such as squeeze-outs that are potentially useful vent-proximity indicators are below the resolution of seismic data. However, compound and simple flows have been distinguished from seismic data in the FSB (Jerram et al. 2009) and can be diagnostic of vent proximity (Nelson et al. 2009b).

2.6.1.2 Basaltic lavas in well data

FMI and its precursor the Formation micro-scanner (FMS) are tools commonly used to collect well data. FMS can distinguish pillow lavas (Brewer et al. 1999). FMI data can recognise the vesicular flow tops characteristic of pāhoehoe lavas (Watton et al. 2014). ‘A‘ā lavas remain uncharacterised in well log, although it is hypothesised that their rubbly crusts could be recognised in FMI data (Watton et al. 2014). However, these breccias may be difficult to distinguish from coarse-grained pyroclastic deposits, identified in FMI as angular volcanic breccias (Watton et al. 2014). FMI can recognise cooling joints and their

orientation (Watton et al. 2014). This may help locate the vents of rootless cones that are surrounded by cooling joints atypical of the rest of the flow field (see Chapter 3).

Subaerial basalt and submarine basalts can be distinguished by their magnetic susceptibility and natural remnant magnetization (NRM) profiles (Delius et al. 2003). Tabular classic (P-type) lava flows and compound flows are recognised by their velocity and density characteristics (Nelson et al. 2009b). Flow type can be then used to constrain the 3D architecture of a basaltic province and provide better control on intra-basalt seismic imaging (Nelson et al. 2009b). Velocity variations within lava flows are also recognised by Planke and Cambray (1998) and record variations in total porosity, pore geometry and alteration. These variations can be used to determine lava flow structure (e.g. the presence of vesicular crusts) in volcanic-affected basins.

2.6.2 Volcanic edifices

Pyroclastic edifices are important features of volcanic-affected hydrocarbon basins (see Chapter 1). Their seismic characteristics and well data signature is outlined below.

2.6.2.1 Volcanic edifices in seismic data

A range of volcanic edifices have been imaged in seismic data (e.g. Gatliff et al. 1984; Faustmann 1995; Bell and Butcher 2002; Planke et al. 2005). However, our understanding of volcanic edifices in seismic data is incomplete and the diversity of volcanoes observed in the field (e.g. tuff rings, scoria cones, flat topped seamounts) has not been recognised in seismic datasets yet. In addition, numerous polygenetic structures are recognised but lack rigorous classification and distinction from monogenetic structures. The seismic characteristics of these edifices are outlined below (see also Table 2.3 and Fig. 2.18).

2.6.2.1.1 Monogenetic volcanoes

Surtsey is the only contemporary volcanic edifice for which seismic data is available (Thors and Jakousson 1982). However, this study is largely focused on the stratigraphy of the surrounding areas and gives sparse detail of the internal structure of the volcano itself. Spatter cones/ramparts, tuff rings and rootless cones are not currently recognised in seismic data. Ancient examples of tuff cones, scoria cones and maars include the study of Faustmann (1995) off the coast of Australia in the Bass Basin. Again, the internal structure of the edifices is not described in detail. Further studies in the South North Sea by Wall et

al. (2010) identified numerous elongate and circular craters that overly dykes and interpreted them to be maars. These structures are 200–2500 m wide and no details are given on the internal structure or the seismic facies of the vents. The craters are inferred to result from phreatomagmatic interaction in a water column 50–100 m deep. Fissures are recognised in the FSB (Thomson 2007) as a ridge-like feature, linked to underlying sills and dykes. The architecture of the edifices overlying the fissure is not described, and the products of the eruption are unknown. Volcanic edifices are also identified by Cukur et al. (2010) and Zhao et al. (2014) in 2D and 3D seismic data, although the genesis of the features is unclear. These edifices have high amplitude tops, and chaotic inner parts with variable amplitude.

Currently the most detailed description of volcanoes in seismic data is from monogenetic shield edifices in the Ceduna sub-basin offshore Australia (Magee et al. 2013). These cones have slightly rounded or flat tops, and concave/convex slope profiles. They range from ~2–19 km in basal diameter, with summit heights 0.02–1 km high. Three principal seismic facies were identified within the vents. Their lowermost parts were composed of high amplitude, early lava flows, overlain by continuous reflectors of varying amplitude. Their seismic velocities varied from 2365–6739 m s⁻¹. Some vents showed a plug-like chaotic internal region. The large size of these vents in comparison with other monogenetic vents (e.g. Walker 1993) is not discussed. They also have a wider range of morphologies (e.g. relationship between summit height and basal diameter) than other shield volcanoes (e.g. Rossi 1996). These vents were found within a sequence of limestone, implying a shallow marine environment – not the subaerial environment in which true monogenetic shield volcanoes form (e.g. Rossi 1996; Walker 2000).

2.6.2.1.2 Polygenetic volcanoes

Several polygenetic volcanoes have been described from seismic data. The Kora field, offshore New Zealand, has been subject to intense investigation owing to the presence of hydrocarbons within the structure (e.g. Bergman et al. 1991). However, there is little description of its internal architecture. Hübscher et al. (2015) describe the evolution of the Kolumbo polygenetic volcano in the southern Aegean Sea. Kolumbo is 1 km in height and 11 km in basal diameter. Explosive underwater eruptions of rhyolitic magma produced volcanoclastic units, forming several overlapping cones. The volcano has a combination of chaotic and weak internal reflections, with prograding reflectors in the edifice flanks. Studies in the North Atlantic have identified volcanic edifices thought to be polygenetic

shield volcanoes that are 2–4 km wide in basal diameter (Gatliff et al. 1984; Thomson 2005) and 400 m high (Gatliff et al. 1984). Internally, they have reflectors that dip radially outwards at $\leq 20^\circ$. The relationship of edifices to underlying sills is unknown, although the Erlend complex, NAIP, overlies a 14 km-wide pluton at 4 km depth (Gatliff et al. 1984). The edifice described by Thomson (2005) is underlain by a 2 km wide ring dyke or fault and has lava flows emanating from its summit and flanks.

2.6.2.1.3 Seamounts

Seismic data reveals that seamounts have high amplitude reflectors that dip outwards at $< 15^\circ$ and an onion ring geometry in plan view (Bell and Butcher 2002; Davies et al. 2002). Their internal reflectors downlap onto the underlying sediments (Thors and Jakousson 1982; Bell and Butcher 2002; Davies et al. 2002). They are found < 1200 m above sill tips (Bell and Butcher 2002; Davies et al. 2002) whilst those observed along active regions suggest that magma chambers are > 1400 m beneath the seafloor (Kent et al. 2003). However, the “hyaloclastite” edifice described by Davies et al. (2002) has been re-interpreted as a sedimentary hydrothermal edifice since drill core recovered from the edifice was composed of quartz, siltstone and dolerite sands, some of which preserve sedimentary laminations (Grove 2013).

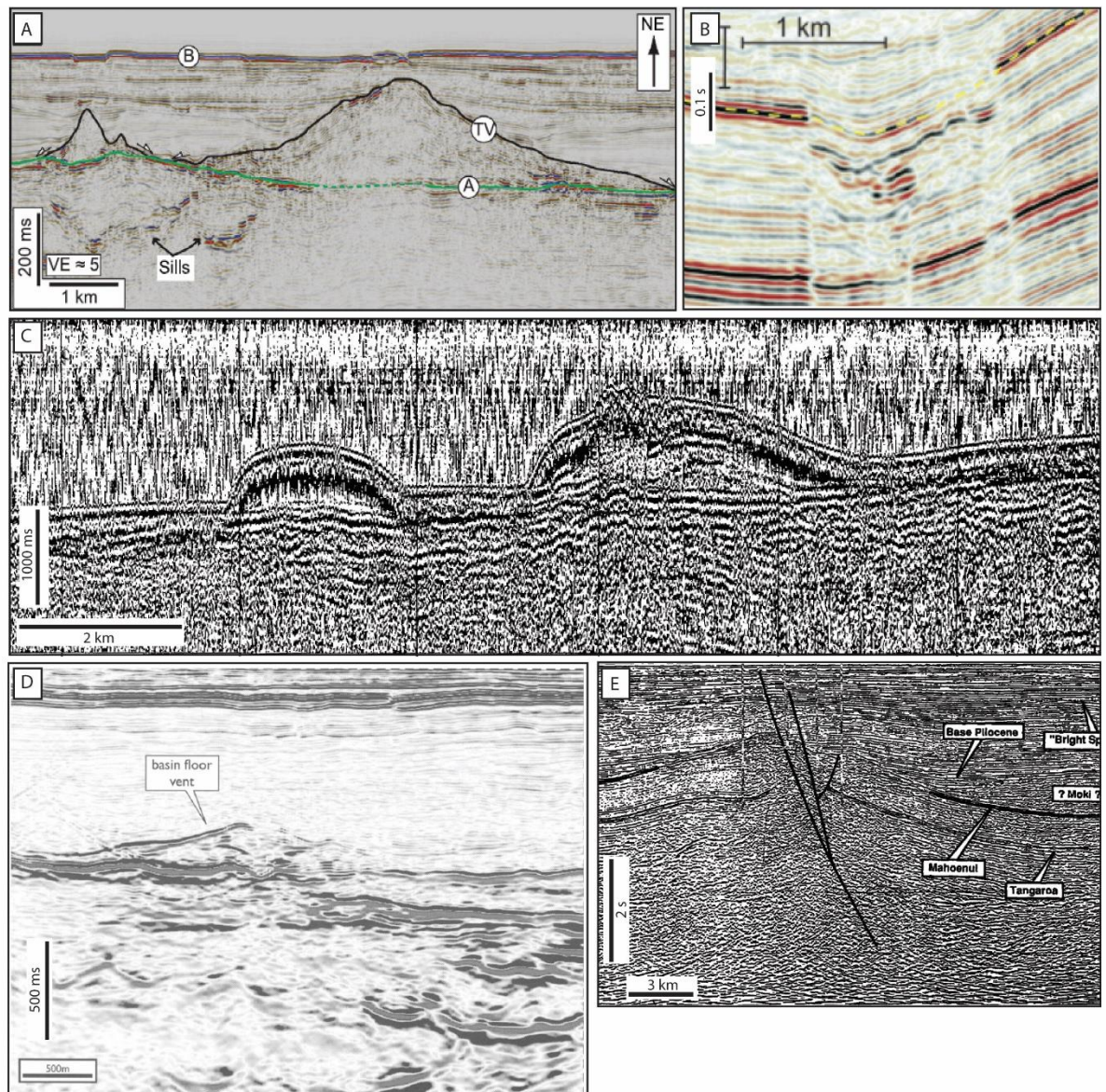


Figure 2.18. A comparison of the volcanoes currently recognised in seismic data. (A) Shield volcano, taken from Magee et al. (2013). (B) Maar crater, described by Wall et al. (2010). (C) Seismic line from Jólnir (left) and Stóra-Hraun (right) in the vicinity of Surtsey. Modified from Thors and Jakousson (1982). (D) Seamount in the Faroe-Shetland Basin, modified from Bell and Butcher (2002). (E) Kora andesitic stratovolcano, offshore New Zealand, modified from Bergman et al. (1991).

| Edifice type | Basal relationship | Internal structure | Faulting | Relative Amplitude | Overlying stratigraphic relationship | Example in seismic data |
|----------------------------|---|---|-------------------------------|---------------------------|---|--|
| Shield-like volcano | May cause pull-up, sometimes masked by basalt | Radially outwards dipping intra-basalt reflectors, dip approaching $\leq 12-20^\circ$ | No data | No data | No data | North of Shetland and Ceduna Sub-Basin |
| Tuff cone | Concordant | Prograding flanks, chaotic central region, occasionally with a plug | No data | Not described | Unknown | Surtsey |
| Maar | Crater and diatreme truncate surrounding sediment | Filled with low amplitude sediments | Not described | Not described | Concordant | Southern North Sea |
| Polygenetic cone | Not described | Outwardly dipping prograding reflectors; some regions poorly imaged | Associated with normal faults | Not described | Onlapped | Kora, New Zealand |
| Seamount | Concordant | Onion ring in plan view, outward dipping reflectors in cross section | Unknown | Not detailed | Not detailed | NE Atlantic Margin |

Table 2.3. Summary of the seismic characteristics of volcanic edifices in seismic section. Data from Thors and Jakousson (1982); Bergman et al. (1991); Bell and Butcher (2002); Thomson (2005); Wall et al. (2010) and Magee et al. (2013).

2.6.2.2 Volcanic edifices in well data

Basaltic volcanoclastic and pyroclastic rocks are poorly classified in well data. Their high resistivities and high FeO values are diagnostic of a basaltic component (Delius et al. 1998). Pyroclasts can be identified in FMI as angular volcanic breccias, but may appear similar to the rubbly tops of 'a'ā lavas (Watton et al. 2014). Cooling joints can be recognised from FMI (Watton et al. 2014); these are found in welded pyroclastic units (e.g. Brown et al. 2014). However, successions typical of volcanic edifices have yet to be characterised in well data.

2.7 Non-volcanic edifices found in hydrocarbon basins

In addition to the volcanic edifices found in hydrocarbon basins, there are also a range of non-volcanic edifices that have similar seismic characteristics. These edifices include mud volcanoes and hydrothermal vents. Their morphology and seismic characteristics are summarised below (see also Tables 2.4 and 2.5).

| Vent type | Mean Basal D (km) | Crater/plateau D (km) | Vertical scale of edifice (km) | Calculated height/basal diameter ratio | Volume (km ³) | Height/rim ratio |
|--------------------------|--|--|--------------------------------|---|---------------------------|------------------|
| Mud volcano | 2–10 | 0.5–2 | 0.1–5 | 0.05–0.5 | ≤ 25 | No data |
| Hydrothermal vent | 0.40–11 | ≤ 11 | 0.03–0.45 | 0.12 | Mean of 0.38 | No data |
| | Plumbing system | External morphology | Formation environment | Lithology | Flank dip (°) | |
| Mud volcano | <10 m diameter feeder conduit contained within downward tapering conduit system, overly diapirs at depth | Circular, lenticular to biconic with flat, convex and concave tops | Sub aerial and sub marine | Argillaceous muds, pebbly muds with silt – sand sized matrix, occasionally brecciated blocks | >5 | |
| Hydrothermal vent | Overly sill tips, with diatreme – like vertical feeder of fluidised sediment | Pit craters, dome and eye shaped | Sub aerial and sub marine | Mudstones, shales, sandstones, country rock boulders and zeolite cements, sediment/magma mixtures | 2–13 | |

Table 2.4. Summary of the morphology of sedimentary edifices. Data from Kopf et al. (1998); Yusifov and Rabinowitz (2004); Davies and Stewart (2005); Planke et al. (2005); MØller Hansen (2006); Svensen et al. (2006); Svensen et al. (2007); Huuse et al. (2010); Grove (2013).

| Edifice type | Basal relationship | Internal structure | Faulting | Relative Amplitude | Overlying stratigraphic relationship | Example in seismic data |
|--------------------------|------------------------------------|--|---|---|---|--------------------------------|
| Mud volcano | Down warped, concordant | Poorly imaged central chimney; outward dipping internal reflectors, central caldera, onion ring in plan view | Concentric, defining caldera, may overly faults linking to mud source | Varying across top surface, lows indicating mud flows | Onlapping, divergent | South Caspian Sea |
| Hydrothermal vent | Down warped, flat lying, truncated | Chaotic, downlapping, onion ring in plan view | Overly deep seated fault terminations | High amplitude top reflector | Onlapping, divergent and concordant | NE Atlantic Margin |

Table 2.5. Summary of the seismic characteristics of sediment type vents in seismic section. Data from Kopf et al. (1998); Davies and Stewart (2005) Stewart and Davies (2006); Evans et al. (2007) and Roberts (2011).

2.7.1 Mud volcanoes

Mud volcanoes (Fig. 2.19) extrude fine-grained sediment and water onto the Earth's surface. They are found in marine and sub-aerial environments and have a spatial and genetic relationship to oil and gas fields (Kopf et al. 1998; Planke et al. 2003; Yusifov and Rabinowitz 2004; Davies and Stewart 2005; Roberts et al. 2011). They are common in extensional and collisional tectonic regimes and form due to overpressure at depth (Kopf et al. 1998; Kopf 2002). Many are found in regions that also contain numerous volcanic edifices (e.g. Lusi in Java and Dashgil in Azerbaijan; see Hovland et al. 1997; Roberts et al. 2011).

Each mud volcano is composed of a central edifice with numerous individual vents. The central edifice may be lenticular to circular or biconic in shape, occasionally with flat tops (Kopf 2002). The mudflows which construct the edifice are composed of poor- to well-sorted, mud- to sand-grade material containing pebbles and gravels. The sediment erupted is a mixture of muds, fluids and gases of varying proportions (Kopf et al. 1998; Deville et al. 2003; Evans et al. 2007; Roberts et al. 2011). These sediments are derived from the elutriation, stoping and brecciation of buried sediments sourced from deep clastic reservoirs up to 10 km beneath the edifice (e.g. Kopf et al. 1998; Graue 2000; Huuse et al.

2010). The edifice is constructed during successive eruptions that may build numerous cones on top of each other (Davies and Stewart 2005; Evans et al. 2007). Meanwhile slumping of unstable vent walls can degrade the edifice.

Originally, mud volcanoes were thought to have been fed by deep mud reservoirs and shale diapirs exploiting fault systems (Graue 2000; Planke et al. 2003). However, recent studies suggest that they are underlain by a root zone that feeds fluids, mud and gases along faults (Davies and Stewart 2005; Roberts et al. 2011). This root zone is considered to be composed of numerous fluidisation pipes and an underlying downward tapering cone of faulted country rock that focuses on buried aquifers (Davies and Stewart 2005). Other studies suggest that they are linked to thrust-cored anticlines at depth (Huuse et al. 2010).

Mud volcanoes reach up to 10 km in basal diameter and may be 10's of metres to 5 km in height. Their craters and calderas can be 0.5–2 km wide and 0.5 km deep (Graue 2000; Davies and Stewart 2005; Evans et al. 2007). They commonly align along faults and the hinges of anticlines with individual vents on the volcano changing orientation and elongation with time as they exploit localized faults and regional structures (Planke et al. 2003; Roberts et al. 2011). Individual vents are 0.01–360 m in diameter (Roberts et al. 2011).

When viewed in cross section in seismic data sets, mud volcanoes look extremely chaotic, with high amplitude tops and central chimney structures that allow gas (and fluid?) escape (Graue 2000; Evans et al. 2007). Low amplitude anomalies on the vent flanks form lobate and linear features that may represent mud flows (Evans et al. 2007). Internally mud volcanoes exhibit outwardly down-lapping reflectors giving them an onion-ring structure, and inward dipping reflectors in their central area (Fig. 2.20; Kopf et al. 1998).

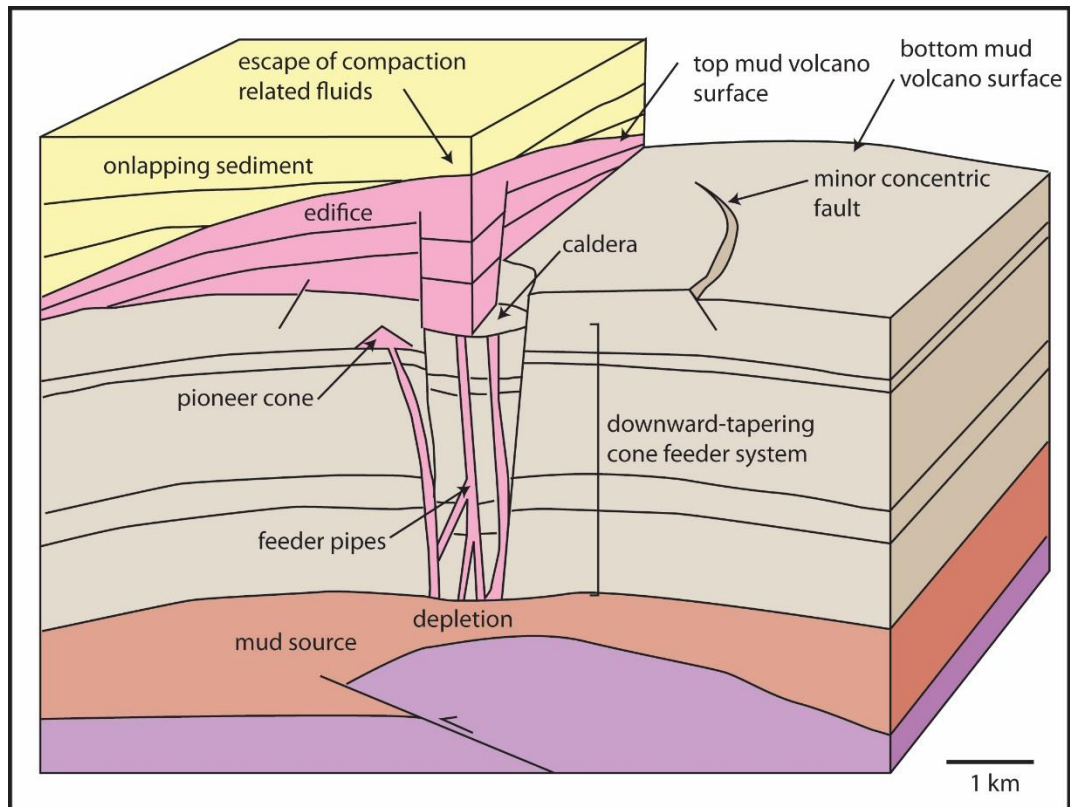


Figure 2.19. Schematic cross section of a mud volcano. The vertical scale varies from hundreds to thousands of metres. Modified from Evans et al. (2007).

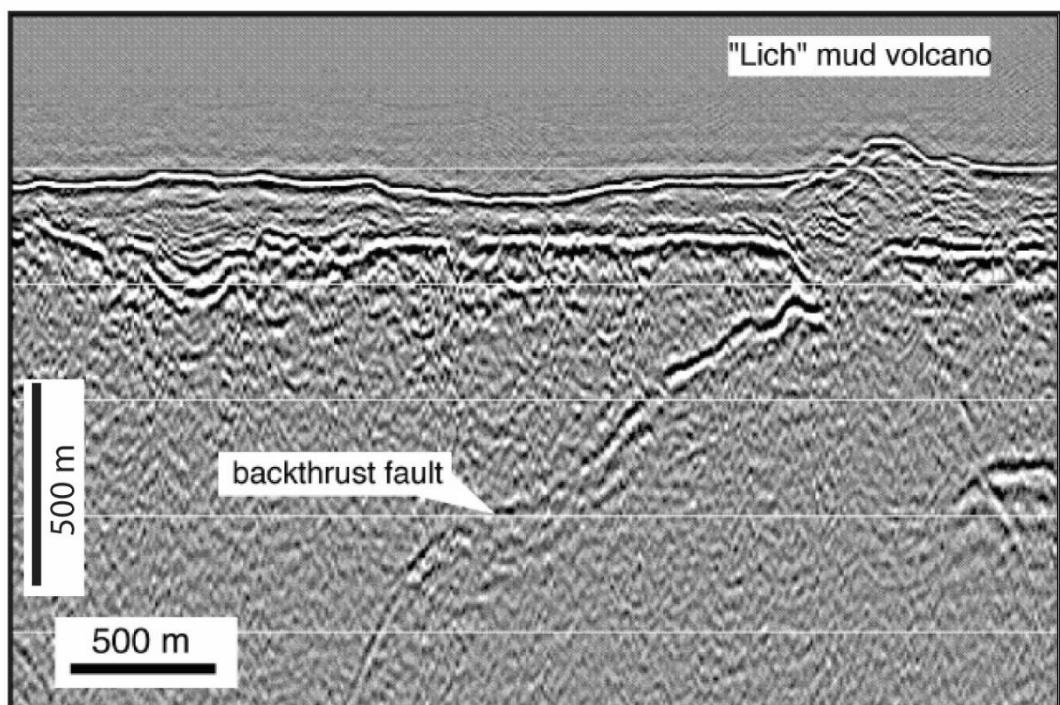


Figure 2.20. Seismic cross section of Lich mud volcano. Modified from Kopf (2002).

2.7.2 Hydrothermal vents

Hydrothermal vents (Fig. 2.21) are common in marine and fluvial environments. They are eye, crater or dome shaped in cross-section (Jamtveit et al. 2004; Svensen et al. 2006; Svensen et al. 2007; Grove 2013). Many hydrothermal vents occur within basins affected by igneous activity (e.g. the Karoo and Faroe Shetland Basin; see Svensen et al. 2006; Grove 2013). They form due to explosive brecciation of host strata and extrusion of fluidised sediment (Jamtveit et al. 2004; Grove 2013). The vents commonly overlie sills (Jamtveit et al. 2004). Thus, it is considered that sill emplacement leads to the boiling of pore fluids in the host rock. This boiling creates overpressure in the host rock due to vapour expansion and results in fluidisation (Jamtveit et al. 2004). Numerical models indicate that discharge occurs shortly after sill emplacement and is thought to occur whilst the magma in the sill is molten (Jamtveit et al. 2004). Fluid discharge continues until the steam is exhausted (Jamtveit et al. 2004).

Individual cones range in height from 30–450 m and are 0.4–11 km in basal diameter, displaying central craters up to 5 km wide (Svensen et al. 2006). The largest vents are underlain by the deepest intrusions (Planke et al. 2005). Vents form above the edges of sill tips (Planke et al. 2005) and may overlap to form linear chains (Grove 2013) similar to monogenetic volcanic edifices aligned along an igneous dyke. Their abundance varies from 1/40 km² to 1/130 km² (Svensen et al. 2006) and they are often found above the termination of deep seated faults. The vents are most common above sills that are layer-parallel rough (i.e. discontinuous with varying inclinations), planar transgressive and slightly saucer-shaped (Planke et al. 2005).

Hydrothermal vents are dominantly composed of loosely consolidated sediment and porous sedimentary rock (Jamtveit et al. 2004; Huuse et al. 2010). Fine to medium grained quartz sand is common since it is easily fluidised (Huuse et al. 2010) although laminated and bedded sandstone, mudstones, shale and country rock boulders are also found in vent structures (Svensen et al. 2006; Svensen et al. 2007; Grove 2013). Component lithologies are sourced from both the horizons in which sills were emplaced and the overlying stratigraphy (Svensen et al. 2003; Svensen et al. 2007). Drill core from breccia pipes beneath hydrothermal vents reveal that these vents can be composed of sediments that contain appreciable quantities of fragmented magma (i.e. peperite), which forms during the intrusion of the sill (Svensen et al. 2007).

In seismic datasets hydrothermal vents exhibit high amplitude tops (Davies et al. 2002; Grove 2013) and onion ring structures in plan view (Fig. 2.22; see Davies et al. 2002),

similar to mud volcanoes. They may have flat-lying, downwarped, truncated or concordant basal reflectors, and the overburden will commonly onlap, diverge or be concordant with the vent structure (Planke et al. 2005). Internally the vents may be chaotic or have progradational, downlapping reflectors (Planke et al. 2005). The vents also disturb underlying reflections (Planke et al. 2005).

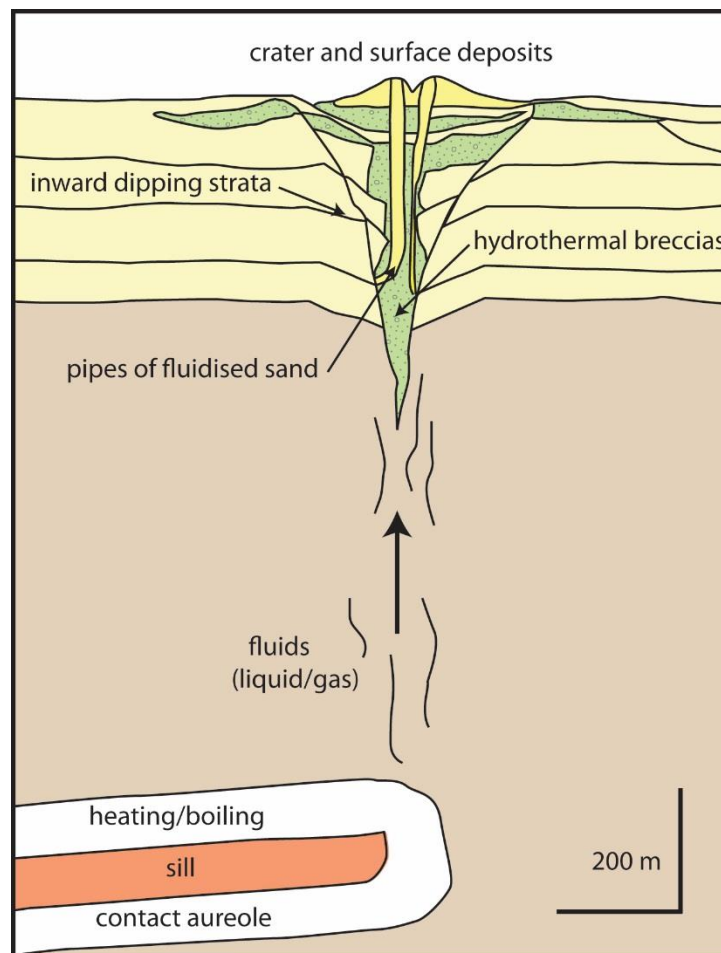


Figure 2.21. Schematic cross section of a hydrothermal vent. Vent formation is linked to the heating of pore fluids adjacent to the sill. Modified from Jamtveit et al. (2004).

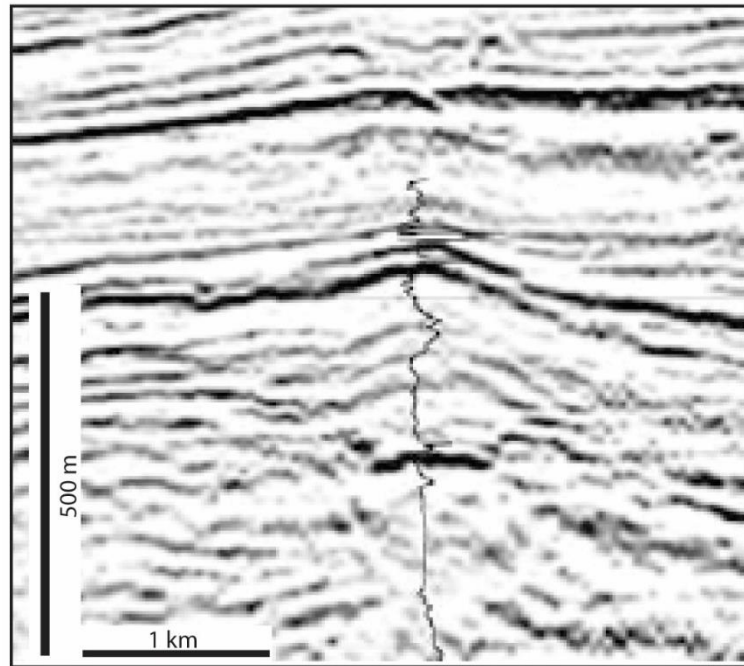


Figure 2.22. Seismic cross section of an eye-type hydrothermal vent. Modified from Svensen et al. (2003).

2.7.3 Comparison between types of sedimentary edifices

Mud volcanoes and hydrothermal vents can be distinguished based on field characteristics and by the inferred method that drove sediment effusion. Sediment effusion in both types is driven by pressure differences between the pore fluid pressure within a sub-surface permeable sedimentary layer and a lower pressurised layer (usually) nearer the surface (Huuse et al. 2010). In the case of hydrothermal vents, the increase in pressure is driven by vapour expansion caused by heating during igneous intrusion (Jamtveit et al. 2004). In mud volcanoes, fluid flow is driven by overpressure in the water phase (Huuse et al. 2010).

An initial assessment of hydrothermal vents and mud volcanoes would suggest that the two are easily distinguished by the larger size of mud volcanoes, their structural characteristics (e.g. calderas and exploitation of underlying faults) and the lithology of the effused sediment. However, the relationship of hydrothermal vents to structural features and the presence of calderas are as-yet unreported (e.g. Svensen et al. 2006). Also, an inherent flaw using field observations to distinguish between the two vent types is the inability to observe magmatic sills underlying mud volcanoes, which are thought to be a key feature in the formation of hydrothermal vents (Jamtveit et al. 2004; Svensen et al. 2006). Furthermore, there is currently no classification scheme that defines each vent type

based on its component lithologies. Both types may effuse sand and silt-sized rock fragments (Kopf et al. 1998; Huuse et al. 2010; Grove 2013).

Distinguishing between different edifices in seismic data is problematic since they have similar seismic responses (e.g. outward dipping internal layering, vertical chimneys of disturbed reflections, chaotic internal zones and high amplitude reflectors; see Graue 2000; Planke et al. 2005; Evans et al. 2007). The vents can be morphologically similar due to constructional processes (sediment effusion) and compactional processes at the seafloor governing morphology in both edifice types (Planke et al. 2005). Given these similarities, eye-shaped hydrothermal vents in seismic data from the Vøring Basin have also been interpreted as mud volcanoes (Jamtveit et al. 2004).

2.8 Summary

This chapter has provided a summary of the controls, styles and deposit of basaltic volcanism. In addition I have outlined the volcanic components of basaltic volcanism-affected basins. These components include feeder dykes, lavas and volcanic edifices. I have also outlined the difficulties in trying to identify volcanic edifices in volcanic-affected hydrocarbon basins. Recognising and distinguishing these edifices from hydrothermal vents remains a significant challenge in regions of hydrocarbon exploration.

2.9 References

- Alparone S, Andronico D, Lodato L, Sgroi T (2003) Relationship between tremor and volcanic activity during the Southeast Crater eruption on Mount Etna in early 2000. *Journal of Geophysical Research: Solid Earth* (1978–2012) 108(B5)
- Anderson SW, Stofan ER, Smrekar SE, Guest JE, Wood B (1999) Pulsed inflation of pahoehoe lava flows: implications for flood basalt emplacement. *Earth and Planetary Science Letters* 168(1-2):7-18
- Andronico D, Scollo S, Cristaldi A, Lo Castro M (2014) Representivity of incompletely sampled fall deposits in estimating eruption source parameters: a test using the 12–13 January 2011 lava fountain deposit from Mt. Etna volcano, Italy. *B Volcanol* 76(10):1-14
- Arrighi S, Principe C, Rosi M (2001) Violent strombolian and subplinian eruptions at Vesuvius during post-1631 activity. *B Volcanol* 63(2-3):126-150
- Batiza R, White JDL (2000) Submarine lavas and hyaloclastite. In: Sigurdsson H (ed) *Encyclopedia of volcanoes*. Academic Press, San Diego, pp 361-381
- Bell B, Butcher H (2002) On the emplacement of sill complexes: evidence from the Faroe-Shetland Basin. *Geological Society, London, Special Publications* 197(1):307-329
- Bergman SC, Talbot JP, Thompson PR (1991) The Kora Miocene submarine andesite stratovolcano hydrocarbon reservoir, Northern Taranaki Basin, New Zealand. In: *New Zealand Oil Exploration Conference Proceedings Ministry of Economic Development, New Zealand*, pp 178 - 206
- Bondre N, Duraiswami R, Dole G (2004a) Morphology and emplacement of flows from the Deccan Volcanic Province, India. *B Volcanol* 66(1):29-45

- Bondre N, Duraiswami R, Dole G (2004b) A brief comparison of lava flows from the Deccan Volcanic Province and the Columbia-Oregon Plateau Flood Basalts: Implications for models of flood basalt emplacement. *Journal of Earth System Science* 113(4):809-817
- Booth B, Self S (1973) Rheological Features of the 1971 Mount Etna Lavas. *Philosophical Transactions of the Royal Society of London. Series A, Mathematical and Physical Sciences* 274(1238):99-106
- Branca S, Del Carlo P, Lo Castro MD, De Beni E, Wijbrans J (2009) The occurrence of Mt Barca flank eruption in the evolution of the NW periphery of Etna volcano (Italy). *B Volcanol* 71(1):79-94
- Branney MJ, Kokelaar P (1992) A Reappraisal of Ignimbrite Emplacement - Progressive Aggradation and Changes from Particulate to Nonparticulate Flow during Emplacement of High-Grade Ignimbrite. *B Volcanol* 54(6):504-520
- Branney MJ, Kokelaar P (1994) Volcanotectonic faulting, soft-state deformation, and rheomorphism of tuffs during development of a piecemeal caldera, English Lake District. *Geol Soc Am Bull* 106(4):507-530
- Brewer TS, Harvey PK, Haggas S, Pezard PA, Goldberg D (1999) The role of borehole images in constraining the structure of the ocean crust: case histories from the Ocean Drilling Program. In: Lovell MA, Williamson G, Harvey PK (eds) *Borehole Imaging: Case Histories*. Geological Society, Special Publications, London, p 283-294
- Brown D, Holohan E, Bell B (2009) Sedimentary and volcano-tectonic processes in the British Paleocene Igneous Province: a review. *Geol Mag* 146(3):326-352
- Brown RJ, Blake S, Thordarson T, Self S (2014) Pyroclastic edifices record vigorous lava fountains during the emplacement of a flood basalt flow field, Roza Member, Columbia River Basalt Province, USA. *Geol Soc Am Bull* 126:875-891
- Bruce PM, Huppert HE (1989) Thermal control of basaltic fissure eruptions. *Nature* 342(6250):665-667
- Bryan SE, Ernst RE (2008) Revised definition of large igneous provinces (LIPs). *Earth-Science Reviews* 86(1):175-202
- Burns E, Williams C, Ingebritsen S, Voss C, Spane F, DeAngelo J (2014) Understanding heat and groundwater flow through continental flood basalt provinces: insights gained from alternative models of permeability/depth relationships for the Columbia Plateau, USA. *Geofluids*
- Burns ER, Snyder DT, Haynes JV, Waibel MS (2012) Groundwater Status and Trends for the Columbia Plateau Regional Aquifer System, Washington, Oregon, and Idaho.
- Calvari S, Pinkerton H (1998) Formation of lava tubes and extensive flow field during the 1991-1993 eruption of Mount Etna. *J. Geophys. Res.* 103(B11):27291-27301
- Calvari S, Pinkerton H (1999) Lava tube morphology on Etna and evidence for lava flow emplacement mechanisms. *J Volcanol Geoth Res* 90(3-4):263-280
- Capaccioni B, Cuccoli F (2005) Spatter and welded air fall deposits generated by fire-fountaining eruptions: Cooling of pyroclasts during transport and deposition. *J Volcanol Geoth Res* 145(3-4):263-280
- Carey R, Houghton B, Thordarson T (2008) Contrasting styles of welding observed in the proximal Askja 1875 eruption deposits II: Local welding. *J Volcanol Geoth Res* 171(1):20-44
- Carracedo Sánchez M, Sarrionandia F, Arostegui J, Eguiluz L, Gil Ibarguchi JI (2012) The transition of spatter to lava-like body in lava fountain deposits: features and examples from the Cabezo Segura volcano (Calatrava, Spain). *J Volcanol Geoth Res* 227-228(0):1-14
- Cas RAF, Wright JV (1987) *Volcanic Successions, Modern and Ancient: a Geological Approach to Processes, Products and Successions*. Allen and Unwin, London
- Cashman K, Kerr R, Griffiths R (2006) A laboratory model of surface crust formation and disruption on lava flows through non-uniform channels. *B Volcanol* 68(7):753-770
- Cashman KV, Thornber C, Kauahikaua JP (1999) Cooling and crystallization of lava in open channels, and the transition of Pāhoehoe Lava to 'A'ā. *B Volcanol* 61(5):306-323
- Cattermole P (1986) Linear volcanic features at Alba Patera, Mars-Probable spatter ridges. *Journal of Geophysical Research: Solid Earth* (1978-2012) 91(B13):E159-E165
- Ceramicola S, Stoker M, Praeg D, Shannon P, De Santis L, Hoult R, Hjelstuen B, Laberg S, Mathiesen A (2005) Anomalous Cenozoic subsidence along the 'passive' continental margin from Ireland to mid-Norway. *Marine and petroleum geology* 22(9):1045-1067

- Chadwick WW, Geist DJ, Jónsson S, Poland M, Johnson DJ, Meertens CM (2006) A volcano bursting at the seams: inflation, faulting, and eruption at Sierra Negra Volcano, Galápagos. *Geology* 34(12):1025-1028
- Chouet B, Hamisevicz N, McGetchin TR (1974) Photoballistics of Volcanic Jet Activity at Stromboli, Italy. *J. Geophys. Res.* 79(32):4961-4976
- Chough S, Sohn Y (1990) Depositional mechanics and sequences of base surges, Songaksan tuff ring, Cheju Island, Korea. *Sedimentology* 37(6):1115-1135
- Cimarelli C, Di Traglia F, de Rita D, Torrente DG (2013) Space–time evolution of monogenetic volcanism in the mafic Garrotxa Volcanic Field (NE Iberian Peninsula). *B Volcanol* 75(11):1-18
- Clague DA, Moore JG, Reynolds JR (2000) Formation of submarine flat-topped volcanic cones in Hawai'i. *B Volcanol* 62(3):214-233
- Clark SJ (2014) Constraining diagenetic timings, processes and reservoir quality in igneous-affected basins. PhD Thesis, Durham University, Department of Earth Sciences.
- Coffin MF, Eldholm O (1994) Large igneous provinces: crustal structure, dimensions, and external consequences. *Reviews of Geophysics* 32(1):1-36
- Cole P, Guest J, Duncan A, Pacheco J-M (2001) Capelinhos 1957–1958, Faial, Azores: deposits formed by an emergent surtseyan eruption. *B Volcanol* 63(2-3):204-220
- Connor CB, Conway MF (2000) Basaltic volcanic fields. In: Sigurdsson H (ed) *Encyclopedia of Volcanoes*. Academic Press, San Diego, pp 331-343
- Crisp J, Baloga S (1994) Influence of crystallization and entrainment of cooler material on the emplacement of basaltic aa lava flows. *J. Geophys. Res.* 99(B6):11819-11831
- Cukur D, Horozal S, Kim DC, Lee GH, Han HC, Kang MH (2010) The distribution and characteristics of the igneous complexes in the northern East China Sea Shelf Basin and their implications for hydrocarbon potential. *Marine Geophysical Researches* 31(4):299-313
- Das P, Iyer SD, Kodagali VN (2007) Morphological characteristics and emplacement mechanism of the seamounts in the Central Indian Ocean Basin. *Tectonophysics* 443(1–2):1-18
- Davidson J, De Silva S (2000) Composite volcanoes. p 679
- Davies R, Bell BR, Cartwright JA, Shoulders S (2002) Three-dimensional seismic imaging of Paleogene dike-fed submarine volcanoes from the northeast Atlantic margin. *Geology* 30(3):223-226
- Davies RJ, Stewart SA (2005) Emplacement of giant mud volcanoes in the South Caspian Basin: 3D seismic reflection imaging of their root zones. *J Geol Soc London* 162(1):1-4
- Davison I, Stasiuk S, Nuttall P, Keane P (2010) Sub-basalt hydrocarbon prospectivity in the Rockall, Faroe–Shetland and Møre basins, NE Atlantic. *Geological Society, London, Petroleum Geology Conference series* 7:1025-1032
- Dean K, McLachlan K, Chambers A (1999) Rifting and the development of the Faeroe-Shetland Basin. In: *Geological Society, London, Petroleum Geology Conference series*. Geological Society of London, pp 533-544
- Degraff JM, Long PE, Aydin A (1989) Use of joint-growth directions and rock textures to infer thermal regimes during solidification of basaltic lava flows. *J Volcanol Geoth Res* 38(3-4):309-324
- Delaney PT, Pollard DD (1981) Deformation of host rocks and flow of magma during growth of minette dikes and breccia-bearing intrusions near Ship Rock, New Mexico. *US Geol Surv Prof Pap* 1202
- Delius H, Bucker C, Wohlenberg J (1998) Determination and characterization of volcanoclastic sediments by wireline logs: Sites 953, 955, and 956, Canary Islands. *Proceedings of the Ocean Drilling, Scientific Results* 157:29-37
- Delius H, Brewer T, Harvey P (2003) Evidence for textural and alteration changes in basaltic lava flows using variations in rock magnetic properties (ODP Leg 183). *Tectonophysics* 371(1):111-140
- Deville E, Battani A, Griboulard R, Guerlais S, Herbin JP, Houzay JP, Muller C, Prinzhofer A (2003) The origin and processes of mud volcanism: new insights from Trinidad. *Geological Society, London, Special Publications* 216(1):475-490
- Dickson LD (1997) Volcanology and geochemistry of pliocene and quaternary basalts on Citadel Mountain, Lunar Crater Volcanic field, Pancake Range, Nevada.
- Doré AG, Lundin ER, Jensen LN, Birkeland Ø, Eliassen PE, Fichler C (1999). Principal tectonic events in the evolution of the northwest European Atlantic margin. In *Geological Society, London, Petroleum Geology Conference series* 5:41-61 Geological Society of London.

- Doubik P, Hill BE (1999) Magmatic and hydromagmatic conduit development during the 1975 Tolbachik Eruption, Kamchatka, with implications for hazards assessment at Yucca Mountain, NV. *J Volcanol Geoth Res* 91(1):43-64
- Dragoni M, Piombo A, Tallarico A (1995) A model for the formation of lava tubes by roofing over a channel. *J. Geophys. Res.* 100(B5):8435-8447
- Duraiswami RA, Dole G, Bondre N (2003) Slabby pahoehoe from the western Deccan Volcanic Province: evidence for incipient pahoehoe–aa transitions. *J Volcanol Geoth Res* 121(3-4):195-217
- Duraiswami RA, Bondre NR, Managave S (2008) Morphology of rubbly pahoehoe (simple) flows from the Deccan Volcanic Province: Implications for style of emplacement. *J Volcanol Geoth Res* 177(4):822-836
- Eldholm O, Grue K (1994) North Atlantic volcanic margins: dimensions and production rates. *Journal of Geophysical Research: Solid Earth* (1978–2012) 99(B2):2955-2968
- Ellis D, Bell BR, Jolley DW, O’Callaghan M (2002) The stratigraphy, environment of eruption and age of the Faroes Lava Group, NE Atlantic Ocean. Geological Society, London, Special Publications 197(1):253-269
- Ellis D, Passey S, Jolley D, Bell B (2009) Transfer zones: The application of new geological information from the Faroe Islands applied to the offshore exploration of intra basalt and sub-basalt strata. In: Faroe Islands Exploration Conference: Proceedings of the 2nd Conference. *Annales Societatis Scientiarum Færoensis, Tórshavn*. pp 205-226
- Evans RJ, Davies RJ, Stewart SA (2007) Internal structure and eruptive history of a kilometre-scale mud volcano system, South Caspian Sea. *Basin Research* 19(1):153-163
- Fagents SA, Lanagan P, Greeley R (2002) Rootless cones on Mars: a consequence of lava-ground ice interaction. Geological Society, London, Special Publications 202(1):295-317
- Fagents SA, Thordarson T (2007) Rootless cones in Iceland and on Mars. In: Chapman M, Skilling IP (eds) *The Geology of Mars: Evidence from Earth-Based Analogues*. Cambridge University Press, pp 151–177
- Faustmann C (1995) The seismic expression of volcanism in the Bass Basin referring to western Victorian analogues.
- Fletcher R, Kuszniir N, Roberts A, Hunsdale R (2013) The formation of a failed continental breakup basin: The Cenozoic development of the Faroe-Shetland Basin. *Basin Research* 25(5):532-553
- Fliedner MM, White RS (2001) Sub-basalt imaging in the Faeroe-Shetland Basin with large-offset data. *First Break* 19(5)
- Forbes, AES, Blake S, Mc Garvie, DW, Tuffen H (2012) Pseudopillow fracture systems in lavas: insights into cooling mechanisms and environments from lava flow fractures *J Volcanol Geoth Res* 245 (2012): 68-80.
- Forbes AES, Blake S, Tuffen H (2014) Entablature: fracture types and mechanisms. *B Volcanol* 76(5):1-13
- Friese N, Bense FA, Tanner DC, Gústafsson LE, Siegesmund S (2013) From feeder dykes to scoria cones: the tectonically controlled plumbing system of the Rauðhólar volcanic chain, Northern Volcanic Zone, Iceland. *B Volcanol* 75(6):1-19
- Galindo I, Gudmundsson A (2012) Basaltic feeder dykes in rift zones: geometry, emplacement, and effusion rates. *Natural Hazards and Earth System Sciences* 12(12):3683-3700
- Gatliff RW, Hitchen K, Ritchie JD, Smythe DK (1984) Internal structure of the Erlend Tertiary volcanic complex, north of Shetland, revealed by seismic reflection. *J Geol Soc London* 141(3):555-562
- Geiki A (1897) *The Ancient Volcanoes of Great Britain*. Macmillan, London
- Genareau K, Valentine G, Moore G, Hervig R (2010) Mechanisms for transition in eruptive style at a monogenetic scoria cone revealed by microtextural analyses (Lathrop Wells volcano, Nevada, U.S.A.). *B Volcanol* 72(5):593-607
- Geshi N, Kusumoto S, Gudmundsson A (2010) Geometric difference between non-feeder and feeder dikes. *Geology* 38(3):195-198
- Geshi N, Oikawa T (2014) The spectrum of basaltic feeder systems from effusive lava eruption to explosive eruption at Miyakejima volcano, Japan. *B Volcanol* 76(3):1-14
- Gibson IL, Kinsman D, Sugurdsson H, Walker G (1966) *Geology of the Faskruds fjörður area, eastern Iceland*.

- Goehring L, Morris SW, Lin Z (2006) Experimental investigation of the scaling of columnar joints. *Physical Review E* 74(3):036115
- Goehring L, Morris SW (2008) Scaling of columnar joints in basalt. *J. Geophys. Res.* 113(B10):B10203
- Goff F (1996) Vesicle cylinders in vapor-differentiated basalt flows. *J Volcanol Geoth Res* 71(2–4):167-185
- Graettinger A, Valentine G, Sonder I, Ross PS, White J, Taddeucci J (2014) Maar-diatreme geometry and deposits: Subsurface blast experiments with variable explosion depth. *Geochemistry, Geophysics, Geosystems* 15(3):740-764
- Graue K (2000) Mud volcanoes in deepwater Nigeria. *Marine and Petroleum Geology* 17(8):959-974
- Green J, Short NM (1971) *Volcanic landforms and surface features: A photographic atlas and glossary*. Springer-Verlag
- Gregg TKP, Fink JH (2000) A laboratory investigation into the effects of slope on lava flow morphology. *J Volcanol Geoth Res* 96(3-4):145-159
- Grosse P, van Wyk de Vries B, Petrinovic IA, Euillades PA, Alvarado GE (2009) Morphometry and evolution of arc volcanoes. *Geology* 37(7):651-654
- Grove C (2013) Submarine hydrothermal vent complexes in the Paleocene of the Faroe-Shetland Basin: Insights from three-dimensional seismic and petrographical data. *Geology* 41(1):71-74
- Grove C (2014) Direct and Indirect Effects of Flood Basalt Volcanism on Reservoir Quality Sandstone. PhD Thesis, Durham University, Department of Earth Sciences.
- Gudmundsson A, Friese N, Galindo I, Philipp SL (2008) Dike-induced reverse faulting in a graben. *Geology* 36(2):123-126
- Guilbaud M-N, Self S, Thordarson T, Blake S (2005) Morphology, surface structures, and emplacement of lavas produced by Laki, A.D. 1783–1784. *Geological Society of America Special Papers* 396:81-102
- Hamilton CW, Fagents SA, Thordarson T (2010a) Explosive lava–water interactions II: self-organization processes among volcanic rootless eruption sites in the 1783–1784 Laki lava flow, Iceland. *B Volcanol* 72(4):469-485
- Hamilton CW, Thordarson T, Fagents SA (2010b) Explosive lava–water interactions I: architecture and emplacement chronology of volcanic rootless cone groups in the 1783–1784 Laki lava flow, Iceland. *B Volcanol* 72(4):449-467
- Hansen J, Jerram D, McCaffrey K, Passey S (2009) The onset of the North Atlantic Igneous Province in a rifting perspective. *Geol Mag* 146(03):309-325
- Harris A, Rowland SR (2001) FLOWGO: a kinematic thermo-rheological model for lava flowing in a channel. *B Volcanol* 63(1):20-44
- Harris AJ, Dehn J, Calvari S (2007) Lava effusion rate definition and measurement: a review. *B Volcanol* 70(1):1-22
- Head JW, Bryan W, Greeley R, Guest J, Shultz P, Sparks R, Walker G, Whitford-Stark J, Wood C, Carr M (1981) Distribution and morphology of basalt deposits on planets. *Basaltic Volcanism on the Terrestrial Planets*:702-887
- Head JW, Wilson L (1989) Basaltic pyroclastic eruptions: Influence of gas-release patterns and volume fluxes on fountain structure, and the formation of cinder cones, spatter cones, rootless flows, lava ponds and lava flows. *J Volcanol Geoth Res* 37(3–4):261-271
- Heliker C, Mangan M, Mattox T, Kauahikaua J, Helz R (1998) The character of long-term eruptions: inferences from episodes 50–53 of the Pu'u'Ō'ō-Kūpaianaha eruption of Kīlauea Volcano. *B Volcanol* 59(6):381-393
- Heliker C, Mattox T (2003) The first two decades of the Pu'u 'Ō'o-Kupaianaha eruption: chronology and selected bibliography. *US Geol Surv Prof Pap* 1676:1-28
- Heslop S, Wilson L, Pinkerton H, Head J, III (1989) Dynamics of a confined lava flow on Kilauea volcano, Hawaii. *B Volcanol* 51(6):415-432
- Hintz AR, Valentine GA (2012) Complex plumbing of monogenetic scoria cones: New insights from the Lunar Crater Volcanic Field (Nevada, USA). *J Volcanol Geoth Res*
- Hirano N, Koppers AAP, Takahashi A, Fujiwara T, Nakanishi M (2008) Seamounts, knolls and petit-spot monogenetic volcanoes on the subducting Pacific Plate. *Basin Research* 20(4):543-553

- Hjartardóttir ÁR, Einarsson P, Bramham E, Wright TJ (2012) The Krafla fissure swarm, Iceland, and its formation by rifting events. *B Volcanol* 74(9):2139-2153
- Holford S, Schofield N, MacDonald J, Duddy I, Green P (2012) Seismic analysis of igneous systems in sedimentary basins and their impacts on hydrocarbon prospectivity: examples from the Southern Australian margin. *Australian Petroleum Production and Exploration Association Journal* 52:229-252
- Holm RF (1987) Significance of agglutinate mounds on lava flows associated with monogenetic cones: An example at Sunset Crater, northern Arizona. *Geol Soc Am Bull* 99(3):319-324
- Holmes A, Griffith C, Scotchman I (1999) The Jurassic petroleum system of the West of Britain Atlantic margin—an integration of tectonics, geochemistry and basin modelling. In: Geological Society, London, Petroleum Geology Conference series. Geological Society of London, pp 1351-1365
- Hon K, Kauahikaua J, Delinger R, Mackay K (1994) Emplacement and inflation of pahoehoe sheet flows: Observations and measurements of active lava flows on Kilauea Volcano, Hawaii. *Geol Soc Am Bull* 106(3):351-370
- Hon K, Gansecki C, Kauahikaua JP (2003) The transition from 'a'ā to pāhoehoe crust on flows emplaced during the Pu'u 'O'ō-Kūpaianaha eruption. *US Geol Surv Prof Pap* 1676: 89–103
- Hooper PR (2000) Flood Basalt Provinces. In: Sigurdsson H (ed) *Encyclopedia of Volcanoes*.
- Houghton BF, Schmincke HU (1989) Rothenberg scoria cone, East Eifel: a complex Strombolian and phreatomagmatic volcano. *B Volcanol* 52(1):28-48
- Hovland M, Hill A, Stokes D (1997) The structure and geomorphology of the Dashgil mud volcano, Azerbaijan. *Geomorphology* 21(1):1-15
- Hübscher C, Ruhnau M, Nomikou P (2015) Volcano-tectonic evolution of the polygenetic Kolumbo submarine volcano/Santorini (Aegean Sea). *J Volcanol Geoth Res* 291:101-111
- Huuse M, Jackson CAL, Van Rensbergen P, Davies RJ, Flemings PB, Dixon RJ (2010) Subsurface sediment remobilization and fluid flow in sedimentary basins: an overview. *Basin Research* 22(4):342-360
- James AVG (1920) Factors Producing Columnar Structure in Lavas and Its Occurrence near Melbourne, Australia. *The Journal of Geology* 28(5):458-469
- Jamtveit B, Svensen H, Podladchikov YY, Planke S (2004) Hydrothermal vent complexes associated with sill intrusions in sedimentary basins. *Physical geology of high-level magmatic systems* 234:233-241
- Jaupart C, Vergnolle S (1988) Laboratory models of Hawaiian and Strombolian eruptions. *Nature* 331(6151):58-60
- Jaupart C, Vergnolle S (1989) The generation and collapse of a foam layer at the roof of a basaltic magma chamber. *Journal of Fluid Mechanics* 203:347-380
- Jerram DA (2002) Volcanology and facies architecture of flood basalts. *Geological Society of America Special Papers* 362:119-132
- Jerram DA, Stollhofen H (2002) Lava–sediment interaction in desert settings; are all peperite-like textures the result of magma–water interaction? *J Volcanol Geoth Res* 114(1–2):231-249
- Jerram DA, Widdowson M (2005) The anatomy of Continental Flood Basalt Provinces: geological constraints on the processes and products of flood volcanism. *Lithos* 79(3-4):385-405
- Jerram DA, Single RT, Hobbs RW, Nelson CE (2009) Understanding the offshore flood basalt sequence using onshore volcanic facies analogues: an example from the Faroe–Shetland basin. *Geol Mag* 146(03):353
- Jolley DW, Bell BR (2002) Genesis and age of the Erlend Volcano, NE Atlantic Margin. Geological Society, London, Special Publications 197(1):95-109
- Jolley DW, Morton AC (2007) Understanding basin sedimentary provenance: evidence from allied phytogeographic and heavy mineral analysis of the Palaeocene of the NE Atlantic. *J Geol Soc London* 164(3):553-563
- Keating G, Valentine G, Krier D, Perry F (2008) Shallow plumbing systems for small-volume basaltic volcanoes. *B Volcanol* 70(5):563-582
- Kent G, Harding A, Babcock J, Orcutt J, Detrick R, Canales J, Van Ark E, Carbotte S, Diebold J, Nedimovic M (2003) A new view of 3-D magma chamber structure beneath axial seamount and coaxial segment: Preliminary results from the 2002 Multichannel Seismic Survey of the Juan de Fuca Ridge. In: AGU Fall Meeting Abstracts. p 0755

- Kent RW, Thomson BA, Skelhorn RR, Kerr AC, Norry MJ, Walsh JN (1998) Emplacement of Hebridean Tertiary flood basalts: evidence from an inflated pahoehoe lava flow on Mull, Scotland. *J Geol Soc London* 155(4):599-607
- Keszthelyi L (1994) Calculated effect of vesicles on the thermal properties of cooling basaltic lava flows. *J Volcanol Geoth Res* 63(3):257-266
- Keszthelyi L, Denlinger R (1996) The initial cooling of pahoehoe flow lobes. *B Volcanol* 58(1):5-18
- Keszthelyi L, Self S (1998) Some physical requirements for the emplacement of long basaltic lava flows. *J. Geophys. Res.* 103(B11):27447-27464
- Kilburn CRJ (2000) Lava flows and flow fields. In: Sigurdsson H (ed) *Encyclopedia of Volcanoes*. Academic Press, San Diego, pp 291-305
- Kokelaar BP, Durant GP (1983) The submarine eruption and erosion of Surtla (Surtsey), Iceland. *J Volcanol Geoth Res* 19(3-4):239-246
- Kokelaar P (1986) Magma-water interactions in subaqueous and emergent basaltic. *B Volcanol* 48(5):275-289
- Kopf A, Robertson AHF, Clennell MB, Flecker R (1998) Mechanisms of mud extrusion on the Mediterranean Ridge Accretionary Complex. *Geo-Marine Letters* 18(2):97-114
- Kopf AJ (2002) Significance of mud volcanism. *Reviews of Geophysics* 40(2):1005
- Krauskopf KB (1948) Mechanism of eruption at Paricutin Volcano, Mexico *Geol Soc Am Bull* 59(8):711-732
- Larsen LM, Waagstein R, Pedersen AK, Storey M (1999) Trans-Atlantic correlation of the Palaeogene volcanic successions in the Faeroe Islands and East Greenland. *J Geol Soc London* 156(6):1081-1095
- Lefebvre N, Kurszlaukis S (2008) Contrasting eruption styles of the 147 Kimberlite, Fort à la Corne, Saskatchewan, Canada. *J Volcanol Geoth Res* 174(1):171-185
- Lefebvre NS, White JDL, Kjarsgaard BA (2012) Spatter-dike reveals subterranean magma diversions: Consequences for small multivert basaltic eruptions. *Geology* 40(5):423-426
- Leverington D (2002) New pahoehoe toes on the flanks of Kilauea. Texas Tech University, Department of Geosciences photographic collection.
- Lipman PW, Banks NG, Rhodes JM (1985) Degassing-induced crystallization of basaltic magma and effects on lava rheology.
- Long PE, Wood BJ (1986) Structures, textures, and cooling histories of Columbia River basalt flows. *Geol Soc Am Bull* 97(9):1144-1155
- Lorenz V (1975) Formation of phreatomagmatic maar-diatreme volcanoes and its relevance to kimberlite diatremes. *Physics and Chemistry of the Earth* 9:17-27
- Lorenz V (1986) On the growth of maars and diatremes and its relevance to the formation of tuff rings. *B Volcanol* 48(5):265-274
- Macdonald GA (1953) Pahoehoe, aa, and block lava. *American Journal of Science* 251(3):169-191
- Macdonald GA (1972) *Volcanoes*. Prentice-Hall, Englewood Cliffs, N.J.
- Macedonio G, Dobran F, Neri A (1994) Erosion processes in volcanic conduits and application to the AD 79 eruption of Vesuvius. *Earth and Planetary Science Letters* 121(1-2):137-152
- Magee C, Hunt-Stewart E, Jackson CAL (2013) Volcano growth mechanisms and the role of sub-volcanic intrusions: Insights from 2D seismic reflection data. *Earth and Planetary Science Letters* 373(0):41-53
- Maresh J, White RS (2005) Seeing through a glass, darkly: strategies for imaging through basalt. *First Break* 23(5)
- Maresh J, White RS, Hobbs RW, Smallwood JR (2006) Seismic attenuation of Atlantic margin basalts: Observations and modeling. *Geophysics* 71(6):B211-B221
- McClintock M, White JD (2006) Large phreatomagmatic vent complex at Coombs Hills, Antarctica: wet, explosive initiation of flood basalt volcanism in the Ferrar-Karoo LIP. *B Volcanol* 68(3), 215-239.
- McGetchin TR, Settle M, Chouet BA (1974) Cinder Cone Growth Modeled After Northeast Crater, Mount Etna, Sicily. *J. Geophys. Res.* 79(23):3257-3272
- McKee C, Harpp K, Geist D, Mittelstaedt E, Fornari D, Soule S (2010) Morphology, Size, and Spatial Distribution of Seamounts in the Northern Galápagos. In: *AGU Fall Meeting Abstracts*. p 2255

- McKerrow W, Mac Niocaill C, Dewey J (2000) The Caledonian orogeny redefined. *J Geol Soc London* 157(6):1149-1154
- McNutt SR, Miller TP, Taber JJ (1991) Geological and seismological evidence of increased explosivity during the 1986 eruptions of Pavlof volcano, Alaska. *B Volcanol* 53(2):86-98
- Millett J (2015) Offshore drilling through basaltic sequences: geological heterogeneity and its implications for drilling complications, VMSG, Norwich
- Mitchell N, Stretch R, Oppenheimer C, Kay D, Beier C (2012) Cone morphologies associated with shallow marine eruptions: east Pico Island, Azores. *B Volcanol* 74(10):2289-2301
- Møller Hansen D (2006) The morphology of intrusion-related vent structures and their implications for constraining the timing of intrusive events along the NE Atlantic margin. *J Geol Soc London* 163(5):789-800
- Moore JG, Nakamura K, Alcaraz A (1966) The 1965 Eruption of Taal Volcano. *Science* 151(3713):955-960
- Moore JG (1985) Structure and eruptive mechanisms at Surtsey Volcano, Iceland. *Geol Mag* 122(06):649-661
- Moore RB, Helz RT, Dzurisin D, Eaton GP, Koyanagi RY, Lipman PW, Lockwood JP, Puniwai GS (1980) The 1977 eruption of Kilauea volcano, Hawaii. *J Volcanol Geoth Res* 7(3):189-210
- Mourão C, Mata J, Doucelance R, Madeira J, Silveira ABd, Silva LC, Moreira M (2010) Quaternary extrusive calciocarbonatite volcanism on Brava Island (Cape Verde): A nephelinite-carbonatite immiscibility product. *Journal of African Earth Sciences* 56(2–3):59-74
- Moy D, Imber J (2009) A critical analysis of the structure and tectonic significance of rift-oblique lineaments ('transfer zones') in the Mesozoic–Cenozoic succession of the Faroe–Shetland Basin, NE Atlantic margin. *J Geol Soc London* 166(5):831-844
- Naylor PH, Bell BR, Jolley DW, Durnall P, Fredsted R (1997) Palaeogene magmatism in the Faeroe–Shetland Basin: influences on uplift history and sedimentation. 545-558
- Nelson CE, Jerram DA, Single RT, Hobbs RW (2009a) Understanding the facies architecture of flood basalts and volcanic rifted margins and its effect on geophysical properties, Faroe Islands Exploration Conference: Proceedings of the 2nd Conference,
- Nelson CE, Jerram DA, Hobbs RW (2009b) Flood basalt facies from borehole data: implications for prospectivity and volcanology in volcanic rifted margins. *Petroleum Geoscience* 15(4):313-324
- Németh K, Martin U, Harangi S (2001) Miocene phreatomagmatic volcanism at Tihany (Pannonian Basin, Hungary). *J Volcanol Geoth Res* 111(1–4):111-135
- Németh K, Martin U (2007) Shallow sill and dyke complex in western Hungary as a possible feeding system of phreatomagmatic volcanoes in “soft-rock” environment. *J Volcanol Geoth Res* 159(1–3):138-152
- Németh K, Risso C, Nullo F, Kereszturi G (2011) The role of collapsing and cone rafting on eruption style changes and final cone morphology: Los Morados scoria cone, Mendoza, Argentina. *Central European Journal of Geosciences* 3(2):102-118
- Ogilvie JS, Crompton R, Hardy NM (2001) Characterization of volcanic units using detailed velocity analysis in the Atlantic Margin, West of Shetlands, United Kingdom. *The Leading Edge* 20(1):34-50
- Opheim JA, Gudmundsson A (1989) Formation and geometry of fractures, and related volcanism, of the Krafla fissure swarm, northeast Iceland. *Geol Soc Am Bull* 101(12):1608-1622
- Óskarsson BV, Riishuus MS (2013) The mode of emplacement of Neogene flood basalts in Eastern Iceland: Facies architecture and structure of the Hólmar and Grjóta olivine basalt groups. *J Volcanol Geoth Res* 267(0):92-118
- Otterloo J, Cas RF, Sheard M (2013) Eruption processes and deposit characteristics at the monogenetic Mt. Gambier Volcanic Complex, SE Australia: implications for alternating magmatic and phreatomagmatic activity. *B Volcanol* 75(8):1-21
- Oze C, Winter JD (2005) The occurrence, vesiculation, and solidification of dense blue glassy pahoehoe. *J Volcanol Geoth Res* 142(3–4):285-301
- Parcheta C, Houghton B, Swanson D (2012) Hawaiian fissure fountains 1: decoding deposits—episode 1 of the 1969–1974 Mauna Ulu eruption. *B Volcanol* 74(7):1729-1743
- Parfitt EA, Wilson L (1995) Explosive volcanic eruptions—IX. The transition between Hawaiian-style lava fountaining and Strombolian explosive activity. *Geophysical Journal International* 121(1):226-232

- Parfitt EA (1998) A study of clast size distribution, ash deposition and fragmentation in a Hawaiian-style volcanic eruption. *J Volcanol Geoth Res* 84(3):197-208
- Parfitt EA (2004) A discussion of the mechanisms of explosive basaltic eruptions. *J Volcanol Geoth Res* 134(1-2):77-107
- Passey SR, Bell BR (2007) Morphologies and emplacement mechanisms of the lava flows of the Faroe Islands Basalt Group, Faroe Islands, NE Atlantic Ocean. *B Volcanol* 70(2):139-156
- Passey SR, Jolley DW (2008) A revised lithostratigraphic nomenclature for the Palaeogene Faroe Islands Basalt group, NE Atlantic Ocean. *Earth and Environmental Science Transactions of the Royal Society of Edinburgh* 99(3-4):127-158
- Patrick MR, Harris AJ, Ripepe M, Dehn J, Rothery DA, Calvari S (2007) Strombolian explosive styles and source conditions: insights from thermal (FLIR) video. *B Volcanol* 69(7):769-784
- Paulsen TS, Wilson TJ (2010) New criteria for systematic mapping and reliability assessment of monogenetic volcanic vent alignments and elongate volcanic vents for crustal stress analyses. *Tectonophysics* 482(1-4):16-28
- Pendred V (2011) Entrail pahoehoe, Hawaii. Personal photographic collection.
- Peterson DW, Tilling RI (1980) Transition of basaltic lava from pahoehoe to aa, Kilauea Volcano, Hawaii: Field observations and key factors. *J Volcanol Geoth Res* 7(3-4):271-293
- Philpotts AR, Lewis CL (1987) Pipe vesicles—An alternate model for their origin. *Geology* 15(10):971-974
- Pinkerton H, Wilson L (1994) Factors controlling the lengths of channel-fed lava flows. *B Volcanol* 56(2):108-120
- Pioli L, Erlund E, Johnson E, Cashman K, Wallace P, Rosi M, Delgado Granados H (2008) Explosive dynamics of violent Strombolian eruptions: The eruption of Parícutin Volcano 1943–1952 (Mexico). *Earth and Planetary Science Letters* 271(1-4):359-368
- Pittari A, Cas R, Lefebvre N, Robey J, Kurszlaukis S, Webb K (2008) Eruption processes and facies architecture of the Orion Central kimberlite volcanic complex, Fort à la Corne, Saskatchewan; kimberlite mass flow deposits in a sedimentary basin. *J Volcanol Geoth Res* 174(1):152-170
- Planke S, Eldholm O (1994) Seismic response and construction of seaward dipping wedges of flood basalts: Vøring volcanic margin. *Journal of Geophysical Research: Solid Earth* (1978–2012) 99(B5):9263-9278
- Planke S, Cambray H (1998) Seismic properties of flood basalts from hole 917A downhole data, southeast Greenland volcanic margin. *Proceedings of the Ocean Drilling Program, Scientific Results* 152
- Planke S, Symonds PA, Alvestad E, Skogseid J (2000) Seismic volcanostratigraphy of large-volume basaltic extrusive complexes on rifted margins. *J. Geophys. Res.* 105(B8):19335-19351
- Planke S, Svensen H, Hovland M, Banks D, Jamtveit B (2003) Mud and fluid migration in active mud volcanoes in Azerbaijan. *Geo-Marine Letters* 23(3-4):258-268
- Planke S, Rasmussen T, Rey SS, Myklebust R (2005) Seismic characteristics and distribution of volcanic intrusions and hydrothermal vent complexes in the Vøring and Møre basins. *Geological Society, London, Petroleum Geology Conference series* 6:833-844
- Praeg D, Stoker M, Shannon P, Ceramicola S, Hjelstuen B, Laberg J, Mathiesen A (2005) Episodic Cenozoic tectonism and the development of the NW European 'passive' continental margin. *Marine and Petroleum Geology* 22(9):1007-1030
- Rateau R, Schofield N, Smith M (2013) The potential role of igneous intrusions on hydrocarbon migration, West of Shetland. *Petroleum Geoscience* 19(3):259-272
- Reidel SP, Tolan TL (1992) Eruption and emplacement of flood basalt: An example from the large-volume Teepee Butte Member, Columbia River Basalt Group. *Geol Soc Am Bull* 104(12):1650-1671
- Richter DH (1970) Chronological narrative of the 1959-60 eruption of Kilauea Volcano, Hawaii: A detailed and pictorial account of an eruptive sequence consisting of a summit eruption, a flank eruption, and a summit collapse. US Government Printing Office
- Riedel C, Ernst GGJ, Riley M (2003) Controls on the growth and geometry of pyroclastic constructs. *J Volcanol Geoth Res* 127(1-2):121-152

- Riggs NR, Duffield WA (2008) Record of complex scoria cone eruptive activity at Red Mountain, Arizona, USA, and implications for monogenetic mafic volcanoes. *J Volcanol Geoth Res* 178(4):763-776
- Ritchie J, Hitchen K (1996) Early Paleogene offshore igneous activity to the northwest of the UK and its relationship to the North Atlantic Igneous Province. Geological Society, London, Special Publications 101(1):63-78
- Ritchie J, Gatliff R, Richards P (1999) Early Tertiary magmatism in the offshore NW UK margin and surrounds. In: Geological Society, London, Petroleum Geology Conference series. Geological Society of London, pp 573-584
- Ritchie J, Ziska H, Johnson H, Evans D (2011) Geology of the Faroe-Shetland Basin and adjacent areas. Nottingham, UK, British geological Survey, pp317.
- Ritchie JD, Gatliff RW, Richards PC (1997) Early Tertiary magmatism in the offshore NW UK margin and surrounds. 573-584
- Roberts D, Thompson M, Mitchener B, Hossack J, Carmichael S, Bjørnseth H-M (1999) Palaeozoic to Tertiary rift and basin dynamics: mid-Norway to the Bay of Biscay—a new context for hydrocarbon prospectivity in the deep water frontier. In: Geological Society, London, Petroleum Geology Conference series. Geological Society of London, pp 7-40
- Roberts KS (2011) Mud volcano systems: structure, evolution and processes. PhD thesis, Durham University, Department of Earth Sciences.
- Roberts KS, Davies RJ, Stewart SA, Tingay M (2011) Structural controls on mud volcano vent distributions: examples from Azerbaijan and Lusi, east Java. *J Geol Soc London* 168(4):1013-1030
- Rohrman M (2007) Prospectivity of volcanic basins: Trap delineation and acreage de-risking. *AAPG bulletin* 91(6):915-939
- Ross GM (1986) Eruptive style and construction of shallow marine mafic tuff cones in the Narakay Volcanic Complex (Proterozoic, Hornby Bay Group, Northwest Territories, Canada). *J Volcanol Geoth Res* 27(3-4):265-297
- Ross P-S, Ukstins Peate I, McClintock M, Xu Y, Skilling I, White J, Houghton B (2005) Mafic volcanoclastic deposits in flood basalt provinces: a review. *J Volcanol Geoth Res* 145(3):281-314
- Ross P-S, White J, Valentine G, Taddeucci J, Sonder I, Andrews R (2013) Experimental birth of a maar–diatreme volcano. *J Volcanol Geoth Res* 260:1-12
- Rossi M (1996) Morphology and mechanism of eruption of postglacial shield volcanoes in Iceland. *B Volcanol* 57(7):530-540
- Rowland SK, Walker GPL (1987) Toothpaste lava: Characteristics and origin of a lava structural type transitional between pahoehoe and aa. *B Volcanol* 49(4):631-641
- Rowland SK, Walker GPL (1990) Pahoehoe and aa in Hawaii: volumetric flow rate controls the lava structure. *B Volcanol* 52(8):615-628
- Ryan MP, Sammis CG (1978) Cyclic fracture mechanisms in cooling basalt. *Geol Soc Am Bull* 89(9):1295-1308
- Rymer H, de Vries BvW, Stix J, Williams-Jones G (1998) Pit crater structure and processes governing persistent activity at Masaya Volcano, Nicaragua. *B Volcanol* 59(5):345-355
- Sable J, Houghton B, Wilson C, Carey R (2006) Complex proximal sedimentation from Plinian plumes: the example of Tarawera 1886. *B Volcanol* 69(1):89-103
- Sánchez MC, Sarrionandia F, Ibarguchi JIG (2014) Post-depositional intrusion and extrusion through a scoria and spatter cone of fountain-fed nephelinite lavas (Las Herrerías volcano, Calatrava, Spain). *B Volcanol* 76(9):1-17
- Schmidt R, Schmincke HU (2000) Seamounts and island building. In: Sigurdsson H (ed) *Encyclopedia of Volcanoes*. Academic Press, San Diego, pp 383-402
- Schnur SR (2007) An Analysis of the Morphology and Physical Properties of Pillow Lavas of the Nicasio Reservoir Terrace, Marin County, California: Implications for Seamount Formation and Structure. Masters dissertation, Carleton College, Minnesota.
- Schofield N, Jolley DW (2013) Development of intra-basaltic lava-field drainage systems within the Faroe–Shetland Basin. *Petroleum Geoscience* 19(3):273-288
- Schutter SR (2003) Occurrences of hydrocarbons in and around igneous rocks. Geological Society, London, Special Publications 214(1):35-68
- Self S, Keszthelyi L, Thordarson T (1998) The importance of pahoehoe. *Annu. Rev. Earth Planet. Sci.* 26:81-110

- Shaw F, Worthington M, White R, Andersen M, Petersen U (2008) Seismic attenuation in Faroe Islands basalts. *Geophysical Prospecting* 56(1):5-20
- Sheriff RE, Geldart L (1995) *Exploration seismology*. Cambridge University Press
- Sheth H (2006) The emplacement of pahoehoe lavas on Kilauea and in the Deccan Traps. *Journal of earth system science* 115(6):615-629
- Simkin T (1972) Origin of some flat-topped volcanoes and guyots. *Geol. Soc. Am. Mem* 132:183-193
- Skogseid J, Planke S, Faleide JJ, Pedersen T, Eldholm O, Neverdal F (2000) NE Atlantic continental rifting and volcanic margin formation. *Geological Society, London, Special Publications* 167(1):295-326
- Sohn YK, Chough SK (1989) Depositional processes of the Suwolbong tuff ring, Cheju Island (Korea). *Sedimentology* 36(5):837-855
- Sohn YK, Chough SK (1992) The Ilchulbong tuff cone, Cheju Island, South Korea. *Sedimentology* 39(4):523-544
- Sohn YK, Chough SK (1993) The Udo tuff cone, Cheju Island, South Korea: transformation of pyroclastic fall into debris fall and grain flow on a steep volcanic cone slope. *Sedimentology* 40(4):769-786
- Sohn YK (1996) Hydrovolcanic processes forming basaltic tuff rings and cones on Cheju Island, Korea. *Geol Soc Am Bull* 108(10):1199-1211
- Solana MC, Kilburn CRJ, Rodriguez Badiola E, Aparicio A (2004) Fast emplacement of extensive pahoehoe flow-fields: the case of the 1736 flows from Montaña de las Nueces, Lanzarote. *J Volcanol Geoth Res* 132(2-3):189-207
- Soper N, Woodcock N (2003) The lost Lower Old Red Sandstone of England and Wales: a record of post-Iapetan flexure or Early Devonian transtension? *Geol Mag* 140(06):627-647
- Sørensen AB (2003) Cenozoic basin development and stratigraphy of the Faroes area. *Petroleum Geoscience* 9(3):189-207
- Soule SA, Cashman KV (2005) Shear rate dependence of the pāhoehoe-to-‘a‘ā transition: Analog experiments. *Geology* 33(5):361-364
- Stevenson J, Mitchell N, Cassidy M, Pinkerton H (2012) Widespread inflation and drainage of a pāhoehoe flow field: the Nesjahraun, Þingvellir, Iceland. *B Volcanol*:1-17
- Stewart SA, Davies RJ (2006) Structure and emplacement of mud volcano systems in the South Caspian Basin. *AAPG Bulletin* 90(5):771-786
- Stoker M, Hitchen K, Graham C (1993) The geology of the Hebrides and West Shetland shelves, and adjacent deep-water areas. The Stationery Office/Tso
- Stovall W, Houghton B, Gonnermann H, Fagents S, Swanson D (2011) Eruption dynamics of Hawaiian-style fountains: the case study of episode 1 of the Kīlauea Iki 1959 eruption. *B Volcanol* 73(5):511-529
- Suiting I, Schmincke H-U (2009) Internal vs. external forcing in shallow marine diatreme formation: A case study from the Iblean Mountains (SE-Sicily, Central Mediterranean). *J Volcanol Geoth Res* 186(3):361-378
- Sumner JM (1998) Formation of clastogenic lava flows during fissure eruption and scoria cone collapse: the 1986 eruption of Izu-Oshima Volcano, eastern Japan. *B Volcanol* 60(3):195-212
- Sumner JM, Blake S, Matela RJ, Wolff JA (2005) Spatter. *J Volcanol Geoth Res* 142(1-2):49-65
- Svensen H, Planke S, Jamtveit B, Pedersen T (2003) Seep carbonate formation controlled by hydrothermal vent complexes: a case study from the Vøring Basin, the Norwegian Sea. *Geo-Marine Letters* 23(3-4):351-358
- Svensen H, Jamtveit B, Planke S, Chevallier L (2006) Structure and evolution of hydrothermal vent complexes in the Karoo Basin, South Africa. *J Geol Soc London* 163(4):671-682
- Svensen H, Planke S, Chevallier L, Malthe-Sørenssen A, Corfu F, Jamtveit B (2007) Hydrothermal venting of greenhouse gases triggering Early Jurassic global warming. *Earth and Planetary Science Letters* 256(3-4):554-566
- Swanson D (1974) USGS Photographic Library.
- Swanson D, Duffield WA, Jackson DB, Peterson DW (1979) Chronological narrative of the 1969 - 1971 Mauna Ulu eruption of Kilauea volcano, Hawaii. U.S Geological Survey Professional Paper 1065:55

- Swanson DA (1973) Pahoehoe Flows from the 1969–1971 Mauna Ulu Eruption, Kilauea Volcano, Hawaii. *Geol Soc Am Bull* 84(2):615-626
- Swanson DA, Wright TL, Helz RT (1975) Linear vent systems and estimated rates of magma production and eruption for the Yakima Basalt on the Columbia Plateau. *American Journal of Science* 275(8):877-905
- Thomson K (2005) Extrusive and intrusive magmatism in the North Rockall Trough. Geological Society, London, Petroleum Geology Conference series 6:1621-1630
- Thomson K (2007) Determining magma flow in sills, dykes and laccoliths and their implications for sill emplacement mechanisms. *B Volcanol* 70(2):183-201
- Thorarinsson S (1966) The Surtsey eruption course of events and the development of the new island. In: Museum of Natural History, Reykjavik, Iceland
- Thorarinsson S, Steinthorsson S, Einarsson T, Kristmannsdottir H, Oskarsson N (1973) The eruption on Heimaey, Iceland. *Nature* 241:372-375
- Thordarson T, Self S (1993) The Laki (Skaftár Fires) and Grímsvötn eruptions in 1783–1785. *B Volcanol* 55(4):233-263
- Thordarson T, Self S (1998) The Roza Member, Columbia River Basalt Group: A gigantic pahoehoe lava flow field formed by endogenous processes? *J. Geophys. Res.* 103(B11):27411-27445
- Thors K, Jakousson SP (1982) Two seismic reflection profiles from the vicinity of Surtsey, Iceland. Surtsey research progress report 9:149
- Tomkeieff S (1940) The basalt lavas of the Giant's Causeway district of Northern Ireland. *B Volcanol* 6(1):89-143
- Valentine G, Cortés J (2013) Time and space variations in magmatic and phreatomagmatic eruptive processes at Easy Chair (Lunar Crater Volcanic Field, Nevada, USA). *B Volcanol* 75(9):1-13
- Valentine GA, Groves KR (1996) Entrainment of Country Rock during Basaltic Eruptions of the Lucero Volcanic Field, New Mexico. *The Journal of Geology* 104(1):71-90
- Valentine GA, Krier D, Perry FV, Heiken G (2005) Scoria cone construction mechanisms, Lathrop Wells volcano, southern Nevada, USA. *Geology* 33(8):629-632
- Valentine GA, Krogh KEC (2006) Emplacement of shallow dikes and sills beneath a small basaltic volcanic center – The role of pre-existing structure (Paiute Ridge, southern Nevada, USA). *Earth and Planetary Science Letters* 246(3–4):217-230
- Valentine GA, Perry FV, Krier D, Keating GN, Kelley RE, Cogbill AH (2006) Small-volume basaltic volcanoes: Eruptive products and processes, and post-eruptive geomorphic evolution in Crater Flat (Pleistocene), southern Nevada. *Geol Soc Am Bull* 118(11-12):1313-1330
- Valentine GA, Keating GN (2007) Eruptive styles and inferences about plumbing systems at Hidden Cone and Little Black Peak scoria cone volcanoes (Nevada, USA). *B Volcanol* 70(1):105-113
- Valentine GA, Krier DJ, Perry FV, Heiken G (2007) Eruptive and geomorphic processes at the Lathrop Wells scoria cone volcano. *J Volcanol Geoth Res* 161(1-2):57-80
- Valentine GA, Gregg TKP (2008) Continental basaltic volcanoes — Processes and problems. *J Volcanol Geoth Res* 177(4):857-873
- Valentine GA (2012) Shallow plumbing systems for small-volume basaltic volcanoes, 2: Evidence from crustal xenoliths at scoria cones and maars. *J Volcanol Geoth Res* 223–224(0):47-63
- Valerio A, Tallarico A, Dragoni M (2008) Mechanisms of formation of lava tubes. *J. Geophys. Res.* 113(B8):B08209
- Vergnolle S, Jaupart C (1986) Separated two-phase flow and basaltic eruptions. *J. Geophys. Res.* 91(B12):12842-12860
- Vergnolle S, Mangan MT (2000) Hawaiian and Strombolian Eruptions. In: Sigurdsson H (ed) *Encyclopedia of Volcanoes*. Academic press, San Diego, pp 447-461
- Verwoerd WJ, Chevallier L (1987) Contrasting types of surtseyan tuff cones on Marion and Prince Edward islands, southwest Indian Ocean. *Bull Volcanol* 49(1), 399-413.
- Vespermann D, Schmincke H-U (2000) Scoria cones and tuff rings. In: Sigurdsson H (ed) *Encyclopedia of Volcanoes*. Academic Press, San Diego. Academic Press, San Diego, pp 683-694
- Wadge G (1981) The variation of magma discharge during basaltic eruptions. *J Volcanol Geoth Res* 11(2–4):139-168

- Waichel B, de Lima E, Lubachesky R, Sommer C (2006) Pahoehoe flows from the central Paraná Continental Flood Basalts. *B Volcanol* 68(7):599-610
- Walker G (1971) Compound and simple lava flows and flood basalts. *B Volcanol* 35(3):579-590
- Walker G (1973) Explosive volcanic eruptions — a new classification scheme. *Geologische Rundschau* 62(2):431-446
- Walker G (1991) Structure, and origin by injection of lava under surface crust, of tumuli, “lava rises”, “lava-rise pits”, and “lava-inflation clefts” in Hawaii. *B Volcanol* 53(7):546-558
- Walker GPL (1958) Geology of the Rydarfjörður area, eastern Iceland. *Quarterly Journal of the Geological Society* 114(1-4):367-391
- Walker GPL, Self S, Wilson L (1984) Tarawera 1886, New Zealand — A basaltic plinian fissure eruption. *J Volcanol Geoth Res* 21(1-2):61-78
- Walker GPL (1989) Spongy pahoehoe in Hawaii: A study of vesicle-distribution patterns in basalt and their significance. *B Volcanol* 51(3):199-209
- Walker GPL (1993) Basaltic-volcano systems. Geological Society, London, Special Publications 76(1):3-38
- Walker GPL (1995) Flood basalts versus central volcanoes and the British Tertiary volcanic Province. Geological Society, London, Memoirs 16(1):195-202
- Walker GPL, Cañón-Tapia E, Herrero-Bervera E (1999) Origin of vesicle layering and double imbrication by endogenous growth in the Birkett basalt flow (Columbia river plateau). *J Volcanol Geoth Res* 88(1-2):15-28
- Walker GPL (2000) Basaltic volcanoes and volcanic systems. In: Sigurdsson H (ed) *Encyclopedia of volcanoes*. Academic Press, San Diego, pp 283-289
- Wall M, Cartwright J, Davies R, McGrandle A (2010) 3D seismic imaging of a Tertiary Dyke Swarm in the Southern North Sea, UK. *Basin Research* 22(2):181-194
- Watton TJ (2013) A multidisciplinary assessment of hyaloclastite deposits in petroleum systems using field studies, drill core, borehole image and wire-line log datasets.
- Watton TJ, Cannon S, Brown RJ, Jerram DA, Waichel BL (2014) Using formation micro-imaging, wireline logs and onshore analogues to distinguish volcanic lithofacies in boreholes: examples from Palaeogene successions in the Faroe–Shetland Basin, NE Atlantic. Geological Society, London, Special Publications 397
- Waythomas CF, Haney MM, Fee D, Schneider DJ, Wech A (2014) The 2013 eruption of Pavlof Volcano, Alaska: a spatter eruption at an ice-and snow-clad volcano. *B Volcanol* 76(10):1-12
- Wessel P, Sandwell DT, Kim S-S (2010) The global seamount census. *Oceanography* 23(1):24
- White JDL (1991) Maar-diatreme phreatomagmatism at Hopi Buttes, Navajo Nation (Arizona), USA. *B Volcanol* 53(4):239-258
- White JDL, Houghton B (2000) Surtseyan and related phreatomagmatic eruptions. In: Sigurdsson H (ed) *Encyclopedia of volcanoes*. Academic Press, San Diego, pp 495-511
- White JDL, Ross PS (2011) Maar-diatreme volcanoes: A review. *J Volcanol Geoth Res* 201(1-4):1-29
- White RS, Smallwood JR, Fliedner MM, Boslaugh B, Maresh J, Fruehn J (2003) Imaging and regional distribution of basalt flows in the Faeroe-Shetland Basin. *Geophysical Prospecting* 51(3):215-231
- Wilch T (2011) Glassy pahoehoe. In: Albion College Geology
- Wilmoth RA, Walker GPL (1993) P-type and S-type pahoehoe: a study of vesicle distribution patterns in Hawaiian lava flows. *J Volcanol Geoth Res* 55(1-2):129-142
- Wilson L, Head JW, III (1981) Ascent and Eruption of Basaltic Magma on the Earth and Moon. *J. Geophys. Res.* 86(B4):2971-3001
- Wilson L, Parfitt E, Head J (1995) Explosive volcanic eruptions—VIII. The role of magma recycling in controlling the behaviour of Hawaiian-style lava fountains. *Geophysical Journal International* 121(1):215-225
- Wohletz KH, Sheridan MF (1983) Hydrovolcanic explosions; II, Evolution of basaltic tuff rings and tuff cones. *American Journal of Science* 283(5):385-413
- Wohletz KH (1983) Mechanisms of hydrovolcanic pyroclast formation: Grain-size, scanning electron microscopy, and experimental studies. *J Volcanol Geoth Res* 17(1-4):31-63

- Wolfe WE, Neal AC, Banks GN, Toni DJ (1988) The Puu Oo Eruption of Kilauea Volcano, Hawaii: Episodes 1 Through 20, January 3, 1983, Through June 8, 1984. U.S Geological Survey Professional Paper 1463
- Wolff J, Sumner J (2000) Lava fountains and their products. In: Sigurdsson H (ed) Encyclopedia of volcanoes. Academic Press, San Diego, pp 321-329
- Wood CA (1980) Morphometric evolution of cinder cones. *J Volcanol Geoth Res* 7(3–4):387-413
- Woods AW, Bursik MI (1991) Particle fallout, thermal disequilibrium and volcanic plumes. *B Volcanol* 53(7):559-570
- Wright K (2013) Seismic Stratigraphy and Geomorphology of Palaeocene Volcanic Rocks, Faroe-Shetland Basin. PhD Thesis, Durham University, Department of Earth Sciences.
- Wright KA, Davies RJ, Jerram DA, Morris J, Fletcher R (2012) Application of seismic and sequence stratigraphic concepts to a lava-fed delta system in the Faroe-Shetland Basin, UK and Faroes. *Basin Research* 24(1):91-106
- Wylie JJ, Helfrich KR, Dade B, Lister JR, Salzig JF (1999) Flow localization in fissure eruptions. *B Volcanol* 60(6):432-440
- Yusifov M, Rabinowitz PD (2004) Classification of mud volcanoes in the South Caspian Basin, offshore Azerbaijan. *Marine and Petroleum Geology* 21(8):965-975
- Zhao F, Wu S, Sun Q, Huuse M, Li W, Wang Z (2014) Submarine volcanic mounds in the Pearl River Mouth Basin, northern South China Sea. *Mar Geol* 355(0):162-172

Chapter 3: The Evolution of the 6–8 kyr R-K Basaltic Fissure Eruption, Northeast Iceland

3.1 Introduction

Basaltic fissure eruptions occur in many tectonic settings (e.g. Fedotov et al. 1980; Karhunen 1988; Wolfe et al. 1988; Carracedo et al. 1992; Thordarson and Self 1993; Parcheta et al. 2012). They are common throughout the geologic record and in historic times (e.g. Carracedo et al. 1992; Thordarson and Self 1993; Thordarson et al. 2001; Gudmundsson et al. 2010; Németh and Cronin 2011; Wendel 2014). Whilst eruptions are usually low explosivity Hawaiian-type events, large-volume fissure eruptions can have significant environmental and climatic effects. Ash fall can cause crop failure (e.g. Thordarson and Self 1993), whilst sulphurous gases associated with vigorous eruption columns penetrate the lower stratosphere and impact the climate (e.g. Thordarson and Self 1993; Thordarson et al. 2001). Fissure eruptions have also produced some of the largest basaltic lava flows in historical times (Thordarson and Self 1993) and produce the lava flow fields that are the “building blocks” of flood basalt provinces (Swanson et al. 1975; Walker 1995; Reidel 1998; Bondre et al. 2004a; Brown et al. 2014).

The feeder dykes for fissures initiate eruptions from linear vents. With time, magma flow along a dyke localises to numerous point sources (e.g. Bruce and Huppert 1989), around which pyroclastic edifices are built. The type and geometry of the edifice produced during dry eruptions (i.e. without magma-water interaction) is largely controlled by the dynamics of the lava fountain. Lava fountains are the most common subaerial eruption mechanism on Earth (Sumner et al. 2005) and also occur on other planetary bodies (e.g. Io; see Keszthelyi et al. 2001). The spread angle of lava fountains is controlled by magma gas content and volume flux (Head and Wilson 1989). Hawaiian-style lava fountains are frequently 500 m in height (Wolff and Sumner 2000) although the height and intensity of the fountain often varies during an eruption (e.g. Wolfe et al. 1988; Thordarson and Self 1993; Parcheta et al. 2012; Valentine and Cortés 2013). The fountains produce a range of welded, non-welded and coalesced deposits depending on factors such as fountain collimation (i.e. spread from vertical) and wind profile (Head and Wilson 1989). These deposits vary in character with distance from the fissure, with welded and agglutinated deposits dominant in proximal regions (e.g. Head and Wilson 1989).

Despite their common occurrence, volumetric importance in the rock record and environmental and climatic impacts, the temporal evolution of fissure eruptions has

received little attention. Although there are observations of historic eruptions (e.g. Steingrímsson and Ólafsson 1783; Steingrímsson 1788; Swanson et al. 1979; Fedotov et al. 1980; Aramaki et al. 1986; Wolfe et al. 1988; Sumner 1998; Gudmundsson et al. 2010; Wendel 2014), few studies have access to the entire eruptive stratigraphy. The products of most fissure eruptions only allow examination of the most recent, last erupted surface deposits (e.g. the Laki fissure; see Thordarson and Self 1993), as earlier deposits are buried. The deposits of older, highly eroded sequences of basaltic fissure eruptions with good cross sectional exposure commonly cannot be correlated laterally (e.g. Tertiary fissure-fed lavas; see Kent et al. 1998). Thus there is a poor understanding of how the deposits from fissure eruptions transition laterally into a lava flow field, and how the eruptive sequence varies with time.

The aim of this study is to provide insights into the spatial and temporal variability of a Holocene basaltic fissure eruption. Erosional dissection has exposed the feeder dyke and a near-complete record of the vent-proximal erupted products. Geologic mapping and stratigraphic analysis are used to understand the construction of a scoria-agglutinate cone, scoria and spatter ramparts, sheet-like fall deposits and rootless cones. Documentation of these edifices can be used to identify vent-proximal locations in other settings, and link observed eruptive processes with deposits.

3.2 Geological setting

Iceland is located above a spreading plate boundary and a mantle plume (Thordarson and Larsen 2007). Active faulting and volcanism is confined to a 15–50 km wide axial zone that crosses Iceland from southwest to the north (Thordarson and Larsen 2007). The axial zone is the loci of active spreading and plate growth and is typified by tholeiitic magmatism (Thordarson and Larsen 2007). One of the core features of the axial zone is the Northern Volcanic Zone (NVZ; Thordarson and Larsen 2007). This zone forms the most northerly emergent part of the Mid-Atlantic ridge and is composed of numerous individual volcanic systems (Frieese et al. 2013). It is linked to the offshore Mid-Atlantic ridge by the northwest-southeast striking Tjörnes Fracture Zone (TFV; Fig. 3.1; Gudmundsson 2007; Thordarson and Larsen 2007).

The 6–8 kyr Rauduborgir-Kvensödul (R-K) fissure is located in the NVZ (Figs. 3.1 and 3.2). Here, the Kraeduborgir, Rauðhólar and R-K fissures form an en-echelon, 150 km long fissure complex. This is part of either the Fremri-Namur or Askja volcanic system, extending from Melrakkasletta in the northeast to Utbruni in the southwest (Tentler and

Temperley 2007). There is no postglacial active central volcano associated with the fissure, but the presence of a magma chamber is indicated by the presence minor acidic volcanic rocks in a geothermally active zone (Tentler and Temperley 2007).

The R-K fissure strikes 025°, changing to 015° where it enters the Sveinar graben (Fig. 3.2); thus it is thought that the graben captured the fissure (Thorarinsson 1959). The fissure is marked by a 75 km-long row of pyroclastic edifices including scoria cones, spatter cones, half cones and hybrids there-of. This “mixed cone row” is typical of both large and small volume Icelandic eruptions (Thordarson and Larsen 2007).

Aphyric olivine tholeiite lavas associated with the fissure merge northwards with lavas from the 9 kyr Rauðhólar eruption (Thorarinsson 1959; Waite 2009; Friese et al. 2013). The aphyric R-K lavas are easily distinguished from the underlying columnar-jointed plagioclase porphyritic lavas, erupted 70 kyr BP (Slater et al. 1998). The study area consists of a 3 km² sections of the fissure (Figs. 3.3 and 3.4) along which 35 pyroclastic edifices are identified (Fig. 3.5).

The fissure is dissected by the Jökulsá canyon. This canyon exploits a fault that strikes sub-parallel to the TFZ (Figs. 3.1 and 3.4; see Gudmundsson 2007) and is thought to have partly existed before the Holocene (Kirkbride et al. 2006). The canyon has since hosted 16 glacial outbursts between 2–9 kyr BP (Alho et al. 2005; Kirkbride et al. 2006; Waite 2009). The largest of these were between 2–7 kyr BP, and just after deglaciation at 8–9 kyr BP (Alho et al. 2005; Kirkbride et al. 2006; Waite 2009). West of the river, the fissure is confined within the 30 km long, 0.5–1 km wide Sveinar graben that developed prior-to and during the R-K eruption (Thorarinsson 1959).

Previous work on the R-K fissure indicates that the dyke on the eastern Jökulsá a Fjöllum canyon wall led to reverse faulting along a pre-existing normal fault (Gudmundsson et al. 2008). Friese et al. (2013) briefly examined this dyke, stating that its flaring morphology was consistent with other nearby dykes in the shallow subsurface.

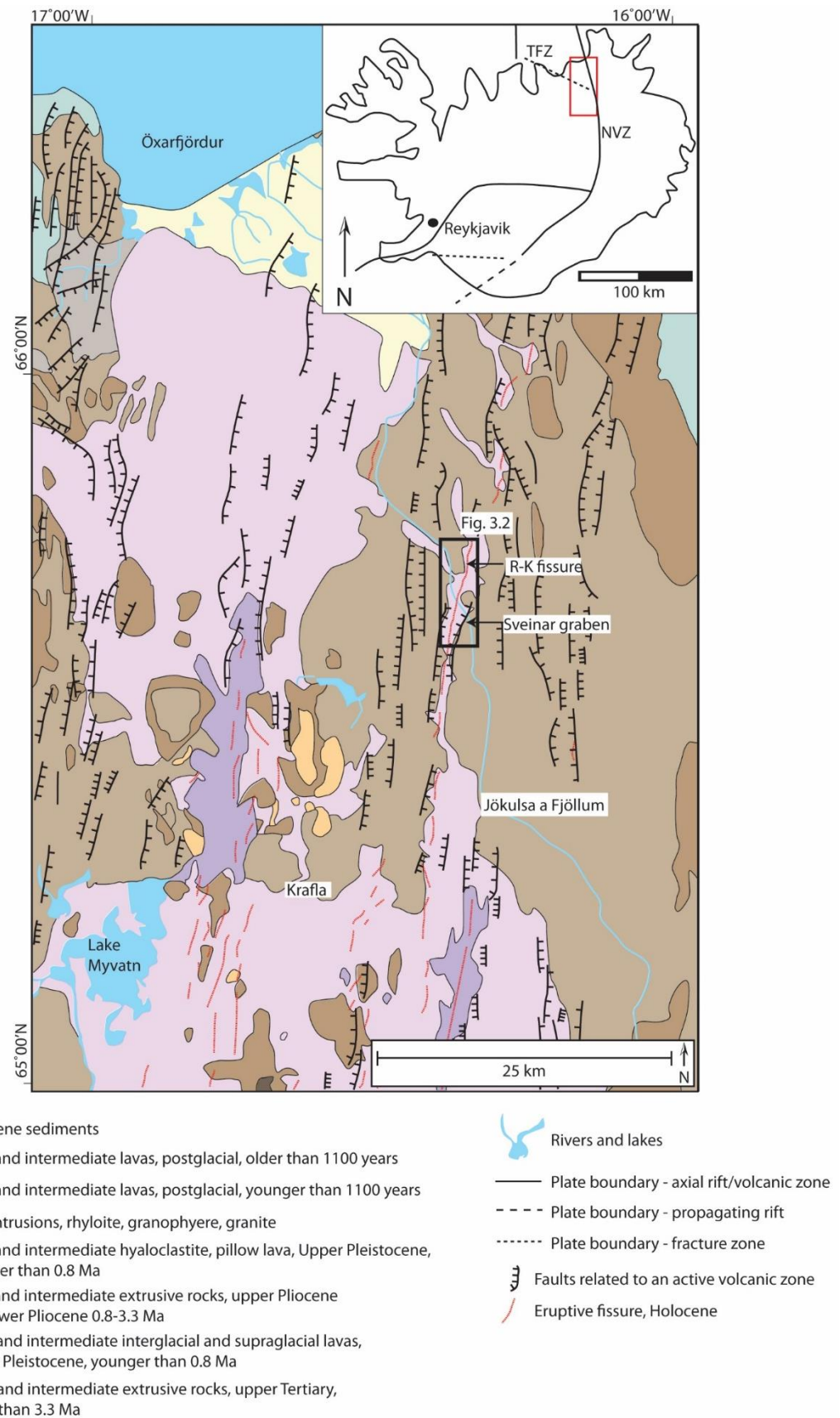


Figure 3.1. Location of the Sveinar graben in the Holocene rift zone of Northern Iceland. Inset map shows the location of the study area outlined in red and the Tjörnes Fracture Zone (TFZ). Adapted from Gudmundsson et al. (2008).

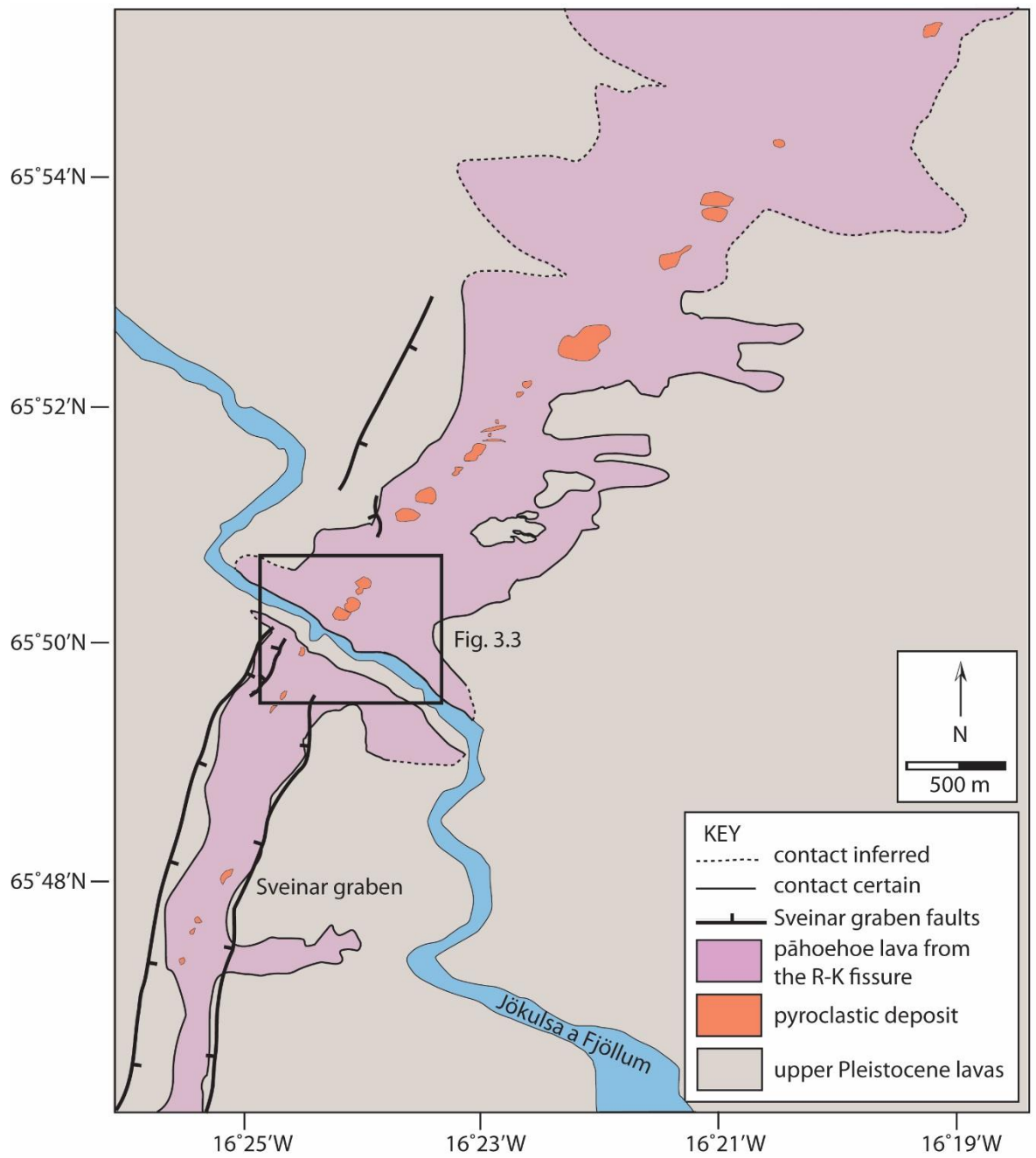


Figure 3.2. Regional geology map of the Rauduborgir-Kvensödul fissure. See Fig. 3.1 for location. Lavas produced during the eruption pond in the Sveinar graben towards the south.

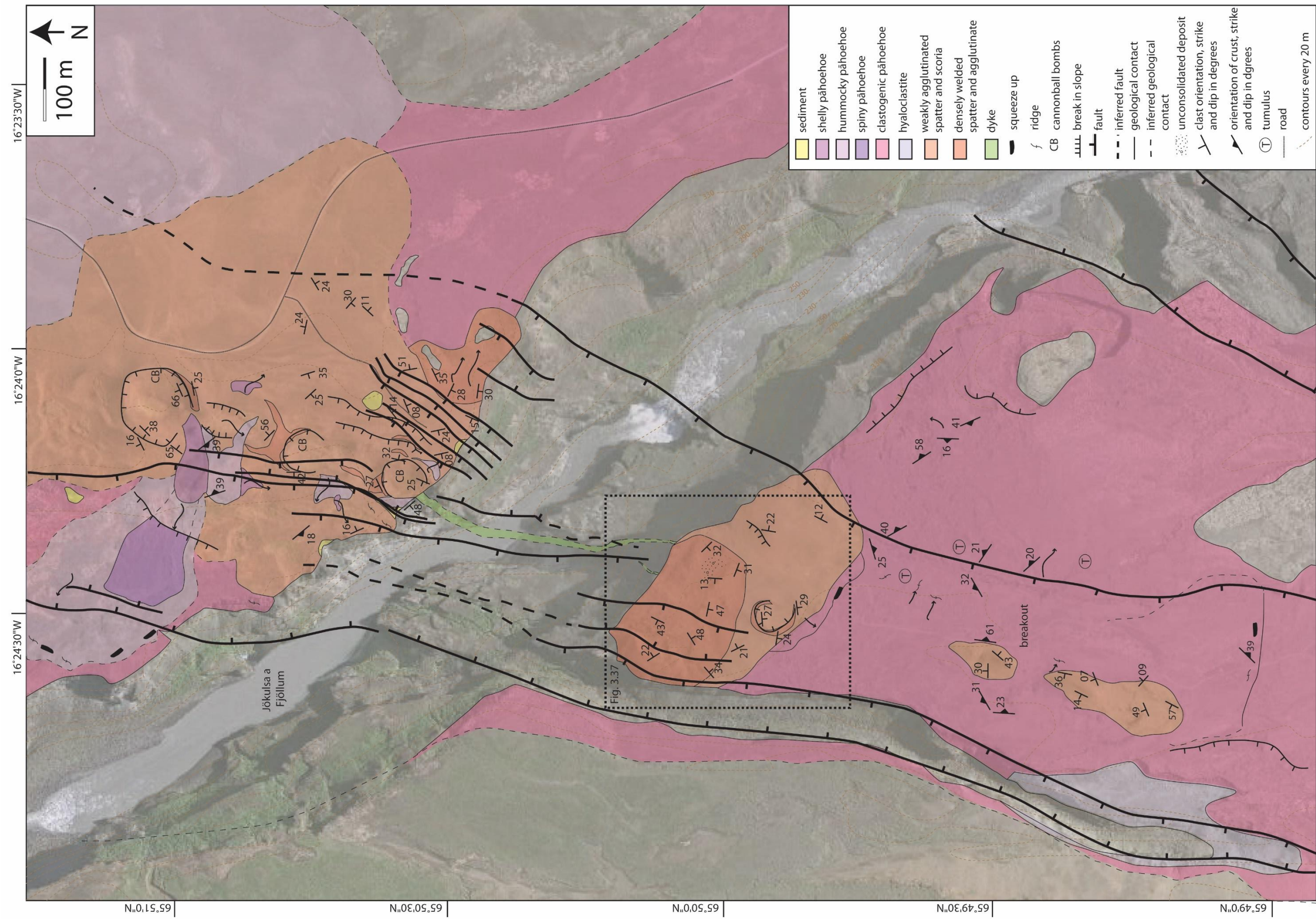


Figure 3.3 Geological map of the study area. See Fig. 3.2 for location.

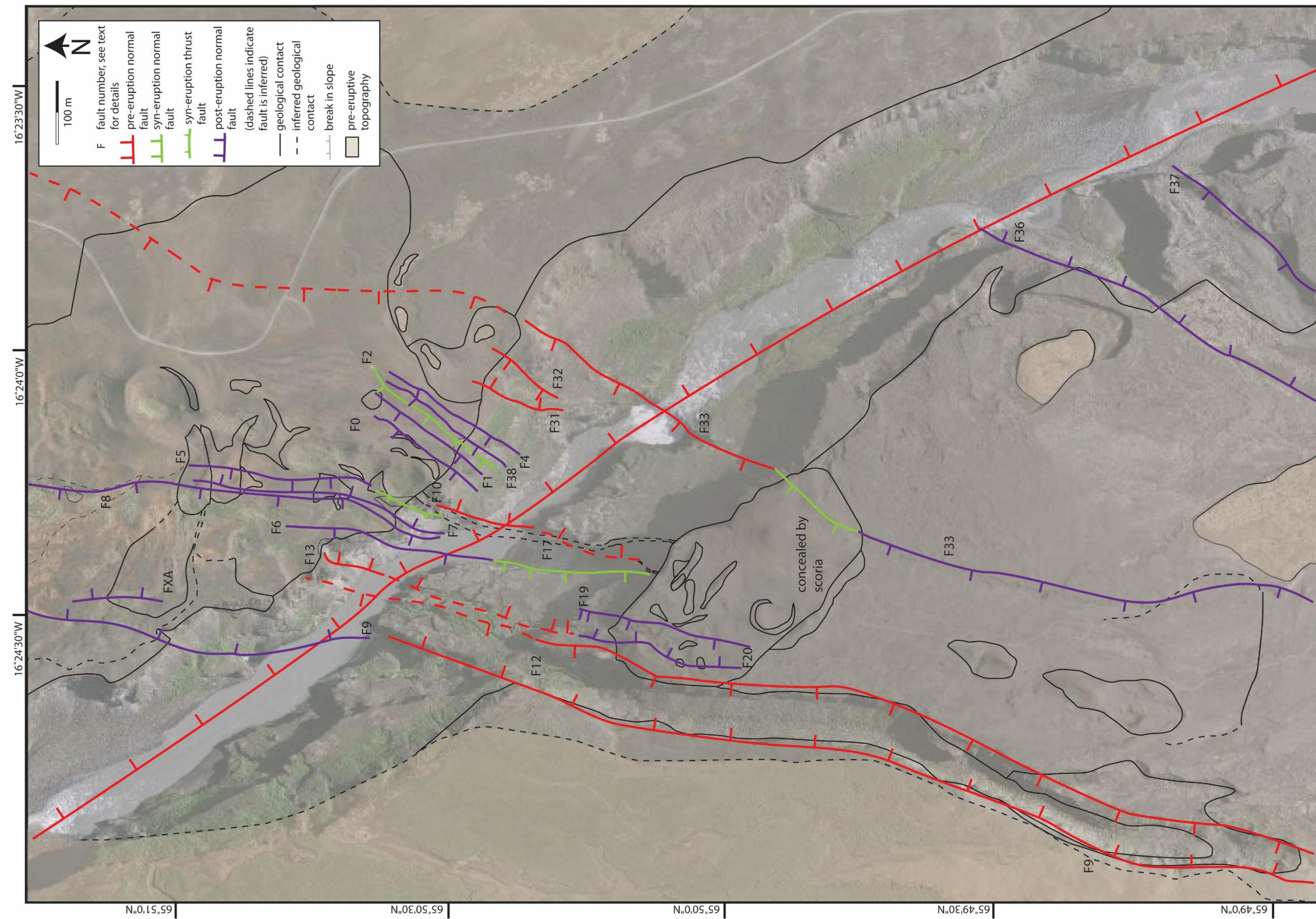


Fig. 3.4. Map of faults in the study area. The faults are coloured to indicate formation prior to, during, or post eruption. Black outline indicates the limit of the R-K stratigraphy. See text for details. See Fig. 3.2 for location.

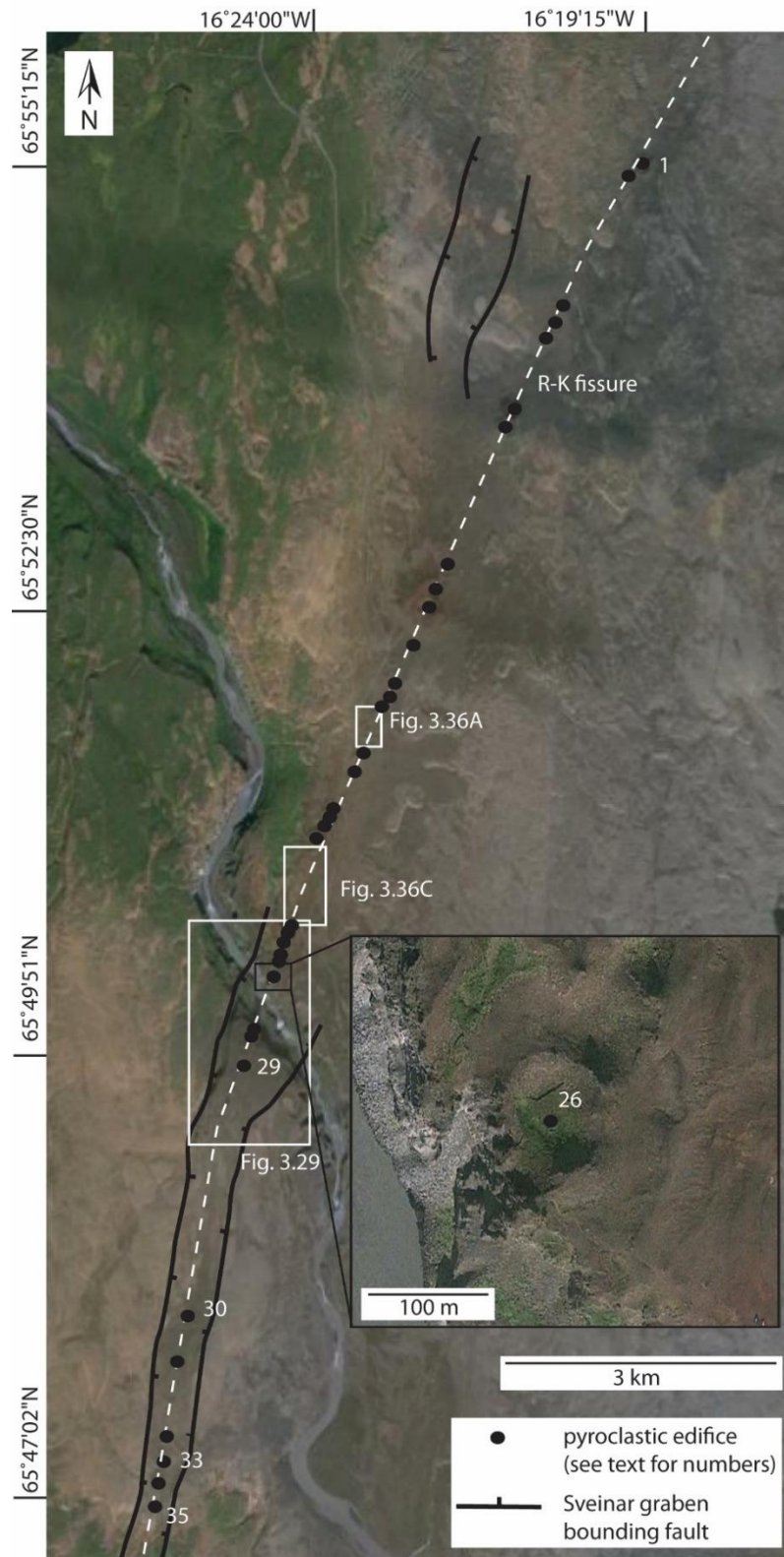


Figure 3.5. Google Earth image showing the change in strike of the R-K fissure as it is captured by the Sveinar graben. Pyroclastic edifices are shown; not all edifices are numbered for clarity. Note the large (3.5 km) gap between edifices 29 and 30, perhaps resulting from post-eruption erosion. Edifice 35 is located at the end of this section of the fissure.

3.3 Methods

The R-K pyroclastic deposits and lavas have been mapped at a 1:5000 scale. Geospatial data were recorded using a handheld global positioning system (GPS) with an accuracy of ± 5 m. Aerial photographs (extracted from Google Earth) were used to map small-scale features and were ground-truthed in the field. Much of the stratigraphy exposed on the canyon wall is inaccessible and has been mapped using photographs. Vertical sections that were measured in the field were then used to calibrate and analyse the photographs via image analysis (software ImageJ, <http://imagej.nih.gov/ij/>). Using this method, the expected errors are <5%. Exposures that allow detailed examination were logged on a centimetre scale to facilitate the identification of lithofacies and establish correlations across the study area.

Representative samples were used to calculate the density of pyroclasts using the method of Houghton and Wilson (1989). Most pyroclastic deposits are at least incipiently welded and sieving was unsuitable for determining the grain size distributions. Instead, the mean largest clast size was calculated by measuring the ten largest clasts per m². The lithic clast contents of the deposits were calculated using the method outlined by Valentine and Groves (1996). Since there is little exposure of the pyroclastic deposits away from the Jökulsá a Fjöllum canyon, isopleth and isopach maps were not constructed. The R-K volcanic sequence is described using the terminology as defined in Table 3.1.

| Term | Definition |
|--|---|
| <i>Petrographic texture (after Thordarson and Self 1998 and references there-in)</i> | |
| Holocrystalline | (90–100% crystalline) |
| Hypocrystalline | (50–90% crystalline) |
| Hypohyaline | (10 – 50% crystalline) |
| Holohyaline | (0 – 10% crystalline) |
| <i>Vesicularity (after Houghton and Wilson 1989)</i> | |
| Non-vesicular | 0 – 5 % |
| Incipiently vesicular | 5 – 20 % |
| Poorly vesicular | 20 – 40 % |
| Moderately vesicular | 40 – 60 % |
| Highly vesicular | 60 – 80 % |
| Extremely vesicular | >80 % |
| <i>Agglutination textures (after Sumner 1998; Wolff and Sumner 2000)</i> | |
| Agglutinate | Moderate flattening, complete clast outlines preserved |
| Deformed agglutinate | Extreme flattening, clast outlines retained |
| Highly deformed agglutinate | <50% of individual clast outlines preserved, deformation into swirling shapes |
| Coalesced | Patchy vesiculation, no unequivocal clast outlines |
| Agglutinated | Clasts that have become adjoined on deposition |
| Welded | Agglutinated pyroclastic deposits in which clasts are flattened and have partially or totally lost their outlines |
| <i>Pyroclastic textures (after Sumner et al. 2005)</i> | |
| Spatter | An accumulation of originally hot, fluid pyroclasts which agglutinate on landing |
| <i>Lava flow field architecture (after Self et al. 1998)</i> | |
| Lava lobe | The smallest individual package of a lava flow |
| Lava flow | The product of a single outpouring of lava |
| Lava flow field | The largest descriptive unit of a single or numerous lava flows |

Table 3.1. Terminology and definitions.

3.4 Pyroclastic lithofacies

A variety of pyroclastic lithofacies are exposed along the R-K fissure. They are composed of numerous clasts (Fig. 3.6) and range from clast-supported, non-welded scoria lapilli (ScL) to clast-supported, densely welded spatter bombs (dwSp; Figs. 3.7 and 3.8). All juvenile material is composed of aphyric hypocrySTALLine to hypohyaline primitive olivine tholeiitic basalt (Jökulsárgljúfur Information Centre; Friese et al. 2013). The lithofacies vary in their componentry, crystallinity, vesicularity, texture and clast aspect ratio. Density histograms for selected pyroclastic deposits indicate that density increases with welding intensity and there is a positive correlation between the clast aspect ratio and density (Fig. 3.9). Primary features within the lithofacies are well preserved. A summary of lithofacies descriptions and interpretations are given in Table 3.2 and 3.3. Detailed stratigraphic logs reveal significant complexity to the architecture of the lithofacies (Figs. 3.10 and 3.11) and are used to infer depositional processes and the dynamics of the lava fountain along the fissure.

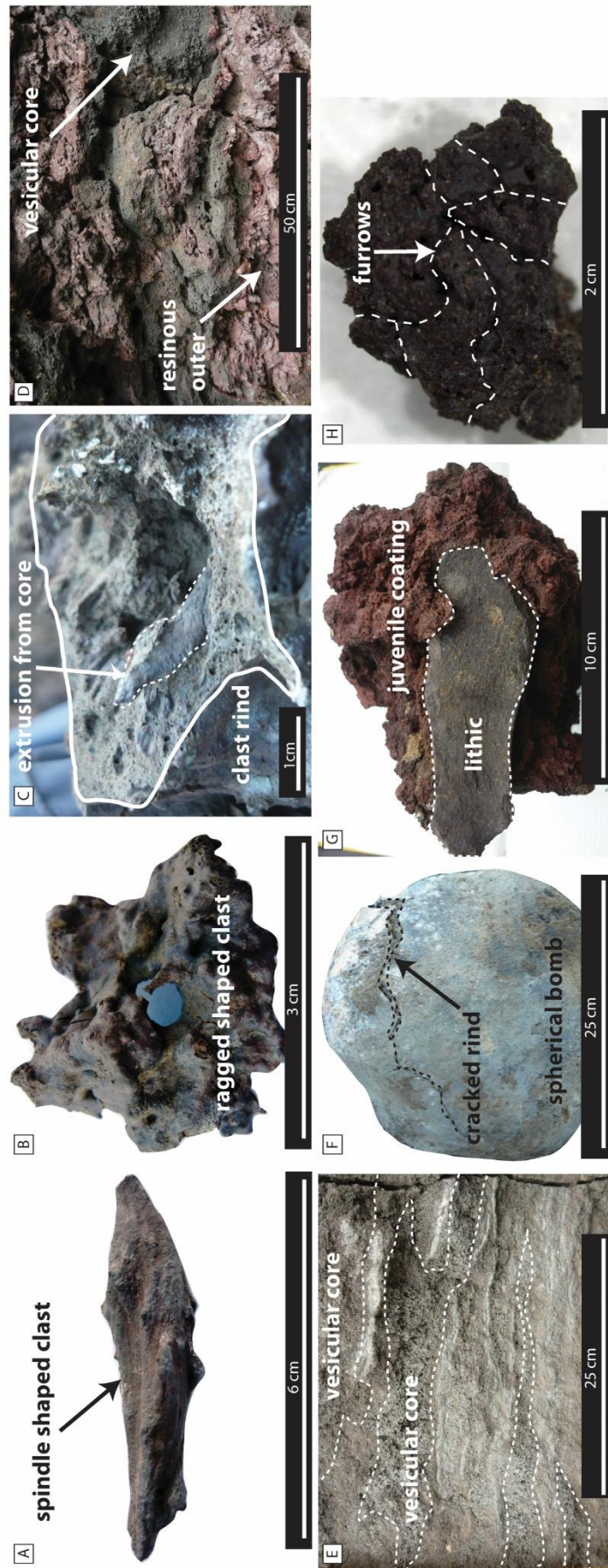


Figure 3.6. Pyroclast types identified in the study area. (A) Spindle-shaped and (B) ragged clast, typical of Hawaiian and Strombolian activity. (C) Clast with a brittle rind (outlined) extruding melt from its interiors (arrowed). (D) Fluid clasts that agglutinate, produced from the inner part of the lava fountain or a low fountain. (E) Fluid clasts that coalesce, produced from the inner lava fountain or a low fountain. (F) Cored bombs produced by the recycling of clasts within an edifice. They have a core of cognate lithic clasts and a 10 mm thick coating of lava. (G) An armoured clast with an accidental or cognate lithic core and a partial coating of lava. (H) Scoria lapilli produced from a rootless lava fountain. Notice the furrows in the crust, similar to those in breadcrust bombs.

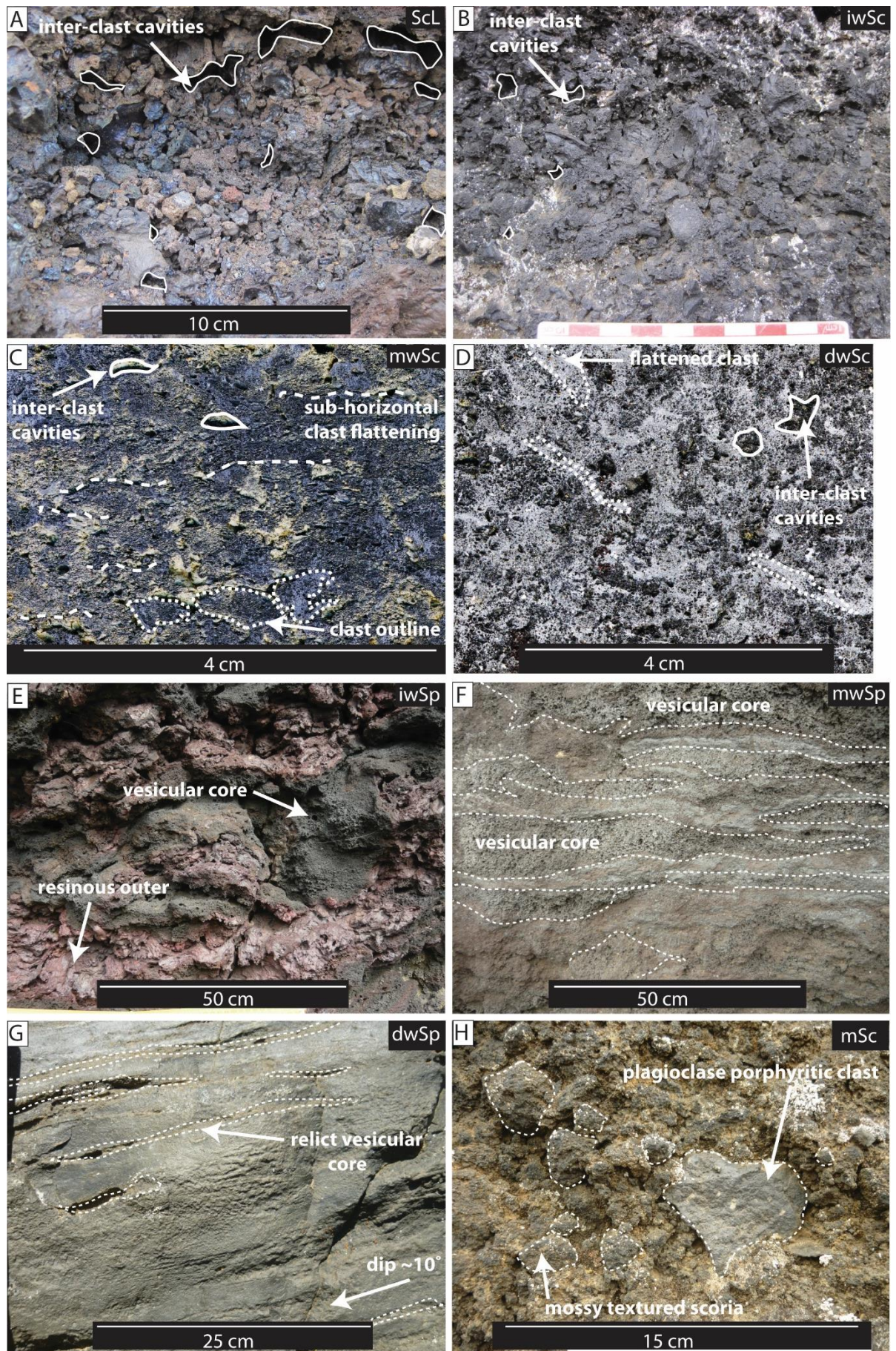


Figure 3.7 (overleaf). Pyroclastic lithofacies observed in the study area. (A) Non-welded scoria lapilli. Inter-clast cavities are visible (outlined). Note the absence of clast flattening. (UTM 557085/7264940). (B) Incipiently welded scoria. Inter-clast cavities are visible (outlined) and clasts are sintered at contacts. Minor clast flattening is observed. (UTM 557442/7264902). (C) Moderately welded scoria. Clast outlines are visible (dashed outline) and some inter-clast cavities (circled) remains. Sub-horizontal clast flattening is parallel to the dashed lines. (UTM 557356/7265748). (D) Densely welded scoria. Flattened clasts (dashed outline) are visible. Small (<1 cm diameter) inter-clast cavities remain. (UTM 563879/7301531). (E) Incipiently welded spatter. Resinous clast rinds are visible (arrowed). (UTM 557433/7264891). (F) Moderately welded spatter. Vesicular cores of clasts remain (dashed outline) and define the bedding. (UTM 557442/7264902). (G) Densely welded spatter. Thin relict vesicular cores (dashed outline) are visible between densely welded zones. The ghost clasts dip ~10°. (UTM 557356/7265748). (H) Massive scoria lapilli and bombs. The clasts are incipiently welded. Armoured clasts with an accidental lithic clast core are common in these deposits. (UTM: 557790/7264865).

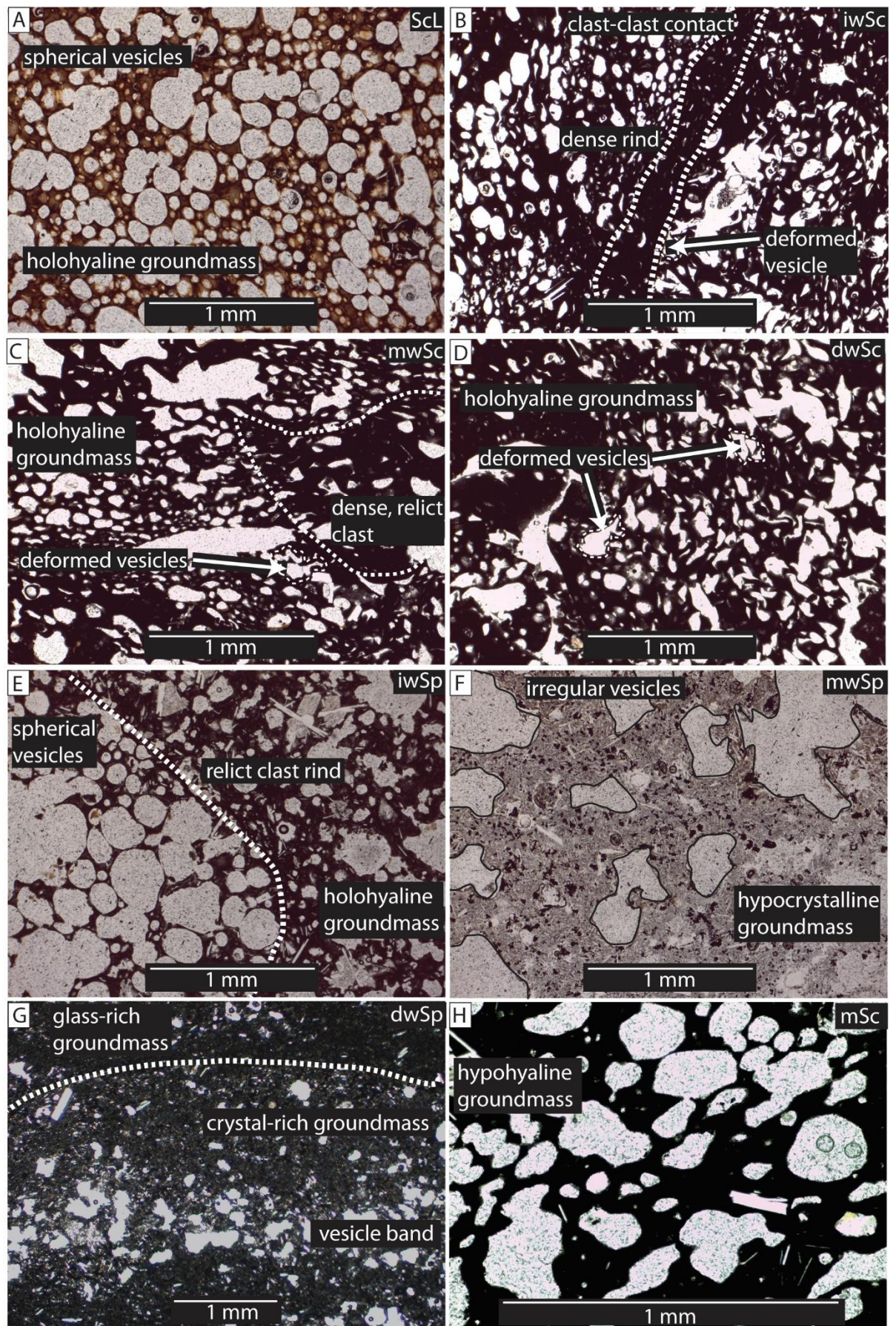


Figure 3.8 (overleaf). Thin section images of pyroclastic lithofacies (plane polarised light). (A) Non-welded scoria lapilli. Note the sphericity of the vesicles compared to the other lithofacies. (B) Incipiently welded scoria. The dashed line indicates an inferred contact between welded clasts. (C) Moderately welded scoria. Domains of less vesicular scoria (dashed outline) are inferred to represent welded clasts. (D) Densely welded scoria. The lithofacies appears texturally similar to clast-supported moderately welded scoria lapilli and bombs (mwSc). (E) Incipiently welded spatter. The dashed line indicates a clast rind folded into the clast core. (F) Moderately welded spatter. Note the increasing crystal content relative to (D) and (E). (G) Densely welded spatter. Note the laminated appearance of the groundmass. The crystal-rich groundmass contains a band of vesicles and is interpreted as the relict core of a spatter bomb. (H) Massive scoria lapilli and bombs. Note the thick bubble septae relative to A and B.

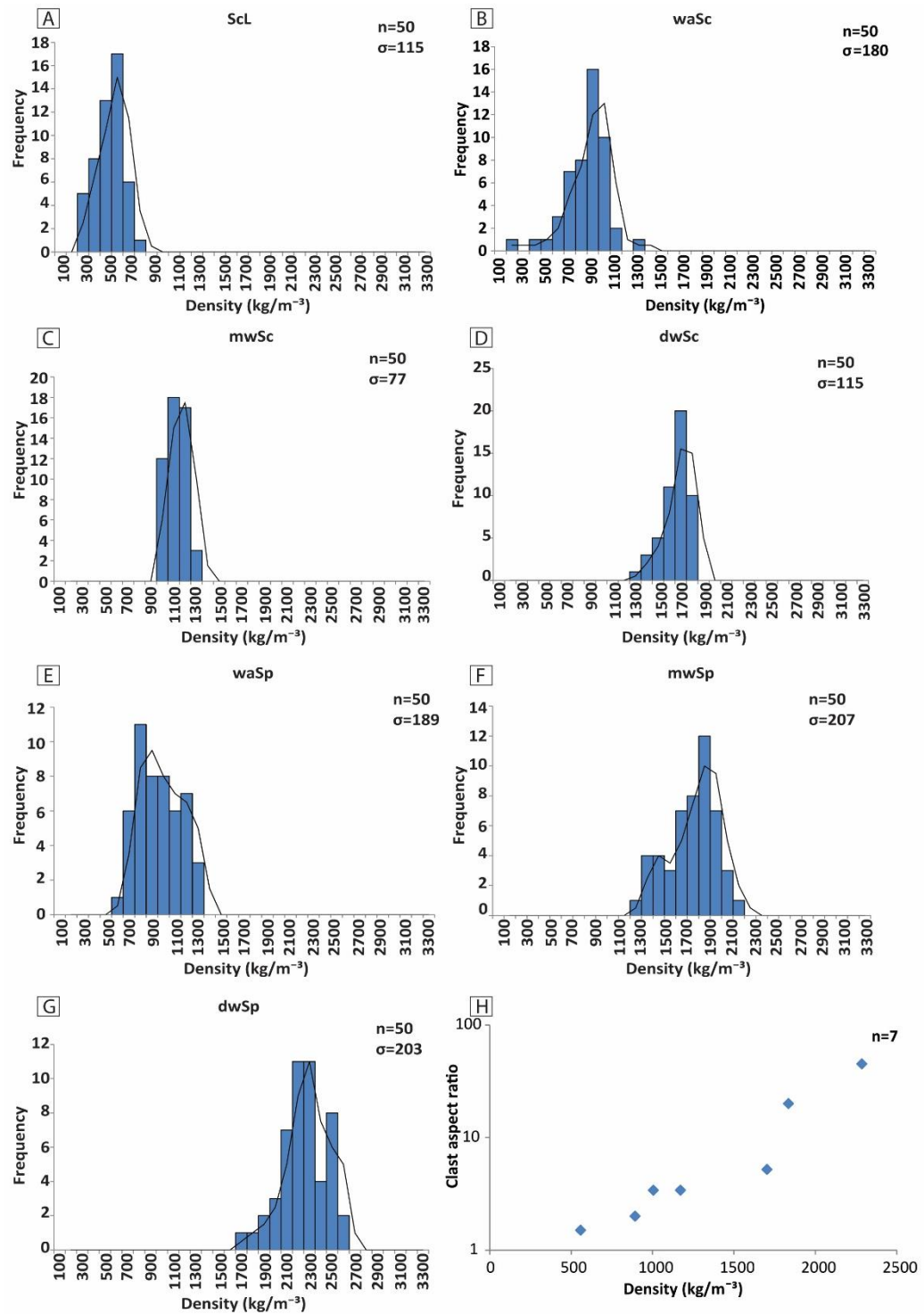


Figure 3.9. Density histograms for the pyroclastic lithofacies. (A) Scoria lapilli. (B) Incipiently welded scoria. (C) Moderately welded scoria. (D) Densely welded scoria. (E) Incipiently welded spatter. (F) Moderately welded spatter. (G) Densely welded spatter. (H) Graph showing that clast aspect ratio increases with density for the pyroclastic lithofacies (each point represents the mean of 50; see Table. 3.2).

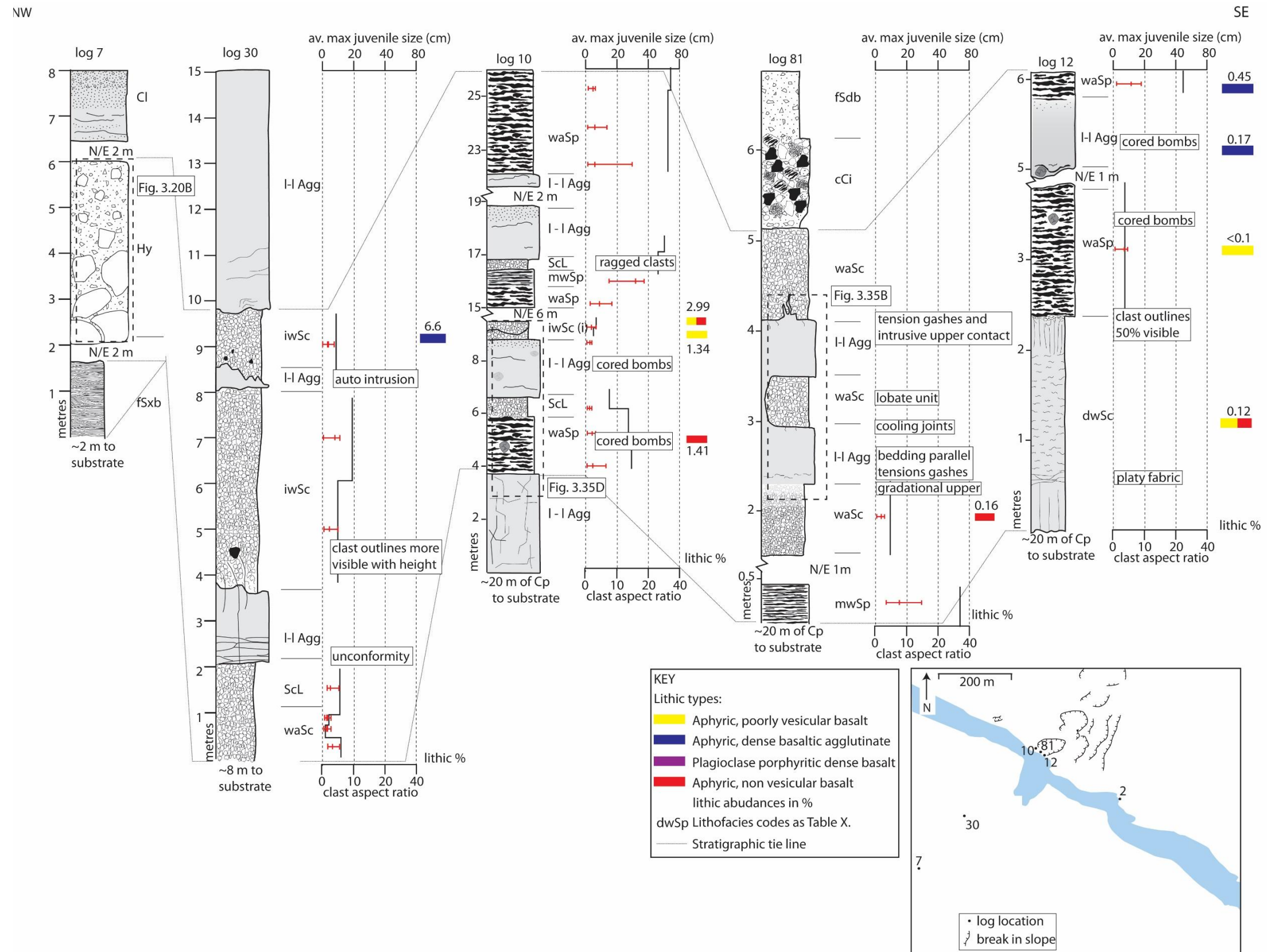


Figure 3.10. Stratigraphic logs showing variations in grain size (black line) and clast aspect ratio (red line); each the average of 10 measurements. Abbreviations for lithofacies are given in Table 3.2.

Note the restriction of the lithic clasts to within the crater.

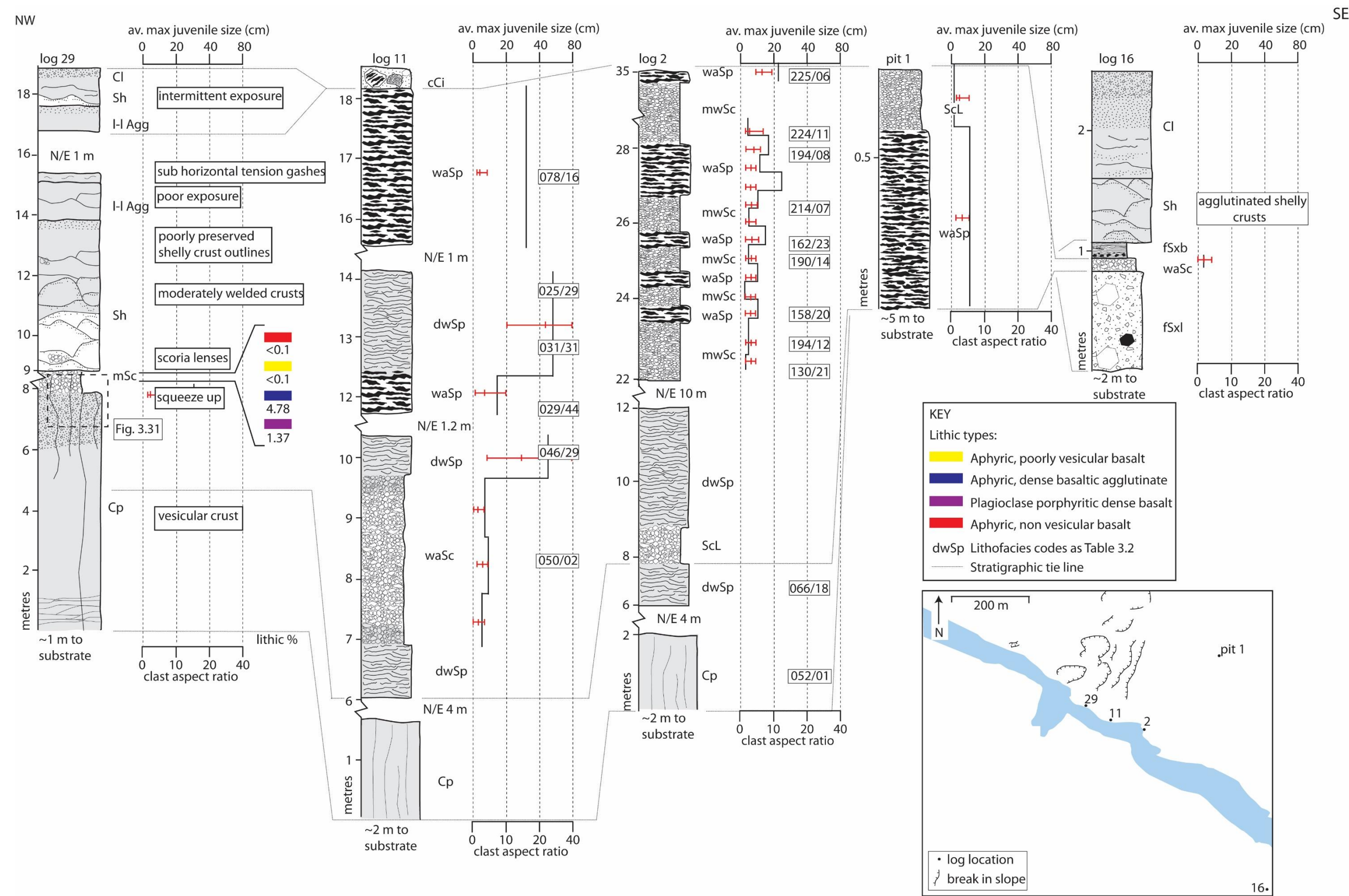


Figure 3.11. Stratigraphic logs showing variations in grain size (black line) and clast aspect ratio (red line); each the average of 10 measurements. Abbreviations for lithofacies are given in Table 3.2.

| Lithofacies | Description | Componentry | Occurrence | Structure | Interpretation |
|-------------|---|---|---|--|---|
| ScL | Non-welded scoria lapilli | Spindle shaped or ragged scoria lapilli | The crater of edifice 26; the scoria rampart (location 280); surrounding the spatter ramparts | Unconsolidated deposit or clast-supported; moderately well sorted; bedding defined by stratigraphic contacts and minor clast size fluctuations | Fall deposit from a lava fountain; Hawaiian or Strombolian activity |
| waSc (i) | Weakly agglutinated scoria lapilli; inversely graded sub facies (i) | Agglutinated spindle-shaped scoria lapilli and bombs; armoured clasts with cognate-clast cores | The crater of edifice 26; scoria ramparts (locations 280) beneath lava flows in medial and distal locations | Clast-supported; moderately well sorted; bedding defined by stratigraphic contacts and clast flattening | Fall deposit from the outer part or a high (>100 m) lava fountain; agglutination promoted by burst cores of clasts and rapid accumulation. Sub facies (i): results from grain flow avalanches |
| mwSc | Moderately welded scoria lapilli | Spindle bombs with burst rinds; scoria lapilli/bombs that agglutinate | The scoria rampart at location 280 | Clast-supported; moderately well sorted; bedding defined by stratigraphic contacts, minor clast size variation and clast flattening | Fall deposit from the inner part of a lava fountain or a high (>100 m) lava fountain |
| dwSc | Densely welded scoria lapilli | Agglutinated scoria lapilli and bombs | The crater of edifice 26 | Clast-supported; moderately well sorted; bedding defined by stratigraphic contacts and clast flattening; often with cooling joints | Fall deposit from the inner part of a lava fountain or a high (>100 m) lava fountain; cooling joints formed as a result of rapid accumulation |
| waSp | Weakly agglutinated spatter | Agglutinated cowpat and ribbon-shaped spatter bombs; armoured clasts and cored bombs with cognate-clast cores | The crater of edifice 26; the scoria rampart at location 280 | Clast-supported; well sorted; bedding defined by stratigraphic contacts and clast flattening | Fall deposit from the inner part of a lava fountain or a low fountain |
| mwSp | Moderately welded spatter | Agglutinated cowpat and ribbon-shaped spatter bombs | The crater of edifice 26; the scoria rampart at location 280 | Clast-supported; well sorted; bedding defined by stratigraphic contacts and clast flattening | As waSp; rapid accumulation promotes agglutination |
| dwSp | Densely welded spatter | Agglutinated and coalesced spatter bombs | The scoria rampart at location 280 | Clast-supported; well sorted; bedding defined by stratigraphic contacts and clast flattening | As waSp; rapid accumulation rate promotes coalescence of clasts |
| mSc | Massive scoria lapilli and bombs | Cauliflower-textured scoria lapilli and bombs; armoured clasts with accidental and cognate-clast cores | The vents of rootless cones | Clast-supported; moderately well sorted; massive; gradational contacts with underlying Cp | Fall deposit from a rootless lava fountain |
| vSpb | Volcaniclastic sandstone with planar bedding | Yellow/beige sand-grade matrix, blocks and cobbles of unknown provenance | Base of the R-K volcanic sequence along the strike of the dyke | Forms planar beds 100 mm thick | Fluvial sandstone or palagonitised tuff |

Table 3.2. Summary descriptions of pyroclastic lithofacies.

| Lithofacies | Crystallinity (%) | Clast aspect ratio | Density Mean (kg m ⁻³) | Density range (kg m ⁻³) | Vesicularity mean (%) | Vesicularity range (%) | Vesicle diameter (mm) | Av. Max clast size (mm) | Lithofacies thickness range (mm) | Maximum dispersal distance from fissure (m) |
|---|-------------------|--------------------|------------------------------------|-------------------------------------|-----------------------|------------------------|-----------------------|-------------------------|----------------------------------|---|
| SeL | 2 | 1 | 572 | 344–827 | 80 | 72–88 | <0.1–1.5 | 35 | 100–1750 | 464 |
| waSc (i) | 5 | 2 | 889 | 290–1332 | 70 | 55–90 | <0.1–2.4 | 55 | 50–3800 | 1247 |
| mwSc | 6 | 3 | 1172 | 1037–1349 | 60 | 57–82 | <0.1–2.6 | 48 | 75–1500 | 500 |
| dwSc | 8 | 5 | 1703 | 1332–1891 | 43 | 36–55 | <0.1–1.5 | 23 | 80–380 | 500 |
| waSp | 48 | 3 | 1005 | 623–1466 | 66 | 51–79 | <0.1–2.5 | 244 | 170–8000 | 420 |
| mwSp | 77 | 20 | 1835 | 1374–2218 | 38 | 26.0–38.8 | <0.1–3.3 | 823 | 340–2400 | 210 |
| dwSp | 86 | 45 | 2286 | 1705–2633 | 23 | 12–43 | <0.1–0.9 | >1000 | 470–1620 | 205 |
| mSc | 13 | 1.4 | - | - | - | - | <0.001–2.04 | 80 | 250–4000 | 130 |
| Table 3.3. Summary table of the texture, distribution and petrography of the pyroclastic lithofacies | | | | | | | | | | |

3.4.1 Lithofacies Descriptions

Lithofacies ScL – Clast-supported non-welded scoria lapilli

This lithofacies is composed of either spindle-shaped or ragged scoria lapilli (Fig. 3.6) that are often fragmented into angular fracture-bound clasts. Clasts are red, purple or black in colour. Their groundmass is holohyaline. Their brittle external rinds are <0.5 mm thick and glassy with hairline fractures. Clasts have a mean vesicularity of 80 %, ranging from 72–88% (see Appendix 1). The vesicles are <0.1–1.5 mm diameter and bubble septae are <0.5 mm thick (see Appendix 1).

The lithofacies is clast-supported and moderately well sorted. The constituent lapilli are non-welded and are easily dislodged by hand. Lithofacies density ranges from 344–827 kg m⁻³ (mean 572 kg m⁻³; Table 3.3). No clast flattening is observed (mean aspect ratio 1:1) and bedding is defined by distinct contacts with overlying lithofacies and minor clast size fluctuations between fine and coarse lapilli. The lithofacies occurs in units 100–1750 mm thick (see Appendix 1). Unconsolidated clast-supported non-welded scoria lapilli (ScL) surround the spatter ramparts west of the river (Fig. 3.3). The lithofacies occurs in the upper 20 m of the crater of cone 26 (log 10; Fig. 3.10) and ~400 m southeast from the fissure (pit 1; Fig. 3.11). It commonly over/underlies clast-supported weakly agglutinated scoria lapilli and bombs (waSc) and clast-supported incipiently welded spatter bombs (waSp) within edifice 26 and adjacent deposits.

Interpretation:

This lithofacies is interpreted as a fall deposit from a lava fountain (Head and Wilson 1989; Sumner et al. 2005). The spindle- and ragged-shaped clasts are typical of Strombolian and Hawaiian activity (Valentine and Gregg 2008). The absence of welding indicates that clasts were cool and brittle on deposition and they are inferred to have accumulated at a low rate from the upper and outer part of a lava fountain (e.g. Walker and Croasdale 1971; Head and Wilson 1989; Sumner et al. 2005). This fountain may have been intermittent, since intermittence promotes low-rate accumulation.

The association of this lithofacies with clast-supported weakly agglutinated scoria lapilli and bombs (waSc) and clast-supported weakly agglutinated spatter bombs (waSp; pit 1; Fig. 3.10) suggests that deposition from different parts of the fountain occurred in rapid succession due to rapidly changing fountain conditions (see section 3.4).

Lithofacies waSc(i) – Clast-supported weakly agglutinated scoria lapilli and bombs with inversely graded (i) sub facies

This lithofacies is composed of agglutinated spindle-shaped scoria lapilli (as described for clast-supported non-welded scoria lapilli; ScL), spindle bombs with fractured rinds and armoured clasts (<7 vol. %). The spindle bombs are red or black and have a holohyaline groundmass (see Appendix 1). Their brittle external rinds are <0.5 mm thick, resinous and often fractured, exposing a ~66% vesicular core that has extruded melt (Fig. 3.6). Clasts range from 55–90% vesicular (mean 70%) and vesicles are <0.1–2.4 mm diameter (see Appendix 1). Their septa are <0.5 mm thick and vesicles commonly have a flattened, eye-like shape. The armoured clasts are lapilli to bomb sized and have a core of cognate incipiently welded scoria lapilli or cognate dense agglutinate/lava. Their angular shape is formed by a singular coating of vesicular juvenile lava that partly encapsulates the core. These clasts are confined to the upper 15 m of the crater of cone 26.

The lapilli and bombs in this lithofacies are clast-supported and moderately well sorted. The scoria lapilli and bombs are incipiently welded, and some exhibit moderate amount clast flattening (mean aspect ratio 1:2). Lithofacies density ranges from 290–1332 kg m⁻³ (mean 889 kg m⁻³; Table 3.3). Bedding is defined by small variations in mean clast size and by the welding fabric. The lithofacies occurs in units 50–3800 mm thick and may have gradational or distinct contacts with over/underlying lithofacies (e.g. log 11; Fig. 3.11). This lithofacies occurs up to 1.2 km from the fissure (e.g. log 16; Fig. 3.10) and at the top of the R-K volcanic sequence (e.g. log 81; Fig. 3.10). It is also found beneath the oldest lavas west of the river (log 16; Fig. 3.11). The inversely graded sub facies (i) occurs within the crater of edifice 26 on moderate slopes (~10°). The lithofacies is commonly associated with clast-supported non-welded scoria lapilli (ScL) and spatter-dominated lithofacies (e.g. clast-supported incipiently welded spatter bombs; waSp; see Fig. 3.11).

Interpretation:

This lithofacies is interpreted as a fall deposit from the outer part of a lava fountain during Strombolian or Hawaiian-style activity. The spindle bombs are inferred to have fallen from the outer part of a lava fountain (e.g. Sumner et al. 2005). The cores of the burst bombs remained molten after deposition due to their large size. Impact-induced leakage of melt from the clasts resulted in the partial agglutination of adjacent and subjacent clasts (e.g. Sumner et al. 2005).

The armoured clasts indicate the ballistic ejection of lithic clasts during a single fountaining event. The bombs show no evidence of ductile deformation or impactation (e.g. a cowpat shape), thus are inferred to have cooled in-flight. They were formed in a fountain which was sufficiently spread to allow in-flight clast cooling. The cognate clast cores of the armoured clasts indicate removal of clasts from the vent region by collapse or remobilisation of pyroclasts into the vent.

Inversely graded scoria beds are typical of Hawaiian and Strombolian deposits (Valentine and Gregg 2008). Grading is inferred to result from grain flow avalanches (e.g. McGetchin et al. 1974); subsequent agglutination may have been promoted by the bursting of large bombs with molten cores. The abundance of the lithofacies across the study area indicates that it was produced from multiple sources along the fissure.

Lithofacies mwSc – Clast-supported moderately welded scoria lapilli and bombs

This lithofacies is composed of clast-supported and moderately well sorted spindle bombs with burst rinds (as described for clast-supported weakly agglutinated scoria lapilli and bombs; waSc) and agglutinated scoria lapilli/bombs. Agglutinated clasts are elongate (Fig. 3.6), with resinous purple/red rinds <0.5 mm thick. Clasts have a holohyaline groundmass and have a mean vesicularity of 60%, ranging from 57–82% (see Appendix 1). Vesicles are <0.1–2.6 mm in diameter and have a flattened eye-like shape. Their septae are <0.5 mm thick. Some clasts have folded rinds inside their cores.

The clasts are clast-supported and moderately well sorted. Lithofacies density ranges from 1037–1349 kg m⁻³ (mean 1172 kg m⁻³; Table 3.3). Moderate welding is indicated by clast mean aspect ratios of 1:3 and an associated loss of deposit pore space. The lithofacies forms planar beds 75–1500 mm thick (see Appendix 1), defined by stratigraphic contacts, clast flattening and clast size variation. The lithofacies is restricted to within 500 m of the fissure toward the southeast. It occurs ≤250 m from the fissure (e.g. log 2; Fig. 3.11) and has gradational contacts with overlying clast-supported incipiently welded spatter bombs (waSp).

Interpretation:

Agglutinated clasts are inferred to have been sourced from the inner part of a lava fountain during Hawaiian or Strombolian activity (e.g. Head and Wilson 1989; Sumner et al. 2005). The presence of internal rinds indicate recycling of clasts within the fountain (e.g. Sumner et al. 2005). Clast flattening indicates rapid accumulation of molten clasts.

Internal grain size variations may result from a variety of factors, as described for clast-supported non-welded scoria lapilli (ScL).

Lithofacies dwSc – Clast-supported densely welded scoria

This lithofacies is composed of densely welded clast-supported and moderately well sorted agglutinated scoria lapilli and bombs. Agglutinated clasts have resinous purple/red rinds <0.5 mm thick. The groundmass of the clasts is holohyaline (see Appendix 1). Clasts have a mean vesicularity of 43%, ranging from 36–55% (see Appendix 1). Vesicles are <0.1–1.5 mm in diameter and have a flattened eye-like shape. Bubble wall septae are <0.5 mm thick.

Lithofacies density ranges from 1332–1891 kg m⁻³ (mean 1703 kg m⁻³; Table 3.3). A distinctive fabric formed by clast flattening is visible (mean clast aspect ratio 1:5), although clast outlines are sometimes unclear due to dense welding. Clast flattening and stratigraphic contacts define beds 80–380 mm thick. Beds often have cooling joints spaced ~50 mm that penetrate the entire deposit thickness. The lithofacies occurs within the crater of edifice 26 (log 12, Fig. 3.10) and up to 500 m southeast of the fissure. It has distinct contacts with clast-supported incipiently welded spatter bombs (waSp), lava-like agglutinate (l-l Agg) and clastogenic pāhoehoe (Cl) and occurs in the upper 15 m of stratigraphy.

Interpretation:

This lithofacies is formed by the rapid accumulation of clasts, as described for clast-supported moderately welded scoria lapilli and bombs (mwSc). High accumulation rates are indicated by the dense welding and the formation of cooling joints which indicate that the beds cooled as a single unit.

Lithofacies waSp – Clast-supported weakly agglutinated spatter bombs

This lithofacies is composed of clast-supported and well sorted cored bombs (<5 vol. %) and agglutinated cowpat and ribbon-shaped spatter bombs with purple/red resinous rinds that are <0.5 mm thick. The spatter bombs are commonly >300 mm in diameter and overlap, often obscuring clast margins. Their groundmass is hypohyaline (see Appendix 1). Clasts have a mean vesicularity of 66%, ranging from 51–79% (see Appendix 1). Vesicles are <0.01–2.5 mm in size. Bubble septae are <0.5 mm thick and vesicles have a flattened, eye-like shape. Cored bombs are also found.

The cored bombs are sub-spherical and are often fractured and broken into jigsaw-fit fragments. Their sub-spherical shape is given by a 10 mm thick rind of multiple ~3 mm thick coatings of incipiently vesicular lava. The core of the bomb consists of cognate incipiently welded scoria lapilli or cognate dense agglutinate/lava.

The density of the lithofacies ranges from 623–1461 kg m⁻³ (mean 1005 kg m⁻³; Table 3.3). Weak agglutination has resulted in the minor flattening of clasts (mean aspect ratio 1:3). Clast flattening and stratigraphic contacts define planar beds which are 170–8000 mm thick (see Appendix 1). The lithofacies occurs up to 400 m from the fissure toward the southeast, and ~200 m toward the northwest. The lithofacies is common in the uppermost parts of the stratigraphy and is associated with edifice building sequences (e.g. log 2; Fig. 3.11). It rapidly grades vertically into densely welded lithofacies (e.g. clast-supported densely welded spatter bombs; dwSp, log 11; Fig. 3.11), and has sharp contacts with densely-welded lithofacies (e.g. clast-supported densely welded scoria; dwSc, log 12; Fig. 3.11).

Interpretation:

Spatter bombs are commonly deposited via fallout from the inner parts of the lava fountain or from low fountains during Hawaiian or Strombolian activity (Wolfe et al. 1988; Head and Wilson 1989; Sumner et al. 2005). The accumulation rate of pyroclasts was sufficiently low to prevent significant welding and allowed clast outlines to be preserved (Head and Wilson 1989; Sumner et al. 2005).

Cored bombs are formed by the recycling of pyroclasts or wall rock during Hawaiian or Strombolian activity (e.g. White and Houghton 2006; Valentine and Gregg 2008). The cognate clast cores of the cored bombs indicate removal of clasts from the vent region by collapse or remobilisation of pyroclasts into the vent. Their spherical shape is attained by: ball milling within the crater of an edifice during intermittent explosions (e.g. McGetchin et al. 1974); rolling down the outer slopes of a cone (e.g. Francis 1973); the presence of large clasts near the centre of the bomb (Rosseel et al. 2006) or moulding by surface tension (e.g. Macdonald 1972; Fisher and Schmincke 1984). These processes are not mutually exclusive. The multiple rinds suggest that the clasts were recycled within the vent during numerous fountaining events. The abundance of fractured and fragmented clasts indicates that traction occurred after the clast had cooled.

Lithofacies mwSp – Clast-supported moderately welded spatter bombs

This lithofacies is composed of clast-supported and well sorted agglutinated cowpat and ribbon-shaped spatter bombs. Their groundmass is hypocrySTALLINE. Clasts are commonly >300 mm length (see Appendix 1); they are recognised by their relict vesicular cores. Their purple/red rinds are difficult to discern, where visible they are <0.5 mm thick and deformed. Clasts have a mean vesicularity of 38%, ranging from 26–38% (see Appendix 1). Vesicles are <0.1–3.3 mm in size. The vesicles are often isolated in the groundmass and have a flattened, eye-like shape.

Lithofacies density ranges from 1374–2218 kg m⁻³ (mean 1835 kg m⁻³; Table 3.3). The lithofacies is moderately welded and clasts have mean aspect ratios of 1:20. Clast flattening and stratigraphic fabrics define 340–2400 mm thick beds which are common in the uppermost parts of the R-K volcanic sequence (see Appendix 1). The lithofacies occurs within the upper 10 m of the R-K volcanic sequence and is associated with edifice building sequences (e.g. log 81; Fig. 3.10), rapidly grading into more/less densely welded deposits. Alternatively, the lithofacies may have distinct stratigraphic contacts (e.g. log 10; Fig. 3.10). It is located ≤210 m from the fissure toward the southeast and 195 m from the fissure toward the northwest.

Interpretation:

Spatter bombs are commonly deposited via fallout from the inner parts of the lava fountain or from low fountains during Hawaiian or Strombolian activity (Wolfe et al. 1988; Head and Wilson 1989; Sumner et al. 2005). Clast flattening indicates rapid accumulation of molten clasts and suggests increased accumulation rates relative to clast-supported incipiently welded spatter bombs (waSp).

Lithofacies dwSp – Clast-supported densely welded spatter bombs

This lithofacies is composed of clast-supported and well sorted agglutinated and coalesced spatter bombs. Clasts are often difficult to recognise; where discernible ghost clasts are commonly >300 mm length. The groundmass of this lithofacies is hypocrySTALLINE (see Appendix 1) and has a laminated appearance due to variations in groundmass crystallinity. The laminations are 0.5 mm thick and are sub-parallel. Vesicles occur within the more crystalline laminations and have an irregular shape. The lithofacies has a mean vesicularity of 23%, ranging from 12–43%. Vesicles are <0.1–0.9 mm in size (see Appendix 1).

The density of the lithofacies ranges from 1705–2633 kg m⁻³ (mean 2286 kg m⁻³; Table 3.3). Dense welding is recognised by intensely flattened clasts with mean aspect ratios of 1:45. Clast flattening and stratigraphic contacts define 470–1620 mm thick beds which are common throughout the R-K volcanic sequence (see Appendix 1). The lithofacies occurs in the upper 30 m of the R-K volcanic sequence and is associated with edifice building sequences (e.g. log 11; Fig. 3.11). The lithofacies rapidly grades into more/less densely welded deposits. Alternatively, it may have distinct contacts with other lithofacies (e.g. log 11; Fig. 3.11). It occurs in the crater of edifice 26 and up to 205 m southeast from the fissure. It also found west of the river, ~150 m from the fissure toward the southeast.

Interpretation:

This lithofacies is interpreted to have formed under similar conditions as clast-supported moderately welded spatter bombs (mwSp) but is inferred to have accumulated more rapidly. The laminated textured is inferred to result from intense welding. The crystal-rich laminations that contain vesicles are interpreted as the relict cores of spatter bombs. The crystal-poor laminations are interpreted as the relict chilled margins of flattened clasts.

Lithofacies vSpb – volcanoclastic sandstone with planar bedding

Outcrops of this lithofacies have only been observed with binoculars due its inaccessibility. It has an apparent yellow/beige sand-grade matrix and ~20 % blocks and cobbles. It forms planar beds ~100 mm thick that dip ~12° to the east (see Appendix 1). The lithofacies occurs towards the base of the R-K volcanic sequence and forms a lenticular deposit ~5 m thick and ~20 m in length. Its contacts with the adjacent and overlying lithofacies (clast-supported weakly agglutinated scoria lapilli and bombs; waSc) are defined by a distinct yellow/beige–brown colour change. Its basal contact is not exposed. It outcrops only on the west of the river along the strike of the fissure.

Interpretation:

I am unable to determine the genesis of the lithofacies from its geometry, contacts or componentry. It is probably a fluvial sandstone or a palagonitised tuff. If the lithofacies represents palagonitised tuff the blocks and cobbles are accidental clasts removed during explosive magma-interaction. Its occurrence only along the base of the R-K volcanic

sequence suggests protracted magma-water interaction during opening of the fissure. The deposits could be fall deposits or pyroclastic density current deposits (e.g. Wohletz and Sheridan 1983).

If the lithofacies represents a fluvial deposit the blocks and cobbles are clasts eroded from the underlying R-K volcanic sequence (see section 3.4). The distribution of the lithofacies at the base of the R-K volcanic sequence would be consistent with deposition in a river channel (e.g. Stow 2005).

Lithofacies mSc – Massive scoria lapilli and bombs

This lithofacies is composed of clast-supported and moderately well sorted scoria lapilli and bombs and armoured clasts (<5 vol. %). The scoria lapilli and bombs have a convoluted, cauliflower-like surface texture defined by furrows in the clast rind (Fig. 3.6). Clasts are often fragmented into angular shapes. Their groundmass is hypohyaline (see Appendix 1). Vesicles are <0.1–2.0 mm in diameter (see Appendix 1). Some clasts may have thick (≤ 10 mm) bubble septae. The armoured clasts are similar to those described for clast-supported weakly agglutinated scoria lapilli and bombs (waSc), but their lithic cores are composed variably of 1) aphyric, non-vesicular basaltic lava; 2) plagioclase porphyritic dense basalt; 3) aphyric, dense basaltic agglutinate; 4) plagioclase porphyritic, poorly vesicular basalt; 5) aphyric, poorly vesicular basalt.

Clasts are without flattening (clast aspect ratio 1:1; Table 3.3). The lithofacies forms a 1 cm thick margin on the columnar-jointed pāhoehoe with which it is always associated (see section 3.5). It was impossible to sample sufficient quantities of this lithofacies to calculate its density. The lithofacies has cooling joints spaced ~20 mm apart that penetrate into the underlying columnar-jointed pāhoehoe (Cp; Fig. 3.11). This lithofacies is only found 95 m southeast of the fissure (location 285; log 29, Fig. 3.11). It has gradational contacts with the columnar-jointed pāhoehoe (Cp) and is restricted to the lower 10 m of the R-K volcanic sequence.

Interpretation:

This lithofacies has many similar features to the proximal deposits of rootless eruptions, including a lapilli–bomb sized pyroclast population (e.g. Chapter 4; Hamilton et al. 2010); abundant lithic clasts (e.g. Chapter 4; Mattox and Mangan 1997) and an association with inflated lava flows (e.g. Chapter 4; Fagents et al. 2002; Fagents and Thordarson 2007; Hamilton et al. 2010). The component juvenile clasts differ from those

of other weakly agglutinated lithofacies (e.g. clast-supported weakly agglutinated scoria lapilli; waSc) since they have a cauliflower-like surface texture (Fig. 3.6). This surface texture suggests that cooling was partly water induced, similar to the bulbous and bread-crust clasts described by Kokelaar (1986) and Mattox and Mangan (1997) respectively. The clasts also have thicker bubble walls than clast-supported weakly agglutinated scoria lapilli and bombs (waSc), suggesting that clasts are denser and underwent degassing prior to fragmentation (Fig. 3.9). The scoria clasts are thus interpreted to be a fall deposit from a rootless lava fountain (e.g. Mattox and Mangan 1997; Hamilton et al. 2010).

The rootless fountains formed during rootless explosions proximal to the fissure, suggesting that there was abundant surface water during the R-K eruption. (e.g. Jurado-Chichay et al. 1996; Mattox and Mangan 1997; Hamilton et al. 2010). The association of the massive scoria with the columnar-jointed pāhoehoe (Cp) indicates a genetic link between the two lithofacies; the columnar-jointed pāhoehoe (Cp) is inferred to be the host lava flow for rootless eruptions (see section 3.7.2).

The aphyric lithic cores of the armoured clasts are interpreted as clasts sourced from the crust of the host lava flow during rootless cone formation. The plagioclase porphyritic cores are interpreted as accidental clasts removed during rootless activity. The clasts are not thought to represent accidental clasts removed from the conduit region for two reasons. Firstly, the clasts are more than twice as abundant as those reported in other Hawaiian eruptions (e.g. Valentine and Groves 1996; Valentine 2012). Secondly, if the clasts represent clasts removed from the conduit, it is necessary to account for their occurrence in the rootless deposits. Perhaps the clasts had been removed from the conduit, deposited, and then erupted again from beneath the columnar-jointed pāhoehoe (Cp) during rootless activity. However, the clasts show no evidence of having been erupted twice (i.e. multiple coatings of lava).

3.4.2 Distribution of the pyroclastic lithofacies

Many of the pyroclastic lithofacies are asymmetrically distributed towards the east (e.g. clast-supported moderately welded scoria lapilli and bombs, mwSc; clast-supported weakly agglutinated scoria lapilli and bombs, waSc; clast-supported non-welded scoria lapilli, ScL). North westerly winds are dominant in Iceland today (Einarsson 1984) and were dominant in the mid-Holocene (e.g. Mauri et al. 2013 and references there-in). Therefore, the asymmetric distribution may result from the clasts stripping of the lava fountain by north-westerly winds. Alternatively, the asymmetry may suggest that the

fountain was inclined (e.g. Capaccioni and Cuccoli 2005). Some lava fountains are both inclined and affected by strong winds (e.g. Geist et al. 2008). The asymmetric distribution is not inferred to result from post-eruption fluvial erosion (see section 3.4.1). The observed R-K tephra thickness distribution (Fig. 3.12) is comparable to that of the 1959 Hawaiian-style Kilauea Iki eruption, which thinned to ≥ 150 cm at a distance of 1 km from the vent (Houghton et al. 2006). This eruption had a maximum fountain height of 570 m (Parfitt 1998). The restriction of clasts 1 m in size to within 600 m of the vent (Fig. 3.12) is similar to that of the Tavuyaga tephra, also the product of a Hawaiian-style eruption (Cronin and Neall 2001).

3.4.3 Temporal variations in pyroclast welding intensity, bedding and contacts

The aspect ratio of clasts and the bulk density of a lithofacies can be used to indicate welding intensity. Progressive increases in welding intensity can result from increases in the rate of accumulation of pyroclasts from a lava fountain. Increases in accumulation rates can result from increases in fountaining intensity, sustained fountaining or a more collimated fountain (i.e. less widely spread; see Head and Wilson 1989; Wolff and Sumner 2000; Sumner et al. 2005). Bedding (defined by minor clast size fluctuations) can also result from variations in the height and inclination of the fountain. In the R-K volcanic sequence, the gradational and distinct contacts with over/underlying lithofacies suggest both gradual and sudden changes in fountain conditions.

3.4.4 Variations in componentry

Cored bombs with cognate-clast cores are only found in the crater of edifice 26 in the lava-like agglutinate lithofacies (l-l Agg) and clast-supported weakly agglutinated spatter bombs lithofacies (waSp; e.g. log 10 and 12; Fig. 3.10). Cored bombs are absent from early pyroclastic deposits but become common in the upper ~15 m of the deposits of the R-K eruption sequence. These bombs indicate intermittent lava fountaining, perhaps triggered by decreasing magma flux in the later stages of the eruption (e.g. Swanson et al. 1979; Thordarson and Self 1993; Parfitt 2004) or bursting of gas bubbles in the conduit (e.g. Wolfe et al. 1988).

Armoured clasts with cognate cores in lithofacies massive scoria lapilli and bombs (mSc) account for <1–5 vol. % of the clast population (logs 29, Fig. 3.10). They are interpreted fragments of the host lava flow and indicate widening of rootless vents. Armoured clasts are also common (<1–7 vol. %) in lithofacies clast-supported weakly

agglutinated spatter bombs (waSp) and clast-supported weakly agglutinated scoria lapilli and bombs (waSc) towards the top of the R-K volcanic sequence. They are inferred to indicate the collapse of R-K pyroclasts back into the vent. Collapse processes and grain flow avalanches, common during many scoria cone eruptions, provide a mechanism for generating the cognate clasts (e.g. McGetchin et al. 1974; Heiken 1978; Valentine et al. 2005; Mattsson and Tripoli 2011; Alvarado et al. 2011).

Armoured clasts with accidental lithics as cores are restricted to the massive scoria lapilli and bombs (mSc) in the lower 10 m of the R-K volcanic sequence. This lithofacies is interpreted as rootless tephra (see section 3.4). The accidental clasts occur in low abundances (1–2 vol. %; log 29, Fig. 3.11). They are interpreted as clasts fragmented from the pre-R-K eruption lavas during rootless eruptions. Their restriction to the lowermost deposits of the R-K eruption sequence suggests that their deposition is dependent on rootless activity whilst surface water was abundant.

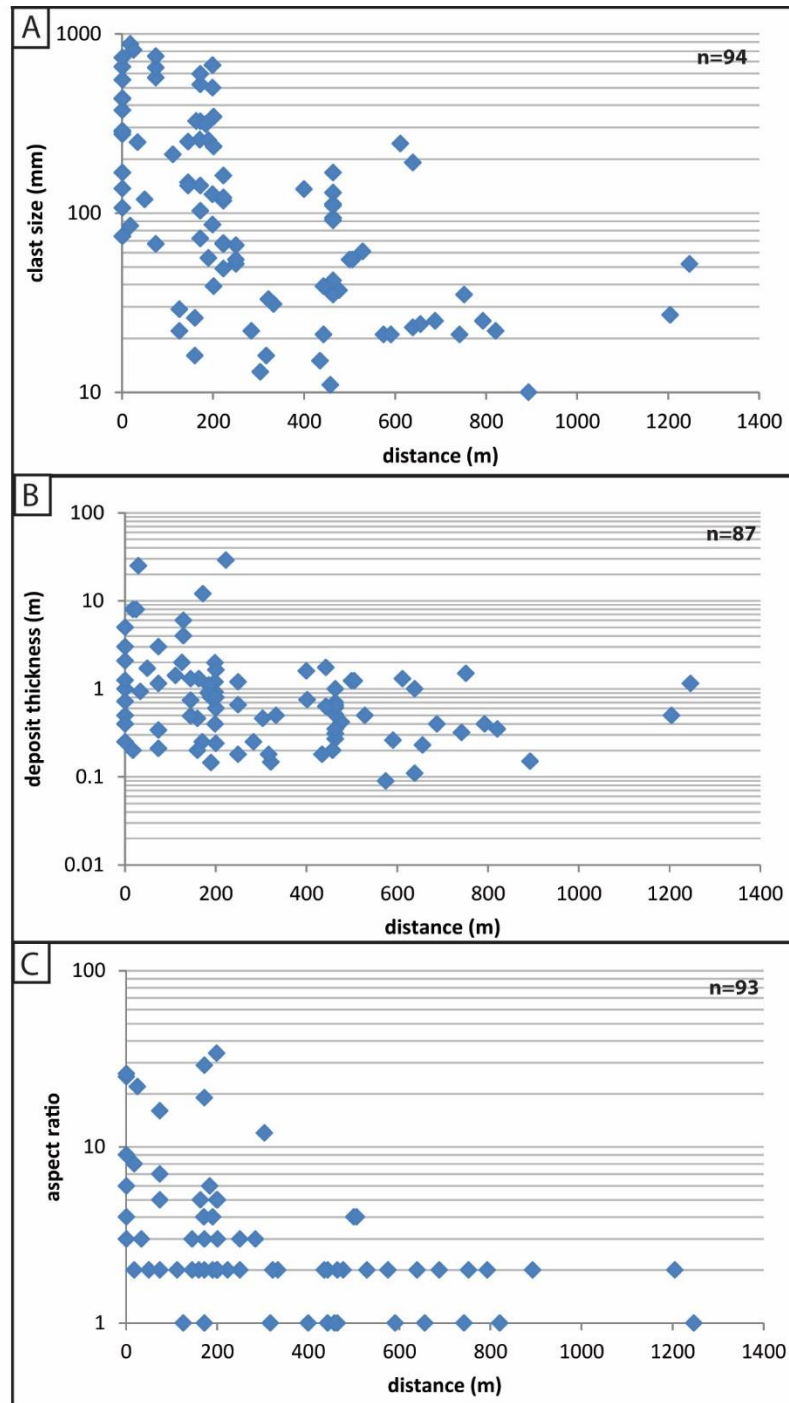


Figure 3.12. Dispersal and welding characteristics of the tephra and lavas. (A) Graph to show the relationship between distance from the fissure (m) and pyroclast size (mm). Pyroclasts decrease in size with distance. (B) Graph to show the relationship between distance from the fissure (m) and pyroclast lithofacies thickness (m). Deposits thin with distance. (C) Graph to show the relationship between distance from the fissure (m) and aspect ratio. Clast aspect ratio (i.e. welding intensity) decreases with distance. For descriptions of lithofacies see Tables 3.1 and 3.2.

3.5 Lava flow field architecture

A variety of lavas were emplaced during the R-K eruption (Figs. 3.13). The lavas are generally confined within the Sveinar graben. Assuming an average thickness of 15 m for the lavas, an average width of 750 m for the graben and a length of 75 km for the R-K fissure, I estimate that the R-K eruption produced $<1 \text{ km}^3$ of lava. This calculation ignores the contribution from pyroclasts, commonly considered a minor contribution during basaltic fissure eruptions (Thordarson and Self 1993). The lavas are differentiated by crust morphology, vesicle structure, internal texture and jointing. The groundmasses of the lavas also display differences in crystallinity and texture (Fig. 3.14). The density of lavas with an inferred pyroclastic origin is shown in Fig. 3.15. Their petrography is summarised in Table 3.4.

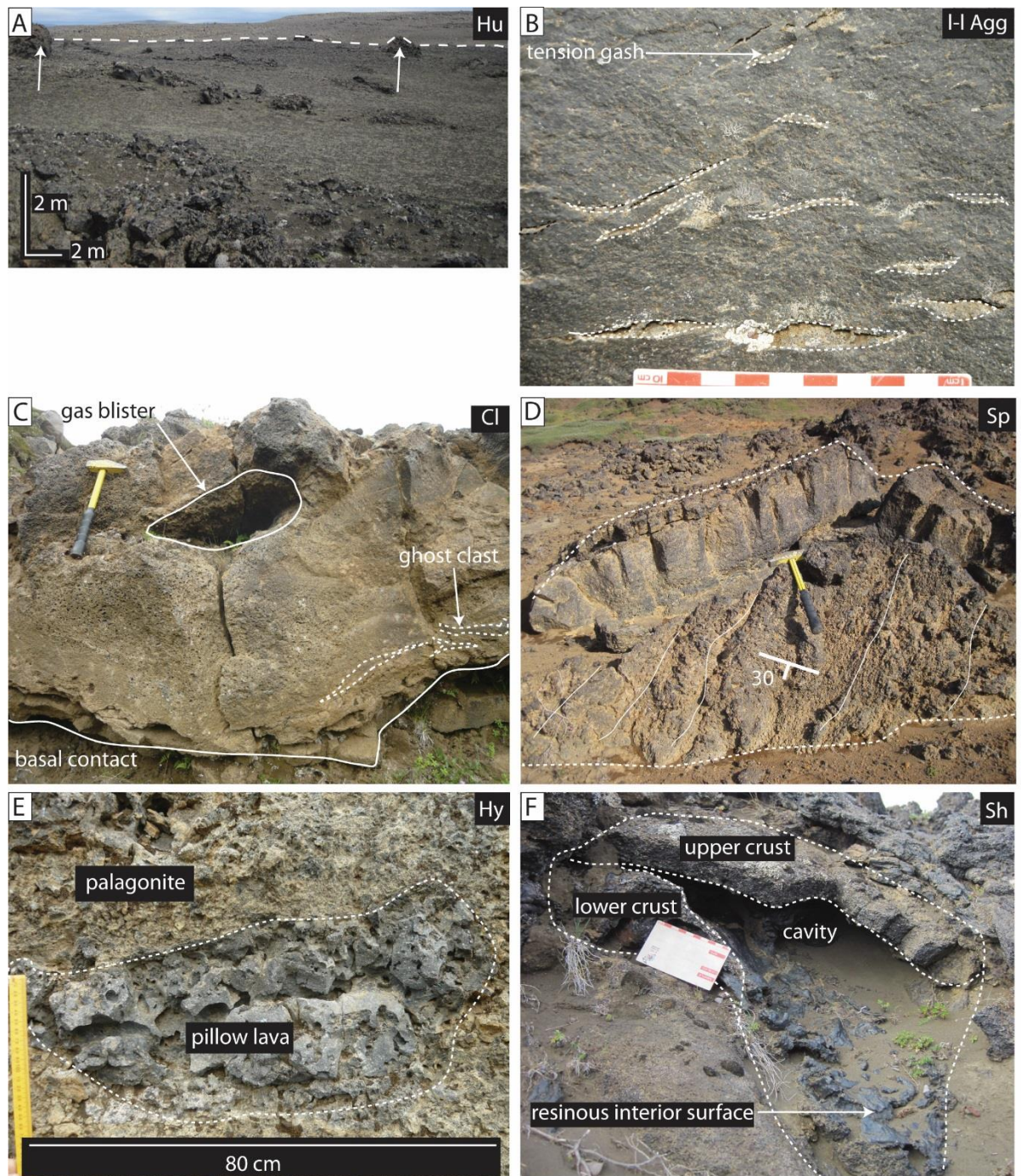


Figure 3.13. Lavas observed in the study area. (A) Hummocky lava (Hu) with little erosional dissection. Tumuli and squeeze outs (arrowed) create the hummocky topography. The contact with pre-existing topography is marked by the dashed line. (UTM 556219/7266138). (B) Lava-like agglutinate. Tension gashes (dashed outline) are sub-parallel to the basal contact (UTM 557447/7264902). (C) Clastogenic pāhoehoe (Cl). Gas blisters (outlined) are common. Ghost clasts are identified by intensely deformed non- and incipiently vesicular patches (dashed outline). (UTM 556985/7264113). (D) Crust of spiny pāhoehoe (dashed outline). The crust dips 30°

toward the viewer. Spines on the surface of the crust are oriented parallel to the solid white lines. Hammer for scale. (UTM 557457/7265092). (E) Hyaloclastite. The pillow lava (dashed outline) occurs in a matrix of palagonitised pillow fragments. (UTM 558272/7263904). (F) Shelly pāhoehoe. The crusts and internal cavity is visible. The resinous interior surface is thought to be caused by draining of lava from the lobe (UTM 557463/7264067).

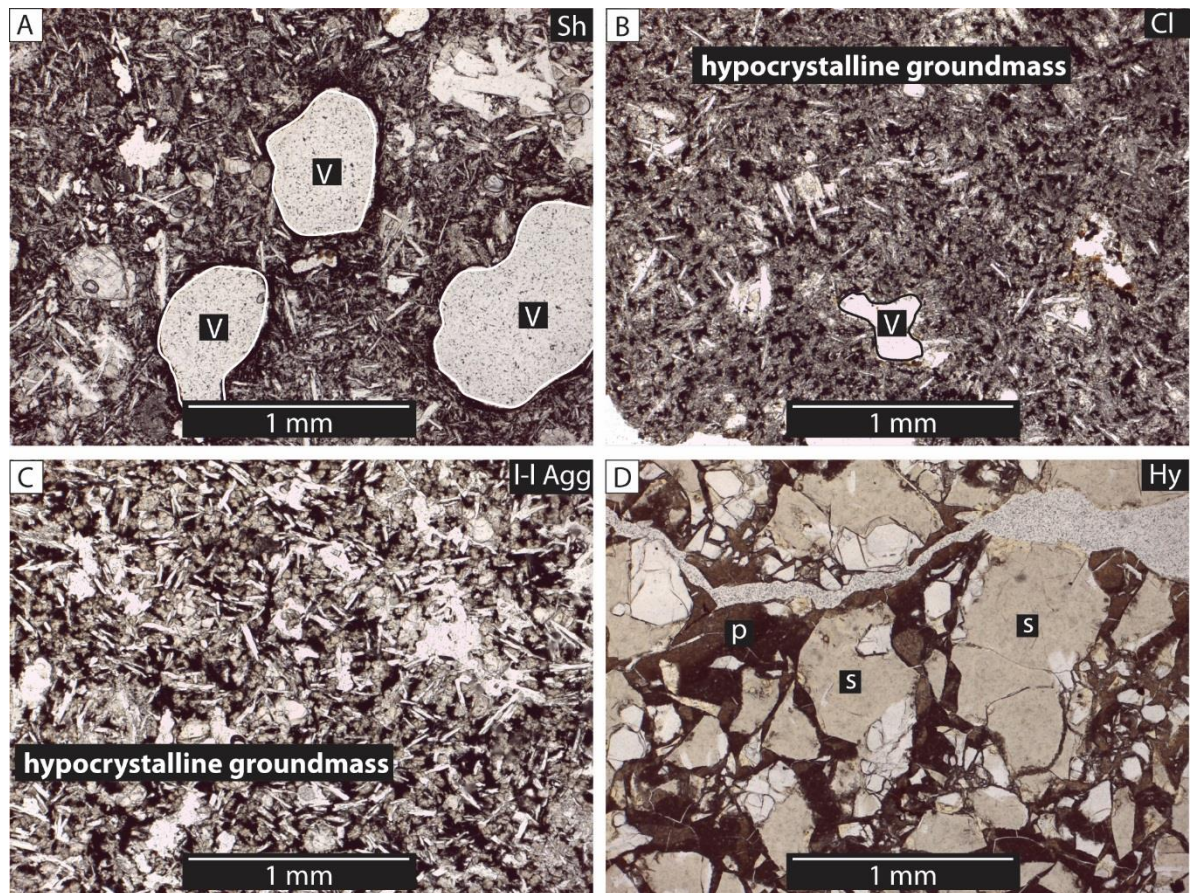


Figure 3.14. Thin section images of lavas (plane polarised light). (A) Shelly pāhoehoe. Note the large vesicles. (B) Clastogenic pāhoehoe. (C) Lava-like agglutinate. (D) Hyaloclastite. The thin section is taken from the palagonite matrix. Vesicles are labelled v; sideromelane fragments are labelled s and palagonite is labelled p.

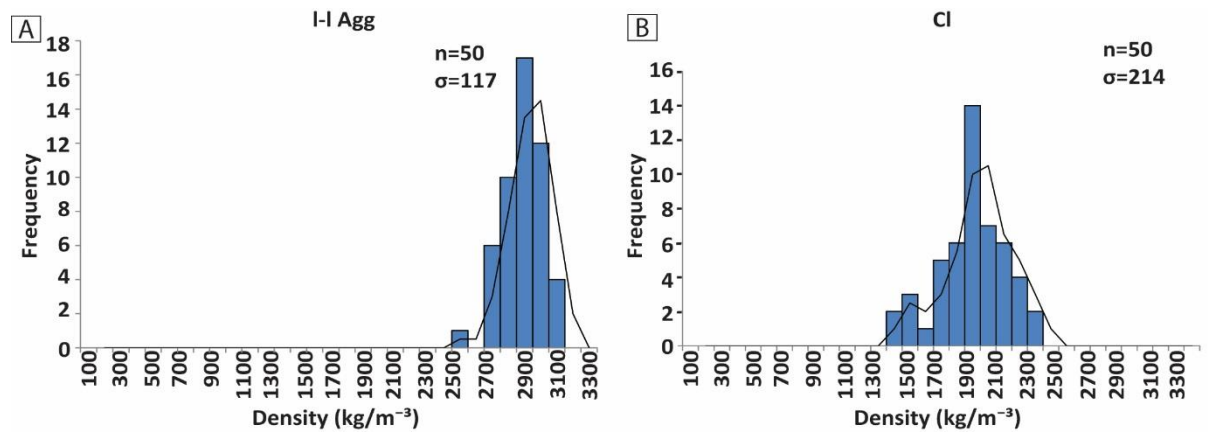


Figure 3.15. Density histograms for lava lithofacies with a pyroclastic origin. (A) Lava-like agglutinate. (B) Clastogenic lava.

| Lava type | Crystallinity (%) | Density Mean (kg m ⁻³) | Density range (kg m ⁻³) | Vesicularity mean (%) | Vesicularity range (%) | Vesicle diameter (mm) | Lithofacies thickness range (mm) | Interpretation |
|---|-------------------|------------------------------------|-------------------------------------|-----------------------|------------------------|-----------------------|----------------------------------|---|
| Cp | - | - | - | 30 | - | - | 1500–20000 | Inflated pāhoehoe lava, sheet-like or hummocky flows |
| Cl | 85 | 1943 | 1450–2322 | 35 | 22–51 | - | 510–3700 | Produced by coalescence and subsequent flow of pyroclasts from the inner part of the lava fountain or a low fountain; lava possessed a yield strength on degassing; likely to contain a component of effused lava |
| Hu | - | - | - | - | - | - | - | Inflated pāhoehoe lava |
| I-I Agg | 75 | 2747 | 2461–2964 | 8 | 1–17 | <0.1–0.55 | 500–29000 | Produced by coalescence and subsequent flow of pyroclasts from the inner part of the lava fountain or a low fountain |
| Sp | - | - | - | - | - | - | - | Down-flow transition of pāhoehoe caused by increase in substrate inclination |
| Hy | - | - | - | - | - | - | - | Formed by the entry of lava into bodies of surface water |
| Sh | 34 | - | - | - | - | - | 255 – 1620 | Gas rich lava effused from vents, also found as rafted debris and/or breakouts from parent clastogenic flows |
| Dyke* | 86 | - | - | - | - | - | - | Feeder dyke for the R-K eruption |
| Table 3.4. Summary table of lavas and dyke (* sample depth 80 m beneath paleo-surface) | | | | | | | | |

Cp – Columnar-jointed pāhoehoe

Columnar-jointed pāhoehoe outcrops on the Jökulsá canyon walls and many of the outcrops are inaccessible. Where accessible, the flows are characterised by a layered structure defined by vesicle abundance. The upper vesicular crust constitutes 25% of the flow thickness (Fig. 3.11) and is ~30 % vesicular (visual estimate). Megavesicles (Fig. 3.16) occur at the base of the crust (e.g. Thordarson and Self 1998). The dense core of the flows constitutes 75% of the flow thickness. The lower 10% of the core often has a sub-horizontal platy fabric, defined by fractures spaced 5–30 mm (Fig. 3.16). Vesicle cylinders are also found within the core (Fig. 3.16). The bases of the flows have not been observed. The flows are characterised by columnar joints that define a colonnade and an entablature. The joints are spaced 15–215 mm in the crust (mean 131 mm) and 250–450 mm in the cores (mean 352 mm). The basalt occurs on sub-horizontal slopes and has a morphology that varies from hummocky to sheet-like. The sheet-like units (Fig. 3.16) maintain a near-constant thickness across their length and have sub-parallel upper and lower contacts. The hummocky flows (Fig. 3.16) have an irregular shape and complex contacts between their cores and crusts.

The pāhoehoe flows vary from 1.5–20 m in thickness. They occur throughout the R-K volcanic sequence, though sheet-like units are dominant towards the base. The basalt often forms ≥ 50 % of the total stratigraphic thickness of the R-K eruption products. Spatially, the columnar-jointed pāhoehoe is generally confined within the Sveinar graben. The eastern Sveinar graben fault is poorly defined south of the river and occurs as segmented faults (F 31–33; Fig. 3.4). Fault 31 dips sub-vertically southeast whilst faults 32 and 33 dip sub-vertically northwest. The faults do not offset the R-K volcanic sequence but create thickness variations in the columnar-jointed pāhoehoe (Cp). West of the river fault 33 offsets the pre-eruptive topography by up to 20 m and the columnar-jointed pāhoehoe (Cp) pinches out against the footwall. There is 6 m of displacement of the columnar-jointed pāhoehoe (Cp) which has been emplaced on the graben footwall.

Northwest of the dyke the columnar-jointed pāhoehoe (Cp) has a distinct, sub-horizontal upper contact with the overlying clast-supported incipiently welded spatter bombs (waSp), clast-supported weakly agglutinated scoria lapilli and bombs (waSc) and hummocky pāhoehoe (Hu). The basalt contains lenses of clast-supported weakly agglutinated scoria lapilli and bombs (waSc) up to 10 m in diameter. At location 292 contacts are distinct with the overlying massive scoria lapilli and bombs (mSc).

Interpretation:

The vesicle-defined layered structure indicates that the columnar-jointed pāhoehoe inflated. Inflation requires emplacement on low angle slopes, a continued and sustained input of lava beneath a cooled crust and low effusion rates (e.g. Hon et al. 1994; Self et al. 1998). Many inflated lavas are also clastogenic in origin, but little evidence of their clastogenic origin is retained (Thordarson and Self 1993). The platy zone of the lavas records late stage horizontal shear along internal velocity boundaries in active lavas (Mackin 1961). The presence of entablature jointing suggests water-induced cooling (e.g. Long and Wood 1986; Forbes et al. 2012; Forbes et al. 2014), possibly caused by the lavas damming rivers. However, there are no foreset-bedded pillow breccias associated with the lavas (e.g. Huscroft et al. 2004) or lava channelization Hamblin (1994), commonly associated with lava dams.

The sheet-like flows are inferred to result from higher effusion rates and/or lower gradient slopes (Self et al. 1998). The hummocky flows indicate a moderate effusion rate/lava flux and/or increased substrate inclination. These factors resulted in differential inflation and the failure of numerous lobes to coalesce (Self et al. 1998; Guilbaud et al. 2005).

The stratigraphic thickness and abundance of the columnar-jointed pāhoehoe (Cp) suggests that inflation of pāhoehoe lobes was the dominant emplacement mechanism during the early stages of the R-K eruption. The pinching out of the columnar-jointed pāhoehoe (Cp) against the footwall of fault 33 suggests that the fault existed prior to the eruption. Thickness variations in the columnar-jointed pāhoehoe (Cp) overlying faults 31–33 suggest that either the faults developed during the eruption and the overlying lavas were viscous enough to have deformed in a ductile fashion, or that the faults pre-dated the eruption.

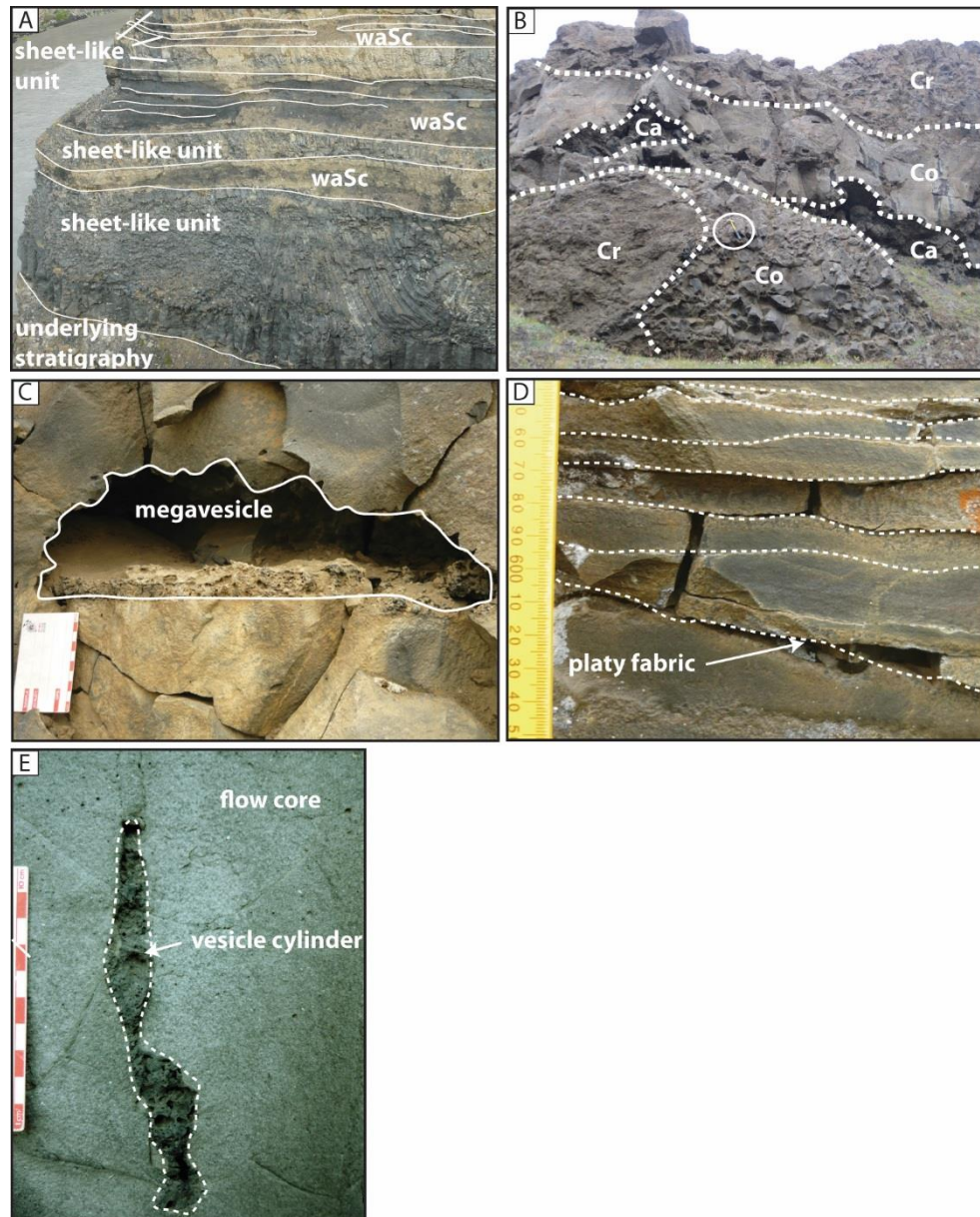


Figure 3.16. Features of the columnar-jointed pāhoehoe. (A) Alternating beds of sheet-like columnar-jointed pahoehoe (Cp) and clast-supported weakly agglutinated scoria lapilli and bombs (waSc) (UTM 557469/7264936). (B) Hummocky morphology flow (sensu Self et al. 1998); Cr: crust, Co: core, Ca: cavity. The hammer (circled) is 30 cm long. (UTM 557145/7265409). (C) Megavesicle in the flow core. Graticules on the scale card are 10 cm. (UTM 557772/7265756). (D) Platy fabric observed towards the base of the flow. The scale on the ruler is mm. (UTM 557772/7265756). (E) Vesicle cylinder in the core of a flow. Graticules on the scale card are 1 cm. (UTM 557544/72651054).

Cl – Clastogenic pāhoehoe

These lava flows have a ropey upper surface. Their groundmass is composed of hypocrySTALLINE, highly deformed and coalesced agglutinate with rare cored bomb ghost clasts (Fig. 3.17). They have a mean vesicularity of 35%, ranging from 22–51%. Vesicles are sub-horizontally aligned in bands ~10 cm thick or are randomly oriented. Vesicles are distributed throughout the flows. The density of the lava ranges from 1450–2322 kg m⁻³ (mean 1943 kg m⁻³). Ghost clasts occur throughout the entire thickness of the flow but are more common toward the base. They are 80–3700 mm in length with aspect ratios of 1:2–1:93. Gas blisters ~190 × 220 mm in size occur in many of the flows, often at or above the horizontal medial plane. The vesicularity of the lava increases towards the gas blisters forming an upper, spongy-type crust. This spongy crust lacks ghost clasts and is ~20 cm thick. Numerous shelly pāhoehoe crusts occur overlying the gas blisters and merge laterally with the clastogenic flows.

Many of the flows have columnar cooling joints spaced 230–1000 mm that penetrate downwards from the crust through 10–100% of the thickness of the flow. Lavas found within northwest/southwest oriented grabens display hackly jointing (Fig. 3.17). The hackly jointing is composed of two joint sets: master joints (spaced 8–108 cm) and sub-set joints (spaced 25–180 mm) that splay from the master joints.

Clastogenic lava occurs up to ~2 km from the vents. The lava flows thicken into topographic lows forming flows 51–370 cm in thickness. Between faults F9 and F12 (Fig. 3.4) the lava overlies hyaloclastite. The flows onlap onto the base of pyroclastic deposits (location 477; see section 3.7) and are dominant towards the South of the study area. The flow field is faulted by the F33 west of river (Fig. 3.4) but is unaffected by faulting east of the river. The clastogenic lava is overlain by hummocky lava in the north of the study area; in the south it is overlain by the spatter and scoria ramparts (Figs. 3.3 and 3.11).

Interpretation:

The clastogenic origin of the lava is evidenced by abundant ghost clasts sourced from the inner part of the lava fountain or from a low fountain that yielded a high proportion of spatter bombs (e.g. Wolfe et al. 1988; Head and Wilson 1989; Sumner et al. 2005). These lavas may also contain a component of effused lava, as observed in contemporary eruptions (Wolfe et al. 1988).

The pāhoehoe morphology indicates relatively low shear rates during emplacement. The sub-horizontal alignment of vesicles suggests late stage flow of lava causing

unidirectional simple shear (e.g. Walker 1989; Polacci et al. 1999). The medial gas blisters are a feature common to P-type, S-type and toothpaste pāhoehoe (Rowland and Walker 1987; Walker 1989; Wilmoth and Walker 1993) and indicate that the lavas possessed a yield strength on degassing (Walker 1989). This yield strength may result from the partial cooling and crystallisation of constituent pyroclasts during flight. Yield strength can also be acquired when lava vesicularity is >30% and forms a foam (Wilmoth and Walker 1993). The shelly pāhoehoe crusts that overlie the lavas may have been rafted from proximal regions. Alternatively, they may be breakouts or overspills from the parent clastogenic flow.

The absence of a tri-partite pāhoehoe structure within the flows suggests that they did not inflate and instead the clastogenic flow field grew exogenously. The hackly jointing suggests interaction between the cooling flows and surface water (Long and Wood 1986), likely related to flooding by rivers. These joints are similar to pseudopillow fracture systems (e.g. Forbes et al 2012), and may suggest that at some locations lava flows penetrated into bodies of open water.

In the north the lava was produced prior to the emplacement of hummocky lava. The clastogenic lava is the youngest lava in the south. The displacement of the lava by fault 33 indicates that slip occurred after the eruption.

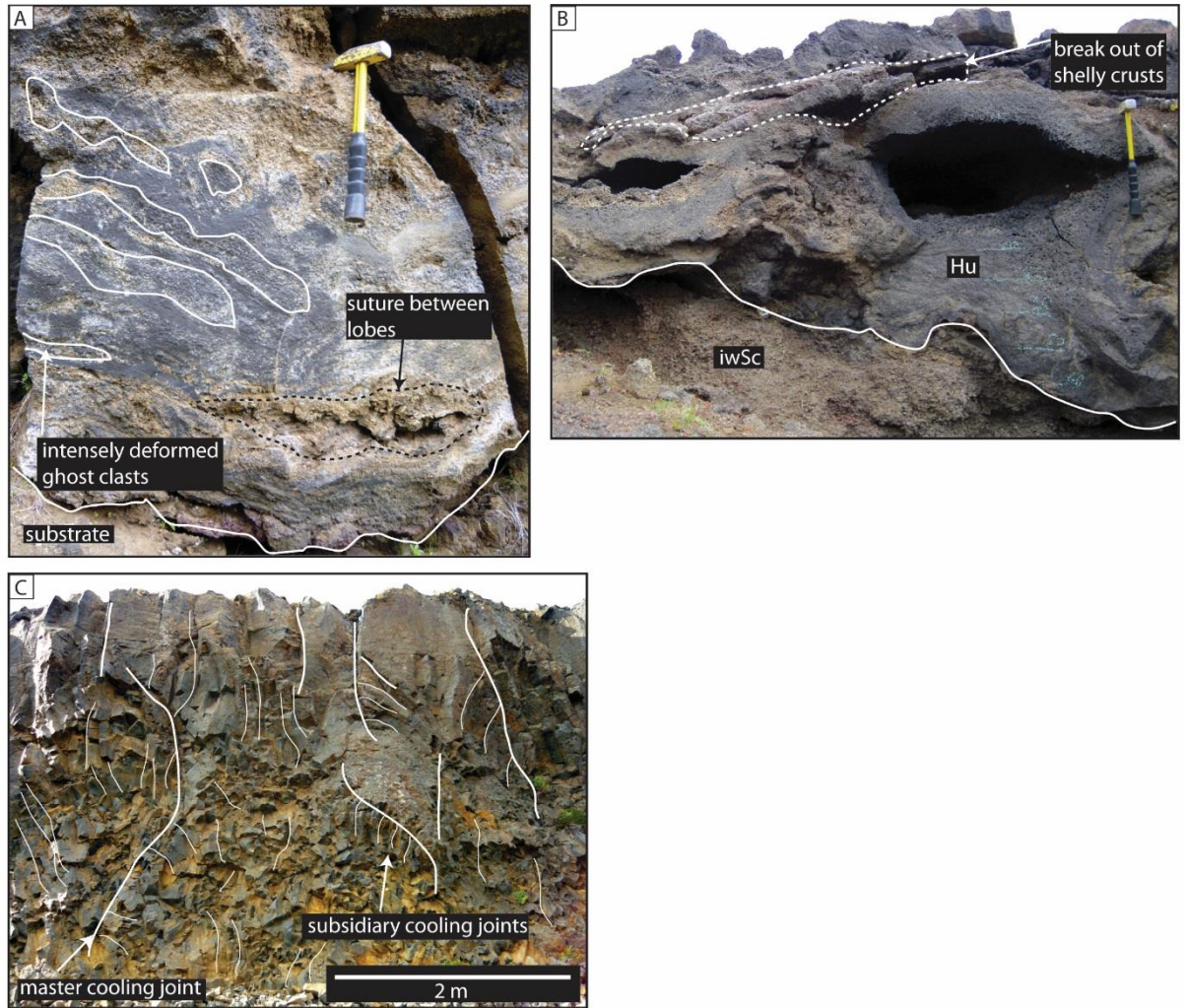


Figure 3.17. Features of the clastogenic lava. (A) Photograph showing the internal texture of the clastogenic flows, with highly deformed ghost clasts and a suture between lobes towards the base. Hammer for scale. (B) Clastogenic lava with a break out of shelly lava. The shelly lava has been subsequently covered by later clastogenic breakouts. Hammer for scale. (UTM 556985/7264113). (UTM 557465/7266307). (C) Clastogenic lava that has been flooded with water during cooling. The lava has a distinctive entablature comprised of two dominant sets of joints, in which the subsidiary set radiate from the master set. (UTM 556935/7263621).

Hu – Hummocky pāhoehoe

Hummocky pāhoehoe is recognised solely by surface textures and topography because there are no sections through the lava flow (Hu; Fig. 3.3). Numerous tumuli and squeeze-outs (Fig. 3.18) are observed throughout the flow field (Fig. 3.3). The tumuli range from 0.5–1 m in height and 1–2 m in diameter. They have a sub-circular shape in plan view. The squeeze-outs range from 1.5–2.5 m in height and are 1–4 m in diameter. They are sub-

circular to elongate in plan view and are composed of numerous ~10 cm thick crusts that dip radially outwards from their centre (Fig. 3.18). Sub-parallel ~3 mm deep grooves 1–3 mm wide occur on the outer surfaces of crusts, oriented parallel to the direction of dip.

Lava tubes 1 m in diameter occur east of the river and strike 280° (approximately perpendicular to the fissure). There is no evidence for overlying tumuli. The tubes have horizontal grooves along their internal surfaces and lava benches at 0.2 and 0.4 m height (Fig. 3.18). Channels occur west of the river (Fig. 3.18). They are <0.5 m in depth and ~4 m wide and their internal surfaces dip ~3°. The internal surfaces of the channels are marked by sub-vertical striations. The channels plunge 025° and 100° (Fig. 3.3).

Hummocky pāhoehoe outcrops over >0.25 km² to the north of the study area. It forms the uppermost unit of the R-K eruption sequence in medial and distal regions and overlies clastogenic lava (Cl, see above; Fig. 3.3). Within 600 m of the fissure, hummocky pāhoehoe is locally overlain by spiny pāhoehoe (Sp; see below) and shelly pāhoehoe (Sh; see below) and by clast-supported, incipiently–densely welded scoria and spatter bombs (waSc–dwSc; waSp–dwSp; Fig. 3.3). Outcrops in the northeast of the study area show that hummocky pāhoehoe passes downstream into spiny pāhoehoe where the slope increases; transitions in surface morphology have not been observed elsewhere.

Interpretation:

Tumuli indicate that the hummocky lava grew by inflation (e.g. Walker 1991) and the tubes indicate that the lava was fed by an arterial network on the east of the river. These arterial networks suggest that the lava was emplaced over slopes of >1–2° (e.g. Hon et al. 1994). The squeeze-outs indicate regions in a compressional regime (e.g. Sumner 1998) and are used to infer the margins of the flow. Scours on the flow crusts are inferred to have formed during extrusion of lava. The channels represent paleoflow networks in the flow field; their dip indicates the lava paleoflow direction (i.e. northeast and southeast; see Fig. 3.3). The vertical striations on the internal channel walls indicate draining of lava and sliding of solid crust during flow.

The hummocky pāhoehoe is inferred to have been sourced from vents in the north. It is the youngest R-K product in medial and distal regions. The down-flow transition from hummocky to spiny pāhoehoe suggests an increase in shear rate within the lava, caused by steeper slopes (e.g. Peterson and Tilling 1980).



Figure 3.18. Hummocky lava features. (A) A tumulus, with the upper crust partially eroded and the core exposed. Hammer for scale. (UTM 556481/7266232). (B) A lava channel on the surface of the flow field. The channel has resinous walls with vertical striations caused by the draining of lava within the channel. Direction of flow is inferred from the slope (toward viewer). The channel is ~3 m wide. (UTM 547155/7208827). (C) An elongate squeeze out at the margin of the flow field. The squeeze out is composed of numerous crusts that dip radially from the centre of the structure. Hammer for scale. (UTM 556215/7266339). (D) Photograph of the inside of a lava tube. Backpack for scale. (UTM 557462/7265995).

l-l Agg – Lava-like agglutinate

This lava is composed of dense to incipiently vesicular, highly deformed to coalesced hypocrySTALLINE agglutinate. Relict pyroclasts with vague outlines are present and account for ≤ 2 vol. % of the lava. These clasts are elongate (aspect ratios 1:8–1:40), 16–480 mm in

diameter and contain irregular vesicles <1 mm size. These clasts are occasionally overprinted by spherical vesicles 1–5 mm in diameter. The clasts are oriented parallel to the upper surface. Rectangular clasts are 70–200 mm in size and have spherical vesicles >1 mm size separated by ~1 mm thick septae (Fig. 3.19). They have no preferred orientation. 100–200 mm sized ghost clasts of non-vesicular, sub-spherical cored bombs are also found (Fig. 3.19). The agglutinate has mean vesicularity of 8% (range 1–17) and its mean density is 2747 kg m⁻³ (range 2461–2964 kg m⁻³).

The lava flows commonly exhibit ~100 mm long tension gashes that penetrate from their upper surface toward their centre (Fig. 3.19). Tension gashes also occur within the cores of lavas and are oriented sub-parallel to the upper and lower surfaces. The basal contacts of the agglutinate dip ≤5–60°. They form sheet-like flows with sub-parallel upper and lower contacts. They maintain a near-constant thickness across their length.

The lava-like agglutinate varies from 0.5–2.9 m in thickness. It is only found in the upper 15 m of the R-K volcanic sequence (in the crater of edifice 26) and within the spatter ramparts. Contacts with other units are complex: they may be gradational, distinct or locally intrusive into overlying pyroclastic units (e.g. clast-supported weakly agglutinated scoria lapilli and bombs; waSc), as observed within the crater of edifice 26 (log 81, Fig. 3.10).

Interpretation:

Ghost clasts indicate the agglutinate is clastogenic in origin. They are interpreted to have rapidly accumulated from the inner part of a lava fountain during high intensity fountaining, or from low fountains that yielded a high proportion of spatter bombs (e.g. Wolfe et al. 1988). The rectangular ghost clasts have a similar vesicularity and vesicle shape to pāhoehoe lava crust and are interpreted as fragments of entrained lava crust. Cored bombs are interpreted as for clast-supported weakly agglutinated spatter bombs (waSp).

The absence of a vesicular crust in the agglutinate flows suggests that they did not inflate and instead grew exogenously, most likely via the coalescence and subsequent flow of pyroclasts. Tension gashes are the result of shear within moving mass (e.g. Sumner 1998) and thus indicate late stage flow. The restriction of the agglutinate to within the edifices suggests that they formed only from the accumulation of clasts from the lower and inner parts of the fountain during the edifice-forming stages of the eruption.

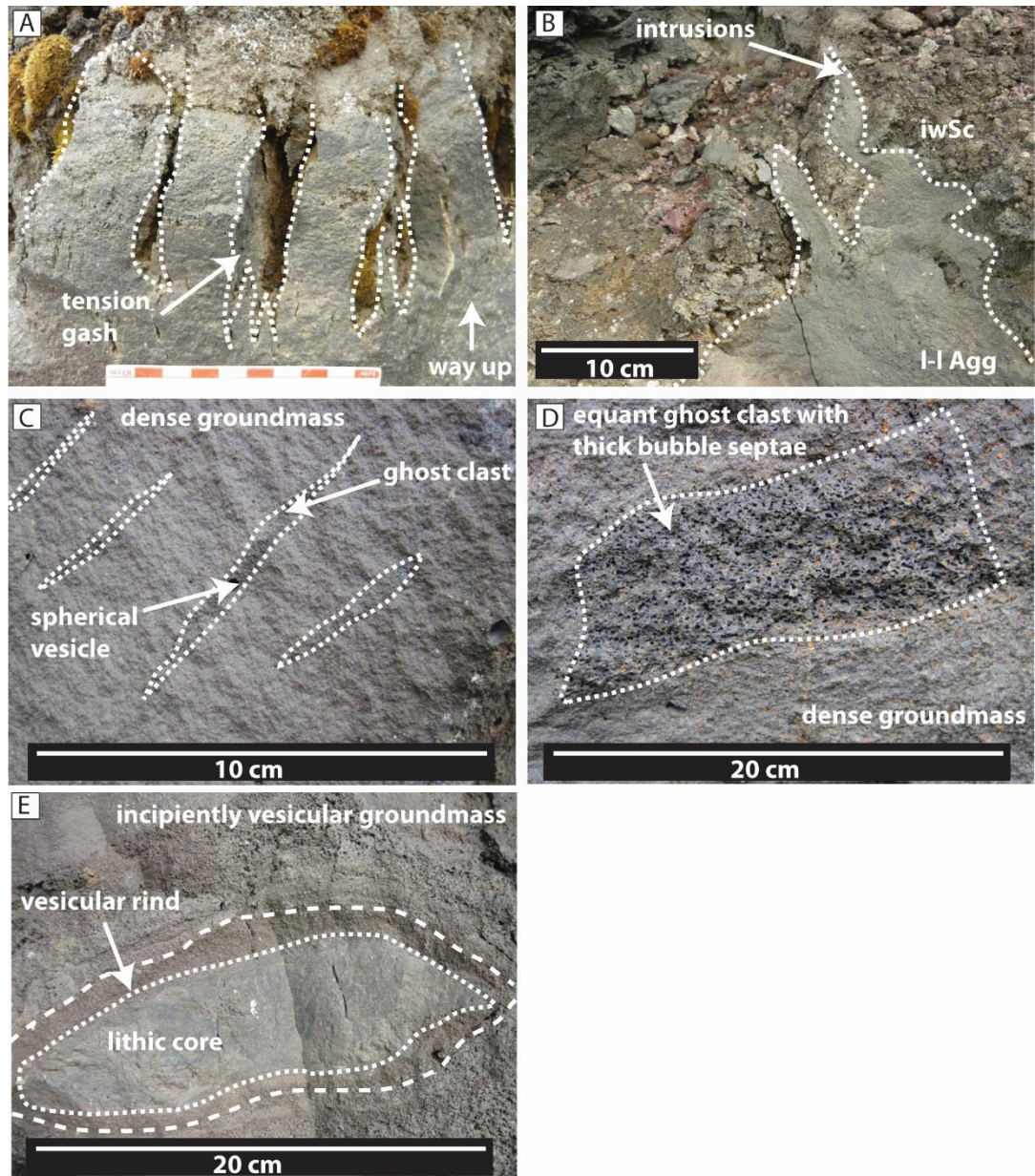


Figure 3.19. Features of the lava-like agglutinate (l-l Agg). (A) Tension gashes at the top of unit 5 in log 81. Graticules on the scale card are 1 cm, the arrow indicates up. (UTM 557442/7264902). (B) Intrusion of lava-like agglutinate (l-l Agg) into overlying clast-supported weakly agglutinated scoria lapilli and bombs (waSc). Dashed line indicates contact. (UTM 557442/7264902). (C) Ghost clasts (outlined) in lava-like agglutinate (l-l Agg), overprinted by a spherical vesicle (arrowed). These spherical vesicles suggest post depositional vesiculation of the lava. (UTM 557772/7265756). (D) Equant ghost clast (outlined) interpreted to represent a lava crust lithic. Compare this ghost clast with those in C and clast-supported moderately welded spatter bombs (mwSp; Fig. 3.7). (UTM 557772/7265756). (E) Cored bomb with a rind of vesicular juvenile magma. The core is composed of dense agglutinate. (UTM 557442/7264902).

Sp – Spiny pāhoehoe

Spiny pāhoehoe is recognised by its spinose surface that forms lineations parallel to the direction of effusion (Fig. 3.13). It occurs at the base of a slope near vent 22. Its up-flow morphology is unclear. The lava covers an area 0.05 km² in size. The lack of cross sectional exposure means that the internal features of the lava cannot be determined.

Interpretation:

Spiny pāhoehoe is transitional between pāhoehoe and a’ā lava types (Rowland and Walker 1987). The occurrence of the spiny pāhoehoe at the base of a break in slope suggests that the change in slope increased the shear rate within the lava (e.g. Peterson and Tilling 1980).

Hy – Hyaloclastite and pillow lavas

Hyaloclastite is composed of pillow lavas in a palagonitised matrix of pillow fragments. There is an upwards transition from coherent (pillow-dominated) to fragmental (palagonite-dominated) deposits (log 7, Figs. 3.10 and 3.20). The coherent units are 0.5–1 m thick and are composed of interlocking, sub-circular pillows that are 900 × 900 mm size. At their margins they have 2–4 cm thick chilled rinds which are often detached from the pillow (Fig. 3.20). Grading towards the core is a 5 cm wide zone characterised by 20 vol. % elongate vesicles that have their longest axis aligned parallel to the margin of the pillow. These vesicles are <1 cm in diameter. The cores of the pillows are characterised by large (~10 cm diameter) irregular vesicles that account for 10 vol. %. The fragmental deposits are 3.4–4 m thick and are composed of similar sized pillows with irregular shapes. These pillows are clast-supported in a lapilli–ash size palagonitised matrix of brittle quench fragments with pebble–block sized pillow fragments. The pillow fragments are commonly portions of the core or spalled rinds. The hyaloclastite deposits are 4.4–4.5 m thick. No structure (e.g. layering or dipping pillows) is observed. The hyaloclastite is overlain by clastogenic pāhoehoe (Cl) and underlain by fSxb (Figs. 3.11, 3.21 and 3.22). It occurs in the southern section of a graben that strikes 015° and is confined within faults F9 and F12 (Fig. 3.4).

Interpretation:

This lithofacies indicates interaction between pāhoehoe lava and bodies of surface water. Based on the thickness and extent of the hyaloclastite, the water body is inferred to

have been ≥ 4 m in depth and have extended laterally for ≥ 630 m. The pillow-dominated deposits are inferred to indicate the progressive penetration of small lobes of lava into water (the hP facies of Watton et al. 2013). The overlying fragmental deposits are interpreted as pillows engulfed by quenched debris during the passage of debris slurries from up-flow (the iP facies of Watton et al. 2013). Thus, the upwards transition from pillow-dominated to fragmental deposits is representative of a lava delta developing in a basin with steep banks (e.g. Watton et al. 2013). This delta may have temporarily dammed the water body (e.g. Hamblin 1992; Huscroft et al. 2004).

The overlying contact with the clastogenic pāhoehoe (Cl) indicates that early lavas interacted with water forming hyaloclastite, whilst later lava flows did not. Whether the pillow lavas are lateral transitions of the clastogenic pāhoehoe (Cl) or other lava flows produced during the eruption is unknown. The surface water supply was later cut-off (e.g. by lava damming of a river) or exhausted before emplacement of later lavas. Pillow lavas built up out of the water – essentially pushing the ‘shoreline’ backwards. The occurrence of the hyaloclastite within a graben suggests that the hyaloclastite is occupying a location that previously represented a river channel. The river channel existed prior to the eruption and occupied a graben formed by faults 9 and 12.



Figure 3.20. Features of the hyaloclastite. (A) Photograph showing the stratigraphic relationship of hyaloclastite and pillow lavas (Hy) with clastogenic pāhoehoe (Cl) and fSxb (UTM 557949/7263864). (B) Vertical section through the pillow-dominated and fragmental hyaloclastite. This section is also represented in log 7; Fig. 3.10 (UTM 557908/7263830). (C) Detail of a pillow lava. The chilled rinds have spalled or been abraded from the majority of the pillow. The aligned vesicles occur in a zone 5 cm wide. The core has large, irregular vesicles (UTM 558272/7263904).

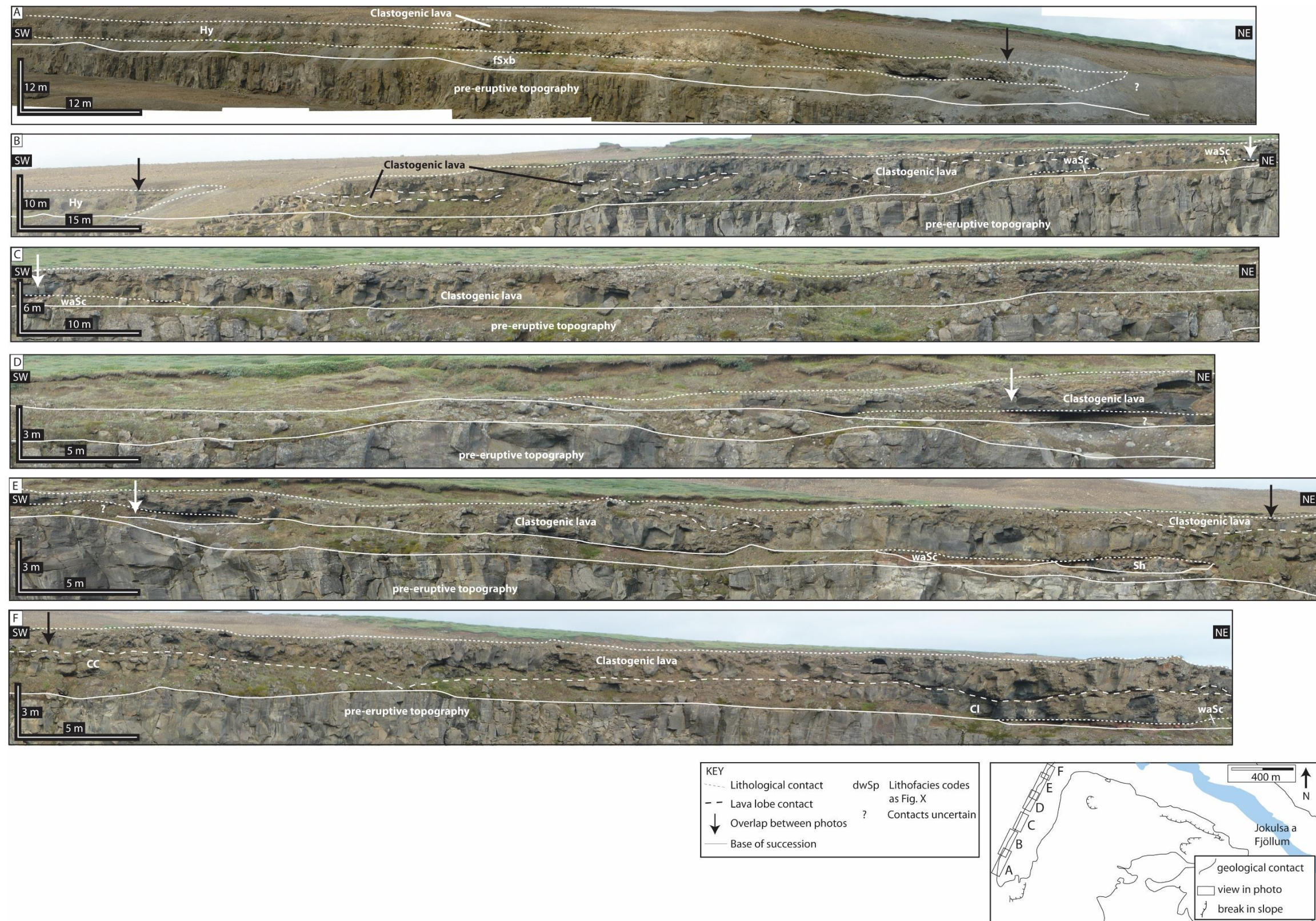


Figure 3.21. Panoramic photos of the western wall of the graben formed by faults F9 and F12. The photos show that the area is dominantly composed of clastogenic lavas underlain by lobate beds of clast-supported weakly agglutinated scoria lapilli and bombs (waSc) <0.5 m in thickness. 3 m wide flows of shelly pāhoehoe are also observed. Hyaloclastite thickens towards the southwest (Fig. 3.3) and is inferred to be underlain by fSxb, as observed on the east of the graben (Fig. 3.22). (A: UTM557585/7264214; B: UTM557595/7264181; C: UTM557601/7264125; D: UTM557616/7264059; E: UTM557649/726; F: UTM 557656/7263914).

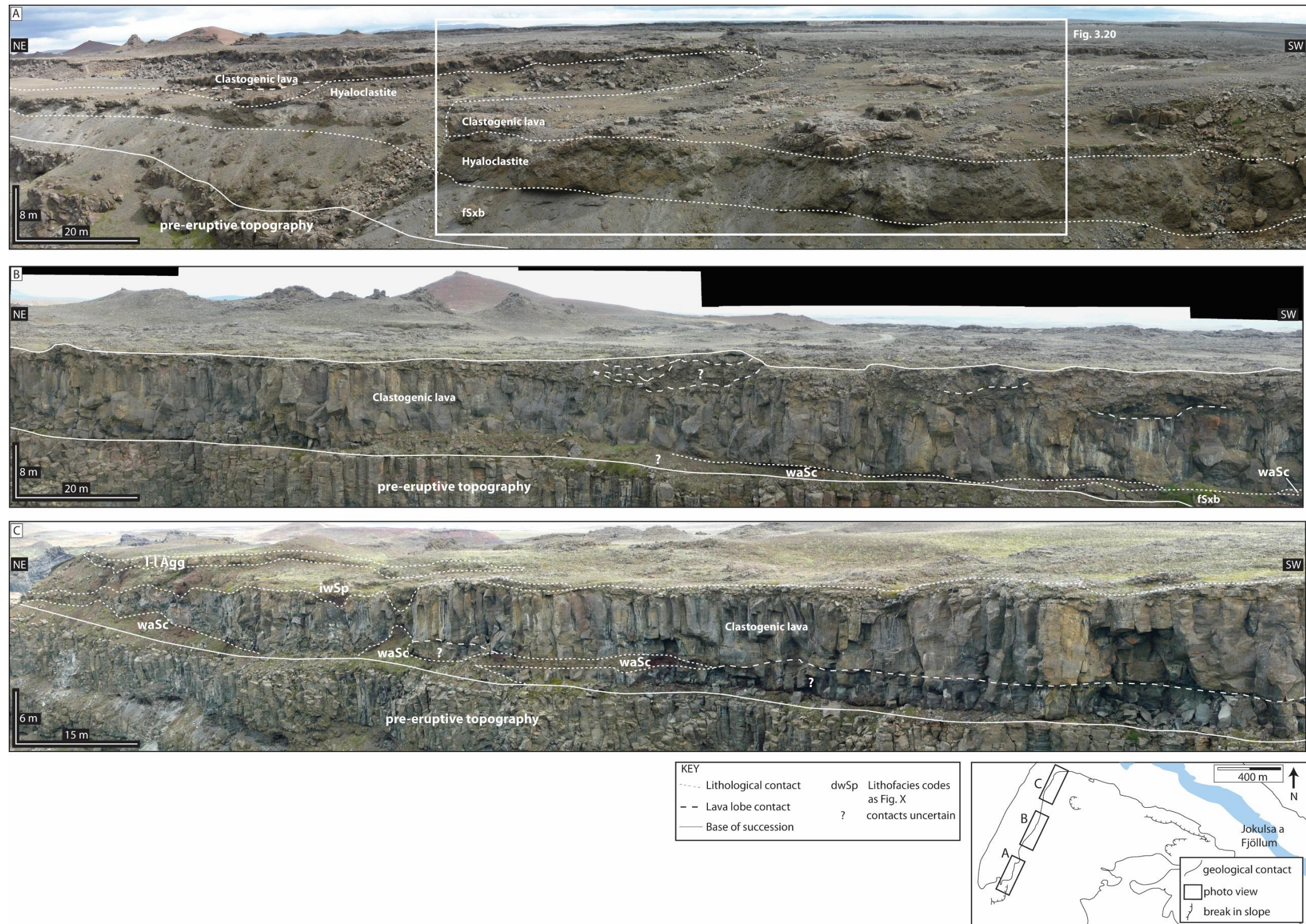


Figure 3.22. Panoramic photos of the eastern wall of the graben formed by faults F9 and F12. The photos show that the area is composed of clastogenic and hummocky lavas underlain by lobate beds of clast-supported weakly agglutinated scoria lapilli and bombs (waSc) <0.5 m in thickness. The contacts between the hummocky and clastogenic lavas are unclear. Numerous lobes 1–5 m thick are observed within the clastogenic lavas. Hyaloclastite thickens towards the southwest (Fig. 3.3) and is underlain by fSxb. Note the absence of Clast-supported weakly agglutinated scoria lapilli and bombs (waSc) at the base of the stratigraphy in (A), suggesting either that this section of the fissure was dominated by effusive activity, or that the pyroclasts coalesced to form lava which subsequently interacted with surface water (forming hyaloclastite). (A: UTM 557934/7263920; B: UTM 558083/7264079; C: UTM 557849/7264219).

Sh – Shelly pāhoehoe

Shelly pāhoehoe flows are composed of numerous 10–200 mm thick crusts that are often contorted. The groundmass is hypohyaline to hypocrystalline, and has an estimated vesicularity of 30 % (estimated with a grain size card). Crusts contain homogeneously distributed spherical and distorted vesicles. Flows often have large ($\sim 420 \times 60$ mm) gas cavities in their centres, with resinous surfaces forming the interior surfaces of the crusts. Shelly pāhoehoe occurs as breakouts from clastogenic pāhoehoe (Cl) lava flows and is also found within the openings of horseshoe-shaped scoria cones at the top of the R-K volcanic sequence (Fig. 3.23). The crusts occur in successions ranging from 255–1620 mm in thickness. The lava occurs as broad (>5000 mm wide) or as narrow (300 mm wide) lobes (Fig. 3.3). The flows cover an area 0.2 km^2 in size.

Interpretation:

Shelly pāhoehoe is a gas-rich lava (e.g. Swanson et al. 1975) and its occurrence as break-outs suggests that the parent flow clastogenic pāhoehoe (Cl) was also gas-rich. The resinous interior of the flow is inferred to be caused by lava draining from the flow, perhaps indicating a channel or tube system within the shelly pāhoehoe flows (e.g. Stevenson et al. 2012). Its occurrence at the opening of scoria cones suggests that the lava was effused from the vent late in the development of the fissure, although it may have accumulated from low (<100 m) lava fountains (e.g. Swanson et al. 1975).

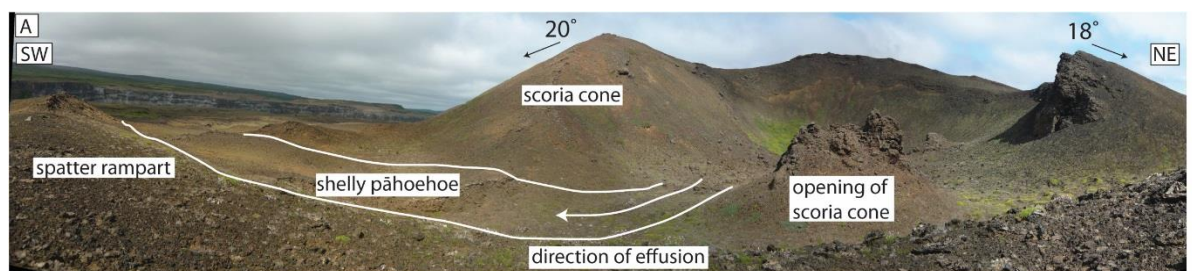


Figure 3.23. Photograph showing shelly pāhoehoe at the opening of a horseshoe-shaped scoria cone (UTM 557647/7265074).

3.6 Sedimentary lithofacies

The sedimentary lithofacies (Fig. 3.24; Table 3.5) are composed of basaltic sandstones and breccias consisting of basaltic pyroclasts and lava flow fragments. East of the river the sediments are confined to the top of the stratigraphy, whilst west of the sediments occur

both beneath and within the R-K volcanic sequence (Fig. 3.10 and 3.11). The sediment outcrops on both sides of the fissure.

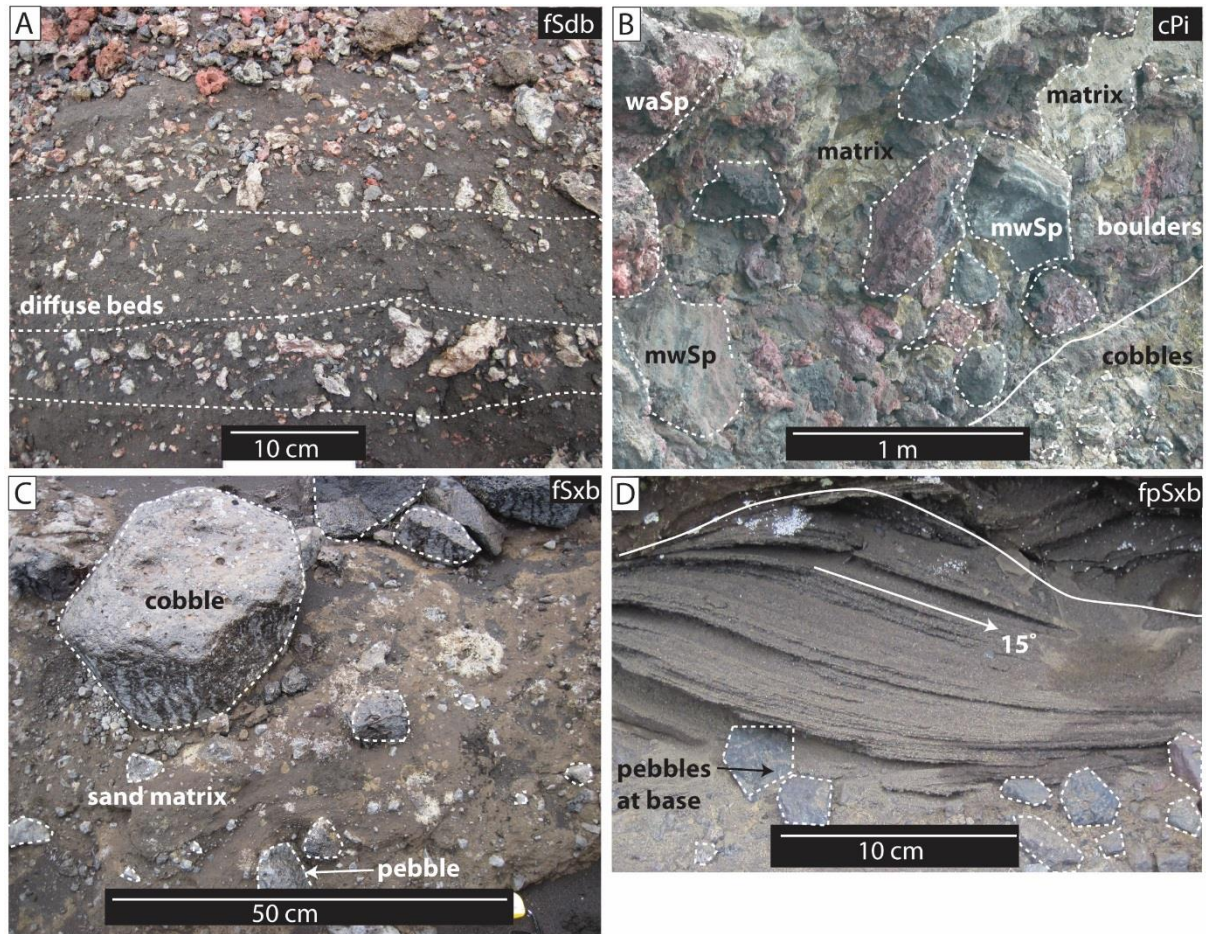


Figure 3.24. Sedimentary lithofacies observed in the study area. (A) Fine, diffusely bedded volcaniclastic pebbly sandstone (pebbles are outlined). See log 16 for stratigraphic position. (UTM 557437/7263977). (B) Inverse-graded cobble breccia. See log 16 for stratigraphic position. (UTM 557437/7263977). (C) Fine, cross bedded volcaniclastic sandstone with gravel, pebbles and cobbles. See log 81 for stratigraphic position. (UTM 557495/7265751). (D) Fine, hummocky cross-stratified pebbly sandstone. Sub-horizontal diffuse beds ~10 cm thick are marked by dashed lines. See log 81 for stratigraphic position. (UTM 557442/7264902). See Tables 3.5 for lithofacies descriptions.

| Lithofacies | Description | Componentry | Structure | Occurrence |
|--|--|---|--|--|
| fSdb | Fine, diffusely bedded sandstone | Angular pebbles of R-K stratigraphy scoria and basaltic sands | Matrix supported; moderately well sorted; ~5 cm thick diffuse beds; units 0.75 m thick | Post eruption; uppermost deposits in the crater of edifice 26 |
| cCi | Cobble conglomerate with inverse grading | Angular pebbles and boulders of R-K stratigraphy pyroclasts | Clast-supported; poorly sorted and inversely graded; units 0.2 – 1 m thick | Post eruption; uppermost deposit in the crater and flank of edifice 26 |
| fSxl | Fine, cross laminated sandstone | Angular – sub-angular granules and cobbles; pyroclasts and dense basalt clasts sourced from R-K and pre-eruptive stratigraphy | Matrix supported; poorly sorted; laminations; units 0.8 – 1 m thick | Pre and post eruption; distal regions west of the river beneath the volcanic stratigraphy and within the flank of edifice 26 |
| fSxb | Fine, trough cross bedded sandstone | Sub-angular granules; pyroclasts and dense basalt clasts sourced from R-K and pre-eruptive stratigraphy | Clast supported; moderately well sorted; 3 mm thick beds with foresets that dip 12°; pebbles of scoria at the base are normally graded; units 0.15 – 1.8 m thick | Pre- and syn-eruption; west of the river overlying iwSc and beneath Hy in distal regions |
| Table 3.5. Summary of sedimentary lithofacies. All lithofacies are interpreted as fluvial deposits, possibly related to glacial floods. | | | | |

Lithofacies fSdb – fine, diffusely bedded volcanoclastic pebbly sandstone

This matrix-supported and moderately well sorted sandstone is composed of fine basaltic sands (95–90 vol. %) of unknown provenance and angular, intraformational scoria pebbles (5–10 vol. %). Diffuse beds defined by variations in pebble abundance are ~5 cm thick and dip 15–20° to the S. The lithofacies occurs in units up to 0.75 m thick within the crater of edifice 26 (log 81, Fig. 3.10).

Lithofacies Cpi – inverse-graded cobble breccia

This breccia is composed of angular intraformational pebbles, cobbles and boulders of the R-K eruption (70 vol. %) and fine basaltic sands (30 vol. %) of unknown provenance. It is matrix-supported, poorly sorted and inversely graded. The beds are 0.2–1 m thick and occur in the crater and flank of edifice 26 (log 81, Fig. 3.10).

Lithofacies fSxb –fine, cross bedded volcanoclastic sandstone with gravel, pebbles and cobbles

This sandstone is matrix-supported and poorly sorted. It is composed of fine sand (80 vol. %) and angular and sub-angular granules, pebbles and cobbles (20 vol. %). These clasts are sourced from the underlying lithologies—either the R-K or pre-eruptive stratigraphy. It is trough cross-stratified with 3 mm thick foresets that dip 19° to the SW. It occurs in distal regions west of the river beneath the R-K volcanic sequence (log 16; location 462; Fig. 3.11) and ~200 m from the fissure (Fig. 3.3) in units 0.8–1 m thick.

Lithofacies fpSxb – fine, hummocky cross-stratified pebbly sandstone

This sandstone is composed of sub-angular granules and pebbles sourced from the underlying lithologies – either the R-K or pre-eruptive stratigraphy. The lithofacies is clast-supported and moderately well sorted. The lithofacies displays hummocky cross-stratification; foresets are 3 mm thick and dips 12° to the E. Scoria pebbles at the base of the unit are inversely graded. Units are 0.15–1.8 m thick and occur west of the river overlying clast-supported weakly agglutinated scoria lapilli and bombs (waSc) and beneath hyaloclastite and pillow lavas (Hy) in distal regions of the study area (logs 7 and 16; Fig. 3.11).

Interpretation:

The sediments exhibit features typical of those deposited in fluvial environments (e.g. sand–cobble grain size, moderate sorting, angular and rounded grains and trough cross-bedding; see Tucker 1995). Fluvial sedimentation is evidenced pre-, syn- and post-eruption, although the thickest deposits are pre- and post-eruption. In proximal regions post-eruption fluvial action has re-worked underlying pyroclastic units. In distal regions pre- and syn-eruptive fluvial action is evident, also re-working the underlying stratigraphy. Post-eruption fluvial action has incised channels in distal regions (e.g. between faults 36 and 37). The sedimentary lithofacies may be related to the glacial outbursts that occurred from 2–9 kyr BP (e.g. Alho et al. 2005; Kirkbride et al. 2006; Waitt 2009; Friese et al. 2013). The presence of the sediments both sides of the fissure suggests that the asymmetric distribution of pyroclastic deposits cannot be accounted for by erosion.

A high energy regime is indicated by the coarse grainsize and cross-bedding of lithofacies Cpi and fSxb (Tucker 1995). The inverse grading in the cobble breccia (Cpi) is common in the deposits of high concentration sediment-water mixtures and commonly occur in the lowest part of debris-flow deposits (Tucker 1995). These debris flows directly overlie the R-K volcanic sequence and record the onset of fluvial deposition. Hummocky cross-stratification suggests rapid aggradation from a uni-directional current (Dumas and Arnott 2006); consistent with high energy fluvial deposition. The presence of lithofacies fSxb within the volcanic R-K volcanic sequence indicates that fluvial deposition west of the river occurred during the eruption. The fluvial system may have flooded lava flows causing the formation of entablature-style jointing.

3.7 Architecture of the pyroclastic deposits

The Jökulsá a Fjöllum canyon exposes a near-complete record of the R-K volcanic sequence and its feeder dyke on both the eastern and western canyon wall (Fig. 3.25). Faults within this sequence occurred prior to, during and after the eruption (Figs 3.26, 3.27 and 3.28). Several pyroclastic constructs are recognised (Fig. 3.29), including rootless cones (location 285), scoria ramparts (locations 280, 477 and 302), a scoria-agglutinate cone (edifice 26, location 289), spatter ramparts (locations Y28, Y29) and sheet-like fall deposits (location 350). The characteristics of these constructs, their feeder dykes and conduit are discussed below (Table 3.6).

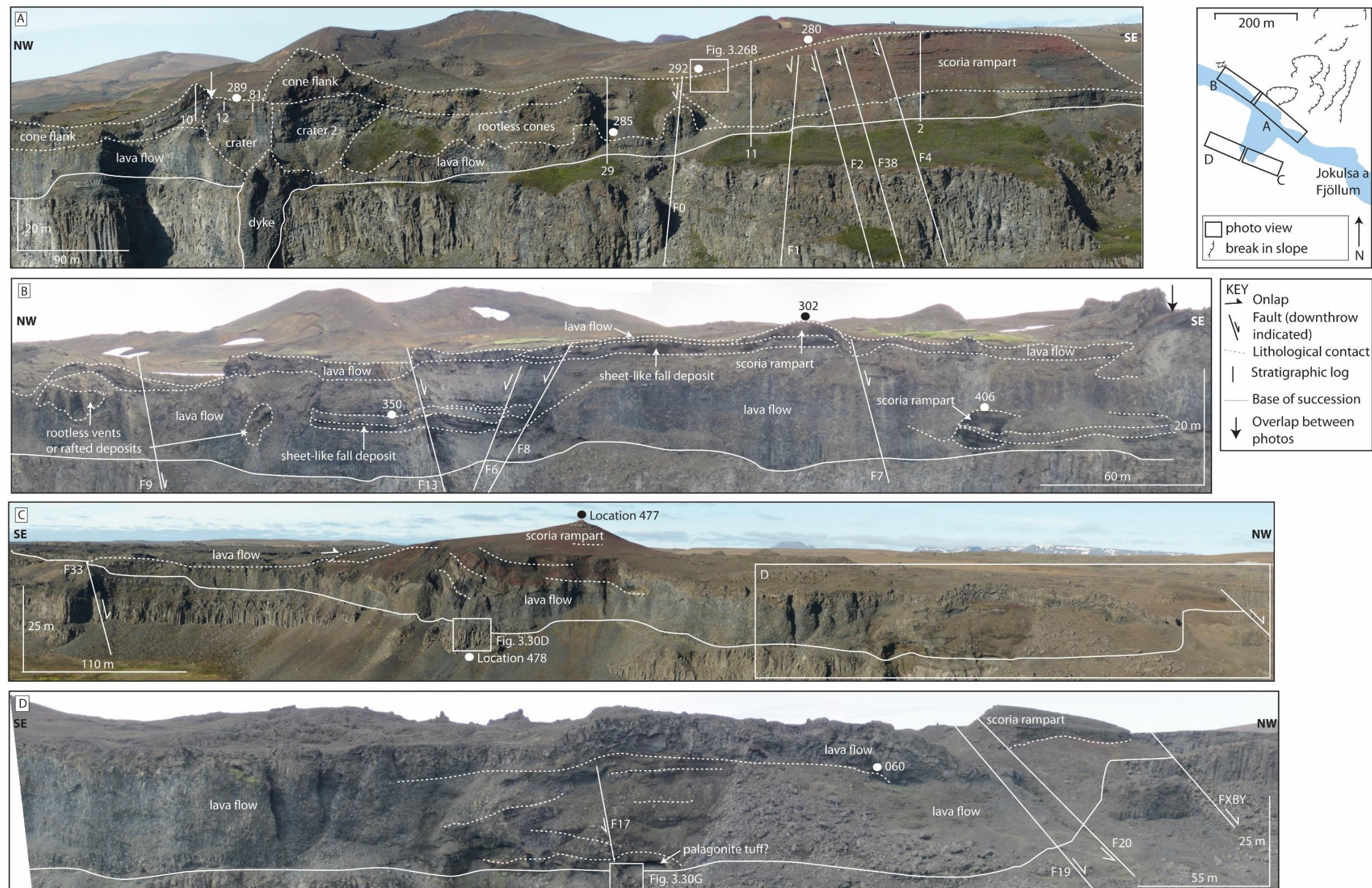


Figure 3.25. Photographs of the canyon walls. (A) Cross section of a scoria-agglutinate cone (location 289; edifice 26) and scoria rampart (location 280). Crater 2 of an overlapping edifice is also shown. (UTM 557542/7264269). (B) Photograph of the canyon wall north of image A. The R-K volcanic sequence is composed of sheet-like fall deposits, scoria ramparts and lava flows of columnar-jointed pāhoehoe (Cp) and clastogenic pāhoehoe (Cl). Numerous faults are visible with throws of ~1 m. The northwestern bounding fault of the Sveinar graben is ~20 m left of the image. (UTM 557617/7265642). (C) Photograph of the western canyon wall. A scoria rampart (Location 477) is observed and has anticlinal bedding at its base. Clastogenic lavas onlap the rampart towards the southeast. Contacts beneath the rampart within crystalline and clastic successions are gradational and beds may pinch-out laterally. The graben bounding fault (F33) is visible toward the southeast. The northwest graben fault is not visible from this location. (UTM 557356/7265748). (D) Photograph of the western canyon wall. The volcaniclastic sandstone with planar bedding (vSpb) is observed at the base of the R-K volcanic sequence. Faults are numbered according to Fig. 3.4. (UTM 557617/7265642).

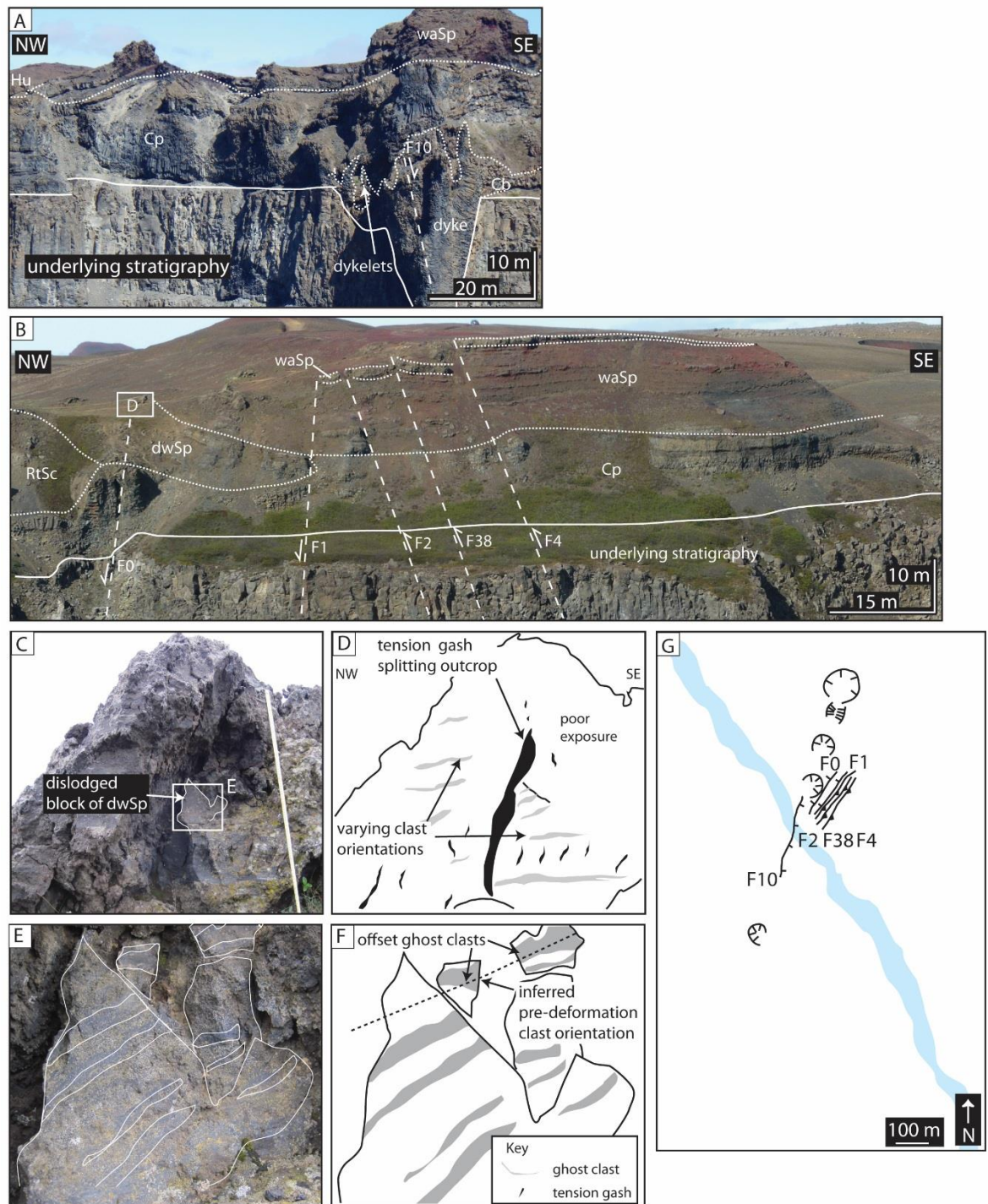


Figure 3.26. Location and orientation of faults associated with edifice 26 and the scoria rampart (location 280). Faults are labelled according to Fig. 3.4 and are indicated by the dashed line. Arrows indicate the direction of downthrown. The contact between the underlying stratigraphy and the R-K stratigraphy is indicated. (A) F10 is exploited by the R-K feeder dyke. Throw is observed to be ~3 m southeast. (UTM 557542/7264269). (B) Numerous faults in the scoria rampart (location 280). Note the throw in the upper pyroclastic units (stippled lines). (UTM 557465/7264189).

Images C–F show deformed blocks of clast-supported densely welded spatter bombs (dwSp) located at the top of normal faults (UTM 564033/7302375). Ghost clasts indicate the original depositional fabric, whilst tension gashes that intersect the bedding suggest ductile deformation in a viscous deposit. Movement was not along the depositional planes, nor confined to the margins of the clast-supported densely welded spatter bombs (dwSp). Ghost clasts are downthrown towards the west (indicated by the dashed line) and suggest extensional deformation. The ruler in C is 70 cm. The block in E is 20 mm wide. Similar features are observed in the clast-supported densely welded spatter bombs (dwSp) at the top of F2. Deformation is interpreted to be the result of syn-eruptive faulting. (G) Map showing location of the faults.

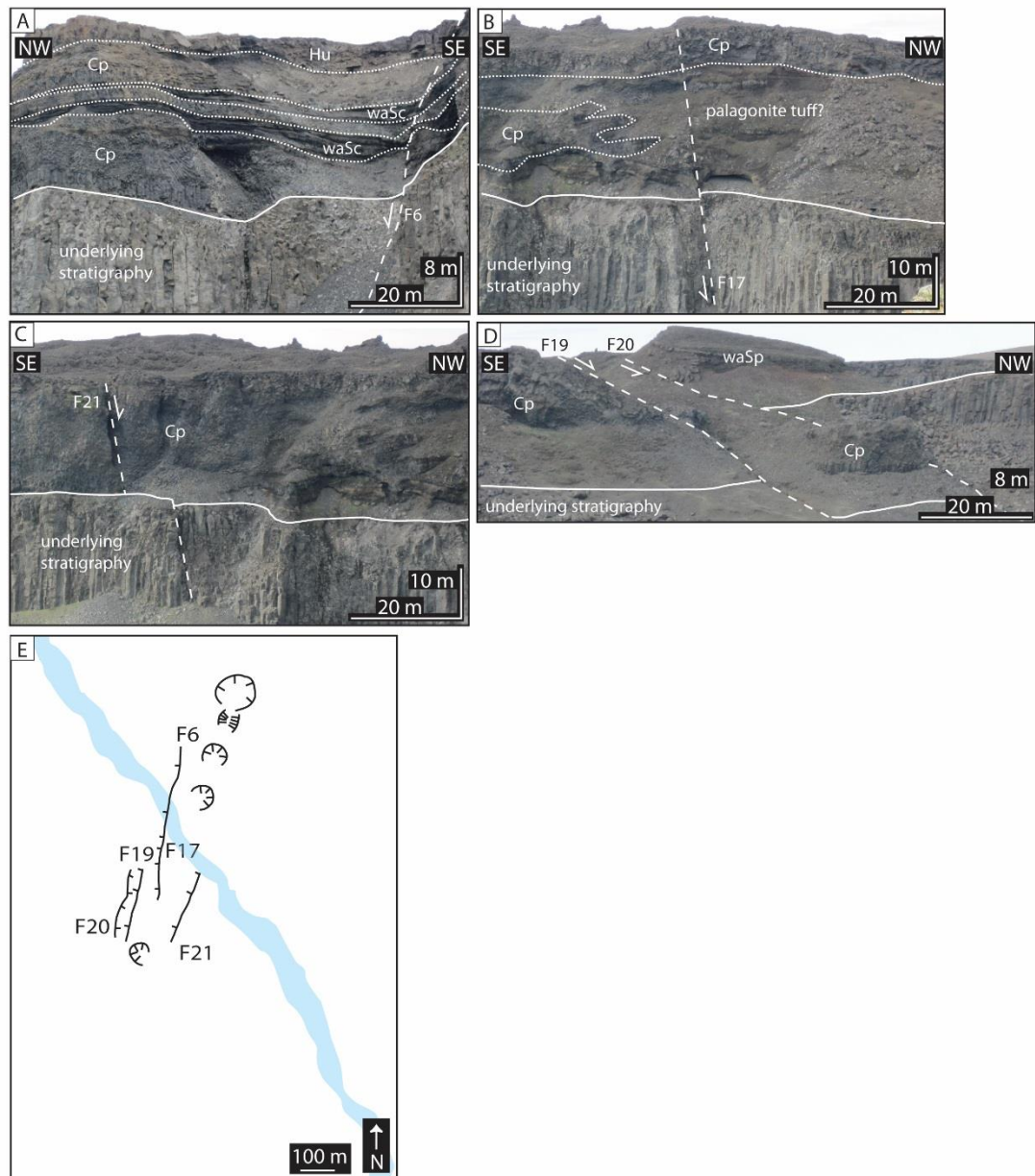


Figure 3.27 (overleaf). Location and orientation of selected faults (dashed lines). Faults are labelled according to Fig. 3.4. Arrows indicate direction of downthrown. The contact between the underlying stratigraphy and the R-K stratigraphy is indicated. (A) F6 forms the margin of an inlet and offsets the upper clastogenic pāhoehoe (Cp). (UTM 557601/7265530). (B) Syn-eruptive slip along F17 is inferred to have resulted in the ductile deformation of the upper agglutinated pyroclastic units resulting in a break in slope at the surface. (UTM 557772/7265756). (C) Fault 21 forms an inlet on the river and forms a gully. There is no topographic expression of the fault in the uppermost lavas. (UTM 557772/7265756). (D) Faults 19 and 20. Columnar-jointed pāhoehoe (Cp) occurs within the graben formed by these faults. (UTM 557601/7265530). (E) Map showing location of the faults.

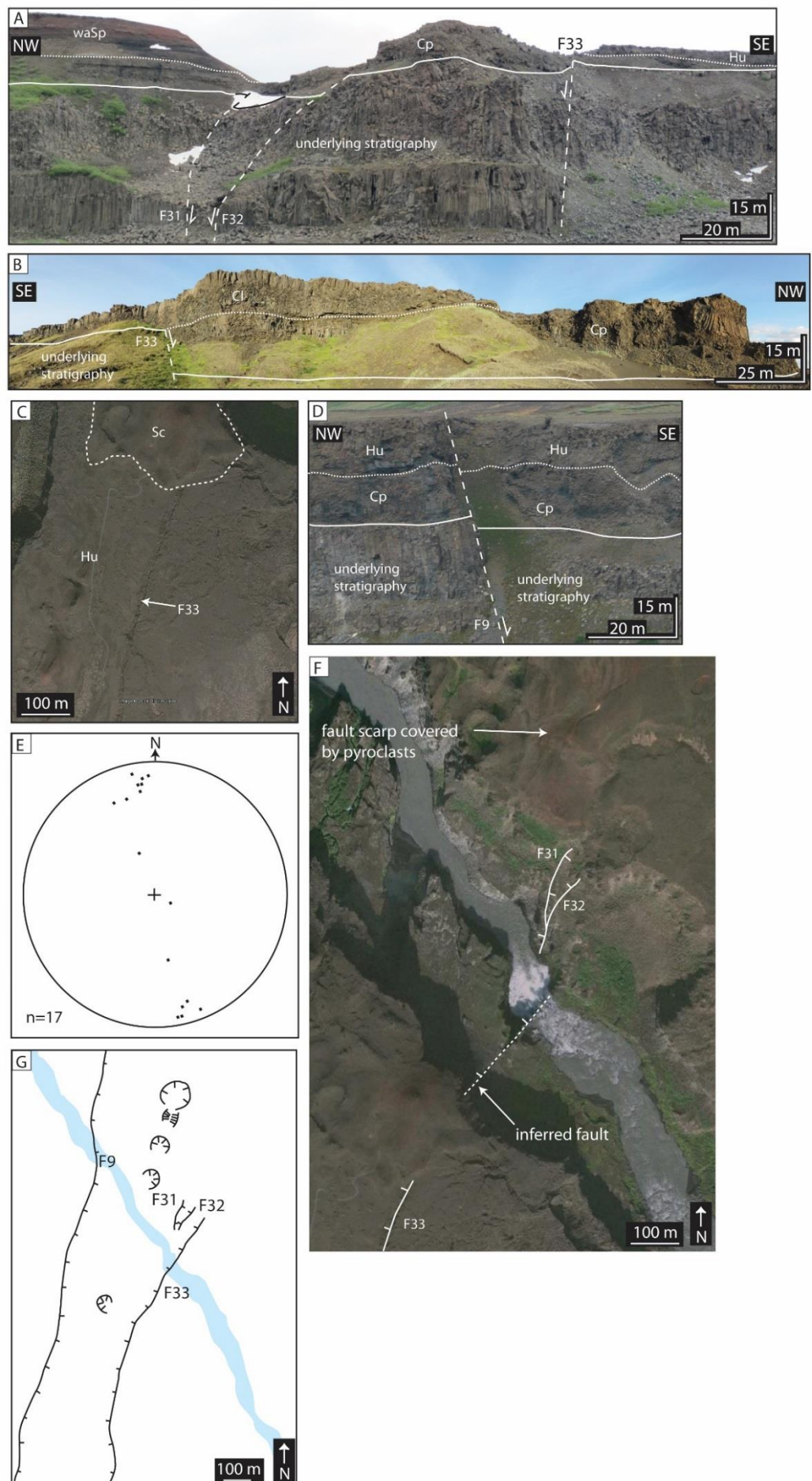


Figure 3.28 (overleaf). Location and orientation of the Sveinar graben bounding faults and stereonet data. Faults are labelled according to Fig. 3.4 and are indicated by the dashed line. Arrows indicate direction of downthrown. The contact between the underlying stratigraphy and the R-K stratigraphy is indicated. (A) Segmented graben bounding faults (F31–33) east of the river. (UTM 557432/7264244). (B) Graben bounding fault west of the river. The lava-like agglutinate (l-l Agg) terminates against the footwall of the graben. The contact between the lava-like agglutinate (l-l Agg) and clastogenic pāhoehoe (Cl) is shown as a stippled line. Note the absence of faulting in the hummocky pāhoehoe (Hu), indicating that the fault existed prior to the eruption. (UTM 563879/7301531). (C) Google Earth image showing F33 (arrowed) faulting the uppermost clastogenic lavas, indicating that the fault had several stages of growth. The fault is concealed further north by scoria (dashed outline). (D) F9 forming the margin of an inlet. The clastogenic pāhoehoe (Cp) is offset by the fault. (UTM 557617/7265642). (E) Pole to plane plot showing the orientation of faults XA, F0,1,4–6,9,13,17, 19–21, 31–33 and 38. (F) Google Earth image showing that F33 (the eastern Sveinar graben bounding fault) does not have a scarp east of the river. This suggests that either: the fault is segmented and slip did not occur on this section of the fault; and/or the eruption continued after faulting. (G) Map showing location of the faults.



Figure 3.29. Google Earth image showing the extent and bedding of the pyroclastic constructs. See text for details.

| Pyroclastic deposit | Characteristic lithofacies | Modal bedding (°) | Geometry | Basal diameter (m) | Thickness (m) | Distance from fissure (m) | Median grain size (cm) | Interpretation |
|--|----------------------------|-------------------|----------|--------------------|---------------|---------------------------|------------------------|--|
| Scoria-agglutinate cone | l-l Agg and waSp | 28 | Circular | 228 | 34 | 0 | 22 | intermittent fountaining from point source |
| Scoria rampart | mwSc and waSp | 10 | Linear | 35–290* | 4–40 | 130–150 | 10 | intermittent fountaining from linear and possibly overlapping source(s) |
| Spatter rampart | l-l Agg | 45 | Linear | 16–25* | <0.5–4.5 | <50 | - | sustained fountaining from linear and possibly overlapping source(s); clastogenic flow |
| Sheet-like fall deposit | waSc | 11 | Linear | - | ≤1.1 | <1300 | 2 | medial/distal fall deposit |
| Rootless Cone | mSc | 20 | Circular | 30 | 14 | 100 | 60 | lava-water interaction |
| Table 3.6. Summary features of pyroclastic deposits. *shortest axis | | | | | | | | |

3.7.1 The R-K feeder dykes

On the east of the Jökulsá canyon edifice 26 is underlain by a conduit 80 m in height which flares upwards, widening from 4 m in diameter at its base to 28 m at its top (Fig. 3.30). The limited vertical exposure does not allow determination of the depth at which the conduit maintains an equal thickness. The northern conduit margin dips 53° while its southern margin dips 15° . Flaring is most pronounced in the upper 40 m of country rock, which is composed of plagioclase porphyritic basalt lava (Fig. 3.30). The conduit is composed of numerous coherent dykes of uniform hypocrySTALLINE, non-vesicular aphyric basalt (Fig. 3.30). The dykes exploit a normal fault (F10; Fig. 3.26) with a throw of ~ 3 m toward the southeast.

On the southern margin the dykes merge laterally with the columnar-jointed pāhoehoe (Cp; Fig. 3.25). On its northern margin the dykes have scallop-shaped contacts with the country rock and breaks up into 5 m thick, contorted dykes 5 m below the paleo-surface (Fig. 3.30). These dykes extend 10 m from the dyke, intruding into the overlying pyroclastic deposits. They thin with distance and have cooling joints across their entire width. The dykes dip $70\text{--}90^\circ$ to the southeast and northwest and fill scalloped shaped depressions within the country rock, merging laterally with the adjacent columnar-jointed pāhoehoe (Cp).

West of the river an 8 m-high section of dyke outcrops at the same elevation as the river (Fig. 3.30; Location 478). The dyke is aphyric and has columnar cooling joints spaced ~ 60 mm. Up to 200 mm from the dyke wall multiple chilled margins form sub-parallel laminations spaced ~ 25 mm apart. 10 m above the river, two ~ 1 m wide segments of dyke outcrop in the canyon walls. The eastern-most segment maintains a constant thickness and coherent texture and merges with the overlying columnar-jointed pāhoehoe (Cp; Fig. 3.30). The western-most segment terminates abruptly within the volcanoclastic sandstone with planar bedding (vS_{pb}) and maintains an equal thickness with height.

Interpretation:

Beneath edifice 26 the conduit is composed of numerous offshoot dykes, typical of monogenetic conduits (Keating et al. 2008). Dyke emplacement resulted in the activation of a pre-existing normal fault (F7; see Gudmundsson et al. 2008), consistent with the observations of Galindo and Gudmundsson (2012) for other feeder dykes. The feeder dykes were emplaced during numerous intrusive events, as evidenced by multiple chilled

margins and by intrusions into the columnar-jointed pāhoehoe (Cp; Fig. 3.30). The morphology of the dykes beneath edifice 26 and at location 478 are typical of effusive eruptions (Geshi and Oikawa 2014) since they merge with adjacent lava flows (columnar-jointed pāhoehoe, Cp) and are coherent beneath the surface. The abrupt termination of the more northerly dyke into the volcaniclastic sandstone with planar bedding (vSpb; Fig. 3.30) indicates that this dyke arrested before reaching the surface. However, it may have reached the surface elsewhere along its strike.

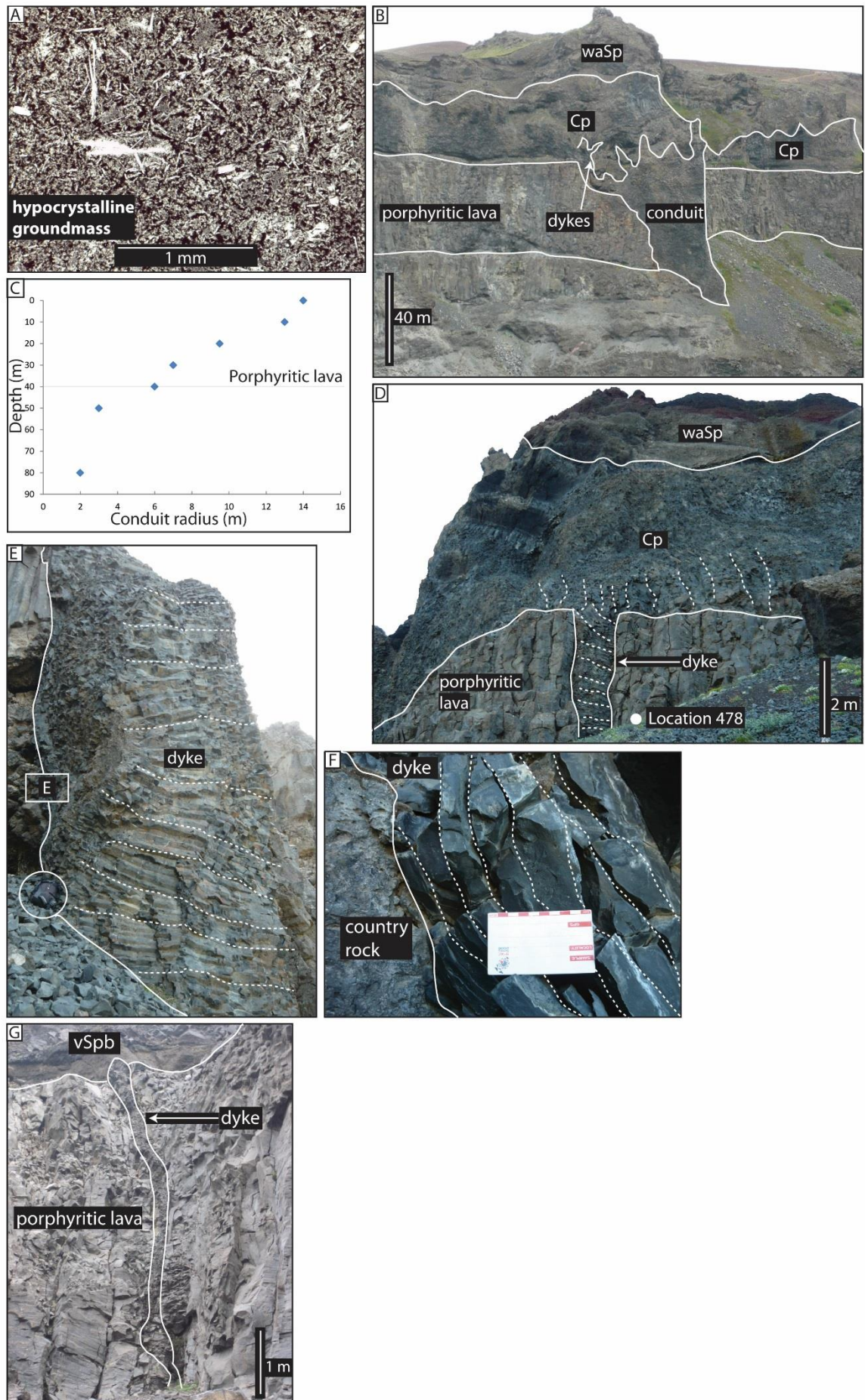


Figure 3.30 (overleaf). Architectural features of the dyke. (A) Thin section image of the dyke (plane polarised light). The sample is taken 30 cm from the country rock contact. (B) View toward the conduit from the west of the canyon. The underlying plagioclase porphyritic lava flows are the source of the lithic clasts in log 29 (Fig. 3.12). Note the scalloped contacts between the dyke and country rock and the numerous intrusions into the overlying pyroclasts. (UTM 557617/7265642). (C) Plot of depth from the top of the canyon vs. conduit radius. The flaring hinge is located at a depth of 40 m at the base of the porphyritic lavas. (D) An effusive dyke on the west of the canyon feeding overlying lava-like agglutinate (l-l Agg). Dashed lines indicate cooling joint orientations. See Fig. 3.25 for location. (UTM 557460/7264234). (E) A section of the dyke adjacent to the river on the west of the canyon. Dashed lines indicate cooling joint orientations. The solid line indicates the contact with the country rock. Bag (circled) is ~0.5 m. See Fig. 3.25 for location. (UTM 557510/7264268). (F) Multiple chilled margins at the dyke/country rock contact. The scale card is 10 cm long. Dashed lines indicate laminations spaced ~ 2 cm. See (D) for location. (UTM 557510/7264268). (G) Arrested dyke intruding into overlying pyroclastics west of the river. See Fig. 3.25 for location. Lithofacies codes are as Figs. 3.8 and 3.13. (UTM 557519/7264280).

3.7.2 Rootless cones

The columnar-jointed pāhoehoe (Cp) on the southeast of the dyke (location 285) has a hummocky, concave-up upper contact. The hummocks are up to 30 m in diameter. Cooling joints become more closely spaced (~10 mm) towards the upper contact, which is gradational with the overlying massive scoria lapilli and bombs (mSc; median grain size 2 cm). The columnar-jointed pāhoehoe is overlain by a 9.5 m-thick sequence of lava-like agglutinate (l-l Agg) and shelly pāhoehoe (Sh) that dips 20° radially outwards (modal value).

Interpretation:

The hummocky, concave-up upper contacts of the columnar-jointed pāhoehoe are interpreted as the vents of rootless cones. They are identical to the vents of rootless cones elsewhere in Iceland and the Columbia River (Fig. 3.31; see Chapter 4). Furthermore, rootless cones are common in the dyke-proximal regions of fissure eruptions (e.g. Thordarson and Self 1993; Hamilton et al. 2010). Since the size of the vent is proportional

to size of the overlying edifice (Fagents and Thordarson 2007; Hamilton et al. 2010), the cones are inferred to have been ≤ 30 m in diameter. The lava-like agglutinate (l-l Agg) and shelly pāhoehoe (Sh) that overly the vents and dip 30–40° radially outwards (Location 285; log 29) are interpreted as the products of rootless eruptions. However, the crater of the cone is inferred to have been flooded by later lavas and is not exposed (Fig. 3.29). Rootless cones are not observed elsewhere along the R-K fissure, suggesting that the studied section either represents a very localised rootless cone field in which surface/open water was particularly abundant, or that cones elsewhere along the fissure have been buried by later-erupted products (see also section 3.9.2).

An alternative suggestion is that the columnar-jointed pahoehoe (Cp) represents a feeder network for lava flows within dyke-fed pyroclastic deposits (e.g. Sánchez et al. 2014). However, this interpretation would provide no explanation for the cauliflower-like texture of the pyroclasts in the massive scoria lapilli and bombs (mSc; Fig. 3.7); the radial dip of the overlying lava-like agglutinate (l-l Agg) and shelly pāhoehoe (Sh) and the occurrence of armoured clasts with a plagioclase porphyritic-clast core.

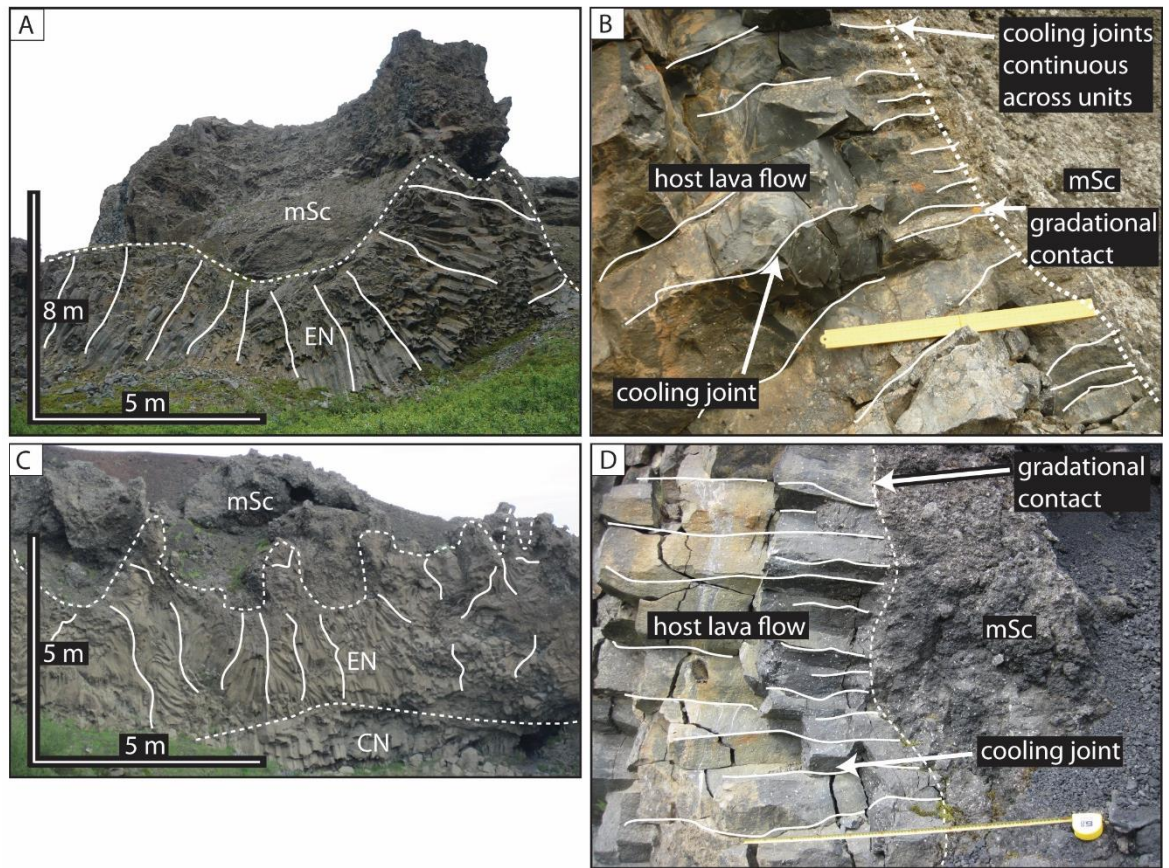


Figure 3.31. Comparison between rootless vents at Hjalparfoss (UTM 402187/7098548) and those along the R-K fissure (UTM 557772/7265756). Images A and C show the vents and the host lavas flows along the R-K fissure and at Hjalparfoss respectively, images B and D show the contact between the columnar jointed pāhoehoe (Cp) lava and massive scoria lapilli and bombs (mSc). Notice the colonnade (CN) and entablature (EN) of the lava flows with cooling joints that radiate from the hummocky, bowl-shaped upper contact. The ruler in B and D is 25 cm.

3.7.3 Scoria ramparts

Numerous small pyroclastic edifices are elongated parallel to the fissure (Fig. 3.29, locations 477, 280 and 077). These deposits have basal diameters of 35–290 m. Feeder dykes are not observed beneath the deposits (except location 477; see following discussion). They are composed of 4–40 m thick bedded sequences of clast-supported incipiently welded spatter bombs (waSp); clast-supported moderately welded scoria lapilli and bombs (mwSc); clast-supported densely welded spatter bombs (dwSp); clast-supported weakly agglutinated scoria lapilli and bombs (waSc) and scoria lapilli (ScL). The ramparts are characterised by low angle dips and are set-back 130–150 m from the fissure (Fig. 3.29). Their median grain size is 10 cm (see Table 3.6).

The ~20 m succession at Location 280 (Figs. 3.25 and 3.29) is represented on Logs 2 and 11 (Fig. 3.11). Log 11 shows that clast-supported densely welded spatter bombs (dwSp) unconformably overly the columnar-jointed pāhoehoe (Cp). The pyroclastic units dip 16–44° to the south and southeast. These beds are truncated on their northwestern margin by the present ground surface (Fig. 3.32). Numerous 10 m wide, sinuous channels occur in the surface of the deposit (Fig. 3.33). These channels are 1–5 m deep and strike 183°, covering an area of 38 m². Log 2 shows that clast-supported incipiently welded spatter bombs (waSp) and clast-supported moderately welded scoria lapilli and bombs (mwSc) unconformably overlie the clast-supported densely welded spatter bombs (dwSp) and columnar-jointed pāhoehoe (Cp). There is an absence of lithic clasts within both logs. Bedding within this succession dips northwest and southeast (see Fig. 3.29).

Faults 1, 2, 4, 38 and 63 occur in this deposit (see logs 2 and 11; Fig. 3.26). Blocks of deformed clast-supported densely welded spatter bombs (dwSp; Fig. 3.26) ~1 m³ in size occur at the tops of faults F 63 and F 1. These blocks contain ghost clasts that dip 11° to the southwest. The ghost clasts are intersected by 70 mm long tension gashes that dip 70° to the southwest. The tension gashes form numerous rotated blocks ~0.08 m³ in size and downthrow the ghost clasts by 2 cm. Other blocks of clast-supported densely welded spatter bombs (dwSp) show similar tension gashes and contain sheared vesicles and have irregular, deformed outer surfaces. Faults 1, 2, 38 and 4 generated a slip of ≤4 m toward the southeast in the upper units (clast-supported incipiently welded spatter bombs, waSp and clast-supported moderately welded scoria lapilli, mwSc; Fig. 3.27). No displacement is observed in the columnar-jointed pāhoehoe (Cp) at the base of the faults, but zones of hackly jointing are developed along the fault plane.

Another 20 m high dissected mound of scoria occurs west of the river. This mound is composed of clast-supported incipiently welded spatter bombs (waSp) that dip 30° northwest and northeast (Location 477; Figs. 3.25 and 3.29). The mound has an antiformal structure at depth, the dip of which shallows to 08° laterally and with height. It has gradational lateral and vertical contacts with the underlying and adjacent columnar-jointed pāhoehoe (Cp) and clast-supported incipiently welded spatter bombs (waSp). The bedding of the clast-supported incipiently welded spatter bombs (waSp) is truncated by the present ground surface. At its base the mound is composed of columnar-jointed pāhoehoe (Cp) which becomes less laterally extensive with height. Towards the southeast, the mound is overlapped by hummocky lavas (Hu).

Other elongate mounds occur further south along the fissure (Fig. 3.29; locations Y22–24). It is unclear whether these mounds are set back from the eastern or western margin of the fissure. Dissected mounds of scoria are also exposed on the eastern canyon wall. Location 302 is composed of clast-supported incipiently welded spatter bombs (waSp) and clast-supported weakly agglutinated scoria lapilli and bombs (waSc). It forms a ridge-like feature 70 m in length and 4.5 m high. Beneath this, another scoria mound occurs (Location 406; Fig. 3.25). This mound is inaccessible, but appears to be composed of columnar-jointed pāhoehoe (Cp) and clast-supported weakly agglutinated scoria lapilli and bombs (waSc) that dips 10° toward the southeast. It is 8 m high and 10 m in length and has a distinctive near-vertical northwest margin. It is overlain and underlain by the columnar-jointed pāhoehoe (Cp), with which it also has distinct lateral contacts.

Interpretation:

These pyroclastic sequences are interpreted as dissected scoria ramparts (the scoria "mounds" of Breed 1964). The ramparts are similar to the "scoria half cones" adjacent to the Laki fissure (Fig. 3.34) which are elongated parallel to the fissure, larger than the adjacent cones and set-back from the fissure. The linear shape of the ramparts in plan view suggests that they accumulated from a linear fountain or from overlapping fountains. The lava fountains were sufficiently collimated or tall to allow the formation of different clasts (e.g. spatter bombs and scoria lapilli). The dominance of juvenile clasts that show no evidence of recycling or ball milling (e.g. cored bombs) indicates that the ramparts formed prior to the adjacent pyroclastic cones. The massive beds defined by minor clast-size fluctuation and absence of rounded clasts suggest that the clasts were deposited in-situ without grain-flow avalanching, typical of Hawaiian activity (Valentine and Gregg 2008).

The abundant welding is also consistent with deposition during Hawaiian-style activity (Valentine and Gregg 2008). The size of the component clasts is typical of the deposits of Strombolian and Hawaiian-style eruptions (Valentine and Gregg 2008).

The pyroclastic sequence at Location 280 is inferred to be eroded, as indicated by the truncated beds and fluvial channels. This rampart may have been constructed as a result of the wind-stripping of pyroclasts from a lava fountain. The size difference between the ramparts at Locations 280 and 302 either side of the fissure (Fig. 3.25) is supportive of this interpretation. The abundance of clast-supported densely welded spatter bombs (dwSp; logs 11 and 2; Fig. 3.11) towards the base of the sequence suggests that deposition was dominated by clasts from the lower part of the fountain, or by a low fountain that contained a high proportion of spatter bombs. Towards the top of the scoria rampart, the abundance of clast-supported moderately welded scoria lapilli and bombs (mwSc) suggests that with time deposition was increasingly dominated by clasts from the outer and upper part of the fountain, or by a wider spread fountain which yielded higher proportion of these clasts. The changing dip directions at location 280 (log 2; Fig. 3.11) suggests that the source of pyroclastic material migrated from dominantly north to dominantly south with time. This may indicate either 1) a subtle change in dominant wind direction or 2) cessation of fountains towards the north.

Faulting is inferred to have altered the architecture of this rampart. Syn-eruptive slip along fault F9 resulted in the ductile extensional deformation of clast-supported densely welded spatter bombs (dwSp), indicated by the displacement of ghost clasts and tension gashes. Slip on faults 1, 2, 38 and 4 are inferred to have occurred post-eruption. Percolation of water down this fault may have initiated the hackly jointing along the fault planes.

The scoria rampart at location 477 has gradational contacts between clast-supported weakly agglutinated spatter bombs (waSp) and columnar-jointed pāhoehoe (Cp). These imply sustained accumulation, and lateral gradational changes result from either 1) pinching out of lenses of pyroclastic material 2) local zones of high or low accumulation rates. Since the other scoria ramparts (e.g. locations 280 and 302) are set-back from the fissure, not directly adjacent to it, this rampart is inferred to have been constructed by deposition from an adjacent section of the fissure, represented at locations Y27–Y32. Thus, the fissure was segmented, and the easterly section (feeding edifice 26; Fig. 3.3) closed prior to the westerly section. This westerly section feeds the southern part of the fissure. The rampart at location 406 is thought to have been deformed during lava flow

emplacement (e.g. Brown et al. in press). However, the exact method of deformation is unclear.

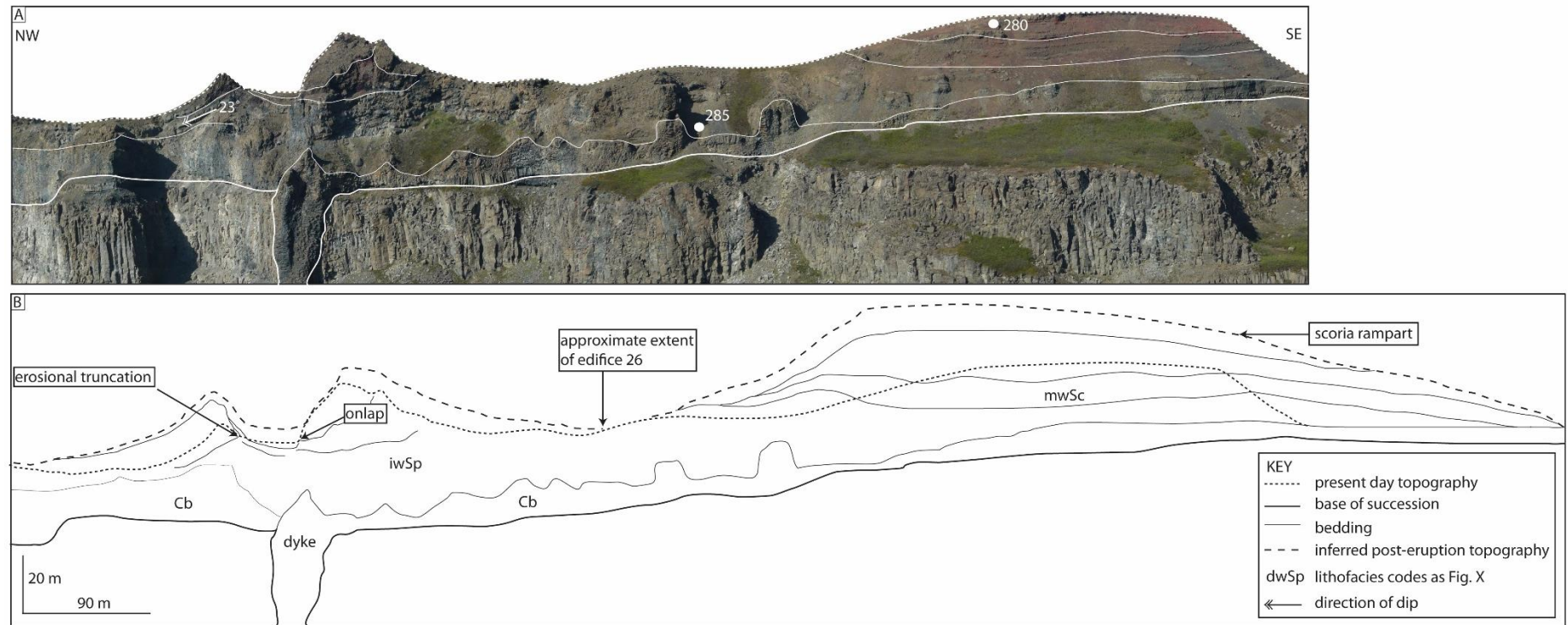


Figure 3.32. Photograph (A) and a reconstruction of the geometry of the pyroclastic constructs immediately after the eruption (B). Truncated beds are visible in the NW margin of the scoria rampart (location 280) and in the crater of cone 26. Field observations suggest ~10 m of stratigraphy is has been eroded from the cone and the rampart. (A: UTM 557542/7264269).



Figure 3.33. Google Earth image showing the inferred location of paleo-channels, contemporary channels and the outcrops of sedimentary lithofacies.

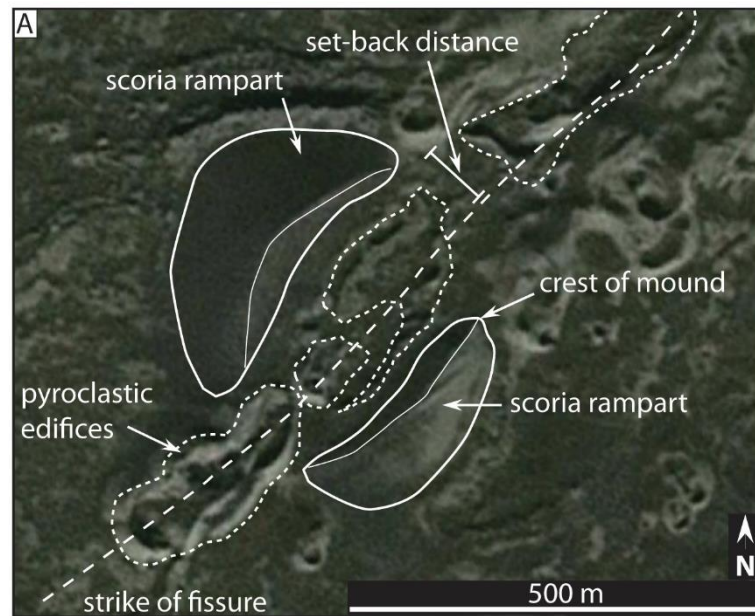


Figure 3.34. Scoria ramparts adjacent to the Laki fissure. (A) Google earth image showing that the ramparts are linear and crescent-shaped, elongated parallel to the fissure. They occur on the outer margin of the cones (UTM 361475/7159674).

3.7.4 Sheet-like fall deposits

Examples of these deposits occur on the eastern canyon wall (Location 350) and beneath the clastogenic lava, west of the river (log 16; location 462; Fig. 3.25). It is unknown whether the deposits on the eastern canyon wall are in-situ; they are found overlying a lava flow and may have been rafted (Sumner 1998; Brown et al. in press). The deposits west of the river (log 16, location 462, Fig. 3.25) overly the pre-eruption substrate, thus are in-situ. This deposit of clast-supported weakly agglutinated scoria lapilli and bombs (waSc) occurs ~500 m from the fissure, is <0.25 cm thick and has a mean grain size of 10 mm. Elsewhere on the southeast of the fissure, deposits ~1 m thick are recorded at ≤1300 m from the fissure (Fig. 3.12).

Interpretation:

The sheet-like fall deposits are interpreted as the medial deposits from a lava fountain. The welded nature of deposits is consistent with Hawaiian-style activity (Valentine and Gregg 2008). Tephra with similar dispersal characteristics is recorded by Aramaki et al. (1986) and Wolfe et al. (1988) during Hawaiian and Strombolian-style eruptions.

3.7.5 Scoria-agglutinate cone

Edifice 26 outcrops on the eastern canyon wall (Figs. 3.25, 3.26 and 3.29). This edifice was fed by the R-K feeder dyke (Figs. 3.3 and 3.26) and has a 90 m wide circular crater; the extent of which is marked by a 5–10 m high crater rim. Beds of lava-like agglutinate (l-l Agg) and clast-supported incipiently welded spatter bombs (waSp) on the northwest margin of the crater are truncated (Fig. 3.32) whilst on its southeast margin these beds onlap against the crater rim. The pyroclastic units are overlain by 2.25 m of sedimentary deposits (lithofacies fSdb and cCi; Fig. 3.32C).

The flanks of the edifice are dominated by spatter-rich lithofacies including lava-like agglutinate (l-l Agg), clast-supported, incipiently, moderately and densely welded spatter bombs (waSp, mwSp and dwSp); clast-supported weakly agglutinated scoria lapilli and bombs sometimes with inverse grading (waSc(i)); clast-supported non-welded scoria lapilli (ScL); and clast-supported densely welded scoria (dwSc). Component clasts range in size from 5–70 cm (median 22 cm). Beds dip inwardly towards the dyke at 12–60°, with units on the southeast of the crater dipping more steeply than those on the northwest. Outwardly dipping beds in the cone flank have a modal dip of 28° (Table 3.6).

The crater is underlain by columnar-jointed pāhoehoe (Cp; logs 10,81 and 12, Figs. 3.10, 3.25 and 3.35). A rosette structure (inferred to be composed of columnar-jointed pāhoehoe; Cp) 15 m in diameter occurs within the crater, with radial cooling joints spaced ~15 cm apart and cuboidal jointing in its core (Fig. 3.35). It occurs ~10 m below the present ground surface and is fed by the dyke. Cooling joints are sub-vertical on the rosettes' upper and lower surfaces but are poorly developed across the mid-section. Joints are longer and more widely spaced at the rosettes' base. At its margins the rosette bifurcates into numerous 1–5 m thick beds of columnar-jointed pāhoehoe (Cp) that dip ~20° to the SW.

The stratigraphic sequence within the crater is shown in logs 81 and 12 (Fig. 3.10). There are gradational and distinct contacts between the various pyroclastic lithofacies which include lava-like agglutinate (l-l Agg), clast-supported, incipiently and moderately welded spatter bombs (waSp and mwSp), clast-supported weakly agglutinated scoria lapilli and bombs (waSc) and clast-supported densely welded scoria (dwSc). Cored bombs and armoured clasts with aphyric lava and agglutinate cores are common within the upper 15 m of the R-K volcanic sequence. Lava-like agglutinate (l-l Agg) is also common and forms a bifurcating network of 0.5–2 m thick beds that intrude into the adjacent clast-supported incipiently welded scoria lapilli (waSc; log 81, Fig. 3.10). This creates 8 m wide and 1 m

thick lenses of clast-supported weakly agglutinated scoria lapilli and bombs (waSc) within the lava-like agglutinate (Fig. 3.32B). Tension gashes occur at the margins of the lava-like agglutinate (l-l Agg).

The southeast cone flank is dominated by clast-supported, incipiently welded spatter bombs (waSp). The northwest cone flank is composed of 27–50 cm thick variably welded, inversely graded and massive pyroclastic deposits and lava-like agglutinate (l-l Agg; logs 9 and 10; Figs. 3.11 and 3.35). Both the pyroclastic units and lava-like agglutinate (l-l Agg) contain cored bombs and aphyric basalt lithics. Beds of the lava-like agglutinate (l-l Agg) thicken with distance from the crater and merge laterally, dipping 13° west-northwest. Normally graded sequences of clast-supported incipiently welded spatter bombs (waSp) and clast-supported non-welded scoria lapilli (ScL) are also present (Fig. 3.35). These sequences contain ragged, Hawaiian-type scoria clasts that become abundant towards the top of the section. At distances of 20–100 m southeast from the dyke the cone flank is composed of columnar-jointed pāhoehoe (Cp) and clastogenic and shelly pāhoehoe (log 29, Fig. 3.11). Numerous outcrops of fine, cross bedded volcanoclastic sandstone with gravel, pebbles and cobbles (fSxb) occur in this area (Figs. 3.3 and 3.33).

Interpretation:

The present dimensions of edifice 26 are not thought to be representative of its original size. The sedimentary lithofacies (e.g. fSdb and cCi) and the truncated beds within the NW margin of the crater indicate that it has been eroded. Projecting the dip of the eroded crater beds upwards, an estimated ~10 m of stratigraphy has been removed. Extending the outward dipping units at 28° from this reconstructed height gives edifice dimensions of 34 m high and 228 m in basal diameter. These dimensions and the cone height–width relationship (0.15) is similar to that reported for scoria cones (e.g. Wood 1980). The circular crater suggests that the cone was formed beneath a point-sourced fountain rather than a fissure.

Evidence for grain flow avalanches (i.e., lithofacies waSc(i); log 10, Fig. 3.10) indicates that cone building occurred partly via talus slope formation (e.g. McGetchin et al. 1974). Steep bedding on the south-eastern crater rim indicates that material was accumulating more rapidly on this side of the cone. The coarse bombs, rapid variations in welding and thick, densely welded units are typical of Hawaiian-style activity (Valentine and Gregg 2008). The size of the component clasts is typical of the deposits of Strombolian and Hawaiian-style eruptions (Valentine and Gregg 2008).

Accumulation of pyroclasts (e.g. spatter and cowpat bombs; Fig. 3.10, logs 10, 12 and 81) occurred dominantly from the inner and lower part of the fountain, or from a fountain <100 m in height (similar to those observed by Wolfe et al. 1988). Steeply dipping intrusive contacts between the lava-like agglutinate (l-l Agg) and pyroclastic units (lithofacies log 81; Fig. 3.10) may represent a section through a network of lava sills and dykes that fed flows outside the cone (e.g. Sánchez et al. 2014). Normally graded sequences of clast-supported weakly agglutinated spatter bombs (waSp) and clast-supported non-welded scoria lapilli (ScL) towards the top of the crater could represent the weakening of fountaining intensity with time. The rosette structure (Fig. 3.35) is interpreted as the remnants of a lava lake in an adjacent edifice, which was subsequently eroded by the Jökulsá River. Outcrops of fSxb at the base of the cone flank indicate fluvial erosion in this region.

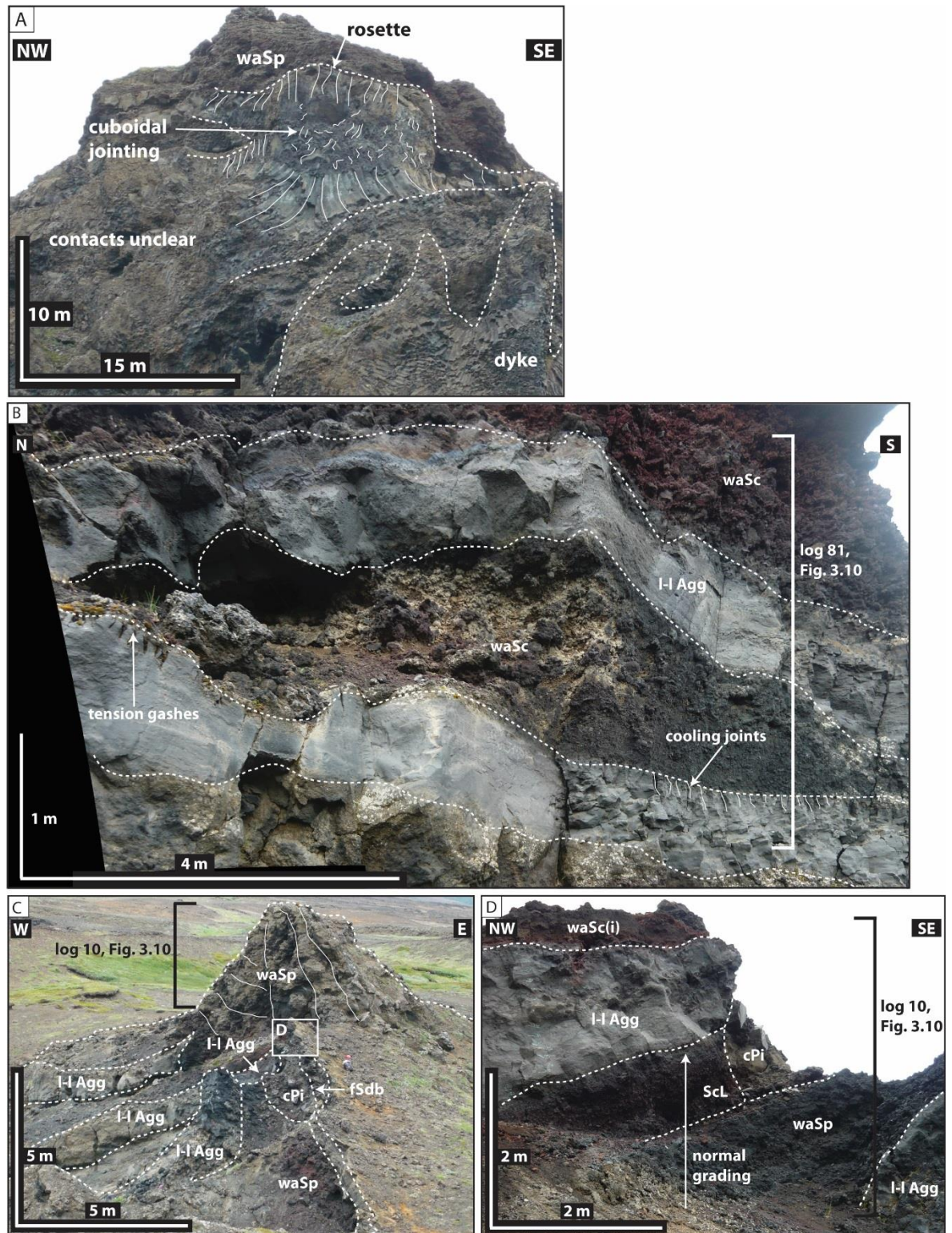


Figure 3.35. Photographs showing the architecture of edifice 26. (A) The rosette structure is located above the feeder dyke. The cooling joints at the top of the rosette are more closely spaced and shorter than those at the base, implying that the rosette cooled from the top downwards. (UTM 557498/7264870). (B) A lobate lense of clast-supported weakly agglutinated scoria lapilli and bombs (waSc) within the lava-like agglutinate (I-I Agg). The lava-like agglutinate (I-I Agg) has distinct contacts with the

clast-supported weakly agglutinated scoria lapilli and bombs (waSc) and is interpreted to be part of a lava sill/dyke network. (UTM 557447/7264902). (C) View of the northern crater rim showing the outwardly dipping units of lava-like agglutinate (l-l Agg) which merge further west. Inverse-graded cobble breccia (cPi) and fine, diffusely bedded volcanoclastic pebbly sandstone (fSdb) are visible inside the crater. (UTM 557438/7264880). (D) Photo of the outwardly dipping lithofacies on the crater rim. (UTM 557447/7264902).

3.7.6 The spatter ramparts

Spatter ramparts form 28–270 m long linear features along the fissure (Fig. 3.36). They are oriented both perpendicular and parallel to the strike of the fissure. They vary from <0.5–4.5 m in height and 16–25 m in width. Erosion exposes the internal architecture of a series of similar ridge-like features west of the river (Fig. 3.37). They are dominantly composed of lava-like agglutinate (l-l Agg) with minor components of clast-supported, incipiently, moderately and densely welded spatter bombs (waSp, mwSp and dwSp). Bedding in the ramparts has a modal dip of 45° (Table 3.6). They occur in a 100 m-wide zone centred above the strike of the fissure. Unconsolidated achneliths are common around the ramparts (Fig. 3.3).

The largest of these outcrops (Location Y29; Fig. 3.37) is 4.5 m high and 80 m in length. The southern face of the outcrop dips 40° to the south whilst its northern face dips up to 58° to the north and northwest. Both faces are composed of numerous discontinuous slabs of lava-like agglutinate (l-l Agg) and clast-supported weakly agglutinated spatter bombs (waSp). The agglutinate slabs are up to 4 m in length and 3 m in width and have a jigsaw-fit arrangement. At the apex of the rampart and where the dip changes from 08° to 55°, fractures 200 mm in width separate the slabs (Fig. 3.38). In some instances the slabs are missing, and lava-like agglutinate (l-l Agg) with a rubbly surface texture is exposed beneath. The slabs have resinous rinds 10 mm thick with ~3 mm deep scours on their external surfaces (Fig. 3.38). Some of these scours are overprinted by tension gashes oriented sub-perpendicular to the external surface dip direction. Many of these scours are oriented obliquely to the external surface dip direction (Fig. 3.38).

On the southern outcrop face, the texture of the crust on the uppermost agglutinate slab varies with height up the rampart. The upper 3 m of the slab has a scoured crust (Fig. 3.38), while the down-dip front (i.e. “snout”) of the slab has a rugose outer crust. This rugose crust is formed by ragged protrusions that vary in height and width from 10–40 mm

and 10–50 mm respectively. The protrusions are separated by tension gashes which form preferentially towards the snout of the agglutinate beds (Fig. 3.38). The tension gashes decrease in width with distance from the snout (Fig. 3.38).

Internally the slab has a vesicular upper and lower crust. Each of the crusts comprises ~30 % of the thickness of the slab. The crusts have homogeneously distributed <1–3 cm diameter vesicles that have a mean abundance of 15% (Fig. 3.39). The vesicles are irregular and elongate, with the direction of elongation sub-parallel to the crust surface. Underlying beds of spatter are discordant with the uppermost slab and give the rampart a “patchwork” internal character (Fig. 3.39). These beds dip 27–56° to the southwest and some have scoured upper surfaces similar to the outermost surface. Individual beds vary from 150–2500 mm thick and pinch out after ≤ 1 m. Relict pyroclasts are occasionally visible; where preserved they are ≤ 100 mm long and 10 mm thick, oriented parallel to the upper contact with the lava-like agglutinate (l-l Agg).

Location Y28 (Figs. 3.37 and 3.40) is another ridge-like outcrop that is 3 m high and 28 m in length. Its outer surface dips sub-vertically on the southern face and 47° on the northern face (Fig. 3.37). Internally the outcrop is composed of clast-supported weakly agglutinated spatter bombs (waSp) overlain by lava-like agglutinate (l-l Agg). The lowermost 240 mm of lava-like agglutinate (l-l Agg) is non vesicular and has 4 mm thick resinous laminations and tension gashes that dip 42° to the south. The lava-like agglutinate (l-l Agg) grades upwards into massive, incipiently vesicular lava-like agglutinate (l-l Agg). It is incipiently vesicular with a patchy, heterogeneous distribution of <1–10 mm diameter vesicles. 20 mm long ghost clasts that dip 20° to the SE are observed in the upper 400 mm. Tension gashes up to 170 mm in length intersect the 70 mm thick outer crust and fragment it into equant ~200 × 150 mm sized jigsaw-fit plates. Agglutinated, non-welded scoria lapilli cover <5% of the surface.

Interpretation:

The ridge-like features west of the river are interpreted as spatter rampart and cone-like features (e.g. Thordarson and Self 1993). They preserve delicate surface features (e.g. mm-scale scours and crustal protrusions; Fig. 3.38) indicating that there has been minimal erosion. It is possible that these ramparts represent the early aborted stages of scoria cone growth (e.g. Wolfe et al. 1988; Valentine and Cortés 2013). The ramparts are dominantly composed of lava-like agglutinate (l-l Agg) and provide no evidence of subsidence into the underlying columnar-jointed pāhoehoe (Cp) that would suggest rafting (e.g. squeeze-ups at

the margins of the rafted fragments; see Sumner 1998; Valentine et al. 2006). Their location within a 100 m-wide zone centred on the strike of the fissure (Fig. 3.37) suggests that they are in-situ and dyke-fed. There is no evidence to suggest that they formed above a lava tube, as required for hornito formation (Németh 2014).

Cross sectional exposure of the ramparts suggests that they accumulated rapidly from pyroclasts sourced from the inner part of the lava fountain, or from low fountains that yielded a high proportion of spatter bombs. Although the depositional processes are hard to discern due to the high degree of welding, a combination of post-depositional modification processes are observed. These processes include flow, scouring, brittle failure and gravitational spreading.

Numerous tension gashes in the agglutinate deposits indicate that they started to flow. Tension gashes become more abundant and widen towards the snout of agglutinate beds (e.g. Fig. 3.35) suggesting that that shear strain was concentrated here. Scours (location Y29) are inferred to result from the slip of solidified agglutinate sheets and/or pyroclastic deposits down the outer surface. Cross-sections through the rampart expose numerous scoured surfaces within the deposit, suggesting this process was repeated during rampart construction. The varying orientation of the scours suggests that material slid downwards as numerous separate sheets, as opposed to whole scale collapse of the external rampart face. The absence of lateral scours on the surfaces suggests that the scours were not caused by lava flow along the fissure (e.g. Parcheta et al. 2012). The tension gashes that overprint the scours suggest brittle deformation of the external surfaces of the rampart after material has scoured them. Location Y29 is inferred to have been constructed by the accumulation and coalescence of spatter bombs, which subsequently underwent clastogenic flow (Fig. 3.41). Brittle failure of the agglutinate is indicated by the angular external margins of the agglutinate slabs at location Y29 (Fig. 3.38). The brittle failure of the slab at the change in dip magnitude suggests failure was initiated by over-steepened depositional slopes.

Unstable agglutinate piles underwent gravitational spreading (Locality Y28, Fig. 3.42) as inferred from the tension gashes at the base of the deposit and those which fracture the crust into numerous jigsaw-fit plates. The non-vesicular base of the agglutinate may have acted as a slip plane during deformation (e.g. Sumner 1998). Spreading was induced by the steep dips maintained by the accumulating agglutinate pile. The outer crust and the ghost clasts have differing orientations, suggesting that the crust represents a cooling surface and not a depositional surface (e.g. bedding plane).

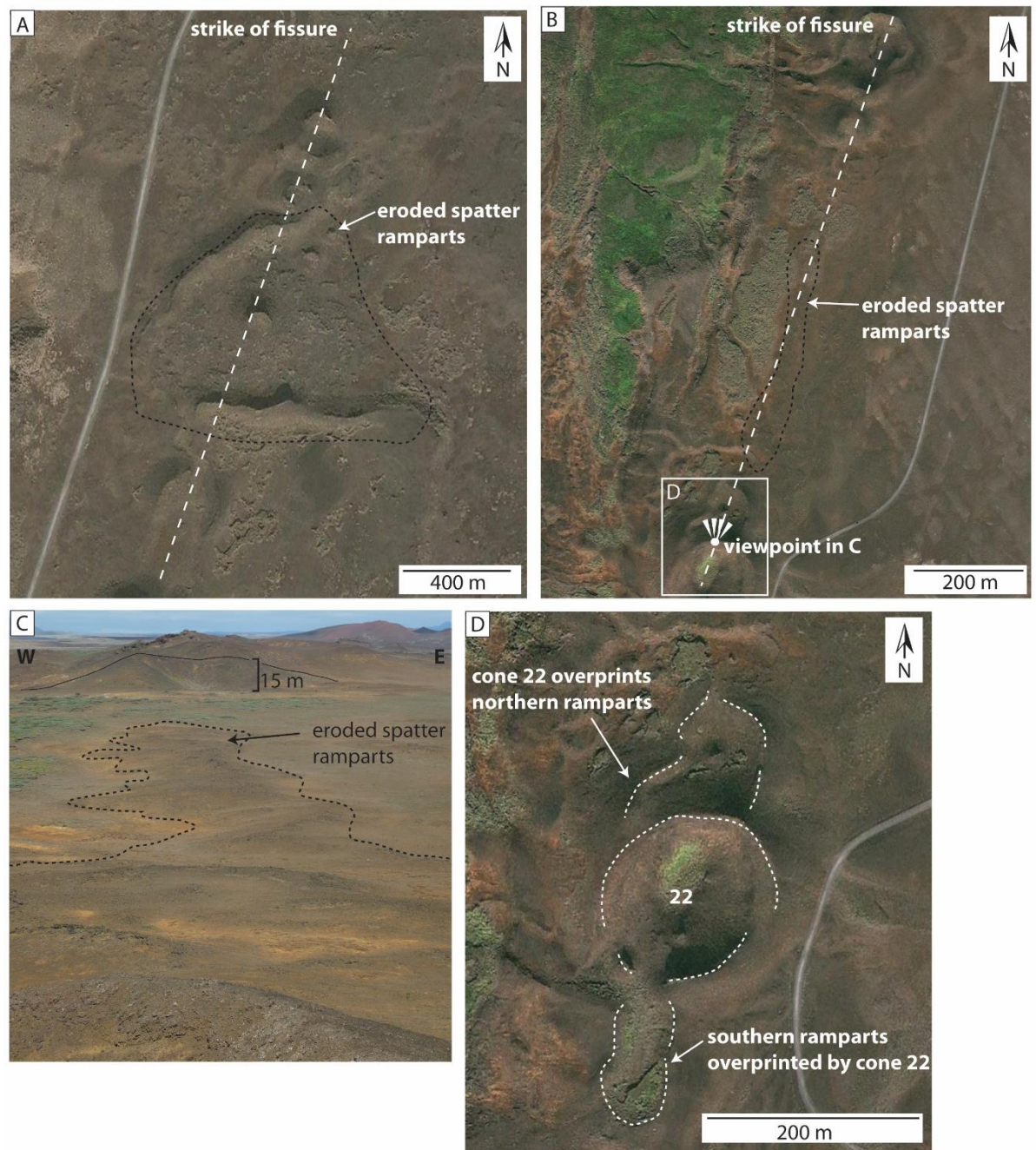


Figure 3.36. Orientation and onlap relationships of the spatter ramparts. (A) Google Earth image showing that some spatter ramparts are oriented perpendicular to the strike of the fissure. **(B)** Google Earth image of eroded spatter ramparts that are oriented parallel to the strike of the fissure. **(C)** Photograph of the spatter ramparts shown in B. **(D)** Google Earth image of scoria cone 22 overprinting adjacent spatter ramparts. The onlapping relationship of the edifices cannot be used to constrain the direction in which the fissure propagated. See Fig. 3.5 for location.

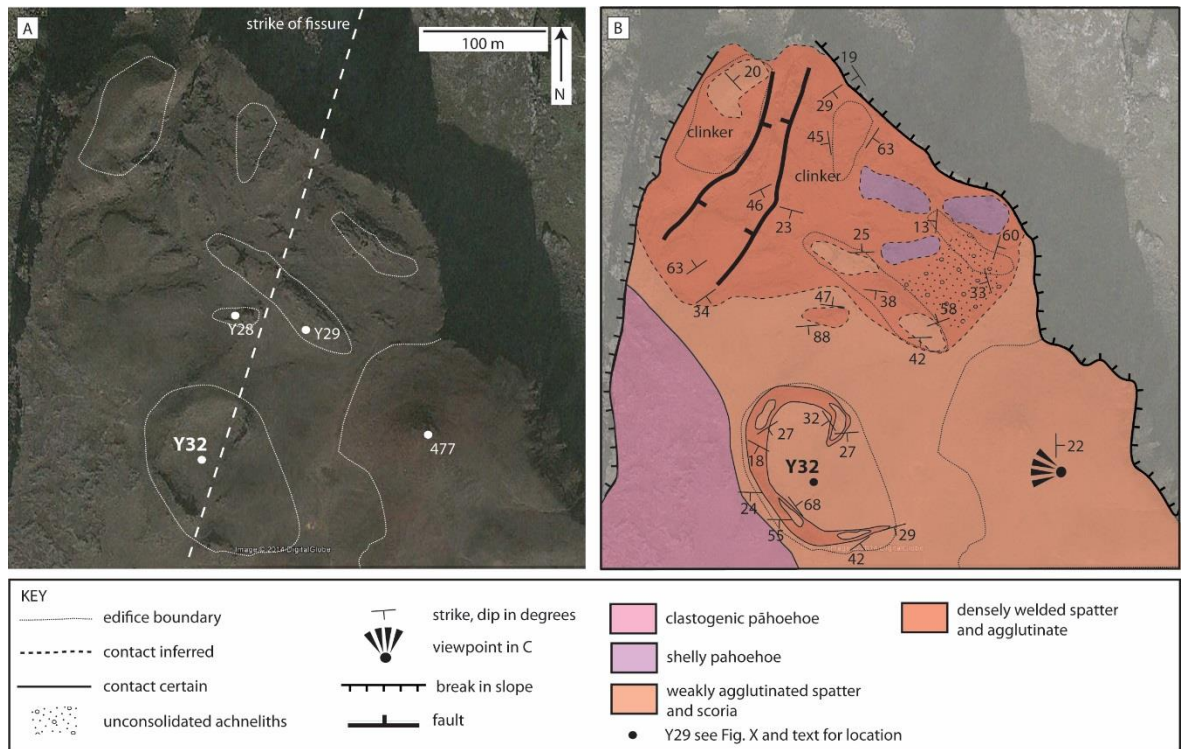


Figure 3.37. Google Earth image (A) and geological map (B) of the spatter ramparts west of the river. See Fig. 3.3 for location.

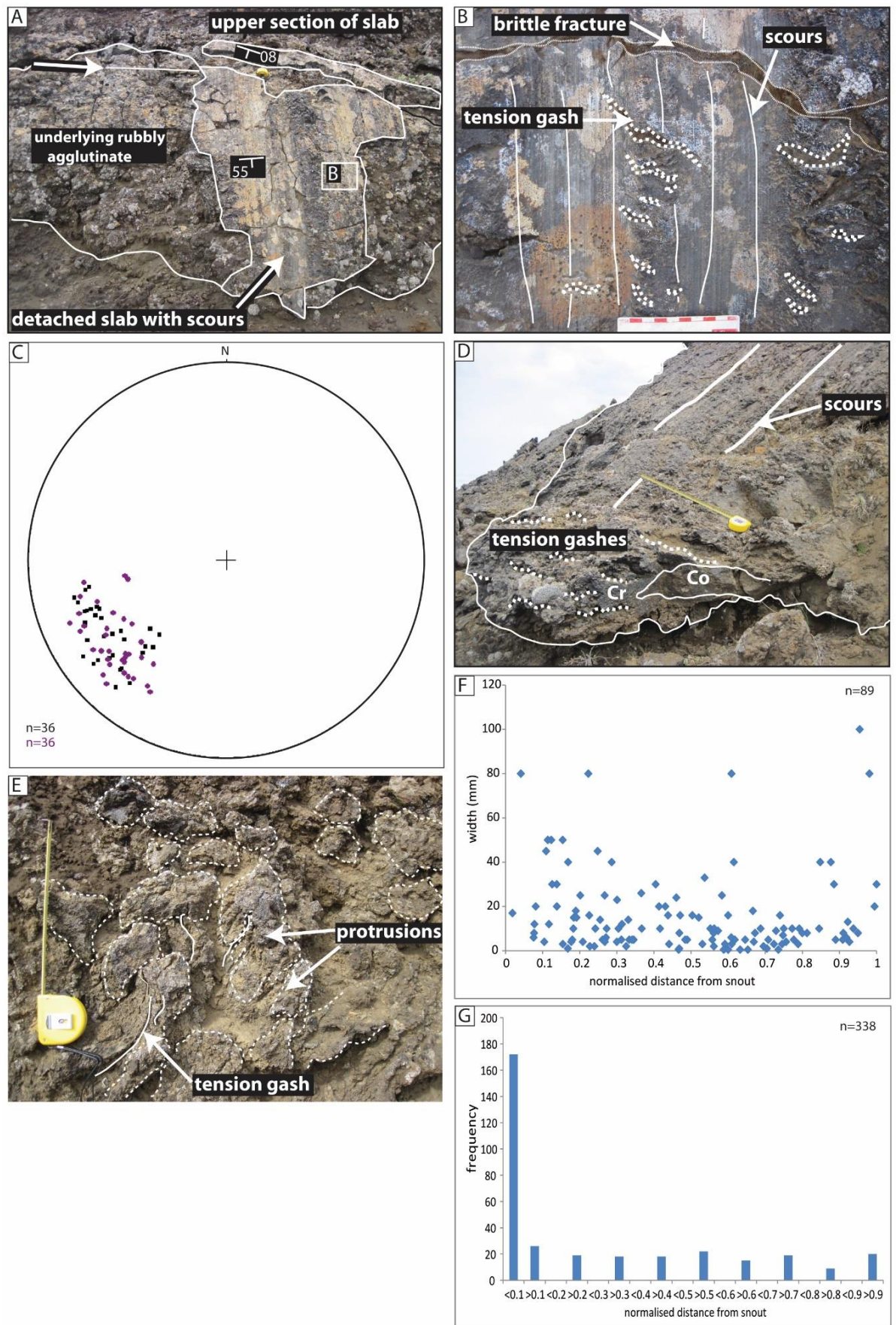


Figure 3.38 (overleaf). Features and measurements associated with location Y29. (A) Scoured agglutinate slab with adjacent sections missing, exposing underlying rubbly agglutinate. The slab has detached from the upper section (arrowed) where the dip of the outcrop changes. The tape measure (arrowed) is 1 m long. (UTM 564346/7301822). (B) Close up of the scours overprinted by tension gashes (outlined), indicating deformation of the agglutinate after the external surface was scoured. Graticules on the scale card are 1 cm. (UTM 564346/7301822). (C) Stereonet plot to show orientation of bedding (black) and scours (purple) on the southwest face of location Y29. The scour plunges are not parallel to the bedding dip direction suggesting that sliding from the outer face occurred in numerous directions with a component of lateral movement. (D) Cross sectional view of the snout of an agglutinate bed. The tension gashes (dashed lines) on the crust (Cr) are perpendicular to the scours (sub vertical striations) and give the snout a rugose texture. The core of the bed (Co) is also exposed (see Fig. 3.39 for details). The tape measure is 1 m long. (UTM 564346/7301822). (E) A rugose textured surface, showing irregular protrusions separated by tension gashes. The ruler is 10 cm long. (UTM 557584/72664247). (F) Graph showing that tension gashes are most abundant towards the snout of the agglutinate sheets, where 0 = the snout tip. (G) Graph showing that crenulation width tends to decrease with distance from the snout of agglutinate beds, where 0 = the snout tip. Graphs F and G suggest that strain is greatest towards the snout of the beds.

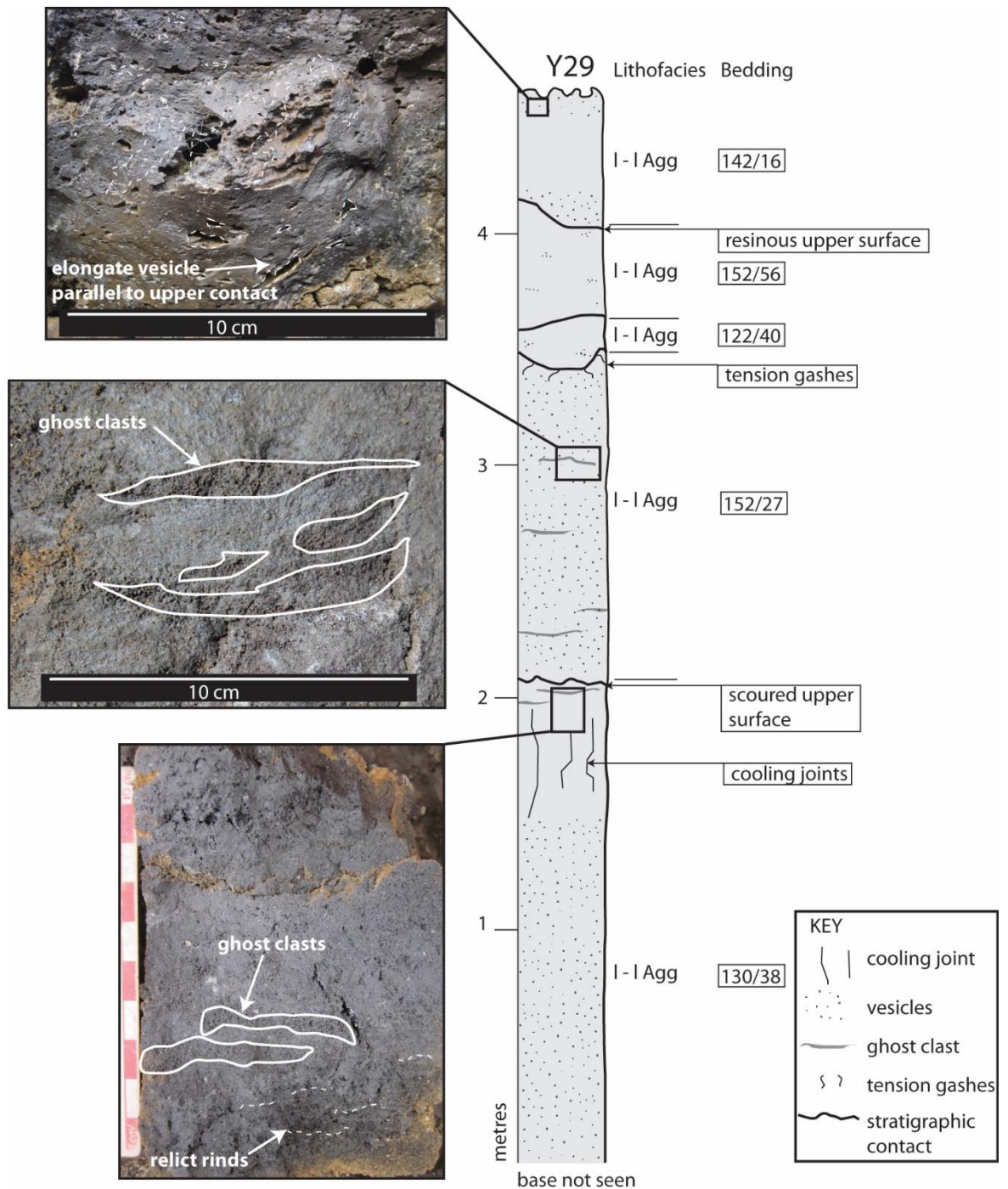


Figure 3.39. Stratigraphic log showing the internal componentry of location Y29. The outcrop is composed of numerous discordant slabs of agglutinate. The upper unit of agglutinate is shown in Fig. 3.38D. See Fig. 3.37 for the location.

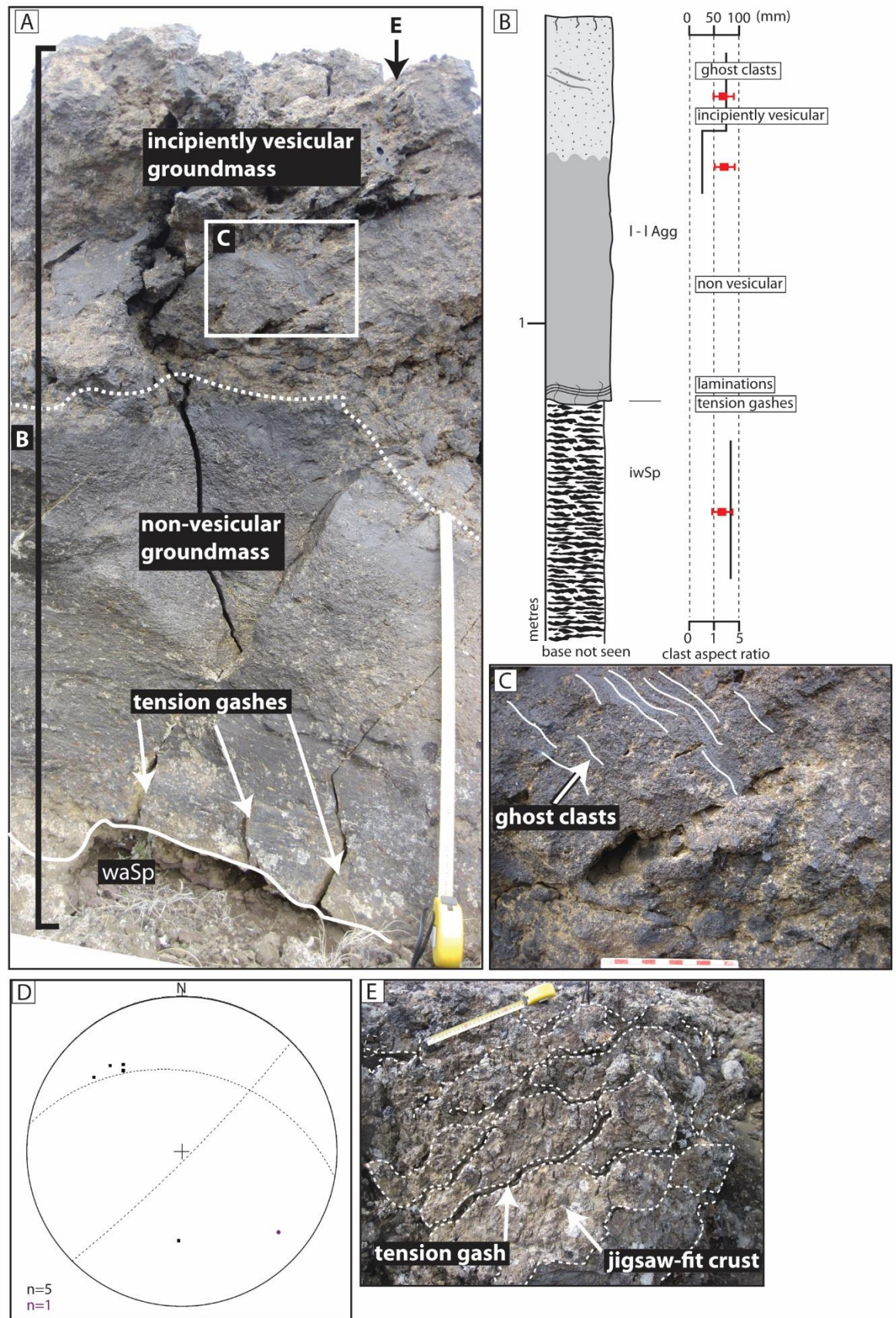


Figure 3.40. Photographs and measurements associated with location Y28. (UTM 564390/7301820). (A) Cross section of the agglutinate, with clast-supported incipiently

welded spatter bombs (waSp) beneath. The agglutinate becomes more vesicular with height and has a 70 mm thick platy crust. Tension gashes occur at the base (arrowed) and in the incipiently vesicular agglutinate in the upper 0.5 m. The tape measure is 50 cm long. (B) Log showing the internal stratigraphy of A. Clast aspect ratio is shown in red, juvenile clast size in black. (C) Details of the ghost clasts (solid lines). Graticules on the scale card are 1 cm. (D) Stereonet to show the orientation of the crust (great circles) tension gashes (black) and ghost clasts (purple). The tension gashes are approximately perpendicular to the outer crust. (E) Photo of the upper crust showing the jigsaw-fit plates. The tape measure is 25 cm long.

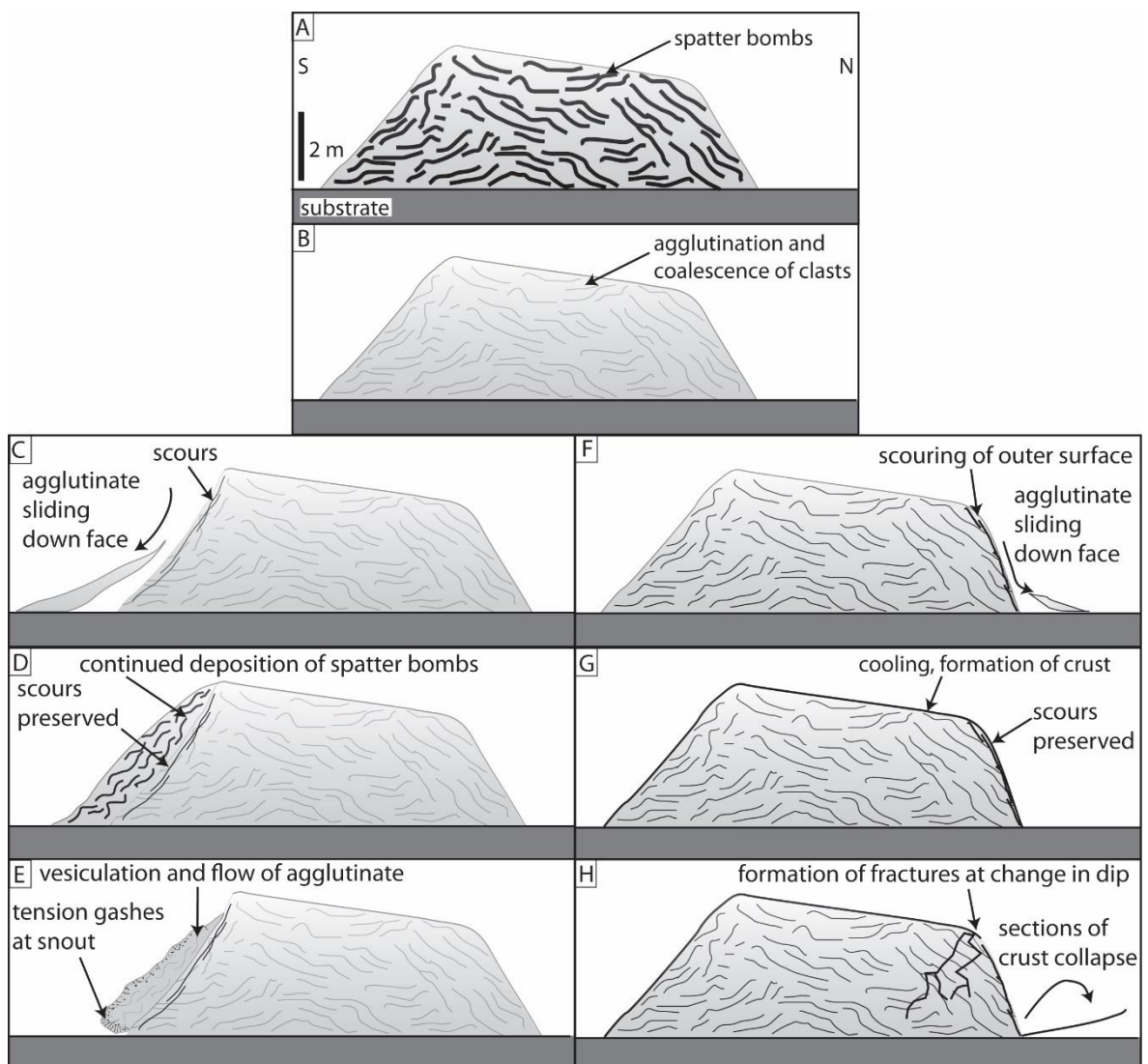


Figure 3.41. Schematic diagram to show the development of Location Y29. Images A and B show the accumulation and coalescence of constituent spatter bombs during Hawaiian-style activity. Images C–E show the evolution of the south face, whilst images F–H show the evolution of the north face of the rampart. (C) Agglutinate

slides down the rampart, scouring the underlying face. The material that causes the scouring is not observed. (D) Continued lava fountaining deposits spatter bombs atop the scoured surface. (E) The spatter bombs coalesce forming a slab of agglutinate, on which a crust develops. This crust is deformed by tension gashes (found dominantly towards the snout of the slab) during clastogenic flow. This slab has scours on its outer surface, suggesting repeating episodes of deposition and flow (not shown). The absence of material at the toe of the slab may suggest collapse of the slab in stages. (F) On the northern slope scouring occurs due to sliding of material down the outer rampart face. (G) The scours are preserved as the rampart cools and a brittle crust develops. (H) Fractures form at the change in dip amplitude and sections of the outer crust collapse due to gravitational instability.

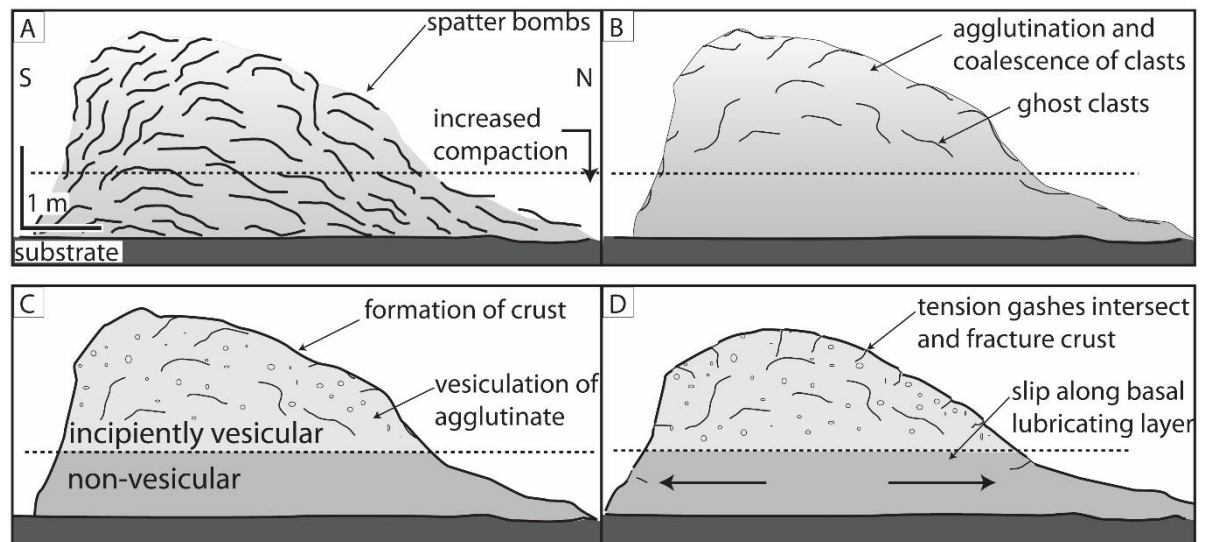


Figure 3.42. Interpretive picture to show the development of location Y28. (A) High rate accumulation of spatter bombs during lava fountaining. Welding intensity is greatest beneath the dashed line. (B) Agglutination and coalescence of pyroclasts. Ghost clasts remain in the upper part of the deposit. (C) Bubbles migrate upwards in the deposit and a crust forms. (D) Gravitational spreading is initiated along the basal lubricating layer. The crust is fractured into numerous plates. Note that stages A and B are contemporaneous: welding and coalescence occurring during deposition.

3.8 Evolution of the fissure

The R-K eruption was characterised by Hawaiian activity. The eruption chronology (Fig. 3.43) is described below.

Phase 0: Pre-eruption topography

The Sveinar graben and numerous other normal faults existed prior to the R-K eruption. The orientation of these faults was influenced by the regional northeast-southwest trending extensional tectonic regime and the TFZ (e.g. F9, F12, Figs. 3.4, 3.28 and 3.29). These faults controlled the location of surface water bodies.

Phase I: Initial eruption, effusion of lava flows and rootless cone explosions

The dyke fed numerous en-echelon fissure segments that propagated north-south. The fissure produced abundant flows of columnar-jointed pāhoehoe (Cp) which were largely confined to the southeast margin of the graben (F33). Interaction between inflating lava flows and surface water resulted in rootless explosions. Lava fountains were >100 m in height and constructed scoria ramparts (Location 406).

Phase II: Constriction of the fissure

Continued lava effusion deformed and buried early scoria ramparts. The fissure began to evolve to numerous point sources due to thermal instabilities along the fissure (e.g. Bruce and Huppert 1989; Thordarson and Self 1993; Keating et al. 2008; Brown et al. 2014). The decreasing abundance of columnar-jointed pāhoehoe (Cp) with time suggests that the magma flux decreased with time. Fountain heights may have increased due to narrowing of the conduit (e.g. Valentine and Cortés 2013). Scoria ramparts were constructed in proximal regions by fountains >100 m in height (location 280) and scoria fall deposits were dispersed ≥ 1 km from the fissure (location 462).

Phase III: Cone construction and flow of lava flows into water

Edifice 26 was constructed by fountains ≤ 100 m in height. Synchronous with the development of cone 26 was the development of an adjacent edifice, now eroded by the Jökulsá River. Further south, this section of the fissure began to close and an adjacent westerly section opened. Deposits from this lava fountain formed a scoria rampart (location 477). Clastogenic pāhoehoe (Cl) was also produced via a combination of effusion and pyroclast coalescence under fountains. Towards the south lavas entering bodies of

surface water (e.g. between F9 and F12) transformed into hyaloclastite and pillow lavas and filled these basins. Decreasing surface water abundance with time restricted hyaloclastite and pillow lavas to the base of the R-K volcanic sequence.

Phase IV: Spatter rampart formation and drowning of the topography

In the north of the study area, hummocky lava was emplaced. Further south, continued deposition from the westerly section of the fissure created spatter ramparts during Hawaiian-style activity. Clastogenic lava flooded the topography and was largely confined within the Sveinar graben. At the end of the eruption shelly lavas were effused from edifices (Fig. 3.3) during phases of low (<100 m) or absent fountains.

Phase V: Extensional faulting and fluvial erosion

Pyroclastic constructs were deformed by slip along faults 1, 2, 38 and 4. Post-eruption faulting associated with the Sveinar graben continued (faults 33 and 9). Flooding and percolation of water into cooling volcanic deposits resulted in the formation of hackly jointing (e.g. within the columnar-jointed pāhoehoe (Cp) in the scoria rampart; Fig. 3.25). Fluvial erosion, in part linked to glacial floods (e.g. Alho et al. 2005; Kirkbride et al. 2006; Waitt 2009) eroded the upper parts of the R-K volcanic sequence. Drainage channels became established along former pathways (e.g. between faults 9 and 12). Deepening of the Jökulsá a Fjöllum canyon exposed the feeder dyke, as observed today.

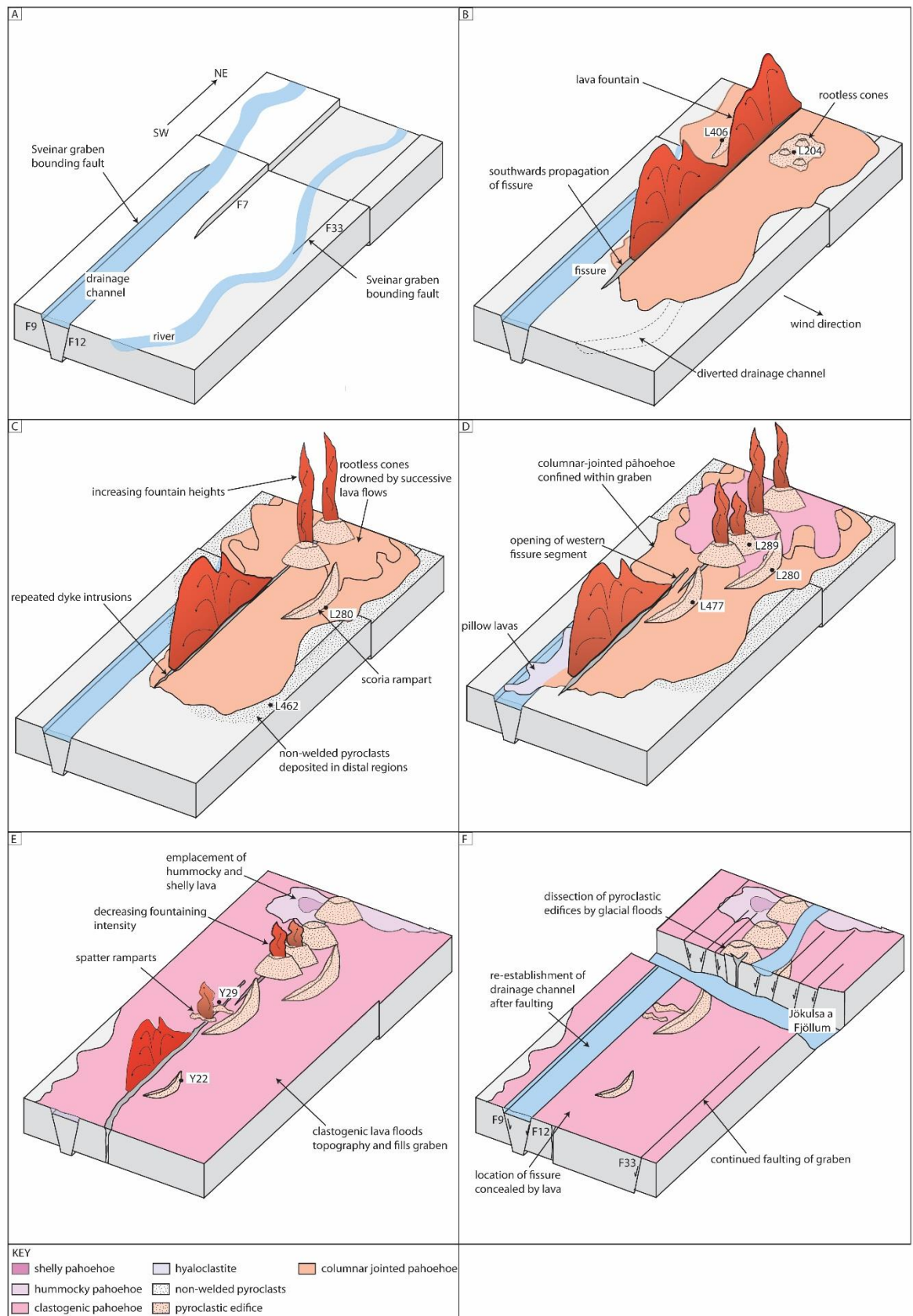


Figure 3.43 (overleaf). Schematic diagram to show the development of the R-K fissure. (A) Phase 0: The Sveinar graben pre-dates the fissure. Drainage patterns are controlled by pre-existing faults. (B) Phase I: The dyke fed numerous en-echelon fissure segments that propagated north-south. (C) Phase II: Lava flows buried scoria ramparts. The fissure began to evolve to numerous point sources due to thermal instabilities. (D) Phase III: Low fountains ≤ 100 m in height constructed edifice 26 (location 289). (E) Phase IV: In the north of the study area, hummocky lava was emplaced. (F) Phase V: Pyroclastic constructs were deformed by slip along faults. Post-eruption faulting associated with the Sveinar graben continued. Diagram not to scale.

3.9 Discussion

3.9.1 Feeder dyke and conduit morphology

The single set of cooling joints within the R-K feeder dyke is consistent with emplacement during a single injection (Sheth and Cañón-Tapia 2014). Widening of the conduit beneath the scoria-agglutinate cone dominantly occurs in the upper 50 m, as observed elsewhere (e.g. Keating et al. 2008; Geshi et al. 2010; Hintz and Valentine 2012). The conduit was enlarged by multiple intrusive events, and/or by dyke intrusion into the conduit when the eruption had ceased (e.g. Friese et al. 2013). Country rock lithics are absent from the dyke-fed R-K volcanic products, suggesting that dyke and conduit widening occurred without host rock removal. The evidence of syn-eruptive faulting throughout the R-K volcanic sequence suggests that graben development played an important role in accommodating dyke and conduit widening (e.g. Rubin 1992; Valentine and Krogh 2006), likely in tandem with free-surface effects (e.g. Galindo and Gudmundsson 2012).

I agree with the conclusions of Galindo and Gudmundsson (2012) and Geshi et al. (2010) that feeder dykes are segmented, sheet-shaped, widen towards the surface and trigger slip on existing faults (e.g. Gudmundsson et al. 2008). However, due to access, I am unable to observe if the dykes beneath edifice 26 contain cavities or vesicles in their uppermost sections (e.g. Galindo and Gudmundsson 2012). No vesicles or cavities were observed in the dyke at location 478; the significance of this (if any) is unknown.

3.9.2 Rootless eruption mechanisms

The rootless tephra deposits adjacent to the dyke (massive scoria lapilli and bombs; mSc; Figs. 3.11 and 3.31) have several features that are atypical of rootless tephra in other settings. The initiation of rootless explosions require a compressible, granular and water-saturated substrate; this substrate is commonly erupted along with the rootless tephra derived from the fragmentation of an inflating lava flow (Hamilton et al. 2010). No such substrate is observed within rootless tephra deposits. Although the lower contact of the columnar-jointed pāhoehoe (Cp) is not observed, there is <1 m between the base of the lava-like agglutinate and the underlying topography. This suggests that there is little or no sediment is present beneath the columnar-jointed pāhoehoe (Cp). Therefore, it is unlikely that rootless explosions occurred by penetration of lava into an unconsolidated substrate and another method is required. One hypothesis is that the influx of water post-dated the emplacement of the lava, but that explosive interaction occurred only after sufficient water had percolated beneath the inflating lava flow. Alternatively, a high water table in the underlying columnar-jointed plagioclase-porphyrific flows could have provided a reservoir of water. These mechanisms for rootless cone formation are as yet untested, but may provide insights into the diversity of lava-water mechanisms. These mechanisms have potential implications for hazard assessments and for the ability of rootless cones to form on other planetary bodies (Fagents et al. 2002; Fagents and Thordarson 2007).

Another hypothesis is that the features represent the vents of littoral-style cones, resulting from the penetration of lava flows into open water (e.g. Mattox and Mangan 1997). In this case, explosive interaction could have resulted from the collapse of a lava delta system (e.g. Mattox and Mangan 1997). I find no evidence of the delta system at this location; however this could have been removed during creation of the Jökulsá canyon.

3.9.3 Scoria ramparts

The R-K fissure is rare in exposing the internal architecture of scoria ramparts generated during basaltic fissure eruptions. The ramparts are inferred to have been produced by a fountain that was >100 m in height; fountains <100 m in height produce little tephra (Wolfe et al. 1988). The ramparts are composed of similar lithofacies to the cones (e.g. clast-supported incipiently welded spatter bombs, waSp; clast-supported moderately welded scoria lapilli and bombs, mwSc; clast-supported densely welded spatter bombs, dwSp; clast-supported weakly agglutinated scoria lapilli and bombs, waSc; and scoria lapilli, ScL). They are inferred to pre-date the formation of adjacent cones (e.g.

Thordarson and Self 1993). Scoria ramparts are observed elsewhere along the R-K fissure, suggesting that the section proximal to the Jökulsá canyon was not unique in terms of eruptional style.

Unlike scoria cones the ramparts lack lithic clasts, likely the result of poor thermal coupling of the lithic clasts with the lava fountain (see section 3.4). In ancient, heavily eroded examples, distinction between scoria ramparts and scoria cones is important because scoria ramparts are not always underlain by dykes (e.g. Location 280). Therefore, they do not necessarily provide insights into the subsurface geology. Furthermore, the ramparts form under different fountain conditions to cones. Misinterpreting eroded ramparts as cones may therefore lead to erroneous conclusions about eruption dynamics (e.g. fountain height).

3.9.4 Scoria-agglutinate cone

The componentry of edifice 26 is lithologically similar to that of spatter cones, which are commonly composed of large, deformed and strongly welded spatter bombs, deposited under fountains <100 m in height (Wolfe et al. 1988; Riedel et al. 2003; Cimarelli et al. 2013). However, edifice 26 is significantly larger spatter cones reported in the literature (10–40 m high and 5–15 m in diameter; see Green and Short 1971; Opheim and Gudmundsson 1989; Thordarson and Self 1993; Rymer et al. 1998; Heliker et al. 1998). The edifice is also smaller than the agglutinate cones described by Brown et al. (2014) and does not have the same characteristic low angle bedding. The edifice has a similar bedding dip, size and height:basal diameter relationship to that of a scoria cone (e.g. Wood 1980). However, scoria cones are typically composed of welded and non-welded beds of scoria lapilli (e.g. McGetchin et al. 1974; Houghton and Schmincke 1989; Valentine et al. 2006) with a median grain size of 1 cm (Riedel et al. 2003); unlike edifice 26.

Since the architecture of edifice 26 shares compositional similarities with spatter cones and is similar to a scoria cone in size, the term “scoria-agglutinate cone” is applied (e.g. Vespermann and Schmincke 2000). The edifice is thought to have formed under a fountain that favoured the high rate accumulation of spatter, likely <100 m in height (e.g. Wolfe et al. 1988). Based on an accumulation rate of >20 cm/min to produce the welded deposits (e.g. lava-like agglutinate and clast-supported moderately welded spatter bombs; see Sparks and Wright 1979; Thomas and Sparks 1992) the cone would have taken 3 hours to construct. Morphologically similar edifices that appear to be dominantly composed of

spatter-rich lithofacies are found elsewhere along the R-K fissure, suggesting that this section of the fissure was not unique in terms of eruption style.

3.9.5 Spatter ramparts

This is the first study to provide document the evolution of spatter ramparts. The Hawaiian-style volcanism that dominated during rampart construction is complementary to observations of historic eruptions (e.g. Parcheta et al. 2012). Spatter ramparts are commonly produced by fountains <100 m in height (Wolfe et al. 1988; Parcheta et al. 2012) and may develop to form spatter cones (e.g. Wolfe et al. 1988). Their preservation indicates that activity along this section of the fissure was not prolonged enough to allow a cone to develop. Activity ends along sections of the fissure when magma flow is focused elsewhere (Bruce and Huppert 1989; Keating et al. 2008), implying that this section of the fissure closed earlier than more southerly sections.

The ramparts have similarities with the spatter cones described by Thordarson and Self (1993), which are superimposed on adjacent scoria cones and half cones. These features commonly merge and intersect in a complex fashion. The ramparts are also comparable with those described by Dickson (1997); Moore et al. (1980) and Parcheta et al. (2012); all of which have heights of ≤ 5 m. However, unlike the ramparts described by Parcheta et al. (2012), some of the ramparts in this study are oriented perpendicular to the fissure. This may suggest the R-K ramparts are preserved at a stage of growth transitional between true ramparts and cones. The lengths of the features described in this study are considerably longer than those described elsewhere (e.g. Parcheta et al. 2012). The reason for this is speculative given the sparse data, but may relate to the length of the active fissure. Ramparts described by Parcheta et al. (2012) are located adjacent to the fissure, or set-back up to 30 m. The set-back of the ramparts in this study is difficult to determine as the location of the dyke is concealed: it is also impossible to determine which of the rampart faces is the inner face as described by Parcheta et al. (2012).

The post-depositional modification processes detailed in this study are broadly comparable to processes observed in contemporary eruptions. Location Y28 evidences the early stages of post-depositional flow at an asymmetric, over-steepened rampart (e.g., McNutt et al. (1991). However, the collapse observed by McNutt et al. (1991) occurred on steep slopes, unlike the shallow slopes on which the ramparts in this study were constructed. Partial collapse in this study is inferred to have been triggered by the

presence of a basal lubricating layer, similar to that described by Sumner (1998) during the collapse of the Izu-Oshima scoria cone.

The processes that resulted in the internal variability of the R-K ramparts are comparable with processes observed by Heslop et al. (1989) and Andronico et al. (2014), who describe lava flows issuing from spatter ramparts. We note the similarity with Location Y29 which exhibits lava-like agglutinate (l-l Agg) that seems to have flowed from the rampart. Furthermore, Heslop et al. (1989) suggest that ramparts can be composed of a molten core and brittle crust, similar to Y28 which had a jigsaw-fit, platy crust and molten interior.

Understanding the formation of spatter ramparts is important for helping us identify the locations of vents in the geological record. Understanding the methods by which they grow also has implications when modelling the growth of monogenetic constructs (Riedel et al. 2003). Furthermore, the post-depositional modification processes observed in this study has implications for our assessment of hazards associated with monogenetic edifices.

3.9.6 Comparison with flood basalt and high-volume (>1 km³) fissure eruptions

The R-K fissure is typical of fissure systems in Iceland; it is a mixed cone row composed of overlapping and merging scoria and spatter cones (e.g. Thordarson and Larsen 2007). High volume eruptions that produce >1km³ of lava (e.g. Laki in 1783–1785 and Eldgjá in 934), are also characterised by these mixed cone rows (Thordarson and Self 1993; Thordarson and Larsen 2007). The types of cones rows formed during flood basalt eruptions are poorly known. The best preserved example of a cone row in a flood basalt province (FBP) is the row of agglutinate cones along the Roza fissure in the Columbia River Flood Basalt Province (CRFBP). A number of features presumed to be shield volcanoes are also found discontinuously along the Roza fissure (Swanson et al. 1975). No other types of edifices are documented. Thus, the diversity of edifices that commonly typifies mixed cone rows (Thordarson and Larsen 2007) are not found from the Roza example. The assemblage of cones along the Roza fissure could be analogous to the rows of spatter-like cones found above the Threngslaborgir and Lúdentborgir fissures (Thordarson and Larsen 2007). Alternatively, the abundance of the agglutinate cones could reflect preservation bias. This preservation bias is a result of componentry of the cones; they are dominated by densely welded scoria and spatter (Brown et al. 2014). These lithofacies are less susceptible to erosion than more vesicular rocks (e.g. scoria, see Manville et al. 2009), therefore the cones stand a higher chance of preservation.

Furthermore, since rafting is dependent on the mass of the collapsing material and the yield strength of the underlying lava (Valentine and Gregg 2008), the agglutinate cones would have been less susceptible to syn-eruptive destruction and transport than edifices composed of vesicular pyroclasts (e.g. scoria cones).

The R-K edifices have many similarities with the edifices formed in flood basalt eruptions (Swanson et al. 1975; Reidel and Tolan 1992; Thordarson et al. 2001; Thordarson and Larsen 2007; Brown et al. 2014). These similarities include an abundance of clasts formed during Hawaiian-style lava fountaining (e.g. achneliths, cowpat bombs) that have similar vesicularities (Thordarson and Self 1993; Brown et al. 2014). In all examples there is an abundance of clastogenic and shelly pāhoehoe, as well as welded deposits. Furthermore, the R-K deposits indicate fluctuating fountaining intensity, as documented during the Laki and Roza eruptions (Thordarson and Self 1993; Brown et al. 2014). As in many examples, the R-K, Columbia River and Laki edifices are commonly asymmetric due to either wind (Reidel and Tolan 1992; Thordarson and Self 1993; Brown et al. 2014) or angled fountains (Brown et al. 2014). The R-K edifices are also found within a graben that developed during the eruption, as documented in Iceland and the CRFBP (Swanson et al. 1975; Thordarson and Self 1993). This is typical of many volcanic systems in which dyke intrusion causes faulting (Pollard et al. 1983; Rubin and Pollard 1988; Rubin 1992; Chadwick and Embley 1998).

The R-K feeder dyke is a single injection dyke, analogous to that for the 1783 Laki eruption (Sheth and Cañón-Tapia 2014 and references there-in). This is in contrast to the Joseph Creek dykes (Reidel and Tolan 1992) which have a similar appearance to the “multiple dykes” found in the Deccan Volcanic Province (Sheth and Cañón-Tapia 2014). These dykes indicate multiple intrusions during a single eruption (Sheth and Cañón-Tapia 2014). The different feeder systems for contemporary and flood basalt eruptions may explain the complex geochemical variation and magma storage problems that are not associated with large volume contemporary eruptions (Sheth and Cañón-Tapia 2014).

An important difference between the deposits of the R-K and high volume fissure eruptions is the character of the sheet-form fall deposits. The R-K eruption produced deposits ~1 m thick at ~1 km distance from the vents. These deposits are typical of Hawaiian eruptions (e.g. Aramaki et al. 1986; Houghton et al. 2006) in which lava fountains are commonly ~500 m high (Wolfe et al. 1988; Parfitt 1998; Vergnolle and Mangan 2000). In contrast, sheet-like fall deposits from the Laki, Roza and Eldgjá eruptions extend ≥ 1.7 km from the fissure and are >2 m thick, typical of Sub-Plinian and

violent Strombolian activity (Thordarson and Self 1993; Thordarson and Larsen 2007; White et al. 2009; Brown et al. 2014). This indicates that the studies section of the R-K fissure was not characterised by the high fountains that typified the Roza, Laki and Eldgjá eruptions. The absence of agglutinate cones, as found along the Roza fissure (Brown et al. 2014) further suggests that the R-K eruption was not characterised by $\gg 1$ km-high fountains.

The R-K volcanic sequence provides insights into the early stages of fissure eruptions that produce mixed cone rows. The deposits from these stages are not commonly observed along other fissures (e.g. Laki). The early stages of the R-K eruption were dominated by the production of lava flows. This is analogous to the high rate discharge of lava that occurred early in the Laki eruption and during the early stages of each eruption episode (Thordarson and Self 1993). The R-K lava flows then deformed and buried early pyroclastic deposits (e.g. Brown et al. in press). Thordarson and Self (1993) have been unable to recognise pyroclastic deposits buried in the proximal region of the Laki fissure. Some pyroclastic edifices formed during high volume fissure eruptions preserve evidence of unique fountaining conditions (Brown et al. 2014). Therefore similar edifices, perhaps preserved beneath the Laki lava flow field and within FBPs, may preserve evidence of fountaining conditions unique to high volume fissure eruptions.

The early R-K lava flows were also the hosts for rootless explosions in proximal regions; as evidenced by the dissected rootless conduits. These explosions may have occurred within the first few weeks of the eruption (as shown in Chapter 4). Rootless explosions are also observed in the Laki flow field, especially in the proximal region (Thordarson and Self 1993). The significance of these rootless eruptions in the proximal region is unknown. Rootless eruptions are thought to be controlled by lava and water availability (Chapter 4; Fagents and Thordarson 2007; Hamilton et al. 2010). Given that surface water was abundant across the Laki lava flow field, it is uncertain why these rootless explosions should be particularly common in the proximal region. This may be because the site of rootless interaction is thought to be partly controlled by substrate compressibility (Hamilton et al. 2010). In regions of high lithostatic load (i.e. thick sequences of lava, as found within the proximal region), the substrate would be more easily compressed. This would increase the likelihood of rootless interaction. However, the absence of a compressible substrate beneath the rootless conduit is noted in the R-K eruption. This suggests that factors such as local water percolation may be important in initiating rootless interactions (see section 3.9.2).

Development of the R-K lava flow field was followed by edifice construction. The R-K scoria-agglutinate cone, scoria ramparts and spatter ramparts have specific similarities with the edifices formed during the Laki eruption. Scoria half-cones are common features along the Laki fissure and in other low volume eruptions (Thordarson and Self 1993; Thordarson and Larsen 2007). The half-cones are elongated parallel to the fissure, are set-back from the fissure and are larger than the spatter cones superimposed on them. These features are similar to those of the scoria ramparts of the R-K eruption. The stratigraphy of the R-K rampart is also near identical to that preserved within the Laki scoria cones (Thordarson and Self 1993). The R-K scoria ramparts are composed of alternating layers of 0.5–1.5 m thick scoria overlain by 0.5–1 m thick spatter (log 2). Local spatter-rich successions in the R-K scoria ramparts (log 11) could suggest deposition from multiple sources along the fissure, or that log 11 represents part of an overlapping spatter cone that has been eroded (e.g. Thordarson and Self 1993). The similarity between the Laki scoria cones and half-cones and the R-K scoria ramparts suggest both were formed during Hawaiian activity that dominated towards the end of the eruption and each eruption episode (e.g. Thordarson and Self 1993).

The Laki scoria cones and half-cones are commonly overlain by spatter cones which intersect and merge in a complex fashion (Thordarson and Self 1993). These spatter cones are the most common feature along the Laki fissures (Thordarson and Self 1993) and are also formed during low volume fissure eruptions (Thordarson and Larsen 2007). These cones overly the fissure and are 10–40 m high (Thordarson and Self 1993). The cones increase in size towards the site of highest lava discharge (Thordarson and Self 1993). The Laki spatter cones form in the dying stages of the eruption (Thordarson and Self 1993). However, the internal features of these cones are not well described, and there are currently no studies describing the internal architecture and textures of these edifices. The R-K scoria-agglutinate cone and spatter ramparts have similar morphologic characteristics to the Laki spatter cones. Furthermore, the R-K scoria-agglutinate cone and spatter ramparts also post-date the scoria ramparts that are analogous to the Laki scoria half-cones. The R-K scoria-agglutinate cone suggests that the dying stages of the eruption are characterised by deposition from low and pulsating fountains, evidenced by the cored bombs and abundant spatter-dominated lithofacies. Since the R-K scoria agglutinate cone is not the largest cone along this section of the fissure, it suggests that the cone is not located on the site of highest discharge (e.g. Thordarson and Self 1993). The R-K scoria-agglutinate cone may also be representative of the Ice Harbor cones in the CRFBP, which are composed of

subaerial pāhoehoe flows and welded spatter (Swanson et al. 1975). This is speculative given the sparse data, but may suggest that the emplacement of the Ice Harbor member was similarly associated with the construction of scoria-agglutinate or spatter cones.

In summary, the R-K volcanic stratigraphy and edifices preserve many similarities with the products of high volume fissure eruptions. In particular, the R-K edifices are similar to those produced during the Laki eruption and evidence Hawaiian-style activity. The products of the Laki eruption and its dynamics are a useful analogue for the emplacement of flood basalts (Thordarson and Self 1998; Thordarson and Larsen 2007; White et al. 2009; Brown et al. 2014). The R-K edifices therefore serve as useful analogues for the edifices that may form during flood basalt eruptions. These edifices suggest that flood basalt eruptions could be associated with periods of Hawaiian-style activity (e.g. Reidel and Tolan 1992). This style of activity contrasts with that evidenced by the Roza agglutinate cones, suggesting significant temporal and spatial variation during flood basalt emplacement. Such variation is expected, given that FBP evidence a variety of emplacement styles (Jerram 2002; Bondre et al. 2004b) and that high volume Icelandic fissure eruptions produce a range of edifices and cone rows (Thordarson and Self 1993; Thordarson and Larsen 2007).

3.10 Summary

The low volume R-K fissure eruption produced a mixed cone row. This cone row contains a scoria-agglutinate cone, scoria and spatter ramparts and rootless cones, as well as sheet-like fall deposits. The architecture of these features and their feeder dyke has not been described before, and allows us to link processes observed in historic eruptions with preserved deposits. The scoria-agglutinate cone, scoria and spatter ramparts are analogous to those formed in high volume fissure eruptions and suggest that flood basalt eruptions may also be associated with periods of Hawaiian activity. This study also helps us to recognise fissure-derived edifices in other settings.

3.11 References

- Alho P, Russell AJ, Carrivick JL, Käyhkö J (2005) Reconstruction of the largest Holocene jökulhlaup within Jökulsá á Fjöllum, NE Iceland. *Quaternary Science Reviews* 24(22):2319-2334
- Alvarado GE, Pérez W, Vogel TA, Gröger H, Patiño L (2011) The Cerro Chopo basaltic cone (Costa Rica): An unusual completely reversed graded pyroclastic cone with abundant low vesiculated cannonball juvenile fragments. *J Volcanol Geoth Res* 201(1–4):163-177

- Andronico D, Scollo S, Cristaldi A, Lo Castro M (2014) Representivity of incompletely sampled fall deposits in estimating eruption source parameters: a test using the 12–13 January 2011 lava fountain deposit from Mt. Etna volcano, Italy. *B Volcanol* 76(10):1-14
- Aramaki S, Hayakawa Y, Fujii T, Nakamura K, Fukuoka T (1986) The October 1983 eruption of Miyakejima volcano. *J Volcanol Geoth Res* 29(1):203-229
- Bondre N, Duraiswami R, Dole G (2004a) Morphology and emplacement of flows from the Deccan Volcanic Province, India. *B Volcanol* 66(1):29-45
- Bondre N, Duraiswami R, Dole G (2004b) A brief comparison of lava flows from the Deccan Volcanic Province and the Columbia-Oregon Plateau Flood Basalts: Implications for models of flood basalt emplacement. *Journal of Earth System Science* 113(4):809-817
- Breed WJ (1964) Morphology and lineation of cinder cones in the San Francisco Volcanic Field. *Mus. North. Ariz. Bull* 40:65-71
- Brown RJ, Blake S, Thordarson T, Self S (2014) Pyroclastic edifices record vigorous lava fountains during the emplacement of a flood basalt flow field, Roza Member, Columbia River Basalt Province, USA. *Geol Soc Am Bull* 126:875-891
- Brown RJ, Thordarson T, Self S, Blake S (in press) Physical Disruption of Sheet-form Fall Deposits during Basaltic Eruptions.
- Bruce PM, Huppert HE (1989) Thermal control of basaltic fissure eruptions. *Nature* 342(6250):665-667
- Capaccioni B, Cuccoli F (2005) Spatter and welded air fall deposits generated by fire-fountaining eruptions: Cooling of pyroclasts during transport and deposition. *J Volcanol Geoth Res* 145(3–4):263-280
- Carracedo JC, Rodriguez Badiola E, Soler V (1992) The 1730–1736 eruption of Lanzarote, Canary Islands: a long, high-magnitude basaltic fissure eruption. *J Volcanol Geoth Res* 53(1–4):239-250
- Chadwick WW, Embley RW (1998) Graben formation associated with recent dike intrusions and volcanic eruptions on the mid-ocean ridge. *Journal of Geophysical Research: Solid Earth* 103(B5):9807-9825
- Cimarelli C, Di Traglia F, de Rita D, Torrente DG (2013) Space–time evolution of monogenetic volcanism in the mafic Garrotxa Volcanic Field (NE Iberian Peninsula). *B Volcanol* 75(11):1-18
- Cronin SJ, Neall VE (2001) Holocene volcanic geology, volcanic hazard, and risk on Taveuni, Fiji. *New Zealand Journal of Geology and Geophysics* 44(3):417-437
- Dickson LD (1997) Volcanology and geochemistry of pliocene and quaternary basalts on Citadel Mountain, Lunar Crater Volcanic field, Pancake Range, Nevada.
- Dumas S, Arnott RWC (2006) Origin of hummocky and swaley cross-stratification— The controlling influence of unidirectional current strength and aggradation rate. *Geology* 34(12):1073-1076
- Einarsson MA (1984) Climate of Iceland. In: Van Loon H (ed) *World Survey of Climatology: 15 : Climates of the Oceans*. Elsevier, Amsterdam, pp 673-697
- Fagents SA, Lanagan P, Greeley R (2002) Rootless cones on Mars: a consequence of lava-ground ice interaction. *Geological Society, London, Special Publications* 202(1):295-317
- Fagents SA, Thordarson T (2007) Rootless cones in Iceland and on Mars. In: Chapman M, Skilling IP (eds) *The Geology of Mars: Evidence from Earth-Based Analogues*. Cambridge University Press, pp 151–177
- Fedotov S, Chirkov A, Gusev N, Kovalev G, Slezin Y (1980) The large fissure eruption in the region of Plosky Tolbachik volcano in Kamchatka, 1975–1976. *B Volcanol* 43(1):47-60
- Fisher RV, Schmincke HU (1984) *Pyroclastic Rocks*. Springer, Berlin, Heidelberg, New York
- Forbes AES, Blake S, Mc Garvie DW, Tuffen H (2012) Pseudopillow fracture systems in lavas: insights into cooling mechanisms and environments from lava flow fractures *J Volcanol Geoth Res* 245 (2012): 68-80
- Forbes AES, Blake S, Tuffen H (2014) Entablature: fracture types and mechanisms. *B Volcanol* 76(5):1-13
- Francis PW (1973) Cannonball Bombs, A New Kind of Volcanic Bomb from the Pacaya Volcano, Guatemala. *Geol Soc Am Bull* 84(8):2791-2794
- Friese N, Bense FA, Tanner DC, Gústafsson LE, Siegesmund S (2013) From feeder dykes to scoria cones: the tectonically controlled plumbing system of the Rauðhólar volcanic chain, Northern Volcanic Zone, Iceland. *B Volcanol* 75(6):1-19

- Galindo I, Gudmundsson A (2012) Basaltic feeder dykes in rift zones: geometry, emplacement, and effusion rates. *Natural Hazards and Earth System Sciences* 12(12):3683-3700
- Geist DJ, Harpp KS, Naumann TR, Poland M, Chadwick WW, Hall M, Rader E (2008) The 2005 eruption of Sierra Negra volcano, Galápagos, Ecuador. *B Volcanol* 70(6):655-673
- Geshi N, Kusumoto S, Gudmundsson A (2010) Geometric difference between non-feeder and feeder dikes. *Geology* 38(3):195-198
- Geshi N, Oikawa T (2014) The spectrum of basaltic feeder systems from effusive lava eruption to explosive eruption at Miyakejima volcano, Japan. *B Volcanol* 76(3):1-14
- Green J, Short NM (1971) Volcanic landforms and surface features: A photographic atlas and glossary. Springer-Verlag
- Gudmundsson A (2007) Infrastructure and evolution of ocean-ridge discontinuities in Iceland. *Journal of Geodynamics* 43(1):6-29
- Gudmundsson A, Friese N, Galindo I, Philipp SL (2008) Dike-induced reverse faulting in a graben. *Geology* 36(2):123-126
- Gudmundsson MT, Pedersen R, Vogfjörð K, Thorbjarnardóttir B, Jakobsdóttir S, Roberts MJ (2010) Eruptions of Eyjafjallajökull Volcano, Iceland. *Eos, Transactions American Geophysical Union* 91(21):190-191
- Guilbaud M-N, Self S, Thordarson T, Blake S (2005) Morphology, surface structures, and emplacement of lavas produced by Laki, A.D. 1783–1784. *Geological Society of America Special Papers* 396:81-102
- Hamblin WK (1994) Late Cenozoic lava dams in the western Grand Canyon. *Geol Soc Am Mem* (183):1-142
- Hamilton CW, Thordarson T, Fagents SA (2010) Explosive lava–water interactions I: architecture and emplacement chronology of volcanic rootless cone groups in the 1783–1784 Laki lava flow, Iceland. *B Volcanol* 72(4):449-467
- Head JW, Wilson L (1989) Basaltic pyroclastic eruptions: Influence of gas-release patterns and volume fluxes on fountain structure, and the formation of cinder cones, spatter cones, rootless flows, lava ponds and lava flows. *J Volcanol Geoth Res* 37(3–4):261-271
- Heiken G (1978) Characteristics of tephra from cinder cone, Lassen volcanic National Park, California. *B Volcanol* 41(2):119-130
- Heliker C, Mangan M, Mattox T, Kauahikaua J, Helz R (1998) The character of long-term eruptions: inferences from episodes 50–53 of the Pu'u'Ō'ō-Kūpaianaha eruption of Kīlauea Volcano. *B Volcanol* 59(6):381-393
- Heslop S, Wilson L, Pinkerton H, Head J, III (1989) Dynamics of a confined lava flow on Kilauea volcano, Hawaii. *B Volcanol* 51(6):415-432
- Hintz AR, Valentine GA (2012) Complex plumbing of monogenetic scoria cones: New insights from the Lunar Crater Volcanic Field (Nevada, USA). *J Volcanol Geoth Res* 239–240:19-32
- Hon K, Kauahikaua J, Delinger R, Mackay K (1994) Emplacement and inflation of pahoehoe sheet flows: Observations and measurements of active lava flows on Kilauea Volcano, Hawaii. *Geol Soc Am Bull* 106(3):351-370
- Houghton BF, Schmincke HU (1989) Rothenberg scoria cone, East Eifel: a complex Strombolian and phreatomagmatic volcano. *B Volcanol* 52(1):28-48
- Houghton BF, Wilson CJN (1989) A vesicularity index for pyroclastic deposits. *B Volcanol* 51(6):451-462
- Houghton BF, Bonadonna C, Gregg CE, Johnston DM, Cousins WJ, Cole JW, Del Carlo P (2006) Proximal tephra hazards: Recent eruption studies applied to volcanic risk in the Auckland volcanic field, New Zealand. *J Volcanol Geoth Res* 155(1–2):138-149
- Huscroft CA, Ward BC, Barendregt RW, Jackson Jr, LE, Opdyke ND (2004) Pleistocene volcanic damming of Yukon River and the maximum age of the Reid Glaciation, west-central Yukon. *Canadian Journal of Earth Sciences* 41(2):151-164.
- Jerram DA (2002) Volcanology and facies architecture of flood basalts. *Geological Society of America Special Papers* 362:119-132
- Jurado-Chichay Z, Rowland S, Walker GL (1996) The formation of circular littoral cones from tube-fed pāhoehoe: Mauna Loa, Hawai'i. *B Volcanol* 57(7):471-482

- Karhunen R (1988) Eruption mechanism and rheomorphism during the basaltic fissure eruption in Biskupsfell, Kverkfjöll, North-central Iceland, Lic. Phil. thesis, University of Iceland, Department of Geology and Mineralogy.
- Keating G, Valentine G, Krier D, Perry F (2008) Shallow plumbing systems for small-volume basaltic volcanoes. *B Volcanol* 70(5):563-582
- Kent RW, Thomson BA, Skelhorn RR, Kerr AC, Norry MJ, Walsh JN (1998) Emplacement of Hebridean Tertiary flood basalts: evidence from an inflated pahoehoe lava flow on Mull, Scotland. *J Geol Soc London* 155(4):599-607
- Keszthelyi L, McEwen A, Phillips C, Milazzo M, Geissler P, Turtle E, Radebaugh J, Williams D, Simonelli D, Breneman H (2001) Imaging of volcanic activity on Jupiter's moon Io by Galileo during the Galileo Europa Mission and the Galileo Millennium Mission. *Journal of Geophysical Research: Planets* (1991–2012) 106(E12):33025-33052
- Kirkbride MP, Dugmore AJ, Brazier V (2006) Radiocarbon dating of mid-Holocene megaflood deposits in the Jokulsa a Fjollum, north Iceland. *The Holocene* 16(4):605-609
- Kokelaar P (1986) Magma-water interactions in subaqueous and emergent basaltic. *B Volcanol* 48(5):275-289
- Long PE, Wood BJ (1986) Structures, textures, and cooling histories of Columbia River basalt flows. *Geol Soc Am Bull* 97(9):1144-1155
- Macdonald GA (1972) *Volcanoes*. Prentice-Hall, Englewood Cliffs, N.J.
- Mackin JH (1961) A stratigraphic section in the Yakima basalt and the Ellensburg Formation in south-central Washington. *Rep. Invest., Wash. Div. Mines Geol.*, 19:45
- Manville V, Németh K, Kano K (2009) Source to sink: a review of three decades of progress in the understanding of volcanoclastic processes, deposits, and hazards. *Sedimentary Geology* 220(3):136-161
- Mattox TN, Mangan MT (1997) Littoral hydrovolcanic explosions: a case study of lava–seawater interaction at Kilauea Volcano. *J Volcanol Geoth Res* 75(1–2):1-17
- Mattsson HB, Tripoli BA (2011) Depositional characteristics and volcanic landforms in the Lake Natron–Engaruka monogenetic field, northern Tanzania. *J Volcanol Geoth Res* 203(1–2):23-34
- Mauri A, Davis B, Collins P, Kaplan J (2013) The influence of atmospheric circulation on the mid-Holocene climate of Europe: a data-model comparison. *Climate of the Past Discussions* 9(5):5569-5592
- McGetchin TR, Settle M, Chouet BA (1974) Cinder Cone Growth Modeled After Northeast Crater, Mount Etna, Sicily. *J. Geophys. Res.* 79(23):3257-3272
- McNutt SR, Miller TP, Taber JJ (1991) Geological and seismological evidence of increased explosivity during the 1986 eruptions of Pavlof volcano, Alaska. *B Volcanol* 53(2):86-98
- Moore RB, Helz RT, Dzurisin D, Eaton GP, Koyanagi RY, Lipman PW, Lockwood JP, Puniwai GS (1980) The 1977 eruption of Kilauea volcano, Hawaii. *J Volcanol Geoth Res* 7(3):189-210
- Németh K, Cronin SJ (2011) Drivers of explosivity and elevated hazard in basaltic fissure eruptions: the 1913 eruption of Ambrym Volcano, Vanuatu (SW-Pacific). *J Volcanol Geoth Res* 201(1):194-209
- Németh K (2014) Rootless Cone/Vent. In: *Encyclopedia of Planetary Landforms*. Springer New York, pp 1-7
- Opheim JA, Gudmundsson A (1989) Formation and geometry of fractures, and related volcanism, of the Krafla fissure swarm, northeast Iceland. *Geol Soc Am Bull* 101(12):1608-1622
- Parcheta C, Houghton B, Swanson D (2012) Hawaiian fissure fountains 1: decoding deposits—episode 1 of the 1969–1974 Mauna Ulu eruption. *B Volcanol* 74(7):1729-1743
- Parfitt EA (1998) A study of clast size distribution, ash deposition and fragmentation in a Hawaiian-style volcanic eruption. *J Volcanol Geoth Res* 84(3):197-208
- Parfitt EA (2004) A discussion of the mechanisms of explosive basaltic eruptions. *J Volcanol Geoth Res* 134(1-2):77-107
- Peterson DW, Tilling RI (1980) Transition of basaltic lava from pahoehoe to aa, Kilauea Volcano, Hawaii: Field observations and key factors. *J Volcanol Geoth Res* 7(3-4):271-293
- Polacci M, Cashman KV, Kauahikaua JP (1999) Textural characterization of the pāhoehoe–‘a‘a transition in Hawaiian basalt. *B Volcanol* 60(8):595-609
- Pollard DD, Delaney PT, Duffield WA, Endo ET, Okamura AT (1983) Surface deformation in volcanic rift zones. *Tectonophysics* 94(1–4):541-584

- Reidel SP, Tolan TL (1992) Eruption and emplacement of flood basalt: An example from the large-volume Teepee Butte Member, Columbia River Basalt Group. *Geol Soc Am Bull* 104(12):1650-1671
- Reidel SP (1998) Emplacement of Columbia River flood basalt. *J. Geophys. Res.* 103(B11):27393-27410
- Riedel C, Ernst GGJ, Riley M (2003) Controls on the growth and geometry of pyroclastic constructs. *J Volcanol Geoth Res* 127(1–2):121-152
- Rosseel J-B, White JDL, Houghton BF (2006) Complex bombs of phreatomagmatic eruptions: Role of agglomeration and welding in vents of the 1886 Rotomahana eruption, Tarawera, New Zealand. *J. Geophys. Res.* 111(B12):B12205
- Rowland SK, Walker GPL (1987) Toothpaste lava: Characteristics and origin of a lava structural type transitional between pahoehoe and aa. *B Volcanol* 49(4):631-641
- Rubin AM, Pollard DD (1988) Dike-induced faulting in rift zones of Iceland and Afar. *Geology* 16(5):413-417
- Rubin AM (1992) Dike-induced faulting and graben subsidence in volcanic rift zones. *Journal of Geophysical Research: Solid Earth* 97(B2):1839-1858
- Rymer H, de Vries BvW, Stix J, Williams-Jones G (1998) Pit crater structure and processes governing persistent activity at Masaya Volcano, Nicaragua. *B Volcanol* 59(5):345-355
- Sánchez MC, Sarrionandia F, Ibarra JIG (2014) Post-depositional intrusion and extrusion through a scoria and spatter cone of fountain-fed nephelinite lavas (Las Herrerías volcano, Calatrava, Spain). *B Volcanol* 76(9):1-17
- Self S, Keszthelyi L, Thordarson T (1998) The importance of pahoehoe. *Annu. Rev. Earth Planet. Sci.* 26:81-110
- Sheth H, Cañón-Tapia E (2014) Are flood basalt eruptions monogenetic or polygenetic? *International Journal of Earth Sciences*:1-16
- Slater L, Jull M, McKenzie D, Gronvöld K (1998) Deglaciation effects on mantle melting under Iceland: results from the northern volcanic zone. *Earth and Planetary Science Letters* 164(1):151-164
- Sparks R, Wright J (1979) Welded air-fall tuffs. *Geological Society of America Special Papers* 180:155-166
- Steingrímsson J, Ólafsson S (1783) Einföld og sönn frásaga um jardeldshlaupid í Skaftafellssyslu árid 1783 (A simple, but true narrative of the eruption in Skaftafell county in the year 1783), . *Safn til Sögu Íslands IV*(Copenhagen, 1907-1915):58-69
- Steingrímsson J (1788) Fulkomid Skrif um Sídueld (A complete description of the Síða volcanic fire), . *Safn til Sögu Íslands IV* (Copenhagen 1907-1915):58-69
- Stevenson J, Mitchell N, Cassidy M, Pinkerton H (2012) Widespread inflation and drainage of a pāhoehoe flow field: the Nesjahraun, Þingvellir, Iceland. *B Volcanol*:1-17
- Stow DA (2005) *Sedimentary rocks in the field*, Manson Publishing Ltd. London, pp320.
- Sumner JM (1998) Formation of clastogenic lava flows during fissure eruption and scoria cone collapse: the 1986 eruption of Izu-Oshima Volcano, eastern Japan. *B Volcanol* 60(3):195-212
- Sumner JM, Blake S, Matela RJ, Wolff JA (2005) Spatter. *J Volcanol Geoth Res* 142(1-2):49-65
- Swanson D, Duffield WA, Jackson DB, Peterson DW (1979) Chronological narrative of the 1969 - 1971 Mauna Ulu eruption of Kilauea volcano, Hawaii. *U.S Geological Survey Professional Paper* 1065:55
- Swanson DA, Wright TL, Helz RT (1975) Linear vent systems and estimated rates of magma production and eruption for the Yakima Basalt on the Columbia Plateau. *American Journal of Science* 275(8):877-905
- Tentler T, Temperley S (2007) Magmatic fissures and their systems in Iceland: A tectonomagmatic model. *Tectonics* 26(5):TC5019
- Thomas R, Sparks R (1992) Cooling of tephra during fallout from eruption columns. *B Volcanol* 54(7):542-553
- Thorarinsson S (1959) Some Geological Problems Involved in the Hydroelectric Development of the Jokulsa a Fjöllum. Report to the State Electricity Authority, Reykjavik.:35
- Thordarson T, Self S (1993) The Laki (Skaftár Fires) and Grímsvötn eruptions in 1783–1785. *B Volcanol* 55(4):233-263

- Thordarson T, Self S (1998) The Roza Member, Columbia River Basalt Group: A gigantic pahoehoe lava flow field formed by endogenous processes? *J. Geophys. Res.* 103(B11):27411-27445
- Thordarson T, Miller D, Larsen G, Self S, Sigurdsson H (2001) New estimates of sulfur degassing and atmospheric mass-loading by the 934 AD Eldgjá eruption, Iceland. *J Volcanol Geoth Res* 108(1):33-54
- Thordarson T, Larsen G (2007) Volcanism in Iceland in historical time: Volcano types, eruption styles and eruptive history. *Journal of Geodynamics* 43(1):118-152
- Tucker M (1995) *Sedimentary rocks in the field*, Wiley, Chichester.
- Valentine G, Cortés J (2013) Time and space variations in magmatic and phreatomagmatic eruptive processes at Easy Chair (Lunar Crater Volcanic Field, Nevada, USA). *B Volcanol* 75(9):1-13
- Valentine GA, Groves KR (1996) Entrainment of Country Rock during Basaltic Eruptions of the Lucero Volcanic Field, New Mexico. *The Journal of Geology* 104(1):71-90
- Valentine GA, Krier D, Perry FV, Heiken G (2005) Scoria cone construction mechanisms, Lathrop Wells volcano, southern Nevada, USA. *Geology* 33(8):629-632
- Valentine GA, Krogh KEC (2006) Emplacement of shallow dikes and sills beneath a small basaltic volcanic center – The role of pre-existing structure (Paiute Ridge, southern Nevada, USA). *Earth and Planetary Science Letters* 246(3–4):217-230
- Valentine GA, Perry FV, Krier D, Keating GN, Kelley RE, Cogbill AH (2006) Small-volume basaltic volcanoes: Eruptive products and processes, and post-eruptive geomorphic evolution in Crater Flat (Pleistocene), southern Nevada. *Geol Soc Am Bull* 118(11-12):1313-1330
- Valentine GA, Gregg TKP (2008) Continental basaltic volcanoes — Processes and problems. *J Volcanol Geoth Res* 177(4):857-873
- Valentine GA (2012) Shallow plumbing systems for small-volume basaltic volcanoes, 2: Evidence from crustal xenoliths at scoria cones and maars. *J Volcanol Geoth Res* 223–224(0):47-63
- Vergnolle S, Mangan MT (2000) Hawaiian and Strombolian Eruptions. In: Sigurdsson H (ed) *Encyclopedia of Volcanoes*. Academic press, San Diego, pp 447-461
- Vespermann D, Schmincke H-U (2000) Scoria cones and tuff rings. In: Sigurdsson H (ed) *Encyclopedia of Volcanoes*. Academic Press, San Diego. Academic Press, San Diego, pp 683-694
- Waite R (2009) Great Holocene floods along Jökulsá á Fjöllum, north Iceland. *Flood and Megaflood Processes and Deposits: Recent and Ancient Examples*, International Association of Sedimentologists special publication 32:37-51
- Walker G, Croasdale R (1971) Characteristics of some basaltic pyroclastics. *B Volcanol* 35(2):303-317
- Walker GPL (1989) Spongy pahoehoe in Hawaii: A study of vesicle-distribution patterns in basalt and their significance. *B Volcanol* 51(3):199-209
- Walker GPL (1991) Structure, and origin by injection of lava under surface crust, of tumuli, “lava rises”, “lava-rise pits”, and “lava-inflation clefts” in Hawaii. *B Volcanol* 53(7):546-558
- Walker GPL (1995) Flood basalts versus central volcanoes and the British Tertiary volcanic Province. *Geological Society, London, Memoirs* 16(1):195-202
- Watton TJ, Jerram DA, Thordarson T, Davies RJ (2013) Three-dimensional lithofacies variations in hyaloclastite deposits. *J Volcanol Geoth Res* 250(0):19-33
- Wendel J (2014) Continuing Bardarbunga eruption fuels scientific research. *Eos, Transactions American Geophysical Union* 95(44):401-401
- White J, Bryan S, Ross P, Self S, Thordarson T (2009) Physical volcanology of continental large igneous provinces: update and review. *Studies in Volcanology: The Legacy of George Walker*. Special Publications of IAVCEI 2:291-321
- White JDL, Houghton BF (2006) Primary volcanoclastic rocks. *Geology* 34(8):677-680
- Wilmoth RA, Walker GPL (1993) P-type and S-type pahoehoe: a study of vesicle distribution patterns in Hawaiian lava flows. *J Volcanol Geoth Res* 55(1-2):129-142
- Wohletz KH, Sheridan MF (1983) Hydrovolcanic explosions; II, Evolution of basaltic tuff rings and tuff cones. *American Journal of Science* 283(5):385-413
- Wolfe WE, Neal AC, Banks GN, Toni DJ (1988) The Puu Oo Eruption of Kilauea Volcano, Hawaii: Episodes 1 Through 20, January 3, 1983, Through June 8, 1984. U.S Geological Survey Professional Paper 1463

- Wolff J, Sumner J (2000) Lava fountains and their products. In: Sigurdsson H (ed) Encyclopedia of volcanoes. Academic Press, San Diego, pp 321-329
- Wood CA (1980) Morphometric evolution of cinder cones. J Volcanol Geoth Res 7(3–4):387-413

Chapter 4: Rootless Cone Processes Informed from Dissected Vent and Tephra Deposits

4.1 Introduction

Explosive interaction between water-logged sediments (or volcanoclastic deposits) and molten lava can result in the formation of rootless cones, also known as ‘pseudocraters’ (Fig. 4.1; Thorarinsson 1953). Rootless cones are present within flow fields where the lava advanced over lacustrine, marsh and fluvial environments (Fagents and Thordarson 2007; Hamilton et al. 2010a; Hamilton et al. 2010b). Explosions are driven by the interaction of molten lava with a water-saturated, unconsolidated substrate. Explosions initiated by interaction of molten lava with substrate pore water eject clasts composed of lava crust, disrupted liquid lava and substrate-derived sediment onto a stationary surface of an active lava flow, thereby building a cone. Similar rootless edifices, known as littoral cones, form when lava flows interact with seawater in a littoral environment (Moore and Ault 1965; Fisher 1968; Jurado-Chichay et al. 1996; Mattox and Mangan 1997; Jaeger et al. 2007). Rootless cone-like structures have also been observed on the surface of Mars near the Martian equator (Lanagan et al. 2001; Bruno et al. 2004; Fagents and Thordarson 2007; Hamilton et al. 2010a) and have been used to infer the former presence of fluids in the Martian substrate.

Two models for rootless eruptions have been proposed; one assuming static heat transfer and the other inferring dynamic heat transfer. The static heat transfer model infers rapid emplacement of lava above a water-logged substrate. Water trapped beneath the lava flow is converted to steam producing eruptions that are analogous to phreatic explosions (Thorarinsson 1951, 1953).

In contrast, the dynamic heat transfer model of Fagents and Thordarson (2007) argues that the explosive interactions are driven by physical (dynamic) mixing of the lava and the water-logged substrate. The model is based on observations that sediment from the substrate is physically mixed into the rootless cone deposits and found between the core and the rim in armoured bombs. Furthermore, the cones feature multiple layers of tephra, which increase upwards in grain size from coarse ash/fine lapilli to bomb-size clasts (Fagents and Thordarson 2007; Hamilton et al. 2010a). The presence of layering implies sustained eruptions (estimated to have lasted for hours to days; Thordarson and Höskuldsson 2008), maintained by quasi-steady input of molten lava to the explosion site.

During rootless cone activity on pāhoehoe lavas, initial sedimentation occurs from explosions that produce pyroclastic density currents (PDCs) that deposit broad, sheet-like platform deposits around the vent (Hamilton et al. 2010a). Later tephra jets and lava fountains deposit lapilli- to bomb-sized scoria and spatter that build a cone (Thordarson et al. 1998; Fagents and Thordarson 2007; Hamilton et al. 2010a). The deposits of rootless activity are usually unconsolidated, except in proximal regions (Hamilton et al. 2010a). Rootless cones vary from 1–40 m in height and 2–450 m in basal diameter. The cones are crudely bedded, inversely graded, and may contain layers of rheomorphic spatter. The degree of explosivity is controlled by a variety of factors including the explosion site geometry, the dynamics of melt and coolant, the percentage of solids in the coolant matrix, magma rheology and vesicularity, the rate of lava influx, and the amount and availability of external water. Tephra deposits within rootless cone fields can cover areas of up to 150 km² and may exhibit complex stratigraphic relationships (Fagents and Thordarson 2007; Hamilton et al. 2010a and references therein).

Despite the abundance of rootless cones (e.g. Lanagan et al. 2001; Greeley and Fagents 2001; Fagents et al. 2002; Fagents and Thordarson 2007; Hamilton et al. 2010a; Hamilton et al. 2010b; Hamilton et al. 2010c; Hamilton et al. 2011; Keszthelyi and Jaeger 2014), there is little documentation of their constituent pyroclasts and the characteristics of their host lava flows (e.g. Melchior Larsen et al. 2006; Hamilton et al. 2010a; Hamilton et al. 2010b). Furthermore, rootless cones are superficially similar to small scoria cones and spatter cones, both in size and componentry (e.g. Fagents and Thordarson 2007). They may also have a linear spatial arrangement, similar to that of edifices along a dyke (e.g. Hamilton et al. 2010a). The limited knowledge of the internal stratigraphy of rootless cones coupled with their similarity to other volcanic edifices means that it can be difficult to distinguish rootless tephra from tephra generated during dyke-fed eruptions. This is particularly the case in flood basalt provinces, where pyroclastic successions are usually poorly preserved and poorly exposed during the main and dying phases of volcanism (e.g. Swanson et al. 1975; Reidel and Tolan 1992; Brown et al. 2014).

In this chapter, I document a newly discovered rootless cone field within the 8.5 Ma Ice Harbor pāhoehoe lava flow field in the Columbia River Flood Basalt Province (CRFBP), USA. Erosional dissection allows me to examine the tephra deposits and conduits of the rootless cones. I use these features to inform on the nature of the explosions that created the

rootless cones and to help define criteria that distinguish the deposits of rootless cones from those of dyke-fed eruptions.

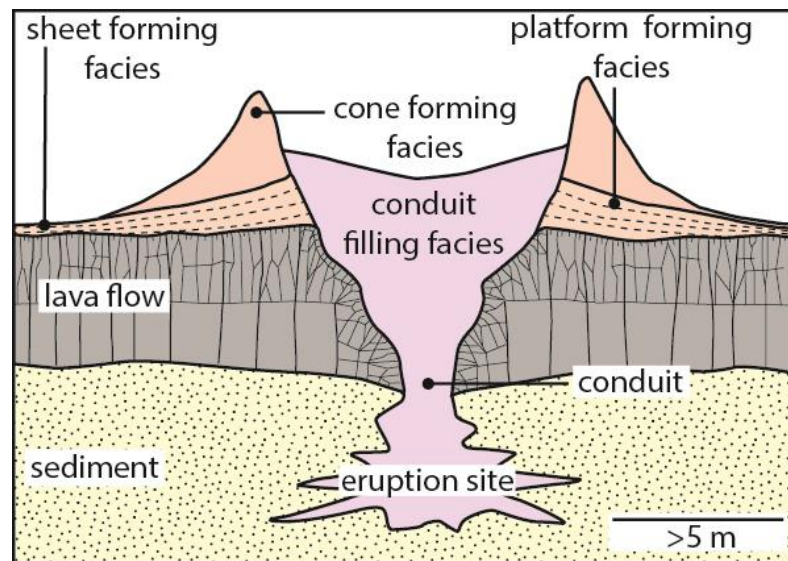


Figure 4.1. Generalised structure of a rootless cone. The cones form on active lava flows. The conduits in the host lava flow are irregular funnels that widen upwards. The upper parts of the conduits are filled with tephra. Cooling joints in the host lava flow radiate from the conduit. Cone forming deposits are composed of lapilli- to bomb-sized material that is often reversely graded and formed by fallout. Platform and sheet deposits are formed by fallout and deposition from pyroclastic density currents. Adapted from Hamilton et al. (2010a).

4.2 Geological setting of the Columbia River Basalt Province

Flood basalt volcanism in the NW USA initiated c. 17 m.y. ago in the Steens Mountain region, Oregon. Over the following ~11 m.y. the volume of erupted mafic magma exceeded $>210\,000\text{ km}^3$ across Oregon and Washington (now considered part of the CRFBP; Camp et al. 2003; Reidel et al. 2013). Eruptions were fed by ~300 km-long dyke swarms from crustal magma chambers under east-central Oregon/west-central Idaho (Wolff et al. 2008; Ramos et al. 2013). Pyroclastic rocks in the CRFBP are generally scarce, although exceptionally preserved examples of proximal tephra deposits (Swanson et al. 1975; Reidel and Tolan 1992; Brown et al. 2014), inferred rootless deposits (Thordarson and Self 1998) and drowned rootless cones (Keszthelyi and Jaeger 2014) are known.

The rootless cone deposits in this study occur in the 8.5 Ma Ice Harbor Member (Fig. 4.2), which is composed of three pāhoehoe lava flow fields that are the youngest products ascribed to the CRFBP (McKee et al. 1977; Swanson et al. 1979). The lavas have been divided into three chemically distinct types that were fed from a dyke system that was up to 90 km in length and on average <15 km in width (Swanson et al. 1975). The lava flow field has a minimum volume of 1.2 km³ (Swanson et al. 1975) and individual lava flows are typically <15 m thick. The pāhoehoe lavas are interbedded with the Ellensburg Formation sediments – diatomaceous muds, lacustrine sands and silts, volcanoclastic silt, conglomerates, and silicic volcanic ash probably sourced from eruptions of volcanoes in the NW USA. These sediments record deposition both within extensive lava-dammed lakes and by ephemeral and established rivers (Schminke 1967; Smith 1988; Tolan et al. 2002).

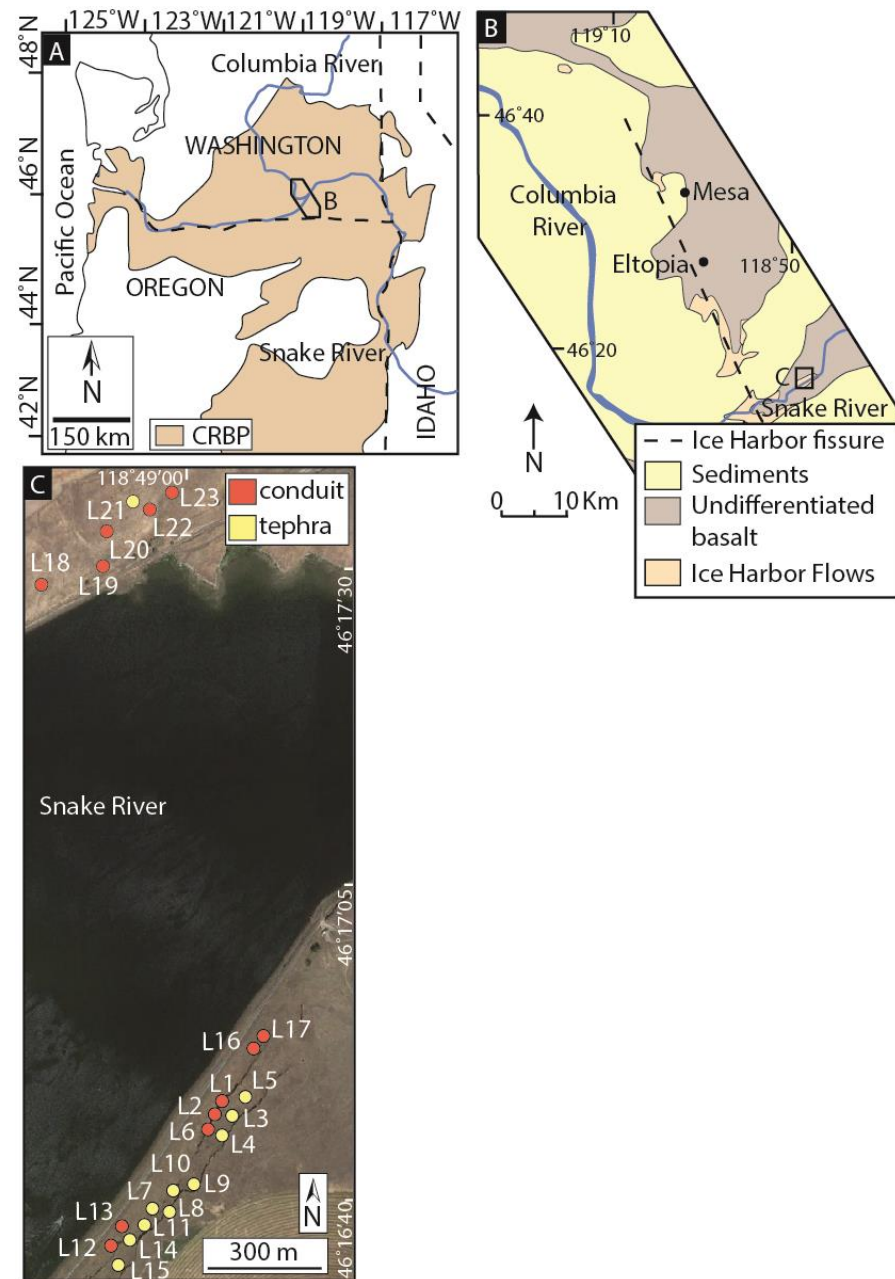


Figure 4.2. Location of the study area. (A) The CRFBP in the NW USA, adapted from Brown et al. (2014). (B) Map of the area showing the Ice Harbor fissure as described by Swanson et al. (1975) and the field area on the banks of the Snake River. (C) Sites of the tephra and conduit deposits described in this study.

4.3 Method

Field studies involved detailed sedimentary logging of tephra successions, lithofacies analysis, geological mapping and sampling. Locations were recorded using a handheld GPS

unit with an accuracy of ± 5 m. Petrographic characterisation was undertaken by optical microscopy on representative thin sections. Vesicle and clast dimensions and abundances were calculated using the image analysis software ImageJ (<http://imagej.nih.gov/ij/>) with representative samples and outcrop photographs. The crystal content of the cone deposits was calculated by point-counting representative samples. Clast densities were calculated on clasts >16 mm across using the method of Houghton and Wilson (1989). Grain size was determined by sieving.

4.4 Ice Harbor rootless cone field

The Ice Harbor rootless cone field is composed of: 1) the substrate over which the lava flows were emplaced (silicic volcanic ash); 2) the host pāhoehoe lava flows; 3) rootless cone conduits within the lava flows; 4) rootless cone- and platform-forming tephra deposits. The cone field is inferred to have occupied an area of ≥ 1 km², based on the distribution of the conduits and associated tephra. The cone field is overlain by later Ice Harbor lava flows.

4.4.1 Volcanic ash substrate

The pre-eruption substrate beneath the Ice Harbor flow field does not crop out in the study area, and the nature of the substrate has been inferred from analysis of material incorporated into the rootless cone tephra deposits. This material is composed of white, silicic, volcanic ash and forms 10–85 vol. % of all rootless cone tephra deposits (see Appendix 2). The volcanic ash is well-sorted ($1.2 \sigma\Phi$) and individual particles are platy, angular or cusped in shape and occasionally preserve vesicles (see Appendix 2). The volcanic ash has a median diameter of <0.25 mm. Smaller particles are blade shaped, whilst coarser particles have complex morphologies and exhibit bubble junctures.

Interpretation

The silicic volcanic ash is interpreted as a pyroclastic fall deposit within the Ellensburg Formation (Schminke 1967). The monolithologic character of the volcanic ash and the absence of organic matter or detrital sediment indicate that the volcanic ash had not been substantially reworked and that burial by the Ice Harbor lava may have occurred shortly after fallout. I infer that the volcanic ash fell out onto a flood plain or shallow lake; common features across the plateau-like CRFBP during the Miocene (e.g. Schminke 1967; Smith 1988;

Tolan et al. 2002). These environments are conducive to the formation of rootless cones (e.g. Thorarinsson 1951; Thorarinsson 1953; Fagents and Thordarson 2007; Hamilton et al. 2010a; Hamilton et al. 2010b).

4.4.2 Ice Harbor lava flows

The rootless cone field crops out along the banks of the Snake River (Fig. 4.2). The flow field is composed of pāhoehoe sheet lobes that reach 8 m thick and exhibit the tripartite structure typical of pāhoehoe sheet lobes in the CRFBP (e.g. Self et al. 1998; Thordarson and Self 1998). They have lower crusts that contain distorted pipe vesicles, massive, dense cores with columnar joints and vesicular upper crusts. The groundmass of the flows is composed of interstitial glass, and plagioclase and pyroxene microlites. Pyroxene and rare swallow-tail plagioclase phenocrysts and glomerocrysts 0.1–3 mm in diameter constitute 1–4 vol. % of the rock (see Appendix 2). Vesicles are partially filled with zeolite minerals. The Ice Harbor sheet lobes that contain the rootless cones have poorly vesicular cores and incipiently vesicular crusts (as defined by Houghton and Wilson 1989) that exhibit hackly, entablature-style joints spaced 11–21 cm apart (see Appendix 2).

Interpretation

I infer that inflation of the flows took several weeks, based on a lava upper crust thickness of ≥ 2 m and the relationship: $t = 164.8C^2$; where t = time in hours and C = crustal thickness in metres (see Hon et al. 1994). The presence of entablature-style jointing in the lava indicates that the flows were subjected to water enhanced cooling, implying emplacement in an environment where surface water was abundant (e.g. Long and Wood 1986). The swallow tail plagioclase microlites indicate that the lava cooled rapidly; this texture is also found in pillow lavas (e.g. Bryan 1972; Jafri and Charan 1992).

4.4.3 Rootless cone conduits

Cliffs along the Snake River reveal funnel-shaped, upward-flaring features in the Ice Harbor sheet lobes (Fig. 4.3). These features range from 1–4 m in diameter, are up to 4 m deep and have cross-sectional areas of 8–12 m². Their walls dip inwards $\sim 60^\circ$. All the funnels appear to terminate ≥ 0.5 m above the bases of the sheet lobes and sometimes form irregular, isolated cavities; these are likely 2D section effects (Fig. 4.3). Hackly cooling joints spaced

~16 cm apart radiate away from the funnel walls and extend up to ~4 m into the surrounding lava core (Fig. 4.3).

The inner surfaces of the funnels are coated with ropey-textured and bread-crust spatter that is ≤ 6 cm thick. The spatter has a hypohyaline groundmass texture, contains sheared vesicles and has multiple chilled rinds. The surface of the spatter has angular, hypocrySTALLINE and hypohyaline clasts of upper lava crust embedded in it. These clasts cover 10–30% of each funnel wall (see Appendix 2). There is a patchy, heterogeneous distribution of silicic volcanic ash across the surfaces; typically $< 5\%$. These funnels are often partially filled with tephra with a similar composition to the overlying cone deposits (massive spatter bombs, mSp; see below).

Twelve of these features have been recognised along a 450 m transect (Fig. 4.2); five on the north bank of the river and seven on the south. The features are spaced 3–206 m apart with tephra deposits exposed above them. Exposures spaced less than 5 m apart may represent irregular sections through the same feature.

Interpretation

I interpret these funnel-shaped features as remnants of rootless conduits because they have spatter, angular lapilli and patches of silicic ash plastered onto their inner wall which can only have occurred via explosive interactions. They are also filled with lapilli- to bomb-sized tephra. These features distinguish them from features described within rubbly pāhoehoe flows (e.g. Duraiswami et al. 2008; Keszthelyi et al. 2009). Sheared vesicles and rope-like textures on the conduit wall result from rheomorphic flow of spatter. The funnel shape of the conduits and their radiating cooling joints are similar to features seen in rootless cones in Iceland (e.g. Hamilton et al. 2010a).

Based on the abundance of conduits and the possibility that some locations represent irregular cross sections through the same conduit (e.g. L16/17; L1/2/6; L12/13) I suggest that the flow field hosted at least eight rootless cones. Since the size of the conduits is proportional to the size of the overlying cone (e.g. Hamilton et al. 2010a), the cones were likely to have been ≥ 5 m in basal diameter.

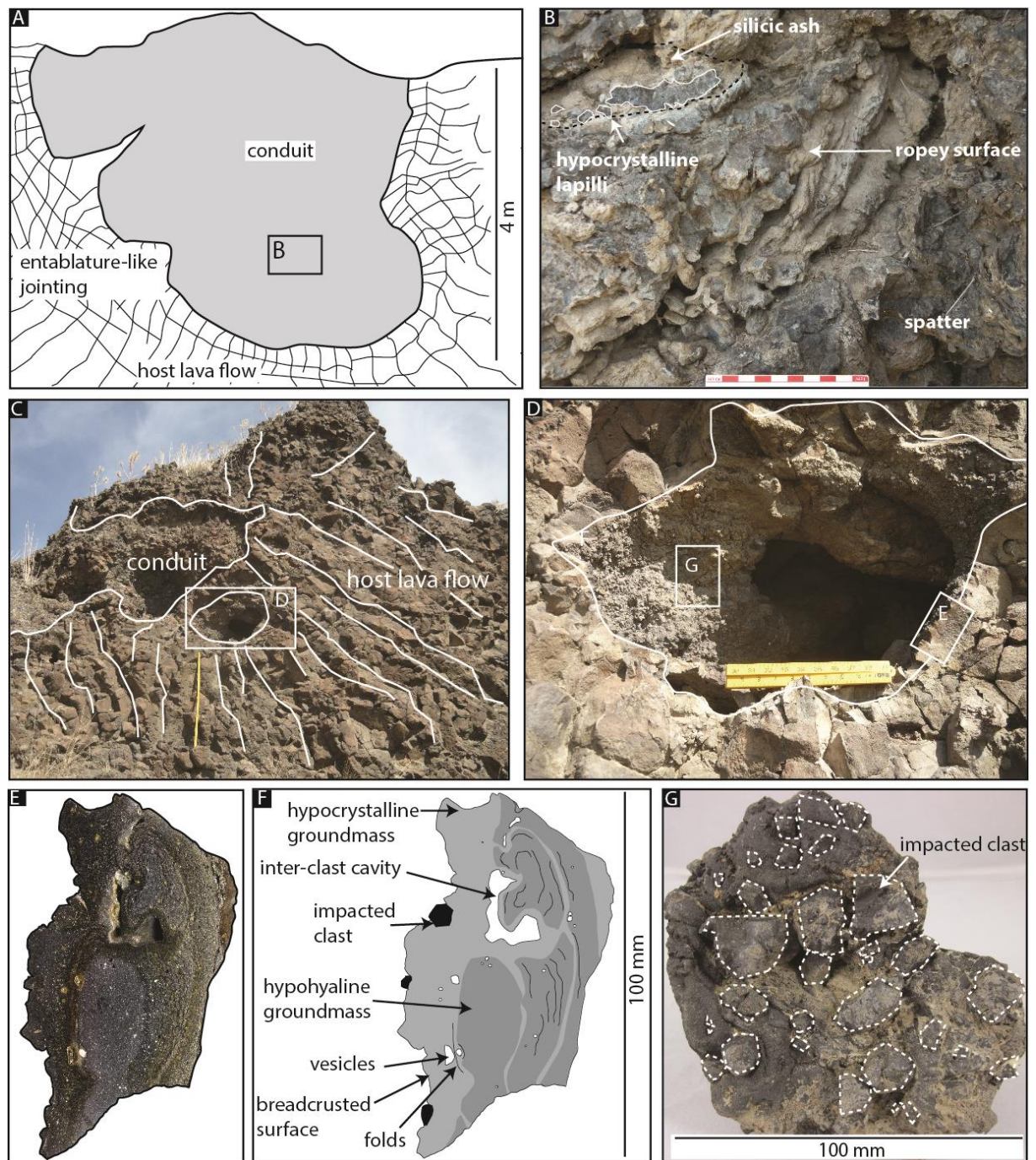


Figure 4.3. Field photographs and schematic diagrams showing the varying geometries of rootless conduits. (A) Field sketch showing the upper part of a funnel-shaped conduit at location 6 (UTM Nad83 zone 11T, 359 987 E/5 126 647 N). View to the southwest. (B) Field photograph of massive spatter (mSp) within the conduit in a, composed of spatter bombs, silicic volcanic ash and hypocrySTALLINE lapilli. (C) Irregular lower part of a conduit in the lava flow at location 22 (UTM Nad83 zone 11T, 359 724 E/5 128 162 N)

with cooling joints (white) radiating from the conduit/lava core contact (outlined). The ruler is 1 m. Inset D shows a close up of the conduit inner wall with embedded juvenile and lava crust lithic clasts. The ruler is 25 cm. Image E shows a cross section through the conduit wall, with hypohyaline lapilli embedded into the surface. (F) Interpretive sketch of E. (G) Plan view of a section of conduit wall, approximately 100 mm across, showing clasts that are inferred to have become embedded in the conduit wall during explosions (dashed outlines).

4.4.4 Rootless cone tephra deposits

Proximal rootless platform and cone-forming deposits are widely exposed over a 450 m-long transect along the south bank of the Snake River, and are intermittently exposed along the north bank of the river (Fig. 4.2). The tephra deposits are composed of juvenile pyroclasts (described below), silicic volcanic ash and fragmented lava crust.

4.4.4.1 Juvenile pyroclast types

The tephra deposits contain four different pyroclast types derived from the fragmentation and modification of the host lava flow (Fig. 4.4; Table 4.1). These juvenile clasts are (1) sideromelane ash and lapilli of both blocky and fluidal morphologies; (2) hypocrySTALLINE bombs (with both ventricular and globular morphologies) and angular lapilli; (3) armoured scoria bombs and lapilli; and (4) spatter bombs. All clasts have hypohyaline to hypocrySTALLINE groundmasses and are mineralogically similar to the host lava. The pyroclasts are incipiently to poorly vesicular, ranging between 15–36% vesicles, and are non to incipiently welded (see Appendix 2). The density of pyroclasts ranges from 1700–2300 kg m⁻³. The pyroclast types and their occurrence is summarised in Table 1.

Interpretation

The density of the Ice Harbor rootless tephra is significantly higher than that of non-welded basaltic pyroclasts produced during dyke-fed eruptions (typically 240–1440 kg m⁻³; see Chapter 3; Houghton and Wilson 1989; Parcheta et al. 2013). This suggests that the pyroclasts were sourced from lava that had already degassed at the source fissure and during transport to the rootless cone site. The ventricular and globular bombs are atypical of the deposits of fissure eruptions (e.g. Valentine and Gregg 2008); they are interpreted as water-

quenched globules of lava ejected from beneath the lava flow during explosive activity. These bombs were subsequently mechanically fragmented into angular lapilli upon eruption and deposition, enhanced by cooling contraction fractures. The spatter bombs are interpreted as proximal deposits from rootless lava fountains (e.g. as observed during the 1783–1785 Laki eruptions, see Thordarson et al. 1998) . Recycling by intermittent fountains appears necessary to form the armoured bombs. The blocky sideromelane clasts indicate cooling-contraction granulation and/or mechanical fragmentation. The fluidal, elongate sideromelane clasts indicate ductile disruption of molten lava and are common components of deposits from magmatic volatile driven eruptions (e.g. Walker and Croasdale 1971), MFCI (e.g. Zimanowski et al. 1997; Morrissey et al. 2000; Büttner et al. 2002) and peperite (see section 4.4.3; Skilling et al. 2002).

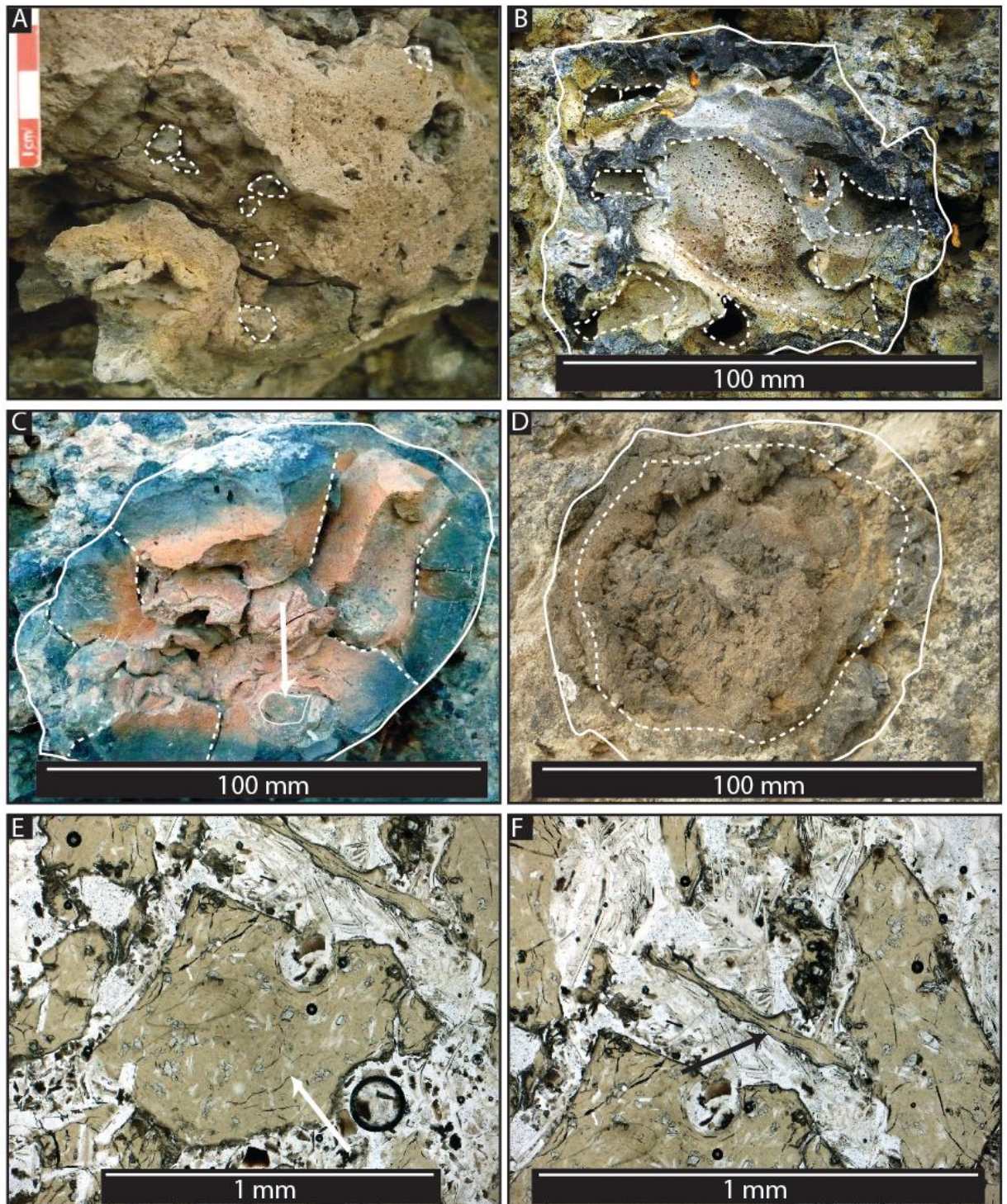


Figure 4.4. Clast types recognised in this study. (A) Folded spatter bomb with embedded lapilli (dashed outline). Graticules on the scale card are 1 cm (UTM Nad83 zone 11T, 359 942 E/5 126 519 N). (B) Ventricular clast (outlined). The clast has an amoeboid shape with a hypohyaline rind approx. 10 mm thick that grades inwards into the core. Vesicles up to 8 cm in diameter (dashed outline) have angular shapes and give clasts their

characteristic ventricular morphology (UTM Nad83 zone 11T, 359 942 E/5 126 519 N). (C) Globular bomb (outlined). The bombs have a sub-spherical shape and a black hypohyaline rind ~1 cm thick that becomes more orange in colour toward the core. Sub angular, dull black coloured basaltic lapilli (arrowed) are contained within the cores of the bombs. Cooling joints (dashed lines) penetrate from the clast margin up to 10 mm towards the core (UTM Nad83 zone 11T, 359 942 E/5 126 519 N). (D) Armoured bomb (solid outline) with 1 cm thick dense rind and vesicular core (dashed outline) (UTM Nad83 zone 11T, 360 015 E/5 126 664 N). (E) Sideromelane clast (arrowed) formed by fragmentation in a brittle state (arrowed). (F) Sideromelane clast (arrowed) formed by ductile disruption of molten lava.

| Juvenile clast type | Description | Mean Density (kg m ⁻³) | Mean Vesicularity (%) | Mean Crystallinity (%) | Interpretation |
|--|---|---------------------------------------|--------------------------|---------------------------|--|
| Spatter bombs | Lithology: Forms irregular bombs with fluidal and ropey exteriors Structure: Clast supported (spBr); clast supported beds are parallel and dip 20°; flattening with distance from vent. Massive in lithofacies mspBr. Occurrence: Tephra deposits ((m)spBr); extends a maximum distance of ~70 m from source vent. | 2200 | 19 | 31 | Bombs indicate proximal fall deposition from a littoral-style lava fountain. |
| Hypocrystalline lapilli and ventricular or globular bombs | Lithology: Forming ventricular and globular shaped bombs frequently fragmented into blocky and equant clasts that occasionally preserve ropey textures on relict exterior surfaces; dominantly lapilli to bomb size; occasionally with radial fractures. Structure: Generally clast supported, occasionally matrix supported; forms cross stratified, massive and graded units (xsLA and m/nLA); also lenses and channels (lensLA). Occurrence: All tephra and conduit facies. | 2300 | 15 | 44 | Clasts represent quenched globules of lava, ejected from beneath/within the host lava flow during tephra jetting. Bombs were mechanically fragmented into angular shapes upon eruption and deposition, and due to cooling contraction granulation. |
| Cored scoria bombs and lapilli | Lithology: Black resinous rinds up to 10 mm thick and black scoriaceous cores; forming rounded bombs frequently fragmented into blocky and equant clasts; dominantly lapilli to bomb size. Structure: Clast-matrix supported; massive Occurrence: All tephra deposits. | 1700 | 36 | 52 | Produced by recycling of clasts in the conduit during intermittent and/or dry tephra jetting when surface water was less abundant. |
| Blocky or fluidal sideromelane ash and lapilli | Lithology: Clast shapes vary from blocky and equant to fluidal and elongate. Structure: Varying from matrix to clast supported; massive (spBr and xsLA), graded (m/nLA) and lenses and channels (lensLA). Occurrence: All tephra and conduit facies. | - | - | 28 | Blocky and equant clasts indicate cooling contraction granulation; fluidal, elongate shapes indicates free-air ductile fragmentation during MFCI. Bedding structures are interpreted to record deposition during the passage of density currents. |
| Table 4.1. Summary descriptions of pyroclast types. | | | | | |

4.4.4.2 Pyroclastic lithofacies

The tephra deposits can be sub-divided into four lithofacies according to their componentry, grain size and depositional structures (Fig. 4.5; Table 4.2). In general the pyroclastic lithofacies appear moderately to very poorly sorted and are composed of juvenile clasts with <10–85 vol. % silicic volcanic ash (see Appendix 2). Lithofacies with the largest juvenile clasts tend to have the least silicic volcanic ash (Fig. 4.6). The lithofacies form proximal platform, cone or conduit-filling deposits. Sheet deposits are not found; these are commonly unconsolidated (Hamilton et al. 2010a). Contacts between the tephra deposits and underlying lavas are not exposed (Fig. 4.6).

Platform deposits include massive or normally graded lapilli-ash (m/nLAf), lenses of lapilli-ash (lensLA) and cross-stratified lapilli-ash (xsLA; Table 4.2; Fig. 4.5). These deposits are 1–5.5 m in thickness (Fig. 4.7) and are present beneath the parallel-bedded spatter (//bSp; Figs. 4.6 and 4.7). Pyroclasts within the deposits are dominantly of lapilli size. They are exposed over a ~600 m long transect. Bedding dips vary from 10–20°.

Cone deposits are composed of parallel-bedded spatter (//bSp; Table 4.2) that is 1–3 m thick (Fig. 4.6) and contains predominantly bomb-sized clasts. Deposits are exposed over a ~200 m long transect. The spatter varies from horizontally bedded to dipping up to 20°; whether this is towards or away from a conduit is unclear (Figs. 4.6 and 4.7).

The conduits are partially filled with massive spatter (mSp; Table 4.2) and are not observed in contact with overlying cone and/or platform deposits.

Interpretation

The Ice Harbor platform deposits are inferred to have been deposited from both PDCs and by fallout (e.g. Hamilton et al. 2010a). The occurrence of massive/normally graded lapilli-ash (m/nLAf), lenses of lapilli-ash (lensLA) and cross-stratified lapilli-ash (xsLA) beneath the spatter-rich deposits (e.g. //bSp) suggests that the platform was constructed prior to cone formation. Intermittent deposits of normally-graded lapilli ash (nLA) and cross-stratified lapilli-ash (xsLA; Fig. 4.6) overlying the spatter layers suggests that the cone field is composed of numerous overlapping cones formed in a sequence of rootless eruptions (e.g. Fagents and Thordarson 2007). The thickness and spatial distribution of the exposures suggest that the tephra platforms were ~5 m thick and were likely to be laterally extensive over 100's

of metres. Cone-forming and conduit-filling deposits of rootless cones commonly contain spatter-rich lithofacies (Hamilton et al. 2010a), as observed in this study. These coarse-grained deposits are produced as the explosivity of the eruptions decreases (Fagents and Thordarson 2007).

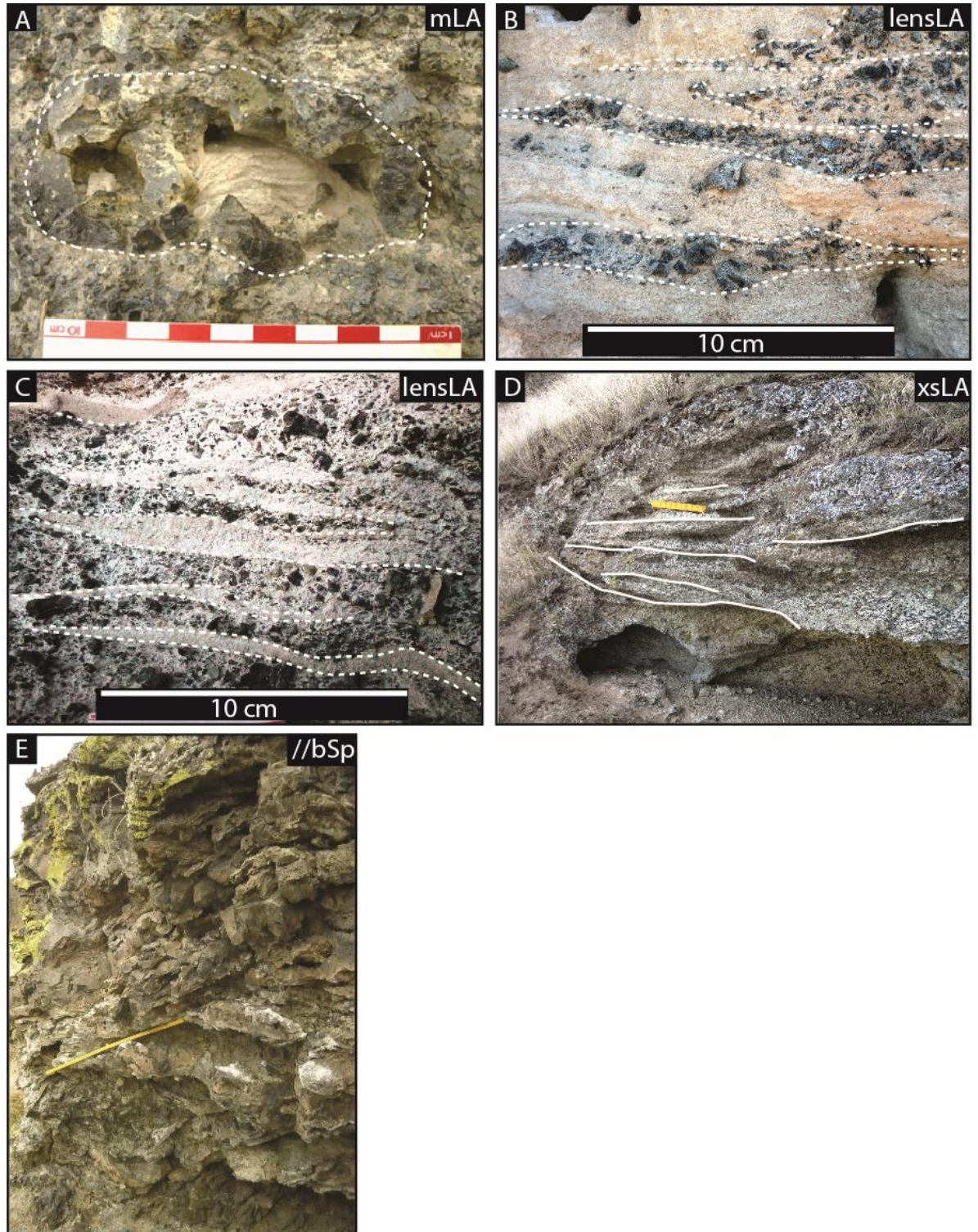


Figure 4.5 (overleaf). Lithofacies found in the study area. (A) mLA with ventricular bomb (outlined) enclosing laminated silicic volcanic ash. Graticules on the scale card are 1 cm (UTM Nad83 zone 11T, 359 881 E/5 126 506 N) (B) lensLA with hypocrySTALLINE lapilli-rich lenses. Dashed white outlines indicate lenses (UTM Nad83 zone 11T, 359 868 E/5 126 485 N) (C) lensLA with silicic ash-rich lenses. White outlines indicate lenses (UTM Nad83 zone 11T, 359 868 E/5 126 485 N) (D) xsLA, white outlines indicate beds. The ruler is 25 cm long (UTM Nad83 zone 11T, 359 868 E/5 126 485 N) (E) //bSp, showing bedded spatter bombs. The ruler is 50 cm (UTM Nad 83 zone 11T, 359 942 E/5 126 519 N).

| Lithofacies | Components | Description | Av. max clast size (mm) | % silicic ash | Interpretation |
|---|---|---|-------------------------|---------------|---|
| LA Sub facies: n (normal graded), m (massive) f (fabric) | Hypocrystalline lapilli and bombs, sideromelane ash, silicic volcanic ash, clasts of lava crust | Very poorly sorted, hypocrystalline lapilli with rare ash sized fragments; clast supported in silicic ash. | 128 | 20–75 | Platform forming deposit. The general lack of evidence for traction sedimentation in the juvenile clasts suggest proximal fall deposition, localised fabrics suggest a minor amount of lateral transport. The coarse nature of some deposits results from the ballistic emplacement of bombs. |
| lensLA | Hypocrystalline lapilli, sideromelane ash, silicic volcanic ash, clasts of lava crust | Lenses and channels of moderately well sorted, sideromelane and hypocrystalline lapilli; clast supported in silicic volcanic ash; and lenses and channels of substrate within sideromelane and hypocrystalline lapilli dominated rock. Irregular lower contact. | 60 | 25–85 | Platform forming deposit. Indicates deposition from dilute PDC. Erosion and transportation of material occurred in locally confined channels. Irregular lower contacts may suggest local erosion of underlying units. |
| xsLA | Hypocrystalline lapilli and bombs, sideromelane ash, silicic volcanic ash, clasts of lava crust | Cross stratified, moderately sorted sideromelane and hypocrystalline lapilli; clast supported in silicic volcanic ash; beds approximately 5 cm thick. | 70 | 20–55 | Platform forming deposit. Crude cross-bedding formed during deposition from PDC's, currents were locally erosive. |
| //bSp Sub facies: m (massive) | Spatter bombs, hypocrystalline lapilli, silicic volcanic ash, clasts of lava crust | Parallel-bedded spatter bombs with embedded angular hypocrystalline lapilli and silicic volcanic ash. Sub facies is massive. | >1000 | <10 | Cone forming deposit; sub facies (mSp) conduit fill deposit. Bomb beds indicate proximal fall deposition from rootless lava fountains. Large grain size indicates decreasing explosivity when water availability was decreasing towards the end of the eruptions. |

Table 4.2 Summary descriptions of cone-forming and conduit deposits.

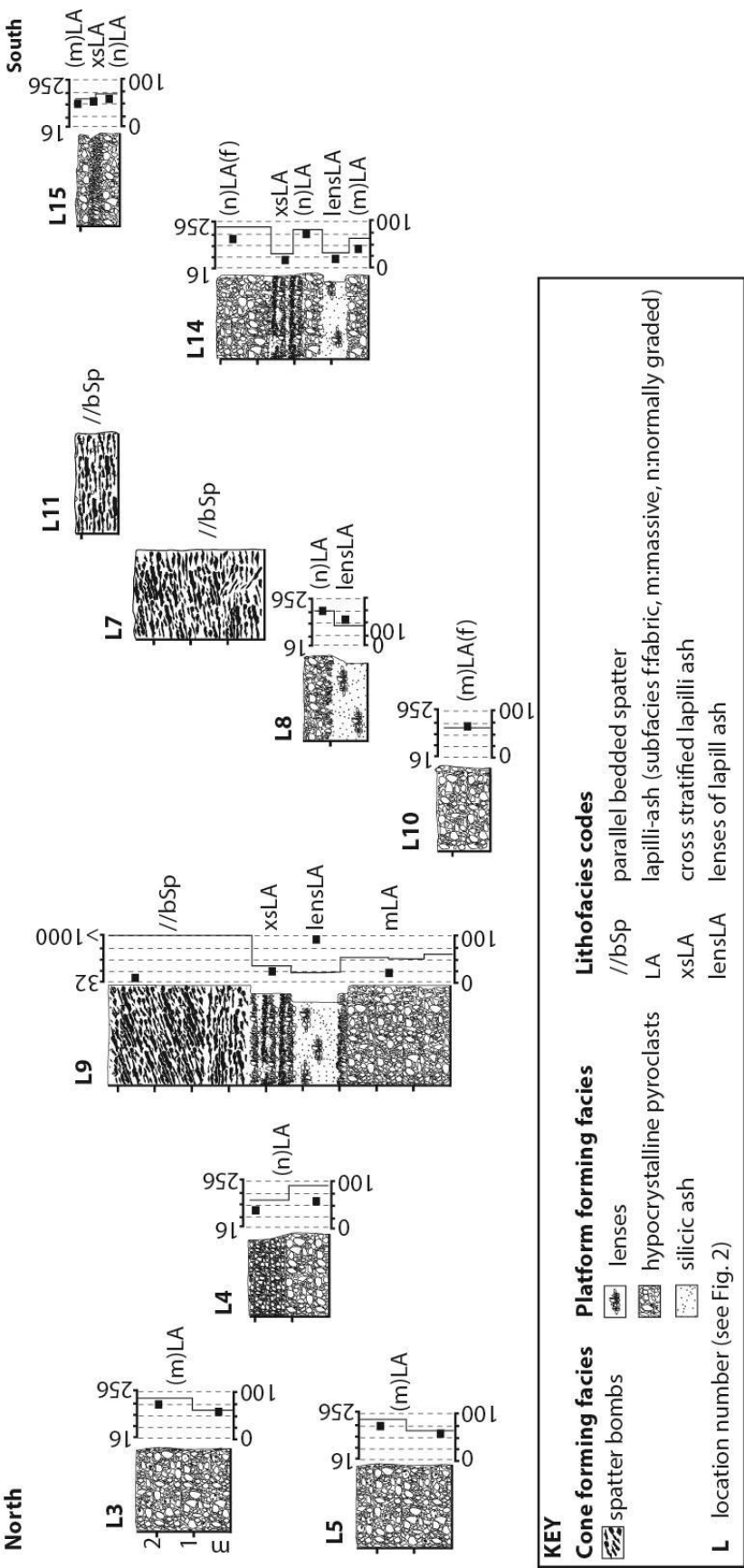


Figure 4.6. Lithofacies logs of tephra deposits south of the Snake River. Clast size is shown on the top axis with divisions at 32, 64, 128 and 256 mm (Location 9 uses 32, 64, 128, 256 and >1000 mm divisions). Silicic volcanic ash abundance (black squares; %) is shown across the bottom axis in 25% gradations. Logs are shown at relative altitudes. For locations of the sections see Fig. 4.2.

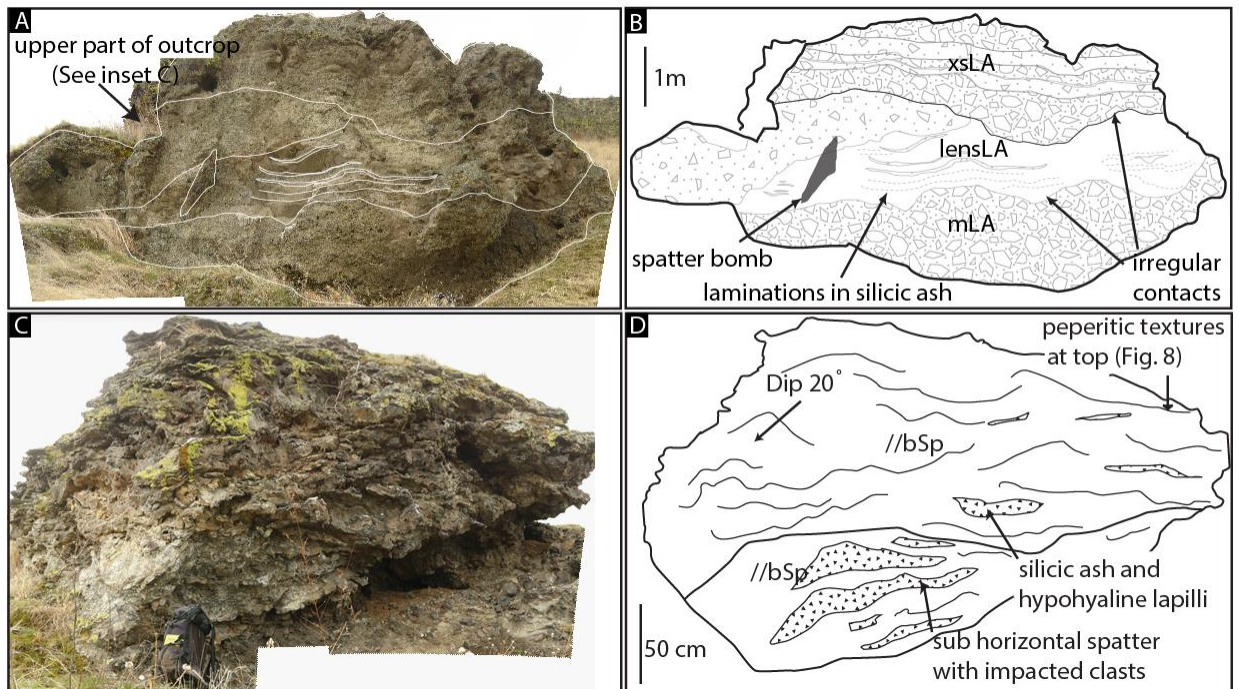


Figure 4.7. Photographs and interpretive pictures of Location 9 (UTM Nad 83 zone 11T, 359 942 E/5 126 519 N). a, b Outcrop of platform-forming admixed tephra and silicic volcanic ash. c,d Outcrop of cone-forming tephra composed of lithofacies //bSp.

4.4.4.3 Lava-silicic volcanic ash interaction textures in tephra deposits

A variety of peperite-like textures are observed in the tephra deposits (Fig. 4.8). Fluidal textures include spatter bombs that inter-finger with the silicic volcanic ash and associated globular and elongate spatter lapilli and ash found intimately mixed with the silicic volcanic ash. Within 2 cm of the spatter, the silicic volcanic ash is often thermally altered, becoming dark in colour and fused (e.g. Schminke 1967). Where fused, the silicic volcanic ash contains vesicles ≤ 2 mm in diameter. Vesicles in the spatter also contain silicic ash. Blocky textures include jigsaw-fit bombs; these clasts have hairline fractures filled with silicic volcanic ash. Other bombs have rinds that are partially separated from their core, encapsulating a 2 mm-thick domain of silicic volcanic ash between rind and core. These domains contain mm-scale globules of lava.

Interpretation

Peperite-like textures indicate interaction between hot juvenile clasts and unconsolidated sediment (e.g. Skilling et al. 2002). Vesicles in the fused silicic volcanic ash indicate that gas was generated during interaction (e.g. Kokelaar 1982; Skilling et al. 2002; Squire and McPhie 2002). Silicic ash-filled vesicles in the spatter indicate that the sediment was mobilised during interaction (e.g. Goto and McPhie 1996 and references there-in; Skilling et al. 2002). The fluidal and blocky textures indicate variations in mechanical stress, movement of lava, lava-silicic ash density contrasts and variations in lava viscosity and clast size (e.g. Skilling et al. 2002; Squire and McPhie 2002). These textures may represent a failed phreatomagmatic fragmentation process formed beneath the lava flow (e.g. Busby-Spera and White 1987; Hooten and Ort 2002). The bombs with encapsulated silicic volcanic ash are interpreted as intrusions of lava into the underlying substrate. Lava globules in the silicic volcanic ash domain indicate that the cores of these bombs were molten during intrusion.

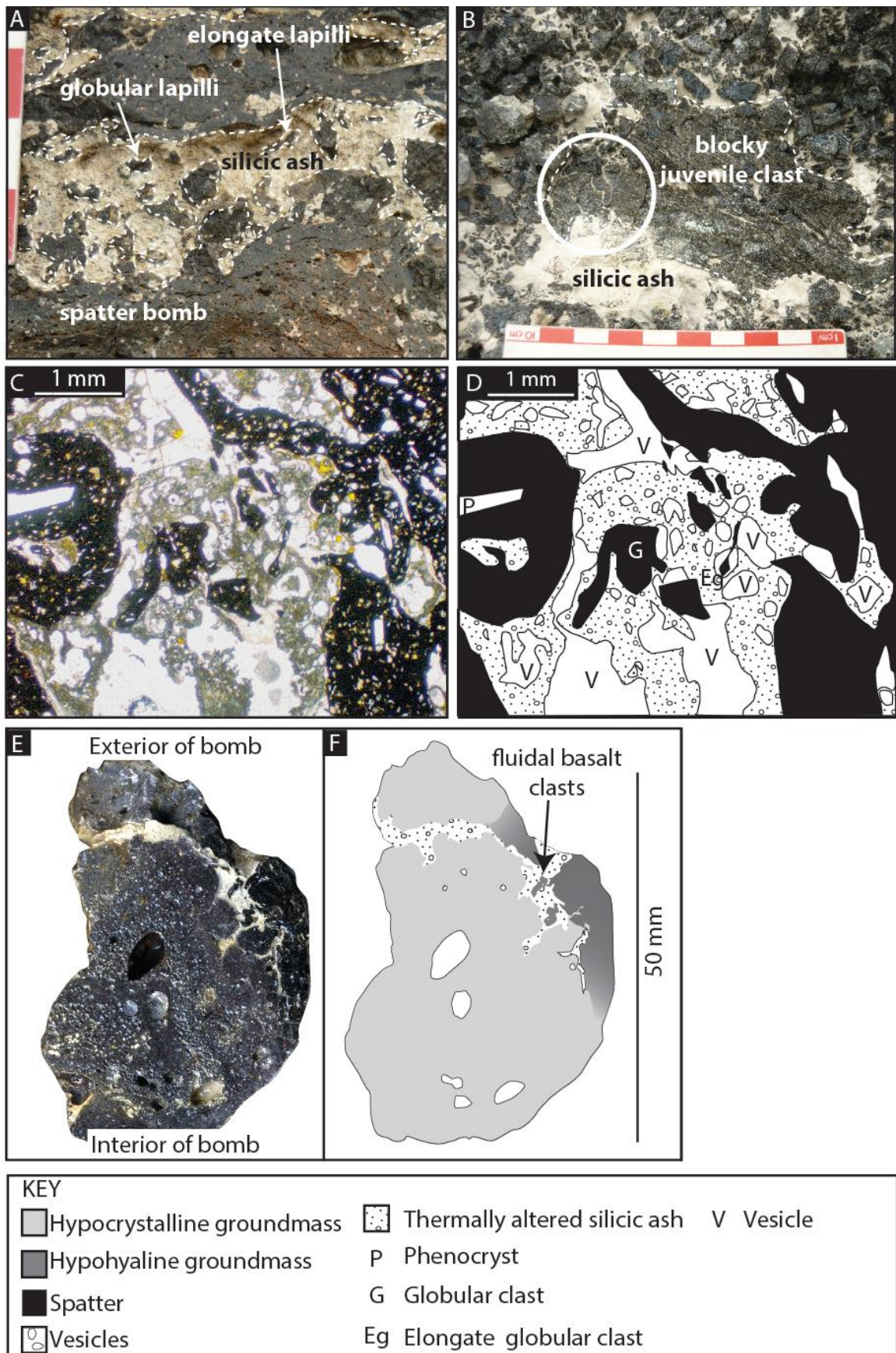


Figure 4.8 (overleaf). Peperite-like textures produced by the interaction of juvenile clasts and silicic volcanic ash. (A) Fluidal peperite with elongate and globular clasts in lithofacies //bSp (UTM Nad 83 zone 11T, 359 942 E/5 126 519 N). (B) Blocky peperite with jigsaw-fit fractures (circled). Graticules are 1 cm (UTM Nad 83 zone 11T, 360 014 E/5 126 649 N). Thin section C and interpretive sketch D shows section of mingled spatter and silicic volcanic ash. The spatter clasts exhibit elongate and globular morphologies. The silicic ash is thermally altered and contains vesicles. Vesicles within the spatter clasts enclose silicic volcanic ash. Section of a ventricular bomb E and interpretive sketch F are also shown. The hypohyaline rind is spalling from the core and has encapsulated a domain of silicic volcanic ash. Fluidal basalt clasts are found within the silicic ash domain (arrowed) indicating that the core of the bomb was molten when the sediment was encapsulated.

4.5 Emplacement of the Ice Harbor rootless cones

We infer that the Ice Harbor lava flows traversed a lacustrine or floodplain environment (Fig. 4.9). The ground was mantled by a layer of silicic volcanic ash fall derived from a major explosive eruption. As the lava flows inflated they developed brittle basal crusts (Hon et al. 1994). These crusts were weakened by the development of cooling fractures (Thordarson and Self 1998) which created a zone of weakness along the base of the flows. Cracking and subsequent failure of the crust would have been facilitated by heterogeneous subsidence of the flows during inflation (e.g. Fagents and Thordarson 2007; Hamilton et al. 2010a). Failure of the basal crust allowed extrusion of lava, analogous to the axial cleft of a tumulus (e.g. Walker 1991; Rossi and Gudmundsson 1996; Hamilton et al. 2010a).

Extrusion of lava through the basal crust resulted in the intimate mixing of molten lava with the water-saturated silicic volcanic ash. This mixing of the lava and sediment is evidenced by the peperite-like textures and abundance of silicic volcanic ash (i.e. substrate) in the tephra deposits. Lava-substrate mixing was followed by explosions. These explosions fragmented the lower lava crust and burst through the molten lava core creating transient conduits. The preservation of conduits requires the cooling and solidification of the conduit walls over time to prevent pressure-driven collapse of the walls between explosions. The presence of spatter lining the walls of the conduits indicates that they were stabilised from both material ejected during the explosions, as well as from the chilling of the molten lava

core. Explosive activity deposited the massive/normally graded lapilli-ash (lithofacies m/nLA (f)) on top of the lava flow. Some of the pyroclastic material formed PDCs (depositing lithofacies lensLA and xsLA; Table 4.2). These processes constructed the tephra platforms.

Spatter-rich lithofacies (e.g. //bSp and mSp; Table 4.2) were produced during rootless lava fountaining and cap the rootless cone successions and fill some conduits. The coarse clast size of these lithofacies indicates decreasing explosivity as water availability declined. Explosions also embedded juvenile clasts and lava crust lithics into the hot and ductile conduit walls.

The presence of the cones on top of sheet lobes suggests that the cones developed repelled, non-aligned spatial distributions (e.g. Hamilton et al. 2010a; Hamilton et al. 2010b). The cones were likely to have formed in topographic lows where lava and water were most abundant, and in regions of enhanced substrate compressibility (Hamilton et al. 2010a; Hamilton et al. 2010b). Exposures do not allow determination of the symmetry of the cones (e.g. radial or elongate). Growth of the cones was terminated by the decreasing availability of ground water, or by water being prevented from gaining access to the explosion site. Continued cooling stabilised the conduit walls and over time cooling joints radiated out into the core (e.g. Fig. 4.9).

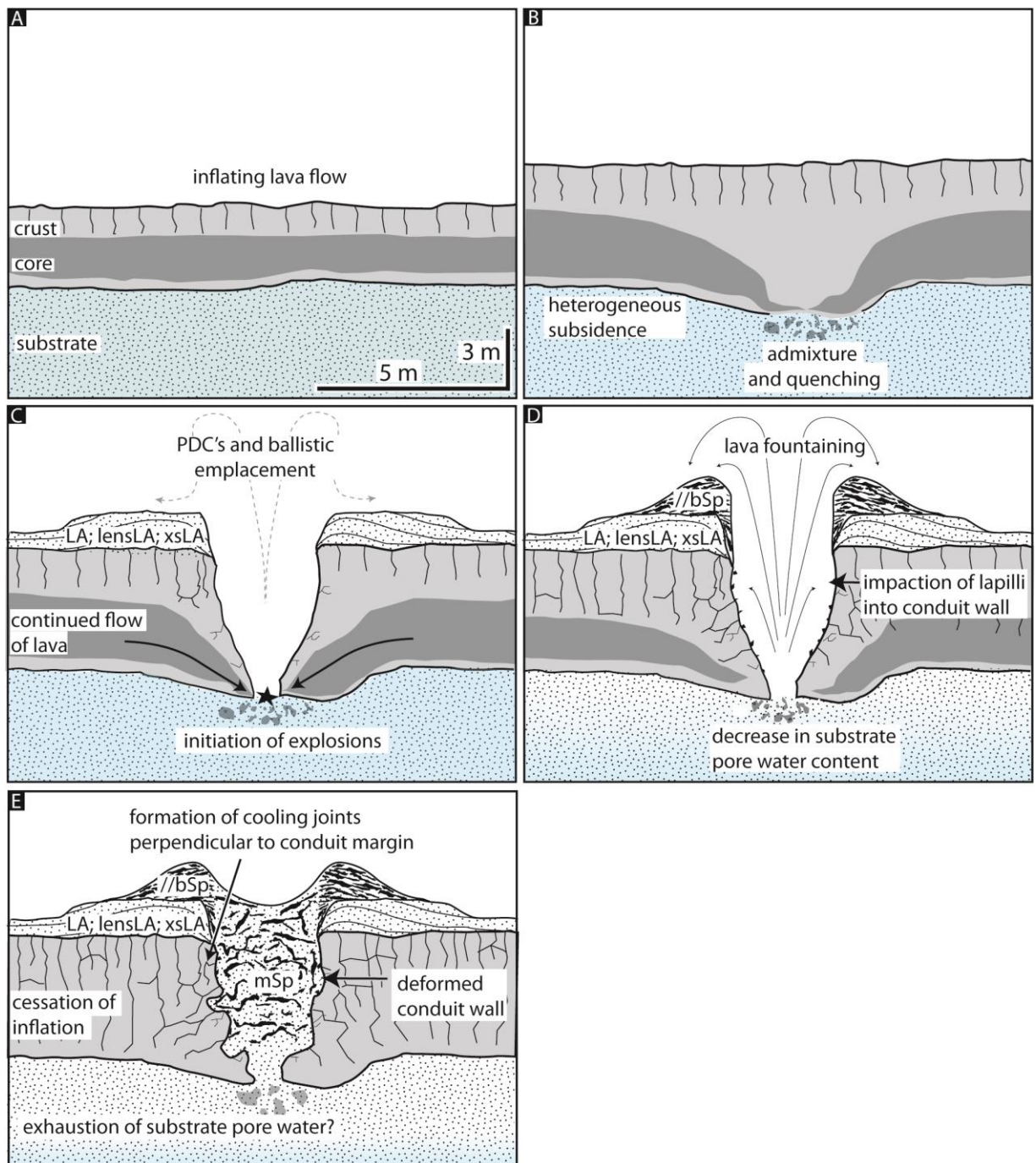


Figure 4.9. Inferred eruption chronology for the cones. (A) Lava flow traverses wet ground and subsides heterogeneously into the underlying silicic volcanic ash. (B) Initial mingling of lava with the silicic ash results in the formation of globular and ventricular juveniles and peperite-like textures. (C) Interaction between molten lava and water saturated silicic volcanic ash results in explosive brecciation of the host lava flow and fragmentation of the globular and ventricular juveniles into lapilli and ash sized clasts.

Episodic eruptions and dilute PDC's deposit poorly sorted juveniles and clasts sourced from the host lava flow, forming sheet and platform deposits (lithofacies m/nLA(f), lensLA, xsLA). Minor clast recycling may occur, producing armoured bombs. Substrate pore water is gradually depleted beneath the lava flow. (D) Decreasing water availability results in less efficient fragmentation and lava fountains are generated. These fountains produce lithofacies //bSp that builds a cone. Lapilli are also impacted into the cooling conduit walls. (E) With time water availability decreases and eruptions cease. The lava flow may continue to inflate and deform the conduit. Post-eruption cooling of the lava promotes the formation of cooling joints that radiate from the conduit.

4.6 Comparison with other rootless cones

The deposits in this study are comparable with the platform and cone-building deposits of rootless cones in Iceland (e.g. Table 4.3; Fig. 4.10), which show a similar pattern of sediment-rich PDC deposits overlain by coarse-grained fall deposits. These PDC and fall deposits are composed of scoria lapilli and bombs, spatter bombs and clastogenic lava, all intimately mixed with silt- to cobble-sized sediment. The coarse grainsize of the platform deposits in this study relative to others described in Iceland (Hamilton et al. 2010a) may result from the proximity of the Ice Harbor tephra platforms to the explosion source, or from less efficient magma-water interaction. Whilst the importance of sediment properties (e.g. grainsize distribution and thermal conductivity) in governing the explosivity of dyke-fed eruptions is recognised (e.g. Sohn 1996; White 1996; Auer et al. 2007; Ort and Carrasco-Nuñez 2009) the effect of sediment properties on rootless eruptions is as-yet unknown. Furthermore, the properties of the substrate would have evolved during the eruptions, due to mixing of basaltic pyroclasts and silicic volcanic ash beneath the lava flow.

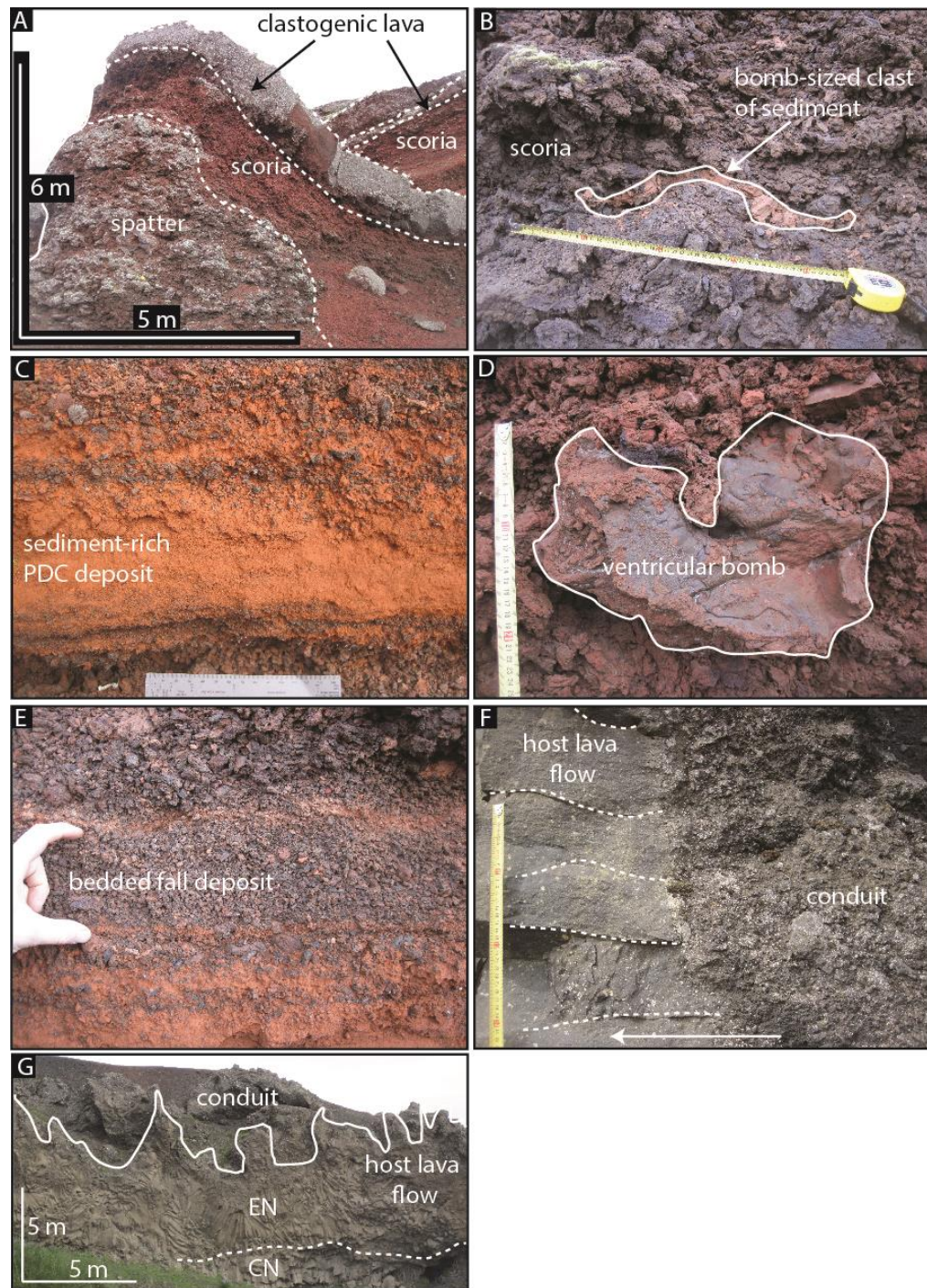


Figure 4.10. Photographs of Leitín and Búrfell rootless cones in southern Iceland (UTM Nad 83, zone 27, 500 000 E/7 097 014 N; 402 187 E/7 098 548 N respectively). (A) Overlapping cone stratigraphies composed of crudely bedded spatter and scoria bombs and lapilli and clastogenic lava. The sequence is ~6 m thick. (B) Bomb-sized clast of sediment (outlined) within a sequence of scoria and spatter. The ruler is 40 cm long. (C) Sediment-rich pyroclastic density current deposit at the base of the cone forming

stratigraphy. The reddish colour is given by the agglutinated sediment (inferred to be a lacustrine siltstone), not oxidation of the pyroclasts. The scale card is 120 mm long. (D) Bomb-sized, ventricular-type pyroclast (outlined) within the bedded spatter and scoria. The ruler is ~25 cm long. (E) Initial cone-forming fall deposit, composed of scoria lapilli. Beds often form inversely-graded couplets. The bed indicated is ~6 cm thick. Beds thickness and clast size increases up-section. (F) Cross section of the conduit wall, with lapilli sized pyroclasts agglutinated to the outer wall. Cooling joints (dashed lines) radiate from the contact and are perpendicular to the conduit contact. The arrow points towards the core of the lava flow. The ruler is 30 cm long. (G) A lava flow affected by rootless cone formation. The lava flow can be divided into a colonnade (CN) and an entablature (EN), and has an irregular upper contact that forms the rootless conduit. The lava is ~10 m thick.

| Field Area | Cone height (m) | Cone basal diameter (m) | Structure | Juvenile Clast types | Environmental setting | Grading | Bedding | Deposition method | Substrate inclusions |
|--------------------------------------|-----------------|-------------------------|--|--|-----------------------------|--------------------|--|--|--|
| Greenland | 25 | 100– 200 | Fines upwards into ash layers rich in shale, largest clasts proximal, central sediment filled chimney | Pillows and pillow fragments up to 0.5 m size at base of the unit, glass rich clasts with fluidal outlines and yellow brown sand sized volcanic at top | Subaqueous lacustrine | Normal | Bedding seen as clast alignment, flanks dip 20° | (No data) | Partly consolidated shale; 10–20 vol. % |
| Iceland | 1–35 | 2– 450 | Capped by spatter 1–2 m thick, inverse grading is common, occasionally with rheomorphic layers, form steep hornitos or broad cinder/tuff cones | Scoria and spatter, ash, lapilli and bombs | Lakes, marshes etc. | Inverse | <0.2 m thick beds of mud and ash, decimetre to metre thick beds of juveniles | PDC and fall | Common in lower sequences as beds, inclusions and coatings; no amounts given |
| Columbia River Ice Harbor lava flows | ≥ 3 | ≥ 5 | Sediment-rich tephra platforms at base, overlain by 1–3 m thick spatter sequences | Angular hypocrySTALLine ash and lapilli, armoured and spatter bombs | Flood plain or shallow lake | Inverse | Decimetre to metre thick beds of juveniles, rich in substrate | PDC and fall | Common in all except uppermost beds, admixed with juveniles; 20– 90 vol. % |
| Hawaii | 10– 90 | 20– 100’s | Monomictic, variably welded and agglutinated, often form crescent shaped ridges at the shoreline | Scoria and spatter, ash, lapilli and cored bombs, Limu-o-Pele , lava crust lithics | Entry of lava into ocean | Normal and inverse | Massive to crudely bedded in proximal facies; poorly to moderately bedded in distal facies | Tephra jets, littoral lava fountains, lithic blasts, lava squeeze up and flow from cone, bubble bursts | (No data) |

Table 4.3. Comparison of rootless and littoral cone structures using data from Simpson and McPhie (2001); Mattox and Mangan (1997); Moore and Ault (1965); Fisher (1968); Hamilton et al. (2010a); Melchior Larsen et al. (2006); Jurado-Chichay et al. (1996); and this study.

4.7 Conclusions

The Ice Harbor tephra deposits provide insights into the construction and componentry of a rootless cone field. Cross sections of conduits suggest that ≥ 8 cones were present in a cone field ≥ 1 km² in area. Cone- and platform-forming deposits are composed of admixed juvenile clasts, clasts from the host lava flow and silicic volcanic ash from an earlier, major explosive eruption in NW USA. Construction of the cone field occurred through a combination of deposition from PDCs and lava fountaining. Explosivity decreased with time as a result of decreasing water availability in the underlying silicic volcanic ash. This study demonstrates juvenile clast morphology and clast density are useful criteria for distinguishing between rootless tephra and tephra produced above an erupting dyke. Furthermore, the abundance of sediment (in this case, silicic volcanic ash) in the tephra can help distinguish rootless cones from superficially similar scoria cones.

4.8 References

- Auer A, Martin U, Nemeth, K (2007) The Fekete-hegy (Balaton Highland Hungary) “soft-substrate” and “hard-substrate” maar volcanoes in an aligned volcanic complex—Implications for vent geometry, subsurface stratigraphy and the palaeoenvironmental setting. *J Volcanol Geoth Res* 159(1), 225-245.
- Brown RJ, Blake S, Thordarson T, Self S (2014) Pyroclastic edifices record vigorous lava fountains during the emplacement of a flood basalt flow field, Roza Member, Columbia River Basalt Province, USA. *Geol Soc Am Bull* 126:875-891
- Bruno BC, Fagents S, Thordarson T, Baloga SM, Pilger E (2004) Clustering within rootless cone groups on Iceland and Mars: Effect of nonrandom processes. *Journal of geophysical research* 109(E7):1991-2012
- Bryan WB (1972) Morphology of quench crystals in submarine basalts. *Journal of Geophysical Research* 77(29):5812-5819
- Busby-Spera C, White JL (1987) Variation in peperite textures associated with differing host-sediment properties. *B Volcanol* 49(6):765-776
- Büttner R, Dellino P, La Volpe L, Lorenz V, Zimanowski B (2002) Thermohydraulic explosions in phreatomagmatic eruptions as evidenced by the comparison between pyroclasts and products from Molten Fuel Coolant Interaction experiments. *J. Geophys. Res.* 107(B11):2277
- Camp VE, Ross ME, Hanson WE (2003) Genesis of flood basalts and Basin and Range volcanic rocks from Steens Mountain to the Malheur River Gorge, Oregon. *Geol Soc Am Bull* 115(1):105-128
- Duraiswami RA, Bondre NR, Managave S (2008) Morphology of rubbly pahoehoe (simple) flows from the Deccan Volcanic Province: Implications for style of emplacement. *J Volcanol Geoth Res* 177(4):822-836
- Fagents SA, Lanagan P, Greeley R (2002) Rootless cones on Mars: a consequence of lava-ground ice interaction. *Geological Society, London, Special Publications* 202(1):295-317
- Fagents SA, Thordarson T (2007) Rootless cones in Iceland and on Mars. In: Chapman M, Skilling IP (eds) *The Geology of Mars: Evidence from Earth-Based Analogues*. Cambridge University Press, pp 151–177
- Fisher RV (1968) Puu Hou littoral cones, Hawaii. *Geologische Rundschau* 57(3):837-864

- Goto Y, McPhie J (1996) A Miocene basanite peperitic dyke at Stanley, northwestern Tasmania, Australia. *J Volcanol Geoth Res* 74(1):111-120
- Greeley R, Fagents SA (2001) Icelandic pseudocraters as analogs to some volcanic cones on Mars. *J. Geophys. Res.* 106(E9):20527-20546
- Hamilton CW, Thordarson T, Fagents SA (2010a) Explosive lava–water interactions I: architecture and emplacement chronology of volcanic rootless cone groups in the 1783–1784 Laki lava flow, Iceland. *B Volcanol* 72(4):449-467
- Hamilton CW, Fagents SA, Thordarson T (2010b) Explosive lava–water interactions II: self-organization processes among volcanic rootless eruption sites in the 1783–1784 Laki lava flow, Iceland. *B Volcanol* 72(4):469-485
- Hamilton CW, Fagents SA, Wilson L (2010c) Explosive lava-water interactions in Elysium Planitia, Mars: Geologic and thermodynamic constraints on the formation of the Tartarus Colles cone groups. *Journal of Geophysical Research: Planets* (1991–2012) 115(E9)
- Hamilton CW, Fagents SA, Thordarson T (2011) Lava–ground ice interactions in Elysium Planitia, Mars: Geomorphological and geospatial analysis of the Tartarus Colles cone groups. *Journal of Geophysical Research: Planets* (1991–2012) 116(E3)
- Hon K, Kauahikaua J, Delinger R, Mackay K (1994) Emplacement and inflation of pahoehoe sheet flows: Observations and measurements of active lava flows on Kilauea Volcano, Hawaii. *Geol Soc Am Bull* 106(3):351-370
- Hooten J, Ort M (2002) Peperite as a record of early-stage phreatomagmatic fragmentation processes: an example from the Hopi Buttes volcanic field, Navajo Nation, Arizona, USA. *J Volcanol Geoth Res* 114(1):95-106
- Houghton BF, Wilson CJN (1989) A vesicularity index for pyroclastic deposits. *B Volcanol* 51(6):451-462
- Jaeger WL, Keszthelyi LP, McEwen AS, Dundas CM, Russell PS (2007) Athabasca Valles, Mars: A Lava-Draped Channel System. *Science* 317(5845):1709-1711
- Jafri SH, Charan SN (1992) Quench textures in pillow basalt from the Andaman-Nicobar Islands, Bay of Bengal, India. *Proc. Indian Acad. Sci. (Earth Planet Sci.)* 101(1):99-107
- Jurado-Chichay Z, Rowland S, Walker GL (1996) The formation of circular littoral cones from tube-fed pāhoehoe: Mauna Loa, Hawai'i. *B Volcanol* 57(7):471-482
- Keszthelyi LP, Baker VR, Jaeger WL, Gaylord DR, Bjornstad BN, Greenbaum N, Self S, Thordarson T, Porat N, Zreda MG (2009) Floods of water and lava in the Columbia River Basin: Analogs for Mars. *Field Guides* 15:845-874
- Keszthelyi LP, Jaeger WL (2014) A field investigation of the basaltic ring structures of the Channeled Scabland and the relevance to Mars. *Geomorphology*
- Kokelaar BP (1982) Fluidization of wet sediments during the emplacement and cooling of various igneous bodies. *J Geol Soc London* 139(1):21-33
- Lanagan PD, McEwen AS, Keszthelyi LP, Thordarson T (2001) Rootless cones on Mars indicating the presence of shallow equatorial ground ice in recent times. *Geophysical Research Letters* 28(12):2365-2367
- Long PE, Wood BJ (1986) Structures, textures, and cooling histories of Columbia River basalt flows. *Geol Soc Am Bull* 97(9):1144-1155
- Mattox TN, Mangan MT (1997) Littoral hydrovolcanic explosions: a case study of lava–seawater interaction at Kilauea Volcano. *J Volcanol Geoth Res* 75(1–2):1-17
- McKee E, Swanson D, Wright T (1977) Duration and volume of Columbia River basalt volcanism, Washington, Oregon and Idaho. In: *Geol. Soc. Am. Abstr. Programs*. pp 463-464
- Melchior Larsen L, Ken Pedersen A, Krarup Pedersen G (2006) A subaqueous rootless cone field at Niuluut, Disko, Paleocene of West Greenland. *Lithos* 92(1-2):20-32
- Moore JG, Ault WU (1965) Historic littoral cones in Hawaii. *Pacific science* XIX(3-11)
- Morrissey M, Zimanowski B, Wohletz KH, Buettner R (2000) Phreatomagmatic fragmentation. In: Sigurdsson H (ed) *Encyclopedia of volcanoes*. Academic Press, San Diego, pp 431-445

- Ort MH, Carrasco-Núñez G (2009) Lateral vent migration during phreatomagmatic and magmatic eruptions at Tecuitlapa Maar, east-central Mexico. *J Volcanol Geoth Res* 181(1), 67-77.
- Parcheta CE, Houghton BF, Swanson DA (2013) Contrasting patterns of vesiculation in low, intermediate, and high Hawaiian fountains: A case study of the 1969 Mauna Ulu eruption. *J Volcanol Geoth Res* 255(0):79-89
- Ramos FC, Wolff JA, Starkel W, Eckberg A, Tollstrup DL, Scott S (2013) The changing nature of sources associated with Columbia River flood basalts: Evidence from strontium isotope ratio variations in plagioclase phenocrysts. *Geological Society of America Special Papers* 497:231-257
- Reidel SP, Tolan TL (1992) Eruption and emplacement of flood basalt: An example from the large-volume Teepee Butte Member, Columbia River Basalt Group. *Geol Soc Am Bull* 104(12):1650-1671
- Reidel SP, Camp VE, Tolan TL, Martin BS (2013) The Columbia River flood basalt province: stratigraphy, areal extent, volume, and physical volcanology. *Geological Society of America Special Papers* 497:1-43
- Rossi M, Gudmundsson A (1996) The morphology and formation of flow-lobe tumuli on Icelandic shield volcanoes. *J Volcanol Geoth Res* 72(3):291-308
- Schminke H-U (1967) Fused Tuff and Pépérites in South-Central Washington. *Geol Soc Am Bull* 78(3):319-330
- Self S, Keszthelyi L, Thordarson T (1998) The importance of pahoehoe. *Annu. Rev. Earth Planet. Sci.* 26:81-110
- Skilling IP, White JDL, McPhie J (2002) Peperite: a review of magma–sediment mingling. *J Volcanol Geoth Res* 114(1–2):1-17
- Smith GA (1988) Neogene synvolcanic and syntectonic sedimentation in central Washington. *Geol Soc Am Bull* 100(9):1479-1492
- Sohn YK (1996) Hydrovolcanic processes forming basaltic tuff rings and cones on Cheju Island, Korea. *Geol Soc Am Bull* 108(10):1199-1211
- Squire RJ, McPhie J (2002) Characteristics and origin of peperite involving coarse-grained host sediment. *J Volcanol Geoth Res* 114(1–2):45-61
- Swanson D, Wright TL, Hooper PR, Bentley RD (1979) Revisions in stratigraphic nomenclature of the Columbia River Basalt Group. *U.S Geological Survey Bulletin* 1457G:G1 - G59
- Swanson DA, Wright TL, Helz RT (1975) Linear vent systems and estimated rates of magma production and eruption for the Yakima Basalt on the Columbia Plateau. *American Journal of Science* 275(8):877-905
- Thorarinsson S (1951) Laxargljufur and Laxarhraun: a tephrochronological study. *Geograf Annal* 2:1–89
- Thorarinsson S (1953) The crater groups in Iceland. *B Volcanol* 14(1):3-44
- Thordarson T, Self S (1998) The Roza Member, Columbia River Basalt Group: A gigantic pahoehoe lava flow field formed by endogenous processes? *J. Geophys. Res.* 103(B11):27411-27445
- Thordarson T, Miller D, Larsen G (1998) New data on the Leidolfssfell cone group in South Iceland. *Jökull* 46:3-15
- Thordarson T, Höskuldsson Á (2008) Postglacial volcanism in Iceland. *Jökull* 58:197-228
- Tolan TL, Beeson MH, Lindsey KA (2002) The Effects of Volcanism and Tectonism on the Evolution of the Columbia River System. In: *A Field Guide to Selected Localities in the South-western Columbia River Plateau and Columbia River Gorge of Washington and Oregon State*. Northwest Geological Society,
- Valentine GA, Gregg TKP (2008) Continental basaltic volcanoes — Processes and problems. *J Volcanol Geoth Res* 177(4):857-873
- Walker G, Croasdale R (1971) Characteristics of some basaltic pyroclastics. *B Volcanol* 35(2):303-317
- Walker GPL (1991) Structure, and origin by injection of lava under surface crust, of tumuli, “lava rises”, “lava-rise pits”, and “lava-inflation clefts” in Hawaii. *B Volcanol* 53(7):546-558
- White JDL (1996) Impure coolants and interaction dynamics of phreatomagmatic eruptions. *J Volcanol Geoth Res* 74(3–4):155-170

- Wolff J, Ramos F, Hart G, Patterson J, Brandon A (2008) Columbia River flood basalts from a centralized crustal magmatic system. *Nature geoscience* 1(3):177-180
- Zimanowski B, Büttner R, Lorenz V (1997) Premixing of magma and water in MFCI experiments. *B Volcanol* 58(6):491-495

Chapter 5: The Construction of Submarine Volcanoes: Insights from 3D Seismic Data

5.1 Introduction

The use of three-dimensional (3D) seismic data within hydrocarbon basins has provided a unique opportunity to investigate the architecture of buried volcanoes (e.g. Gatliff et al. 1984; Ritchie and Hitchen 1996; Bell and Butcher 2002; Lee et al. 2006; Wall et al. 2010; Jackson 2012; Magee et al. 2013; Zhao et al. 2014). These edifices form in sub aerial and submarine environments (Chapter 2). Seismic data allows us to remotely interrogate these edifices externally and internally, without the requirement of erosional dissection. We are therefore able to examine the development of volcanoes (e.g. Magee et al. 2013), their magmatic plumbing system (e.g. Bell and Butcher 2002; Thomson 2007; Wall et al. 2010; Zhao et al. 2014) and their links to structural features within a basin (e.g. Zhao et al. 2014). These data also grant access to regions of the Earth inaccessible in the field (Thors and Jakousson 1982; Magee et al. 2013; Zhao et al. 2014). Previous studies using seismic data have identified shield volcanoes (Magee et al. 2013), diatremes (Wall et al. 2010) and seamounts (Bell and Butcher 2002; see Chapter 2). A range of volcanic edifices underlain by dykes are also recognised (e.g. Jackson 2012; Zhao et al. 2014), the genesis of which is unclear.

However, the location and structure of volcanoes can be concealed due to poor seismic imaging within and beneath layers of basaltic lava (e.g. Jerram 2002). Poor imaging is the result of the scattering and attenuation of seismic waves (see Chapter 2) and velocity contrasts between the edifice (composed of volcanoclastic rock and lavas) and the surrounding lava flows. As a result, few of the monogenetic edifices recognised in field data are also documented in seismic data. This is particularly true of edifices formed during submarine eruptions. Bathymetric data can be used to study the morphology of these features, but their internal architecture is not commonly exposed. Examples of dissected polygenetic submarine volcanoes exist (e.g. Schmidt and Schminke 2000), but these do not highlight the complexity of monogenetic eruptions commonly observed in subaerial examples (e.g. Valentine and Gregg 2008). Furthermore, observations of contemporary submarine eruptions are often limited to the emergent stages of activity (e.g. Thorarinsson 1966; Fiske et al. 1998; Baker et al. 2002; Németh et al. 2006), inhibiting our understanding of the early depositional mechanisms.

5.1.1 Aims

The aim of this study is to detail the seismic characteristics, morphology and plumbing system of submarine monogenetic volcanoes, offshore Australia. These edifices are free from overlying basalt lava cover and are also relatively young, making them ideal candidates to study. Through comparison with field analogues, I demonstrate that the volcanoes were constructed via a combination of explosive and effusive activity; evolving through initial maar-forming to later tuff cone-building stages. Transitions in eruptive style are thought to have been controlled by the site of magma fragmentation, intrinsic magma properties and decreasing hydrostatic pressure as the edifices grew towards the sea surface. This study can be used to understand the processes by which submarine edifices are constructed. Furthermore, it can help recognise volcanoes in other regions affected by basaltic volcanism, and differentiate them from similar hydrothermal vents. These hydrothermal vents are the result of phreatic eruptions (e.g. Jamtveit et al. 2004) and are dominantly composed of sediment (see Chapter 2). This study also has useful implications for understanding the feeder system underlying the edifices, and associated impacts on underlying hydrocarbon systems.

5.2 Geological setting

The southeastern Australian margin is associated with the Southern Rift System separating Australia from Antarctica. Opening of the rift was associated with onshore and offshore volcanism (Johnson 1989; Price et al. 2003; Sutherland 2003), much of which was monogenetic (Johnson 1989; Otterloo et al. 2013). The Bass Basin (Fig. 5.1) represents a failed intra-cratonic rift basin that formed along the margin (Blevin 2003). The basin consists of a series of Cretaceous northwest-southeast trending half-grabens (Cas et al. 1993) and contains a transgressive sequence of Cretaceous, Paleocene and Eocene siltstones, shales and sandstones, overlain by the Oligocene–Quaternary aged Torquay Group limestone. Numerous petroleum exploration wells have been drilled, targeting the late Cretaceous to early Miocene Eastern View Coal Measures (EVCN).

In addition to rift-related sediments, the basin also contains Cretaceous–Miocene aged lava flows, edifices and sills. Onshore Eocene–Miocene lava flows are tholeiitic to alkali basalts (e.g. Sutherland and Wellman 1986; Vogel and Keays 1997). The earliest evidence

of volcanism is Cretaceous volcanoclastic sandstones, although the source of these is unclear. Subsequent Mid-Cretaceous volcanism produced a series of edifices, flows and sills (Trigg et al. 2003; Cummings and Blevin 2003; Holford et al. 2007). Volcanism associated with syn- and post-rift activity peaked in the Paleocene and Oligocene-Miocene, (Cummings and Blevin 2003). This activity was widespread through the central and north-east Bass basin (Cummings and Blevin 2003) and emplaced lavas, sills, dykes and volcanoes (Faustmann 1995). These features are commonly associated with rift faults and structural accommodation zones (Trigg et al. 2003; Cummings and Blevin 2003).

The subject of this study is a series of Late Cretaceous lava flows and Miocene-aged sills and edifices, located within the EVCM and Torquay limestone sequence respectively. The edifices are overlapped by neritic claystones and are inferred to have been emplaced in water depths of 90–140 m, as indicated by biostratigraphic data (Geoscience Australia 2010; Holford and Schofield in review). Previous workers have suggested the edifices represent pyroclastic edifices, analogous to onshore volcanoes in the Otway Basin (Faustmann 1995; Holford et al. 2012). However, these studies have not provided a detailed assessment of the edifices' architecture, nor have they investigated the mechanisms by which they were constructed.

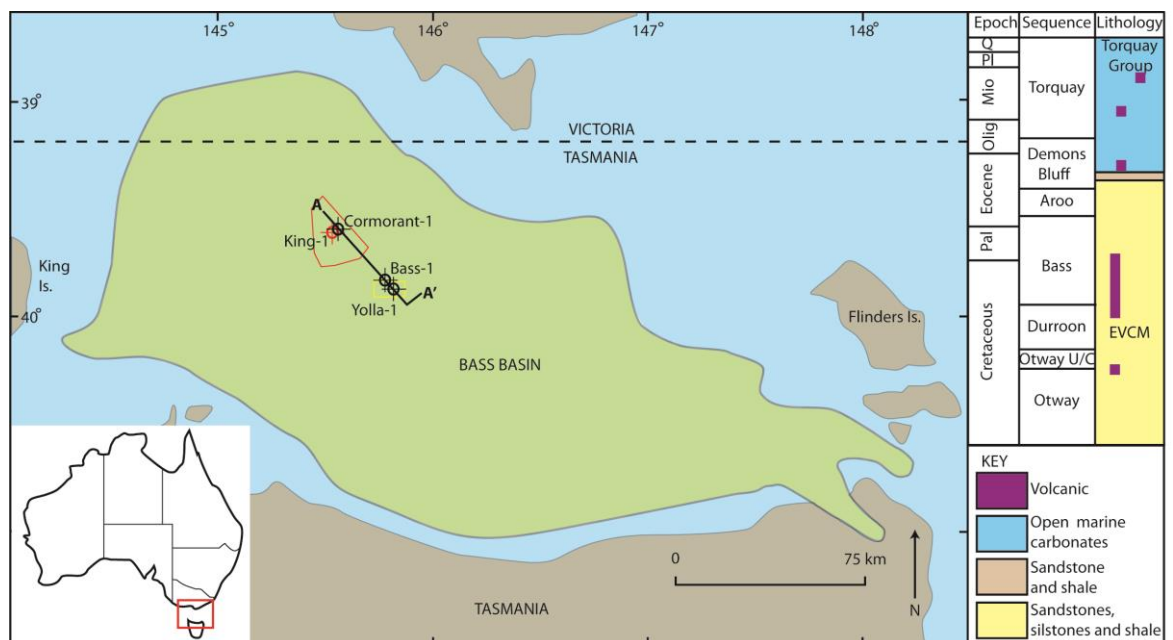


Figure 5.1. Location of the study area. The Bass Basin is shown in green, the red outline delimits the Labatt survey and the yellow delimits Yolla survey. Bass-1, King-1, Yolla-1 and Cormorant-1 wells are also shown. A 2D seismic line (A–A'; Fig. 5.2)

between the surveys is shown. A simplified stratigraphy of the Bass Basin is also shown. Modified from Boral Energy Resources Ltd. (1998).

5.3 Dataset and methodology

5.3.1 Seismic and well data

This study utilises 3D seismic data from the Yolla and Labatt surveys which were acquired in 1994 and 2008 respectively. The 525 km² Labatt survey has a bin size of 25 × 12.5 m (Tap Oil Ltd. 2008). The Yolla survey is smaller, covering 260 km² with a 12.5 × 25 m bin size (Boral Energy Resources Ltd. 1998). A 2D seismic line between these surveys shows the Bass-1, Yolla-1 and Cormorant-1 wells (section A–A', Figs. 5.1 and 5.2). The Bass-1 well was drilled to test the hydrocarbon potential of a Miocene “reef complex” at a depth of 790 m (Esso Exploration Australia Inc. 1965). This reef complex was proven to be a volcano, as the well intersected a 185 m thick sequence of volcanic rocks (Figs. 5.2 and 5.3). Core data recovered buff and light grey brown, finely grained and vesicular rocks with abundant zeolites (Esso Exploration Australia Inc. 1965). 80 m of gabbro was found deeper in the well at 2584 m, and 320 m of basalt was found at 3031 m (Figs. 5.2 and 5.3). These intervals were interpreted as intrusions and lava flows (Wheeler and Kjellgren 1986). The Yolla-1 well intersected volcanic rock at a depth of 1237 m (Figs. 5.2 and 5.3). This 68 m-thick sequence was interpreted to represent highly altered pyroclastics (Wheeler and Kjellgren 1986). Intrusions were also found in the Cormorant-1 well, which intersected 130 m of weathered volcanic rocks at a depth of 2470 m (Esso Exploration Australia Inc. 1970). All volcanic intervals produced decreases in Gamma Ray and increases in Sonic wireline data (Fig. 5.3). King-1 did not intersect any volcanic rock.

Petrophysical data from the Yolla-1 and Cormorant-1 wells has been used to constrain seismic events. The Miocene Top Volcanic (TV) and Base Volcanic (BV) were identified at 0.70 and 0.82 s Two-Way-Travel-Time (TWTT) in the Labatt data, and 1.01 and 1.15 s in the Yolla data respectively. The Oligocene (OH) and Eocene-aged Demons Bluff (DB) horizons were defined from the Yolla-1 well (Boral Energy Resources Ltd. 1998). The Lower Mid Miocene (LMM), Base Volcanic (BV) and Cretaceous Eastern View Coal

Measures (EVCN), Top Aroo (TR) and Base Aroo (BA) horizons were defined from the Cormorant-1 well (Tap Oil Ltd. 2010). High amplitude reflections in the Labatt survey were identified at depths of 1.5 s; these reflections represent lava flows and define the Cretaceous-aged Lower Volcanic (LV) horizon. The TV and BV horizons were picked in the Labatt (Figs. 5.4 and 5.5) and Yolla surveys (Figs. 5.6 and 5.7) to allow further investigation of the edifices.

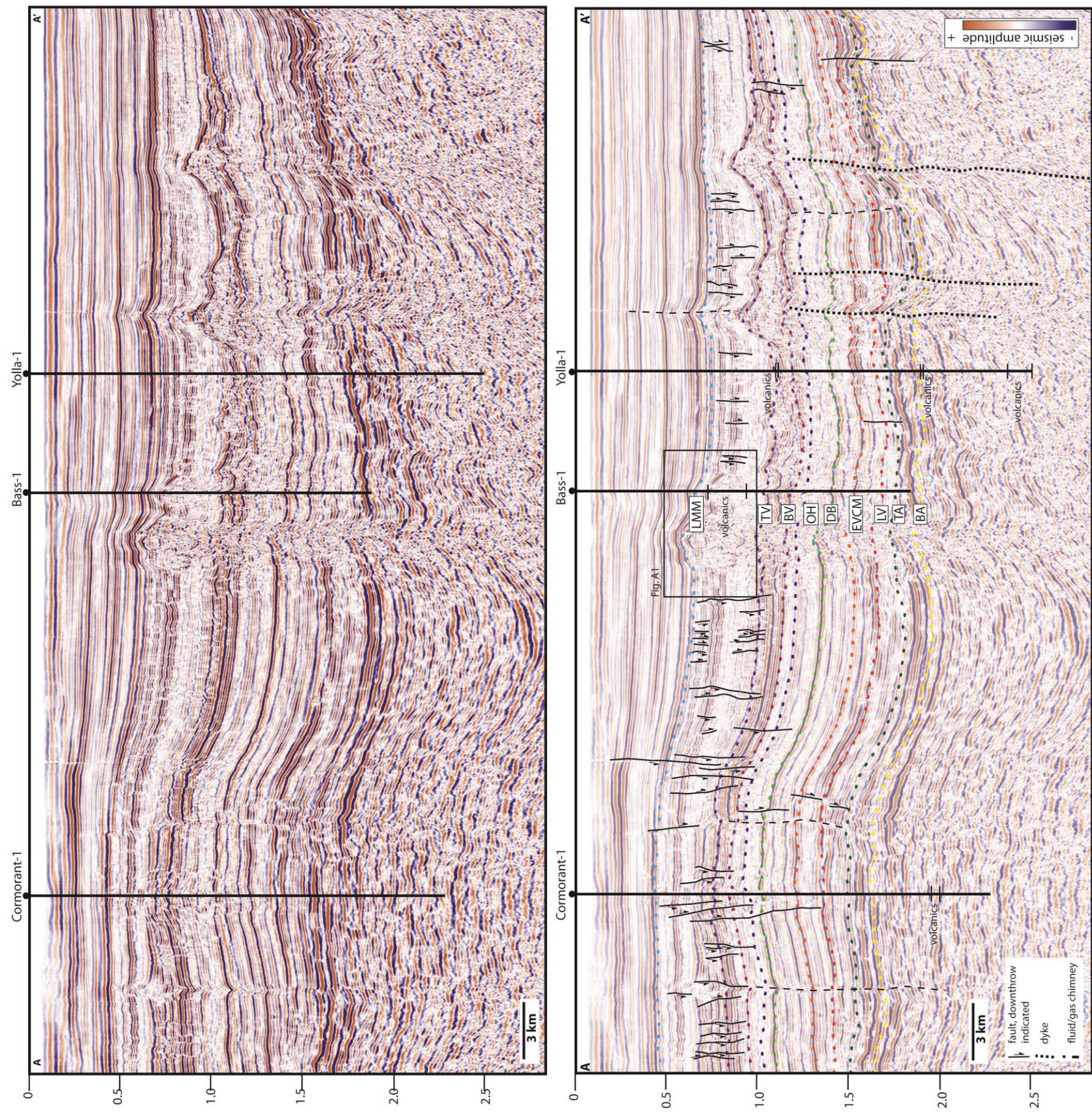


Figure 5.2. Seismic line A–A' and interpretation intersecting the Cormorant-1, Bass-1 and Yolla-1 wells. Correlated horizons are also shown.

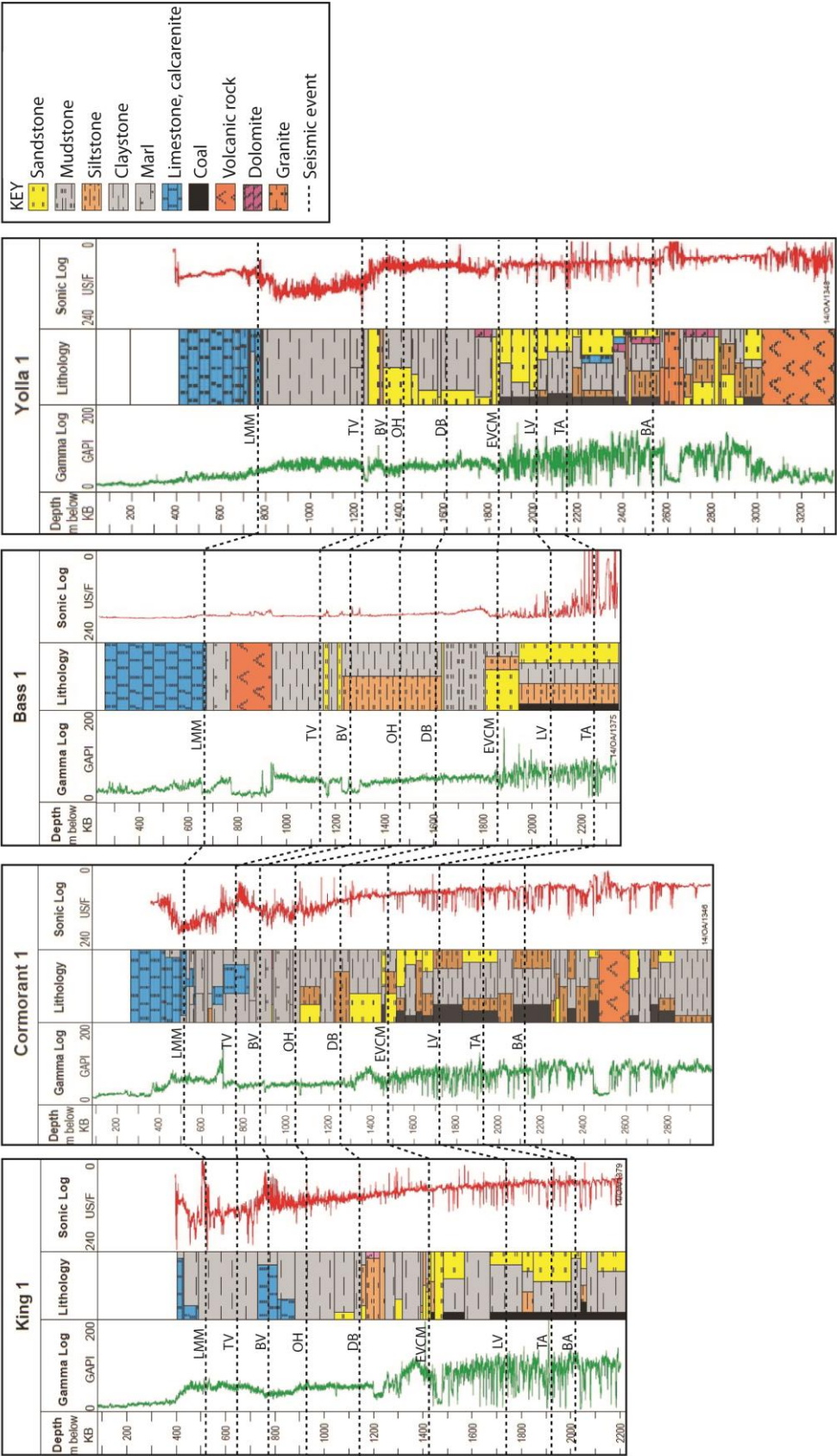


Figure 5.3. Well logs for King-1, Cormorant-1, Bass-1 and Yolla-1. Seismic horizons are also shown: LMM=Lower Mid Miocene, TV=Top Volcanic, BV=Base Volcanic, OH=Oligocene, Demons Bluff=DB, EVC=Eastern View Coal Measures, LV=Lower Volcanic, TA=Top Aroo and BA=Base Aroo. Adapted from Trigg et al. (2003).

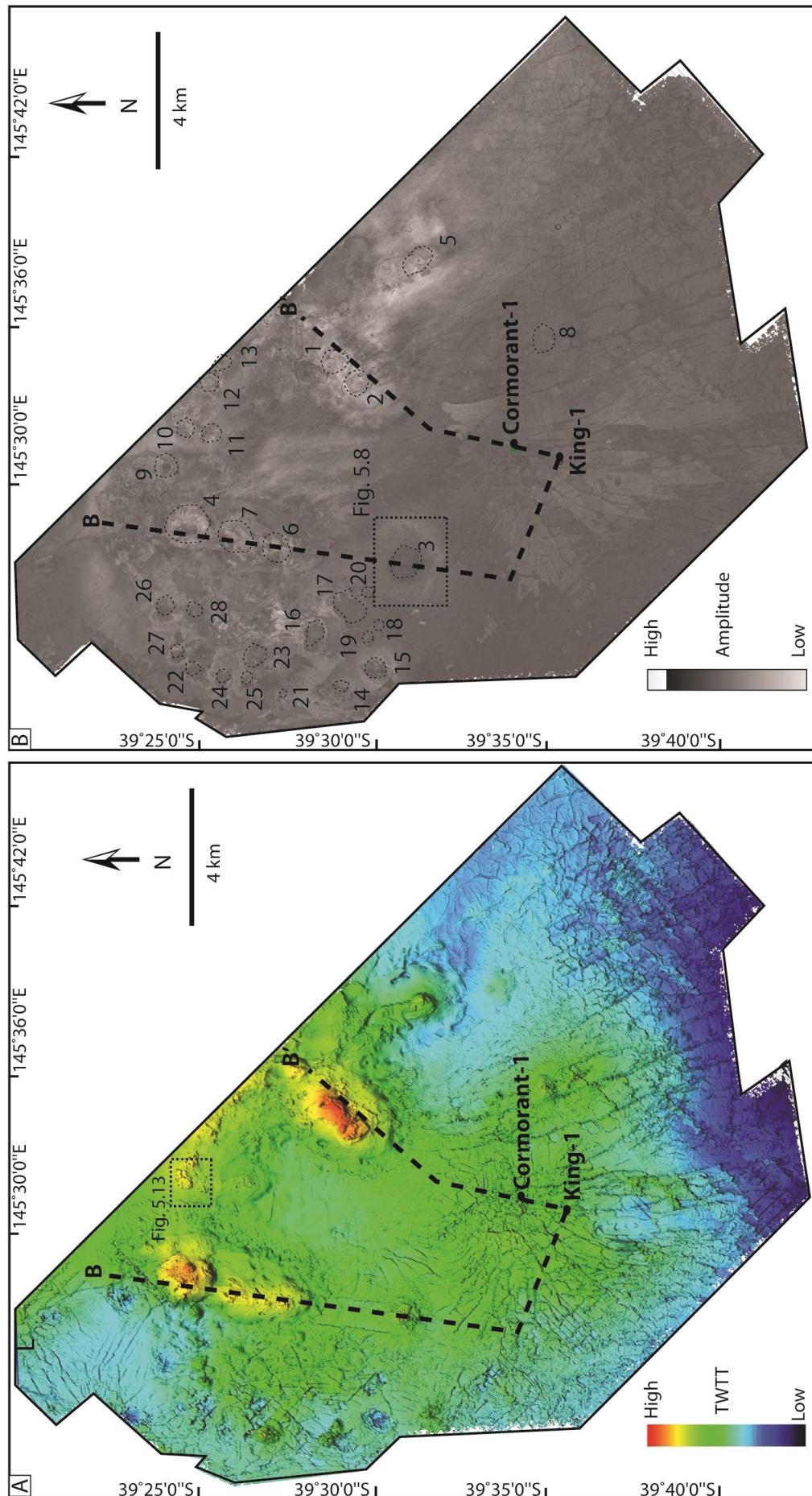


Figure 5.4. Time (A) and amplitude (B) maps of the TV horizon in the Labatt survey. The edifices (dashed outline) are numbered in B. See Fig. 5.5 for cross section.

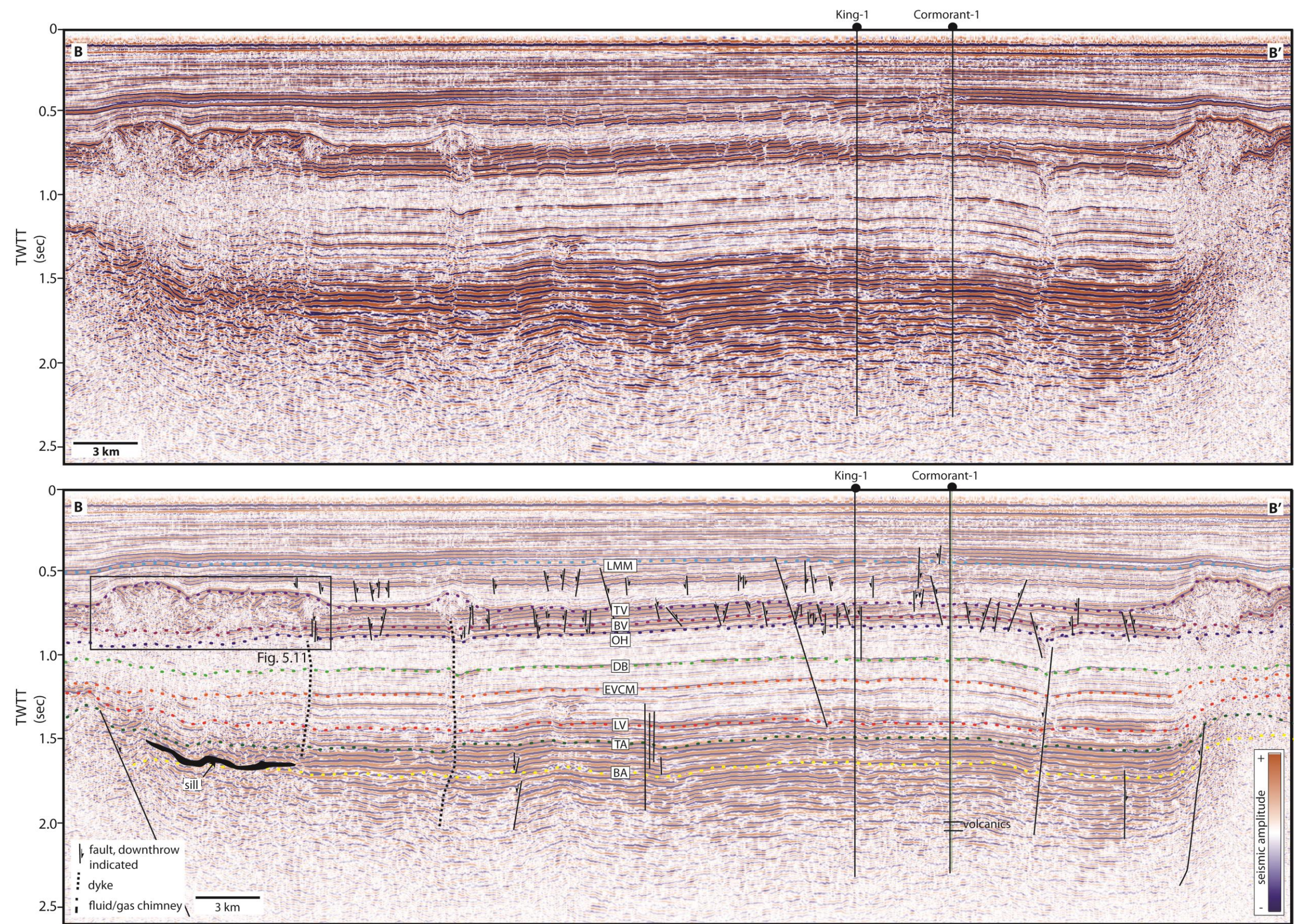


Figure 5.5. Seismic line B–B’ and interpretation in the Labatt survey. See Fig. 5.4 for location.

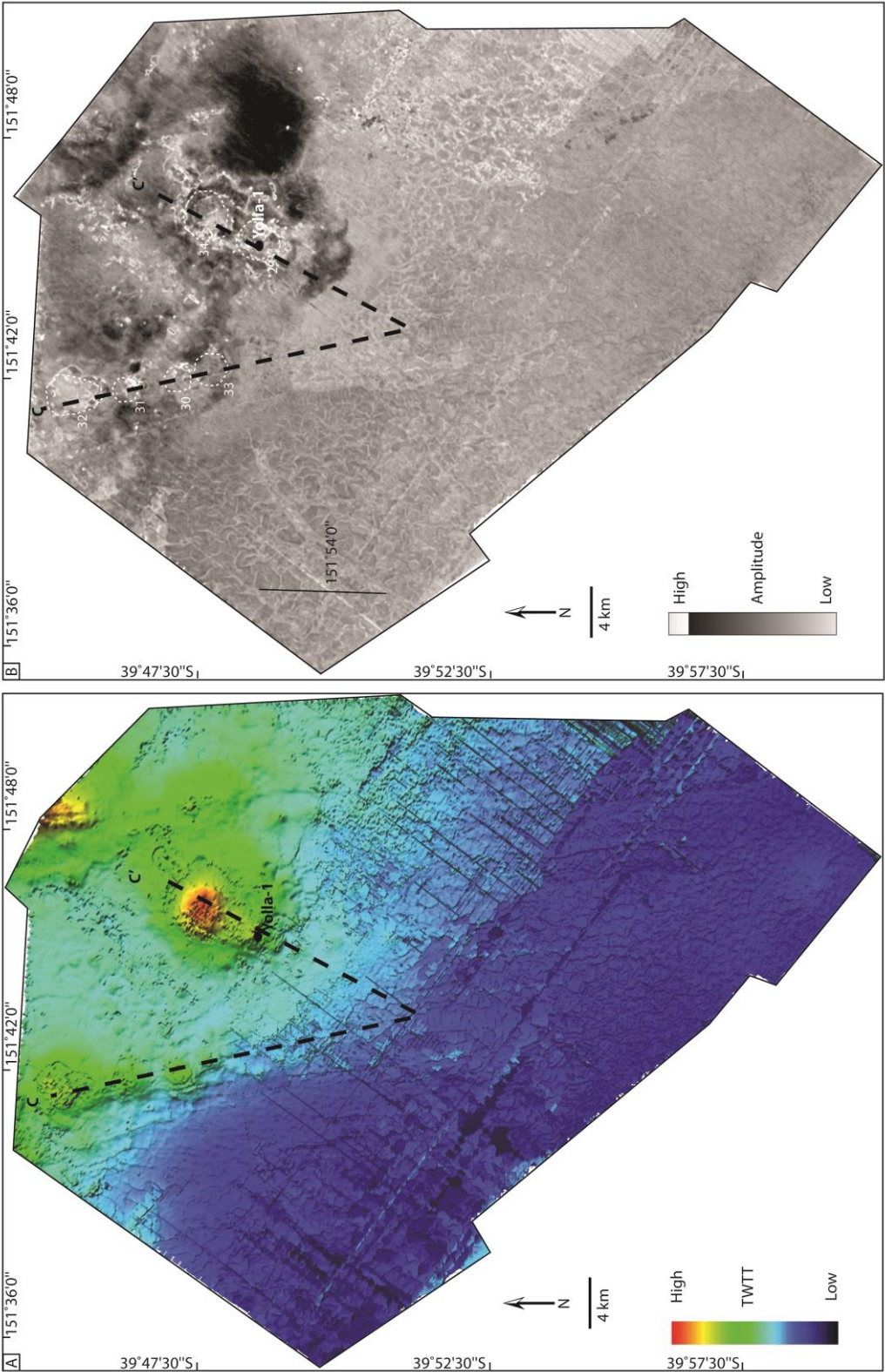


Figure 5.6. Time (A) and amplitude (B) maps of the TV horizon in the Yolla survey. The edifices (dashed outline) are numbered in B. See Fig. 5.7 for cross section.

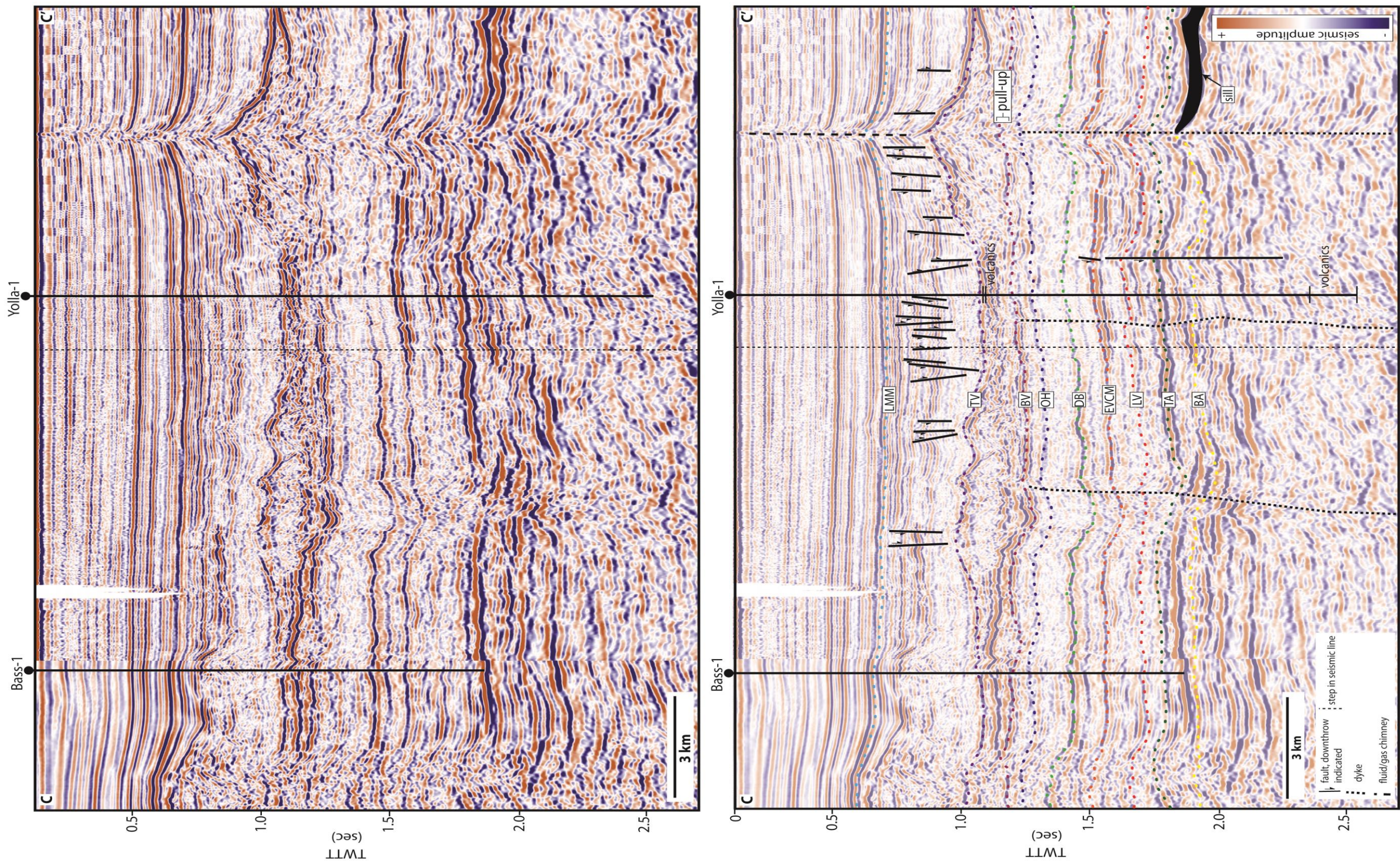


Figure 5.7. Seismic line C-C' and interpretation in the Yolla survey. See Fig. 5.6 for location.

5.3.2 Composition of the edifices

Time extractions of the TV surface define 34 edifices that are either cone-shaped topographic highs (positive TWTT anomalies) or pit craters (negative TWTT anomalies; Figs. 5.4 and 5.6). The Yolla-1 and Bass-1 wells indicate that the cone-shaped edifices are composed of volcanic rock. The edifices also have seismic characteristics typical of volcanic lithologies; they have high amplitude top reflections and reduce the quality of imaging beneath them (Figs. 5.4 and 5.6; see Planke et al. 2000; Jerram 2002; Bell and Butcher 2002; Wright et al. 2012; Schofield and Jolley 2013). Pull-ups beneath the edifices are typical of volcanic rocks within a sedimentary sequence (Jackson 2012; Magee et al. 2013). Many of the cone-shaped edifices and pit craters are underlain by sills, further suggesting a volcanic origin. Edifices beneath which the sills are not visible are inferred to be underlain by sills below the resolution of the data. These edifices were emplaced in a shallow marine environment, as indicated by the transgressive sequence within which the edifices are found, and by biostratigraphic data (see section 5.2).

5.3.3 Calculating edifice dimensions

Cone-shaped edifices are sub-circular to elongate in shape and often overlap in linear clusters. The pit craters are sub-circular in plan view. The diameters of the cone-shaped edifices were determined from amplitude maps and cross sections by the change in the seismic expression of the cone (Fig. 5.8), interpreted to represent a lateral transition from the cone to surrounding basin deposits. Variations in amplitude were used to measure the diameter of the pit craters.

The internal velocity of the edifices was calculated either from the thickness of pull ups beneath the edifice (see Magee et al. 2013) or from the Yolla-1 well data in cases where pull ups were absent. (Boral Energy Resources Ltd. 1998). Using this method, I calculate that the internal velocity of the edifices ranges between 2090–4025 m s⁻¹. This range is lower than that of lava flows (commonly 3300–6800 m s⁻¹; see Planke and Eldholm 1994; Berndt et al. 2000; Calvès et al. 2011; Magee et al. 2013), suggesting that the volcanic material is dominantly fragmental (e.g. pyroclasts and hyaloclastite), consistent with core descriptions. The velocities were used to calculate the heights of the edifices.

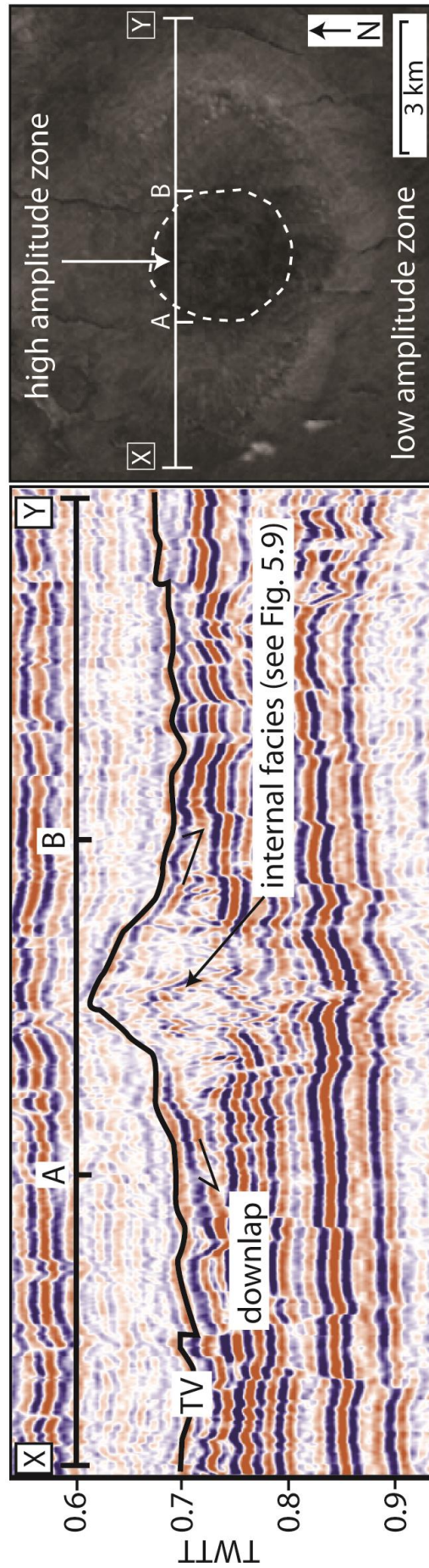


Figure 5.8. Seismic line X–Y showing that the basal diameter of the edifices (A–B) is calculated from the change in seismic facies and amplitude of the edifice. See Fig. 5.4 for location.

5.3.4 Seismic facies analysis

Four seismic facies have been recognised within the edifices based on the geometry, amplitude and continuity of the internal reflections (Table 5.1). Seismic facies indicate variation in the structure and composition of the volcanic succession (e.g. Planke et al. 2000; Calvès et al. 2011; Wright et al. 2012; Watton et al. 2013b). The reflections within the edifices lap out and are not truncated.

The hummocky facies (***Hu***) forms wedge-shaped bodies and only occurs within the flanks of cone-shaped edifices. The reflections are moderate to low amplitude and vary from semi-continuous to continuous. They grade outwards from the chaotic conduit zone of the edifices and prograde laterally, downlapping underlying facies. They are overlain by ***PHA*** facies (see below). ***Hu***-type facies are reported in other seismic datasets from volcanic margins, and represent fragmental igneous material (e.g. Planke et al. 2000; Thomson 2005; Jerram et al. 2009; Wright et al. 2012). I infer a similar origin for the ***Hu*** facies in this study, and suggest that the facies represents low velocity, fragmental igneous rocks such as hyaloclastite and/or pyroclasts; commonly produced during shallow submarine eruptions (e.g. Kokelaar 1986; Cas et al. 1989; Sohn 1995; White 2001; Suiting and Schmincke 2009; Watton et al. 2013b).

Planar, moderate amplitude facies (***PMA***) are composed of moderate amplitude, continuous and parallel reflections in a sub-horizontal or inclined orientation. They are found within all parts of the stratigraphy and commonly onlap the cone-shaped edifices. The facies has distinct contacts with overlying and underlying facies, but can inter-finger with ***Hu***. This facies is interpreted to represent non-volcanic lithologies, since they are found throughout the stratigraphy. However, within the edifices they may also represent volcanoclastic material with a lower velocity than coherent rocks, resulting in moderate amplitude reflections (e.g. Planke et al. 2000). The sub-parallel reflections represent sub-parallel interfaces between lithologies (e.g. Bacon et al. 2007) indicating that the component sediments are bedded.

The planar high amplitude facies (***PHA***) is composed of high amplitude, continuous reflections in a sub-horizontal or inclined orientation. They form the TV and BV horizon, as well as sills and the Late Cretaceous lava flows. The tops of cone-shaped edifices composed of this facies may appear segmented. This facies is typically thin and forms distinct contacts between over and underlying facies, although it can grade laterally into the ***PMA*** and ***Ch*** facies. They are overlain by ***PMA*** facies. Edifices with high amplitude, continuous reflections of ***PHA*** facies are interpreted as high velocity, dominantly coherent subaerial and/or submarine lava flows and hyaloclastite (e.g. Planke et al. 2000; Jerram et al. 2009;

Wright 2013). The sheet-like nature of the reflections suggests the flows form sub-planar units that maintain a near-constant thickness (e.g. Planke et al. 2000). Their sheet-like morphology may result from higher effusion rates relative to the hummocky facies (e.g. Gregg and Fink 1995; Self et al. 2000; Batiza and White 2000). **PHA** facies has a higher amplitude than **Hu** because **PHA** facies is overlain by **PMA**, whilst **Hu** is overlain by **PHA**. Therefore, the velocity contrast is greater for **PHA**. The presence of **PHA** or **PMA** facies on the tops of the edifices is interpreted to result from the variable grain size and vesicularity of hyaloclastite (e.g. Watton et al. 2013a; Watton et al. 2013b), both of which affect the velocity and hence seismic amplitude of the facies.

Chaotic facies (**Ch**) are low amplitude; discontinuous reflections found beneath and within cone-shaped edifices. The facies forms plug-like bodies and grades laterally into **Hu**. **Ch** facies represents the central region of the edifices that is poorly imaged. Poor imaging may result from the high impedance contrast of the uppermost **PHA** facies (e.g. Jerram 2002; Maresh et al. 2006). This central region may also contain numerous dykes intruded into the edifice (e.g. Moore 1985), creating high velocity contrasts between fragmental and coherent igneous material.

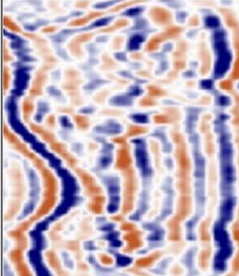
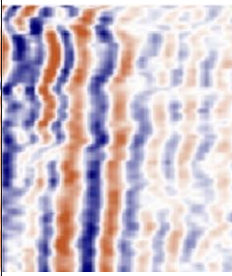
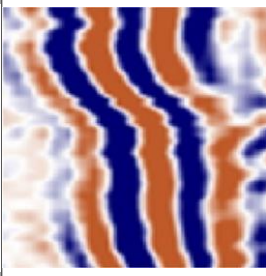
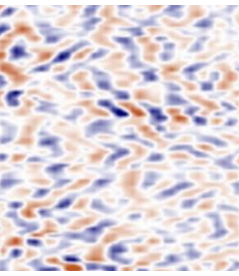
| Seismic facies | Seismic reflections | Characteristics | Interpretation |
|----------------------------------|---|--|---|
| Hummocky (Hu) |  | Moderate – low amplitude, semi-continuous – continuous reflectors. Form prograding, wedge-like bodies. Oriented sub-horizontally and may dip up to $\sim 18^\circ$. Found in the flanks of cratered and flat topped vents, also within isolated vents between the TV and BV horizons. Gradational into chaotic facies. | Low velocity, fragmental volcanic rock such as hyaloclastite and pyroclasts. |
| Planar, Moderate Amplitude (PMA) |  | Moderate – low amplitude, semi-continuous – continuous reflectors. Form sheet – like, sub-parallel units beneath the TV and BV, and occasionally forms the TV itself. Oriented sub-horizontally and may dip up to $\sim 11^\circ$. Found within isolated vents and pit craters. | Siliciclastic sediments and volcanoclastic sediments with a limited component of volcanic rock. |
| Planar, High Amplitude (PHA) |  | High amplitude, continuous reflectors with sheet-like geometries. May be segmented in the TV, and lap out and diverge. Found in cratered and flat topped vents; may form bowl-shaped reflectors that are offset at their tips and define the crater. Oriented sub-horizontally and may dip up to $\sim 18^\circ$. Commonly form the TV, BV and sills. | Dominantly coherent, sheet-like subaerial and/or submarine lava flows and associated hyaloclastite. |
| Chaotic (Ch) |  | Moderate – low amplitude, discontinuous reflectors that form plug-like bodies in vent conduits. Found beneath the TV and BV horizons within all vent types. Gradational into hummocky facies. | Poorly imaged conduit region of the edifices composed of coherent and fragmental volcanic rock. |

Table 5.1. Summary characteristics and interpretation of seismic facies.

5.4 Edifice characteristics

5.4.1 Pit craters

Pit craters (n=15) are negative TWTT anomalies in the TV surface (Fig. 5.4). In cross section the pit craters are funnel-shaped, with conduits that truncate underlying **PHA** reflections. The conduits contain **PMA** reflections that onlap the conduit margin. Concentric, arcuate normal faults surround the conduit (Fig. 5.9A). The pit craters may be overlain by pointed edifices (Fig. 5.9B). The sub-circular craters of these vents range from 341–1166 m in diameter and the conduits extend 0.05–0.11 km into the subsurface (Table A3.1). Pit craters have a clustered distribution (Fig. 5.4) and are only found in the Labatt survey.

5.4.2 Cone-shaped edifices

The cone-shaped edifices can be categorised into 3 distinct types according to their profile and internal seismic characteristics: 1) cratered (n=5); 2) flat topped (n=7) and 3) pointed edifices (n=7; Fig. 5.9; Table 5.2). The flanks of these edifices dip outwards 5–18° (Table A3.1). All of the cone shaped edifices have flat lying, concordant basal surfaces. Cone-shaped edifices are also observed on the 2D seismic section between the Yolla and Labatt surveys (see Appendix C).

5.4.2.1 Pointed edifices

Pointed edifices (Fig. 5.9B) have a conical morphology and are identified by an upper unit of **PMA** or **PHA** facies that overlies internal **Ch** facies. These reflections grade laterally into **Hu** facies. The edifices are roughly symmetrical in plan view. Time slices beneath edifice 3 (Fig. 5.10) at 0.82 s TWT and 0.9 s TWT show concentric faulting and an upward flaring central conduit; identical to pits crater in cross-section (Fig. 5.9A). The pointed edifices also have a distinctive onion ring structure (Fig. 5.10). These edifices have a height/basal diameter ratio of 0.04–0.15 (heights 0.13–0.16 km, diameters 1.67–3.03 km; see Table A3.1). They have volumes of 0.4–1.1 km³. They are found in both surveys.

5.4.2.2 Flat-topped edifices

Flat-topped edifices (Fig. 5.9C) have a sub-horizontal, upper **PHA** facies gives the vents their characteristic flat top. Internally, **Hu** and **PMA** reflections emanate from a source within the BV and grade outwards from an internal plug-like **Ch** zone. Time slices of the edifices reveal an onion ring structure beneath the TV horizon. **PMA** reflections within the edifice onlap onto a central unconformity surface beneath the TV. These reflections become

fainter and more chaotic with depth. Imaging beneath the BV horizon is poor. These edifices have a height/basal diameter ratio of 0.06–0.16 (heights 0.12–0.52 km, diameters of 1.08–3.98 km; see Table 5.2). They range in volume from 1–1.4 km³. They are only found in the Labatt survey.

5.4.2.3 Cratered edifices

Cratered edifices (Fig. 5.9D) are characterised by an upper bowl shaped **PHA** reflector that defines a ~30 m deep crater in the centre of the edifice. Internally, their facies are similar to the flat-topped edifices. They have an onion ring structure and are often asymmetric with steeper slopes on their eastern flank. They have height/basal diameter ratios of 0.04–0.09, with heights of 0.20–0.31 km and diameters of 3.41–4.85 km (Table 5.2). They range in volume from 0.07–1.36 km³. Their craters are 380–950 m diameter. These edifices are found in both surveys.

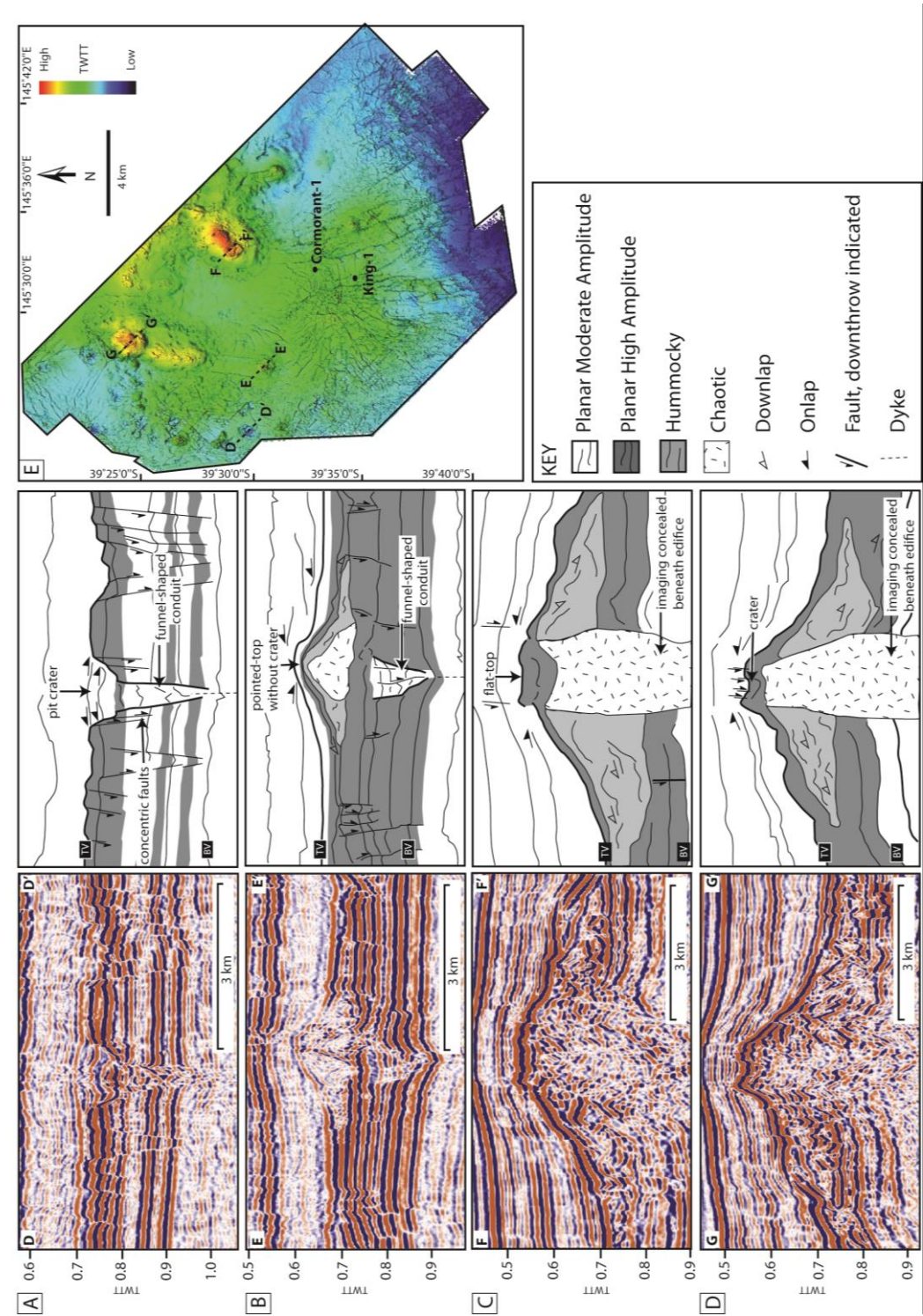


Figure 5.9. Seismic sections showing the seismic facies of the pit craters (A), pointed (B), flat-topped (C) and cratered (D) edifices. The location of the sections is shown in the time map of the Labatt survey (E).

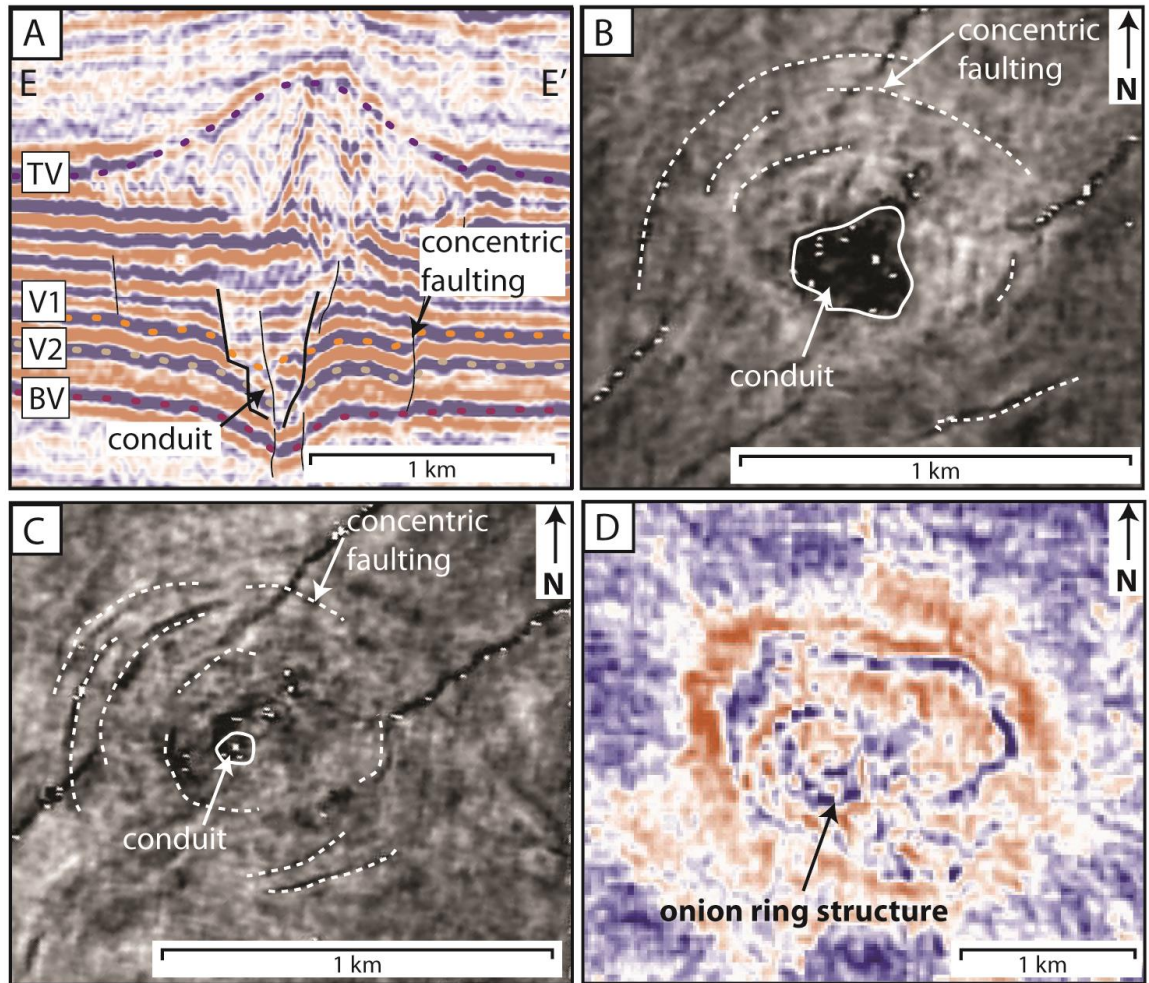


Figure 5.10. Features associated with the pointed edifices. Seismic line (A). Horizons V1 and V2 are shown in B and C respectively. See Fig. 5.9 for location. (B) Concentric faulting (dashed lines) in horizon V1 around the underlying conduit. (C) Concentric faulting (dashed lines) in horizon V2 around the underlying conduit. (D) Time slice at 0.63 s TWTT beneath the edifice showing an onion-ring structure.

5.4.3 Edifice distribution

The edifices occur in linear clusters, as isolated edifices, and in apparently randomly distributed clusters (Figs. 5.4 and 5.6). Linear and randomly distributed clusters overlap, whilst isolated edifices do not. Isolated edifices include structures 3, 5 and 8, which are pointed and flat topped in morphology (Fig. 5.4). Clustered edifices include all pit craters (14–28) and the flat topped edifices 10–13. Linear clusters include cratered, pointed and flat topped edifices that are spaced ~800–3000 m apart. The linear clusters of edifices may contain up to four individual edifices, which onlap in a northerly direction and decrease in volume towards the south (Fig. 5.11). The onlap relationship suggests the edifices young

north-south. Linear cluster 1 includes edifices 1 and 2, linear cluster 2 includes edifices 2, 7 and 6 and linear cluster 3 includes edifices 30–33.

There is a spatial relationship between the edifices, underlying sills and lava flows. Saucer-shaped and smooth layer-parallel sills (e.g. Planke et al. 2005) occur at depths of 495–1207 m beneath the BV. The lateral tips of these sills are linked to the centre of the overlying edifices (Fig. 5.12). In the north of the Labatt survey, lavas in the LV horizon were effused from a north-south trending linear source (Fig. 5.13). Spectral decomposition (using frequencies Red:17 Hz; Green: 24 Hz; Blue:60 Hz) clearly images these flows (Fig. 13). Edifices 4–7 in linear cluster 1 directly overly the lava flows (Fig. 5.4; Appendix C) and also have a north-south strike. No relationship is recognised between basement highs and the edifices.

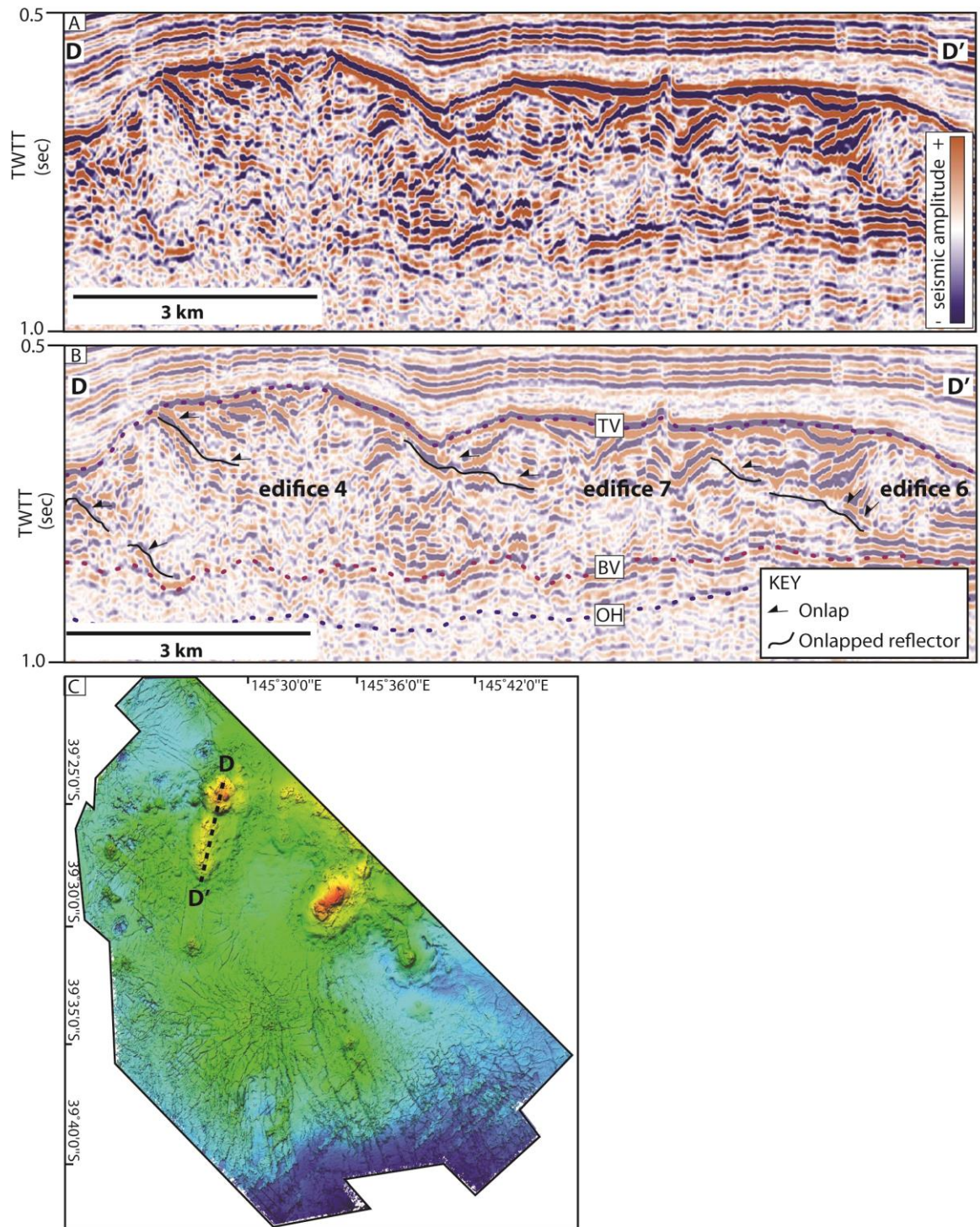


Figure 5.11. Seismic line (A) and interpretation (B) showing that the edifices in linear clusters young towards the south.

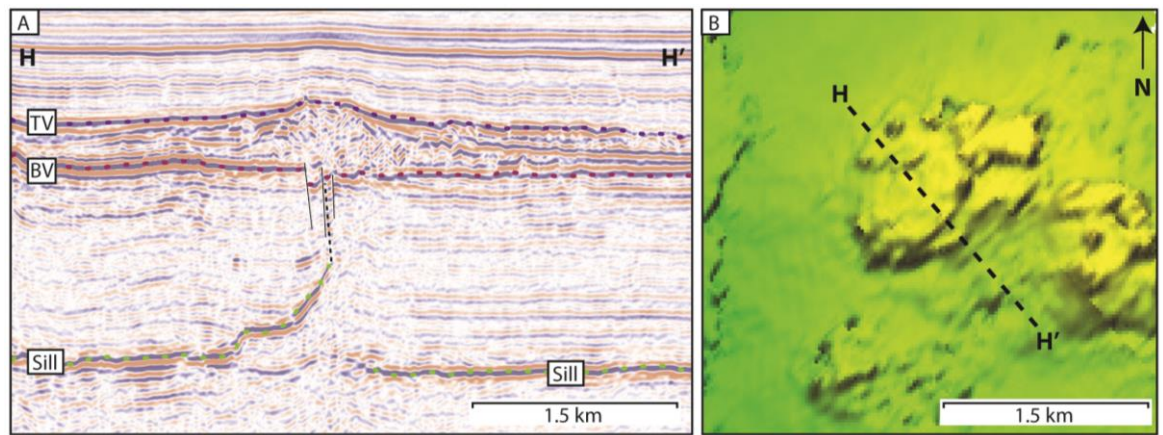


Figure 5.12. Seismic section (A) and time map (B) of a flat-topped edifice fed by a sill/dyke system. See Fig. 5.4 for location.

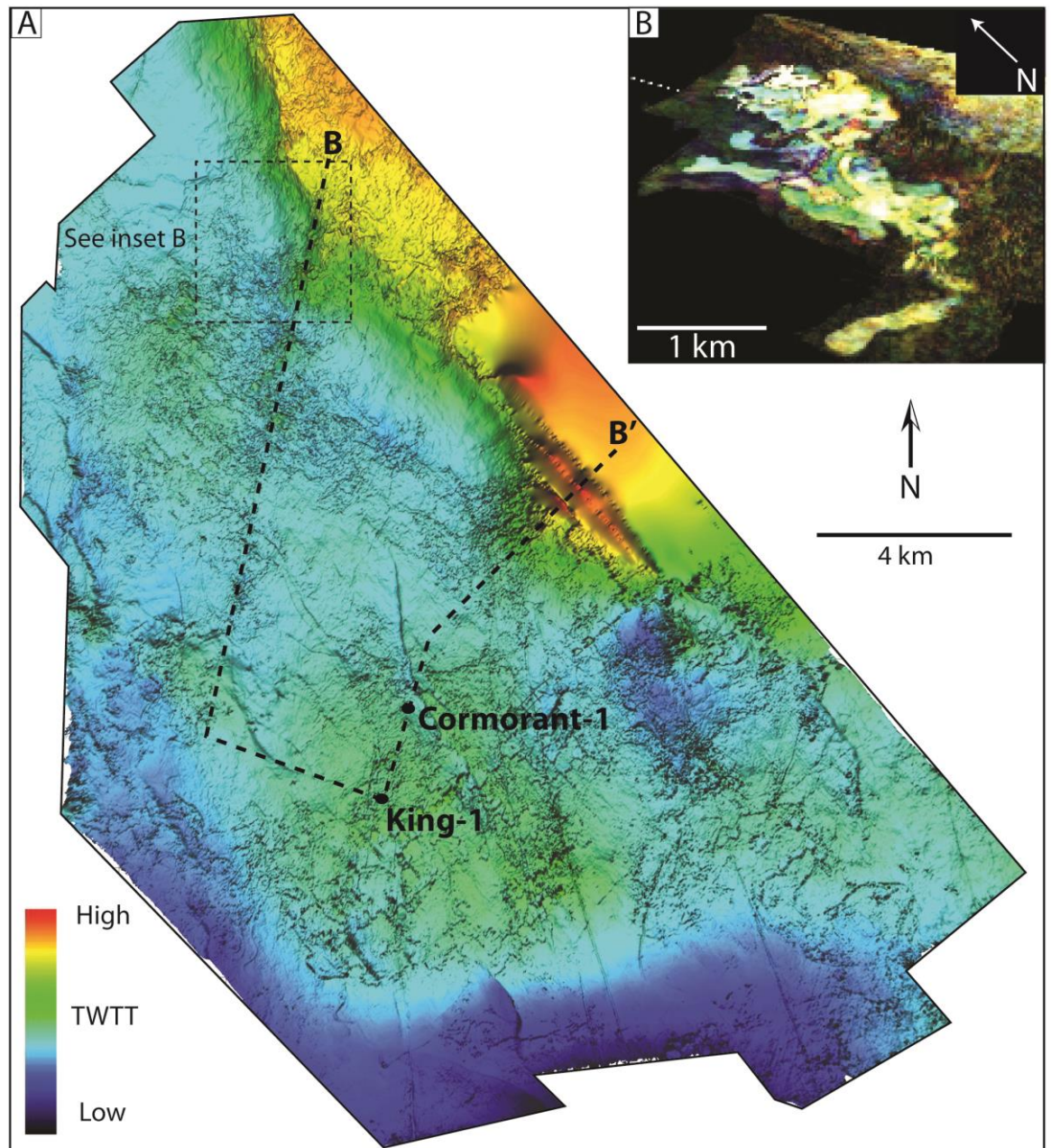


Figure 5.13. Amplitude map of the LV horizon. Inset B shows a RGB decomposition image of the lava flows.

5.5 Discussion

The edifices are interpreted as monogenetic volcanoes due to their low volumes (commonly $<1 \text{ km}^3$; Table 5.2); typical of these edifices (Walker 1993; Connor and Conway 2000; White and Ross 2011). The formation of the volcanoes is discussed below.

5.5.1 Physical volcanology of the edifices

The pit crater volcanoes are interpreted as maars; these are explosion craters in the country rock with diameters of 0.2–3 km (e.g. Urrutia-Fucugauchi and Uribe-Cifuentes 1999; Roger et al. 2000; Pirrung et al. 2003; Haller et al. 2006; Gençalioglu-Kuşcu et al. 2007; Kwon and Sohn 2008; White and Ross 2011; Ross et al. 2011; Suiting and Schmincke 2012). Maars also commonly overlap (White and McClintock 2001; Németh and White 2003; McClintock and White 2006; White and Ross 2011), as do the pit crater volcanoes in this study. The ejecta rings that surround maars are commonly <30 m in height (White and Ross 2011) and are not recognised; either they have been eroded or they are below the resolution of the data. Maar-forming eruptions result from magma-water interaction and subsurface magma fragmentation. This interaction produces Taalian-style eruptions (e.g. Kokelaar 1986; Vespermann and Schmincke 2000; White and Ross 2011).

The funnel-shaped conduits beneath the pit crater volcanoes are interpreted as diatremes (downward-tapering conduits), based on their similar morphology, dimensions and their relationship to the overlying maars (e.g. Lorenz 1975; White 1991; White and McClintock 2001; Lorenz and Kurszlauskis 2007; Kwon and Sohn 2008; Suiting and Schmincke 2010; White and Ross 2011; Suiting and Schmincke 2012). The funnel-shaped conduits observed in this study are surrounded by concentric and radial faults (Fig. 5.10), similar to diatremes described by Suiting and Schmincke (2009). Diatremes are filled by syn- and post-eruptive sediments (Lorenz 1986; White and Ross 2011). These sediments may be syn-eruptive debris flows or the products of eruption columns (e.g. Suiting and Schmincke 2009) and are bedded or massive (Francis 1970; White and Ross 2011). Bedded diatreme fill deposits indicate that the diatreme were open at the surface (White and Ross 2011). In the conduits beneath the pit crater volcanoes, these sediments are represented by the **PMA** reflections (see section 3.4). Underlying lower diatreme deposits are massive (White and Ross 2011); these are poorly imaged. The pit craters and their conduits are interpreted to have formed in a submarine environment, consistent with other studies (e.g. Lefebvre and Kurszlauskis 2008; Pittari et al. 2008; Suiting and Schmincke 2009; Kjarsgaard et al. 2009; Calvari and Tanner 2011; Suiting and Schmincke 2012; Elliott et al. 2015). Volcanoes similar to maars are known to effuse lavas later during their development (e.g. Brown et al. 2012).

The pointed edifices are interpreted as pillow volcanoes—a type of submarine volcano that forms during effusive activity. Pillow volcanoes are 100–400 m in height and lack a crater (Batiza and White 2000), as observed for the pointed edifices. Pillow volcanoes are commonly composed of hyaloclastite and pillow lavas (Skilling 1994; Smellie and Hole

1997; Batiza and White 2000), consistent with well data and the seismic facies in this study. The effusive, shallow water eruptions that typify these edifices are thought to be pre-cursors to tuff cone-building, Surtseyan activity (e.g. Moore 1985).

The flat-topped and cratered edifices are interpreted as tuff cones: the products of emergent submarine and ice-confined volcanism (e.g. Wohletz and Sheridan 1983; Moore 1985; Sohn 1996; Skilling 2009; White and Ross 2011). Tuff cones are also formed during high discharge fissure eruptions (Thordarson and Self 1993). Tuff cones are of a similar size and have craters of similar dimensions to the edifices in this study. Tuff cones are also composed of fragmental volcanic rock (e.g. tephra and hyaloclastite), consistent with well data and the seismic facies of the flat-topped and cratered edifices. Tuff cone-forming eruptions may effuse lava in the later stages (Thorarinsson 1966; Moore 1985) and the upper *PHA* facies that typifies the cratered and flat-topped edifices are interpreted as a carapace of lava flows and/or pillow lavas. The flat-tops of the edifices are interpreted as lava flows that ponded in the summit crater. The flat-topped and cratered edifices are larger than the pointed edifices, indicating that they formed from longer-lived eruptions or eruptions with higher effusion rates.

5.5.2 Temporal and spatial evolution of the Bass Basin volcanic field

The age relationships of the edifices provides insights into the transition from maar-forming to tuff cone-building activity (Fig. 5.14). The first stage of the eruption is recorded by the maar-diatreme complexes (represented by the pit crater volcanoes). Whether all maars within the field formed at the same time is uncertain; the age relationship between the clustered maars in the west of the basin and the cone-shaped edifices is unknown. However, a maar within the linear cluster is overlain by a pointed edifice (Fig. 5.9), indicating that in this instance the maar represents the edifice that formed earliest in the eruption. The superposition of the pointed edifice is interpreted to result from cone construction atop the maar during the same eruption (e.g. White 1991; Lefebvre and Kurszlaukis 2008). This records the transition from pit-crater-forming to effusive activity, as observed at other maar-like monogenetic volcanoes (e.g. Brown et al. 2012). The transition from maar-forming to pillow volcano-building activity indicates that magma ceased to fragment beneath the paleosurface. This may have resulted from decreased efficiency of magma-water interaction, caused by variations in magma flux and/or crystallinity and composition (e.g. Brown et al. 1994; Gutmann 2002; Nemeth et al. 2003; Houghton and Gonnermann 2008; Büchner and Tietz 2012; Graettinger et al. 2013; Valentine and Cortés 2013; Augustín-Flores et al. 2014).

Alternatively, water may have been prevented from gaining access to the vent (e.g. Calvari and Tanner 2011).

The pointed edifices are interpreted to represent the early stages of tuff cone growth. The subsequent onset of Surtseyan activity (building the cratered and flat-topped edifices) could have resulted from a variety of processes. These include: 1) collapse of the growing submarine edifice (e.g. Lonsdale and Batiza 1980; Fujibayashi and Sakai 2003; Wohletz 2003; Watton et al. 2013b) causing depressurisation of the feeder system (e.g. Fujibayashi and Sakai 2003; Riggs and Duffield 2008); 2) decreased hydrostatic pressure as the volcano grew towards the sea surface (e.g. Skilling 2009; Graettinger et al. 2013); 3) variations in magma flux (e.g. Brown et al. 1994; Gutmann 2002; Büchner and Tietz 2012; Valentine and Cortés 2013; Agustín-Flores et al. 2014); 4) variations in volatile content; 5) variations in magma crystallinity (Houghton and Gonnermann 2008; Graettinger et al. 2013) and; 6) variations in the composition of the magma (Nemeth et al. 2003).

In addition to the development of the Miocene edifices, I also highlight that the underlying Late Cretaceous LV lava flows in the Bass Basin are located along the same north-south trending source as the edifices 4, 7 and 6 (Fig. 5.4). These lava flows are located in an early transgressional part of the basin stratigraphy, possibly in subaerial conditions (Cummings and Blevin 2003). Given the absence of a central edifice (e.g. a shield volcano), the lavas are interpreted to have erupted from fissures (Thordarson and Self 1993; Brown et al. 2014). Subsequent Miocene eruptions occurred above this fissure, but were fed by a different dyke. This indicates that the dykes exploited the same pathways over tens of millions of years (e.g. Takada 1994; Connor and Conway 2000; Németh 2010). Dyke locations may reflect shallow crustal processes or deeper melt processes (Takada 1994; Connor and Conway 2000; Brown and Valentine 2013; Le Corvec et al. 2013). This spatial relationship also indicates that monogenetic eruptions can be spatially linked over millions of years, and could represent a novel style of polygenetic volcanism (Nemeth et al. 2003; Brenna et al. 2010; Németh 2010; Brenna et al. 2011; Moorhouse et al. 2015).

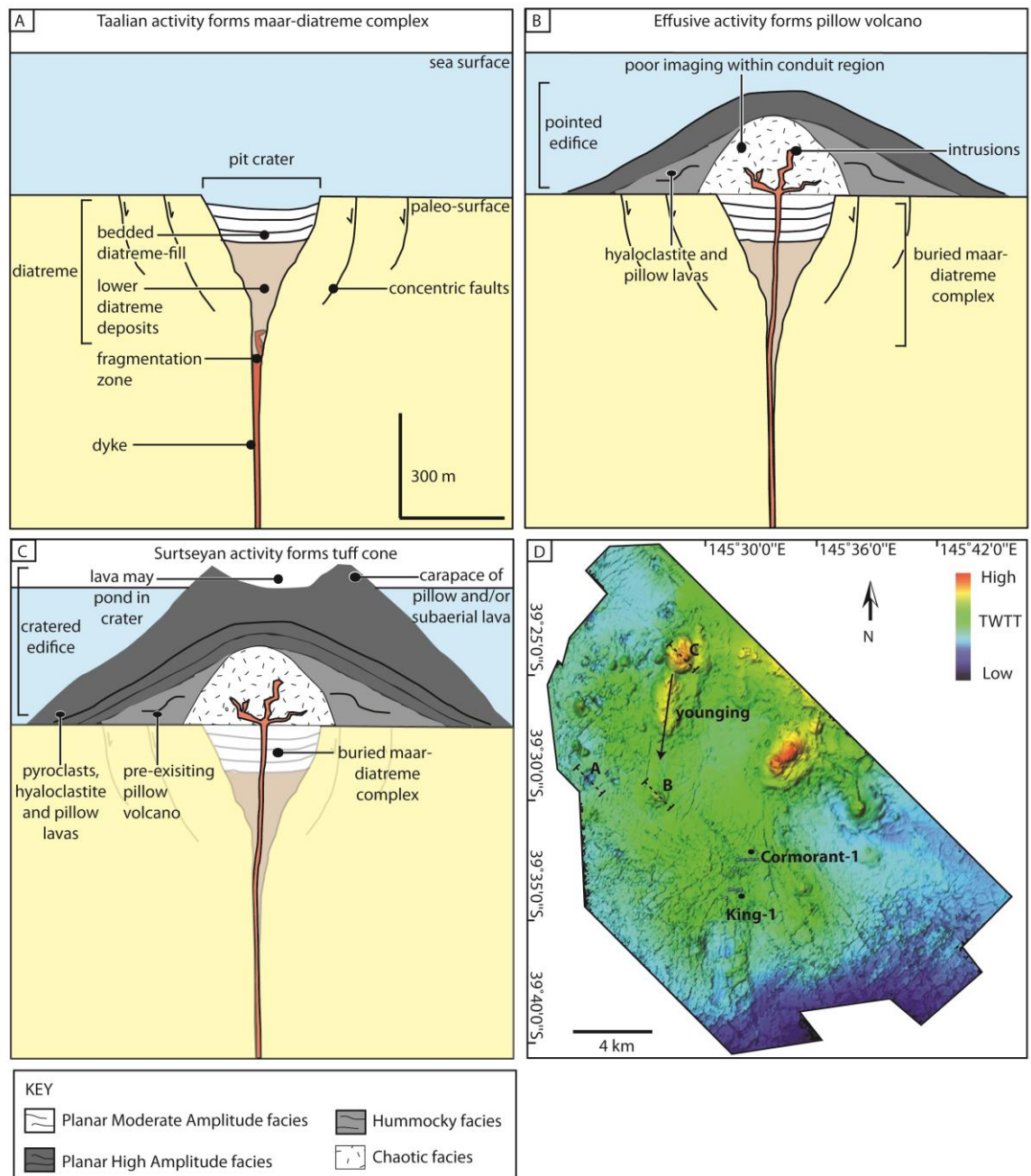


Figure 5.14. Schematic diagram to show the evolution of a submarine monogenetic volcano (A) Submarine maar-diatreme complexes form during Taalian-style activity. Syn- and post-eruptive sediments fill the craters. These are represented by the pit crater volcanoes. (B) Continued activity results in the submarine effusion of lavas, building pillow volcanoes. These are represented by the pointed edifices. (C) Tuff cones, represented by the flat-topped and cratered edifices, are formed during later Surtseyan activity. Ponding of lavas within the crater resulted in the formation of flat-topped volcanoes. These edifices may have been emergent. Image (D) shows the location of diagrams A–C.

5.5.3 Comparison with other volcanoes in seismic data

Volcanoes are reported in other seismic data sets in other tectonic settings worldwide (see Chapter 2). The pit craters in this study have a similar size, funnel-shaped geometry and facies to the maars described by Wall et al. (2010), in which the dyke is clearly imaged beneath the maar. This further supports a volcanic origin for the crater-type vents in this study. The facies and architecture of the edifices identified in this study are broadly similar to those of the submarine volcanoes and shield volcanoes described by Bell and Butcher (2002) and Magee et al. (2013). These edifices have onion ring structures in plan view, high amplitude tops and prograding reflections in their flanks. However, these features are not necessarily diagnostic of a volcanic origin. Zhao et al. (2014) describe “volcanic mounds” from the South China Sea, which have a similar size and depth relationship to sills to the edifices I describe. However, since detailed description of the edifices’ internal architecture is lacking, I am unable to provide further comparison.

There are a range of sedimentary edifices recognised in seismic data that can have similar morphologies, including mud volcanoes and hydrothermal vents. A volcanic origin for the edifices in this study is indicated by the presence of volcanic material in wells, and by the high velocities (2090–4025 m s⁻¹) of the volcanoes. Furthermore, unlike mud volcanoes, the volcanoes in this study have steep (>10°) slopes. The volcanoes also lack the inwardly dipping reflectors in their central area that are found within mud volcanoes (Kopf et al. 1998). The edifices I describe have chaotic and hummocky reflections that differentiate them from similar-sized hydrothermal edifices imaged by Grove (2013) that are composed of sediment. The Bass Basin edifices have superficially similar morphologies (i.e. a cone- or crater-like shape) and reflection characteristics (i.e. prograding internal reflections) to the hydrothermal vents documented by Planke et al. (2005). These vents have velocities of 1800 m s⁻¹ and are composed of diatomitic siltstone and carbonate (Svensen et al. 2003), unlike the edifices in this study. There are also several morphological features which distinguish the vents. Firstly, the eye-type hydrothermal vents described by Planke et al. (2005) have inwardly dipping reflections in their lower parts, unlike the cone-shaped edifices in this study. The dome-type vents described by Planke et al. (2005) also lack an underlying diatrema-like feature, as observed in this study. Instead, the dome-type vents are underlain by a cylindrical conduit zone (Planke et al. 2005). I also note the absence of sedimentary cones within the craters of the crater-type vents (e.g. Jamtveit et al. 2004). Furthermore, the hydrothermal vents described by Planke et al. (2005) are located above sills at ≥2000 m

depth. The edifices in this study are located above sills at 400–1200 m depth. Thus, the edifices in this study are fed by much shallower sills than the hydrothermal vents.

5.5.4 Implications for the identification of submarine volcanoes

This chapter provides insights into the growth of submarine edifices, volcanic fields and their plumbing systems. This information can be used to inform on plumbing systems and host rock interactions in other seismic data sets where imaging is concealed beneath edifices (e.g. Magee et al. 2013; Zhao et al. 2014).

The similarity between the edifices in this study and hydrothermal vents has important implications for structures not penetrated by wells (e.g. Lee et al. 2006; Rocchi et al. 2007; Inoue et al. 2008; Sun et al. 2014). Hydrothermal vents have been proposed as hydrocarbon plays (e.g. Grove 2013) and are underlain by sediment-filled breccia pipes (Svensen et al. 2006). They are thought to form during the early stages of volcanic continental rifting (e.g. Planke et al. 2005). In contrast, volcanoes represent sources of volcanic material that could potentially contaminate reservoir rocks. Furthermore, volcanoes are underlain by dykes that may compartmentalise underlying reservoirs or facilitate fluid flow (e.g. Rateau et al. 2013).

The data also suggests that the early stages of tuff cone growth may be characterised by pillow volcano construction. This highlights the usefulness of seismic data in helping constrain volcanic processes which may otherwise be inaccessible.

5.5.5 Edifice Preservation

The edifices are ≤ 550 m in height and were constructed in 90–140 m of water (Boral Energy Resources Ltd. 1998), suggesting that they were emergent. Emergent monogenetic edifices are rapidly eroded. For instance, a Surtla was eroded 10's of meters in decades leaving a plateau of pyroclastic material (e.g. Kokelaar and Durant 1983). However, the edifices in this study retain little evidence for erosion. Several factors are thought to have contributed to their preservation. Firstly, the seismic facies indicate the edifices had a protective carapace of hyaloclastite or lava (e.g. Kokelaar and Durant 1983; Andrews 2013). Secondly, the edifices are located in a basin, a site of sediment accumulation (Williamson et al. 1987). Furthermore, the results presented in this study suggest that water depth may have been deeper than inferred from biostratigraphic data, and/or that local areas of deep water existed.

5.5.6 Limitations of the study

Seismic interpretation is strongly dependent on the detection limit and resolution of the data. Detection and resolution are commonly on a scale of 10's of metres, thus seismic data represents a low resolution proxy for geologic interfaces (Sheriff and Geldart 1995). The resolution is affected by the depth of the interface, bed thickness, the impedance contrast across interfaces (i.e. lithology and the presence of fluids) and processing techniques (Sheriff and Geldart 1995). Processing techniques are capable of correcting seismic data to account for near-surface effects (e.g. irregular topography), improving the signal-noise ratio and correcting for offset between the recorded location of a seismic event and its location of the Earth's surface (Sheriff and Geldart 1995). However, since processing occurs before interpretation, and no processing reports were provided with the dataset, it is impossible to determine how the data may have appeared given different processing techniques and better resolution.

5.6 Conclusion

3D seismic and well data from the Bass Basin, offshore Australia, constrains the architecture and emplacement mechanisms of submarine volcanoes. The edifices evolved through a series of explosive and effusive stages, forming maar-diatreme complexes and volcanoclastic-dominated conical, flat-topped and cratered volcanoes. The pristine preservation of the edifices can be accounted for by a combination of a protective carapace on top of the edifices, sediment accumulation within the basin and basin subsidence concomitant with edifice growth. These volcanoes have different internal facies to morphologically-similar hydrothermal vents, and are located above shallow sills. These characteristics can be used to recognise similar volcanic features in other basins, and to distinguish these features from similar hydrothermal vents.

5.7 References

- Agustín-Flores J, Németh K, Cronin SJ, Lindsay JM, Kereszturi G, Brand BD, Smith IE (2014) Phreatomagmatic eruptions through unconsolidated coastal plain sequences, Maungataketake, Auckland Volcanic Field (New Zealand). *J Volcanol Geoth Res* 276:46-63
- Andrews B (2013) Eruptive and Depositional Mechanisms of an Eocene Shallow Submarine Volcano, Moeraki Peninsula, New Zealand. In: *Explosive Subaqueous Volcanism*. American Geophysical Union, pp 179-188
- Bacon M, Simm R, Redshaw T (2007) *3-D Seismic Interpretation*. Cambridge University Press
- Baker ET, Massoth GJ, de Ronde CEJ, Lupton JE, McInnes BIA (2002) Observations and sampling of an ongoing subsurface eruption of Kavachi volcano, Solomon Islands, May 2000. *Geology* 30(11):975-978

- Batiza R, White JDL (2000) Submarine lavas and hyaloclastite. In: Sigurdsson H (ed) *Encyclopedia of volcanoes*. Academic Press, San Diego, pp 361-381
- Bell B, Butcher H (2002) On the emplacement of sill complexes: evidence from the Faroe-Shetland Basin. *Geological Society, London, Special Publications* 197(1):307-329
- Berndt C, Skogly O, Planke S, Eldholm O, Mjelde R (2000) High-velocity breakup-related sills in the Vøring Basin, off Norway. *Journal of Geophysical Research: Solid Earth* (1978–2012) 105(B12):28443-28454
- Blevin J (2003) *Petroleum Geology of the Bass Basin - Interpretation Report*. In, Canberra Boral Energy Resources Ltd. (1998) Yolla 2 Well Proposal T/RL1. In: internal report.
- Brenna M, Cronin S, Smith IM, Sohn Y, Németh K (2010) Mechanisms driving polymagmatic activity at a monogenetic volcano, Udo, Jeju Island, South Korea. *Contributions to Mineralogy and Petrology* 160(6):931-950
- Brenna M, Cronin SJ, Németh K, Smith IEM, Sohn YK (2011) The influence of magma plumbing complexity on monogenetic eruptions, Jeju Island, Korea. *Terra Nova* 23(2):70-75
- Brenna M, Cronin SJ, Smith IE, Sohn YK, Maas R (2012) Spatio-temporal evolution of a dispersed magmatic system and its implications for volcano growth, Jeju Island Volcanic Field, Korea. *Lithos* 148:337-352
- Brenna M, Németh K, Cronin SJ, Sohn YK, Smith IE, Wijbrans J (2015) Co-located monogenetic eruptions~ 200 kyr apart driven by tapping vertically separated mantle source regions, Chagwido, Jeju Island, Republic of Korea. *B Volcanol* 77(5):1-17
- Brown RJ, Valentine GA (2013) Physical characteristics of kimberlite and basaltic intraplate volcanism and implications of a biased kimberlite record. *Geol Soc Am Bull* 125(7-8):1224-1238
- Brown RJ, Many S, Buisman I, Fontana G, Field M, Mac Niocaill C, Sparks RSJ, Stuart FM (2012) Eruption of kimberlite magmas: physical volcanology, geomorphology and age of the youngest kimberlitic volcanoes known on earth (the Upper Pleistocene/Holocene Igwisi Hills volcanoes, Tanzania) *B Volcanol* 74 (7) (2012): 1621-1643.
- Brown RJ, Blake S, Thordarson T, Self S (2014) Pyroclastic edifices record vigorous lava fountains during the emplacement of a flood basalt flow field, Roza Member, Columbia River Basalt Province, USA. *Geol Soc Am Bull* 126:875-891
- Brown S, Smith R, Cole J, Houghton B (1994) Compositional and textural characteristics of the strombolian and surtseyan K-Trig basalts, Taupo Volcanic Centre, New Zealand: Implications for eruption dynamics. *New Zealand Journal of Geology and Geophysics* 37(1):113-126
- Büchner J, Tietz O (2012) Reconstruction of the Landeskroner Scoria Cone in the Lusatian Volcanic Field, Eastern Germany—Long-term degradation of volcanic edifices and implications for landscape evolution. *Geomorphology* 151:175-187
- Calvari S, Tanner LH (2011) The Miocene Costa Giardini diatreme, Iblean Mountains, southern Italy: model for maar-diatreme formation on a submerged carbonate platform. *B Volcanol* 73(5):557-576
- Calvès G, Schwab AM, Huuse M, Clift PD, Gaina C, Jolley D, Tabrez AR, Inam A (2011) Seismic volcanostratigraphy of the western Indian rifted margin: The pre-Deccan igneous province. *Journal of Geophysical Research: Solid Earth* (1978–2012) 116(B1)
- Cas R, Landis C, Fordyce R (1989) A monogenetic, surtla-type, Surtseyan volcano from the Eocene-Oligocene Waiareka-Deborah volcanics, Otago, New Zealand: a model. *B Volcanol* 51(4):281-298
- Cas RAF, Simpson C, Sato H (1993) *Newer Volcanics Province - Processes and Products of Phreatomagmatic Activity*. IAVCEI Excursion Guide
- Connor CB, Conway MF (2000) Basaltic volcanic fields. In: Sigurdsson H (ed) *Encyclopedia of Volcanoes*. Academic Press, San Diego, pp 331-343
- Cummings AM, Blevin J (2003) Nature and distribution of igneous rocks. In: Blevin, J. (compiler), *Petroleum Geology of the Bass Basin - Interpretation Report*, an Output of the Western Tasmanian Regional Minerals Program. Geoscience Australia, Record 2003/19
- Elliott H, Gernon T, Roberts S, Hewson C (2015) Basaltic maar-diatreme volcanism in the Lower Carboniferous of the Limerick Basin (SW Ireland). *B Volcanol* 77(5):1-22
- Esso Exploration Australia Inc. (1965) *Esso Bass-1 Well Completion Report*. In,
- Esso Exploration Australia Inc. (1970) *Report - Cormorant 1*. In,
- Faustmann C (1995) The seismic expression of volcanism in the Bass Basin referring to western Victorian analogues.

- Fiske RS, Cashman KV, Shibata A, Watanabe K (1998) Tephra dispersal from Myojinsho, Japan, during its shallow submarine eruption of 1952–1953. *B Volcanol* 59(4):262-275
- Francis E (1970) Bedding in Scottish (Fifeshire) tuff-pipes and its relevance to maars and calderas. *Bull Volcanol* 34(3):697-712
- Fujibayashi N, Sakai U (2003) Vesiculation and eruption processes of submarine effusive and explosive rocks from the Middle Miocene Ogi Basalt, Sado Island, Japan. *Explosive Subaqueous Volcanism*:259-272
- Gatliff RW, Hitchen K, Ritchie JD, Smythe DK (1984) Internal structure of the Erlend Tertiary volcanic complex, north of Shetland, revealed by seismic reflection. *J Geol Soc London* 141(3):555-562
- Gençalioglu-Kuşcu G, Atilla C, Cas RA, Kuşcu İ (2007) Base surge deposits, eruption history, and depositional processes of a wet phreatomagmatic volcano in Central Anatolia (Cora Maar). *J Volcanol Geoth Res* 159(1):198-209
- Geoscience Australia (2010) Yolla Well Report - All Graphs. In: Australian Government, Graettinger AH, Skilling I, McGarvie D, Höskuldsson Á (2013) Subaqueous basaltic magmatic explosions trigger phreatomagmatism: A case study from Askja, Iceland. *J Volcanol Geoth Res* 264:17-35
- Gregg TK, Fink JH (1995) Quantification of submarine lava-flow morphology through analog experiments. *Geology* 23(1):73-76
- Grove C (2013) Submarine hydrothermal vent complexes in the Paleocene of the Faroe-Shetland Basin: Insights from three-dimensional seismic and petrographical data. *Geology* 41(1):71-74
- Gutmann JT (2002) Strombolian and effusive activity as precursors to phreatomagmatism: eruptive sequence at maars of the Pinacate volcanic field, Sonora, Mexico. *J Volcanol Geoth Res* 113(1):345-356
- Haller MJ, de Wall H, Martin U, Németh K (2006) Understanding the evolution of maar craters. Holford S, Schofield N, MacDonald J.D, Duddy I.R, P.F G (2007) Seismic Analysis of Igneous Systems in Sedimentary Basins and their Impacts on Hydrocarbon Prospectivity: Examples from the Southern Australian Margin.
- Holford S, Schofield N, MacDonald J, Duddy I, Green P (2012) Seismic analysis of igneous systems in sedimentary basins and their impacts on hydrocarbon prospectivity: examples from the Southern Australian margin. *Australian Petroleum Production and Exploration Association Journal* 52:229-252
- Holford S, Schofield N (in review) Three-dimensional seismic analysis for non-magmatic reactivation of buried volcanic complexes in sedimentary basins.
- Houghton B, Gonnermann H (2008) Basaltic explosive volcanism: constraints from deposits and models. *Chemie der Erde-Geochemistry* 68(2):117-140
- Inoue H, Coffin MF, Nakamura Y, Mochizuki K, Kroenke LW (2008) Intrabasement reflections of the Ontong Java Plateau: Implications for plateau construction. *Geochemistry, Geophysics, Geosystems* 9(4)
- Jackson CA-L (2012) Seismic reflection imaging and controls on the preservation of ancient sill-fed magmatic vents. *J Geol Soc London* 169(5):503-506
- Jamtveit B, Svensen H, Podladchikov YY, Planke S (2004) Hydrothermal vent complexes associated with sill intrusions in sedimentary basins. *Physical geology of high-level magmatic systems* 234:233-241
- Jerram DA (2002) Volcanology and facies architecture of flood basalts. *Geological Society of America Special Papers* 362:119-132
- Jerram DA, Single RT, Hobbs RW, Nelson CE (2009) Understanding the offshore flood basalt sequence using onshore volcanic facies analogues: an example from the Faroe–Shetland basin. *Geol Mag* 146(03):353
- Johnson RW (1989) Intraplate volcanism in eastern Australia and New Zealand. Cambridge University Press
- Kjarsgaard B, Harvey S, McClintock M, Zonneveld J, Du Plessis P, McNeil D, Heaman L (2009) Geology of the Orion South kimberlite, Fort à la Corne, Canada. *Lithos* 112:600-617
- Kokelaar BP, Durant GP (1983) The submarine eruption and erosion of Surtla (Surtsey), Iceland. *J Volcanol Geoth Res* 19(3–4):239-246

- Kokelaar P (1986) Magma-water interactions in subaqueous and emergent basaltic. *B Volcanol* 48(5):275-289
- Kopf A, Robertson AHF, Clennell MB, Flecker R (1998) Mechanisms of mud extrusion on the Mediterranean Ridge Accretionary Complex. *Geo-Marine Letters* 18(2):97-114
- Kwon CW, Sohn YK (2008) Tephra-filled volcanic neck (diatreme) of a mafic tuff ring at Maegok, Miocene Eoil Basin, SE Korea. *Geosciences Journal* 12(4):317-329
- Le Corvec N, Menand T, Lindsay J (2013) Interaction of ascending magma with pre-existing crustal fractures in monogenetic basaltic volcanism: an experimental approach. *Journal of Geophysical Research: Solid Earth* 118(3):968-984
- Lee GH, Kwon YI, Yoon CS, Kim HJ, Yoo HS (2006) Igneous complexes in the eastern Northern South Yellow Sea Basin and their implications for hydrocarbon systems. *Marine and Petroleum Geology* 23(6):631-645
- Lefebvre N, Kurszlaukis S (2008) Contrasting eruption styles of the 147 Kimberlite, Fort à la Corne, Saskatchewan, Canada. *J Volcanol Geoth Res* 174(1):171-185
- Lonsdale P, Batiza R (1980) Hyaloclastite and lava flows on young seamounts examined with a submersible. *Geol Soc Am Bull* 91(9):545-554
- Lorenz V (1975) Formation of phreatomagmatic maar-diatreme volcanoes and its relevance to kimberlite diatremes. *Physics and Chemistry of the Earth* 9:17-27
- Lorenz V (1986) On the growth of maars and diatremes and its relevance to the formation of tuff rings. *B Volcanol* 48(5):265-274
- Lorenz V, Kurszlaukis S (2007) Root zone processes in the phreatomagmatic pipe emplacement model and consequences for the evolution of maar-diatreme volcanoes. *J Volcanol Geoth Res* 159(1-3):4-32
- Magee C, Hunt-Stewart E, Jackson CAL (2013) Volcano growth mechanisms and the role of sub-volcanic intrusions: Insights from 2D seismic reflection data. *Earth and Planetary Science Letters* 373(0):41-53
- Maresh J, White RS, Hobbs RW, Smallwood JR (2006) Seismic attenuation of Atlantic margin basalts: Observations and modeling. *Geophysics* 71(6):B211-B221
- McClintock M, White J (2006) Large phreatomagmatic vent complex at Coombs Hills, Antarctica: Wet, explosive initiation of flood basalt volcanism in the Ferrar-Karoo LIP. *B Volcanol* 68(3):215-239
- Moore JG (1985) Structure and eruptive mechanisms at Surtsey Volcano, Iceland. *Geol Mag* 122(06):649-661
- Moorhouse B, White J, Scott J (2015) Cape Wanbrow: A stack of Surtseyan-style volcanoes built over millions of years in the Waiareka-Deborah volcanic field, New Zealand. *J Volcanol Geoth Res* 298:27-46
- Nemeth K, White JD, Reay A, Martin U (2003) Compositional variation during monogenetic volcano growth and its implications for magma supply to continental volcanic fields. *J Geol Soc London* 160(4):523-530
- Németh K, White JDL (2003) Reconstructing eruption processes of a Miocene monogenetic volcanic field from vent remnants: Waipiata Volcanic Field, South Island, New Zealand. *J Volcanol Geoth Res* 124(1-2):1-21
- Németh K, Cronin SJ, Charley DT, Harrison MJ, Garae E (2006) Exploding lakes in Vanuatu-"Surtseyan-style" eruptions witnessed on Ambae Island.
- Németh K (2010) Monogenetic volcanic fields: Origin, sedimentary record, and relationship with polygenetic volcanism. *Geological Society of America Special Papers* 470:43-66
- Otterloo J, Cas RF, Sheard M (2013) Eruption processes and deposit characteristics at the monogenetic Mt. Gambier Volcanic Complex, SE Australia: implications for alternating magmatic and phreatomagmatic activity. *B Volcanol* 75(8):1-21
- Pirrung M, Fischer C, Büchel G, Gaupp R, Lutz H, Neuffer FO (2003) Lithofacies succession of maar crater deposits in the Eifel area (Germany). *Terra Nova* 15(2):125-132
- Pittari A, Cas R, Lefebvre N, Robey J, Kurszlaukis S, Webb K (2008) Eruption processes and facies architecture of the Orion Central kimberlite volcanic complex, Fort à la Corne, Saskatchewan; kimberlite mass flow deposits in a sedimentary basin. *J Volcanol Geoth Res* 174(1):152-170

- Planke S, Eldholm O (1994) Seismic response and construction of seaward dipping wedges of flood basalts: Vøring volcanic margin. *Journal of Geophysical Research: Solid Earth* (1978–2012) 99(B5):9263–9278
- Planke S, Symonds PA, Alvestad E, Skogseid J (2000) Seismic volcanostratigraphy of large-volume basaltic extrusive complexes on rifted margins. *J. Geophys. Res.* 105(B8):19335–19351
- Planke S, Rasmussen T, Rey SS, Myklebust R (2005) Seismic characteristics and distribution of volcanic intrusions and hydrothermal vent complexes in the Vøring and Møre basins. Geological Society, London, Petroleum Geology Conference series 6:833–844
- Price R, Nicholls I, Gray C (2003) Cainozoic igneous activity: widespread volcanism resulting from long-term mantle instability and rifting.
- Rateau R, Schofield N, Smith M (2013) The potential role of igneous intrusions on hydrocarbon migration, West of Shetland. *Petroleum Geoscience* 19(3):259–272
- Riggs NR, Duffield WA (2008) Record of complex scoria cone eruptive activity at Red Mountain, Arizona, USA, and implications for monogenetic mafic volcanoes. *J Volcanol Geoth Res* 178(4):763–776
- Ritchie J, Hitchen K (1996) Early Paleogene offshore igneous activity to the northwest of the UK and its relationship to the North Atlantic Igneous Province. Geological Society, London, Special Publications 101(1):63–78
- Rocchi S, Mazzotti A, Marroni M, Pandolfi L, Costantini P, Giuseppe B, Biase Dd, Federici F, Lô PG (2007) Detection of Miocene saucer-shaped sills (offshore Senegal) via integrated interpretation of seismic, magnetic and gravity data. *Terra Nova* 19(4):232–239
- Roger S, Coulon C, Thouveny N, Féraud G, Van Velzen A, Fauquette S, Cocheme JJ, Prevot M, Verosub K (2000) $^{40}\text{Ar}/^{39}\text{Ar}$ dating of a tephra layer in the Pliocene Senèze maar lacustrine sequence (French Massif Central): constraint on the age of the Réunion–Matuyama transition and implications on paleoenvironmental archives. *Earth and Planetary Science Letters* 183(3):431–440
- Ross P-S, Delpit S, Haller MJ, Németh K, Corbella H (2011) Influence of the substrate on maar–diatreme volcanoes—an example of a mixed setting from the Pali Aike volcanic field, Argentina. *J Volcanol Geoth Res* 201(1):253–271
- Schmidt R, Schminke HU (2000) Seamounts and island building. In: Sigurdsson H (ed) *Encyclopedia of volcanoes*. Academic Press, San Diego, pp 361–381
- Schofield N, Jolley DW (2013) Development of intra-basaltic lava-field drainage systems within the Faroe–Shetland Basin. *Petroleum Geoscience* 19(3):273–288
- Self S, Keszthelyi LP, Thordarson T (2000) Discussion of: “Pulsed inflation of pahoehoe lava flows: implications for flood basalt emplacement”, by S.W. Anderson, E.R. Stofan, E.R. Smrekar, J.E. Guest and B. Wood [*Earth Planet. Sci. Lett.* 168 (1999) 7–18]. *Earth and Planetary Science Letters* 179(2):421–423
- Sheriff RE, Geldart L (1995) *Exploration seismology*. Cambridge University Press
- Skilling I (1994) Evolution of an englacial volcano: Brown Bluff, Antarctica. *B Volcanol* 56(6–7):573–591
- Skilling IP (2009) Subglacial to emergent basaltic volcanism at Hlöðufell, south-west Iceland: a history of ice-confinement *J Volcanol Geoth Res* 185(4): 276–289.
- Smellie J, Hole M (1997) Products and processes in Pliocene–Recent, subaqueous to emergent volcanism in the Antarctic Peninsula: examples of englacial Surtseyan volcano construction. *B Volcanol* 58(8):628–646
- Sohn Y (1995) Geology of Tok Island, Korea: eruptive and depositional processes of a shoaling to emergent island volcano. *B Volcanol* 56(8):660–674
- Sohn YK (1996) Hydrovolcanic processes forming basaltic tuff rings and cones on Cheju Island, Korea. *Geol Soc Am Bull* 108(10):1199–1211
- Suiting I, Schmincke H-U (2009) Internal vs. external forcing in shallow marine diatreme formation: A case study from the Iblean Mountains (SE-Sicily, Central Mediterranean). *J Volcanol Geoth Res* 186(3):361–378
- Suiting I, Schmincke H-U (2010) Iblean diatremes 2: shallow marine volcanism in the Central Mediterranean at the onset of the Messinian Salinity Crisis (Iblean Mountains, SE-Sicily)—a multidisciplinary approach. *International Journal of Earth Sciences* 99(8):1917–1940

- Suiting I, Schmincke H-U (2012) Iblean diatremes 3: volcanic processes on a Miocene carbonate platform (Iblean Mountains, SE-Sicily): a comparison of deep vs. shallow marine eruptive processes. *B Volcanol* 74(1):207-230
- Sun Q, Wu S, Cartwright J, Wang S, Lu Y, Chen D, Dong D (2014) Neogene igneous intrusions in the northern South China Sea: Evidence from high-resolution three dimensional seismic data. *Marine and Petroleum Geology* 54:83-95
- Sutherland F (2003) 'Boomerang' migratory intraplate Cenozoic volcanism, eastern Australian rift margins and the Indian-Pacific mantle boundary. *Geological Society of America Special Papers* 372:203-221
- Sutherland FL, Wellman P (1986) Potassium-argon ages of Tertiary volcanic rocks, Tasmania. *Papers and Proceedings of the Royal Society of Tasmania* 120
- Svensen H, Planke S, Jamtveit B, Pedersen T (2003) Seep carbonate formation controlled by hydrothermal vent complexes: a case study from the Vøring Basin, the Norwegian Sea. *Geo-Marine Letters* 23(3-4):351-358
- Svensen H, Jamtveit B, Planke S, Chevallier L (2006) Structure and evolution of hydrothermal vent complexes in the Karoo Basin, South Africa. *J Geol Soc London* 163(4):671-682
- Takada A (1994) The influence of regional stress and magmatic input on styles of monogenetic and polygenetic volcanism. *Journal of Geophysical Research: Solid Earth* (1978–2012) 99(B7):13563-13573
- Tap Oil Ltd. (2008) Labatt 3D Seismic Survey Acquisition Report. In: Internal report.
- Tap Oil Ltd. (2010) T/47P Bass Basin, Tasmania – 2007 Labatt 3D and 2008 Molson 2D Seismic Interpretation Report. In,
- Thomson K (2005) Volcanic features of the North Rockall Trough: application of visualisation techniques on 3D seismic reflection data. *B Volcanol* 67(2):116-128
- Thomson K (2007) Determining magma flow in sills, dykes and laccoliths and their implications for sill emplacement mechanisms. *B Volcanol* 70(2):183-201
- Thorarinsson S (1966) The Surtsey eruption course of events and the development of the new island. In: Museum of Natural History, Reykjavik, Iceland
- Thordarson T, Self S (1993) The Laki (Skaftár Fires) and Grímsvötn eruptions in 1783–1785. *B Volcanol* 55(4):233-263
- Thors K, Jakousson SP (1982) Two seismic reflection profiles from the vicinity of Surtsey, Iceland. *Surtsey research progress report* 9:149
- Trigg KR, Blevine JE, Boreham CJ (2003) An Audit of Petroleum Exploration Wells in the Bass Basin 1965 - 1999. *Geoscience Australia*
- Urrutia-Fucugauchi J, Uribe-Cifuentes RM (1999) Lower-crustal xenoliths from the Valle de Santiago maar field, Michoacan-Guanajuato volcanic field, central Mexico. *International Geology Review* 41(12):1067-1081
- Valentine GA, Gregg TKP (2008) Continental basaltic volcanoes — Processes and problems. *J Volcanol Geoth Res* 177(4):857-873
- Valentine GA, Cortés J (2013) Time and space variations in magmatic and phreatomagmatic eruptive processes at Easy Chair (Lunar Crater Volcanic Field, Nevada, USA). *B Volcanol* 75(9):1-13
- Vespermann D, Schmincke H-U (2000) Scoria cones and tuff rings. In: Sigurdsson H (ed) *Encyclopedia of Volcanoes*. Academic Press, San Diego. Academic Press, San Diego, pp 683-694
- Vogel DC, Keays RR (1997) The petrogenesis and platinum-group element geochemistry of the Newer Volcanic Province, Victoria, Australia. *Chemical Geology* 136(3):181-204
- Walker GPL (1993) Basaltic-volcano systems. *Geological Society, London, Special Publications* 76(1):3-38
- Wall M, Cartwright J, Davies R, McGrandle A (2010) 3D seismic imaging of a Tertiary Dyke Swarm in the Southern North Sea, UK. *Basin Research* 22(2):181-194
- Watton TJ, Wright KA, Jerram DA, Brown RJ (2013a) The Petrophysical and Petrographical Properties of Hyaloclastite Deposits: Implications for Petroleum Exploration. *AAPG Bulletin* (20,130,909)
- Watton TJ, Jerram DA, Thordarson T, Davies RJ (2013b) Three-dimensional lithofacies variations in hyaloclastite deposits. *J Volcanol Geoth Res* 250(0):19-33
- Wheeler BF, Kjellgren GM (1986) Yolla-1 final well report. In: Amoco Australian Petroleum Company,

- White JD (2001) Eruption and reshaping of Pahvant Butte volcano in Pleistocene Lake Bonneville. *Volcaniclastic Sedimentation in Lacustrine Settings*:(Special Publication 30 of the IAS) 54:61
- White JDL (1991) Maar-diatreme phreatomagmatism at Hopi Buttes, Navajo Nation (Arizona), USA. *B Volcanol* 53(4):239-258
- White JDL, McClintock MK (2001) Immense vent complex marks flood-basalt eruption in a wet, failed rift: Coombs Hills, Antarctica. *Geology* 29(10):935-938
- White JDL, Ross PS (2011) Maar-diatreme volcanoes: A review. *J Volcanol Geoth Res* 201(1–4):1-29
- Williamson P, Pigram C, Colwell J, Scherl A, Lockwood K, Branson J (1987) Review of stratigraphy, structure, and hydrocarbon potential of Bass Basin, Australia. *AAPG bulletin* 71(3):253-280
- Wohletz KH, Sheridan MF (1983) Hydrovolcanic explosions; II, Evolution of basaltic tuff rings and tuff cones. *American Journal of Science* 283(5):385-413
- Wohletz KH (2003) Water/magma interaction: physical considerations for the deep submarine environment. *Explosive subaqueous volcanism*:25-49
- Wright K (2013) Seismic Stratigraphy and Geomorphology of Palaeocene Volcanic Rocks, Faroe-Shetland Basin. PhD Thesis, Durham University, Department of Earth Sciences.
- Wright KA, Davies RJ, Jerram DA, Morris J, Fletcher R (2012) Application of seismic and sequence stratigraphic concepts to a lava-fed delta system in the Faroe-Shetland Basin, UK and Faroes. *Basin Research* 24(1):91-106
- Zhao F, Wu S, Sun Q, Huuse M, Li W, Wang Z (2014) Submarine volcanic mounds in the Pearl River Mouth Basin, northern South China Sea. *Mar Geol* 355(0):162-172

Chapter 6: Discussion

6.1 Introduction

Chapters 3, 4 and 5 describe the architecture of basaltic volcanic edifices. In this chapter, I assess the importance of each edifice for hydrocarbon systems. I also discuss how the fissure-derived and rootless edifices detailed in Chapters 3 and 4 can be recognised in hydrocarbon basins using core, cutting and FMI well data. Since this thesis did not determine the petrophysical properties of pyroclastic rocks in wireline data, this remains a topic worthy of future research (see Chapter 8). I also discuss the challenges associated with recognising the edifices described in Chapters 3 and 4 in seismic data.

6.2 Fissure eruption-derived volcanoes

Chapter 3 details the edifices formed during a low volume fissure eruption. These edifices are analogous to those formed during large-volume fissure eruptions and were formed during Hawaiian-style activity. This suggests that flood basalt emplacement may also be associated with a diversity of eruption styles. The edifices are underlain by dykes that widen towards the surface (e.g. Chapter 3; see also Keating et al. 2008; Geshi et al. 2010; Geshi and Oikawa 2014). Dykes are typified by abundant cooling joints which may form permeable pathways (Rateau et al. 2013). This permeability can subsequently be enhanced or decreased through tectonic fracturing, diagenesis, weathering and hydrothermal alteration (Rateau et al. 2013). Thus, the dykes and conduit could act as a hydrocarbon reservoir (e.g. Schutter 2003), fluid pathway or a barrier to fluid flow (e.g. Rateau et al. 2013). The planes of the graben bounding faults that undergo post-eruption displacement (e.g. Chapter 3) may also act as hydrocarbon migration pathways (e.g. Walker et al. 2013). Thus, the fissure-proximal region could be an important region for hydrocarbon migration. The fissure-proximal region could also act as a reservoir, since 4-way dip closure of sediments above the edifices can form a seal for underlying hydrocarbons (Schutter 2003).

There are not thought to be any effects on hydrocarbon source rock unique to the fissure-proximal region. Fissure-proximal regions are underlain by complex assemblages of sills and dykes (Thomson 2007) which have important effects on source rock maturation (Raymond and Murchison 1988; Bishop and Abbott 1995). However, sills and dykes are found throughout volcanic basins (Planke et al. 2005; Hansen and Cartwright 2006; Polteau et al. 2008; Goultly and Schofield 2008; Galerne et al. 2008; Galerne et al. 2011), and are not unique to the fissure-proximal region.

Features that can be used to recognise the fissure-proximal region from FMI data include variations in vesicle distribution and foliation textures. Vesicles are recognised in FMI by a distinct mottled appearance (Watton et al. 2014). Irregular vesicle patches are common in the core of clastogenic lavas (Chapter 3). These lavas are characteristic of the vent-proximal region in many basaltic settings (e.g. Chapter 3; see also Swanson et al. 1975; Sumner 1998; Thordarson and Self 1998; Carracedo Sánchez et al. 2012; Brown et al. 2014). Alternating vesicle-rich and vesicle-poor zones also indicate welding fabrics such as those found in clast supported densely welded spatter bombs (dwSp) and in the crusts of stacked shelly pāhoehoe lobes. Again, these facies are common in the vent-proximal region (e.g. Chapter 3; see also Swanson et al. 1975; Thordarson and Self 1998; Brown et al. 2014). Foliation textures (i.e. laminations) resulting from welding occur in clast supported densely welded spatter bombs (dwSp). Tension gashes in lava-like agglutinate (l-l Agg; logs 30 and 11, Figs. 10 and 11) also give this lithofacies a foliated appearance. Similar laminations are recognised in sequences <0.25 m thick in FMI logs (Watton et al. 2014) suggesting that vent-proximal sequences can be recognised by their laminated texture. However, it may be difficult to distinguish these features from other foliated textures not diagnostic of a fissure-proximal location, such as the platy zone found at the base of pāhoehoe lava flows (e.g. Thordarson and Self 1998). The petrographic textures documented in Chapter 3 have been reported from other studies of fissure-derived pyroclastic edifices (Thordarson and Self 1998; Brown et al. 2014), thus do not provide further insights into how dyke-fed edifices can be recognised from core and cutting data.

This thesis highlights that the fissure-derived edifices in Chapter 3 will be difficult to detect in seismic data. Seismic data commonly has a resolution of 10's of metres (Sheriff and Geldart 1995). Therefore, the edifices described will be difficult, if not impossible to detect, especially if they are located beneath the "Top Basalt" reflection (Jerram 2002; Roberts et al. 2005).

Furthermore, fissure-derived edifices may not be recognised because of their close association with grabens. Chapter 3 shows that the R-K fissure eruption occurred within the Sveinar graben. Grabens associated with fissure eruptions are thought to form as a result deflation of the underlying feeder system (Tentler and Temperley 2007) and/or intrusion of the feeder dyke (Pollard et al. 1983; Rubin and Pollard 1988; Rubin 1992; Chadwick and Embley 1998). Syn-eruptive graben formation results in the ponding of lavas (e.g. Chapter 3) and drowning of the edifices (e.g. Thordarson and Self 1993; Keszthelyi et al. 2004). These lavas would then mask the underlying reflections (Jerram

2002; Roberts et al. 2005), rendering the edifices unresolvable. Grabens are also likely to be favourable pathways for the re-establishment for drainage systems (e.g. Chapter 3; Ebinghaus et al. 2014) enhancing erosion and degradation of the edifices.

Erosion serves to decrease the likelihood of fissure-proximal locations being recognised from seismic data. Erosion of volcanic edifices is partly linked to the vesicularity and density of the constituent lithofacies, since vesicular clasts are more easily entrained in water than dense clasts (e.g. Manville 2009). Therefore, edifices composed of densely welded lithofacies (e.g. spatter ramparts and scoria-agglutinate cones) are likely to stand a higher chance of preservation than those composed of vesicular lithofacies (e.g. scoria ramparts and rootless cones). However, small edifices such as spatter ramparts are more likely to be buried by lava (e.g. Keszthelyi et al. 2004) and are thus more difficult to resolve from seismic data.

Erosion is also linked to climate, most notably rainfall and temperature (e.g. Wood 1980; Hooper and Sheridan 1998). The flood basalts of the NAIP were predominantly emplaced sub aerially (Brown et al. 2009) during the Paleocene-Eocene Thermal Maximum (Jolley and Widdowson 2005). This period was typified by a warm and wet climate, where fluvial channels were abundant (Brown et al. 2009). These conditions would have favoured rapid erosion of pyroclastic edifices (e.g. Wood 1980; Németh and Cronin 2007; Németh et al. 2009; Manville et al. 2009). This situation is in contrast to the eruptions in the Bass Basin (Chapter 4) which occurred beneath sea level, therefore favouring edifice preservation.

6.3 Rootless cones

Chapter 4 provides quantitative data on rootless juvenile clast morphology, density and lithofacies architecture that can be used to differentiate between dyke-fed and rootless edifices. Differentiating between rootless and dyke-fed edifices is important because dyke-fed edifices can be used to inform on magma plumbing systems (Valentine and Groves 1996; Valentine and Keating 2007; Valentine 2012), conduit conditions (Taddeucci et al. 2004; Genareau et al. 2010), environmental impacts (Thordarson et al. 1996; Thordarson et al. 2001; Brown et al. 2014) and magma flux (Di Traglia et al. 2009; Németh et al. 2011; Valentine and Cortés 2013) and fragmentation processes (Sumner et al. 2005; Valentine and Gregg 2008). If rootless edifices are incorrectly identified as dyke-fed edifices (or vice-versa) incorrect conclusions may be drawn about these processes and conditions. Furthermore, dyke-fed edifices can also be used to identify structural trends (e.g. Connor

and Conway 2000), in contrast to rootless edifices which indicate lava flow pathways (e.g. tubes; see Hamilton et al. 2010). I presume that rootless eruptions were common in the North Atlantic Igneous Province, since the lava flows were emplaced in an environment where ephemeral lakes, swamps and small fluvial channels were common (Brown et al. 2009). However, no rootless cones have been discovered to date.

Rootless vents (as described in Chapter 4) are important features for hydrocarbon migration. The vents occur in lava flow cores, which commonly act as seals in volcanic-affected basins (Schutter 2003; Rohrman 2007). They also create highly anisotropic flow regimes in basalt aquifers (Burns et al. 2014). Although the preservation potential of the void that characterises the vents is unknown, the vents and associated joints extend from the base to the top of a lava flow. This will increase the porosity and permeability of the core, particularly in the vertical plane, providing an efficient vertical migration pathway. The net result will be to decrease the effectiveness of the host lava flow as a seal (e.g. Rohrman 2007). The vents and joints may also provide zones of accelerated fluid loss whilst drilling through the basalt sequence (e.g. Millett 2015). Since rootless cone fields cover areas up to 150 km² (Hamilton et al. 2010), these considerations are important over a basin-wide scale.

My research highlights the importance of rootless cones as paleo-environmental indicators and sources of hydrocarbon reservoir and source rock contamination. Rootless cones form on clay–cobble sized substrates (e.g. Chapter 4; see also Fagents and Thordarson 2007; Hamilton et al. 2010). Sand-sized sediments could act as inter-basalt reservoirs (Schofield and Jolley 2013). These are difficult to detect in seismic data if their thickness is <50 m, or if sub-basalt imaging is sufficiently poor (e.g. Jerram 2002). Therefore rootless cones can be used to identify sediment packages unresolvable in seismic data. Although the effect of cone formation on the sediment is unknown, there is likely to be contamination of the sediment by igneous material during cone formation. Therefore rootless cone formation is detrimental to the quality of underlying reservoirs in a basin. Rootless cone formation is also detrimental to source rock quality. Source rocks are commonly formed in lacustrine environments, in which rootless cone are found (e.g. Chapter 4; see also Fagents and Thordarson 2007; Hamilton et al. 2010). Rootless cones also distribute pyroclastic material throughout the basin, and could contaminate overlying reservoir rocks (e.g. Clark 2014).

However, distinguishing rootless edifices from dyke-fed edifices in well core data would present a significant challenge. The rootless juvenile clasts that have morphologies

atypical of dyke-fed tephra (see Chapter 4) are unlikely to be recognised from core data; angular volcanic “breccias” are often highly fractured during drilling (Watton et al. 2014), thus hampering recognition of clast shape and size. Although the abundance of sediment in the rootless tephra documented in Chapter 4 proves a useful criterion for distinguishing dyke-fed from rootless tephra in field data sets, intimately mixed sediment and tephra is also characteristic of epiclastic successions (Fisher 1961; Fisher 1966; White and Houghton 2006; Clark 2014) and peperite (Skilling et al. 2002) which are found in many settings. Furthermore, diagenesis may alter the porosity and mineralogy of primary volcanoclastic rocks (Clark 2014), thus increasing the difficulty of distinguishing between epiclastic, dyke-fed and rootless pyroclastic successions.

FMI data is also of limited use in distinguishing dyke-fed from rootless tephra. The resolution of FMI is such it does not allow determination of lava fragmentation mechanism, welding or sedimentation processes (Watton et al. 2014). Therefore, it would be difficult to distinguish primary volcanoclastic rocks, dyke-fed and rootless tephra (e.g. Watton et al. 2014). Although the density of an FMI facies can be determined to 0.1 gm/cm^3 (Watton et al. 2014), welding and clast morphology cannot be accurately determined on a scale of $<25 \text{ cm}$ (Watton et al. 2014). Therefore, it would be difficult to determine if dense pyroclastic successions are welded (and potentially dyke-fed) or are composed of fragmented, degassed lava (as is the case for rootless tephra).

As described for dyke-fed edifices, the size of rootless edifices would hamper recognition of these edifices in seismic data. Furthermore, rootless cones have a low preservation potential due to the vesicular and unconsolidated nature of the component lithofacies (e.g. Chapter 4; see also Mattox and Mangan 1997; Melchior Larsen et al. 2006; Hamilton et al. 2010). This would further limit the chances of them being detected in seismic data.

6.4 Monogenetic edifices in seismic data

Chapter 5 provides insights into the seismic facies that characterise submarine volcanic edifices. These facies can be used to recognise volcanic edifices from other seismic data sets. These insights are especially useful in other volcanic-affected basins where the edifices have not been penetrated by wells. Chapter 5 also shows that the edifices directly overlie the site of previous lava extrusion (within the Lower Volcanic horizon, Chapter 5). This spatial relationship exists in other volcanic fields (e.g. Takada

1994; Connor and Conway 2000; Németh 2010) and may exist within FBP (e.g. the FSB; see also White et al. 2009).

Buried volcanic edifices also act as fluid pathways (Holford and Schofield, in review). The edifices described by Holford and Schofield (in review) have been identified in this thesis as tuff cones (Chapter 5); relatively common features along fissures (e.g. Thordarson and Larsen 2007; Zanon et al. 2009; Németh and Cronin 2011). This suggests tuff cones are likely to be important features for vertical fluid migration in other hydrocarbon basins also affected by fissure volcanism. Chapter 5 also shows that the feeder dyke for the Miocene edifices exploited the same vertical pathway as the dyke for the Lower Volcanic (LV) lava flows. Since dykes may act as conduits for fluid migration (Rateau et al. 2013), vertical fluid pathways are also likely to exist between edifices that formed over several millions of years (e.g. Takada 1994; Connor and Conway 2000; Németh 2010).

6.5 References

- Bishop A, Abbott G (1995) Vitrinite reflectance and molecular geochemistry of Jurassic sediments: the influence of heating by Tertiary dykes (northwest Scotland). *Organic Geochemistry* 22(1):165-177
- Brown D, Holohan E, Bell B (2009) Sedimentary and volcano-tectonic processes in the British Paleocene Igneous Province: a review. *Geol Mag* 146(3):326-352
- Brown RJ, Blake S, Thordarson T, Self S (2014) Pyroclastic edifices record vigorous lava fountains during the emplacement of a flood basalt flow field, Roza Member, Columbia River Basalt Province, USA. *Geol Soc Am Bull* 126:875-891
- Burns E, Williams C, Ingebritsen S, Voss C, Spane F, DeAngelo J (2014) Understanding heat and groundwater flow through continental flood basalt provinces: insights gained from alternative models of permeability/depth relationships for the Columbia Plateau, USA. *Geofluids*
- Carracedo Sánchez M, Sarrionandia F, Arostegui J, Eguiluz L, Gil Ibarguchi JI (2012) The transition of spatter to lava-like body in lava fountain deposits: features and examples from the Cabezo Segura volcano (Calatrava, Spain). *J Volcanol Geoth Res* 227–228(0):1-14
- Chadwick WW, Embley RW (1998) Graben formation associated with recent dike intrusions and volcanic eruptions on the mid-ocean ridge. *Journal of Geophysical Research: Solid Earth* 103(B5):9807-9825
- Clark SJ (2014) Constraining diagenetic timings, processes and reservoir quality in igneous-affected basins. PhD Thesis, Durham University, Department of Earth Sciences.
- Connor CB, Conway MF (2000) Basaltic volcanic fields. In: Sigurdsson H (ed) *Encyclopedia of Volcanoes*. Academic Press, San Diego, pp 331-343
- Di Traglia F, Cimorelli C, de Rita D, Gimeno Torrente D (2009) Changing eruptive styles in basaltic explosive volcanism: Examples from Croscat complex scoria cone, Garrotxa Volcanic Field (NE Iberian Peninsula). *J Volcanol Geoth Res* 180(2–4):89-109
- Ebinghaus A, Hartley AJ, Jolley DW, Hole M, Millett J (2014) Lava–Sediment Interaction and Drainage-System Development In A Large Igneous Province: Columbia River Flood Basalt Province, Washington State, USA. *Journal of Sedimentary Research* 84(11):1041-1063
- Fagents SA, Thordarson T (2007) Rootless cones in Iceland and on Mars. In: Chapman M, Skilling IP (eds) *The Geology of Mars: Evidence from Earth-Based Analogues*. Cambridge University Press, pp 151–177
- Fisher RV (1961) Proposed Classification of Volcaniclastic Sediments and Rocks. *Geol Soc Am Bull* 72(9):1409-1414

- Fisher RV (1966) Rocks composed of volcanic fragments and their classification. *Earth-Science Reviews* 1(4):287-298
- Galerne CY, Neumann E-R, Planke S (2008) Emplacement mechanisms of sill complexes: Information from the geochemical architecture of the Golden Valley Sill Complex, South Africa. *J Volcanol Geoth Res* 177(2):425-440
- Galerne CY, Galland O, Neumann E-R, Planke S (2011) 3D relationships between sills and their feeders: evidence from the Golden Valley Sill Complex (Karoo Basin) and experimental modelling. *J Volcanol Geoth Res* 202(3–4):189-199
- Genareau K, Valentine G, Moore G, Hervig R (2010) Mechanisms for transition in eruptive style at a monogenetic scoria cone revealed by microtextural analyses (Lathrop Wells volcano, Nevada, U.S.A.). *B Volcanol* 72(5):593-607
- Geshi N, Kusumoto S, Gudmundsson A (2010) Geometric difference between non-feeder and feeder dikes. *Geology* 38(3):195-198
- Geshi N, Oikawa T (2014) The spectrum of basaltic feeder systems from effusive lava eruption to explosive eruption at Miyakejima volcano, Japan. *B Volcanol* 76(3):1-14
- Goult N, Schofield N (2008) Implications of simple flexure theory for the formation of saucer-shaped sills. *Journal of Structural Geology* 30(7):812-817
- Hamilton CW, Thordarson T, Fagents SA (2010) Explosive lava–water interactions I: architecture and emplacement chronology of volcanic rootless cone groups in the 1783–1784 Laki lava flow, Iceland. *B Volcanol* 72(4):449-467
- Hansen DM, Cartwright J (2006) Saucer-shaped sill with lobate morphology revealed by 3D seismic data: implications for resolving a shallow-level sill emplacement mechanism. *J Geol Soc London* 163(3):509-523
- Holford S, Schofield N (in review) Three-dimensional seismic analysis for non-magmatic reactivation of buried volcanic complexes in sedimentary basins.
- Hooper DM, Sheridan MF (1998) Computer-simulation models of scoria cone degradation. *J Volcanol Geoth Res* 83(3):241-267
- Jerram DA (2002) Volcanology and facies architecture of flood basalts. *Geological Society of America Special Papers* 362:119-132
- Jolley DW, Widdowson M (2005) Did Paleogene North Atlantic rift-related eruptions drive early Eocene climate cooling? *Lithos* 79(3–4):355-366
- Keating G, Valentine G, Krier D, Perry F (2008) Shallow plumbing systems for small-volume basaltic volcanoes. *B Volcanol* 70(5):563-582
- Keszthelyi L, Thordarson T, McEwen A, Haack H, Guilbaud MN, Self S, Rossi MJ (2004) Icelandic analogs to Martian flood lavas. *Geochemistry, Geophysics, Geosystems* 5(11)
- Manville V, Németh K, Kano K (2009) Source to sink: a review of three decades of progress in the understanding of volcanoclastic processes, deposits, and hazards. *Sedimentary Geology* 220(3):136-161
- Mattox TN, Mangan MT (1997) Littoral hydrovolcanic explosions: a case study of lava–seawater interaction at Kilauea Volcano. *J Volcanol Geoth Res* 75(1–2):1-17
- Melchior Larsen L, Ken Pedersen A, Krarup Pedersen G (2006) A subaqueous rootless cone field at Niuluut, Disko, Paleocene of West Greenland. *Lithos* 92(1-2):20-32
- Millett J (2015) Offshore drilling through basaltic sequences: geological heterogeneity and its implications for drilling complications, VMSG, Norwich
- Németh K, Cronin SJ (2007) Syn-and post-eruptive erosion, gully formation, and morphological evolution of a tephra ring in tropical climate erupted in 1913 in West Ambrym, Vanuatu. *Geomorphology* 86(1):115-130
- Németh K, Cronin SJ, Stewart RB, Charley D (2009) Intra- and extra-caldera volcanoclastic facies and geomorphic characteristics of a frequently active mafic island–arc volcano, Ambrym Island, Vanuatu. *Sedimentary Geology* 220(3–4):256-270
- Németh K (2010) Monogenetic volcanic fields: Origin, sedimentary record, and relationship with polygenetic volcanism. *Geological Society of America Special Papers* 470:43-66
- Németh K, Risso C, Nullo F, Kereszturi G (2011) The role of collapsing and cone rafting on eruption style changes and final cone morphology: Los Morados scoria cone, Mendoza, Argentina. *Central European Journal of Geosciences* 3(2):102-118

- Németh K, Cronin SJ (2011) Drivers of explosivity and elevated hazard in basaltic fissure eruptions: the 1913 eruption of Ambrym Volcano, Vanuatu (SW-Pacific). *J Volcanol Geoth Res* 201(1):194-209
- Planke S, Rasmussen T, Rey SS, Myklebust R (2005) Seismic characteristics and distribution of volcanic intrusions and hydrothermal vent complexes in the Vøring and Møre basins. Geological Society, London, Petroleum Geology Conference series 6:833-844
- Pollard DD, Delaney PT, Duffield WA, Endo ET, Okamura AT (1983) Surface deformation in volcanic rift zones. *Tectonophysics* 94(1-4):541-584
- Polteau S, Ferré E, Planke S, Neumann ER, Chevallier L (2008) How are saucer-shaped sills emplaced? Constraints from the Golden Valley Sill, South Africa. *Journal of Geophysical Research: Solid Earth* (1978–2012) 113(B12)
- Rateau R, Schofield N, Smith M (2013) The potential role of igneous intrusions on hydrocarbon migration, West of Shetland. *Petroleum Geoscience* 19(3):259-272
- Raymond AC, Murchison DG (1988) Development of organic maturation in the thermal aureoles of sills and its relation to sediment compaction. *Fuel* 67(12):1599-1608
- Roberts A, White R, Lunnon Z, Christie P, Spitzer R, iSIMM T (2005) Imaging magmatic rocks on the Faroes margin. In: *Petroleum Geology: North-West Europe and Global Perspectives—Proceedings of the 6th Petroleum Geology Conference*. pp 00-01
- Rohrman M (2007) Prospectivity of volcanic basins: Trap delineation and acreage de-risking. *AAPG bulletin* 91(6):915-939
- Rubin AM, Pollard DD (1988) Dike-induced faulting in rift zones of Iceland and Afar. *Geology* 16(5):413-417
- Rubin AM (1992) Dike-induced faulting and graben subsidence in volcanic rift zones. *Journal of Geophysical Research: Solid Earth* 97(B2):1839-1858
- Schofield N, Jolley DW (2013) Development of intra-basaltic lava-field drainage systems within the Faroe–Shetland Basin. *Petroleum Geoscience* 19(3):273-288
- Schutter SR (2003) Occurrences of hydrocarbons in and around igneous rocks. Geological Society, London, Special Publications 214(1):35-68
- Sheriff RE, Geldart L (1995) *Exploration seismology*. Cambridge University Press
- Skilling IP, White JDL, McPhie J (2002) Peperite: a review of magma–sediment mingling. *J Volcanol Geoth Res* 114(1-2):1-17
- Sumner JM (1998) Formation of clastogenic lava flows during fissure eruption and scoria cone collapse: the 1986 eruption of Izu-Oshima Volcano, eastern Japan. *B Volcanol* 60(3):195-212
- Sumner JM, Blake S, Matela RJ, Wolff JA (2005) Spatter. *J Volcanol Geoth Res* 142(1-2):49-65
- Swanson DA, Wright TL, Helz RT (1975) Linear vent systems and estimated rates of magma production and eruption for the Yakima Basalt on the Columbia Plateau. *American Journal of Science* 275(8):877-905
- Taddeucci J, Pompilio M, Scarlato P (2004) Conduit processes during the July–August 2001 explosive activity of Mt. Etna (Italy): inferences from glass chemistry and crystal size distribution of ash particles. *J Volcanol Geoth Res* 137(1-3):33-54
- Takada A (1994) The influence of regional stress and magmatic input on styles of monogenetic and polygenetic volcanism. *Journal of Geophysical Research: Solid Earth* (1978–2012) 99(B7):13563-13573
- Tentler T, Temperley S (2007) Magmatic fissures and their systems in Iceland: A tectonomagmatic model. *Tectonics* 26(5):TC5019
- Thomson K (2007) Determining magma flow in sills, dykes and laccoliths and their implications for sill emplacement mechanisms. *B Volcanol* 70(2):183-201
- Thordarson T, Self S (1993) The Laki (Skaftár Fires) and Grímsvötn eruptions in 1783–1785. *B Volcanol* 55(4):233-263
- Thordarson T, Self S, Oskarsson N, Hulsebosch T (1996) Sulfur, chlorine, and fluorine degassing and atmospheric loading by the 1783–1784 AD Laki (Skaftár Fires) eruption in Iceland. *B Volcanol* 58(2-3):205-225
- Thordarson T, Self S (1998) The Roza Member, Columbia River Basalt Group: A gigantic pahoehoe lava flow field formed by endogenous processes? *J. Geophys. Res.* 103(B11):27411-27445

- Thordarson T, Miller D, Larsen G, Self S, Sigurdsson H (2001) New estimates of sulfur degassing and atmospheric mass-loading by the 934 AD Eldgjá eruption, Iceland. *J Volcanol Geoth Res* 108(1):33-54
- Thordarson T, Larsen G (2007) Volcanism in Iceland in historical time: Volcano types, eruption styles and eruptive history. *Journal of Geodynamics* 43(1):118-152
- Valentine G, Cortés J (2013) Time and space variations in magmatic and phreatomagmatic eruptive processes at Easy Chair (Lunar Crater Volcanic Field, Nevada, USA). *B Volcanol* 75(9):1-13
- Valentine GA, Groves KR (1996) Entrainment of Country Rock during Basaltic Eruptions of the Lucero Volcanic Field, New Mexico. *The Journal of Geology* 104(1):71-90
- Valentine GA, Keating GN (2007) Eruptive styles and inferences about plumbing systems at Hidden Cone and Little Black Peak scoria cone volcanoes (Nevada, USA). *B Volcanol* 70(1):105-113
- Valentine GA, Gregg TKP (2008) Continental basaltic volcanoes — Processes and problems. *J Volcanol Geoth Res* 177(4):857-873
- Valentine GA (2012) Shallow plumbing systems for small-volume basaltic volcanoes, 2: Evidence from crustal xenoliths at scoria cones and maars. *J Volcanol Geoth Res* 223–224(0):47-63
- Walker RJ, Holdsworth RE, Armitage PJ, Faulkner DR (2013) Fault zone permeability structure evolution in basalts. *Geology* 41(1):59-62
- Watton TJ, Cannon S, Brown RJ, Jerram DA, Waichel BL (2014) Using formation micro-imaging, wireline logs and onshore analogues to distinguish volcanic lithofacies in boreholes: examples from Palaeogene successions in the Faroe–Shetland Basin, NE Atlantic. Geological Society, London, Special Publications 397
- White J, Bryan S, Ross P, Self S, Thordarson T (2009) Physical volcanology of continental large igneous provinces: update and review. *Studies in Volcanology: The Legacy of George Walker*. Special Publications of IAVCEI 2:291-321
- White JDL, Houghton BF (2006) Primary volcanoclastic rocks. *Geology* 34(8):677-680
- Wood CA (1980) Morphometric analysis of cinder cone degradation. *J Volcanol Geoth Res* 8(2):137-160
- Zanon V, Pacheco J, Pimentel A (2009) Growth and evolution of an emergent tuff cone: Considerations from structural geology, geomorphology and facies analysis of São Roque volcano, São Miguel (Azores). *J Volcanol Geoth Res* 180(2–4):277-291

Chapter 7: Summary

7.1 Summary and conclusions

Many flood basalt provinces host hydrocarbon reserves. These provinces are constructed as the result of multiple fissure eruptions. This thesis uses data from a dissected subaerial fissure and a submarine volcanic field to help recognise fissure-derived edifices in field, seismic and well data. These edifices are analogous to those produced high volume fissure eruptions. In addition, data from a newly-discovered rootless cone field is used to help distinguish these features from dyke-fed edifices. The edifices described have important implications for hydrocarbon basin development, architecture and fluid flow.

Chapter 3 details the internal architecture of a scoria-agglutinate cone, scoria and spatter ramparts, rootless cones and sheet-like fall deposits produced during a Holocene basaltic fissure eruption. These features formed as a result of variations in lava fountain intensity and lava-water interaction. They allow us to link processes observed in contemporary eruptions with preserved deposits, and inform on the early stages of the eruption which are commonly buried. The scoria-agglutinate cone, spatter ramparts and scoria ramparts have many similarities with edifices produced during high-volume eruptions, suggesting that flood basalt eruptions may also be associated with periods of Hawaiian-style activity. This supports the notion that flood basalt eruptions can be associated with a diversity of emplacement styles.

Chapter 4 provides insights into rootless eruption processes based on dissected tephra deposits and conduits. These eruptions result from explosive lava-water interaction beneath the host lava flow. I have also provided quantitative data on the rootless cone- and platform-building tephra successions, characterising the juvenile clasts and lava-sediment interaction textures that typify these deposits. My research has shown that rootless cones formed in the Columbia River Flood Basalt Province are analogous to rootless cones in Iceland. In both study areas, the explosivity decreases as surface water availability declines. This chapter also shows that juvenile clast morphology and clast density are useful criteria for distinguishing between rootless tephra and tephra generated above an erupting dyke.

Chapter 5 uses well data and exceptional quality 3D seismic data to detail the architecture of submarine basaltic edifices. These edifices are free from overlying basalt cover and are relatively young, making them ideal candidates to inform on the seismic facies and eruption processes that typify submarine monogenetic edifices. I identify three

types of edifice, including maar-diatreme complexes, pillow volcanoes and tuff cones. The edifices are shown to have evolved during a combination of effusive and explosive activity. The spatial relationship of the edifices with underlying lava flows suggests that monogenetic eruptions can be spatially linked over millions of years.

Chapter 8: Future Work

8.1 Directions for future work

Chapter 3 highlights the diversity of lavas and pyroclasts deposited in the fissure-proximal region. Better classifying the petrophysical properties of these deposits will enhance our understanding of the architecture of volcanic-affected basins. Lavas observed include shelly pāhoehoe, clastogenic pāhoehoe, lava-like agglutinate and spiny pāhoehoe. Currently, only hyaloclastite, compound and tabular flows are recognised in wireline data (Nelson et al. 2009). These facies are recognised by variations in P-wave velocity (V_p), a function of vesicularity (Nelson et al. 2009). Shelly pāhoehoe is characterised by vesicular crusts, likely giving them a low V_p response. The clastogenic lavas have variably vesicular cores and vesicular crusts, again likely giving them a low V_p response. Lava-like agglutinate is massive and incipiently vesicular, suggesting it would have a similar V_p response to the cores of tabular classic flows. Spiny pāhoehoe inflates (Guilbaud et al. 2005), thus has a similar internal structure to tabular classic flows. However, the flows described in Chapter 3 are often <10 m thick, suggesting they would be difficult to distinguish from similar-sized compound flows which have variable V_p responses (Nelson et al. 2009).

In order to recognise pyroclasts, it would be necessary to distinguish pyroclastic sequences from other primary volcanoclastic sequences such as hyaloclastite. Hyaloclastite can show spikes in Spectral Gamma Ray responses associated with foraminifera (Watton et al. 2014). Since these microfossils are deposited in a marine environment, they would be uncharacteristic of in-situ subaerial pyroclastic sequences. Hyaloclastite is also recognised by its uniform P-wave distribution (Nelson et al. 2009). However, hyaloclastite is highly variable in its density and componentry (Watton et al. 2013). Therefore, to distinguish pyroclastic sequences from hyaloclastite it would first be necessary to better classify the range of hyaloclastite facies.

Chapter 4 details the products of rootless eruptions. These can be initiated beneath ‘ā‘ā and pāhoehoe lava flows, as well beneath as the deposits of pyroclastic density currents (Moore and Ault 1965; Moyer and Swanson 1987; Fagents et al. 2002; Fagents and Thordarson 2007; Hamilton et al. 2010). Given that ‘ā‘ā lava flows and the deposits of density currents do not inflate, it is possible that rootless eruptions can result from both physical mixing and phreatic-type eruptions (e.g. Mastin 1995; Fagents and Thordarson 2007). However, the substrate beneath the site of rootless eruptions is not commonly exposed. Studies of the substrate may provide insights into the triggering mechanisms for

rootless explosions. It is likely that eruptions resulting from physical mixing preserve evidence of such processes beneath the lava flow, evidenced by peperite-like textures (e.g. Skilling et al. 2002; Hooten and Ort 2002). In contrast, those arising from phreatic-type eruptions may preserve “uncontaminated” sedimentary sequences, or volcanoclastic successions without evidence of molten lava-sediment mixing. Studies could also seek to identify other environmental settings in which rootless cones form (e.g. those without a compressible substrate, see Chapter 3). This would help understand the diversity of settings in which rootless eruptions occur, and better constrain the usefulness of rootless cones as indicators of underlying, water-saturated substrate.

Chapter 5 highlights the superficial similarity of volcanic and hydrothermal edifices in seismic data. Hydrothermal vents are dominated by sedimentary lithologies, but also contain volcanic rocks (e.g. Jamtveit et al. 2004). However, the source and fragmentation mechanism of this material is unknown. A better understanding of the genesis of the volcanic material would have implications for understanding the fragmentation and triggering mechanism for hydrothermal eruptions (e.g. phreatic or MFCI). This could have important implications for understanding the early stages of volcanic activity in rift basins (e.g. Planke et al. 2005).

8.2 References

- Fagents SA, Lanagan P, Greeley R (2002) Rootless cones on Mars: a consequence of lava-ground ice interaction. *Geological Society, London, Special Publications* 202(1):295-317
- Fagents SA, Thordarson T (2007) Rootless cones in Iceland and on Mars. In: Chapman M, Skilling IP (eds) *The Geology of Mars: Evidence from Earth-Based Analogues*. Cambridge University Press, pp 151–177
- Guilbaud M-N, Self S, Thordarson T, Blake S (2005) Morphology, surface structures, and emplacement of lavas produced by Laki, A.D. 1783–1784. *Geological Society of America Special Papers* 396:81-102
- Hamilton CW, Thordarson T, Fagents SA (2010) Explosive lava–water interactions I: architecture and emplacement chronology of volcanic rootless cone groups in the 1783–1784 Laki lava flow, Iceland. *B Volcanol* 72(4):449-467
- Hooten J, Ort M (2002) Peperite as a record of early-stage phreatomagmatic fragmentation processes: an example from the Hopi Buttes volcanic field, Navajo Nation, Arizona, USA. *J Volcanol Geoth Res* 114(1):95-106
- Jamtveit B, Svensen H, Podladchikov YY, Planke S (2004) Hydrothermal vent complexes associated with sill intrusions in sedimentary basins. *Physical geology of high-level magmatic systems* 234:233-241
- Mastin LG (1995) Thermodynamics of gas and steam-blast eruptions. *B Volcanol* 57(2):85-98
- Moore JG, Ault WU (1965) Historic littoral cones in Hawaii. *Pacific science* XIX(3-11)
- Moyer TC, Swanson DA (1987) Secondary hydroeruptions in pyroclastic-flow deposits: Examples from Mount St. Helens. *J Volcanol Geoth Res* 32(4):299-319
- Nelson CE, Jerram DA, Hobbs RW (2009) Flood basalt facies from borehole data: implications for prospectivity and volcanology in volcanic rifted margins. *Petroleum Geoscience* 15(4):313-324

- Planke S, Rasmussen T, Rey SS, Myklebust R (2005) Seismic characteristics and distribution of volcanic intrusions and hydrothermal vent complexes in the Vøring and Møre basins. Geological Society, London, Petroleum Geology Conference series 6:833-844
- Skilling IP, White JDL, McPhie J (2002) Peperite: a review of magma–sediment mingling. *J Volcanol Geoth Res* 114(1–2):1-17
- Watton TJ, Jerram DA, Thordarson T, Davies RJ (2013) Three-dimensional lithofacies variations in hyaloclastite deposits. *J Volcanol Geoth Res* 250(0):19-33
- Watton TJ, Cannon S, Brown RJ, Jerram DA, Waichel BL (2014) Using formation micro-imaging, wireline logs and onshore analogues to distinguish volcanic lithofacies in boreholes: examples from Palaeogene successions in the Faroe–Shetland Basin, NE Atlantic. Geological Society, London, Special Publications 397

Appendix 1: Support Material for Chapter 3

| fault number | strike | dip | fault number | strike | dip | fault number | strike | dip | fault number | strike | dip |
|-----------------|--------|-----|-----------------|--------|-----|-----------------|--------|-----|-----------------|--------|-----|
| XA | 010 | 75 | 13 | 031 | 78 | 31 | 195 | 42 | 9 | 014 | 80 |
| F0 | 191 | 85 | 17 | 007 | 85 | 32 | 047 | 42 | 5 | 187 | 75 |
| 1 | 191 | 85 | 19 | 190 | 78 | 33 | 037 | 80 | 6 | 182 | 85 |
| 2 | 008 | 70 | 20 | 011 | 79 | 38 | 008 | 75 | 21 | 193 | 85 |
| 4 | 010 | 75 | | | | | | | | | |

Table A1.1. Orientations of faults.

| | | | | | | | |
|----------------|-----------|-----------|--------|--------|--------|-------|------------------------|
| waSc | glass | microlite | pyx | olv | lithic | total | matrix crystallinity % |
| count | 734 | 20 | 17 | 1 | 28 | 800 | 4.922 |
| % | 91.7 | 2.5 | 2.1 | 0.1 | 3.5 | | |
| dwSp | glass | microlite | pyx | olv | glass | | 86.1 |
| count | 12 | 181 | 508 | 0 | 99 | 800 | |
| % | 1.5 | 22.6 | 63.5 | 0 | 12.3 | | |
| mwSp | microlite | pyx | glass | glass | | | |
| count | 171 | 447 | 168 | 14 | | 800 | 77.1 |
| % | 21.3 | 55.8 | 21 | 1.7 | | | |
| | | | | | | | |
| waSp | glass | microlite | pyx | olv | | | |
| count | 419 | 302 | 77 | 2 | | 800 | 47.5 |
| % | 52.3 | 37.7 | 9.6 | 0.2 | | | |
| | | | | | | | |
| ScL | glass | microlite | pyx | olv | | | |
| count | 391 | 8 | 1 | 0 | | 400 | 2.25 |
| L-l Agg | 97.75 | 2 | 0.25 | 0 | | | |
| l-l Agg | glass | microlite | pyx | olv | | | |
| count | 198 | 219 | 381 | 2 | | 800 | 75.25 |
| % | 24.75 | 27.375 | 47.625 | 0.25 | | | |
| dwSc | glass | microlite | pyx | olv | | | |
| count | 735 | 46 | 19 | 0 | | 800 | |
| | 91.8 | 5.7 | 2.3 | 0 | | | 8 |
| mwSc | glass | microlite | pyx | olv | plag | | |
| count | 752 | 28 | 10 | 0 | 10 | 800 | |
| | 94 | 3.5 | 1.2 | 0 | 1.2 | | 5.9 |
| Cl | pyx | feld | glass | oxides | | | |
| count | 474 | 206 | 117 | 3 | | 800 | |
| | 59.2 | 25.7 | 14.6 | 0.3 | | | 84.9 |
| dyke | feld | pyx | glass | olv | | | |

| | | | | | | | |
|--|------|------|-------|-----|--|-----|----|
| count | 140 | 546 | 111 | 3 | | | |
| | 17.5 | 68.2 | 13.8 | 0.3 | | 800 | 86 |
| mSc | feld | pyx | glass | olv | | | |
| count | 96 | 8 | 696 | 0 | | | |
| % | 12 | 1 | 87 | 0 | | 800 | 13 |
| Table A1.2. Point count data for lithofacies. | | | | | | | |

| Total unit thickness (mm) | Platy zone spacing (mm) | mean spacing (mm) |
|---|-------------------------|-------------------|
| 12 | 13.45454545 | 7950 |
| 30 | | |
| 14 | | |
| 6 | | |
| 7 | | |
| 10 | | |
| 12 | | |
| 17 | | |
| 14 | | |
| 21 | | |
| 5 | | |
| Table A1.3. Measurements of platy zone in columnar basalt, log 14, unit 4. | | |

| Platy zone spacing (mm) | mean spacing (mm) | Total unit thickness (mm) |
|---|-------------------|---------------------------|
| 65 | 82.22222222 | 1700 |
| 55 | | |
| 70 | | |
| 75 | | |
| 30 | | |
| 90 | | |
| 110 | | |
| 60 | | |
| 60 | | |
| 190 | | |
| Table A1.4. Measurements of platy zone in columnar basalt, Log 30, unit 1. | | |

| Platy zone spacing (mm) | Platy zone spacing (mm) | mean spacing (mm) | Total unit thickness (mm) |
|--|-------------------------|-------------------|---------------------------|
| 25 | 30 | 29.83333333 | 2300 |
| 34 | 29 | | |
| 30 | 16 | | |
| 35 | 69 | | |
| 10 | 65 | | |
| 45 | 12 | | |
| 25 | 16 | | |
| 20 | 46 | | |
| 54 | 10 | | |
| 22 | 42 | | |
| 11 | 10 | | |
| 45 | 14 | | |
| 25 | 16 | | |
| 34 | 30 | | |
| 30 | | | |
| 45 | | | |
| Table A1.5. Measurements of platy zone in columnar basalt, Log 12, unit 11. | | | |

| number | Wc air | | | | Wc+s water | | | Ws water | Wc water | SG | DENSITY kg m ⁻³ | density sorted | density mean of 90 |
|--------|--------------|--------|-------|-------------|------------|------------------|----------|----------------------|--------------------|----------|----------------------------|----------------|--------------------|
| | dry uncoated | coated | wet | ballast wet | clast wet | sheet dry weight | sheet % | sheet wet weight (g) | clast wet no sheet | | | | |
| 1 | 12.06 | 13.42 | 12.24 | 15.78 | -3.54 | 1.36 | 10.13413 | -0.358748137 | -3.181251863 | 0.791274 | 791.2735849 | 623.2091691 | 1007.045387 |
| 2 | 21.77 | 23.06 | 8.12 | 15.78 | -7.66 | 1.29 | 5.594102 | -0.428508239 | -7.231491761 | 0.750651 | 750.6510417 | 634.7634763 | stdev |
| 3 | 5.73 | 6.72 | 13.07 | 15.78 | -2.71 | 0.99 | 14.73214 | -0.399241071 | -2.310758929 | 0.712619 | 712.6193001 | 685.3932584 | 192.7530006 |
| 4 | 13.45 | 14.52 | 18.95 | 15.78 | 3.17 | 1.07 | 7.369146 | 0.233601928 | 2.936398072 | 1.279295 | 1279.295154 | 712.6193001 | |
| 5 | 14.42 | 15.55 | 16.1 | 15.78 | 0.32 | 1.13 | 7.266881 | 0.023254019 | 0.296745981 | 1.021011 | 1021.011162 | 720 | mean of 50 |
| 6 | 14.94 | 16.03 | 14.73 | 15.78 | -1.05 | 1.09 | 6.79975 | -0.07139738 | -0.97860262 | 0.938525 | 938.5245902 | 729.8787211 | 1005.700428 |
| 7 | 8.78 | 9.59 | 14.27 | 15.78 | -1.51 | 0.81 | 8.446298 | -0.127539103 | -1.382460897 | 0.863964 | 863.963964 | 750.6510417 | stdev |
| 8 | 6.98 | 7.67 | 15.16 | 15.78 | -0.62 | 0.69 | 8.996089 | -0.05577575 | -0.56422425 | 0.925211 | 925.2110977 | 788.91258 | 189.3211468 |
| 9 | 4.57 | 5.05 | 14.67 | 15.78 | -1.11 | 0.48 | 9.50495 | -0.10550495 | -1.00449505 | 0.819805 | 819.8051948 | 790.2511078 | |
| 10 | 13.66 | 14.48 | 19.55 | 15.78 | 3.77 | 0.82 | 5.662983 | 0.213494475 | 3.556505525 | 1.352007 | 1352.00747 | 791.2735849 | mean of 30 |
| 11 | 9.7 | 10.86 | 15.11 | 15.78 | -0.67 | 1.16 | 10.6814 | -0.071565378 | -0.598434622 | 0.941891 | 941.8907199 | 796.1165049 | 993.1854134 |
| 12 | 10.36 | 11.17 | 16.73 | 15.78 | 0.95 | 0.81 | 7.251567 | 0.068889884 | 0.881110116 | 1.092955 | 1092.95499 | 806.4516129 | st dev |
| 13 | 7.63 | 8.26 | 14.66 | 15.78 | -1.12 | 0.63 | 7.627119 | -0.085423729 | -1.034576271 | 0.880597 | 880.5970149 | 807.0866142 | 214.3864122 |
| 14 | 8.26 | 8.82 | 12.35 | 15.78 | -3.43 | 0.56 | 6.349206 | -0.217777778 | -3.212222222 | 0.72 | 720 | 811.5653041 | |
| 15 | 10.05 | 10.62 | 17.62 | 15.78 | 1.84 | 0.57 | 5.367232 | 0.098757062 | 1.741242938 | 1.209567 | 1209.567198 | 811.9001919 | vesic |
| 16 | 12.28 | 12.87 | 16.6 | 15.78 | 0.82 | 0.59 | 4.584305 | 0.037591298 | 0.782408702 | 1.06805 | 1068.049793 | 812.2119816 | 66.4766524 |
| 17 | 6.82 | 7.4 | 13.8 | 15.78 | -1.98 | 0.58 | 7.837838 | -0.155189189 | -1.824810811 | 0.788913 | 788.91258 | 819.3717277 | 79.23333333 |
| 18 | 5.62 | 6.15 | 14.31 | 15.78 | -1.47 | 0.53 | 8.617886 | -0.126682927 | -1.343317073 | 0.807087 | 807.0866142 | 819.8051948 | 51.13333333 |
| 19 | 15.84 | 16.47 | 19.55 | 15.78 | 3.77 | 0.63 | 3.825137 | 0.14420765 | 3.62579235 | 1.29685 | 1296.850394 | 821.0639441 | |
| 20 | 9.62 | 10.2 | 16.83 | 15.78 | 1.05 | 0.58 | 5.686275 | 0.059705882 | 0.990294118 | 1.114754 | 1114.754098 | 825.8212376 | |
| 21 | 11.29 | 12.15 | 14.95 | 15.78 | -0.83 | 0.86 | 7.078189 | -0.058748971 | -0.771251029 | 0.936055 | 936.05547 | 839.348903 | |
| 22 | 8.37 | 8.72 | 14.63 | 15.78 | -1.15 | 0.35 | 4.013761 | -0.046158257 | -1.103841743 | 0.883485 | 883.485309 | 841.7266187 | |
| 23 | 13.26 | 13.82 | 18.68 | 15.78 | 2.9 | 0.56 | 4.052098 | 0.117510854 | 2.782489146 | 1.265568 | 1265.567766 | 859.2132505 | |
| 24 | 17.61 | 18.21 | 20.53 | 15.78 | 4.75 | 0.6 | 3.294893 | 0.156507414 | 4.593492586 | 1.352897 | 1352.897474 | 861.0763454 | |
| 25 | 13.44 | 14.13 | 18.38 | 15.78 | 2.6 | 0.69 | 4.883227 | 0.126963907 | 2.473036093 | 1.225499 | 1225.498699 | 863.67713 | |
| 26 | 10.01 | 10.81 | 13.5 | 15.78 | -2.28 | 0.8 | 7.400555 | -0.168732655 | -2.111267345 | 0.825821 | 825.8212376 | 863.963964 | |
| 27 | 5.11 | 5.77 | 12.46 | 15.78 | -3.32 | 0.66 | 11.43847 | -0.379757366 | -2.940242634 | 0.634763 | 634.7634763 | 866.1242604 | |
| 28 | 15.01 | 15.71 | 13.41 | 15.78 | -2.37 | 0.7 | 4.455761 | -0.105601528 | -2.264398472 | 0.868916 | 868.9159292 | 868.9159292 | |
| 29 | 15.29 | 15.78 | 19.31 | 15.78 | 3.53 | 0.49 | 3.105196 | 0.109613435 | 3.420386565 | 1.288163 | 1288.163265 | 871.4285714 | |
| 30 | 7.41 | 7.93 | 16.75 | 15.78 | 0.97 | 0.52 | 6.557377 | 0.063606557 | 0.906393443 | 1.139368 | 1139.367816 | 880.5970149 | |
| 31 | 10 | 10.7 | 12.94 | 15.78 | -2.84 | 0.7 | 6.542056 | -0.185794393 | -2.654205607 | 0.790251 | 790.2511078 | 883.485309 | |
| 32 | 11.2 | 11.88 | 14.35 | 15.78 | -1.43 | 0.68 | 5.723906 | -0.081851852 | -1.348148148 | 0.892562 | 892.5619835 | 892.5619835 | |
| 33 | 20.03 | 20.74 | 20.58 | 15.78 | 4.8 | 0.71 | 3.423337 | 0.164320154 | 4.635679846 | 1.301129 | 1301.129235 | 913.9344262 | |
| 34 | 16.95 | 17.59 | 15.79 | 15.78 | 0.01 | 0.64 | 3.638431 | 0.000363843 | 0.009636157 | 1.000569 | 1000.568828 | 914.3730887 | |
| 35 | 13.5 | 14.1 | 17.67 | 15.78 | 1.89 | 0.6 | 4.255319 | 0.080425532 | 1.809574468 | 1.154791 | 1154.791155 | 925.2110977 | |
| 36 | 22.79 | 23.41 | 18.72 | 15.78 | 2.94 | 0.62 | 2.648441 | 0.077864161 | 2.862135839 | 1.143625 | 1143.624817 | 935.483871 | |
| 37 | 10.25 | 10.98 | 14.16 | 15.78 | -1.62 | 0.73 | 6.648452 | -0.107704918 | -1.512295082 | 0.871429 | 871.4285714 | 936.05547 | |
| 38 | 13.43 | 14.03 | 18.48 | 15.78 | 2.7 | 0.6 | 4.27655 | 0.115466857 | 2.584533143 | 1.238305 | 1238.305384 | 938.4449244 | |

| | | | | | | | | | | | | | |
|----|-------|-------|-------|-------|-------|------|----------|--------------|--------------|----------|-------------|-------------|--|
| 39 | 13.43 | 14.05 | 16.92 | 15.78 | 1.14 | 0.62 | 4.412811 | 0.05030605 | 1.08969395 | 1.088304 | 1088.303641 | 938.5245902 | |
| 40 | 10.22 | 10.84 | 15.97 | 15.78 | 0.19 | 0.62 | 5.719557 | 0.010867159 | 0.179132841 | 1.01784 | 1017.840376 | 941.8907199 | |
| 41 | 4.02 | 4.46 | 15.36 | 15.78 | -0.42 | 0.44 | 9.865471 | -0.041434978 | -0.378565022 | 0.913934 | 913.9344262 | 956.2101911 | |
| 42 | 5.46 | 5.98 | 15.22 | 15.78 | -0.56 | 0.52 | 8.695652 | -0.048695652 | -0.511304348 | 0.914373 | 914.3730887 | 967.1574179 | |
| 43 | 6.42 | 6.82 | 16.25 | 15.78 | 0.47 | 0.4 | 5.865103 | 0.027565982 | 0.442434018 | 1.074016 | 1074.015748 | 980.5886036 | |
| 44 | 6.25 | 7.05 | 14.15 | 15.78 | -1.63 | 0.8 | 11.34752 | -0.184964539 | -1.445035461 | 0.812212 | 812.2119816 | 984.9219171 | |
| 45 | 11.71 | 12.32 | 15.62 | 15.78 | -0.16 | 0.61 | 4.951299 | -0.007922078 | -0.152077922 | 0.987179 | 987.1794872 | 987.1794872 | |
| 46 | 20.22 | 21.02 | 19.25 | 15.78 | 3.47 | 0.8 | 3.805899 | 0.1320647 | 3.3379353 | 1.197721 | 1197.720798 | 987.2611465 | |
| 47 | 7.09 | 9.63 | 14.26 | 15.78 | -1.52 | 2.54 | 26.37591 | -0.400913811 | -1.119086189 | 0.863677 | 863.67713 | 1000.568828 | |
| 48 | 13.49 | 13.92 | 16.94 | 15.78 | 1.16 | 0.43 | 3.08908 | 0.035833333 | 1.124166667 | 1.090909 | 1090.909091 | 1017.840376 | |
| 49 | 11.18 | 11.8 | 17.49 | 15.78 | 1.71 | 0.62 | 5.254237 | 0.089847458 | 1.620152542 | 1.169475 | 1169.474727 | 1021.011162 | |
| 50 | 8.02 | 8.54 | 15.49 | 15.78 | -0.29 | 0.52 | 6.088993 | -0.01765808 | -0.27234192 | 0.967157 | 967.1574179 | 1025.929127 | |
| 51 | 11.36 | 11.85 | 16.12 | 15.78 | 0.34 | 0.49 | 4.135021 | 0.014059072 | 0.325940928 | 1.02954 | 1029.539531 | 1027.681661 | |
| 52 | 9.38 | 9.75 | 16.14 | 15.78 | 0.36 | 0.37 | 3.794872 | 0.013661538 | 0.346338462 | 1.038339 | 1038.338658 | 1029.539531 | |
| 53 | 7.57 | 8.3 | 14.42 | 15.78 | -1.36 | 0.73 | 8.795181 | -0.119614458 | -1.240385542 | 0.859213 | 859.2132505 | 1038.338658 | |
| 54 | 7.18 | 7.75 | 13.92 | 15.78 | -1.86 | 0.57 | 7.354839 | -0.1368 | -1.7232 | 0.806452 | 806.4516129 | 1047.012733 | |
| 55 | 11.3 | 12.01 | 15.23 | 15.78 | -0.55 | 0.71 | 5.91174 | -0.032514571 | -0.517485429 | 0.95621 | 956.2101911 | 1068.049793 | |
| 56 | 11.23 | 11.88 | 16.1 | 15.78 | 0.32 | 0.65 | 5.47138 | 0.017508418 | 0.302491582 | 1.027682 | 1027.681661 | 1074.015748 | |
| 57 | 17.03 | 17.63 | 19.09 | 15.78 | 3.31 | 0.6 | 3.40329 | 0.112648894 | 3.197351106 | 1.231145 | 1231.145251 | 1077.887198 | |
| 58 | 10.97 | 11.6 | 14.98 | 15.78 | -0.8 | 0.63 | 5.431034 | -0.043448276 | -0.756551724 | 0.935484 | 935.483871 | 1081.166273 | |
| 59 | 13.98 | 14.83 | 19.6 | 15.78 | 3.82 | 0.85 | 5.731625 | 0.218948078 | 3.601051922 | 1.346957 | 1346.957312 | 1082.106894 | |
| 60 | 6.17 | 6.88 | 14.67 | 15.78 | -1.11 | 0.71 | 10.31977 | -0.114549419 | -0.995450581 | 0.861076 | 861.0763454 | 1088.303641 | |
| 61 | 15.42 | 16.12 | 18.85 | 15.78 | 3.07 | 0.7 | 4.342432 | 0.133312655 | 2.936687345 | 1.235249 | 1235.249042 | 1090.909091 | |
| 62 | 13.3 | 13.97 | 16.84 | 15.78 | 1.06 | 0.67 | 4.795991 | 0.050837509 | 1.009162491 | 1.082107 | 1082.106894 | 1092.95499 | |
| 63 | 14.71 | 15.52 | 20.49 | 15.78 | 4.71 | 0.81 | 5.219072 | 0.245818299 | 4.464181701 | 1.435708 | 1435.707678 | 1103.673469 | |
| 64 | 13.42 | 14.22 | 17.42 | 15.78 | 1.64 | 0.8 | 5.625879 | 0.092264416 | 1.547735584 | 1.130366 | 1130.36566 | 1114.754098 | |
| 65 | 10.83 | 11.87 | 16.08 | 15.78 | 0.3 | 1.04 | 8.761584 | 0.026284751 | 0.273715249 | 1.025929 | 1025.929127 | 1130.36566 | |
| 66 | 12.79 | 13.72 | 16.81 | 15.78 | 1.03 | 0.93 | 6.778426 | 0.069817784 | 0.960182216 | 1.081166 | 1081.166273 | 1139.367816 | |
| 67 | 14.55 | 15.28 | 12.45 | 15.78 | -3.33 | 0.73 | 4.777487 | -0.159090314 | -3.170909686 | 0.821064 | 821.0639441 | 1143.624817 | |
| 68 | 9.94 | 10.69 | 16.26 | 15.78 | 0.48 | 0.75 | 7.015903 | 0.033676333 | 0.446323667 | 1.047013 | 1047.012733 | 1154.791155 | |
| 69 | 12.78 | 13.52 | 17.05 | 15.78 | 1.27 | 0.74 | 5.473373 | 0.069511834 | 1.200488166 | 1.103673 | 1103.673469 | 1169.474727 | |
| 70 | 6.6 | 7.32 | 12.42 | 15.78 | -3.36 | 0.72 | 9.836066 | -0.330491803 | -3.029508197 | 0.685393 | 685.3932584 | 1176.591376 | |
| 71 | 17.68 | 18.29 | 15.5 | 15.78 | -0.28 | 0.61 | 3.335156 | -0.009338436 | -0.270661564 | 0.984922 | 984.9219171 | 1187.977099 | |
| 72 | 11.13 | 11.86 | 13.51 | 15.78 | -2.27 | 0.73 | 6.155143 | -0.139721754 | -2.130278246 | 0.839349 | 839.348903 | 1197.720798 | |
| 73 | 8.05 | 8.7 | 10.52 | 15.78 | -5.26 | 0.65 | 7.471264 | -0.392988506 | -4.867011494 | 0.623209 | 623.2091691 | 1209.567198 | |
| 74 | 8.6 | 9.39 | 13.71 | 15.78 | -2.07 | 0.79 | 8.413206 | -0.174153355 | -1.895846645 | 0.819372 | 819.3717277 | 1213.496933 | |
| 75 | 5.86 | 6.62 | 13.33 | 15.78 | -2.45 | 0.76 | 11.48036 | -0.281268882 | -2.168731118 | 0.729879 | 729.8787211 | 1225.498699 | |
| 76 | 10.63 | 11.46 | 17.5 | 15.78 | 1.72 | 0.83 | 7.242583 | 0.124572426 | 1.595427574 | 1.176591 | 1176.591376 | 1227.321238 | |
| 77 | 10.84 | 11.71 | 13.97 | 15.78 | -1.81 | 0.87 | 7.429547 | -0.134474808 | -1.675525192 | 0.866124 | 866.1242604 | 1228.571429 | |
| 78 | 7.63 | 8.14 | 13.89 | 15.78 | -1.89 | 0.51 | 6.265356 | -0.118415233 | -1.771584767 | 0.811565 | 811.5653041 | 1231.145251 | |
| 79 | 10.99 | 11.61 | 17.94 | 15.78 | 2.16 | 0.62 | 5.340224 | 0.115348837 | 2.044651163 | 1.228571 | 1228.571429 | 1235.249042 | |
| 80 | 8.51 | 9.36 | 14.02 | 15.78 | -1.76 | 0.85 | 9.081197 | -0.15982906 | -1.60017094 | 0.841727 | 841.7266187 | 1238.305384 | |
| 81 | 9.12 | 9.84 | 13.26 | 15.78 | -2.52 | 0.72 | 7.317073 | -0.184390244 | -2.335609756 | 0.796117 | 796.1165049 | 1265.567766 | |
| 82 | 18.88 | 19.78 | 19.26 | 15.78 | 3.48 | 0.9 | 4.550051 | 0.158341759 | 3.321658241 | 1.213497 | 1213.496933 | 1279.295154 | |
| 83 | 7.82 | 8.46 | 13.82 | 15.78 | -1.96 | 0.64 | 7.565012 | -0.148274232 | -1.811725768 | 0.8119 | 811.9001919 | 1288.163265 | |

| | | | | | | | | | | | | | |
|--|-------|-------|-------|-------|-------|------|----------|--------------|--------------|----------|-------------|-------------|--|
| 84 | 8.55 | 9.3 | 15.66 | 15.78 | -0.12 | 0.75 | 8.064516 | -0.009677419 | -0.110322581 | 0.987261 | 987.2611465 | 1296.850394 | |
| 85 | 7.88 | 8.69 | 15.21 | 15.78 | -0.57 | 0.81 | 9.321059 | -0.053130035 | -0.516869965 | 0.938445 | 938.4449244 | 1301.129235 | |
| 86 | 14.89 | 15.66 | 15.47 | 15.78 | -0.31 | 0.77 | 4.916986 | -0.015242656 | -0.294757344 | 0.980589 | 980.5886036 | 1346.957312 | |
| 87 | 11.3 | 12.04 | 16.65 | 15.78 | 0.87 | 0.74 | 6.146179 | 0.053471761 | 0.816528239 | 1.077887 | 1077.887198 | 1352.00747 | |
| 88 | 20 | 20.89 | 22.43 | 15.78 | 6.65 | 0.89 | 4.260412 | 0.283317377 | 6.366682623 | 1.466994 | 1466.994382 | 1352.897474 | |
| 89 | 10.63 | 11.5 | 17.91 | 15.78 | 2.13 | 0.87 | 7.565217 | 0.16113913 | 1.96886087 | 1.227321 | 1227.321238 | 1435.707678 | |
| 90 | 11.94 | 12.45 | 17.75 | 15.78 | 1.97 | 0.51 | 4.096386 | 0.080698795 | 1.889301205 | 1.187977 | 1187.977099 | 1466.994382 | |
| Table A1.6. Density measurements for waSp. | | | | | | | | | | | | | |

| number | | | | Wc+s water | | | Ws water | Wc water | SG | DENSITY kg m^-3 | density sorted | density range | density mean of 90 |
|--------|-------|-------|-------|------------|------------------|----------|----------------------|--------------------|----------|-----------------|----------------|---------------|--------------------|
| | | | | clast wet | sheet dry weight | sheet % | sheet wet weight (g) | clast wet no sheet | | | | | |
| 1 | 16.3 | 16.75 | 9.07 | 9.07 | 0.45 | 2.686567 | 0.243671642 | 8.826328358 | 2.18099 | 2180.989583 | 1374.331551 | 1374 | 1835.79601 |
| 2 | 12.86 | 13.2 | 6.15 | 6.15 | 0.34 | 2.575758 | 0.158409091 | 5.991590909 | 1.87234 | 1872.340426 | 1459.71564 | 2218 | 208.2805532 |
| 3 | 13.04 | 13.33 | 7.08 | 7.08 | 0.29 | 2.175544 | 0.154028507 | 6.925971493 | 2.1328 | 2132.8 | 1470.760234 | | |
| 4 | 14.45 | 14.72 | 7.32 | 7.32 | 0.27 | 1.834239 | 0.134266304 | 7.185733696 | 1.989189 | 1989.189189 | 1473.537604 | | mean of 50 |
| 5 | 12.4 | 12.73 | 4.81 | 4.81 | 0.33 | 2.592302 | 0.124689709 | 4.685310291 | 1.607323 | 1607.323232 | 1492.783505 | | 1835.79601 |
| 6 | 15.41 | 15.87 | 5.1 | 5.1 | 0.46 | 2.898551 | 0.147826087 | 4.952173913 | 1.473538 | 1473.537604 | 1548.75717 | | stdev |
| 7 | 13.18 | 13.46 | 5.34 | 5.34 | 0.28 | 2.080238 | 0.111084695 | 5.228915305 | 1.657635 | 1657.635468 | 1551.214361 | | 207.7034687 |
| 8 | 14.94 | 15.44 | 6.47 | 6.47 | 0.5 | 3.238342 | 0.209520725 | 6.260479275 | 1.721293 | 1721.2932 | 1581.294964 | | |
| 9 | 29.49 | 30.02 | 13.8 | 13.8 | 0.53 | 1.76549 | 0.243637575 | 13.55636243 | 1.850801 | 1850.80148 | 1582.371459 | | mean of 30 |
| 10 | 21.24 | 21.85 | 10.76 | 10.76 | 0.61 | 2.791762 | 0.300393593 | 10.45960641 | 1.970243 | 1970.243463 | 1607.323232 | | 1880.072076 |
| 11 | 10.93 | 11.22 | 4.89 | 4.89 | 0.29 | 2.58467 | 0.126390374 | 4.763609626 | 1.772512 | 1772.511848 | 1657.635468 | | st dev |
| 12 | 27.18 | 27.7 | 13.75 | 13.75 | 0.52 | 1.877256 | 0.258122744 | 13.49187726 | 1.985663 | 1985.663082 | 1675.115207 | | 207.7316072 |
| 13 | 14.37 | 14.63 | 7.16 | 7.16 | 0.26 | 1.77717 | 0.127245386 | 7.032754614 | 1.958501 | 1958.500669 | 1700.205339 | | |
| 14 | 20.15 | 20.62 | 10.35 | 10.35 | 0.47 | 2.27934 | 0.235911736 | 10.11408826 | 2.00779 | 2007.789679 | 1709.849157 | | vesic |
| 15 | 25.99 | 26.33 | 12.67 | 12.67 | 0.34 | 1.291303 | 0.163608052 | 12.50639195 | 1.927526 | 1927.525622 | 1721.2932 | | 38.80679965 |
| 16 | 9.94 | 10.27 | 5.64 | 5.64 | 0.33 | 3.213242 | 0.181226874 | 5.458773126 | 2.218143 | 2218.142549 | 1738.317757 | | 54.2 |
| 17 | 29.31 | 29.7 | 14.46 | 14.46 | 0.39 | 1.313131 | 0.189878788 | 14.27012121 | 1.948819 | 1948.818898 | 1772.511848 | | 26.06666667 |
| 18 | 17.34 | 17.64 | 8.86 | 8.86 | 0.3 | 1.70068 | 0.150680272 | 8.709319728 | 2.009112 | 2009.111617 | 1773.672055 | | |
| 19 | 6.88 | 7.24 | 2.39 | 2.39 | 0.36 | 4.972376 | 0.118839779 | 2.271160221 | 1.492784 | 1492.783505 | 1775.655022 | | |
| 20 | 6.77 | 7.07 | 3.16 | 3.16 | 0.3 | 4.243281 | 0.134087694 | 3.025912306 | 1.808184 | 1808.184143 | 1801.438849 | | |
| 21 | 14.73 | 14.92 | 7.22 | 7.22 | 0.19 | 1.273458 | 0.0919437 | 7.1280563 | 1.937662 | 1937.662338 | 1802.904564 | | |
| 22 | 17.27 | 17.38 | 7.74 | 7.74 | 0.11 | 0.632911 | 0.048987342 | 7.691012658 | 1.802905 | 1802.904564 | 1808.184143 | | |
| 23 | 14.55 | 15.08 | 5.55 | 5.55 | 0.53 | 3.514589 | 0.195059682 | 5.354940318 | 1.582371 | 1582.371459 | 1850.80148 | | |
| 24 | 13.33 | 13.62 | 6.75 | 6.75 | 0.29 | 2.129222 | 0.143722467 | 6.606277533 | 1.982533 | 1982.532751 | 1870.198675 | | |
| 25 | 19.06 | 19.33 | 10.41 | 10.41 | 0.27 | 1.396793 | 0.145406105 | 10.2645939 | 2.16704 | 2167.040359 | 1872.340426 | | |
| 26 | 15.85 | 16.15 | 8.14 | 8.14 | 0.3 | 1.857585 | 0.15120743 | 7.98879257 | 2.01623 | 2016.229713 | 1874.055416 | | |
| 27 | 9.79 | 10.06 | 3.22 | 3.22 | 0.27 | 2.683897 | 0.086421471 | 3.133578529 | 1.47076 | 1470.760234 | 1887.675507 | | |
| 28 | 11.81 | 12.1 | 5.69 | 5.69 | 0.29 | 2.396694 | 0.136371901 | 5.553628099 | 1.887676 | 1887.675507 | 1924.348379 | | |

| | | | | | | | | | | | | | |
|----|-------|-------|-------|-------|------|----------|-------------|-------------|----------|-------------|-------------|--|--|
| 29 | 7.15 | 7.44 | 3.47 | 3.47 | 0.29 | 3.897849 | 0.135255376 | 3.334744624 | 1.874055 | 1874.055416 | 1926.486486 | | |
| 30 | 11.55 | 11.82 | 6.18 | 6.18 | 0.27 | 2.284264 | 0.141167513 | 6.038832487 | 2.095745 | 2095.744681 | 1927.525622 | | |
| 31 | 17.42 | 17.82 | 8.57 | 8.57 | 0.4 | 2.244669 | 0.192368126 | 8.377631874 | 1.926486 | 1926.486486 | 1935.135135 | | |
| 32 | 31.9 | 32.53 | 14.21 | 14.21 | 0.63 | 1.936674 | 0.275201353 | 13.93479865 | 1.775655 | 1775.655022 | 1937.662338 | | |
| 33 | 13.66 | 13.95 | 7.08 | 7.08 | 0.29 | 2.078853 | 0.147182796 | 6.932817204 | 2.030568 | 2030.567686 | 1948.324022 | | |
| 34 | 13.72 | 14.12 | 6.57 | 6.57 | 0.4 | 2.832861 | 0.18611898 | 6.38388102 | 1.870199 | 1870.198675 | 1948.818898 | | |
| 35 | 15.08 | 15.36 | 6.7 | 6.7 | 0.28 | 1.822917 | 0.122135417 | 6.577864583 | 1.773672 | 1773.672055 | 1958.500669 | | |
| 36 | 15.02 | 15.4 | 4.85 | 4.85 | 0.38 | 2.467532 | 0.119675325 | 4.730324675 | 1.459716 | 1459.71564 | 1970.243463 | | |
| 37 | 24.56 | 25.04 | 11.14 | 11.14 | 0.48 | 1.916933 | 0.213546326 | 10.92645367 | 1.801439 | 1801.438849 | 1982.532751 | | |
| 38 | 18.82 | 19.27 | 8 | 8 | 0.45 | 2.335236 | 0.186818889 | 7.813181111 | 1.709849 | 1709.849157 | 1985.663082 | | |
| 39 | 14.38 | 14.69 | 5.22 | 5.22 | 0.31 | 2.110279 | 0.110156569 | 5.109843431 | 1.551214 | 1551.214361 | 1989.189189 | | |
| 40 | 6.91 | 7.16 | 3.46 | 3.46 | 0.25 | 3.49162 | 0.120810056 | 3.339189944 | 1.935135 | 1935.135135 | 2007.789679 | | |
| 41 | 13.71 | 13.95 | 6.79 | 6.79 | 0.24 | 1.72043 | 0.116817204 | 6.673182796 | 1.948324 | 1948.324022 | 2009.111617 | | |
| 42 | 9.65 | 9.91 | 5 | 5 | 0.26 | 2.623613 | 0.131180626 | 4.868819374 | 2.01833 | 2018.329939 | 2016.229713 | | |
| 43 | 9.35 | 9.61 | 4.91 | 4.91 | 0.26 | 2.705515 | 0.132840791 | 4.777159209 | 2.044681 | 2044.680851 | 2018.329939 | | |
| 44 | 7.4 | 7.71 | 2.1 | 2.1 | 0.31 | 4.020752 | 0.084435798 | 2.015564202 | 1.374332 | 1374.331551 | 2030.567686 | | |
| 45 | 10.71 | 10.99 | 4.04 | 4.04 | 0.28 | 2.547771 | 0.102929936 | 3.937070064 | 1.581295 | 1581.294964 | 2044.680851 | | |
| 46 | 16.32 | 16.56 | 6.82 | 6.82 | 0.24 | 1.449275 | 0.09884058 | 6.72115942 | 1.700205 | 1700.205339 | 2095.744681 | | |
| 47 | 7.19 | 7.44 | 3.16 | 3.16 | 0.25 | 3.360215 | 0.106182796 | 3.053817204 | 1.738318 | 1738.317757 | 2132.8 | | |
| 48 | 7 | 7.27 | 2.93 | 2.93 | 0.27 | 3.713893 | 0.108817056 | 2.821182944 | 1.675115 | 1675.115207 | 2167.040359 | | |
| 49 | 7.8 | 8.1 | 2.87 | 2.87 | 0.3 | 3.703704 | 0.106296296 | 2.763703704 | 1.548757 | 1548.75717 | 2180.989583 | | |
| 50 | 29.83 | 30.27 | 14.54 | 14.54 | 0.44 | 1.453584 | 0.211351173 | 14.32864883 | 1.924348 | 1924.348379 | 2218.142549 | | |
| 51 | 25.64 | 26.13 | 13.63 | 13.63 | 0.49 | 1.875239 | 0.255595101 | 13.3744049 | 2.0904 | 2090.4 | | | |
| 52 | 26.33 | 26.92 | 12.61 | 12.61 | 0.59 | 2.191679 | 0.276370728 | 12.33362927 | 1.881202 | 1881.201957 | | | |
| 53 | 20.99 | 21.33 | 10.72 | 10.72 | 0.34 | 1.593999 | 0.170876699 | 10.5491233 | 2.010368 | 2010.367578 | | | |
| 54 | 19.16 | 19.61 | 8.26 | 8.26 | 0.45 | 2.294748 | 0.18954615 | 8.07045385 | 1.727753 | 1727.753304 | | | |
| 55 | 16.07 | 16.45 | 7.24 | 7.24 | 0.38 | 2.31003 | 0.167246201 | 7.072753799 | 1.786102 | 1786.102063 | | | |
| 56 | 14.54 | 14.91 | 7.59 | 7.59 | 0.37 | 2.481556 | 0.188350101 | 7.401649899 | 2.036885 | 2036.885246 | | | |
| 57 | 22.12 | 22.52 | 11.01 | 11.01 | 0.4 | 1.776199 | 0.195559503 | 10.8144405 | 1.95656 | 1956.559513 | | | |
| 58 | 17.32 | 17.69 | 8.4 | 8.4 | 0.37 | 2.091577 | 0.175692482 | 8.224307518 | 1.904198 | 1904.198062 | | | |
| 59 | 14.2 | 14.52 | 5.86 | 5.86 | 0.32 | 2.203857 | 0.129146006 | 5.730853994 | 1.676674 | 1676.674365 | | | |
| 60 | 16.11 | 16.4 | 6.84 | 6.84 | 0.29 | 1.768293 | 0.12095122 | 6.71904878 | 1.715481 | 1715.481172 | | | |
| 61 | 17.39 | 17.75 | 8.18 | 8.18 | 0.36 | 2.028169 | 0.165904225 | 8.014095775 | 1.854754 | 1854.754441 | | | |
| 62 | 18.42 | 18.94 | 6.25 | 6.25 | 0.52 | 2.745512 | 0.171594509 | 6.078405491 | 1.492514 | 1492.51379 | | | |
| 63 | 13.45 | 13.75 | 6.31 | 6.31 | 0.3 | 2.181818 | 0.137672727 | 6.172327273 | 1.848118 | 1848.11828 | | | |
| 64 | 16.65 | 16.94 | 8.13 | 8.13 | 0.29 | 1.711924 | 0.139179457 | 7.990820543 | 1.922815 | 1922.814983 | | | |
| 65 | 15.46 | 15.8 | 8.48 | 8.48 | 0.34 | 2.151899 | 0.182481013 | 8.297518987 | 2.15847 | 2158.469945 | | | |
| 66 | 22.69 | 23.12 | 12.43 | 12.43 | 0.43 | 1.859862 | 0.231180796 | 12.1988192 | 2.162769 | 2162.768943 | | | |
| 67 | 20.16 | 20.63 | 8.71 | 8.71 | 0.47 | 2.278236 | 0.198434319 | 8.511565681 | 1.730705 | 1730.704698 | | | |
| 68 | 14.27 | 14.56 | 6.98 | 6.98 | 0.29 | 1.991758 | 0.139024725 | 6.840975275 | 1.920844 | 1920.844327 | | | |
| 69 | 19.42 | 19.73 | 9.63 | 9.63 | 0.31 | 1.571211 | 0.151307653 | 9.478692347 | 1.953465 | 1953.465347 | | | |
| 70 | 14.05 | 14.32 | 6.2 | 6.2 | 0.27 | 1.885475 | 0.116899441 | 6.083100559 | 1.763547 | 1763.546798 | | | |
| 71 | 11.82 | 12.11 | 5.79 | 5.79 | 0.29 | 2.394715 | 0.138654005 | 5.651345995 | 1.916139 | 1916.139241 | | | |
| 72 | 8.32 | 8.61 | 3.87 | 3.87 | 0.29 | 3.368177 | 0.130348432 | 3.739651568 | 1.816456 | 1816.455696 | | | |
| 73 | 17.63 | 17.89 | 9.42 | 9.42 | 0.26 | 1.453326 | 0.136903298 | 9.283096702 | 2.112161 | 2112.160567 | | | |

| | | | | | | | | | | | | | |
|--|-------|-------|-------|-------|------|----------|-------------|-------------|----------|-------------|--|--|--|
| 74 | 16.48 | 16.75 | 8.4 | 8.4 | 0.27 | 1.61194 | 0.135402985 | 8.264597015 | 2.005988 | 2005.988024 | | | |
| 75 | 9.18 | 9.46 | 3.95 | 3.95 | 0.28 | 2.959831 | 0.116913319 | 3.833086681 | 1.716878 | 1716.878403 | | | |
| 76 | 16.75 | 17.04 | 9.48 | 9.48 | 0.29 | 1.701878 | 0.161338028 | 9.318661972 | 2.253968 | 2253.968254 | | | |
| 77 | 15.41 | 15.71 | 8.34 | 8.34 | 0.3 | 1.909612 | 0.159261617 | 8.180738383 | 2.131615 | 2131.614654 | | | |
| 78 | 26.9 | 27.48 | 14.2 | 14.2 | 0.58 | 2.110626 | 0.299708879 | 13.90029112 | 2.069277 | 2069.277108 | | | |
| 79 | 20.39 | 20.73 | 9.56 | 9.56 | 0.34 | 1.640135 | 0.156796913 | 9.403203087 | 1.855864 | 1855.863921 | | | |
| 80 | 21.65 | 22.12 | 11.85 | 11.85 | 0.47 | 2.124774 | 0.251785714 | 11.59821429 | 2.153846 | 2153.846154 | | | |
| 81 | 34.4 | 34.85 | 8.57 | 8.57 | 0.45 | 1.291248 | 0.110659971 | 8.459340029 | 1.326104 | 1326.103501 | | | |
| 82 | 23.79 | 24.17 | 11.08 | 11.08 | 0.38 | 1.572197 | 0.174199421 | 10.90580058 | 1.846448 | 1846.44767 | | | |
| 83 | 14.06 | 14.38 | 5.19 | 5.19 | 0.32 | 2.225313 | 0.115493741 | 5.074506259 | 1.564744 | 1564.744287 | | | |
| 84 | 14.65 | 15.05 | 5.9 | 5.9 | 0.4 | 2.657807 | 0.156810631 | 5.743189369 | 1.644809 | 1644.808743 | | | |
| 85 | 25.02 | 25.48 | 13.1 | 13.1 | 0.46 | 1.805338 | 0.236499215 | 12.86350078 | 2.058158 | 2058.15832 | | | |
| 86 | 17.7 | 18.15 | 7.83 | 7.83 | 0.45 | 2.479339 | 0.194132231 | 7.635867769 | 1.758721 | 1758.72093 | | | |
| 87 | 17.43 | 17.85 | 7.13 | 7.13 | 0.42 | 2.352941 | 0.167764706 | 6.962235294 | 1.665112 | 1665.11194 | | | |
| 88 | 17.6 | 18.01 | 8.36 | 8.36 | 0.41 | 2.276513 | 0.190316491 | 8.169683509 | 1.866321 | 1866.321244 | | | |
| 89 | 25.6 | 26.03 | 12.96 | 12.96 | 0.43 | 1.65194 | 0.214091433 | 12.74590857 | 1.991584 | 1991.58378 | | | |
| 90 | 9.81 | 10.1 | 3.28 | 3.28 | 0.29 | 2.871287 | 0.094178218 | 3.185821782 | 1.480938 | 1480.938416 | | | |
| Table A1.7. Density measurements for mwSp. | | | | | | | | | | | | | |

| number | | | | | | Wc+s water | | | Ws water | Wc water | SG | DENSITY kg m^-3 | | density range | density mean of 90 |
|--------|-----------|-----------|-----------|----------------|----------------|---------------|---------------------|--------------|-------------------------|-----------------------|--------------|--------------------|-----------------|------------------|-----------------------|
| | | | | ballast dry | ballast wet | clast wet | sheet dry weight | sheet % | sheet wet weight (g) | clast wet no sheet | | | | | |
| 1 | 27. 77 | 28.0 4 | 18.0 1 | | | 18.01 | 0.27 | 0.96291 | 0.173420114 | 17.83657989 | 2.79561 3 | 2795.613161 | 2461.02449 9 | 2461.02449 9 | 2680.640285 |
| 2 | 23. 66 | 23.9 5 | 15.6 8 | | | 15.68 | 0.29 | 1.21085 6 | 0.189862213 | 15.49013779 | 2.89601 | 2896.009674 | 2533.61344 5 | 2964 | stdev |
| 3 | 24. 14 | 24.4 4 | 15.9 1 | | | 15.91 | 0.3 | 1.22749 6 | 0.195294599 | 15.7147054 | 2.86518 2 | 2865.181712 | 2565.21739 1 | | 118.0170483 |
| 4 | 19. 65 | 19.9 | 12.6 1 | | | 12.61 | 0.25 | 1.25628 1 | 0.158417085 | 12.45158291 | 2.72976 7 | 2729.766804 | 2566.55844 2 | | |
| 5 | 24. 71 | 25.0 5 | 16.9 7 | | | 16.97 | 0.34 | 1.35728 5 | 0.230331337 | 16.73966866 | 3.10024 8 | | 2590.72978 3 | | mean of 50 |
| 6 | 17. 72 | 17.9 5 | 11.6 3 | | | 11.63 | 0.23 | 1.28133 7 | 0.149019499 | 11.4809805 | 2.84019 | 2840.189873 | 2590.73842 3 | | 2751.971105 |
| 7 | 14. 7 | 14.9 2 | 9.77 | | | 9.77 | 0.22 | 1.47453 1 | 0.144061662 | 9.625938338 | 2.89708 7 | 2897.087379 | 2597.96672 8 | | stdev |
| 8 | 15. 69 | 16 | 10.2 7 | | | 10.27 | 0.31 | 1.9375 | 0.19898125 | 10.07101875 | 2.79232 1 | 2792.321117 | 2621.66962 7 | | 117.3245864 |
| 9 | 13. 47 | 13.7 6 | 8.84 | | | 8.84 | 0.29 | 2.10755 8 | 0.18630814 | 8.65369186 | 2.79674 8 | 2796.747967 | 2626.24035 3 | | |
| 10 | 14. 69 | 14.9 8 | 9.62 | | | 9.62 | 0.29 | 1.93591 5 | 0.18623498 | 9.43376502 | 2.79477 6 | 2794.776119 | 2626.30792 2 | | mean of 30 |
| 11 | 12. 9 | 13.2 2 | 8.71 | | | 8.71 | 0.32 | 2.42057 5 | 0.210832073 | 8.499167927 | 2.93126 4 | 2931.263858 | 2655.17241 4 | | 2790.214219 |

| | | | | | | | | | | | | | | | |
|----|-----------|-----------|-----------|--|--|-------|-------|--------------|--------------|-------------|--------------|-------------|-----------------|--|-------------|
| 12 | 11. 89 | 12.1 8 | 8.13 | | | 8.13 | 0.29 | 2.38095 2 | 0.193571429 | 7.936428571 | 3.00740 7 | | 2656.71641 8 | | stdev |
| 13 | 13. 54 | 13.0 6 | 8.43 | | | 8.43 | -0.48 | - 3.67534 | -0.309831547 | 8.739831547 | 2.82073 4 | 2820.734341 | 2664.60587 3 | | 83.9472812 |
| 14 | 12. 8 | 13.0 8 | 8.43 | | | 8.43 | 0.28 | 2.14067 3 | 0.180458716 | 8.249541284 | 2.81290 3 | 2812.903226 | 2666.01562 5 | | |
| 15 | 17. 7 | 17.9 9 | 11.6 7 | | | 11.67 | 0.29 | 1.61200 7 | 0.188121178 | 11.48187882 | 2.84651 9 | 2846.518987 | 2669.03073 3 | | vesic |
| 16 | 9.9 8 | 10.2 6 | 6.59 | | | 6.59 | 0.28 | 2.72904 5 | 0.179844055 | 6.410155945 | 2.79564 | 2795.640327 | 2689.61201 5 | | 10.64532383 |
| 17 | 9.9 9 | 10.2 6 | 6.58 | | | 6.58 | 0.27 | 2.63157 9 | 0.173157895 | 6.406842105 | 2.78804 3 | 2788.043478 | 2692.30769 2 | | 17.96585004 |
| 18 | 13. 31 | 13.6 2 | 8.63 | | | 8.63 | 0.31 | 2.27606 5 | 0.196424376 | 8.433575624 | 2.72945 9 | 2729.458918 | 2704.86656 2 | | 1.2 |
| 19 | 8.8 1 | 9.1 | 5.72 | | | 5.72 | 0.29 | 3.18681 3 | 0.182285714 | 5.537714286 | 2.69230 8 | 2692.307692 | 2716.75531 9 | | |
| 20 | 10. 9 | 11.2 9 | 7.06 | | | 7.06 | 0.39 | 3.45438 4 | 0.243879539 | 6.816120461 | 2.66903 1 | 2669.030733 | 2723.64217 3 | | |
| 21 | 20. 13 | 20.4 3 | 12.9 1 | | | 12.91 | 0.3 | 1.46842 9 | 0.189574156 | 12.72042584 | 2.71675 5 | 2716.755319 | 2724.23398 3 | | |
| 22 | 16. 74 | 17.0 5 | 10.7 9 | | | 10.79 | 0.31 | 1.81818 2 | 0.196181818 | 10.59381818 | 2.72364 2 | 2723.642173 | 2729.19818 5 | | |
| 23 | 17. 74 | 18.0 4 | 11.4 3 | | | 11.43 | 0.3 | 1.66297 1 | 0.190077605 | 11.23992239 | 2.72919 8 | 2729.198185 | 2729.45891 8 | | |
| 24 | 14. 77 | 15.0 2 | 9.69 | | | 9.69 | 0.25 | 1.66444 7 | 0.161284953 | 9.528715047 | 2.81801 1 | 2818.011257 | 2729.76680 4 | | |
| 25 | 22. 4 | 22.7 | 14.5 2 | | | 14.52 | 0.3 | 1.32158 6 | 0.191894273 | 14.32810573 | 2.77506 1 | 2775.061125 | 2734.58149 8 | | |
| 26 | 13. 34 | 13.6 5 | 8.53 | | | 8.53 | 0.31 | 2.27106 2 | 0.193721612 | 8.336278388 | 2.66601 6 | 2666.015625 | 2765.84734 8 | | |
| 27 | 18. 43 | 18.5 9 | 12.3 2 | | | 12.32 | 0.16 | 0.86067 8 | 0.106035503 | 12.2139645 | 2.96491 2 | 2964.912281 | 2775.06112 5 | | |
| 28 | 18. 7 | 19.0 2 | 12.2 4 | | | 12.24 | 0.32 | 1.68244 | 0.205930599 | 12.0340694 | 2.80531 | 2805.309735 | 2786.68942 | | |
| 29 | 25. 89 | 26.2 7 | 16.1 3 | | | 16.13 | 0.38 | 1.44651 7 | 0.233323182 | 15.89667682 | 2.59073 | 2590.729783 | 2788.04347 8 | | |
| 30 | 22. 32 | 22.6 | 14.6 5 | | | 14.65 | 0.28 | 1.23893 8 | 0.181504425 | 14.46849558 | 2.84276 7 | 2842.767296 | 2792.32111 7 | | |
| 31 | 16. 05 | 16.3 3 | 10.4 7 | | | 10.47 | 0.28 | 1.71463 6 | 0.179522352 | 10.29047765 | 2.78668 9 | 2786.68942 | 2794.77611 9 | | |
| 32 | 21. 09 | 21.3 8 | 13.6 5 | | | 13.65 | 0.29 | 1.35640 8 | 0.185149673 | 13.46485033 | 2.76584 7 | 2765.847348 | 2795.61316 1 | | |
| 33 | 20. 94 | 21.2 5 | 13.8 | | | 13.8 | 0.31 | 1.45882 4 | 0.201317647 | 13.59868235 | 2.85234 9 | 2852.348993 | 2795.64032 7 | | |
| 34 | 16. 76 | 17.0 1 | 11.1 3 | | | 11.13 | 0.25 | 1.46972 4 | 0.163580247 | 10.96641975 | 2.89285 7 | 2892.857143 | 2796.74796 7 | | |
| 35 | 15. 18 | 15.4 6 | 10.2 4 | | | 10.24 | 0.28 | 1.81112 5 | 0.18545925 | 10.05454075 | 2.96168 6 | 2961.685824 | 2805.30973 5 | | |
| 36 | 21. 27 | 21.5 3 | 14.2 6 | | | 14.26 | 0.26 | 1.20761 7 | 0.172206224 | 14.08779378 | 2.96148 6 | 2961.485557 | 2812.90322 6 | | |

| | | | | | | | | | | | | | | | |
|----|-------|-------|-------|--|--|-------|------|----------|-------------|-------------|----------|-------------|-------------|--|--|
| 37 | 16.91 | 17.24 | 10.77 | | | 10.77 | 0.33 | 1.914153 | 0.206154292 | 10.56384571 | 2.664606 | 2664.605873 | 2818.011257 | | |
| 38 | 29.11 | 29.52 | 18.26 | | | 18.26 | 0.41 | 1.388889 | 0.253611111 | 18.00638889 | 2.62167 | 2621.669627 | 2820.734341 | | |
| 39 | 27.66 | 28.11 | 17.29 | | | 17.29 | 0.45 | 1.600854 | 0.27678762 | 17.01321238 | 2.597967 | 2597.966728 | 2840.189873 | | |
| 40 | 12.2 | 12.39 | 7.56 | | | 7.56 | 0.19 | 1.533495 | 0.115932203 | 7.444067797 | 2.565217 | 2565.217391 | 2842.767296 | | |
| 41 | 10.78 | 11.05 | 6.56 | | | 6.56 | 0.27 | 2.443439 | 0.160289593 | 6.399710407 | 2.461024 | 2461.024499 | 2846.518987 | | |
| 42 | 24.54 | 24.83 | 15.75 | | | 15.75 | 0.29 | 1.167942 | 0.183950866 | 15.56604913 | 2.734581 | 2734.581498 | 2852.348993 | | |
| 43 | 17.31 | 17.57 | 10.88 | | | 10.88 | 0.26 | 1.479795 | 0.161001707 | 10.71899829 | 2.626308 | 2626.307922 | 2865.181712 | | |
| 44 | 23.55 | 23.82 | 14.75 | | | 14.75 | 0.27 | 1.133501 | 0.167191436 | 14.58280856 | 2.62624 | 2626.240353 | 2892.857143 | | |
| 45 | 13.96 | 14.24 | 8.88 | | | 8.88 | 0.28 | 1.966292 | 0.174606742 | 8.705393258 | 2.656716 | 2656.716418 | 2896.009674 | | |
| 46 | 17.81 | 18.09 | 10.95 | | | 10.95 | 0.28 | 1.547816 | 0.169485904 | 10.7805141 | 2.533613 | 2533.613445 | 2897.087379 | | |
| 47 | 19.28 | 19.56 | 12.38 | | | 12.38 | 0.28 | 1.431493 | 0.177218814 | 12.20278119 | 2.724234 | 2724.233983 | 2931.263858 | | |
| 48 | 20.46 | 20.71 | 12.71 | | | 12.71 | 0.24 | 1.15942 | 0.147362319 | 12.56263768 | 2.590738 | 2590.738423 | 2961.485557 | | |
| 49 | 21.18 | 21.49 | 13.5 | | | 13.5 | 0.31 | 1.442531 | 0.19474174 | 13.30525826 | 2.689612 | 2689.612015 | 2961.685824 | | |
| 50 | 13.57 | 13.86 | 8.64 | | | 8.64 | 0.29 | 2.092352 | 0.180779221 | 8.459220779 | 2.655172 | 2655.172414 | 2964.912281 | | |
| 51 | 15.5 | 15.81 | 9.65 | | | 9.65 | 0.31 | 1.960784 | 0.189215686 | 9.460784314 | 2.566558 | 2566.558442 | | | |
| 52 | 16.92 | 17.23 | 10.86 | | | 10.86 | 0.31 | 1.799187 | 0.195391759 | 10.66460824 | 2.704867 | 2704.866562 | | | |
| 53 | 12.11 | 12.37 | 7.87 | | | 7.87 | 0.26 | 2.101859 | 0.16541633 | 7.70458367 | 2.748889 | 2748.888889 | | | |
| 54 | 8.49 | 8.77 | 5.57 | | | 5.57 | 0.28 | 3.192702 | 0.177833523 | 5.392166477 | 2.740625 | 2740.625 | | | |
| 55 | 11.74 | 12.03 | 7.57 | | | 7.57 | 0.29 | 2.41064 | 0.182485453 | 7.387514547 | 2.697309 | 2697.309417 | | | |
| 56 | 15.41 | 15.72 | 9.6 | | | 9.6 | 0.31 | 1.97201 | 0.189312977 | 9.410687023 | 2.568627 | 2568.627451 | | | |
| 57 | 11.82 | 12.08 | 7.29 | | | 7.29 | 0.26 | 2.152318 | 0.156903974 | 7.133096026 | 2.521921 | 2521.920668 | | | |
| 58 | 22.1 | 22.36 | 13.89 | | | 13.89 | 0.26 | 1.162791 | 0.161511628 | 13.72848837 | 2.639906 | 2639.905549 | | | |
| 59 | 14.88 | 15.16 | 9.53 | | | 9.53 | 0.28 | 1.846966 | 0.176015831 | 9.353984169 | 2.692718 | 2692.717584 | | | |
| 60 | 22.73 | 23.25 | 14.45 | | | 14.45 | 0.52 | 2.236559 | 0.323182796 | 14.1268172 | 2.642045 | 2642.045455 | | | |
| 61 | 8.14 | 8.43 | 5.29 | | | 5.29 | 0.29 | 3.440095 | 0.18198102 | 5.10801898 | 2.684713 | 2684.713376 | | | |

| | | | | | | | | | | | | | | | |
|----|-------|-------|-------|--|--|-------|------|----------|-------------|-------------|----------|-------------|--|--|--|
| 62 | 21.95 | 22.23 | 13.75 | | | 13.75 | 0.28 | 1.259559 | 0.173189384 | 13.57681062 | 2.621462 | 2621.462264 | | | |
| 63 | 24.21 | 24.46 | 15.51 | | | 15.51 | 0.25 | 1.022077 | 0.158524121 | 15.35147588 | 2.732961 | 2732.960894 | | | |
| 64 | 27.5 | 27.88 | 17.4 | | | 17.4 | 0.38 | 1.362984 | 0.237159254 | 17.16284075 | 2.660305 | 2660.305344 | | | |
| 65 | 29.13 | 29.43 | 18.68 | | | 18.68 | 0.3 | 1.019368 | 0.190417941 | 18.48958206 | 2.737674 | 2737.674419 | | | |
| 66 | 33.04 | 33.37 | 21.14 | | | 21.14 | 0.33 | 0.988912 | 0.209056038 | 20.93094396 | 2.728536 | 2728.536386 | | | |
| 67 | 23.44 | 23.77 | 14.79 | | | 14.79 | 0.33 | 1.388305 | 0.205330248 | 14.58466975 | 2.646993 | 2646.993318 | | | |
| 68 | 21.02 | 21.31 | 13.24 | | | 13.24 | 0.29 | 1.360863 | 0.18017832 | 13.05982168 | 2.640644 | 2640.644362 | | | |
| 69 | 30.01 | 30.36 | 18.87 | | | 18.87 | 0.35 | 1.152833 | 0.217539526 | 18.65246047 | 2.642298 | 2642.29765 | | | |
| 70 | 31.69 | 32.06 | 19.91 | | | 19.91 | 0.37 | 1.154086 | 0.22977854 | 19.68022146 | 2.638683 | 2638.683128 | | | |
| 71 | 31.33 | 31.69 | 15.5 | | | 15.5 | 0.36 | 1.136005 | 0.176080783 | 15.32391922 | 1.957381 | 1957.381099 | | | |
| 72 | 23.12 | 23.43 | 14.72 | | | 14.72 | 0.31 | 1.32309 | 0.194758856 | 14.52524114 | 2.690011 | 2690.011481 | | | |
| 73 | 21.79 | 22.04 | 12.98 | | | 12.98 | 0.25 | 1.134301 | 0.147232305 | 12.8327677 | 2.432671 | 2432.671082 | | | |
| 74 | 20.34 | 20.7 | 12.1 | | | 12.1 | 0.36 | 1.73913 | 0.210434783 | 11.88956522 | 2.406977 | 2406.976744 | | | |
| 75 | 20.11 | 20.4 | 12.76 | | | 12.76 | 0.29 | 1.421569 | 0.181392157 | 12.57860784 | 2.670157 | 2670.157068 | | | |
| 76 | 26.08 | 26.35 | 16 | | | 16 | 0.27 | 1.024668 | 0.163946869 | 15.83605313 | 2.545894 | 2545.89372 | | | |
| 77 | 27.42 | 27.7 | 16.88 | | | 16.88 | 0.28 | 1.01083 | 0.170628159 | 16.70937184 | 2.560074 | 2560.073937 | | | |
| 78 | 15.76 | 16 | 9.49 | | | 9.49 | 0.24 | 1.5 | 0.14235 | 9.34765 | 2.457757 | 2457.757296 | | | |
| 79 | 12.17 | 12.42 | 7.61 | | | 7.61 | 0.25 | 2.012882 | 0.153180354 | 7.456819646 | 2.582121 | 2582.120582 | | | |
| 80 | 18.28 | 18.52 | 11.43 | | | 11.43 | 0.24 | 1.295896 | 0.14812095 | 11.28187905 | 2.61213 | 2612.12976 | | | |
| 81 | 16.04 | 16.34 | 9.95 | | | 9.95 | 0.3 | 1.835985 | 0.182680539 | 9.767319461 | 2.557121 | 2557.120501 | | | |
| 82 | 10.03 | 10.3 | 5.76 | | | 5.76 | 0.27 | 2.621359 | 0.150990291 | 5.609009709 | 2.268722 | 2268.722467 | | | |
| 83 | 12.79 | 13.07 | 7.64 | | | 7.64 | 0.28 | 2.142311 | 0.163672533 | 7.476327467 | 2.406998 | 2406.998158 | | | |
| 84 | 30.41 | 30.74 | 18.89 | | | 18.89 | 0.33 | 1.07352 | 0.202787899 | 18.6872121 | 2.594093 | 2594.092827 | | | |
| 85 | 35.82 | 36.08 | 22.39 | | | 22.39 | 0.26 | 0.720621 | 0.161347007 | 22.22865299 | 2.6355 | 2635.500365 | | | |
| 86 | 30.96 | 31.28 | 19.25 | | | 19.25 | 0.32 | 1.023018 | 0.196930946 | 19.05306905 | 2.600166 | 2600.166251 | | | |

| | | | | | | | | | | | | | | | |
|---|-------|-------|-------|--|--|-------|------|----------|-------------|-------------|----------|-------------|--|--|--|
| 87 | 24.92 | 25.28 | 15.71 | | | 15.71 | 0.36 | 1.424051 | 0.223718354 | 15.48628165 | 2.641588 | 2641.588297 | | | |
| 88 | 51.17 | 51.67 | 32.23 | | | 32.23 | 0.5 | 0.96768 | 0.311883104 | 31.9181169 | 2.657922 | 2657.921811 | | | |
| 89 | 32.51 | 32.95 | 20.44 | | | 20.44 | 0.44 | 1.335357 | 0.272946889 | 20.16705311 | 2.633893 | 2633.892886 | | | |
| 90 | 28.7 | 29.04 | 18.01 | | | 18.01 | 0.34 | 1.170799 | 0.210860882 | 17.79913912 | 2.63282 | 2632.819583 | | | |
| Table A1.8. Density measurements for l-l Agg. | | | | | | | | | | | | | | | |

| number | | | | Wc+s water | | | Ws water | Wc water | SG | DENSITY kg m^-3 | density sorted | density range | density mean of 50 |
|--------|-------|-------|-------|------------|------------------|----------|----------------------|--------------------|----------|-----------------|----------------|---------------|--------------------|
| | | | | clast wet | sheet dry weight | sheet % | sheet wet weight (g) | clast wet no sheet | | | | | |
| 1 | 34.51 | 35.11 | 19.46 | 19.46 | 0.6 | 1.708915 | 0.332554828 | 19.12744517 | 2.24345 | 2243.450479 | 1705.270007 | 1705 | 2286.2697 |
| 2 | 21.09 | 21.36 | 13.25 | 13.25 | 0.27 | 1.264045 | 0.167485955 | 13.08251404 | 2.633785 | 2633.78545 | 1828.729282 | 2633 | stdev |
| 3 | 28.84 | 29.14 | 17.17 | 17.17 | 0.3 | 1.029513 | 0.17676733 | 16.99323267 | 2.434419 | 2434.419382 | 1905.30303 | | 203.4711388 |
| 4 | 14.29 | 14.6 | 7.98 | 7.98 | 0.31 | 2.123288 | 0.169438356 | 7.810561644 | 2.205438 | 2205.438066 | 1936.144578 | | |
| 5 | 11.76 | 12.05 | 6.67 | 6.67 | 0.29 | 2.406639 | 0.160522822 | 6.509477178 | 2.239777 | 2239.776952 | 2002.533784 | | vesic |
| 6 | 17.88 | 18.18 | 10.99 | 10.99 | 0.3 | 1.650165 | 0.181353135 | 10.80864686 | 2.528512 | 2528.511822 | 2059.299191 | | 23.79101 |
| 7 | 20.79 | 21.04 | 12.83 | 12.83 | 0.25 | 1.188213 | 0.152447719 | 12.67755228 | 2.562728 | 2562.72838 | 2085.477178 | | 43.16666667 |
| 8 | 22.82 | 23.17 | 10.5 | 10.5 | 0.35 | 1.510574 | 0.158610272 | 10.34138973 | 1.828729 | 1828.729282 | 2110.009911 | | 12.23333333 |
| 9 | 12.95 | 13.22 | 7.57 | 7.57 | 0.27 | 2.04236 | 0.154606657 | 7.415393343 | 2.339823 | 2339.823009 | 2117.256637 | | |
| 10 | 31.85 | 32.16 | 18.59 | 18.59 | 0.31 | 0.96393 | 0.179194652 | 18.41080535 | 2.369934 | 2369.933677 | 2136.363636 | | |
| 11 | 18.85 | 19.14 | 10.1 | 10.1 | 0.29 | 1.515152 | 0.153030303 | 9.946969697 | 2.117257 | 2117.256637 | 2155.868545 | | |
| 12 | 24.67 | 24.95 | 15.11 | 15.11 | 0.28 | 1.122244 | 0.169571142 | 14.94042886 | 2.535569 | 2535.569106 | 2159.847245 | | |
| 13 | 21.78 | 22.1 | 12.16 | 12.16 | 0.32 | 1.447964 | 0.176072398 | 11.9839276 | 2.22334 | 2223.34004 | 2169.522092 | | |
| 14 | 17.91 | 18.18 | 10.97 | 10.97 | 0.27 | 1.485149 | 0.162920792 | 10.80707921 | 2.521498 | 2521.49792 | 2186.734694 | | |
| 15 | 15.8 | 16.06 | 8.92 | 8.92 | 0.26 | 1.618929 | 0.144408468 | 8.775591532 | 2.2493 | 2249.29972 | 2203.052422 | | |
| 16 | 22.77 | 23.09 | 13.23 | 13.23 | 0.32 | 1.385881 | 0.1833521 | 13.0466479 | 2.341785 | 2341.78499 | 2205.438066 | | |
| 17 | 21.01 | 21.29 | 11.2 | 11.2 | 0.28 | 1.315171 | 0.147299202 | 11.0527008 | 2.11001 | 2110.009911 | 2223.34004 | | |
| 18 | 32.81 | 33.2 | 18.13 | 18.13 | 0.39 | 1.174699 | 0.212972892 | 17.91702711 | 2.203052 | 2203.052422 | 2225.683408 | | |
| 19 | 39.03 | 39.59 | 21.26 | 21.26 | 0.56 | 1.414499 | 0.300722405 | 20.9592776 | 2.159847 | 2159.847245 | 2235.9447 | | |
| 20 | 42.37 | 42.86 | 23.26 | 23.26 | 0.49 | 1.143257 | 0.265921605 | 22.99407839 | 2.186735 | 2186.734694 | 2239.776952 | | |
| 21 | 36.12 | 36.65 | 21.88 | 21.88 | 0.53 | 1.446112 | 0.316409277 | 21.56359072 | 2.481381 | 2481.381178 | 2240.619902 | | |
| 22 | 45.44 | 45.92 | 24.62 | 24.62 | 0.48 | 1.045296 | 0.257351916 | 24.36264808 | 2.155869 | 2155.868545 | 2243.450479 | | |
| 23 | 31.44 | 31.86 | 19.25 | 19.25 | 0.42 | 1.318267 | 0.253766478 | 18.99623352 | 2.526566 | 2526.566217 | 2249.29972 | | |
| 24 | 25.68 | 26.21 | 10.84 | 10.84 | 0.53 | 2.022129 | 0.219198779 | 10.62080122 | 1.70527 | 1705.270007 | 2256.768559 | | |
| 25 | 34.51 | 35.01 | 19.28 | 19.28 | 0.5 | 1.428163 | 0.2753499 | 19.0046501 | 2.225683 | 2225.683408 | 2275.316456 | | |
| 26 | 41.7 | 42.11 | 24.05 | 24.05 | 0.41 | 0.97364 | 0.234160532 | 23.81583947 | 2.331672 | 2331.672204 | 2314.058957 | | |
| 27 | 35.03 | 35.43 | 20.47 | 20.47 | 0.4 | 1.128987 | 0.231103585 | 20.23889642 | 2.368316 | 2368.315508 | 2318.623785 | | |
| 28 | 47.94 | 48.49 | 28.78 | 28.78 | 0.55 | 1.134254 | 0.326438441 | 28.45356156 | 2.460173 | 2460.172501 | 2331.672204 | | |
| 29 | 40.25 | 40.82 | 23.18 | 23.18 | 0.57 | 1.396374 | 0.323679569 | 22.85632043 | 2.314059 | 2314.058957 | 2339.823009 | | |
| 30 | 40.53 | 41.05 | 23.63 | 23.63 | 0.52 | 1.266748 | 0.299332521 | 23.33066748 | 2.356487 | 2356.486797 | 2341.78499 | | |
| 31 | 40.62 | 41.1 | 24.73 | 24.73 | 0.48 | 1.167883 | 0.288817518 | 24.44118248 | 2.51069 | 2510.690287 | 2356.486797 | | |
| 32 | 25.38 | 25.84 | 14.39 | 14.39 | 0.46 | 1.780186 | 0.256168731 | 14.13383127 | 2.256769 | 2256.768559 | 2368.315508 | | |

| | | | | | | | | | | | | | |
|--|-------|-------|-------|-------|-------|----------|--------------|-------------|----------|-------------|-------------|--|--|
| 33 | 27.18 | 27.47 | 15.21 | 15.21 | 0.29 | 1.055697 | 0.160571533 | 15.04942847 | 2.24062 | 2240.619902 | 2369.863014 | | |
| 34 | 27.09 | 27.36 | 16.06 | 16.06 | 0.27 | 0.986842 | 0.158486842 | 15.90151316 | 2.421239 | 2421.238938 | 2369.933677 | | |
| 35 | 25.99 | 26.24 | 16.2 | 16.2 | 0.25 | 0.952744 | 0.154344512 | 16.04565549 | 2.613546 | 2613.545817 | 2371.342079 | | |
| 36 | 30.45 | 31 | 17.63 | 17.63 | 0.55 | 1.774194 | 0.312790323 | 17.31720968 | 2.318624 | 2318.623785 | 2375.523013 | | |
| 37 | 22.21 | 22.49 | 13 | 13 | 0.28 | 1.244998 | 0.161849711 | 12.83815029 | 2.369863 | 2369.863014 | 2421.238938 | | |
| 38 | 22.47 | 22.71 | 13.15 | 13.15 | 0.24 | 1.056803 | 0.138969617 | 13.01103038 | 2.375523 | 2375.523013 | 2434.419382 | | |
| 39 | 23.72 | 24.06 | 12.97 | 12.97 | 0.34 | 1.413134 | 0.183283458 | 12.78671654 | 2.169522 | 2169.522092 | 2460.172501 | | |
| 40 | 23.23 | 23.5 | 13.59 | 13.59 | 0.27 | 1.148936 | 0.156140426 | 13.43385957 | 2.371342 | 2371.342079 | 2481.381178 | | |
| 41 | 21.27 | 21.57 | 12.09 | 12.09 | 0.3 | 1.390821 | 0.168150209 | 11.92184979 | 2.275316 | 2275.316456 | 2510.690287 | | |
| 42 | 29.25 | 24.53 | 14.87 | 14.87 | -4.72 | -19.2417 | -2.861247452 | 17.73124745 | 2.539337 | 2539.337474 | 2521.49792 | | |
| 43 | 19.38 | 19.68 | 11.9 | 11.9 | 0.3 | 1.52439 | 0.181402439 | 11.71859756 | 2.529563 | 2529.562982 | 2526.566217 | | |
| 44 | 23.95 | 24.26 | 13.41 | 13.41 | 0.31 | 1.277824 | 0.171356142 | 13.23864386 | 2.235945 | 2235.9447 | 2528.511822 | | |
| 45 | 24.7 | 25.13 | 13.08 | 13.08 | 0.43 | 1.711102 | 0.223812177 | 12.85618782 | 2.085477 | 2085.477178 | 2529.562982 | | |
| 46 | 20.39 | 20.68 | 11 | 11 | 0.29 | 1.402321 | 0.154255319 | 10.84574468 | 2.136364 | 2136.363636 | 2535.569106 | | |
| 47 | 14.96 | 15.28 | 7.86 | 7.86 | 0.32 | 2.094241 | 0.16460733 | 7.69539267 | 2.059299 | 2059.299191 | 2539.337474 | | |
| 48 | 9.76 | 10.06 | 4.78 | 4.78 | 0.3 | 2.982107 | 0.142544732 | 4.637455268 | 1.905303 | 1905.30303 | 2562.72838 | | |
| 49 | 23.42 | 23.71 | 11.87 | 11.87 | 0.29 | 1.223113 | 0.145183467 | 11.72481653 | 2.002534 | 2002.533784 | 2613.545817 | | |
| 50 | 15.7 | 16.07 | 7.77 | 7.77 | 0.37 | 2.302427 | 0.178898569 | 7.591101431 | 1.936145 | 1936.144578 | 2633.78545 | | |
| Table A1.9. Density measurements for dwSp. | | | | | | | | | | | | | |

| number | | | | | Wc+s water | | | Ws water | Wc water | SG | DENSITY kg m^-3 | density sorted | density range | density mean of 90 |
|--------|------|------|-------|----------------|---------------|------------------------|----------|-------------------------|-----------------------|----------|--------------------|----------------|------------------|--------------------|
| | | | | ballast wet | clast wet | sheet dry weight | sheet % | sheet wet weight (g) | clast wet no sheet | | | | | |
| 1 | 3.67 | 4.16 | 12.03 | 15.78 | -3.75 | 0.49 | 11.77885 | -0.441706731 | -3.308293269 | 0.525917 | 525.9165613 | 344.1589918 | 344.1589918 | 558.4204358 |
| 2 | 4.03 | 4.32 | 14.17 | 15.78 | -1.61 | 0.29 | 6.712963 | -0.108078704 | -1.501921296 | 0.728499 | 728.4991568 | 353.5911602 | 827 | stdev |
| 3 | 3.38 | 3.84 | 8.76 | 15.78 | -7.02 | 0.46 | 11.97917 | -0.8409375 | -6.1790625 | 0.353591 | 353.5911602 | 371.1340206 | | 115.1955497 |
| 4 | 6.84 | 7.34 | 11.96 | 15.78 | -3.82 | 0.5 | 6.811989 | -0.260217984 | -3.559782016 | 0.657706 | 657.7060932 | 382.6754386 | | |
| 5 | 3.03 | 3.49 | 10.15 | 15.78 | -5.63 | 0.46 | 13.18052 | -0.742063037 | -4.887936963 | 0.382675 | 382.6754386 | 384.6908734 | | mean of 50 |
| 6 | 6.84 | 7.1 | 2.25 | 15.78 | -13.53 | 0.26 | 3.661972 | -0.495464789 | -13.03453521 | 0.344159 | 344.1589918 | 404.2792793 | | 572.2514541 |
| 7 | 3.23 | 3.63 | 12.35 | 15.78 | -3.43 | 0.4 | 11.01928 | -0.377961433 | -3.052038567 | 0.514164 | 514.1643059 | 416.091954 | | stdev |
| 8 | 5.51 | 5.92 | 8 | 15.78 | -7.78 | 0.41 | 6.925676 | -0.538817568 | -7.241182432 | 0.432117 | 432.1167883 | 420.8074534 | | 122.948321 |
| 9 | 2.88 | 3.32 | 11.68 | 15.78 | -4.1 | 0.44 | 13.25301 | -0.543373494 | -3.556626506 | 0.447439 | 447.4393531 | 426.744186 | | vesic |
| 10 | 6.51 | 7.01 | 13.01 | 15.78 | -2.77 | 0.5 | 7.132668 | -0.197574893 | -2.572425107 | 0.716769 | 716.7689162 | 432.1167883 | | 80.92495153 |
| 11 | 5.19 | 5.59 | 12.26 | 15.78 | -3.52 | 0.4 | 7.155635 | -0.251878354 | -3.268121646 | 0.613611 | 613.611416 | 447.4393531 | | 88.52803361 |
| 12 | 2.25 | 2.71 | 12.05 | 15.78 | -3.73 | 0.46 | 16.97417 | -0.633136531 | -3.096863469 | 0.420807 | 420.8074534 | 455.6786704 | | 72.43333333 |
| 13 | 3.19 | 3.59 | 10.49 | 15.78 | -5.29 | 0.4 | 11.14206 | -0.589415042 | -4.700584958 | 0.404279 | 404.2792793 | 472.1407625 | | |

| | | | | | | | | | | | | | | |
|----|------|------|-------|-------|-------|------|----------|--------------|--------------|----------|-------------|-------------|--|--|
| 14 | 4.27 | 4.78 | 12.89 | 15.78 | -2.89 | 0.51 | 10.66946 | -0.30834728 | -2.58165272 | 0.623207 | 623.2073012 | 505.0505051 | | |
| 15 | 4.69 | 5.08 | 11.46 | 15.78 | -4.32 | 0.39 | 7.677165 | -0.331653543 | -3.988346457 | 0.540426 | 540.4255319 | 513.8568129 | | |
| 16 | 4.85 | 5.29 | 12.55 | 15.78 | -3.23 | 0.44 | 8.31758 | -0.268657845 | -2.961342155 | 0.620892 | 620.8920188 | 514.1643059 | | |
| 17 | 1.42 | 1.81 | 13.24 | 15.78 | -2.54 | 0.39 | 21.54696 | -0.547292818 | -1.992707182 | 0.416092 | 416.091954 | 525.9165613 | | |
| 18 | 4.38 | 4.95 | 12.9 | 15.78 | -2.88 | 0.57 | 11.51515 | -0.331636364 | -2.548363636 | 0.632184 | 632.183908 | 540.4255319 | | |
| 19 | 7.25 | 7.79 | 11.8 | 15.78 | -3.98 | 0.54 | 6.931964 | -0.275892169 | -3.704107831 | 0.661852 | 661.8521665 | 540.8805031 | | |
| 20 | 6.77 | 7.28 | 11.8 | 15.78 | -3.98 | 0.51 | 7.005495 | -0.278818681 | -3.701181319 | 0.646536 | 646.5364121 | 540.9153953 | | |
| 21 | 4.66 | 5.22 | 12.93 | 15.78 | -2.85 | 0.56 | 10.72797 | -0.305747126 | -2.544252874 | 0.64684 | 646.8401487 | 545.5519829 | | |
| 22 | 1.74 | 2.16 | 12.12 | 15.78 | -3.66 | 0.42 | 19.44444 | -0.711666667 | -2.948333333 | 0.371134 | 371.1340206 | 547.7792732 | | |
| 23 | 4.63 | 5.09 | 11.54 | 15.78 | -4.24 | 0.46 | 9.037328 | -0.383182711 | -3.856817289 | 0.545552 | 545.5519829 | 569.9570815 | | |
| 24 | 3.86 | 4.45 | 11.57 | 15.78 | -4.21 | 0.59 | 13.25843 | -0.558179775 | -3.651820225 | 0.513857 | 513.8568129 | 573.7298637 | | |
| 25 | 3.16 | 3.67 | 10.85 | 15.78 | -4.93 | 0.51 | 13.89646 | -0.685095368 | -4.244904632 | 0.426744 | 426.744186 | 583.0429733 | | |
| 26 | 4.13 | 4.51 | 13.71 | 15.78 | -2.07 | 0.38 | 8.425721 | -0.174412417 | -1.895587583 | 0.68541 | 685.4103343 | 587.0445344 | | |
| 27 | 4.23 | 4.63 | 12.34 | 15.78 | -3.44 | 0.4 | 8.639309 | -0.297192225 | -3.142807775 | 0.57373 | 573.7298637 | 600.3787879 | | |
| 28 | 3.62 | 4.07 | 12.42 | 15.78 | -3.36 | 0.45 | 11.05651 | -0.371498771 | -2.988501229 | 0.547779 | 547.7792732 | 600.9389671 | | |
| 29 | 3.88 | 4.29 | 13.88 | 15.78 | -1.9 | 0.41 | 9.55711 | -0.181585082 | -1.718414918 | 0.693053 | 693.0533118 | 613.611416 | | |
| 30 | 4.59 | 5.05 | 12.98 | 15.78 | -2.8 | 0.46 | 9.108911 | -0.255049505 | -2.544950495 | 0.643312 | 643.3121019 | 620.8920188 | | |
| 31 | 3.92 | 4.3 | 12.13 | 15.78 | -3.65 | 0.38 | 8.837209 | -0.32255814 | -3.32744186 | 0.540881 | 540.8805031 | 622.0930233 | | |
| 32 | 5.27 | 5.76 | 13.46 | 15.78 | -2.32 | 0.49 | 8.506944 | -0.197361111 | -2.122638889 | 0.712871 | 712.8712871 | 623.2073012 | | |
| 33 | 4.29 | 4.83 | 10.38 | 15.78 | -5.4 | 0.54 | 11.18012 | -0.603726708 | -4.796273292 | 0.472141 | 472.1407625 | 632.183908 | | |
| 34 | 3.39 | 3.84 | 13.23 | 15.78 | -2.55 | 0.45 | 11.71875 | -0.298828125 | -2.251171875 | 0.600939 | 600.9389671 | 632.3687031 | | |
| 35 | 6.19 | 6.64 | 10.77 | 15.78 | -5.01 | 0.45 | 6.777108 | -0.339533133 | -4.670466867 | 0.569957 | 569.9570815 | 636.7346939 | | |
| 36 | 5.88 | 6.34 | 11.56 | 15.78 | -4.22 | 0.46 | 7.255521 | -0.306182965 | -3.913817035 | 0.600379 | 600.3787879 | 643.3121019 | | |
| 37 | 2.81 | 3.29 | 11.85 | 15.78 | -3.93 | 0.48 | 14.58967 | -0.57337386 | -3.35662614 | 0.455679 | 455.6786704 | 646.5364121 | | |
| 38 | 5.58 | 6.06 | 14.52 | 15.78 | -1.26 | 0.48 | 7.920792 | -0.09980198 | -1.16019802 | 0.827869 | 827.8688525 | 646.8401487 | | |
| 39 | 5.5 | 5.9 | 12.35 | 15.78 | -3.43 | 0.4 | 6.779661 | -0.232542373 | -3.197457627 | 0.632369 | 632.3687031 | 648.9361702 | | |
| 40 | 4.54 | 5.02 | 12.19 | 15.78 | -3.59 | 0.48 | 9.561753 | -0.343266932 | -3.246733068 | 0.583043 | 583.0429733 | 657.7060932 | | |
| 41 | 3.34 | 3.9 | 12.47 | 15.78 | -3.31 | 0.56 | 14.35897 | -0.475282051 | -2.834717949 | 0.540915 | 540.9153953 | 661.8521665 | | |
| 42 | 3.57 | 4 | 11.86 | 15.78 | -3.92 | 0.43 | 10.75 | -0.4214 | -3.4986 | 0.505051 | 505.0505051 | 685.4103343 | | |
| 43 | 4.03 | 4.45 | 14.5 | 15.78 | -1.28 | 0.42 | 9.438202 | -0.120808989 | -1.159191011 | 0.776614 | 776.6143106 | 693.0533118 | | |
| 44 | 3.84 | 4.27 | 13.47 | 15.78 | -2.31 | 0.43 | 10.07026 | -0.232622951 | -2.077377049 | 0.648936 | 648.9361702 | 712.8712871 | | |
| 45 | 3.85 | 4.28 | 13.18 | 15.78 | -2.6 | 0.43 | 10.04673 | -0.261214953 | -2.338785047 | 0.622093 | 622.0930233 | 716.7689162 | | |
| 46 | 4.21 | 4.68 | 13.11 | 15.78 | -2.67 | 0.47 | 10.04274 | -0.268141026 | -2.401858974 | 0.636735 | 636.7346939 | 728.4991568 | | |
| 47 | 3.4 | 3.92 | 9.51 | 15.78 | -6.27 | 0.52 | 13.26531 | -0.831734694 | -5.438265306 | 0.384691 | 384.6908734 | 776.6143106 | | |
| 48 | 6.17 | 6.69 | 13.98 | 15.78 | -1.8 | 0.52 | 7.772795 | -0.139910314 | -1.660089686 | 0.787986 | 787.9858657 | 787.9858657 | | |
| 49 | 1.19 | 1.45 | 14.76 | 15.78 | -1.02 | 0.26 | 17.93103 | -0.182896552 | -0.837103448 | 0.587045 | 587.0445344 | 796.0444994 | | |
| 50 | 5.97 | 6.44 | 14.13 | 15.78 | -1.65 | 0.47 | 7.298137 | -0.120419255 | -1.529580745 | 0.796044 | 796.0444994 | 827.8688525 | | |
| 51 | 5.19 | 5.77 | 10.85 | 15.78 | -4.93 | 0.58 | 10.05199 | -0.495563258 | -4.434436742 | 0.539252 | 539.2523364 | | | |
| 52 | 3.25 | 3.63 | 13.07 | 15.78 | -2.71 | 0.38 | 10.46832 | -0.28369146 | -2.42630854 | 0.572555 | 572.555205 | | | |
| 53 | 3.29 | 3.65 | 9.66 | 15.78 | -6.12 | 0.36 | 9.863014 | -0.603616438 | -5.516383562 | 0.373593 | 373.5926305 | | | |
| 54 | 3.24 | 3.66 | 13.22 | 15.78 | -2.56 | 0.42 | 11.47541 | -0.293770492 | -2.266229508 | 0.588424 | 588.4244373 | | | |
| 55 | 4.2 | 4.58 | 13.87 | 15.78 | -1.91 | 0.38 | 8.296943 | -0.158471616 | -1.751528384 | 0.705701 | 705.7010786 | | | |
| 56 | 2.98 | 3.43 | 12.87 | 15.78 | -2.91 | 0.45 | 13.11953 | -0.381778426 | -2.528221574 | 0.541009 | 541.0094637 | | | |
| 57 | 3.02 | 3.42 | 14.24 | 15.78 | -1.54 | 0.4 | 11.69591 | -0.180116959 | -1.359883041 | 0.689516 | 689.516129 | | | |
| 58 | 2.3 | 2.83 | 12.22 | 15.78 | -3.56 | 0.53 | 18.72792 | -0.666713781 | -2.893286219 | 0.442879 | 442.8794992 | | | |

| | | | | | | | | | | | | | | |
|----|------|------|-------|-------|-------|------|----------|--------------|--------------|----------|-------------|--|--|--|
| 59 | 5.46 | 6.02 | 13.08 | 15.78 | -2.7 | 0.56 | 9.302326 | -0.251162791 | -2.448837209 | 0.690367 | 690.3669725 | | | |
| 60 | 4.97 | 5.43 | 12.43 | 15.78 | -3.35 | 0.46 | 8.471455 | -0.283793738 | -3.066206262 | 0.618451 | 618.4510251 | | | |
| 61 | 4.18 | 4.67 | 12.97 | 15.78 | -2.81 | 0.49 | 10.49251 | -0.2948394 | -2.5151606 | 0.624332 | 624.3315508 | | | |
| 62 | 3.31 | 3.69 | 14.19 | 15.78 | -1.59 | 0.38 | 10.2981 | -0.163739837 | -1.426260163 | 0.698864 | 698.8636364 | | | |
| 63 | 4.45 | 4.86 | 12.44 | 15.78 | -3.34 | 0.41 | 8.436214 | -0.281769547 | -3.058230453 | 0.592683 | 592.6829268 | | | |
| 64 | 3.3 | 3.73 | 11.92 | 15.78 | -3.86 | 0.43 | 11.52815 | -0.444986595 | -3.415013405 | 0.491436 | 491.4361001 | | | |
| 65 | 5.17 | 5.62 | 10.67 | 15.78 | -5.11 | 0.45 | 8.007117 | -0.409163701 | -4.700836299 | 0.523765 | 523.7651445 | | | |
| 66 | 2.97 | 3.27 | 12.98 | 15.78 | -2.8 | 0.3 | 9.174312 | -0.256880734 | -2.543119266 | 0.538715 | 538.7149918 | | | |
| 67 | 3.48 | 3.86 | 12.76 | 15.78 | -3.02 | 0.38 | 9.84456 | -0.297305699 | -2.722694301 | 0.561047 | 561.0465116 | | | |
| 68 | 3.3 | 3.69 | 11.32 | 15.78 | -4.46 | 0.39 | 10.56911 | -0.471382114 | -3.988617886 | 0.452761 | 452.7607362 | | | |
| 69 | 3.39 | 3.69 | 13.47 | 15.78 | -2.31 | 0.3 | 8.130081 | -0.187804878 | -2.122195122 | 0.615 | 615 | | | |
| 70 | 3.06 | 3.35 | 13.26 | 15.78 | -2.52 | 0.29 | 8.656716 | -0.218149254 | -2.301850746 | 0.570698 | 570.6984668 | | | |
| 71 | 1.91 | 2.14 | 12.88 | 15.78 | -2.9 | 0.23 | 10.74766 | -0.311682243 | -2.588317757 | 0.424603 | 424.6031746 | | | |
| 72 | 1.98 | 2.26 | 13.61 | 15.78 | -2.17 | 0.28 | 12.38938 | -0.268849558 | -1.901150442 | 0.510158 | 510.1580135 | | | |
| 73 | 2.01 | 2.27 | 13.09 | 15.78 | -2.69 | 0.26 | 11.45374 | -0.308105727 | -2.381894273 | 0.457661 | 457.6612903 | | | |
| 74 | 3.63 | 3.88 | 12.66 | 15.78 | -3.12 | 0.25 | 6.443299 | -0.201030928 | -2.918969072 | 0.554286 | 554.2857143 | | | |
| 75 | 2.77 | 3.02 | 14 | 15.78 | -1.78 | 0.25 | 8.278146 | -0.147350993 | -1.632649007 | 0.629167 | 629.1666667 | | | |
| 76 | 3.3 | 3.6 | 14.01 | 15.78 | -1.77 | 0.3 | 8.333333 | -0.1475 | -1.6225 | 0.670391 | 670.3910615 | | | |
| 77 | 3.21 | 3.54 | 14.29 | 15.78 | -1.49 | 0.33 | 9.322034 | -0.138898305 | -1.351101695 | 0.703777 | 703.777336 | | | |
| 78 | 1.69 | 1.95 | 13.6 | 15.78 | -2.18 | 0.26 | 13.33333 | -0.290666667 | -1.889333333 | 0.472155 | 472.1549637 | | | |
| 79 | 3.17 | 3.47 | 13.81 | 15.78 | -1.97 | 0.3 | 8.645533 | -0.170317003 | -1.799682997 | 0.637868 | 637.8676471 | | | |
| 80 | 1.18 | 1.45 | 12.23 | 15.78 | -3.55 | 0.27 | 18.62069 | -0.661034483 | -2.888965517 | 0.29 | 290 | | | |
| 81 | 3.54 | 3.82 | 13.23 | 15.78 | -2.55 | 0.28 | 7.329843 | -0.186910995 | -2.363089005 | 0.599686 | 599.6860283 | | | |
| 82 | 2.85 | 3.13 | 13.44 | 15.78 | -2.34 | 0.28 | 8.945687 | -0.209329073 | -2.130670927 | 0.572212 | 572.2120658 | | | |
| 83 | 2.62 | 2.99 | 12.74 | 15.78 | -3.04 | 0.37 | 12.37458 | -0.376187291 | -2.663812709 | 0.495854 | 495.854063 | | | |
| 84 | 1.93 | 2.29 | 12.8 | 15.78 | -2.98 | 0.36 | 15.72052 | -0.468471616 | -2.511528384 | 0.434535 | 434.5351044 | | | |
| 85 | 3.36 | 3.83 | 11.38 | 15.78 | -4.4 | 0.47 | 12.27154 | -0.539947781 | -3.860052219 | 0.465371 | 465.3705954 | | | |
| 86 | 1.39 | 1.66 | 11.82 | 15.78 | -3.96 | 0.27 | 16.26506 | -0.644096386 | -3.315903614 | 0.295374 | 295.3736655 | | | |
| 87 | 4.26 | 4.56 | 9.72 | 15.78 | -6.06 | 0.3 | 6.578947 | -0.398684211 | -5.661315789 | 0.429379 | 429.3785311 | | | |
| 88 | 3.07 | 3.48 | 12.39 | 15.78 | -3.39 | 0.41 | 11.78161 | -0.399396552 | -2.990603448 | 0.50655 | 506.5502183 | | | |
| 89 | 3.99 | 4.3 | 12.36 | 15.78 | -3.42 | 0.31 | 7.209302 | -0.24655814 | -3.17344186 | 0.556995 | 556.9948187 | | | |
| 90 | 2.23 | 2.48 | 13.38 | 15.78 | -2.4 | 0.25 | 10.08065 | -0.241935484 | -2.158064516 | 0.508197 | 508.1967213 | | | |

Table A1.10. Density measurements for ScL.

| number | | | | | Wc+s water | | | Ws water | Wc water | SG | DENSITY kg m^- 3 | density sorted | density range | density mean of 90 |
|--------|-----------|-----------|-----------|----------------|---------------|---------------------|--------------|-------------------------|-----------------------|--------------|---------------------|-------------------|------------------|-----------------------|
| | | | | ballast wet | clast wet | sheet dry weight | sheet % | sheet wet weight (g) | clast wet no sheet | | | | | |
| 1 | 6.71 | 6.98 | 12.9 7 | 15.78 | -2.81 | 0.27 | 3.86819 5 | -0.108696275 | -2.701303725 | 0.71297 2 | 712.9724208 | 290.5355833 | 290.535583 3 | #DIV/0! |
| 2 | 6.58 | 6.84 | 15.7 5 | 15.78 | -0.03 | 0.26 | 3.80117 | -0.001140351 | -0.028859649 | 0.99563 3 | 995.6331878 | 480.1297648 | 1332.68608 4 | stdev |
| 3 | 10.9 2 | 11.2 2 | 16.3 2 | 15.78 | 0.54 | 0.3 | 2.67379 7 | 0.014438503 | 0.525561497 | 1.05056 2 | 1050.561798 | 550.5415162 | | #DIV/0! |

| | | | | | | | | | | | | | | |
|----|-----------|-----------|-----------|-------|-------|------|--------------|--------------|--------------|--------------|-------------|-------------|--|-------------|
| 4 | 7.52 | 7.8 | 15.6 5 | 15.78 | -0.13 | 0.28 | 3.58974 4 | -0.004666667 | -0.125333333 | 0.98360 7 | 983.6065574 | 638.5426654 | | |
| 5 | 8.04 | 8.37 | 11.2 9 | 15.78 | -4.49 | 0.33 | 3.94265 2 | -0.17702509 | -4.31297491 | 0.65085 5 | 650.8553655 | 650.8553655 | | mean of 50 |
| 6 | 3.72 | 3.96 | 6.11 | 15.78 | -9.67 | 0.24 | 6.06060 6 | -0.586060606 | -9.083939394 | 0.29053 6 | 290.5355833 | 676.2402089 | | 889.9081384 |
| 7 | 5.36 | 5.65 | 13.6 8 | 15.78 | -2.1 | 0.29 | 5.13274 3 | -0.107787611 | -1.992212389 | 0.72903 2 | 729.0322581 | 712.9724208 | | stdev |
| 8 | 4.89 | 5.18 | 13.3 | 15.78 | -2.48 | 0.29 | 5.59845 6 | -0.138841699 | -2.341158301 | 0.67624 | 676.2402089 | 729.0268456 | | 180.540113 |
| 9 | 8.45 | 8.77 | 15.5 8 | 15.78 | -0.2 | 0.32 | 3.64880 3 | -0.007297605 | -0.192702395 | 0.97770 3 | 977.703456 | 729.0322581 | | vesic |
| 10 | 8.12 | 8.69 | 12.5 5 | 15.78 | -3.23 | 0.57 | 6.55926 4 | -0.211864212 | -3.018135788 | 0.72902 7 | 729.0268456 | 730.5475504 | | 70.33639539 |
| 11 | 5.68 | 5.99 | 15.6 | 15.78 | -0.18 | 0.31 | 5.17529 2 | -0.009315526 | -0.170684474 | 0.97082 7 | 970.8265802 | 748.1108312 | | 90.31548056 |
| 12 | 4.03 | 4.34 | 15.3 6 | 15.78 | -0.42 | 0.31 | 7.14285 7 | -0.03 | -0.39 | 0.91176 5 | 911.7647059 | 765.1057402 | | 55.57713053 |
| 13 | 12.1 6 | 12.4 8 | 16.6 | 15.78 | 0.82 | 0.32 | 2.56410 3 | 0.021025641 | 0.798974359 | 1.07032 6 | 1070.325901 | 768.1623932 | | |
| 14 | 10.6 | 10.9 | 15.0 2 | 15.78 | -0.76 | 0.3 | 2.75229 4 | -0.020917431 | -0.739082569 | 0.93482 | 934.8198971 | 819.7226502 | | |
| 15 | 8.76 | 9.15 | 8.31 | 15.78 | -7.47 | 0.39 | 4.26229 5 | -0.318393443 | -7.151606557 | 0.55054 2 | 550.5415162 | 822.4299065 | | |
| 16 | 8.58 | 9.1 | 15.1 4 | 15.78 | -0.64 | 0.52 | 5.71428 6 | -0.036571429 | -0.603428571 | 0.93429 2 | 934.2915811 | 826.3555251 | | |
| 17 | 6.01 | 6.27 | 16.3 | 15.78 | 0.52 | 0.26 | 4.14673 | 0.021562998 | 0.498437002 | 1.09043 5 | 1090.434783 | 843.75 | | |
| 18 | 5.63 | 5.92 | 9.37 | 15.78 | -6.41 | 0.29 | 4.89864 9 | -0.314003378 | -6.095996622 | 0.48013 | 480.1297648 | 864.1686183 | | |
| 19 | 4.88 | 5.18 | 15.9 5 | 15.78 | 0.17 | 0.3 | 5.79150 6 | 0.00984556 | 0.16015444 | 1.03393 2 | 1033.932136 | 872.9472774 | | |
| 20 | 5.23 | 5.49 | 15.8 6 | 15.78 | 0.08 | 0.26 | 4.73588 3 | 0.003788707 | 0.076211293 | 1.01478 7 | 1014.787431 | 878.5607196 | | |
| 21 | 7.54 | 7.83 | 16.2 1 | 15.78 | 0.43 | 0.29 | 3.70370 4 | 0.015925926 | 0.414074074 | 1.05810 8 | 1058.108108 | 890.7103825 | | |
| 22 | 5.92 | 6.18 | 15.8 3 | 15.78 | 0.05 | 0.26 | 4.20712 | 0.00210356 | 0.04789644 | 1.00815 7 | 1008.156607 | 900.2744739 | | |
| 23 | 7.16 | 7.38 | 14.6 2 | 15.78 | -1.16 | 0.22 | 2.98103 | -0.034579946 | -1.125420054 | 0.86416 9 | 864.1686183 | 911.7647059 | | |
| 24 | 2.97 | 3.26 | 15.5 9 | 15.78 | -0.19 | 0.29 | 8.89570 6 | -0.01690184 | -0.17309816 | 0.94492 8 | 944.9275362 | 925.1101322 | | |
| 25 | 3.95 | 4.2 | 15.4 4 | 15.78 | -0.34 | 0.25 | 5.95238 1 | -0.020238095 | -0.319761905 | 0.92511 | 925.1101322 | 928.1524927 | | |
| 26 | 5.04 | 5.32 | 14.6 1 | 15.78 | -1.17 | 0.28 | 5.26315 8 | -0.061578947 | -1.108421053 | 0.81972 3 | 819.7226502 | 934.2915811 | | |
| 27 | 4.91 | 5.18 | 15.8 8 | 15.78 | 0.1 | 0.27 | 5.21235 5 | 0.005212355 | 0.094787645 | 1.01968 5 | 1019.685039 | 934.8198971 | | |
| 28 | 5.89 | 6.16 | 14.4 5 | 15.78 | -1.33 | 0.27 | 4.38311 7 | -0.058295455 | -1.271704545 | 0.82243 | 822.4299065 | 935.0282486 | | |

| | | | | | | | | | | | | | | |
|----|-----------|-----------|-----------|-------|-------|-------|--------------|--------------|--------------|--------------|-------------|-------------|--|--|
| 29 | 4.8 | 5.07 | 13.9 1 | 15.78 | -1.87 | 0.27 | 5.32544 4 | -0.099585799 | -1.770414201 | 0.73054 8 | 730.5475504 | 944.9275362 | | |
| 30 | 6.42 | 6.66 | 12.0 1 | 15.78 | -3.77 | 0.24 | 3.60360 4 | -0.135855856 | -3.634144144 | 0.63854 3 | 638.5426654 | 954.9668874 | | |
| 31 | 6.09 | 6.33 | 15.2 9 | 15.78 | -0.49 | 0.24 | 3.79146 9 | -0.018578199 | -0.471421801 | 0.92815 2 | 928.1524927 | 959.5170455 | | |
| 32 | 2.77 | 2.97 | 14.7 8 | 15.78 | -1 | 0.2 | 6.73400 7 | -0.067340067 | -0.932659933 | 0.74811 1 | 748.1108312 | 964.7546648 | | |
| 33 | 12.9 4 | 13.5 1 | 16.8 1 | 15.78 | 1.03 | 0.57 | 4.21909 7 | 0.043456699 | 0.986543301 | 1.08253 2 | 1082.532051 | 970.8265802 | | |
| 34 | 15.2 8 | 13.0 4 | 14.1 8 | 15.78 | -1.6 | -2.24 | -17.1779 | 0.274846626 | -1.874846626 | 0.89071 | 890.7103825 | 977.703456 | | |
| 35 | 13.8 9 | 14.4 2 | 15.1 | 15.78 | -0.68 | 0.53 | 3.67545 1 | -0.024993065 | -0.655006935 | 0.95496 7 | 954.9668874 | 983.6065574 | | |
| 36 | 19.9 6 | 20.5 9 | 20.9 2 | 15.78 | 5.14 | 0.63 | 3.05973 8 | 0.15727052 | 4.98272948 | 1.33268 6 | 1332.686084 | 987.6847291 | | |
| 37 | 9.54 | 10.1 3 | 12.6 7 | 15.78 | -3.11 | 0.59 | 5.82428 4 | -0.181135242 | -2.928864758 | 0.76510 6 | 765.1057402 | 995.6331878 | | |
| 38 | 13.5 3 | 13.9 6 | 15.2 7 | 15.78 | -0.51 | 0.43 | 3.08022 9 | -0.015709169 | -0.494290831 | 0.96475 5 | 964.7546648 | 1007.371007 | | |
| 39 | 11.5 5 | 12.0 3 | 15.6 3 | 15.78 | -0.15 | 0.48 | 3.99002 5 | -0.005985037 | -0.144014963 | 0.98768 5 | 987.6847291 | 1008.156607 | | |
| 40 | 9.3 | 9.84 | 14.6 9 | 15.78 | -1.09 | 0.54 | 5.48780 5 | -0.059817073 | -1.030182927 | 0.90027 4 | 900.2744739 | 1014.787431 | | |
| 41 | 11.4 6 | 12.0 4 | 13.2 5 | 15.78 | -2.53 | 0.58 | 4.81727 6 | -0.121877076 | -2.408122924 | 0.82635 6 | 826.3555251 | 1019.685039 | | |
| 42 | 12.4 1 | 13 | 17.2 5 | 15.78 | 1.47 | 0.59 | 4.53846 2 | 0.066715385 | 1.403284615 | 1.12749 3 | 1127.493495 | 1033.932136 | | |
| 43 | 6.82 | 7.19 | 13.6 1 | 15.78 | -2.17 | 0.37 | 5.14603 6 | -0.111668985 | -2.058331015 | 0.76816 2 | 768.1623932 | 1050.561798 | | |
| 44 | 11.1 7 | 11.7 2 | 14.1 6 | 15.78 | -1.62 | 0.55 | 4.69283 3 | -0.076023891 | -1.543976109 | 0.87856 1 | 878.5607196 | 1058.108108 | | |
| 45 | 9.55 | 10.1 | 14.3 1 | 15.78 | -1.47 | 0.55 | 5.44554 5 | -0.080049505 | -1.389950495 | 0.87294 7 | 872.9472774 | 1070.325901 | | |
| 46 | 20.0 1 | 20.5 6 | 17.6 8 | 15.78 | 1.9 | 0.55 | 2.67509 7 | 0.050826848 | 1.849173152 | 1.10182 2 | 1101.822079 | 1082.532051 | | |
| 47 | 12.9 6 | 13.5 1 | 15.2 1 | 15.78 | -0.57 | 0.55 | 4.07105 8 | -0.023205033 | -0.546794967 | 0.95951 7 | 959.5170455 | 1090.434783 | | |
| 48 | 11.7 4 | 12.3 | 15.8 7 | 15.78 | 0.09 | 0.56 | 4.55284 6 | 0.004097561 | 0.085902439 | 1.00737 1 | 1007.371007 | 1101.822079 | | |
| 49 | 8.17 | 8.64 | 14.1 8 | 15.78 | -1.6 | 0.47 | 5.43981 5 | -0.087037037 | -1.512962963 | 0.84375 | 843.75 | 1127.493495 | | |
| 50 | 12.7 9 | 13.2 4 | 14.8 6 | 15.78 | -0.92 | 0.45 | 3.39879 2 | -0.031268882 | -0.888731118 | 0.93502 8 | 935.0282486 | 1332.686084 | | |
| 51 | 5.62 | 6.12 | 13.8 2 | 15.78 | -1.96 | 0.5 | 8.16993 5 | -0.160130719 | -1.799869281 | 0.75742 6 | 757.4257426 | | | |
| 52 | 9.12 | 9.73 | 15.2 2 | 15.78 | -0.56 | 0.61 | 6.26927 | -0.035107914 | -0.524892086 | 0.94557 8 | 945.5782313 | | | |
| 53 | 14.2 5 | 14.7 8 | 17.9 7 | 15.78 | 2.19 | 0.53 | 3.58592 7 | 0.0785318 | 2.1114682 | 1.17394 8 | 1173.947577 | | | |

| | | | | | | | | | | | | | | |
|---|-----------|-----------|-----------|-------|-------|------|--------------|--------------|--------------|--------------|-------------|--|--|--|
| 54 | 16.2 2 | 16.8 3 | 13.1 8 | 15.78 | -2.6 | 0.61 | 3.62448 | -0.094236482 | -2.505763518 | 0.86618 6 | 866.1863098 | | | |
| 55 | 7.99 | 8.48 | 15.5 4 | 15.78 | -0.24 | 0.49 | 5.77830 2 | -0.013867925 | -0.226132075 | 0.97247 7 | 972.4770642 | | | |
| 56 | 6.98 | 7.29 | 15.5 8 | 15.78 | -0.2 | 0.31 | 4.25240 1 | -0.008504801 | -0.191495199 | 0.97329 8 | 973.2977303 | | | |
| 57 | 10.7 5 | 11.1 2 | 14.8 | 15.78 | -0.98 | 0.37 | 3.32733 8 | -0.032607914 | -0.947392086 | 0.91900 8 | 919.0082645 | | | |
| 58 | 4.23 | 4.5 | 16.0 4 | 15.78 | 0.26 | 0.27 | 6 | 0.0156 | 0.2444 | 1.06132 1 | 1061.320755 | | | |
| 59 | 3.37 | 3.67 | 14.4 4 | 15.78 | -1.34 | 0.3 | 8.17438 7 | -0.109536785 | -1.230463215 | 0.73253 5 | 732.5349301 | | | |
| 60 | 3.28 | 3.55 | 15.1 9 | 15.78 | -0.59 | 0.27 | 7.60563 4 | -0.044873239 | -0.545126761 | 0.85748 8 | 857.4879227 | | | |
| 61 | 2.2 | 2.52 | 15.3 5 | 15.78 | -0.43 | 0.32 | 12.6984 1 | -0.054603175 | -0.375396825 | 0.85423 7 | 854.2372881 | | | |
| Table A1.11. Density measurements for waSc. | | | | | | | | | | | | | | |

| number | | | | Wc+s water | | | Ws water | Wc water | SG | DENSITY kg m^-3 | density sorted | density range | density mean of 900 |
|--------|-------|-------|------|------------|------------------|----------|----------------------|--------------------|----------|-----------------|----------------|---------------|---------------------|
| | | | | clast wet | sheet dry weight | sheet % | sheet wet weight (g) | clast wet no sheet | | | | | |
| 1 | 10.52 | 11.07 | 1.98 | 1.98 | 0.55 | 4.968383 | 0.098373984 | 1.881626016 | 1.217822 | 1217.821782 | 1037.481259 | 1037.481259 | #DIV/0! |
| 2 | 7.58 | 8.05 | 1.2 | 1.2 | 0.47 | 5.838509 | 0.070062112 | 1.129937888 | 1.175182 | 1175.182482 | 1046.464646 | 1349 | stdev |
| 3 | 5.48 | 5.96 | 0.9 | 0.9 | 0.48 | 8.053691 | 0.072483221 | 0.827516779 | 1.177866 | 1177.865613 | 1049.309665 | | #DIV/0! |
| 4 | 4.22 | 4.54 | 0.74 | 0.74 | 0.32 | 7.048458 | 0.05215859 | 0.68784141 | 1.194737 | 1194.736842 | 1058.252427 | | |
| 5 | 6.18 | 6.53 | 0.74 | 0.74 | 0.35 | 5.359877 | 0.039663093 | 0.700336907 | 1.127807 | 1127.806563 | 1060.606061 | | mean of 50 |
| 6 | 8.6 | 9.09 | 1.33 | 1.33 | 0.49 | 5.390539 | 0.071694169 | 1.258305831 | 1.171392 | 1171.391753 | 1061.776062 | | 1172.542647 |
| 7 | 8.53 | 9.08 | 1.8 | 1.8 | 0.55 | 6.057269 | 0.109030837 | 1.690969163 | 1.247253 | 1247.252747 | 1069.767442 | | stdev |
| 8 | 9.26 | 9.76 | 1.4 | 1.4 | 0.5 | 5.122951 | 0.071721311 | 1.328278689 | 1.167464 | 1167.464115 | 1083.707025 | | 77.73529688 |
| 9 | 4.79 | 5.18 | 0.23 | 0.23 | 0.39 | 7.528958 | 0.017316602 | 0.212683398 | 1.046465 | 1046.464646 | 1084.821429 | | |
| 10 | 7.71 | 8.25 | 0.48 | 0.48 | 0.54 | 6.545455 | 0.031418182 | 0.448581818 | 1.061776 | 1061.776062 | 1089.84375 | | vesicularity |
| 11 | 7.69 | 8.21 | 1.11 | 1.11 | 0.52 | 6.333739 | 0.070304507 | 1.039695493 | 1.156338 | 1156.338028 | 1094.736842 | | 60.9152451 |
| 12 | 5.54 | 5.93 | 1 | 1 | 0.39 | 6.576728 | 0.065767285 | 0.934232715 | 1.20284 | 1202.839757 | 1099.885189 | | 65.41729135 |
| 13 | 7.13 | 7.59 | 1.04 | 1.04 | 0.46 | 6.060606 | 0.063030303 | 0.976969697 | 1.158779 | 1158.778626 | 1101.5625 | | 55.03333333 |
| 14 | 3.88 | 4.2 | 0.24 | 0.24 | 0.32 | 7.619048 | 0.018285714 | 0.221714286 | 1.060606 | 1060.606061 | 1117.194183 | | |
| 15 | 15.96 | 16.53 | 3.85 | 3.85 | 0.57 | 3.448276 | 0.132758621 | 3.717241379 | 1.303628 | 1303.62776 | 1127.806563 | | |
| 16 | 10.42 | 10.99 | 2 | 2 | 0.57 | 5.186533 | 0.103730664 | 1.896269336 | 1.222469 | 1222.46941 | 1128.808864 | | |
| 17 | 4.16 | 4.45 | 0.77 | 0.77 | 0.29 | 6.516854 | 0.050179775 | 0.719820225 | 1.209239 | 1209.23913 | 1131.147541 | | |
| 18 | 5.94 | 6.2 | 1.18 | 1.18 | 0.26 | 4.193548 | 0.049483871 | 1.130516129 | 1.23506 | 1235.059761 | 1153.939394 | | |
| 19 | 3.87 | 4.16 | 0.36 | 0.36 | 0.29 | 6.971154 | 0.025096154 | 0.334903846 | 1.094737 | 1094.736842 | 1156.338028 | | |
| 20 | 4.73 | 5.04 | 0.88 | 0.88 | 0.31 | 6.150794 | 0.054126984 | 0.825873016 | 1.211538 | 1211.538462 | 1158.778626 | | |
| 21 | 12.56 | 13.06 | 1.37 | 1.37 | 0.5 | 3.828484 | 0.05245023 | 1.31754977 | 1.117194 | 1117.194183 | 1160.674157 | | |
| 22 | 8.8 | 9.16 | 1.39 | 1.39 | 0.36 | 3.930131 | 0.054628821 | 1.335371179 | 1.178893 | 1178.893179 | 1167.464115 | | |
| 23 | 6.79 | 7.05 | 1.47 | 1.47 | 0.26 | 3.687943 | 0.054212766 | 1.415787234 | 1.263441 | 1263.44086 | 1171.391753 | | |
| 24 | 12.34 | 12.93 | 1.96 | 1.96 | 0.59 | 4.563032 | 0.089435422 | 1.870564578 | 1.178669 | 1178.669098 | 1175.182482 | | |

| | | | | | | | | | | | | | |
|--|-------|-------|------|------|------|----------|-------------|-------------|----------|-------------|-------------|--|--|
| 25 | 15.22 | 15.73 | 2.74 | 2.74 | 0.51 | 3.242212 | 0.088836618 | 2.651163382 | 1.210931 | 1210.931486 | 1177.865613 | | |
| 26 | 8.6 | 9.2 | 0.6 | 0.6 | 0.6 | 6.521739 | 0.039130435 | 0.560869565 | 1.069767 | 1069.767442 | 1177.94836 | | |
| 27 | 13.47 | 13.95 | 1.15 | 1.15 | 0.48 | 3.44086 | 0.039569892 | 1.110430108 | 1.089844 | 1089.84375 | 1178.669098 | | |
| 28 | 9.36 | 9.89 | 2.25 | 2.25 | 0.53 | 5.358948 | 0.12057634 | 2.12942366 | 1.294503 | 1294.502618 | 1178.893179 | | |
| 29 | 6.66 | 7.05 | 0.65 | 0.65 | 0.39 | 5.531915 | 0.035957447 | 0.614042553 | 1.101563 | 1101.5625 | 1181.603774 | | |
| 30 | 11.56 | 12.04 | 2.09 | 2.09 | 0.48 | 3.986711 | 0.083322259 | 2.006677741 | 1.21005 | 1210.050251 | 1194.736842 | | |
| 31 | 6.63 | 6.95 | 1.8 | 1.8 | 0.32 | 4.604317 | 0.082877698 | 1.717122302 | 1.349515 | 1349.514563 | 1201.447527 | | |
| 32 | 9.04 | 9.58 | 0.87 | 0.87 | 0.54 | 5.636743 | 0.049039666 | 0.820960334 | 1.099885 | 1099.885189 | 1202.839757 | | |
| 33 | 4.68 | 4.83 | 0.56 | 0.56 | 0.15 | 3.10559 | 0.017391304 | 0.542608696 | 1.131148 | 1131.147541 | 1209.23913 | | |
| 34 | 15.95 | 16.88 | 2.55 | 2.55 | 0.93 | 5.509479 | 0.140491706 | 2.409508294 | 1.177948 | 1177.94836 | 1210.050251 | | |
| 35 | 6.62 | 6.92 | 0.25 | 0.25 | 0.3 | 4.33526 | 0.01083815 | 0.23916185 | 1.037481 | 1037.481259 | 1210.931486 | | |
| 36 | 7.96 | 8.23 | 1.78 | 1.78 | 0.27 | 3.28068 | 0.058396112 | 1.721603888 | 1.275969 | 1275.968992 | 1211.538462 | | |
| 37 | 6.13 | 6.44 | 1.13 | 1.13 | 0.31 | 4.813665 | 0.05439441 | 1.07560559 | 1.212806 | 1212.806026 | 1212.806026 | | |
| 38 | 6.15 | 6.44 | 1.33 | 1.33 | 0.29 | 4.503106 | 0.059891304 | 1.270108696 | 1.260274 | 1260.273973 | 1217.821782 | | |
| 39 | 9.66 | 9.96 | 1.67 | 1.67 | 0.3 | 3.012048 | 0.050301205 | 1.619698795 | 1.201448 | 1201.447527 | 1222.46941 | | |
| 40 | 5.79 | 6.06 | 1.51 | 1.51 | 0.27 | 4.455446 | 0.067277228 | 1.442722772 | 1.331868 | 1331.868132 | 1235.059761 | | |
| 41 | 9.16 | 9.46 | 1.91 | 1.91 | 0.3 | 3.171247 | 0.060570825 | 1.849429175 | 1.25298 | 1252.980132 | 1236.842105 | | |
| 42 | 7.54 | 8.15 | 0.93 | 0.93 | 0.61 | 7.484663 | 0.069607362 | 0.860392638 | 1.128809 | 1128.808864 | 1247.252747 | | |
| 43 | 6.29 | 6.58 | 1.26 | 1.26 | 0.29 | 4.407295 | 0.055531915 | 1.204468085 | 1.236842 | 1236.842105 | 1252.980132 | | |
| 44 | 9.76 | 10.33 | 1.43 | 1.43 | 0.57 | 5.517909 | 0.078906099 | 1.351093901 | 1.160674 | 1160.674157 | 1260.273973 | | |
| 45 | 6.71 | 7.25 | 0.56 | 0.56 | 0.54 | 7.448276 | 0.041710345 | 0.518289655 | 1.083707 | 1083.707025 | 1263.44086 | | |
| 46 | 9.45 | 10.02 | 1.54 | 1.54 | 0.57 | 5.688623 | 0.08760479 | 1.45239521 | 1.181604 | 1181.603774 | 1275.968992 | | |
| 47 | 9.02 | 9.52 | 1.27 | 1.27 | 0.5 | 5.252101 | 0.066701681 | 1.203298319 | 1.153939 | 1153.939394 | 1294.502618 | | |
| 48 | 4.6 | 4.86 | 0.38 | 0.38 | 0.26 | 5.349794 | 0.020329218 | 0.359670782 | 1.084821 | 1084.821429 | 1303.62776 | | |
| 49 | 4.06 | 4.36 | 0.24 | 0.24 | 0.3 | 6.880734 | 0.016513761 | 0.223486239 | 1.058252 | 1058.252427 | 1331.868132 | | |
| 50 | 4.93 | 5.32 | 0.25 | 0.25 | 0.39 | 7.330827 | 0.018327068 | 0.231672932 | 1.04931 | 1049.309665 | 1349.514563 | | |
| Table A.1.12. Density measurements for mwSc. | | | | | | | | | | | | | |

| number | | | | Wc+s water | | | Ws water | Wc water | SG | DENSITY kg m^-3 | density sorted | density range | density mean of 90 |
|--------|-------|-------|-------|------------|------------------|----------|----------------------|--------------------|----------|-----------------|----------------|---------------|--------------------|
| | | | | clast wet | sheet dry weight | sheet % | sheet wet weight (g) | clast wet no sheet | | | | | |
| 1 | 13.24 | 13.3 | 7.31 | 7.31 | 0.06 | 0.451128 | 0.032977444 | 7.277022556 | 2.220367 | 2220.367279 | 1450 | 1450 | #DIV/0! |
| 2 | 13.28 | 13.76 | 4.7 | 4.7 | 0.48 | 3.488372 | 0.163953488 | 4.536046512 | 1.518764 | 1518.763797 | 1465.783664 | 2322 | stdev |
| 3 | 12.55 | 13.03 | 6.16 | 6.16 | 0.48 | 3.683807 | 0.226922487 | 5.933077513 | 1.896652 | 1896.652111 | 1518.763797 | | #DIV/0! |
| 4 | 12.05 | 12.26 | 5.99 | 5.99 | 0.21 | 1.712887 | 0.102601958 | 5.887398042 | 1.955343 | 1955.342903 | 1527.777778 | | |
| 5 | 13.52 | 13.79 | 6.32 | 6.32 | 0.27 | 1.957941 | 0.123741842 | 6.196258158 | 1.846051 | 1846.05087 | 1544.850498 | | mean of 50 |
| 6 | 5.13 | 5.43 | 2.19 | 2.19 | 0.3 | 5.524862 | 0.120994475 | 2.069005525 | 1.675926 | 1675.925926 | 1675.925926 | | 1943.681403 |
| 7 | 13.7 | 14.3 | 7.29 | 7.29 | 0.6 | 4.195804 | 0.305874126 | 6.984125874 | 2.039943 | 2039.942939 | 1719.723183 | | stdev |
| 8 | 17.67 | 17.88 | 10.12 | 10.12 | 0.21 | 1.174497 | 0.11885906 | 10.00114094 | 2.304124 | 2304.123711 | 1751.740139 | | 214.4349911 |
| 9 | 7.15 | 7.55 | 3.24 | 3.24 | 0.4 | 5.298013 | 0.171655629 | 3.068344371 | 1.75174 | 1751.740139 | 1778.611632 | | |
| 10 | 11.26 | 11.88 | 6.69 | 6.69 | 0.62 | 5.218855 | 0.349141414 | 6.340858586 | 2.289017 | 2289.017341 | 1785.854617 | | vesicularity |
| 11 | 7.19 | 7.64 | 4.05 | 4.05 | 0.45 | 5.890052 | 0.23854712 | 3.81145288 | 2.128134 | 2128.133705 | 1786.786787 | | 35.2106199 |
| 12 | 10.04 | 10.5 | 5.39 | 5.39 | 0.46 | 4.380952 | 0.236133333 | 5.153866667 | 2.054795 | 2054.794521 | 1816.129032 | | 51.66666667 |

| | | | | | | | | | | | | | |
|----|-------|-------|------|------|------|----------|-------------|-------------|----------|-------------|-------------|--|------|
| 13 | 6.63 | 7.13 | 3.39 | 3.39 | 0.5 | 7.012623 | 0.23772791 | 3.15227209 | 1.906417 | 1906.417112 | 1836.689038 | | 22.6 |
| 14 | 17.74 | 18.28 | 9.61 | 9.61 | 0.54 | 2.954048 | 0.283884026 | 9.326115974 | 2.10842 | 2108.419839 | 1846.05087 | | |
| 15 | 11.24 | 11.55 | 3.99 | 3.99 | 0.31 | 2.683983 | 0.107090909 | 3.882909091 | 1.527778 | 1527.777778 | 1847.727273 | | |
| 16 | 6.65 | 7.06 | 3.85 | 3.85 | 0.41 | 5.807365 | 0.223583569 | 3.626416431 | 2.199377 | 2199.376947 | 1874.58194 | | |
| 17 | 9.49 | 9.9 | 5.28 | 5.28 | 0.41 | 4.141414 | 0.218666667 | 5.061333333 | 2.142857 | 2142.857143 | 1896.652111 | | |
| 18 | 10.8 | 11.21 | 5.23 | 5.23 | 0.41 | 3.657449 | 0.191284567 | 5.038715433 | 1.874582 | 1874.58194 | 1906.417112 | | |
| 19 | 7.77 | 8.28 | 4.24 | 4.24 | 0.51 | 6.15942 | 0.26115942 | 3.97884058 | 2.049505 | 2049.50495 | 1910.958904 | | |
| 20 | 6.41 | 6.98 | 3.83 | 3.83 | 0.57 | 8.166189 | 0.312765043 | 3.517234957 | 2.215873 | 2215.873016 | 1914.691943 | | |
| 21 | 7.52 | 8.13 | 3.73 | 3.73 | 0.61 | 7.503075 | 0.279864699 | 3.450135301 | 1.847727 | 1847.727273 | 1915.09434 | | |
| 22 | 12.49 | 13 | 6.79 | 6.79 | 0.51 | 3.923077 | 0.266376923 | 6.523623077 | 2.093398 | 2093.397746 | 1924.205379 | | |
| 23 | 4.32 | 4.65 | 1.64 | 1.64 | 0.33 | 7.096774 | 0.116387097 | 1.523612903 | 1.54485 | 1544.850498 | 1930.693069 | | |
| 24 | 6.76 | 7.19 | 3.93 | 3.93 | 0.43 | 5.980529 | 0.235034771 | 3.694965229 | 2.205521 | 2205.521472 | 1950.596252 | | |
| 25 | 8.38 | 9.09 | 4 | 4 | 0.71 | 7.810781 | 0.312431243 | 3.687568757 | 1.785855 | 1785.854617 | 1955.342903 | | |
| 26 | 5.31 | 5.58 | 2.66 | 2.66 | 0.27 | 4.83871 | 0.128709677 | 2.531290323 | 1.910959 | 1910.958904 | 1955.357143 | | |
| 27 | 11.11 | 11.42 | 5.61 | 5.61 | 0.31 | 2.714536 | 0.152285464 | 5.457714536 | 1.965577 | 1965.576592 | 1955.451348 | | |
| 28 | 12.95 | 13.19 | 6.57 | 6.57 | 0.24 | 1.81956 | 0.11954511 | 6.45045489 | 1.992447 | 1992.44713 | 1965.576592 | | |
| 29 | 5.88 | 6.01 | 2.97 | 2.97 | 0.13 | 2.163062 | 0.064242928 | 2.905757072 | 1.976974 | 1976.973684 | 1965.859031 | | |
| 30 | 10.48 | 10.85 | 5.54 | 5.54 | 0.37 | 3.410138 | 0.188921659 | 5.351078341 | 2.043315 | 2043.314501 | 1976.973684 | | |
| 31 | 13.99 | 14.4 | 7.2 | 7.2 | 0.41 | 2.847222 | 0.205 | 6.995 | 2 | 2000 | 1992.44713 | | |
| 32 | 8.12 | 8.55 | 4.65 | 4.65 | 0.43 | 5.02924 | 0.233859649 | 4.416140351 | 2.192308 | 2192.307692 | 2000 | | |
| 33 | 4.59 | 4.97 | 2.08 | 2.08 | 0.38 | 7.645875 | 0.159034205 | 1.920965795 | 1.719723 | 1719.723183 | 2039.942939 | | |
| 34 | 7.53 | 7.78 | 4.43 | 4.43 | 0.25 | 3.213368 | 0.142352185 | 4.287647815 | 2.322388 | 2322.38806 | 2043.314501 | | |
| 35 | 4.9 | 5.22 | 1.62 | 1.62 | 0.32 | 6.130268 | 0.099310345 | 1.520689655 | 1.45 | 1450 | 2049.50495 | | |
| 36 | 9.05 | 9.48 | 4.15 | 4.15 | 0.43 | 4.535865 | 0.188238397 | 3.961761603 | 1.778612 | 1778.611632 | 2054.794521 | | |
| 37 | 17.44 | 17.85 | 8.77 | 8.77 | 0.41 | 2.296919 | 0.201439776 | 8.568560224 | 1.965859 | 1965.859031 | 2079.608939 | | |
| 38 | 13.69 | 14.21 | 6.79 | 6.79 | 0.52 | 3.659395 | 0.248472906 | 6.541527094 | 1.915094 | 1915.09434 | 2093.397746 | | |
| 39 | 7.85 | 8.08 | 3.86 | 3.86 | 0.23 | 2.846535 | 0.109876238 | 3.750123762 | 1.914692 | 1914.691943 | 2108.419839 | | |
| 40 | 11.06 | 11.45 | 5.58 | 5.58 | 0.39 | 3.406114 | 0.190061135 | 5.389938865 | 1.950596 | 1950.596252 | 2128.133705 | | |
| 41 | 5.7 | 5.95 | 2.62 | 2.62 | 0.25 | 4.201681 | 0.110084034 | 2.509915966 | 1.786787 | 1786.786787 | 2142.857143 | | |
| 42 | 5.32 | 5.63 | 2.53 | 2.53 | 0.31 | 5.506217 | 0.139307282 | 2.390692718 | 1.816129 | 1816.129032 | 2151.807229 | | |
| 43 | 8.49 | 8.76 | 4.28 | 4.28 | 0.27 | 3.082192 | 0.131917808 | 4.148082192 | 1.955357 | 1955.357143 | 2192.307692 | | |
| 44 | 16.16 | 16.68 | 8.15 | 8.15 | 0.52 | 3.117506 | 0.254076739 | 7.895923261 | 1.955451 | 1955.451348 | 2199.376947 | | |
| 45 | 6.3 | 6.64 | 2.11 | 2.11 | 0.34 | 5.120482 | 0.108042169 | 2.001957831 | 1.465784 | 1465.783664 | 2205.521472 | | |
| 46 | 14.46 | 14.89 | 7.73 | 7.73 | 0.43 | 2.887844 | 0.223230356 | 7.506769644 | 2.079609 | 2079.608939 | 2215.873016 | | |
| 47 | 8.7 | 8.93 | 4.78 | 4.78 | 0.23 | 2.575588 | 0.123113102 | 4.656886898 | 2.151807 | 2151.807229 | 2220.367279 | | |
| 48 | 7.91 | 8.21 | 3.74 | 3.74 | 0.3 | 3.65408 | 0.136662607 | 3.603337393 | 1.836689 | 1836.689038 | 2289.017341 | | |
| 49 | 7.52 | 7.8 | 3.76 | 3.76 | 0.28 | 3.589744 | 0.134974359 | 3.625025641 | 1.930693 | 1930.693069 | 2304.123711 | | |
| 50 | 7.59 | 7.87 | 3.78 | 3.78 | 0.28 | 3.557814 | 0.134485388 | 3.645514612 | 1.924205 | 1924.205379 | 2322.38806 | | |

Table A1.13. Density measurements for Cl.

| number | | | | Wc+s water | | | Ws water | Wc water | SG | DENSITY kg m ⁻³ | density sorted | density range | density mean of 900 |
|--------|-------|-------|-------|------------|------------------|----------|----------------------|--------------------|----------|----------------------------|----------------|---------------|---------------------|
| | | | | clast wet | sheet dry weight | sheet % | sheet wet weight (g) | clast wet no sheet | | | | | |
| 1 | 9.56 | 10 | 4.51 | 4.51 | 0.44 | 4.4 | 0.19844 | 4.31156 | 1.821494 | 1821.493625 | 1332.512315 | 1332.512315 | #DIV/0! |
| 2 | 12.91 | 13.37 | 5.21 | 5.21 | 0.46 | 3.440539 | 0.179252057 | 5.030747943 | 1.63848 | 1638.480392 | 1410.282258 | 1891.156463 | stdev |
| 3 | 16.57 | 17.13 | 6.27 | 6.27 | 0.56 | 3.269119 | 0.20497373 | 6.06502627 | 1.577348 | 1577.348066 | 1476.712329 | | #DIV/0! |
| 4 | 14.44 | 14.93 | 6.52 | 6.52 | 0.49 | 3.281983 | 0.213985265 | 6.306014735 | 1.775268 | 1775.267539 | 1499.51784 | | |
| 5 | 19.45 | 20.02 | 8.74 | 8.74 | 0.57 | 2.847153 | 0.248841159 | 8.491158841 | 1.774823 | 1774.822695 | 1561.759729 | | mean of 50 |
| 6 | 19.75 | 20.29 | 8.87 | 8.87 | 0.54 | 2.66141 | 0.236067028 | 8.633932972 | 1.776708 | 1776.707531 | 1564.924115 | | 1703.560426 |
| 7 | 11.17 | 11.71 | 5.09 | 5.09 | 0.54 | 4.611443 | 0.234722459 | 4.855277541 | 1.768882 | 1768.882175 | 1577.348066 | | stdev |
| 8 | 19.92 | 20.51 | 9.2 | 9.2 | 0.59 | 2.876646 | 0.26465139 | 8.93534861 | 1.813439 | 1813.439434 | 1577.487765 | | 119.2009012 |
| 9 | 10.2 | 10.62 | 4.86 | 4.86 | 0.42 | 3.954802 | 0.19220339 | 4.66779661 | 1.84375 | 1843.75 | 1587.352626 | | vesic |
| 10 | 6.13 | 6.38 | 2.52 | 2.52 | 0.25 | 3.918495 | 0.098746082 | 2.421253918 | 1.65285 | 1652.849741 | 1610.508757 | | 43.21465246 |
| 11 | 10.65 | 11.1 | 4.75 | 4.75 | 0.45 | 4.054054 | 0.192567568 | 4.557432432 | 1.748031 | 1748.031496 | 1612.423447 | | 55.58292282 |
| 12 | 9.22 | 9.64 | 3.67 | 3.67 | 0.42 | 4.356846 | 0.159896266 | 3.510103734 | 1.61474 | 1614.740369 | 1614.740369 | | 36.96145125 |
| 13 | 15.07 | 15.55 | 5.18 | 5.18 | 0.48 | 3.086817 | 0.159897106 | 5.020102894 | 1.499518 | 1499.51784 | 1635.018496 | | |
| 14 | 17.86 | 18.43 | 7 | 7 | 0.57 | 3.092784 | 0.216494845 | 6.783505155 | 1.612423 | 1612.423447 | 1638.480392 | | |
| 15 | 18.69 | 19.34 | 7.08 | 7.08 | 0.65 | 3.36091 | 0.23795243 | 6.84204757 | 1.577488 | 1577.487765 | 1652.849741 | | |
| 16 | 18.24 | 18.71 | 8.01 | 8.01 | 0.47 | 2.512026 | 0.201213255 | 7.808786745 | 1.748598 | 1748.598131 | 1656.580938 | | |
| 17 | 14.35 | 14.81 | 5.48 | 5.48 | 0.46 | 3.106009 | 0.170209318 | 5.309790682 | 1.587353 | 1587.352626 | 1665.384615 | | |
| 18 | 13.64 | 13.99 | 4.07 | 4.07 | 0.35 | 2.501787 | 0.101822731 | 3.968177269 | 1.410282 | 1410.282258 | 1671.985816 | | |
| 19 | 11.49 | 11.97 | 5.39 | 5.39 | 0.48 | 4.010025 | 0.216140351 | 5.173859649 | 1.819149 | 1819.148936 | 1691.566265 | | |
| 20 | 10.97 | 11.38 | 5.34 | 5.34 | 0.41 | 3.602812 | 0.192390158 | 5.147609842 | 1.884106 | 1884.10596 | 1697.443182 | | |
| 21 | 10.55 | 10.95 | 4.34 | 4.34 | 0.4 | 3.652968 | 0.158538813 | 4.181461187 | 1.656581 | 1656.580938 | 1704 | | |
| 22 | 10.85 | 11.25 | 5.01 | 5.01 | 0.4 | 3.555556 | 0.178133333 | 4.831866667 | 1.802885 | 1802.884615 | 1706.970128 | | |
| 23 | 12.12 | 12.57 | 5.85 | 5.85 | 0.45 | 3.579952 | 0.209427208 | 5.640572792 | 1.870536 | 1870.535714 | 1707.943925 | | |
| 24 | 14.15 | 14.62 | 6.06 | 6.06 | 0.47 | 3.214774 | 0.194815321 | 5.865184679 | 1.707944 | 1707.943925 | 1714.457831 | | |
| 25 | 10.77 | 11.26 | 4.88 | 4.88 | 0.49 | 4.351687 | 0.212362345 | 4.667637655 | 1.76489 | 1764.890282 | 1739.783153 | | |
| 26 | 23.74 | 24.24 | 10.55 | 10.55 | 0.5 | 2.062706 | 0.217615512 | 10.33238449 | 1.770636 | 1770.6355 | 1742.362525 | | |
| 27 | 17.38 | 17.87 | 8.13 | 8.13 | 0.49 | 2.742026 | 0.222926693 | 7.907073307 | 1.834702 | 1834.702259 | 1748.031496 | | |
| 28 | 10.72 | 11.12 | 5.24 | 5.24 | 0.4 | 3.597122 | 0.188489209 | 5.051510791 | 1.891156 | 1891.156463 | 1748.598131 | | |
| 29 | 15.71 | 16.15 | 6.97 | 6.97 | 0.44 | 2.724458 | 0.189894737 | 6.780105263 | 1.759259 | 1759.259259 | 1759.259259 | | |
| 30 | 6.67 | 7.02 | 2.87 | 2.87 | 0.35 | 4.985755 | 0.143091168 | 2.726908832 | 1.691566 | 1691.566265 | 1760.830325 | | |
| 31 | 16.65 | 17.11 | 7.29 | 7.29 | 0.46 | 2.688486 | 0.195990649 | 7.094009351 | 1.742363 | 1742.362525 | 1764.890282 | | |
| 32 | 13.69 | 14.23 | 5.93 | 5.93 | 0.54 | 3.7948 | 0.225031623 | 5.704968377 | 1.714458 | 1714.457831 | 1766.326531 | | |
| 33 | 19.04 | 19.51 | 8.43 | 8.43 | 0.47 | 2.409021 | 0.203080472 | 8.226919528 | 1.76083 | 1760.830325 | 1768.421053 | | |
| 34 | 27.29 | 27.84 | 10.05 | 10.05 | 0.55 | 1.975575 | 0.198545259 | 9.851454741 | 1.564924 | 1564.924115 | 1768.882175 | | |
| 35 | 11.3 | 11.76 | 5.11 | 5.11 | 0.46 | 3.911565 | 0.199880952 | 4.910119048 | 1.768421 | 1768.421053 | 1770.6355 | | |
| 36 | 18.75 | 19.31 | 7.32 | 7.32 | 0.56 | 2.900052 | 0.212283791 | 7.107716209 | 1.610509 | 1610.508757 | 1774.822695 | | |
| 37 | 8.83 | 9.23 | 3.32 | 3.32 | 0.4 | 4.333694 | 0.143878657 | 3.176121343 | 1.56176 | 1561.759729 | 1775.267539 | | |
| 38 | 18.09 | 18.58 | 8.33 | 8.33 | 0.49 | 2.637244 | 0.219682454 | 8.110317546 | 1.812683 | 1812.682927 | 1775.376555 | | |
| 39 | 12.83 | 13.26 | 5.15 | 5.15 | 0.43 | 3.242836 | 0.167006033 | 4.982993967 | 1.635018 | 1635.018496 | 1775.675676 | | |
| 40 | 19.26 | 19.71 | 8.61 | 8.61 | 0.45 | 2.283105 | 0.196575342 | 8.413424658 | 1.775676 | 1775.675676 | 1776.707531 | | |
| 41 | 11.56 | 12 | 4.97 | 4.97 | 0.44 | 3.666667 | 0.182233333 | 4.787766667 | 1.70697 | 1706.970128 | 1802.884615 | | |
| 42 | 16.85 | 17.31 | 7.51 | 7.51 | 0.46 | 2.657423 | 0.199572501 | 7.310427499 | 1.766327 | 1766.326531 | 1812.682927 | | |
| 43 | 11.49 | 11.95 | 4.91 | 4.91 | 0.46 | 3.849372 | 0.189004184 | 4.720995816 | 1.697443 | 1697.443182 | 1813.439434 | | |

| | | | | | | | | | | | | | |
|---|-------|-------|-------|-------|------|----------|-------------|-------------|----------|-------------|-------------|--|--|
| 44 | 8.93 | 9.43 | 3.79 | 3.79 | 0.5 | 5.302227 | 0.200954401 | 3.589045599 | 1.671986 | 1671.985816 | 1819.148936 | | |
| 45 | 21.07 | 21.56 | 6.96 | 6.96 | 0.49 | 2.272727 | 0.158181818 | 6.801818182 | 1.476712 | 1476.712329 | 1821.493625 | | |
| 46 | 20.29 | 20.86 | 8.87 | 8.87 | 0.57 | 2.732502 | 0.242372963 | 8.627627037 | 1.739783 | 1739.783153 | 1834.702259 | | |
| 47 | 26.55 | 27.11 | 11.84 | 11.84 | 0.56 | 2.065658 | 0.244573958 | 11.59542604 | 1.775377 | 1775.376555 | 1843.75 | | |
| 48 | 12.57 | 12.99 | 5.19 | 5.19 | 0.42 | 3.233256 | 0.167806005 | 5.022193995 | 1.665385 | 1665.384615 | 1870.535714 | | |
| 49 | 5.14 | 5.41 | 1.35 | 1.35 | 0.27 | 4.990758 | 0.067375231 | 1.282624769 | 1.332512 | 1332.512315 | 1884.10596 | | |
| 50 | 3.98 | 4.26 | 1.76 | 1.76 | 0.28 | 6.57277 | 0.115680751 | 1.644319249 | 1.704 | 1704 | 1891.156463 | | |
| Table A1.14. Density measurements for dwSc. | | | | | | | | | | | | | |

| Edifice | log | dip (°) | dip (°) | dip (°) | dip (°) | dip (°) | dip (°) | dip (°) | dip (°) | dip (°) | dip (°) |
|-----------------|-----|---------|---------|---------|---------|---------|---------|---------|---------|---------|---------|
| cone 26 | 10 | 21 | 28 | 33 | 30 | 40 | 40 | 20 | | | |
| | 81 | 42 | 22 | 28 | 18 | | | | | | |
| | 12 | 28 | 32 | 2 | | | | | | | |
| | 9 | 36 | 45 | 48 | 48 | 40 | 18 | | | | |
| | 8 | 24 | 35 | 33 | 25 | 17 | 20 | 21 | 10 | 11 | 10 |
| | 8 | 16 | 16 | 16 | 6 | 8 | 18 | 14 | 13 | 42 | 72 |
| | 8 | 73 | 74 | 44 | 38 | 33 | 22 | 32 | 31 | 22 | 24 |
| scoria rampart | L8 | 25 | 30 | 10 | 23 | | | | | | |
| | L13 | 39 | 29 | 41 | 50 | 41 | 37 | 41 | 44 | 39 | 35 |
| | L13 | 43 | 31 | 26 | 29 | 19 | 16 | 32 | 21 | | |
| | L17 | 13 | 9 | 15 | | | | | | | |
| | L20 | 34 | 29 | 18 | 24 | 32 | 39 | 30 | 35 | 32 | 34 |
| | L20 | 43 | 55 | 30 | 28 | | | | | | |
| | L21 | 32 | 28 | 22 | 35 | 37 | 24 | 49 | 51 | 53 | 57 |
| | L21 | 63 | 26 | 29 | 25 | 42 | 10 | 24 | 21 | 11 | 17 |
| | L21 | 3 | 12 | 9 | 20 | 14 | 11 | 23 | 1 | 7 | 7 |
| | L21 | 18 | 8 | 8 | 11 | 14 | 6 | 18 | 12 | 8 | |
| | 2 | 10 | 16 | 18 | 18 | 15 | 33 | 16 | 24 | 40 | 14 |
| | 2 | 14 | 40 | 44 | 41 | 43 | 42 | 5 | 26 | 24 | 25 |
| | 2 | 38 | 14 | 32 | 22 | 21 | 34 | | | | |
| | 13 | 21 | 35 | 16 | 9 | 10 | 10 | 11 | 6 | 11 | |
| spatter rampart | | 42 | 31 | 35 | 40 | 16 | 32 | 19 | 32 | 28 | 24 |
| | | 24 | 24 | 22 | 26 | 31 | 48 | 47 | 37 | 22 | 22 |
| | | 29 | 30 | 25 | 36 | 26 | 28 | 40 | 25 | 23 | 20 |
| | | 14 | 28 | 23 | 16 | 31 | 28 | 22 | 18 | 64 | 62 |
| | | 48 | 19 | 53 | 58 | 33 | 45 | 8 | 58 | 51 | 37 |
| | | 46 | 31 | 12 | 46 | 38 | 71 | 39 | 46 | 46 | 38 |
| | | 42 | 42 | 55 | 71 | 69 | 64 | 82 | 82 | 64 | 64 |
| | | 38 | 58 | 46 | 40 | 60 | 37 | 28 | 28 | 85 | 45 |
| | | 35 | 25 | 13 | 35 | 33 | 40 | 48 | 24 | 31 | 31 |
| | | 67 | 38 | 33 | 45 | 44 | 45 | 53 | 45 | 62 | 60 |
| | | 86 | 32 | 35 | 68 | 52 | 74 | 46 | 64 | 44 | 41 |

| | | | | | | | | | | | |
|---|-----|----|----|----|----|----|----|----|----|----|----|
| | | 72 | 70 | 74 | 72 | 71 | 65 | 77 | 81 | 81 | 69 |
| | | 78 | 81 | 67 | 57 | 75 | 60 | 58 | 63 | 62 | 80 |
| | | 65 | 66 | 59 | 65 | 66 | 68 | 68 | 48 | 70 | 71 |
| | | 60 | 58 | 60 | 44 | 68 | 44 | 82 | 52 | | |
| | L3 | 40 | 51 | 10 | | | | | | | |
| | L4 | 45 | 32 | 53 | 39 | 44 | | | | | |
| | L5 | 29 | | | | | | | | | |
| | L6 | 17 | 23 | 34 | 20 | 43 | 47 | | | | |
| | L9 | 27 | 40 | 56 | | | | | | | |
| | L11 | 36 | 53 | 39 | 31 | 49 | 37 | 43 | 25 | 21 | 33 |
| | L11 | 45 | 28 | 30 | 50 | 45 | | | | | |
| sheet-like fall deposit | | 11 | 11 | 5 | 6 | 8 | 10 | 17 | 14 | 3 | 11 |
| | | 19 | 28 | 28 | 28 | 9 | 16 | 6 | 27 | 11 | 6 |
| | | 3 | | | | | | | | | |
| rootless cone | | 33 | 20 | 28 | 35 | 70 | 78 | 46 | 38 | 48 | 38 |
| | | 46 | 64 | 42 | 48 | 28 | 28 | 16 | 35 | 18 | 52 |
| | | 27 | 20 | 41 | 39 | 14 | 41 | 39 | 43 | 32 | 39 |
| | | 58 | 20 | 29 | 24 | 6 | 43 | 26 | 34 | | |
| Table A1.15. Bedding measurements for edifices. | | | | | | | | | | | |

| WP | log | unit | max clast size | unit thickness (mm) | distance from fissure (m) | facies | aspect ratio | thickness (m) |
|-----|-----|------|----------------------|---------------------------|------------------------------------|--------|-----------------|------------------|
| 374 | 8 | 1 | 434 | 1000 | 1 | waSp | 9.3 | 1 |
| 374 | 8 | 2 | 653 | 250 | 1 | dwsp | 24.8 | 0.25 |
| 374 | 8 | 4 | 287 | 2080 | 1 | waSp | 3.6 | 2.08 |
| 374 | 8 | 5 | 137 | 500 | 1 | waSp | 3.1 | 0.5 |
| 374 | 8 | 6 | 107 | 1000 | 1 | waSp | 2.7 | 1 |
| 374 | | 7 | 552.5 | 500 | 1 | mwSp | 26.2 | 0.5 |
| 374 | | 9 | 374.444 4444 | 1250 | 1 | waSp | 6.4 | 1.25 |
| 375 | 10 | 5 | 275 | 3000 | 1 | waSp | 3.1 | 3 |
| 375 | 10 | 7 | 67.2 | 210 | 74 | waSc | 1.7 | 0.21 |
| 375 | 10 | 9 | 569 | 1150 | 74 | waSp | 6.8 | 1.15 |
| 375 | 10 | 10 | 648 | 340 | 74 | mwsp | 16 | 0.34 |
| 375 | 9 | 4 | 750 | 3000 | 74 | waSp | 4.85 | 3 |
| NA | 12 | 2 | 168 | | 1 | waSp | 2.8 | 0 |
| NA | 12 | 3 | 283 | | 1 | waSp | 3.2 | 0 |
| NA | 12 | 5 | 437 | | 1 | waSp | 3.7 | 0 |
| NA | 81 | 1 | 737 | 400 | 1 | mwsp | 9 | 0.4 |
| NA | 81 | 3 | 74 | 720 | 1 | waSc | 2.5 | 0.72 |
| 298 | 28 | 1 | 877 | 8000 | 18 | waSp | 8.2 | 8 |
| 303 | 14 | 5 | 244 | 1300 | 612 | waSp | 2.9 | 1.3 |
| 480 | 21 | 1 | 66 | 180 | 250 | waSc | 2 | 0.18 |
| 480 | 21 | 3 | 52 | 1200 | 250 | waSc | 1.7 | 1.2 |
| 480 | 21 | 5 | 55 | 660 | 250 | mwSc | 3 | 0.66 |
| 406 | 13 | 1 | 86 | 400 | 199 | waSc | 1.7 | 0.4 |
| 406 | 13 | 2-4 | 127 | 1980 | 199 | waSp | 1.7 | 1.98 |
| 406 | 13 | 6 | 500 | 920 | 199 | waSp | 5.2 | 0.92 |
| 406 | 13 | 5 | 667 | 1200 | 199 | mwsp | 34.2 | 1.2 |
| 297 | 3 | 1 | 52 | 1150 | 1247 | waSc | 1.3 | 1.15 |
| 401 | 11 | 1-3 | 103 | | 172 | waSc | 1.3 | 0 |
| 401 | 11 | 4 | 522 | | 172 | dwsp | 18.7 | 0 |
| 401 | 11 | 5 | 142 | | 172 | waSp | 3.2 | 0 |
| 401 | 11 | 6 | 597 | | 172 | dwsp | 28.6 | 0 |
| 401 | 11 | 7 | 325 | | 172 | waSp | 2 | 0 |
| 401 | 11 | 8 | 72 | | 172 | waSc | 1.5 | 0 |
| 293 | 2 | 7-9 | 68 | | 223 | waSc | 2 | 0 |
| 293 | 2 | 10 | 122 | | 223 | waSp | 2.3 | 0 |
| 293 | 2 | 11 | 49 | | 223 | waSc | 1.6 | 0 |
| 293 | 2 | 12 | 117 | | 223 | waSp | 1.5 | 0 |
| 293 | 2 | 13 | 67 | | 223 | waSc | 1.7 | 0 |
| 293 | 2 | 14 | 162 | | 223 | waSp | 1.6 | 0 |
| 293 | 2 | 17 | 122 | | 223 | waSp | | 0 |
| 486 | N | 1 | 37 | 420 | 477 | waSc | 2.2 | 0.42 |

| | A | | | | | | | |
|-----|----------|-----|-----|------|------|------|------|-------|
| 497 | 24 | 4 | 35 | 1500 | 752 | waSc | 1.7 | 1.5 |
| 508 | 26 | 3 | 25 | 400 | 688 | NA | 1.8 | 0.4 |
| 494 | 23 | 1 | 61 | 500 | 529 | waSc | 1.8 | 0.5 |
| 505 | 27 | 2 | 191 | 1000 | 639 | waSc | 1.6 | 1 |
| 505 | 27 | 3 | 23 | 110 | 639 | dwSc | 1.6 | 0.11 |
| 31 | pit | 1 | 112 | 510 | 464 | waSp | 1.3 | 0.51 |
| 31 | | 2-3 | 35 | 270 | 464 | scl | 1.5 | 0.27 |
| 31 | pit 2 | | 94 | 610 | 464 | scl | 1.3 | 0.61 |
| 31 | pit 3 | 1 | 130 | 310 | 464 | waSp | 1.3 | 0.31 |
| 31 | | 2 | 42 | 350 | 464 | scl | 1.6 | 0.35 |
| 31 | pit 4 | | 110 | 700 | 464 | waSp | 1.8 | 0.7 |
| 31 | pit 5 | | 168 | 1000 | 464 | waSp | 1.2 | 1 |
| 31 | pit 6 | | 91 | 650 | 464 | waSp | 1.5 | 0.65 |
| 287 | 29 | 3 | 29 | | 126 | waSc | 1.2 | 0 |
| 287 | | 4 | 22 | 2000 | 126 | waSc | 1.4 | 2 |
| 41 | | 1-3 | 136 | 1600 | 400 | waSp | 1.4 | 1.6 |
| 79 | | | 326 | 1300 | 163 | waSp | 5.1 | 1.3 |
| 81 | | | 256 | 250 | 171 | waSp | 3.8 | 0.25 |
| 84 | | | 314 | 900 | 184 | waSp | 5.7 | 0.9 |
| 297 | | | 27 | 500 | 1205 | scl | 1.8 | 0.5 |
| 141 | 31 | 2 | 31 | 500 | 333 | waSc | 1.5 | 0.5 |
| 145 | | 1 | 56 | 145 | 190 | waSc | 1.7 | 0.145 |
| 145 | | 2 | 254 | 800 | 190 | waSp | 3.5 | 0.8 |
| 147 | 32 | 1 | 33 | 147 | 322 | mwSc | 2.3 | 0.147 |
| 151 | 33 | 1 | 22 | 250 | 284 | mwSc | 3 | 0.25 |
| 158 | 34 | 1 | 55 | 1230 | 500 | mwSc | 3.5 | 1.23 |
| 483 | 22 | 2 | 39 | 630 | 443 | waSc | 1.8 | 0.63 |
| 483 | | 4 | 21 | 1750 | 443 | scl | 1.4 | 1.75 |
| 158 | | | 55 | 1230 | 506 | mwSc | 3.5 | 1.23 |
| 147 | 32 | 2 | 13 | 460 | 304 | dwSc | 12.3 | 0.46 |
| 401 | 15 | 1 | 16 | 200 | 160 | waSc | 2 | 0.2 |
| 401 | 15 | 2-3 | 26 | 460 | 160 | waSc | 2 | 0.46 |
| y48 | 16 | 2 | 21 | 90 | 575 | waSc | 1.6 | 0.09 |
| y42 | 11 | 2-3 | 248 | 930 | 34 | waSp | 2.8 | 0.93 |
| y26 | 6 | 1-3 | 212 | 1420 | 112 | waSp | 2.3 | 1.42 |
| y28 | 3 | 2 | 85 | 200 | 18 | waSp | 2.1 | 0.2 |
| 77 | 8 | 2-3 | 148 | 1300 | 145 | waSp | 2.5 | 1.3 |
| 77 | | 4 | 142 | 740 | 145 | waSp | 2.1 | 0.74 |
| 77 | | 5 | 250 | 490 | 145 | waSp | 3.1 | 0.49 |
| 477 | 17 | 1 | 39 | 240 | 201 | waSc | 1.8 | 0.24 |

| | | | | | | | | |
|---|----|-----|-----|-------|-----|------|------|------|
| | | 2 | 345 | 600 | 201 | waSp | 4.5 | 0.6 |
| | | 4 | 235 | 800 | 201 | waSp | 3.2 | 0.8 |
| y57 | | | 11 | 200 | 458 | scl | 1.3 | 0.2 |
| y58 | | | 21 | 260 | 591 | scl | 1.4 | 0.26 |
| y59 | | | 21 | 320 | 742 | scl | 1.4 | 0.32 |
| y60 | | | 10 | 150 | 893 | scl | 1.6 | 0.15 |
| y61 | | | 22 | 350 | 821 | scl | 1.2 | 0.35 |
| y62 | | | 25 | 400 | 793 | scl | 1.5 | 0.4 |
| pr | | | 119 | 1710 | 50 | scl | 1.8 | 1.71 |
| 477 | 17 | | | 1100 | 185 | dwsp | | 1.1 |
| y56 | | | 16 | 180 | 317 | scl | 1.4 | 0.18 |
| Z22 | | | 24 | 230 | 656 | scl | 1.3 | 0.23 |
| y40 | | | 15 | 180 | 435 | waSc | 1.7 | 0.18 |
| y22 | | | 812 | 8000 | 25 | waSp | 21.5 | 8 |
| y26 | 6 | 1-3 | 212 | 1420 | 112 | waSp | 4.7 | 1.42 |
| point 1 (see AI) | | | | 25000 | 30 | | | 25 |
| 30 | | | | 6000 | 129 | | | 6 |
| 12 | | | | 5000 | 1 | | | 5 |
| 2 | | | | 29000 | 223 | | | 29 |
| 11 | | | | 12000 | 172 | | | 12 |
| pit 1 | | | | | 402 | | | 0.75 |
| 29 | | | | | 129 | | | 4 |
| 477 | | | | 1640 | 201 | | | 1.64 |
| Table A1.16. Dispersal characteristics for the tephra. | | | | | | | | |

| sheet | date | wp | unit | Strike (°) | Dip (°) | modular direction of dip (°) | height from base (mm) |
|-------|--------|-----|------|------------|---------|------------------------------|-----------------------|
| 114 | 24-Jun | 401 | 1 | 358 | 48 | 88 | 300 |
| | | | | 352 | 61 | 82 | |
| | | | | 352 | 63 | 82 | |
| | | | 2 | 3 | 78 | 93 | 1600 |
| | | | | 344 | 73 | 74 | |
| | | | | 350 | 83 | 80 | |
| | | | | 341 | 69 | 71 | |
| | | | 3 | 336 | 78 | 66 | 200 |
| | | | | 342 | 80 | 72 | |
| | | | | 25 | 75 | 115 | |
| | | | 4 | 3 | 75 | 93 | 220 |
| | | | | 5 | 68 | 95 | |
| | | | | 14 | 61 | 104 | |
| | | | | 16 | 75 | 106 | |
| | | | 5 | 5 | 79 | 95 | 75 |
| | | | | 10 | 69 | 100 | |
| | | | | 6 | 72 | 96 | |
| | | | 6 | 6 | 81 | 96 | 180 |
| | | | | 356 | 81 | 86 | |
| | | | | 32 | 71 | 122 | |
| | | | 7 | 32 | 41 | 122 | 260 |
| | | | | 21 | 45 | 111 | |
| | | | 8 | 16 | 52 | 106 | 170 |
| 13 | 23-Jun | y46 | 2 | 24 | 39 | 114 | 8470 |
| | | | 2 | 46 | 29 | 136 | 8470 |
| | | | 2 | 32 | 41 | 122 | 8470 |
| | | | 2 | 25 | 50 | 115 | 8470 |
| | | | 2 | 19 | 41 | 109 | 8470 |
| | | | 2 | 11 | 37 | 101 | 8470 |
| | | | 3 | 20 | 41 | 110 | 8790 |
| | | | 3 | 29 | 44 | 119 | 8790 |
| | | | 3 | 25 | 39 | 115 | 8790 |
| | | | 4 | 16 | 35 | 106 | 11190 |
| | | | 4 | 36 | 43 | 126 | 11190 |
| | | | 4 | 31 | 31 | 121 | 11190 |
| | | | 5 | 57 | 26 | 147 | 11400 |
| | | | 5 | 25 | 29 | 115 | 11400 |
| | | | 5 | 353 | 19 | 83 | 11400 |
| | | | 6 | 78 | 16 | 168 | 11610 |
| | | | 7 | 20 | 21 | 110 | 11610 |
| | | | 7 | 352 | 32 | 82 | 11610 |
| | | | 8 | 20 | 21 | 110 | 12150 |

| | | | | | | | |
|----|--|-----|----|-----|----|-----|-------|
| | | | 8 | 352 | 32 | 262 | 12150 |
| 11 | | 401 | 2 | 284 | 17 | 194 | |
| | | | 2 | 256 | 13 | 166 | |
| 11 | | 401 | 3 | 183 | 20 | 93 | |
| | | | 3 | 150 | 8 | 60 | |
| | | | 3 | 172 | 13 | 82 | |
| | | | 4 | 166 | 40 | 76 | |
| | | | 4 | 144 | 44 | 54 | |
| | | | 4 | 162 | 41 | 72 | |
| | | | 4 | 156 | 43 | 66 | |
| 2 | | 293 | 4 | 59 | 10 | 329 | |
| | | | 4 | 74 | 16 | 344 | |
| | | | 4 | 66 | 18 | 336 | |
| | | | 4 | 64 | 18 | 334 | |
| | | | 7 | 80 | 40 | 350 | |
| | | | 7 | 28 | 14 | 298 | |
| | | | 7 | 29 | 14 | 299 | |
| | | | 9 | 104 | 33 | 14 | |
| | | | 9 | 90 | 16 | 0 | |
| | | | 11 | 66 | 6 | 336 | |
| | | | 11 | 60 | 7 | 330 | |
| | | | 13 | 32 | 2 | 302 | |
| | | | 17 | 130 | 21 | 220 | |
| | | | 17 | 226 | 11 | 316 | |
| | | | 17 | 180 | 17 | 270 | |
| | | | 18 | 195 | 3 | 285 | |
| | | | 18 | 194 | 12 | 284 | |
| | | | 18 | 230 | 9 | 320 | |
| | | | 19 | 158 | 20 | 248 | |
| | | | 21 | 190 | 14 | 280 | |
| | | | 21 | 208 | 11 | 298 | |
| | | | 23 | 162 | 23 | 252 | |
| | | | 23 | 212 | 1 | 302 | |
| | | | 24 | 214 | 7 | 304 | |
| | | | 25 | 222 | 7 | 312 | |
| | | | 26 | 196 | 18 | 286 | |
| | | | 27 | 194 | 8 | 284 | |
| | | | 27 | 195 | 8 | 285 | |
| | | | 29 | 224 | 11 | 314 | |
| | | | 29 | 310 | 14 | 40 | |
| | | | 30 | 225 | 6 | 315 | |
| | | | 32 | 172 | 18 | 262 | |
| | | | 32 | 178 | 12 | 268 | |
| | | | 32 | 218 | 8 | 308 | |

Table A1.17. Bedding measurements in scoria rampart.

| log | unit | X axis (mm) | Y axis (mm) | aspect ratio |
|-----|-------------------|-------------|-------------|--------------|
| 8 | 1 | 800 | 50 | 16 |
| | | 740 | 150 | 4.933333333 |
| | | 480 | 30 | 16 |
| | | 470 | 30 | 15.66666667 |
| | | 430 | 45 | 9.555555556 |
| | | 360 | 50 | 7.2 |
| | | 340 | 60 | 5.666666667 |
| | | 305 | 35 | 8.714285714 |
| | | 220 | 70 | 3.142857143 |
| | | 200 | 30 | 6.666666667 |
| | | | mean | 9.354603175 |
| | av max clast (mm) | 434.5 | 55 | |
| log | unit | X (mm) | Y (mm) | aspect ratio |
| 8 | 2 | 1000 | 25 | 40 |
| | | 800 | 20 | 40 |
| | | 210 | 40 | 5.25 |
| | | 600 | 20 | 30 |
| | | 560 | 30 | 18.66666667 |
| | | 750 | 50 | 15 |
| | | | | #DIV/0! |
| | | | | #DIV/0! |
| | | | | #DIV/0! |
| | | | | #DIV/0! |
| | | | mean | 24.81944444 |
| | av max clast (mm) | 653.3333 | 30.83333333 | |
| log | unit | X (mm) | Y (mm) | aspect ratio |
| 8 | 4 | 610 | 120 | 5.083333333 |
| | | 180 | 150 | 1.2 |
| | | 500 | 70 | 7.142857143 |
| | | 185 | 70 | 2.642857143 |
| | | 400 | 60 | 6.666666667 |
| | | 130 | 70 | 1.857142857 |
| | | 190 | 90 | 2.111111111 |
| | | 220 | 60 | 3.666666667 |
| | | 300 | 110 | 2.727272727 |
| | | 160 | 45 | 3.555555556 |
| | | | mean | 3.66534632 |
| | av max clast (mm) | 287.5 | 84.5 | |
| log | unit | X (mm) | Y (mm) | aspect ratio |
| 8 | 5 | 190 | 60 | 3.166666667 |
| | | 120 | 50 | 2.4 |
| | | 250 | 30 | 8.333333333 |
| | | 150 | 40 | 3.75 |
| | | 170 | 50 | 3.4 |

| | | | | |
|-----|-------------------|--------|--------|--------------|
| | | 70 | 30 | 2.333333333 |
| | | 100 | 90 | 1.111111111 |
| | | 155 | 50 | 3.1 |
| | | 65 | 35 | 1.857142857 |
| | | 100 | 55 | 1.818181818 |
| | | | mean | 3.126976912 |
| | av max clast (mm) | 137 | 49 | |
| log | unit | X (mm) | Y (mm) | aspect ratio |
| 8 | 6 | 90 | 40 | 2.25 |
| | | 65 | 40 | 1.625 |
| | | 150 | 45 | 3.333333333 |
| | | 80 | 40 | 2 |
| | | 85 | 40 | 2.125 |
| | | 90 | 30 | 3 |
| | | 80 | 44 | 1.818181818 |
| | | 130 | 35 | 3.714285714 |
| | | 160 | 70 | 2.285714286 |
| | | 140 | 25 | 5.6 |
| | | | mean | 2.775151515 |
| | av max clast (mm) | 107 | 40.9 | |
| log | unit | X (mm) | Y (mm) | aspect ratio |
| 8 | 7 | 450 | 25 | 18 |
| | | 630 | 63 | 10 |
| | | 750 | 95 | 7.894736842 |
| | | 580 | 11 | 52.72727273 |
| | | 870 | 10 | 87 |
| | | 190 | 20 | 9.5 |
| | | 500 | 70 | 7.142857143 |
| | | 450 | 25 | 18 |
| | | | | |
| | | | | |
| | | | mean | 26.28310834 |
| | av max clast (mm) | 552.5 | 39.875 | |
| log | unit | X (mm) | Y (mm) | aspect ratio |
| 8 | 9 | 250 | 80 | 3.125 |
| | | 220 | 160 | 1.375 |
| | | 200 | 30 | 6.666666667 |
| | | 270 | 100 | 2.7 |
| | | 320 | 30 | 10.66666667 |
| | | 550 | 170 | 3.235294118 |
| | | 520 | 30 | 17.33333333 |
| | | 640 | 100 | 6.4 |
| | | 400 | 60 | 6.666666667 |
| | | | | #DIV/0! |
| | | | mean | 6.463180828 |

| | | | | |
|-----|-------------------|----------|------------|--------------|
| | av max clast (mm) | 374.4444 | 84.4444444 | |
| log | unit | X (mm) | Y (mm) | aspect ratio |
| 10 | 5 | 460 | 60 | 7.666666667 |
| | m1 | 250 | 40 | 6.25 |
| | | 250 | 200 | 1.25 |
| | | 240 | 160 | 1.5 |
| | | 140 | 100 | 1.4 |
| | | 400 | 100 | 4 |
| | | 340 | 70 | 4.857142857 |
| | | 150 | 130 | 1.153846154 |
| | | 220 | 105 | 2.095238095 |
| | | 300 | 200 | 1.5 |
| | | | mean | 3.167289377 |
| | av max clast (mm) | 275 | 116.5 | |
| log | unit | X (mm) | Y (mm) | aspect ratio |
| 10 | 5 | 400 | 130 | 3.076923077 |
| | m2 | 300 | 55 | 5.454545455 |
| | | 500 | 80 | 6.25 |
| | | 120 | 35 | 3.428571429 |
| | | 100 | 55 | 1.818181818 |
| | | 150 | 60 | 2.5 |
| | | 70 | 60 | 1.166666667 |
| | | 200 | 55 | 3.636363636 |
| | | 155 | 70 | 2.214285714 |
| | | 320 | 150 | 2.133333333 |
| | | | mean | 3.167887113 |
| | av max clast (mm) | 231.5 | 75 | |
| log | unit | X (mm) | Y (mm) | aspect ratio |
| 10 | 5 | 45 | 30 | 1.5 |
| | m3 | 60 | 30 | 2 |
| | | 70 | 55 | 1.272727273 |
| | | 60 | 50 | 1.2 |
| | | 50 | 50 | 1 |
| | | 45 | 35 | 1.285714286 |
| | | 50 | 30 | 1.666666667 |
| | | 30 | 15 | 2 |
| | | 100 | 20 | 5 |
| | | 30 | 30 | 1 |
| | | | mean | 1.376406926 |
| | av max clast (mm) | 54 | 34.5 | |
| | | | | |
| log | unit | X (mm) | Y (mm) | aspect ratio |
| 10 | 7 | 30 | 22 | 1.363636364 |
| | | 15 | 10 | 1.5 |
| | | 13 | 10 | 1.3 |

| | | | | |
|-----|-------------------|----------|------------|--------------|
| | | 15 | 9 | 1.666666667 |
| | | 55 | 40 | 1.375 |
| | | 30 | 18 | 1.666666667 |
| | | 20 | 20 | 1 |
| | | 290 | 60 | 4.833333333 |
| | | 20 | 12 | 1.666666667 |
| | | 20 | 14 | 1.428571429 |
| | | | mean | 1.780054113 |
| | av max clast (mm) | 50.8 | 21.5 | |
| log | unit | X (mm) | Y (mm) | aspect ratio |
| 10 | 8 | 95 | 25 | 3.8 |
| | | 50 | 20 | 2.5 |
| | | 55 | 22 | 2.5 |
| | | 29 | 10 | 2.9 |
| | | 140 | 24 | 5.833333333 |
| | | 120 | 65 | 1.846153846 |
| | | 79 | 25 | 3.16 |
| | | 19 | 15 | 1.266666667 |
| | | 25 | 20 | 1.25 |
| | | 60 | 36 | 1.666666667 |
| | | | mean | 2.672282051 |
| | av max clast (mm) | 67.2 | 26.2 | |
| log | unit | X (mm) | Y (mm) | aspect ratio |
| 10 | 9 | 490 | 70 | 7 |
| | | 640 | 110 | 5.818181818 |
| | | 600 | 80 | 7.5 |
| | | 950 | 100 | 9.5 |
| | | 240 | 40 | 6 |
| | | 90 | 30 | 3 |
| | | 490 | 70 | 7 |
| | | 640 | 110 | 5.818181818 |
| | | 600 | 80 | 7.5 |
| | | 950 | 100 | 9.5 |
| | | | mean | 6.863636364 |
| | av max clast (mm) | 569 | 79 | |
| log | unit | X (mm) | Y (mm) | aspect ratio |
| 10 | 10 | 1150 | 55 | 20.90909091 |
| | | 800 | 30 | 26.66666667 |
| | | 450 | 40 | 11.25 |
| | | 1000 | 35 | 28.57142857 |
| | | 280 | 50 | 5.6 |
| | | 700 | 60 | 11.66666667 |
| | | 160 | 20 | 8 |
| | | | mean | 16.09483612 |
| | av max clast (mm) | 648.5714 | 41.4285714 | |

| log | unit | X (mm) | Y (mm) | aspect ratio |
|-----|-------------------|--------|------------|--------------|
| 9 | 4 | 460 | 80 | 5.75 |
| | m1 | 1000 | 250 | 4 |
| | | 1000 | 80 | 12.5 |
| | | 250 | 70 | 3.571428571 |
| | | 700 | 200 | 3.5 |
| | | 440 | 200 | 2.2 |
| | | 1500 | 105 | 14.28571429 |
| | | 210 | 110 | 1.909090909 |
| | | 0 | 0 | #DIV/0! |
| | | 0 | 0 | #DIV/0! |
| | | | mean | 5.964529221 |
| | av max clast (mm) | 695 | 136.875 | |
| log | unit | X (mm) | Y (mm) | aspect ratio |
| 9 | 4 | 600 | 80 | 7.5 |
| | m2 | 750 | 85 | 8.823529412 |
| | | 290 | 100 | 2.9 |
| | | 500 | 90 | 5.555555556 |
| | | 750 | 100 | 7.5 |
| | | 660 | 110 | 6 |
| | | 620 | 220 | 2.818181818 |
| | | 800 | 170 | 4.705882353 |
| | | | | #DIV/0! |
| | | | | #DIV/0! |
| | | | mean | 5.725393642 |
| | av max clast (mm) | 621.25 | 119.375 | |
| log | unit | X (mm) | Y (mm) | aspect ratio |
| 9 | 4 | 500 | 95 | 5.263157895 |
| | m3 | 1250 | 250 | 5 |
| | | 500 | 250 | 2 |
| | | | | #DIV/0! |
| | | | | #DIV/0! |
| | | | | #DIV/0! |
| | | | | #DIV/0! |
| | | | | #DIV/0! |
| | | | | #DIV/0! |
| | | | | #DIV/0! |
| | | | mean | 4.087719298 |
| | av max clast (mm) | 750 | 198.333333 | |
| log | unit | X (mm) | Y (mm) | aspect ratio |
| 12 | 2 | 120 | 70 | 1.714285714 |
| | | 300 | 70 | 4.285714286 |
| | | 160 | 70 | 2.285714286 |
| | | 190 | 65 | 2.923076923 |
| | | 190 | 45 | 4.222222222 |

| | | | | |
|-----|-------------------|----------|------------|--------------|
| | | 200 | 70 | 2.857142857 |
| | | 130 | 50 | 2.6 |
| | | 160 | 50 | 3.2 |
| | | 115 | 45 | 2.555555556 |
| | | 120 | 70 | 1.714285714 |
| | | | mean | 2.835799756 |
| | av max clast (mm) | 168.5 | 60.5 | |
| log | unit | X (mm) | Y (mm) | aspect ratio |
| 12 | 3 | 140 | 90 | 1.555555556 |
| | | 400 | 50 | 8 |
| | | 190 | 120 | 1.583333333 |
| | | 400 | 130 | 3.076923077 |
| | | 190 | 100 | 1.9 |
| | | 380 | 120 | 3.166666667 |
| | | | | #DIV/0! |
| | | | | #DIV/0! |
| | | | | #DIV/0! |
| | | | | #DIV/0! |
| | | | mean | 3.213746439 |
| | av max clast (mm) | 283.3333 | 101.666667 | |
| log | unit | X (mm) | Y (mm) | aspect ratio |
| 12 | 5 | 440 | 90 | 4.888888889 |
| | | 670 | 180 | 3.722222222 |
| | | 230 | 50 | 4.6 |
| | | 120 | 90 | 1.333333333 |
| | | 410 | 100 | 4.1 |
| | | 550 | 130 | 4.230769231 |
| | | 250 | 80 | 3.125 |
| | | 700 | 140 | 5 |
| | | 570 | 180 | 3.166666667 |
| | | | | |
| | | | mean | 3.796320038 |
| | av max clast (mm) | 437.7778 | 115.555556 | |
| log | unit | X (mm) | Y (mm) | aspect ratio |
| 81 | 1 | 410 | 45 | 9.111111111 |
| | | 500 | 100 | 5 |
| | | 1300 | 100 | 13 |
| | | | | #DIV/0! |
| | | | | #DIV/0! |
| | | | | #DIV/0! |
| | | | | #DIV/0! |
| | | | | #DIV/0! |
| | | | | #DIV/0! |
| | | | | #DIV/0! |
| | | | mean | 9.037037037 |

| | | | | |
|-----|-------------------|----------|------------|--------------|
| | av max clast (mm) | 736.6667 | 81.6666667 | |
| log | unit | X (mm) | Y (mm) | aspect ratio |
| 81 | 3 | 55 | 35 | 1.571428571 |
| | | 45 | 30 | 1.5 |
| | | 150 | 50 | 3 |
| | | 110 | 50 | 2.2 |
| | | 80 | 25 | 3.2 |
| | | 70 | 65 | 1.076923077 |
| | | 50 | 10 | 5 |
| | | 70 | 25 | 2.8 |
| | | 50 | 20 | 2.5 |
| | | 65 | 30 | 2.166666667 |
| | | | mean | 2.501501832 |
| | av max clast (mm) | 74.5 | 34 | |
| log | unit | X (mm) | Y (mm) | aspect ratio |
| 81 | 7 | 460 | 250 | 1.84 |
| | | 370 | 100 | 3.7 |
| | | 310 | 100 | 3.1 |
| | | 170 | 90 | 1.888888889 |
| | | 270 | 100 | 2.7 |
| | | 135 | 50 | 2.7 |
| | | 250 | 100 | 2.5 |
| | | 100 | 20 | 5 |
| | | 190 | 20 | 9.5 |
| | | 135 | 40 | 3.375 |
| | | | mean | 3.630388889 |
| | av max clast (mm) | 239 | 87 | |
| log | unit | X (mm) | Y (mm) | aspect ratio |
| 28 | 1 | 910 | 200 | 4.55 |
| | m3 | 430 | 90 | 4.777777778 |
| | | 720 | 130 | 5.538461538 |
| | | 1250 | 120 | 10.41666667 |
| | | 910 | 70 | 13 |
| | | 900 | 80 | 11.25 |
| | | 1170 | 100 | 11.7 |
| | | 1120 | 70 | 16 |
| | | 750 | 140 | 5.357142857 |
| | | 610 | 60 | 10.16666667 |
| | | | mean | 8.25548433 |
| | av max clast (mm) | 877 | 106 | |
| log | unit | X (mm) | Y (mm) | aspect ratio |
| 28 | 1 | 79 | 30 | 2.633333333 |
| | m6 | 34 | 30 | 1.133333333 |
| | | 29 | 20 | 1.45 |
| | | 90 | 60 | 1.5 |

| | | | | |
|-----|-------------------|----------|------------|--------------|
| | | 49 | 22 | 2.227272727 |
| | | 49 | 25 | 1.96 |
| | | 55 | 25 | 2.2 |
| | | 37 | 26 | 1.423076923 |
| | | 130 | 80 | 1.625 |
| | | 60 | 30 | 2 |
| | | | mean | 1.815201632 |
| | av max clast (mm) | 61.2 | 34.8 | |
| log | unit | X (mm) | Y (mm) | aspect ratio |
| 14 | 5 | 370 | 220 | 1.681818182 |
| | | 970 | 90 | 10.77777778 |
| | | 350 | 90 | 3.888888889 |
| | | 40 | 30 | 1.333333333 |
| | | 230 | 100 | 2.3 |
| | | 40 | 30 | 1.333333333 |
| | | 40 | 35 | 1.142857143 |
| | | 85 | 43 | 1.976744186 |
| | | 75 | 35 | 2.142857143 |
| | | | | #DIV/0! |
| | | | mean | 2.953067776 |
| | av max clast (mm) | 244.4444 | 74.7777778 | |
| log | unit | X (mm) | Y (mm) | aspect ratio |
| 21 | 1 | 85 | 40 | 2.125 |
| | | 46 | 39 | 1.179487179 |
| | | 115 | 24 | 4.791666667 |
| | | 59 | 49 | 1.204081633 |
| | | 50 | 40 | 1.25 |
| | | 90 | 35 | 2.571428571 |
| | | 49 | 25 | 1.96 |
| | | 56 | 30 | 1.866666667 |
| | | 55 | 25 | 2.2 |
| | | 55 | 35 | 1.571428571 |
| | | | mean | 2.071975929 |
| | av max clast (mm) | 66 | 34.2 | |
| log | unit | X (mm) | Y (mm) | aspect ratio |
| 21 | 3 | 54 | 40 | 1.35 |
| | | 70 | 45 | 1.555555556 |
| | | 50 | 36 | 1.388888889 |
| | | 54 | 19 | 2.842105263 |
| | | 36 | 20 | 1.8 |
| | | 24 | 20 | 1.2 |
| | | 62 | 45 | 1.377777778 |
| | | 64 | 19 | 3.368421053 |
| | | 50 | 51 | 0.980392157 |
| | | 59 | 40 | 1.475 |

| | | | | |
|-----|----------------------|----------|--------|--------------|
| | | | mean | 1.733814069 |
| | av max clast (mm) | 52.3 | 33.5 | |
| log | unit | X (mm) | Y (mm) | aspect ratio |
| 21 | 5 | 49 | 20 | 2.45 |
| | | 71 | 10 | 7.1 |
| | | 29 | 23 | 1.260869565 |
| | | 40 | 24 | 1.666666667 |
| | | 56 | 15 | 3.733333333 |
| | | 57 | 12 | 4.75 |
| | | 25 | 25 | 1 |
| | | 44 | 24 | 1.833333333 |
| | | 75 | 26 | 2.884615385 |
| | | 34 | 10 | 3.4 |
| | | | mean | 3.007881828 |
| | av max clast (mm) | 48 | 18.9 | |
| | sum avmax clast (mm) | 55.43333 | | |
| log | unit | X (mm) | Y (mm) | aspect ratio |
| 13 | 1 | 100 | 50 | 2 |
| | | 85 | 70 | 1.214285714 |
| | | 70 | 23 | 3.043478261 |
| | | 93 | 70 | 1.328571429 |
| | | 65 | 35 | 1.857142857 |
| | | 70 | 45 | 1.555555556 |
| | | 80 | 70 | 1.142857143 |
| | | 55 | 40 | 1.375 |
| | | 65 | 45 | 1.444444444 |
| | | 185 | 70 | 2.642857143 |
| | | | mean | 1.760419255 |
| | av max clast (mm) | 86.8 | 51.8 | |
| log | unit | X (mm) | Y (mm) | aspect ratio |
| 13 | 2 | 75 | 35 | 2.142857143 |
| | | 250 | 105 | 2.380952381 |
| | | 70 | 64 | 1.09375 |
| | | 90 | 55 | 1.636363636 |
| | | 77 | 50 | 1.54 |
| | | 75 | 65 | 1.153846154 |
| | | 195 | 75 | 2.6 |
| | | 130 | 75 | 1.733333333 |
| | | 130 | 35 | 3.714285714 |
| | | 70 | 40 | 1.75 |
| | | | mean | 1.974538836 |
| | av max clast (mm) | 116.2 | 59.9 | |
| log | unit | X (mm) | Y (mm) | aspect ratio |
| 13 | 3 | 150 | 50 | 3 |
| | | 115 | 80 | 1.4375 |

| | | | | |
|-----|-------------------|--------|--------|--------------|
| | | 160 | 90 | 1.777777778 |
| | | 100 | 80 | 1.25 |
| | | 100 | 60 | 1.666666667 |
| | | 105 | 65 | 1.615384615 |
| | | 160 | 70 | 2.285714286 |
| | | 120 | 95 | 1.263157895 |
| | | 170 | 110 | 1.545454545 |
| | | 92 | 70 | 1.314285714 |
| | | | mean | 1.71559415 |
| | av max clast (mm) | 127.2 | 77 | |
| log | unit | X (mm) | Y (mm) | aspect ratio |
| 13 | 4 | 105 | 90 | 1.166666667 |
| | | 80 | 60 | 1.333333333 |
| | | 135 | 70 | 1.928571429 |
| | | 110 | 74 | 1.486486486 |
| | | 50 | 46 | 1.086956522 |
| | | 110 | 80 | 1.375 |
| | | 120 | 80 | 1.5 |
| | | 75 | 20 | 3.75 |
| | | 160 | 105 | 1.523809524 |
| | | 125 | 70 | 1.785714286 |
| | | | mean | 1.693653825 |
| | av max clast (mm) | 107 | 69.5 | |
| log | unit | X (mm) | Y (mm) | aspect ratio |
| 13 | 6 | 460 | 90 | 5.111111111 |
| | | 400 | 80 | 5 |
| | | 370 | 60 | 6.166666667 |
| | | 590 | 100 | 5.9 |
| | | 680 | 160 | 4.25 |
| | | | | #DIV/0! |
| | | | | #DIV/0! |
| | | | | #DIV/0! |
| | | | | #DIV/0! |
| | | | | #DIV/0! |
| | | | mean | 5.285555556 |
| | av max clast (mm) | 500 | 98 | |
| log | unit | X (mm) | Y (mm) | aspect ratio |
| 13 | 5 | 900 | 20 | 45 |
| | | 820 | 50 | 16.4 |
| | | 650 | 20 | 32.5 |
| | | 710 | 10 | 71 |
| | | 570 | 10 | 57 |
| | | 860 | 60 | 14.33333333 |
| | | 160 | 50 | 3.2 |
| | | | | #DIV/0! |

| | | | | |
|-----|-----------------------|----------|------------|--------------|
| | | | | #DIV/0! |
| | | | | #DIV/0! |
| | | | mean | 34.2047619 |
| | av max clast (mm) | 667.1429 | 31.4285714 | |
| | sum av max clast (mm) | 229.1918 | | |
| log | unit | X (mm) | Y (mm) | aspect ratio |
| 3 | 1 | 78 | 50 | 1.56 |
| | | 60 | 34 | 1.764705882 |
| | | 79 | 69 | 1.144927536 |
| | | 64 | 49 | 1.306122449 |
| | | 39 | 26 | 1.5 |
| | | 34 | 32 | 1.0625 |
| | | 34 | 30 | 1.133333333 |
| | | 44 | 33 | 1.333333333 |
| | | 56 | 34 | 1.647058824 |
| | | 41 | 39 | 1.051282051 |
| | | | mean | 1.350326341 |
| | av max clast (mm) | 52.9 | 39.6 | |
| log | unit | X (mm) | Y (mm) | aspect ratio |
| 11 | 3 | 60 | 50 | 1.2 |
| | m1 | 95 | 55 | 1.727272727 |
| | | 29 | 20 | 1.45 |
| | | 100 | 65 | 1.538461538 |
| | | 55 | 35 | 1.571428571 |
| | | 45 | 35 | 1.285714286 |
| | | 30 | 25 | 1.2 |
| | | 45 | 40 | 1.125 |
| | | 65 | 40 | 1.625 |
| | | 65 | 59 | 1.101694915 |
| | | | mean | 1.382457204 |
| | av max clast (mm) | 58.9 | 42.4 | |
| log | unit | X (mm) | Y (mm) | aspect ratio |
| 11 | 3 | 90 | 50 | 1.8 |
| | m2 | 60 | 69 | 0.869565217 |
| | | 120 | 55 | 2.181818182 |
| | | 65 | 53 | 1.226415094 |
| | | 230 | 40 | 5.75 |
| | | 80 | 35 | 2.285714286 |
| | | 180 | 60 | 3 |
| | | 60 | 25 | 2.4 |
| | | 35 | 30 | 1.166666667 |
| | | 110 | 40 | 2.75 |
| | | | mean | 2.343017945 |
| | av max clast (mm) | 103 | 45.7 | |
| log | unit | X (mm) | Y (mm) | aspect ratio |

| | | | | |
|-----|-------------------|--------|--------|--------------|
| 11 | 3 | 70 | 65 | 1.076923077 |
| | m3 | 100 | 74 | 1.351351351 |
| | | 80 | 80 | 1 |
| | | 54 | 40 | 1.35 |
| | | 96 | 39 | 2.461538462 |
| | | 66 | 30 | 2.2 |
| | | 50 | 45 | 1.111111111 |
| | | 64 | 55 | 1.163636364 |
| | | 60 | 50 | 1.2 |
| | | 82 | 53 | 1.547169811 |
| | | | mean | 1.446173018 |
| | av max clast (mm) | 72.2 | 53.1 | |
| log | unit | X (mm) | Y (mm) | aspect ratio |
| 11 | 4 | 600 | 15 | 40 |
| | | 290 | 18 | 16.11111111 |
| | | 500 | 35 | 14.28571429 |
| | | 820 | 40 | 20.5 |
| | | 480 | 25 | 19.2 |
| | | 870 | 35 | 24.85714286 |
| | | 150 | 50 | 3 |
| | | 470 | 40 | 11.75 |
| | | | | #DIV/0! |
| | | | | #DIV/0! |
| | | | mean | 18.71299603 |
| | av max clast (mm) | 522.5 | 32.25 | |
| log | unit | X (mm) | Y (mm) | aspect ratio |
| 11 | 5 | 335 | 40 | 8.375 |
| | | 135 | 60 | 2.25 |
| | | 140 | 50 | 2.8 |
| | | 155 | 60 | 2.583333333 |
| | | 205 | 50 | 4.1 |
| | | 140 | 50 | 2.8 |
| | | 135 | 60 | 2.25 |
| | | 40 | 20 | 2 |
| | | 55 | 35 | 1.571428571 |
| | | 80 | 20 | 4 |
| | | | mean | 3.27297619 |
| | av max clast (mm) | 142 | 44.5 | |
| log | unit | X (mm) | Y (mm) | aspect ratio |
| 11 | 6 | 500 | 40 | 12.5 |
| | | 540 | 40 | 13.5 |
| | | 800 | 10 | 80 |
| | | 520 | 20 | 26 |
| | | 360 | 20 | 18 |
| | | 520 | 20 | 26 |

| | | | | |
|-----|-------------------|----------|------------|--------------|
| | | 860 | 30 | 28.66666667 |
| | | 630 | 30 | 21 |
| | | 650 | 20 | 32.5 |
| | | | | #DIV/0! |
| | | | mean | 28.68518519 |
| | av max clast (mm) | 597.7778 | 25.5555556 | |
| log | unit | X (mm) | Y (mm) | aspect ratio |
| 11 | 7 | 415 | 170 | 2.441176471 |
| | | 300 | 180 | 1.666666667 |
| | | 250 | 200 | 1.25 |
| | | 400 | 140 | 2.857142857 |
| | | 430 | 320 | 1.34375 |
| | | 280 | 110 | 2.545454545 |
| | | 200 | 100 | 2 |
| | | | | #DIV/0! |
| | | | | #DIV/0! |
| | | | | #DIV/0! |
| | | | mean | 2.014884363 |
| | av max clast (mm) | 325 | 174.285714 | |
| log | unit | X (mm) | Y (mm) | aspect ratio |
| 11 | 8 | 180 | 150 | 1.2 |
| | | 95 | 70 | 1.357142857 |
| | | 60 | 40 | 1.5 |
| | | 55 | 30 | 1.833333333 |
| | | 40 | 30 | 1.333333333 |
| | | 40 | 25 | 1.6 |
| | | 45 | 40 | 1.125 |
| | | 85 | 40 | 2.125 |
| | | 55 | 30 | 1.833333333 |
| | | | | #DIV/0! |
| | | | mean | 1.545238095 |
| | av max clast (mm) | 72.77778 | 50.5555556 | |
| log | unit | X (mm) | Y (mm) | aspect ratio |
| 2 | 7 | 59 | 33 | 1.787878788 |
| | | 75 | 32 | 2.34375 |
| | | 59 | 39 | 1.512820513 |
| | | 49 | 24 | 2.041666667 |
| | | 79 | 20 | 3.95 |
| | | 33 | 22 | 1.5 |
| | | 45 | 19 | 2.368421053 |
| | | 34 | 22 | 1.545454545 |
| | | 75 | 10 | 7.5 |
| | | 23 | 18 | 1.277777778 |
| | | | mean | 2.582776934 |
| | av max clast (mm) | 53.1 | 23.9 | |

| log | unit | X (mm) | Y (mm) | aspect ratio |
|-----|-------------------|----------|------------|--------------|
| 2 | 8 | 46 | 28 | 1.642857143 |
| | | 60 | 45 | 1.333333333 |
| | | 110 | 90 | 1.222222222 |
| | | 75 | 50 | 1.5 |
| | | 69 | 30 | 2.3 |
| | | 65 | 45 | 1.444444444 |
| | | 79 | 51 | 1.549019608 |
| | | 53 | 52 | 1.019230769 |
| | | 62 | 59 | 1.050847458 |
| | | 64 | 29 | 2.206896552 |
| | | | mean | 1.526885153 |
| | av max clast (mm) | 68.3 | 47.9 | |
| log | unit | X (mm) | Y (mm) | aspect ratio |
| 2 | 9 | 70 | 28 | 2.5 |
| | | 100 | 60 | 1.666666667 |
| | | 45 | 36 | 1.25 |
| | | 64 | 40 | 1.6 |
| | | 45 | 25 | 1.8 |
| | | 69 | 30 | 2.3 |
| | | 54 | 24 | 2.25 |
| | | 75 | 73 | 1.02739726 |
| | | 84 | 39 | 2.153846154 |
| | | | | #DIV/0! |
| | | | mean | 1.838656676 |
| | av max clast (mm) | 67.33333 | 39.4444444 | |
| log | unit | X (mm) | Y (mm) | aspect ratio |
| 2 | 10 | 119 | 80 | 1.4875 |
| | | 250 | 50 | 5 |
| | | 99 | 90 | 1.1 |
| | | 120 | 69 | 1.739130435 |
| | | 105 | 52 | 2.019230769 |
| | | 135 | 40 | 3.375 |
| | | 78 | 51 | 1.529411765 |
| | | 99 | 34 | 2.911764706 |
| | | 150 | 55 | 2.727272727 |
| | | 69 | 50 | 1.38 |
| | | | mean | 2.32693104 |
| | av max clast (mm) | 122.4 | 57.1 | |
| log | unit | X (mm) | Y (mm) | aspect ratio |
| 2 | 11 | 44 | 15 | 2.933333333 |
| | | 55 | 30 | 1.833333333 |
| | | 31 | 29 | 1.068965517 |
| | | 50 | 24 | 2.083333333 |
| | | 59 | 40 | 1.475 |

| | | | | |
|-----|-------------------|--------|--------|--------------|
| | | 54 | 31 | 1.741935484 |
| | | 50 | 49 | 1.020408163 |
| | | 60 | 50 | 1.2 |
| | | 49 | 36 | 1.361111111 |
| | | 45 | 25 | 1.8 |
| | | | mean | 1.651742028 |
| | av max clast (mm) | 49.7 | 32.9 | |
| log | unit | X (mm) | Y (mm) | aspect ratio |
| 2 | 12 | 79 | 86 | 0.918604651 |
| | | 110 | 55 | 2 |
| | | 109 | 84 | 1.297619048 |
| | | 125 | 75 | 1.666666667 |
| | | 155 | 80 | 1.9375 |
| | | 155 | 60 | 2.583333333 |
| | | 130 | 90 | 1.444444444 |
| | | 106 | 85 | 1.247058824 |
| | | 130 | 70 | 1.857142857 |
| | | 80 | 79 | 1.012658228 |
| | | | mean | 1.596502805 |
| | av max clast (mm) | 117.9 | 76.4 | |
| log | unit | X (mm) | Y (mm) | aspect ratio |
| 2 | 13 | 85 | 35 | 2.428571429 |
| | | 71 | 70 | 1.014285714 |
| | | 105 | 30 | 3.5 |
| | | 60 | 35 | 1.714285714 |
| | | 59 | 26 | 2.269230769 |
| | | 45 | 30 | 1.5 |
| | | 99 | 79 | 1.253164557 |
| | | 39 | 20 | 1.95 |
| | | 42 | 36 | 1.166666667 |
| | | 65 | 60 | 1.083333333 |
| | | | mean | 1.787953818 |
| | av max clast (mm) | 67 | 42.1 | |
| log | unit | X (mm) | Y (mm) | aspect ratio |
| 2 | 14 | 200 | 183 | 1.092896175 |
| | | 116 | 120 | 0.966666667 |
| | | 199 | 188 | 1.058510638 |
| | | 225 | 100 | 2.25 |
| | | 110 | 60 | 1.833333333 |
| | | 88 | 82 | 1.073170732 |
| | | 288 | 120 | 2.4 |
| | | 135 | 90 | 1.5 |
| | | 78 | 50 | 1.56 |
| | | 185 | 70 | 2.642857143 |
| | | | mean | 1.637743469 |

| | | | | |
|-----|-------------------------|--------|--------|--------------|
| | av max clast (mm) | 162.4 | 106.3 | |
| log | unit | X (mm) | Y (mm) | aspect ratio |
| 2 | 15 | 47 | 27 | 1.740740741 |
| | m3 | 44 | 20 | 2.2 |
| | | 59 | 29 | 2.034482759 |
| | | 124 | 44 | 2.818181818 |
| | | 53 | 44 | 1.204545455 |
| | | 80 | 40 | 2 |
| | | 100 | 79 | 1.265822785 |
| | | 75 | 40 | 1.875 |
| | | 86 | 51 | 1.68627451 |
| | | 55 | 26 | 2.115384615 |
| | | | mean | 1.894043268 |
| | av max clast (mm) | 72.3 | 40 | |
| log | unit | X (mm) | Y (mm) | aspect ratio |
| 2 | 16 | 142 | 72 | 1.972222222 |
| | | 70 | 65 | 1.076923077 |
| | | 115 | 99 | 1.161616162 |
| | | 86 | 36 | 2.388888889 |
| | | 66 | 55 | 1.2 |
| | | 140 | 50 | 2.8 |
| | | 240 | 115 | 2.086956522 |
| | | 130 | 60 | 2.166666667 |
| | | 130 | 70 | 1.857142857 |
| | | 102 | 56 | 1.821428571 |
| | | | mean | 1.853184497 |
| | av max clast (mm) | 122.1 | 67.8 | |
| log | unit | X (mm) | Y (mm) | aspect ratio |
| 2 | 17 | 424 | 119 | 3.56302521 |
| | top m of entire section | 189 | 70 | 2.7 |
| | | 130 | 42 | 3.095238095 |
| | | 99 | 88 | 1.125 |
| | | 99 | 72 | 1.375 |
| | | 260 | 65 | 4 |
| | | 81 | 56 | 1.446428571 |
| | | 177 | 140 | 1.264285714 |
| | | 110 | 55 | 2 |
| | | 150 | 55 | 2.727272727 |
| | | | mean | 2.329625032 |
| | av max clast (mm) | 171.9 | 76.2 | |
| log | unit | X (mm) | Y (mm) | aspect ratio |
| 2 | 17 | 350 | 80 | 4.375 |
| | base | 120 | 100 | 1.2 |
| | | 120 | 40 | 3 |
| | | 70 | 40 | 1.75 |

| | | | | |
|-----|-------------------|--------|------------|--------------|
| | | 90 | 28 | 3.214285714 |
| | | 120 | 60 | 2 |
| | | 140 | 40 | 3.5 |
| | | 105 | 60 | 1.75 |
| | | 130 | 60 | 2.166666667 |
| | | 220 | 60 | 3.666666667 |
| | | | mean | 2.662261905 |
| | av max clast (mm) | 146.5 | 56.8 | |
| log | unit | X (mm) | Y (mm) | aspect ratio |
| 2 | 17 | 360 | 160 | 2.25 |
| | m1 | 240 | 100 | 2.4 |
| | | 180 | 120 | 1.5 |
| | | 350 | 130 | 2.692307692 |
| | | 300 | 160 | 1.875 |
| | | 820 | 140 | 5.857142857 |
| | | 360 | 120 | 3 |
| | | 420 | 100 | 4.2 |
| | | 980 | 90 | 10.88888889 |
| | | 430 | 180 | 2.388888889 |
| | | | mean | 3.705222833 |
| | av max clast (mm) | 444 | 130 | |
| log | unit | X (mm) | Y (mm) | aspect ratio |
| 2 | 17 | 195 | 90 | 2.166666667 |
| | m2 | 280 | 160 | 1.75 |
| | | 550 | 100 | 5.5 |
| | | 190 | 70 | 2.714285714 |
| | | 3800 | 100 | 38 |
| | | 385 | 150 | 2.566666667 |
| | | 2650 | 50 | 53 |
| | | | | #DIV/0! |
| | | | | #DIV/0! |
| | | | | #DIV/0! |
| | | | mean | 15.09965986 |
| | av max clast (mm) | 1150 | 102.857143 | |
| log | unit | X (mm) | Y (mm) | aspect ratio |
| 2 | 17 | 200 | 100 | 2 |
| | m3 | 200 | 150 | 1.333333333 |
| | | 370 | 90 | 4.111111111 |
| | | 260 | 80 | 3.25 |
| | | 620 | 190 | 3.263157895 |
| | | 230 | 80 | 2.875 |
| | | 220 | 180 | 1.222222222 |
| | | 210 | 130 | 1.615384615 |
| | | 280 | 90 | 3.111111111 |
| | | 390 | 60 | 6.5 |

| | | | | |
|-----|----------------------------------|----------|------------|--------------|
| | | | mean | 2.928132029 |
| | av max clast (mm) | 298 | 115 | |
| log | unit | X (mm) | Y (mm) | aspect ratio |
| 2 | 17 | 80 | 25 | 3.2 |
| | 4500-4100 | 105 | 30 | 3.5 |
| | | 65 | 23 | 2.826086957 |
| | | 140 | 40 | 3.5 |
| | | 95 | 35 | 2.714285714 |
| | | 70 | 40 | 1.75 |
| | | 120 | 50 | 2.4 |
| | | 65 | 40 | 1.625 |
| | | 95 | 20 | 4.75 |
| | | 120 | 50 | 2.4 |
| | | | mean | 2.866537267 |
| | av max clast (mm) | 95.5 | 35.3 | |
| log | unit | X (mm) | Y (mm) | aspect ratio |
| 2 | 17 | 330 | 120 | 2.75 |
| | 5000-4500 | 150 | 70 | 2.142857143 |
| | | 140 | 65 | 2.153846154 |
| | | 115 | 80 | 1.4375 |
| | | 270 | 110 | 2.454545455 |
| | | 125 | 60 | 2.083333333 |
| | | 105 | 34 | 3.088235294 |
| | | 115 | 40 | 2.875 |
| | | 80 | 35 | 2.285714286 |
| | | 170 | 60 | 2.833333333 |
| | | | mean | 2.4104365 |
| | av max clast (mm) | 160 | 67.4 | |
| | sum av max red scoria clast (mm) | 198.1431 | | |
| log | unit | X (mm) | Y (mm) | aspect ratio |
| 16 | 2 | 26 | 22 | 1.181818182 |
| | | 20 | 19 | 1.052631579 |
| | | 24 | 21 | 1.142857143 |
| | | 15 | 10 | 1.5 |
| | | 20 | 16 | 1.25 |
| | | 20 | 11 | 1.818181818 |
| | | 18 | 17 | 1.058823529 |
| | | 20 | 17 | 1.176470588 |
| | | 22 | 17 | 1.294117647 |
| | | | | #DIV/0! |
| | | | mean | 1.274988943 |
| | av max clast (mm) | 20.55556 | 16.6666667 | |
| log | unit | X (mm) | Y (mm) | aspect ratio |
| 17 | 1 | 20 | 9 | 2.222222222 |
| | | 13 | 9 | 1.444444444 |

| | | | | |
|----------|-------------------|----------|-------------|--------------|
| | | 14 | 10 | 1.4 |
| | | 21 | 19 | 1.105263158 |
| | | 17 | 12 | 1.416666667 |
| | | 21 | 5 | 4.2 |
| | | 25 | 12 | 2.083333333 |
| | | 21 | 15 | 1.4 |
| | | 21 | 9 | 2.333333333 |
| | | | | #DIV/0! |
| | | | mean | 1.956140351 |
| | av max clast (mm) | 19.22222 | 11.11111111 | |
| log | unit | X (mm) | Y (mm) | aspect ratio |
| 19 | | 40 | 20 | 2 |
| | | 27 | 25 | 1.08 |
| | | 29 | 30 | 0.966666667 |
| | | 21 | 30 | 0.7 |
| | | 16 | 75 | 0.213333333 |
| | | 26 | 25 | 1.04 |
| | | 35 | 10 | 3.5 |
| | | 22 | 17 | 1.294117647 |
| | | 9 | 7 | 1.285714286 |
| | | 14 | 14 | 1 |
| | | | mean | 1.307983193 |
| | av max clast (mm) | 23.9 | 25.3 | |
| log | unit | X (mm) | Y (mm) | aspect ratio |
| | 1 | 25 | 19 | 1.315789474 |
| pg94 bk3 | | 34 | 10 | 3.4 |
| | | 40 | 12 | 3.333333333 |
| | | 26 | 10 | 2.6 |
| | | 49 | 16 | 3.0625 |
| | | 49 | 30 | 1.633333333 |
| | | 40 | 20 | 2 |
| | | 60 | 30 | 2 |
| | | 25 | 20 | 1.25 |
| | | 24 | 16 | 1.5 |
| | | | mean | 2.209495614 |
| | av max clast (mm) | 37.2 | 18.3 | |
| log | unit | X (mm) | Y (mm) | aspect ratio |
| | 2 | 300 | 20 | 15 |
| log | unit | X (mm) | Y (mm) | aspect ratio |
| 24 | 4 | 28 | 25 | 1.12 |
| | | 32 | 17 | 1.882352941 |
| | | 30 | 20 | 1.5 |
| | | 30 | 25 | 1.2 |
| | | 28 | 25 | 1.12 |
| | | 64 | 35 | 1.828571429 |

| | | | | |
|-----|-------------------|--------|--------|--------------|
| | | 50 | 25 | 2 |
| | | 32 | 10 | 3.2 |
| | | 34 | 30 | 1.133333333 |
| | | 28 | 12 | 2.333333333 |
| | | | mean | 1.731759104 |
| | av max clast (mm) | 35.6 | 22.4 | |
| log | unit | X (mm) | Y (mm) | aspect ratio |
| 26 | 3 | 25 | 15 | 1.666666667 |
| | | 42 | 13 | 3.230769231 |
| | | 39 | 15 | 2.6 |
| | | 31 | 20 | 1.55 |
| | | 17 | 9 | 1.888888889 |
| | | 17 | 15 | 1.133333333 |
| | | 32 | 13 | 2.461538462 |
| | | 24 | 15 | 1.6 |
| | | 11 | 7 | 1.571428571 |
| | | 15 | 12 | 1.25 |
| | | | mean | 1.895262515 |
| | av max clast (mm) | 25.3 | 13.4 | |
| log | unit | X (mm) | Y (mm) | aspect ratio |
| 26 | 5 | 10 | 20 | 0.5 |
| | | 35 | 21 | 1.666666667 |
| | | 13 | 9 | 1.444444444 |
| | | 16 | 10 | 1.6 |
| | | 11 | 9 | 1.222222222 |
| | | 34 | 10 | 3.4 |
| | | 20 | 9 | 2.222222222 |
| | | 13 | 10 | 1.3 |
| | | 21 | 19 | 1.105263158 |
| | | 17 | 15 | 1.133333333 |
| | | | mean | 1.559415205 |
| | av max clast (mm) | 19 | 13.2 | |
| log | unit | X (mm) | Y (mm) | aspect ratio |
| 23 | 1 | 43 | 35 | 1.228571429 |
| | | 65 | 70 | 0.928571429 |
| | | 100 | 40 | 2.5 |
| | | 40 | 40 | 1 |
| | | 75 | 30 | 2.5 |
| | | 66 | 60 | 1.1 |
| | | 74 | 30 | 2.466666667 |
| | | 39 | 30 | 1.3 |
| | | 49 | 12 | 4.083333333 |
| | | 62 | 40 | 1.55 |
| | | | mean | 1.865714286 |
| | av max clast (mm) | 61.3 | 38.7 | |

| log | unit | X (mm) | Y (mm) | aspect ratio |
|-------|-------------------|----------|------------|--------------|
| 27 | 2 | 300 | 130 | 2.307692308 |
| | | 100 | 70 | 1.428571429 |
| | | 180 | 170 | 1.058823529 |
| | | 190 | 160 | 1.1875 |
| | | 130 | 90 | 1.444444444 |
| | | 130 | 40 | 3.25 |
| | | 70 | 55 | 1.272727273 |
| | | 250 | 100 | 2.5 |
| | | 160 | 150 | 1.066666667 |
| | | 400 | 340 | 1.176470588 |
| | | | mean | 1.669289624 |
| | av max clast (mm) | 191 | 130.5 | |
| log | unit | X (mm) | Y (mm) | aspect ratio |
| 27 | 3 | 22 | 13 | 1.692307692 |
| | | 22 | 15 | 1.466666667 |
| | | 19 | 10 | 1.9 |
| | | 21 | 13 | 1.615384615 |
| | | 33 | 26 | 1.269230769 |
| | | 26 | 15 | 1.733333333 |
| | | | | #DIV/0! |
| | | | | #DIV/0! |
| | | | | #DIV/0! |
| | | | | #DIV/0! |
| | | | mean | 1.612820513 |
| | av max clast (mm) | 23.83333 | 15.3333333 | |
| log | unit | X (mm) | Y (mm) | aspect ratio |
| 27 | 1 | 120 | 25 | 4.8 |
| | | 86 | 26 | 3.307692308 |
| | | 70 | 30 | 2.333333333 |
| | | 90 | 22 | 4.090909091 |
| | | 70 | 35 | 2 |
| | | 65 | 45 | 1.444444444 |
| | | 95 | 50 | 1.9 |
| | | 110 | 70 | 1.571428571 |
| | | 85 | 25 | 3.4 |
| | | 70 | 45 | 1.555555556 |
| | | | mean | 2.64033633 |
| | av max clast (mm) | 86.1 | 37.3 | |
| log | unit | X (mm) | Y (mm) | aspect ratio |
| wp204 | 1 | 20 | 10 | 2 |
| | | 25 | 15 | 1.666666667 |
| | | 35 | 11 | 3.181818182 |
| | | 26 | 15 | 1.733333333 |
| | | 25 | 19 | 1.315789474 |

| | | | | |
|-------|-------------------|--------|--------|--------------|
| | | 29 | 10 | 2.9 |
| | | 15 | 15 | 1 |
| | | 29 | 15 | 1.933333333 |
| | | 40 | 15 | 2.666666667 |
| | | 19 | 14 | 1.357142857 |
| | | | mean | 1.975475051 |
| | av max clast (mm) | 26.3 | 13.9 | |
| log | unit | X (mm) | Y (mm) | aspect ratio |
| pit 1 | 1 | 96 | 73 | 1.315068493 |
| | | 120 | 67 | 1.791044776 |
| | | 139 | 110 | 1.263636364 |
| | | 106 | 58 | 1.827586207 |
| | | 115 | 99 | 1.161616162 |
| | | 78 | 44 | 1.772727273 |
| | | 139 | 115 | 1.208695652 |
| | | 110 | 100 | 1.1 |
| | | 129 | 113 | 1.14159292 |
| | | 90 | 70 | 1.285714286 |
| | | | mean | 1.386768213 |
| | av max clast (mm) | 112.2 | 84.9 | |
| log | unit | X (mm) | Y (mm) | aspect ratio |
| pit 1 | 2 | 39 | 20 | 1.95 |
| | | 24 | 15 | 1.6 |
| | | 19 | 11 | 1.727272727 |
| | | 29 | 21 | 1.380952381 |
| | | 37 | 31 | 1.193548387 |
| | | 26 | 15 | 1.733333333 |
| | | 33 | 24 | 1.375 |
| | | 29 | 22 | 1.318181818 |
| | | 41 | 32 | 1.28125 |
| | | 36 | 30 | 1.2 |
| | | | mean | 1.475953865 |
| | av max clast (mm) | 31.3 | 22.1 | |
| log | unit | X (mm) | Y (mm) | aspect ratio |
| pit 1 | 3 | 39 | 24 | 1.625 |
| | | 24 | 10 | 2.4 |
| | | 30 | 22 | 1.363636364 |
| | | 36 | 32 | 1.125 |
| | | 35 | 29 | 1.206896552 |
| | | 28 | 20 | 1.4 |
| | | 33 | 22 | 1.5 |
| | | 34 | 23 | 1.47826087 |
| | | 46 | 34 | 1.352941176 |
| | | 45 | 23 | 1.956521739 |
| | | | mean | 1.54082567 |

| | | | | |
|-------|-------------------|--------|--------|--------------|
| | av max clast (mm) | 35 | 23.9 | |
| log | unit | X (mm) | Y (mm) | aspect ratio |
| pit 2 | | 80 | 65 | 1.230769231 |
| | | 110 | 85 | 1.294117647 |
| | | 103 | 72 | 1.430555556 |
| | | 100 | 70 | 1.428571429 |
| | | 75 | 30 | 2.5 |
| | | 144 | 120 | 1.2 |
| | | 75 | 76 | 0.986842105 |
| | | 70 | 70 | 1 |
| | | 110 | 80 | 1.375 |
| | | 77 | 67 | 1.149253731 |
| | | | mean | 1.35951097 |
| | av max clast (mm) | 94.4 | 73.5 | |
| log | unit | X (mm) | Y (mm) | aspect ratio |
| pit 3 | 1 | 199 | 150 | 1.326666667 |
| | | 100 | 95 | 1.052631579 |
| | | 225 | 160 | 1.40625 |
| | | 106 | 66 | 1.606060606 |
| | | 85 | 66 | 1.287878788 |
| | | 160 | 115 | 1.391304348 |
| | | 103 | 80 | 1.2875 |
| | | 115 | 90 | 1.277777778 |
| | | 70 | 60 | 1.166666667 |
| | | 145 | 70 | 2.071428571 |
| | | | mean | 1.3874165 |
| | av max clast (mm) | 130.8 | 95.2 | |
| log | unit | X (mm) | Y (mm) | aspect ratio |
| pit 3 | 2 | 49 | 30 | 1.633333333 |
| | | 46 | 20 | 2.3 |
| | | 51 | 19 | 2.684210526 |
| | | 36 | 29 | 1.24137931 |
| | | 47 | 35 | 1.342857143 |
| | | 39 | 27 | 1.444444444 |
| | | 34 | 22 | 1.545454545 |
| | | 46 | 27 | 1.703703704 |
| | | 39 | 34 | 1.147058824 |
| | | 40 | 25 | 1.6 |
| | | | mean | 1.664244183 |
| | av max clast (mm) | 42.7 | 26.8 | |
| log | unit | X (mm) | Y (mm) | aspect ratio |
| pit 4 | | 76 | 70 | 1.085714286 |
| | | 140 | 85 | 1.647058824 |
| | | 70 | 59 | 1.186440678 |
| | | 90 | 90 | 1 |

| | | | | |
|-------|-----------------------|----------|--------|--------------|
| | | 100 | 45 | 2.222222222 |
| | | 90 | 65 | 1.384615385 |
| | | 95 | 65 | 1.461538462 |
| | | 140 | 25 | 5.6 |
| | | 110 | 75 | 1.466666667 |
| | | 190 | 110 | 1.727272727 |
| | | | mean | 1.878152925 |
| | av max clast (mm) | 110.1 | 68.9 | |
| log | unit | X (mm) | Y (mm) | aspect ratio |
| pit 5 | | 100 | 95 | 1.052631579 |
| | | 100 | 74 | 1.351351351 |
| | | 120 | 100 | 1.2 |
| | | 245 | 150 | 1.633333333 |
| | | 310 | 330 | 0.939393939 |
| | | 240 | 200 | 1.2 |
| | | 170 | 120 | 1.416666667 |
| | | 130 | 120 | 1.083333333 |
| | | 130 | 95 | 1.368421053 |
| | | 135 | 120 | 1.125 |
| | | | mean | 1.237013126 |
| | av max clast (mm) | 168 | 140.4 | |
| log | unit | X (mm) | Y (mm) | aspect ratio |
| pit 6 | | 130 | 100 | 1.3 |
| | | 120 | 71 | 1.690140845 |
| | | 100 | 55 | 1.818181818 |
| | | 160 | 140 | 1.142857143 |
| | | 100 | 40 | 2.5 |
| | | 65 | 55 | 1.181818182 |
| | | 85 | 80 | 1.0625 |
| | | 85 | 60 | 1.416666667 |
| | | 65 | 45 | 1.444444444 |
| | | 90 | 50 | 1.8 |
| | | | mean | 1.53566091 |
| | av max clast (mm) | 100 | 69.6 | |
| | sum av max clast (mm) | 91.61111 | | |
| log | unit | X (mm) | Y (mm) | aspect ratio |
| 29 | 3 | 45 | 48 | 0.9375 |
| | | 20 | 24 | 0.833333333 |
| | | 24 | 37 | 0.648648649 |
| | | 30 | 47 | 0.638297872 |
| | | 28 | 16 | 1.75 |
| | | 18 | 15 | 1.2 |
| | | 43 | 30 | 1.433333333 |
| | | 38 | 23 | 1.652173913 |
| | | 25 | 11 | 2.272727273 |

| | | | | |
|-------|-------------------|----------|------------|--------------|
| | | 19 | 18 | 1.055555556 |
| | | | mean | 1.242156993 |
| | av max clast (mm) | 29 | 26.9 | |
| log | unit | X (mm) | Y (mm) | aspect ratio |
| 29 | 4 | 25 | 20 | 1.25 |
| | | 15 | 9 | 1.666666667 |
| | | 25 | 22 | 1.136363636 |
| | | 20 | 15 | 1.333333333 |
| | | 22 | 15 | 1.466666667 |
| | | 20 | 16 | 1.25 |
| | | 19 | 13 | 1.461538462 |
| | | 20 | 10 | 2 |
| | | 40 | 40 | 1 |
| | | 21 | 14 | 1.5 |
| | | | mean | 1.406456876 |
| | av max clast (mm) | 22.7 | 17.4 | |
| log | unit | X (mm) | Y (mm) | aspect ratio |
| wp041 | 1 | 130 | 125 | 1.04 |
| | | 170 | 120 | 1.416666667 |
| | | 80 | 75 | 1.066666667 |
| | | 105 | 75 | 1.4 |
| | | 126 | 95 | 1.326315789 |
| | | 135 | 75 | 1.8 |
| | | 180 | 110 | 1.636363636 |
| | | 189 | 105 | 1.8 |
| | | 105 | 80 | 1.3125 |
| | | | | #DIV/0! |
| | | | mean | 1.422056973 |
| | av max clast (mm) | 135.5556 | 95.5555556 | |
| log | unit | X (mm) | Y (mm) | aspect ratio |
| wp401 | 2 | 105 | 50 | 2.1 |
| | | 140 | 90 | 1.555555556 |
| | | 145 | 80 | 1.8125 |
| | | 130 | 100 | 1.3 |
| | | 185 | 130 | 1.423076923 |
| | | 155 | 140 | 1.107142857 |
| | | 110 | 85 | 1.294117647 |
| | | 160 | 110 | 1.454545455 |
| | | 125 | 90 | 1.388888889 |
| | | 105 | 70 | 1.5 |
| | | | mean | 1.493582733 |
| | av max clast (mm) | 136 | 94.5 | |
| log | unit | X (mm) | Y (mm) | aspect ratio |
| wp401 | 3 | 135 | 70 | 1.928571429 |
| | | 140 | 90 | 1.555555556 |

| | | | | |
|-----|-----------------------|----------|--------|--------------|
| | | 125 | 70 | 1.785714286 |
| | | 140 | 65 | 2.153846154 |
| | | 90 | 60 | 1.5 |
| | | 55 | 38 | 1.447368421 |
| | | 90 | 35 | 2.571428571 |
| | | 150 | 70 | 2.142857143 |
| | | 120 | 70 | 1.714285714 |
| | | 100 | 60 | 1.666666667 |
| | | | mean | 1.846629394 |
| | av max clast (mm) | 114.5 | 62.8 | |
| | sum av max clast (mm) | 128.6852 | | |
| log | unit | X (mm) | Y (mm) | aspect ratio |
| 30 | 2 | 250 | 200 | 1.25 |
| | | 155 | 90 | 1.722222222 |
| | | 230 | 110 | 2.090909091 |
| | | 110 | 100 | 1.1 |
| | | 270 | 140 | 1.928571429 |
| | | 130 | 60 | 2.166666667 |
| | | 200 | 155 | 1.290322581 |
| | | 100 | 85 | 1.176470588 |
| | | 150 | 110 | 1.363636364 |
| | | 60 | 45 | 1.333333333 |
| | | | mean | 1.542213227 |
| | av max clast (mm) | 165.5 | 109.5 | |
| log | unit | X (mm) | Y (mm) | aspect ratio |
| 30 | 2 | 300 | 140 | 2.142857143 |
| | m4 | 310 | 130 | 2.384615385 |
| | | 150 | 110 | 1.363636364 |
| | | 90 | 60 | 1.5 |
| | | 80 | 50 | 1.6 |
| | | 370 | 110 | 3.363636364 |
| | | 125 | 50 | 2.5 |
| | | 200 | 80 | 2.5 |
| | | 200 | 100 | 2 |
| | | 245 | 150 | 1.633333333 |
| | | | mean | 2.098807859 |
| | av max clast (mm) | 207 | 98 | |
| log | unit | X (mm) | Y (mm) | aspect ratio |
| 30 | 4 | 75 | 50 | 1.5 |
| | | 80 | 65 | 1.230769231 |
| | | 60 | 40 | 1.5 |
| | | 100 | 95 | 1.052631579 |
| | | 165 | 200 | 0.825 |
| | | 110 | 40 | 2.75 |
| | | 70 | 45 | 1.555555556 |

| | | | | |
|-------|-------------------|---------|------------|--------------|
| | | 100 | 65 | 1.538461538 |
| | | 170 | 140 | 1.214285714 |
| | | 70 | 35 | 2 |
| | | | mean | 1.516670362 |
| | av max clast (mm) | 100 | 77.5 | |
| log | unit | X (mm) | Y (mm) | aspect ratio |
| wp079 | | 170 | 40 | 4.25 |
| | | 240 | 85 | 2.823529412 |
| | | 370 | 30 | 12.33333333 |
| | | 360 | 50 | 7.2 |
| | | 390 | 120 | 3.25 |
| | | 280 | 120 | 2.333333333 |
| | | 290 | 60 | 4.833333333 |
| | | 360 | 60 | 6 |
| | | 440 | 120 | 3.666666667 |
| | | 360 | 80 | 4.5 |
| | | | mean | 5.119019608 |
| | av max clast (mm) | 326 | 76.5 | |
| log | unit | X (mm) | Y (mm) | aspect ratio |
| wp081 | | 330 | 120 | 2.75 |
| | | 190 | 85 | 2.235294118 |
| | | 240 | 70 | 3.428571429 |
| | | 280 | 60 | 4.666666667 |
| | | 260 | 50 | 5.2 |
| | | 290 | 60 | 4.833333333 |
| | | | | #DIV/0! |
| | | | | #DIV/0! |
| | | | | #DIV/0! |
| | | | | #DIV/0! |
| | | | mean | 3.852310924 |
| | av max clast (mm) | 265 | 74.1666667 | |
| log | unit | X (mm) | Y (mm) | aspect ratio |
| wp084 | | 280 | 70 | 4 |
| | | 260 | 50 | 5.2 |
| | | 410 | 70 | 5.857142857 |
| | | 200 | 40 | 5 |
| | | 260 | 70 | 3.714285714 |
| | | 295 | 60 | 4.916666667 |
| | | 450 | 50 | 9 |
| | | 360 | 45 | 8 |
| | | | | #DIV/0! |
| | | | | #DIV/0! |
| | | | mean | 5.711011905 |
| | av max clast (mm) | 314.375 | 56.875 | |
| log | unit | X (mm) | Y (mm) | aspect ratio |

| | | | | |
|-------------|-------------------|--------|--------|--------------|
| 297 bk4pg77 | | 26 | 15 | 1.733333333 |
| | | 25 | 12 | 2.083333333 |
| | | 23 | 12 | 1.916666667 |
| | | 21 | 11 | 1.909090909 |
| | | 42 | 35 | 1.2 |
| | | 31 | 16 | 1.9375 |
| | | 24 | 13 | 1.846153846 |
| | | 22 | 12 | 1.833333333 |
| | | 32 | 18 | 1.777777778 |
| | | 26 | 13 | 2 |
| | | | mean | 1.82371892 |
| | av max clast (mm) | 27.2 | 15.7 | |
| log | unit | X (mm) | Y (mm) | aspect ratio |
| 31 | 2 | 45 | 20 | 2.25 |
| | | 35 | 35 | 1 |
| | | 35 | 30 | 1.166666667 |
| | | 45 | 28 | 1.607142857 |
| | | 19 | 19 | 1 |
| | | 42 | 40 | 1.05 |
| | | 25 | 15 | 1.666666667 |
| | | 13 | 5 | 2.6 |
| | | 30 | 16 | 1.875 |
| | | 25 | 20 | 1.25 |
| | | | mean | 1.546547619 |
| | av max clast (mm) | 31.4 | 22.8 | |
| log | unit | X (mm) | Y (mm) | aspect ratio |
| wp145 | 1 | 55 | 24 | 2.291666667 |
| | | 70 | 50 | 1.4 |
| | | 75 | 40 | 1.875 |
| | | 47 | 30 | 1.566666667 |
| | | 59 | 55 | 1.072727273 |
| | | 70 | 30 | 2.333333333 |
| | | 45 | 40 | 1.125 |
| | | 59 | 30 | 1.966666667 |
| | | 35 | 20 | 1.75 |
| | | 50 | 25 | 2 |
| | | | mean | 1.738106061 |
| | av max clast (mm) | 56.5 | 34.4 | |
| log | unit | X (mm) | Y (mm) | aspect ratio |
| wp145 | 2 | 340 | 100 | 3.4 |
| | | 220 | 110 | 2 |
| | | 500 | 130 | 3.846153846 |
| | | 220 | 60 | 3.666666667 |
| | | 240 | 50 | 4.8 |
| | | 370 | 80 | 4.625 |

| | | | | |
|-------|-----------------------|--------|--------|--------------|
| | | 120 | 70 | 1.714285714 |
| | | 200 | 60 | 3.333333333 |
| | | 140 | 30 | 4.666666667 |
| | | 190 | 50 | 3.8 |
| | | | mean | 3.585210623 |
| | av max clast (mm) | 254 | 74 | |
| | sum av max clast (mm) | 155.25 | | |
| log | unit | X (mm) | Y (mm) | aspect ratio |
| 32 | 1 | 25 | 15 | 1.666666667 |
| | | 40 | 16 | 2.5 |
| | | 16 | 5 | 3.2 |
| | | 34 | 9 | 3.777777778 |
| | | 20 | 10 | 2 |
| | | 45 | 16 | 2.8125 |
| | | 26 | 24 | 1.083333333 |
| | | 50 | 13 | 3.846153846 |
| | | 30 | 30 | 1 |
| | | 50 | 36 | 1.388888889 |
| | | | mean | 2.327532051 |
| | av max clast (mm) | 33.6 | 17.4 | |
| log | unit | X (mm) | Y (mm) | aspect ratio |
| 33 | 1 | 22 | 19 | 1.157894737 |
| | | 20 | 6 | 3.333333333 |
| | | 20 | 15 | 1.333333333 |
| | | 21 | 6 | 3.5 |
| | | 23 | 5 | 4.6 |
| | | 32 | 7 | 4.571428571 |
| | | 16 | 5 | 3.2 |
| | | 22 | 14 | 1.571428571 |
| | | 26 | 5 | 5.2 |
| | | 19 | 9 | 2.111111111 |
| | | | mean | 3.057852966 |
| | av max clast (mm) | 22.1 | 9.1 | |
| log | unit | X (mm) | Y (mm) | aspect ratio |
| wp152 | | 27 | 10 | 2.7 |
| | | 12 | 15 | 0.8 |
| | | 30 | 14 | 2.142857143 |
| | | 20 | 12 | 1.666666667 |
| | | 40 | 30 | 1.333333333 |
| | | 15 | 12 | 1.25 |
| | | 44 | 30 | 1.466666667 |
| | | 32 | 11 | 2.909090909 |
| | | 30 | 15 | 2 |
| | | 25 | 15 | 1.666666667 |
| | | | mean | 1.793528139 |

| | | | | |
|-------|-------------------|----------|------------|--------------|
| | av max clast (mm) | 27.5 | 16.4 | |
| log | unit | X (mm) | Y (mm) | aspect ratio |
| 34 | 1 | 64 | 15 | 4.266666667 |
| | | 55 | 25 | 2.2 |
| | | 50 | 20 | 2.5 |
| | | 40 | 10 | 4 |
| | | 65 | 30 | 2.166666667 |
| | | 70 | 20 | 3.5 |
| | | 46 | 6 | 7.666666667 |
| | | 39 | 10 | 3.9 |
| | | 30 | 10 | 3 |
| | | 95 | 45 | 2.111111111 |
| | | | mean | 3.531111111 |
| | av max clast (mm) | 55.4 | 19.1 | |
| log | unit | X (mm) | Y (mm) | aspect ratio |
| wp174 | | 95 | 70 | 1.357142857 |
| | | 99 | 55 | 1.8 |
| | | 70 | 50 | 1.4 |
| | | 120 | 90 | 1.333333333 |
| | | 80 | 65 | 1.230769231 |
| | | 140 | 60 | 2.333333333 |
| | | 85 | 60 | 1.416666667 |
| | | 270 | 100 | 2.7 |
| | | 120 | 100 | 1.2 |
| | | 75 | 50 | 1.5 |
| | | | mean | 1.627124542 |
| | av max clast (mm) | 115.4 | 70 | |
| log | unit | X (mm) | Y (mm) | aspect ratio |
| 22 | 1 | 2000 | 105 | 19.04761905 |
| | | 2250 | 200 | 11.25 |
| | | 1350 | 60 | 22.5 |
| | | | | #DIV/0! |
| | | | | #DIV/0! |
| | | | | #DIV/0! |
| | | | | #DIV/0! |
| | | | | #DIV/0! |
| | | | | #DIV/0! |
| | | | | #DIV/0! |
| | | | mean | 17.59920635 |
| | av max clast (mm) | 1866.667 | 121.666667 | |
| log | unit | X (mm) | Y (mm) | aspect ratio |
| 22 | 2 | 44 | 15 | 2.933333333 |
| | | 34 | 12 | 2.833333333 |
| | | 20 | 15 | 1.333333333 |
| | | 32 | 20 | 1.6 |

| | | | | |
|-------|-----------------------|----------|-------------|--------------|
| | | 35 | 10 | 3.5 |
| | | 60 | 40 | 1.5 |
| | | 60 | 50 | 1.2 |
| | | 25 | 15 | 1.666666667 |
| | | 35 | 35 | 1 |
| | | 45 | 42 | 1.071428571 |
| | | | mean | 1.863809524 |
| | av max clast (mm) | 39 | 25.4 | |
| log | unit | X (mm) | Y (mm) | aspect ratio |
| 22 | 3 | 2000 | 55 | 36.36363636 |
| | | 600 | 15 | 40 |
| | | 500 | 100 | 5 |
| | | 115 | 10 | 11.5 |
| | | 350 | 5 | 70 |
| | | 560 | 5 | 112 |
| | | | | #DIV/0! |
| | | | | #DIV/0! |
| | | | | #DIV/0! |
| | | | | #DIV/0! |
| | | | mean | 45.81060606 |
| | av max clast (mm) | 687.5 | 31.66666667 | |
| log | unit | X (mm) | Y (mm) | aspect ratio |
| 22 | 4 | 35 | 32 | 1.09375 |
| | | 20 | 15 | 1.333333333 |
| | | 30 | 10 | 3 |
| | | 30 | 25 | 1.2 |
| | | 25 | 10 | 2.5 |
| | | 12 | 12 | 1 |
| | | 10 | 12 | 0.833333333 |
| | | 15 | 15 | 1 |
| | | 12 | 10 | 1.2 |
| | | | | #DIV/0! |
| | | | mean | 1.462268519 |
| | av max clast (mm) | 21 | 15.66666667 | |
| | sum av max clast (mm) | 653.5417 | | |
| log | unit | X (mm) | Y (mm) | aspect ratio |
| wp165 | | 1000 | 80 | 12.5 |
| | | 640 | 110 | 5.818181818 |
| | | 550 | 100 | 5.5 |
| | | 900 | 65 | 13.84615385 |
| | | 500 | 120 | 4.166666667 |
| | | | | #DIV/0! |
| | | | | #DIV/0! |
| | | | | #DIV/0! |
| | | | | #DIV/0! |

| | | | | |
|-------|-------------------|----------|------------|--------------|
| | | | | #DIV/0! |
| | | | mean | 8.366200466 |
| | av max clast (mm) | 718 | 95 | |
| log | unit | X (mm) | Y (mm) | aspect ratio |
| wp166 | | 1030 | 120 | 8.583333333 |
| | | 1110 | 160 | 6.9375 |
| | | 750 | 60 | 12.5 |
| | | | | #DIV/0! |
| | | | | #DIV/0! |
| | | | | #DIV/0! |
| | | | | #DIV/0! |
| | | | | #DIV/0! |
| | | | | #DIV/0! |
| | | | | #DIV/0! |
| | | | mean | 9.340277778 |
| | av max clast (mm) | 963.3333 | 113.333333 | |
| log | unit | X (mm) | Y (mm) | aspect ratio |
| wp174 | | 95 | 70 | 1.357142857 |
| | | 99 | 55 | 1.8 |
| | | 70 | 50 | 1.4 |
| | | 120 | 90 | 1.333333333 |
| | | 80 | 65 | 1.230769231 |
| | | 140 | 60 | 2.333333333 |
| | | 85 | 60 | 1.416666667 |
| | | 270 | 100 | 2.7 |
| | | 120 | 100 | 1.2 |
| | | 75 | 50 | 1.5 |
| | | | mean | 1.627124542 |
| | av max clast (mm) | 115.4 | 70 | |
| log | unit | X (mm) | Y (mm) | aspect ratio |
| wp158 | | 64 | 15 | 4.266666667 |
| | | 55 | 25 | 2.2 |
| | | 50 | 20 | 2.5 |
| | | 40 | 10 | 4 |
| | | 65 | 30 | 2.166666667 |
| | | 70 | 20 | 3.5 |
| | | 46 | 6 | 7.666666667 |
| | | 39 | 10 | 3.9 |
| | | 30 | 10 | 3 |
| | | 95 | 45 | 2.111111111 |
| | | | mean | 3.531111111 |
| | av max clast (mm) | 55.4 | 19.1 | |
| 29 | M1 | 15 | 18 | 0.8 |
| | | 70 | 59 | 1.1 |
| | | 29 | 5 | 5.8 |

| | | | | |
|---|-------------------|------|------|-----|
| | | 31 | 13 | 2.3 |
| | | 22 | 11 | 2 |
| | | 25 | 12 | 2 |
| | | 26 | 18 | 1.4 |
| | | 39 | 7 | 5.5 |
| | | 28 | 4 | 7 |
| | | 17 | 13 | 1.3 |
| | Av max clast (mm) | 30.2 | 16 | 2.9 |
| 29 | M6 | 25 | 25 | 1 |
| | | 30 | 22 | 1.3 |
| | | 49 | 35 | 1.4 |
| | | 25 | 30 | 0.8 |
| | | 30 | 20 | 1.5 |
| | | 25 | 24 | 1 |
| | | 25 | 23 | 1.9 |
| | | 31 | 15 | 2 |
| | | 15 | 13 | 1.1 |
| | Av max clast (mm) | 28 | 21 | |
| | | | mean | 1.3 |
| 29 | M7 | 75 | 30 | 2.5 |
| | | 50 | 23 | 2.1 |
| | | 18 | 17 | 1 |
| | | 31 | 20 | 1.5 |
| | | 25 | 19 | 1.3 |
| | | 37 | 23 | 1.6 |
| | | 29 | 25 | 1.1 |
| | | 25 | 16 | 1.5 |
| | | 22 | 14 | 1.5 |
| | | 19 | 18 | 1 |
| | Av max clast (mm) | 33 | 20 | 1.5 |
| | | | mean | 1.5 |
| Table A1.18. Stratigraphic log measurements from 2012. | | | | |

| date | wp | lo g | bk,p g | unit | clast type | x (mm) | y (mm) | unit thickness (mm) | aspect ratio |
|--------|-----|---------|-----------|------|---------------|-----------|-----------|------------------------|-----------------|
| 24-Jun | 401 | 15 | 5,144 | 1 | sc | 16 | 8 | 200 | 2 |
| | | | | | | 28 | 8 | | 3.5 |
| | | | | | | 13 | 11 | | 1.181818 182 |
| | | | | | | 25 | 7 | | 3.571428 571 |
| | | | | | | 32 | 20 | | 1.6 |
| | | | | | | 8 | 7 | | 1.142857 143 |
| | | | | | | 11 | 7 | | 1.571428 |

| | | | | | | | | | |
|--|--|--|--|---|------|--------------|--------------|-----|-----------------|
| | | | | | | | | | 571 |
| | | | | | | 10 | 8 | | 1.25 |
| | | | | | | 10 | 7 | | 1.428571 429 |
| | | | | | | 14 | 4 | | 3.5 |
| | | | | | mean | 16.7 | 8.7 | | 2.074610 39 |
| | | | | | agg | 100 | 60 | | 1.666666 667 |
| | | | | | | 90 | 40 | | 2.25 |
| | | | | | | 110 | 40 | | 2.75 |
| | | | | | | 70 | 20 | | 3.5 |
| | | | | | | 60 | 40 | | 1.5 |
| | | | | | mean | 86 | 40 | | 2.333333 333 |
| | | | | 2 | sc | 20 | 16 | 320 | 1.25 |
| | | | | | | 16 | 8 | | 2 |
| | | | | | | 16 | 4 | | 4 |
| | | | | | | 22 | 16 | | 1.375 |
| | | | | | | 16 | 13 | | 1.230769 231 |
| | | | | | | 23 | 15 | | 1.533333 333 |
| | | | | | | 10 | 8 | | 1.25 |
| | | | | | | 22 | 15 | | 1.466666 667 |
| | | | | | | 16 | 9 | | 1.777777 778 |
| | | | | | | 13 | 4 | | 3.25 |
| | | | | | mean | 17.4 | 10.8 | | 1.913354 701 |
| | | | | 3 | sc | 32 | 6 | 140 | 5.333333 333 |
| | | | | | | 15 | 5 | | 3 |
| | | | | | | 32 | 10 | | 3.2 |
| | | | | | | 32 | 30 | | 1.066666 667 |
| | | | | | | 30 | 21 | | 1.428571 429 |
| | | | | | | 20 | 10 | | 2 |
| | | | | | mean | 26.833 33 | 13.666 67 | | 2.671428 571 |
| | | | | 4 | agg | 80 | 20 | 250 | 4 |
| | | | | | | 80 | 40 | | 2 |
| | | | | | | 60 | 50 | | 1.2 |
| | | | | | | 60 | 20 | | 3 |
| | | | | | | 130 | 54 | | 2.407407 407 |

| | | | | | | | | | |
|------------|-----|--------|-----------|----------|------|------|------|------|-----------------|
| | | | | | | 70 | 50 | | 1.4 |
| | | | | | mean | 80 | 39 | | 2.334567 901 |
| | | | | 6 | agg | 55 | 10 | | 5.5 |
| | | | | | | 60 | 16 | | 3.75 |
| | | | | | | 57 | 17 | | 3.352941 176 |
| | | | | | | 32 | 12 | | 2.666666 667 |
| | | | | | | 80 | 16 | | 5 |
| | | | | | | 50 | 30 | | 1.666666 667 |
| | | | | | | 59 | 8 | | 7.375 |
| | | | | | | 28 | 11 | | 2.545454 545 |
| | | | | | | 43 | 8 | | 5.375 |
| | | | | | | 39 | 20 | | 1.95 |
| | | | | | mean | 50.3 | 14.8 | | 3.918172 906 |
| 23- Jun | y46 | 1 3 | 5, 139 | 3 | sc | 21 | 16 | 320 | 1.3125 |
| | | | | | | 28 | 15 | | 1.866666 667 |
| | | | | | | 22 | 8 | | 2.75 |
| | | | | | | 58 | 21 | | 2.761904 762 |
| | | | | | | 24 | 6 | | 4 |
| | | | | | | 60 | 10 | | 6 |
| | | | | | | 43 | 30 | | 1.433333 333 |
| | | | | | | 120 | 16 | | 7.5 |
| | | | | | | 64 | 33 | | 1.939393 939 |
| | | | | | | 28 | 24 | | 1.166666 667 |
| | | | | | mean | 46.8 | 17.9 | | 3.073046 537 |
| | | | | 4, ml | sc | 190 | 60 | 2400 | 3.166666 667 |
| | | | | | | 105 | 50 | | 2.1 |
| | | | | | | 110 | 50 | | 2.2 |
| | | | | | | 80 | 30 | | 2.666666 667 |
| | | | | | | 150 | 40 | | 3.75 |
| | | | | | | 70 | 30 | | 2.333333 333 |
| | | | | | | 100 | 30 | | 3.333333 333 |

| | | | | | | | | | |
|--|--|--|--|----------|------|--------------|------|------|-----------------|
| | | | | | | 125 | 30 | | 4.166666 667 |
| | | | | | | 70 | 40 | | 1.75 |
| | | | | | mean | 111.11 11 | 40 | | 2.829629 63 |
| | | | | 4, m2 | | 100 | 30 | | 3.333333 333 |
| | | | | | | 75 | 60 | | 1.25 |
| | | | | | | 110 | 20 | | 5.5 |
| | | | | | | 150 | 55 | | 2.727272 727 |
| | | | | | | 110 | 40 | | 2.75 |
| | | | | | | 90 | 40 | | 2.25 |
| | | | | | | 110 | 35 | | 3.142857 143 |
| | | | | | | 70 | 20 | | 3.5 |
| | | | | | | 100 | 40 | | 2.5 |
| | | | | | | 80 | 30 | | 2.666666 667 |
| | | | | | mean | 99.5 | 37 | | 2.962012 987 |
| | | | | 6, m1 | | 63 | 16 | 5000 | 3.9375 |
| | | | | | | 49 | 20 | | 2.45 |
| | | | | | | 100 | 20 | | 5 |
| | | | | | | 102 | 50 | | 2.04 |
| | | | | | | 69 | 20 | | 3.45 |
| | | | | | | 60 | 40 | | 1.5 |
| | | | | | | 36 | 28 | | 1.285714 286 |
| | | | | | | 63 | 24 | | 2.625 |
| | | | | | | 60 | 20 | | 3 |
| | | | | | | 54 | 16 | | 3.375 |
| | | | | | mean | 65.6 | 25.4 | | 2.866321 429 |
| | | | | m2 | | 190 | 60 | | 3.166666 667 |
| | | | | | | 70 | 40 | | 1.75 |
| | | | | | | 130 | 40 | | 3.25 |
| | | | | | | 95 | 30 | | 3.166666 667 |
| | | | | | | 150 | 40 | | 3.75 |
| | | | | | | 90 | 50 | | 1.8 |
| | | | | | | 130 | 45 | | 2.888888 889 |
| | | | | | | 130 | 70 | | 1.857142 857 |

| | | | | | | | | | |
|--|--|--|--|--------------|------|--------------|--------------|------|-----------------|
| | | | | | | 100 | 40 | | 2.5 |
| | | | | | | 80 | 40 | | 2 |
| | | | | | mean | 116.5 | 45.5 | | 2.612936 508 |
| | | | | 1st bomb bed | | 160 | 60 | | 2.666666 667 |
| | | | | | | 120 | 60 | | 2 |
| | | | | | | 80 | 50 | | 1.6 |
| | | | | | | 210 | 50 | | 4.2 |
| | | | | | | 145 | 50 | | 2.9 |
| | | | | | | 230 | 40 | | 5.75 |
| | | | | | mean | 157.5 | 51.666 67 | | 3.186111 111 |
| | | | | m4 | | 100 | 30 | | 3.333333 333 |
| | | | | | | 80 | 55 | | 1.454545 455 |
| | | | | | | 70 | 30 | | 2.333333 333 |
| | | | | | | 64 | 43 | | 1.488372 093 |
| | | | | | | 70 | 28 | | 2.5 |
| | | | | | | 64 | 40 | | 1.6 |
| | | | | | | 70 | 16 | | 4.375 |
| | | | | | | 190 | 40 | | 4.75 |
| | | | | | | 200 | 60 | | 3.333333 333 |
| | | | | | | 135 | 50 | | 2.7 |
| | | | | | | 130 | 40 | | 3.25 |
| | | | | | mean | 106.63 64 | 39.272 73 | | 2.778458 421 |
| | | | | upper 380 | | 130 | 40 | | 3.25 |
| | | | | | | 160 | 60 | | 2.666666 667 |
| | | | | | | 160 | 70 | | 2.285714 286 |
| | | | | | | 170 | 80 | | 2.125 |
| | | | | | | 140 | 60 | | 2.333333 333 |
| | | | | | | 120 | 50 | | 2.4 |
| | | | | | mean | 146.66 67 | 60 | | 2.510119 048 |
| | | | | 10 | | 70 | 28 | 1500 | 2.5 |
| | | | | | | 58 | 11 | | 5.272727 273 |
| | | | | | | 130 | 25 | | 5.2 |
| | | | | | | 90 | 8 | | 11.25 |
| | | | | | | 64 | 25 | | 2.56 |

| | | | | | | | | | |
|--------|-----|-----|------|------|----------|--------|--------|-----|-------------|
| | | | | | | 74 | 32 | | 2.3125 |
| | | | | | | 58 | 16 | | 3.625 |
| | | | | | | 80 | 21 | | 3.80952381 |
| | | | | | | 73 | 16 | | 4.5625 |
| | | | | mean | | 77.444 | 20.222 | | 4.565805676 |
| | | | | 8 | | 28 | 20 | | 1.4 |
| | | | | | | 32 | 14 | | 2.285714286 |
| | | | | | | 80 | 30 | | 2.666666667 |
| | | | | | | 90 | 45 | | 2 |
| | | | | | | 60 | 23 | | 2.608695652 |
| | | | | | | 54 | 30 | | 1.8 |
| | | | | | | 50 | 10 | | 5 |
| | | | | mean | | 56.285 | 24.571 | | 2.537296658 |
| 01-Jul | y48 | 16 | 6,59 | 1 | sediment | 180 | 130 | 800 | 1.384615385 |
| | | | | | | 110 | 80 | | 1.375 |
| | | | | | | 160 | 120 | | 1.333333333 |
| | | | | | | 180 | 80 | | 2.25 |
| | | | | | | 140 | 150 | | 0.933333333 |
| | | | | | | 800 | 670 | | 1.194029851 |
| | | | | mean | | 261.66 | 205 | | 1.41171865 |
| | | | | 2 | sc | 16 | 10 | 90 | 1.6 |
| | | | | | | 19 | 16 | | 1.1875 |
| | | | | | | 20 | 11 | | 1.818181818 |
| | | | | | | 16 | 20 | | 0.8 |
| | | | | | | 21 | 11 | | 1.909090909 |
| | | | | | | 23 | 16 | | 1.4375 |
| | | | | | | 24 | 20 | | 1.2 |
| | | | | | | 30 | 20 | | 1.5 |
| | | | | | | 30 | 8 | | 3.75 |
| | | | | | | 16 | 16 | | 1 |
| | | | | mean | | 21.5 | 14.8 | | 1.620227273 |
| 24-Jun | 401 | 114 | 141 | 1 | spatters | 130 | 60 | 300 | 2.166666667 |
| | | | | | | 190 | 45 | | 4.222222 |

| | | | | | | | | | |
|--|--|--|--|------|----------|------|--------|------|-----------------|
| | | | | | | | | | 222 |
| | | | | | | 100 | 30 | | 3.333333 333 |
| | | | | | | 220 | 80 | | 2.75 |
| | | | | | | 190 | 70 | | 2.714285 714 |
| | | | | | | 200 | 80 | | 2.5 |
| | | | | | | 130 | 50 | | 2.6 |
| | | | | | | 320 | 80 | | 4 |
| | | | | mean | | 185 | 61.875 | | 3.035813 492 |
| | | | | 2 | mwew | 430 | 40 | 1600 | 10.75 |
| | | | | | | 600 | 70 | | 8.571428 571 |
| | | | | | | 400 | 10 | | 40 |
| | | | | | | 400 | 10 | | 40 |
| | | | | | | 680 | 45 | | 15.11111 111 |
| | | | | | | 270 | 40 | | 6.75 |
| | | | | | | 510 | 30 | | 17 |
| | | | | mean | | 470 | 35 | | 19.74036 281 |
| | | | | 3 | spatters | 90 | 30 | 200 | 3 |
| | | | | | | 160 | 15 | | 10.66666 667 |
| | | | | | | 200 | 80 | | 2.5 |
| | | | | | | 130 | 55 | | 2.363636 364 |
| | | | | | | 120 | 10 | | 12 |
| | | | | | mean | 140 | 38 | | 6.106060 606 |
| | | | | 5 | mwscf | 80 | 16 | 75 | 5 |
| | | | | | | 58 | 8 | | 7.25 |
| | | | | | | 59 | 8 | | 7.375 |
| | | | | | | 64 | 30 | | 2.133333 333 |
| | | | | | | 32 | 16 | | 2 |
| | | | | | | 86 | 20 | | 4.3 |
| | | | | | | 64 | 24 | | 2.666666 667 |
| | | | | | | 51 | 20 | | 2.55 |
| | | | | | | 64 | 25 | | 2.56 |
| | | | | | | 50 | 10 | | 5 |
| | | | | | mean | 60.8 | 17.7 | | 4.0835 |
| | | | | 6 | scb | 70 | 50 | 180 | 1.4 |
| | | | | | | 70 | 70 | | 1 |
| | | | | | | 54 | 40 | | 1.35 |

| | | | | | | | | | |
|------------|-----|---------|-----|----|--------------|--------------|--------------|-----------|-----------------|
| | | | | | | 130 | 32 | | 4.0625 |
| | | | | | mean | 81 | 48 | | 1.953125 |
| | | | | 7 | sp | 300 | 120 | 260 | 2.5 |
| | | | | | | 500 | 110 | | 4.545454 545 |
| | | | | | mean | 400 | 115 | | 3.522727 273 |
| | | | | 8 | mwsc1 | 20 | 16 | 170 | 1.25 |
| | | | | | | 39 | 20 | | 1.95 |
| | | | | | | 20 | 16 | | 1.25 |
| | | | | | | 40 | 16 | | 2.5 |
| | | | | | | 50 | 8 | | 6.25 |
| | | | | | | 50 | 12 | | 4.166666 667 |
| | | | | | mean | 36.5 | 14.666 67 | | 2.894444 444 |
| | | | | 9 | sp | 340 | 130 | 450 | 2.615384 615 |
| | | | | 11 | spatter s | 140 | 30 | 1300 | 4.666666 667 |
| | | | | | | 220 | 75 | | 2.933333 333 |
| | | | | | | 150 | 50 | | 3 |
| | | | | | | 210 | 70 | | 3 |
| | | | | | | 180 | 70 | | 2.571428 571 |
| | | | | | | 170 | 50 | | 3.4 |
| | | | | | | 155 | 35 | | 4.428571 429 |
| | | | | | mean | 175 | 54.285 71 | | 3.326923 077 |
| 17- Jun | y42 | 11 1 | 100 | 2 | clots | 130 | 55 | 270 - 500 | 2.363636 364 |
| | | | | | | 170 | 90 | | 1.888888 889 |
| | | | | | | 80 | 60 | | 1.333333 333 |
| | | | | | | 230 | 80 | | 2.875 |
| | | | | | | 330 | 100 | | 3.3 |
| | | | | | | 100 | 80 | | 1.25 |
| | | | | | | 135 | 120 | | 1.125 |
| | | | | | mean | 167.85 71 | 83.571 43 | | 2.019408 369 |
| | | | | 3 | clots | 100 | 70 | | 1.428571 429 |
| | | | | | | 420 | 40 | | 10.5 |
| | | | | | | 160 | 60 | | 2.666666 667 |

| | | | | | | | | | |
|------------|-----|---|------|---|-------|--------------|--------------|----------|-----------------|
| | | | | | | 270 | 60 | | 4.5 |
| | | | | | | 270 | 70 | | 3.857142 857 |
| | | | | | | 220 | 70 | | 3.142857 143 |
| | | | | | | 300 | 70 | | 4.285714 286 |
| | | | | | mean | 248.57 14 | 62.857 14 | | 3.477536 075 |
| 11- Jun | y26 | 6 | 5,41 | 1 | clots | 65 | 20 | 360 | 3.25 |
| | | | | | | 45 | 15 | | 3 |
| | | | | | | 160 | 120 | | 1.333333 333 |
| | | | | | | 70 | 60 | | 1.166666 667 |
| | | | | | | 170 | 80 | | 2.125 |
| | | | | | | 80 | 70 | | 1.142857 143 |
| | | | | | | 150 | 80 | | 1.875 |
| | | | | | | 110 | 70 | | 1.571428 571 |
| | | | | | mean | 106.25 | 64.375 | | 2.322753 608 |
| | | | | 3 | clots | 150 | 80 | 300-1060 | 1.875 |
| | | | | | | 90 | 35 | | 2.571428 571 |
| | | | | | | 90 | 90 | | 1 |
| | | | | | | 60 | 50 | | 1.2 |
| | | | | | | 900 | 30 | | 30 |
| | | | | | | 110 | 60 | | 1.833333 333 |
| | | | | | | 90 | 30 | | 3 |
| | | | | | mean | 212.85 71 | 53.571 43 | | 4.724894 408 |
| | | | | | sp | 60 | 40 | | 1.5 |
| | | | | | | 100 | 50 | | 2 |
| | | | | | | 115 | 30 | | 3.833333 333 |
| | | | | | | 95 | 40 | | 2.375 |
| | | | | | | 95 | 60 | | 1.583333 333 |
| | | | | | | 110 | 90 | | 1.222222 222 |
| | | | | | | 80 | 50 | | 1.6 |
| | | | | | | 110 | 50 | | 2.2 |
| | | | | | | 90 | 60 | | 1.5 |
| | | | | | | 160 | 120 | | 1.333333 |

| | | | | | | | | | |
|------------|-----|----|----|---|--------------|--------------|--------------|-----|-----------------|
| | | | | | | | | | 333 |
| | | | | | | 110 | 100 | | 1.1 |
| | | | | | | 60 | 35 | | 1.714285 714 |
| | | | | | | 110 | 90 | | 1.222222 222 |
| | | | | | mean | 99.615 38 | 62.692 31 | | 1.585039 683 |
| 11- Jun | y35 | 14 | 40 | 1 | | 130 | 65 | 750 | 2 |
| | | | | | | 80 | 40 | | 2 |
| | | | | | | 60 | 30 | | 2 |
| | | | | | | 120 | 70 | | 1.714285 714 |
| | | | | | | 75 | 50 | | 1.5 |
| | | | | | | 120 | 50 | | 2.4 |
| | | | | | | 45 | 40 | | 1.125 |
| | | | | | | 150 | 50 | | 3 |
| | | | | | | 55 | 30 | | 1.833333 333 |
| | | | | | | 65 | 30 | | 2.166666 667 |
| | | | | | mean | 90 | 45.5 | | 1.973928 571 |
| 10- Jun | y28 | 13 | 25 | 2 | spatter s | 55 | 30 | 200 | 1.833333 333 |
| | | | | | | 70 | 20 | | 3.5 |
| | | | | | | 95 | 90 | | 1.055555 556 |
| | | | | | | 120 | 80 | | 1.5 |
| | | | | | | 115 | 30 | | 3.833333 333 |
| | | | | | | 55 | 50 | | 1.1 |
| | | | | | mean | 85 | 50 | | 2.179615 079 |
| | | | | | | 20 | 10 | | 2 |
| | | | | | | 10 | 8 | | 1.25 |
| | | | | | | 5 | 3 | | 1.666666 667 |
| | | | | | | 20 | 8 | | 2.5 |
| | | | | | | 5 | 5 | | 1 |
| | | | | | | 12 | 10 | | 1.2 |
| | | | | | | 10 | 10 | | 1 |
| | | | | | | 20 | 15 | | 1.333333 333 |
| | | | | | | 20 | 17 | | 1.176470 588 |
| | | | | | mean | 13.555 | 9.5555 | | 1.530608 |

| | | | | | | | | | |
|------------|----|---|----|---|--------------|--------------|--------------|-----|-----------------|
| | | | | | | 56 | 56 | | 567 |
| | | | | 5 | agg | 20 | 20 | 210 | 1 |
| | | | | | | 25 | 18 | | 1.388888 889 |
| | | | | | | 17 | 17 | | 1 |
| | | | | | | 55 | 18 | | 3.055555 556 |
| | | | | | | 24 | 20 | | 1.2 |
| | | | | | | 43 | 30 | | 1.433333 333 |
| | | | | | | 20 | 12 | | 1.666666 667 |
| | | | | | | 17 | 12 | | 1.416666 667 |
| | | | | | | 36 | 25 | | 1.44 |
| | | | | | | 10 | 5 | | 2 |
| | | | | | mean | 26.7 | 17.7 | | 1.560111 111 |
| | | | | 6 | agg | 55 | 30 | 190 | 1.833333 333 |
| | | | | | | 70 | 20 | | 3.5 |
| | | | | | | 100 | 50 | | 2 |
| | | | | | | 55 | 25 | | 2.2 |
| | | | | | | 110 | 80 | | 1.375 |
| | | | | | | 20 | 15 | | 1.333333 333 |
| | | | | | | 70 | 40 | | 1.75 |
| | | | | | | 45 | 20 | | 2.25 |
| | | | | | | 70 | 50 | | 1.4 |
| | | | | | mean | 66.111 11 | 36.666 67 | | 1.920177 778 |
| 12- Jun | 77 | 8 | 59 | 2 | spatter s | 165 | 50 | 600 | 3.3 |
| | | | | | | 180 | 50 | | 3.6 |
| | | | | | | 115 | 65 | | 1.769230 769 |
| | | | | | | 160 | 50 | | 3.2 |
| | | | | | | 130 | 60 | | 2.166666 667 |
| | | | | | | 80 | 40 | | 2 |
| | | | | | | 130 | 70 | | 1.857142 857 |
| | | | | | | 130 | 45 | | 2.888888 889 |
| | | | | | | 170 | 40 | | 4.25 |
| | | | | | | 90 | 40 | | 2.25 |
| | | | | | mean | 135 | 51 | | 2.728192 918 |

| | | | | | | | | | |
|--|--|--|--|----|----------|------|------|-----|-------------|
| | | | | 3 | spatters | 90 | 90 | 700 | 1 |
| | | | | | | 100 | 50 | | 2 |
| | | | | | | 310 | 110 | | 2.818181818 |
| | | | | | | 50 | 50 | | 1 |
| | | | | | | 135 | 130 | | 1.038461538 |
| | | | | | | 160 | 150 | | 1.066666667 |
| | | | | | | 125 | 60 | | 2.083333333 |
| | | | | | | 100 | 65 | | 1.538461538 |
| | | | | | | 160 | 55 | | 2.909090909 |
| | | | | | | 250 | 40 | | 6.25 |
| | | | | | mean | 148 | 80 | | 2.17041958 |
| | | | | | sc | 10 | 10 | | 1 |
| | | | | | | 15 | 14 | | 1.071428571 |
| | | | | | | 9 | 6 | | 1.5 |
| | | | | | | 8 | 8 | | 1 |
| | | | | | | 10 | 8 | | 1.25 |
| | | | | | | 14 | 10 | | 1.4 |
| | | | | | | 12 | 10 | | 1.2 |
| | | | | | | 14 | 10 | | 1.4 |
| | | | | | | 6 | 4 | | 1.5 |
| | | | | | | 6 | 3 | | 2 |
| | | | | | mean | 10.4 | 8.3 | | 1.332142857 |
| | | | | 4a | sc | 42 | 16 | 130 | 2.625 |
| | | | | | | 22 | 8 | | 2.75 |
| | | | | | | 22 | 12 | | 1.833333333 |
| | | | | | | 16 | 11 | | 1.454545455 |
| | | | | | | 24 | 10 | | 2.4 |
| | | | | | | 20 | 16 | | 1.25 |
| | | | | | | 8 | 5 | | 1.6 |
| | | | | | | 11 | 6 | | 1.833333333 |
| | | | | | | 13 | 8 | | 1.625 |
| | | | | | | 22 | 16 | | 1.375 |
| | | | | | mean | 20 | 10.8 | | 1.874621212 |
| | | | | 4 | clots | 90 | 85 | 740 | 1.058823 |

| | | | | | | | | | |
|--|--|--|--|---|----------|-------|--------------|-----|-----------------|
| | | | | | | | | | 529 |
| | | | | | | 120 | 50 | | 2.4 |
| | | | | | | 90 | 70 | | 1.285714 286 |
| | | | | | | 270 | 80 | | 3.375 |
| | | | | | mean | 142.5 | 71.25 | | 1.767749 236 |
| | | | | | sp | 110 | 60 | | 1.833333 333 |
| | | | | | | 170 | 30 | | 5.666666 667 |
| | | | | | | 140 | 50 | | 2.8 |
| | | | | | | 105 | 35 | | 3 |
| | | | | | | 90 | 90 | | 1 |
| | | | | | | 120 | 60 | | 2 |
| | | | | | mean | 122.5 | 54.166 67 | | 2.512846 352 |
| | | | | 5 | spatters | 360 | 110 | 490 | 3.272727 273 |
| | | | | | | 210 | 100 | | 2.1 |
| | | | | | | 270 | 90 | | 3 |
| | | | | | | 370 | 90 | | 4.111111 111 |
| | | | | | | 180 | 60 | | 3 |
| | | | | | | 120 | 100 | | 1.2 |
| | | | | | | 200 | 70 | | 2.857142 857 |
| | | | | | | 400 | 90 | | 4.444444 444 |
| | | | | | | 240 | 70 | | 3.428571 429 |
| | | | | | | 150 | 40 | | 3.75 |
| | | | | | | 250 | 82 | | 3.048780 488 |
| | | | | | sc | 42 | 16 | | 2.625 |
| | | | | | | 22 | 8 | | 2.75 |
| | | | | | | 22 | 12 | | 1.833333 333 |
| | | | | | | 16 | 11 | | 1.454545 455 |
| | | | | | | 24 | 10 | | 2.4 |
| | | | | | | 20 | 16 | | 1.25 |
| | | | | | | 8 | 5 | | 1.6 |
| | | | | | | 11 | 6 | | 1.833333 333 |
| | | | | | | 13 | 8 | | 1.625 |
| | | | | | | 22 | 16 | | 1.375 |
| | | | | | mean | 20 | 10.8 | | 1.874621 |

| | | | | | | | | | |
|--------|--------------|----|----|---|------|------|---------|-----|-------------|
| | | | | | | | | | 212 |
| 11-Jun | y30 | 5 | 37 | 1 | agg | 200 | 140 | 600 | 1.428571429 |
| | | | | | | 230 | 130 | | 1.769230769 |
| | | | | | | 280 | 250 | | 1.12 |
| | | | | | | 200 | 160 | | 1.25 |
| | | | | | | 200 | 130 | | 1.538461538 |
| | | | | | | 200 | 100 | | 2 |
| | | | | | | 230 | 160 | | 1.4375 |
| | | | | | | 100 | 75 | | 1.333333333 |
| | | | | | mean | 205 | 143.125 | | 1.484637134 |
| 09-Jul | location 477 | 17 | | 1 | sc | 30 | 20 | 240 | 1.5 |
| | | | | | | 30 | 18 | | 1.666666667 |
| | | | | | | 50 | 21 | | 2.380952381 |
| | | | | | | 53 | 11 | | 4.818181818 |
| | | | | | | 32 | 16 | | 2 |
| | | | | | | 32 | 30 | | 1.066666667 |
| | | | | | | 50 | 33 | | 1.515151515 |
| | | | | | | 35 | 30 | | 1.166666667 |
| | | | | | | 43 | 30 | | 1.433333333 |
| | | | | | | 40 | 35 | | 1.142857143 |
| | | | | | mean | 39.5 | 24.4 | | 1.869047619 |
| | | | | 2 | mwcw | 320 | 70 | 600 | 4.571428571 |
| | | | | | | 370 | 80 | | 4.625 |
| | | | | | mean | 345 | 75 | | 4.598214286 |
| | | | | 4 | mwcw | 350 | 90 | 800 | 3.888888889 |
| | | | | | | 230 | 75 | | 3.066666667 |
| | | | | | | 240 | 50 | | 4.8 |
| | | | | | | 200 | 60 | | 3.333333333 |
| | | | | | | 230 | 80 | | 2.875 |

| | | | | | | | | | |
|------------|-----|--|-----------|---|-------|--------------|--------------|------|-----------------|
| | | | | | | 200 | 70 | | 2.857142 857 |
| | | | | | | 200 | 90 | | 2.222222 222 |
| | | | | | mean | 235.71 43 | 73.571 43 | | 3.291893 424 |
| 23- Jun | 285 | | 5,13 5 | 1 | llagg | 90 | 2 | 1000 | 45 |
| | | | | | | 110 | 2 | | 55 |
| | | | | | | 120 | 2 | | 60 |
| | | | | | | 140 | 2 | | 70 |
| | | | | | | 50 | 1 | | 50 |
| | | | | | | 90 | 2 | | 45 |
| | | | | | | 130 | 1 | | 130 |
| | | | | | | 100 | 1 | | 100 |
| | | | | | | 45 | 1 | | 45 |
| | | | | | | 190 | 2 | | 95 |
| | | | | | | 120 | 2 | | 60 |
| | | | | | mean | 107.72 73 | 1.6363 64 | | 68.63636 364 |
| | | | | | llagg | 64 | 1 | 1000 | 64 |
| | | | | | | 80 | 1 | | 80 |
| | | | | | | 50 | 1 | | 50 |
| | | | | | | 40 | 1 | | 40 |
| | | | | | | 50 | 1 | | 50 |
| | | | | | | 23 | 1 | | 23 |
| | | | | | | 30 | 1 | | 30 |
| | | | | | | 40 | 1 | | 40 |
| | | | | | | 16 | 1 | | 16 |
| | | | | | | 20 | 1 | | 20 |
| | | | | | | | | | 41.3 |
| | | | | | mean | 41.3 | 1 | 1000 | |
| | | | | | llagg | 30 | 1 | | 30 |
| | | | | | | 23 | 1 | | 23 |
| | | | | | | 30 | 3 | | 10 |
| | | | | | | 16 | 2 | | 8 |
| | | | | | | 80 | 2 | | 40 |
| | | | | | | 40 | 1 | | 40 |
| | | | | | | 30 | 2 | | 15 |
| | | | | | | 52 | 2 | | 26 |
| | | | | | | 34 | 1 | | 34 |
| | | | | | | 60 | 3 | | 20 |
| | | | | | mean | 39.5 | 1.8 | | 24.6 |
| | | | | | llagg | 100 | 4 | 5 | 25 |
| | | | | | | 130 | 2 | | 65 |
| | | | | | | 160 | 2 | | 80 |

| | | | | | | | | | |
|--------|-----|--|-----------|--|-------|-------|------|-----|-----------------|
| | | | | | | 130 | 2 | | 65 |
| | | | | | | 18 | 15 | | 1.2 |
| | | | | | | | | | |
| | | | | | | | | | |
| | | | | | | | | | |
| | | | | | | | | | |
| | | | | | | | | | |
| | | | | | mean | 107.6 | 5 | | 47.24 |
| | | | | | llagg | 330 | 20 | 16 | 16.5 |
| | | | | | | 150 | 10 | | 15 |
| | | | | | | 180 | 10 | | 18 |
| | | | | | | 160 | 30 | | 5.333333 333 |
| | | | | | | 270 | 15 | | 18 |
| | | | | | | 140 | 10 | | 14 |
| | | | | | | 100 | 30 | | 3.333333 333 |
| | | | | | | 80 | 20 | | 4 |
| | | | | | | 200 | 10 | | 20 |
| | | | | | | 160 | 24 | | 6.666666 667 |
| | | | | | mean | 177 | 17.9 | | 12.08333 333 |
| | | | | | llagg | 120 | 10 | 6 | 12 |
| | | | | | | 480 | 220 | | 2.181818 182 |
| | | | | | | 240 | 25 | | 9.6 |
| | | | | | | 90 | 35 | | 2.571428 571 |
| | | | | | | 140 | 40 | | 3.5 |
| | | | | | | | | | |
| | | | | | | | | | |
| | | | | | | | | | |
| | | | | | | | | | |
| | | | | | | | | | |
| | | | | | mean | 214 | 66 | | 5.970649 351 |
| 17-Jul | y57 | | 5,14 9 | | sc | 15 | 8 | 100 | 1.875 |
| | | | | | | 9 | 9 | | 1 |
| | | | | | | 10 | 8 | | 1.25 |
| | | | | | | 10 | 8 | | 1.25 |
| | | | | | | 13 | 10 | | 1.3 |
| | | | | | | 10 | 8 | | 1.25 |
| | | | | | | 10 | 8 | | 1.25 |
| | | | | | | 16 | 10 | | 1.6 |
| | | | | | | 9 | 6 | | 1.5 |

| | | | | | | | | | |
|--------|-----|--|-------|--|------|------|------|------|-------------|
| | | | | | | 10 | 8 | | 1.25 |
| | | | | | mean | 11.2 | 8.3 | | 1.3525 |
| 17-Jul | y58 | | 5,150 | | sc | 29 | 24 | >260 | 1.208333333 |
| | | | | | | 21 | 14 | | 1.5 |
| | | | | | | 15 | 9 | | 1.666666667 |
| | | | | | | 23 | 12 | | 1.916666667 |
| | | | | | | 23 | 15 | | 1.533333333 |
| | | | | | | 19 | 11 | | 1.727272727 |
| | | | | | | 22 | 14 | | 1.571428571 |
| | | | | | | 26 | 18 | | 1.444444444 |
| | | | | | | 20 | 19 | | 1.052631579 |
| | | | | | | 20 | 19 | | 1.052631579 |
| | | | | | mean | 21.8 | 15.5 | | 1.46734089 |
| 17-Jul | y59 | | 5,150 | | sc | 12 | 8 | 320 | 1.5 |
| | | | | | | 20 | 16 | | 1.25 |
| | | | | | | 32 | 15 | | 2.133333333 |
| | | | | | | 35 | 20 | | 1.75 |
| | | | | | | 22 | 15 | | 1.466666667 |
| | | | | | | 16 | 15 | | 1.066666667 |
| | | | | | | 22 | 16 | | 1.375 |
| | | | | | | 29 | 18 | | 1.611111111 |
| | | | | | | 10 | 10 | | 1 |
| | | | | | | 20 | 13 | | 1.538461538 |
| | | | | | mean | 21.8 | 14.6 | | 1.469123932 |
| 17-Jul | y60 | | 5,152 | | sc | 8 | 6 | >150 | 1.333333333 |
| | | | | | | 12 | 7 | | 1.714285714 |
| | | | | | | 10 | 7 | | 1.428571429 |
| | | | | | | 8 | 6 | | 1.333333333 |

| | | | | | | | | | |
|------------|-----|----|-----------|---|------|------|------|------|-----------------|
| | | | | | | 10 | 7 | | 1.428571 429 |
| | | | | | | 12 | 10 | | 1.2 |
| | | | | | | 13 | 8 | | 1.625 |
| | | | | | | 10 | 8 | | 1.25 |
| | | | | | | 7 | 2 | | 3.5 |
| | | | | | | 16 | 10 | | 1.6 |
| | | | | | mean | 10.6 | 7.1 | | 1.641309 524 |
| 17- Jul | y61 | | 5,15 2 | | sc | 19 | 17 | <350 | 1.117647 059 |
| | | | | | | 19 | 16 | | 1.1875 |
| | | | | | | 29 | 20 | | 1.45 |
| | | | | | | 17 | 15 | | 1.133333 333 |
| | | | | | | 17 | 15 | | 1.133333 333 |
| | | | | | | 24 | 19 | | 1.263157 895 |
| | | | | | | 21 | 16 | | 1.3125 |
| | | | | | | 24 | 21 | | 1.142857 143 |
| | | | | | | 32 | 30 | | 1.066666 667 |
| | | | | | | 19 | 10 | | 1.9 |
| | | | | | mean | 22.1 | 17.9 | | 1.270699 543 |
| 17- Jul | y62 | | 5,15 3 | | sc | 24 | 21 | <400 | 1.142857 143 |
| | | | | | | 22 | 18 | | 1.222222 222 |
| | | | | | | 21 | 13 | | 1.615384 615 |
| | | | | | | 31 | 16 | | 1.9375 |
| | | | | | | 40 | 20 | | 2 |
| | | | | | | 31 | 29 | | 1.068965 517 |
| | | | | | | 30 | 16 | | 1.875 |
| | | | | | | 20 | 15 | | 1.333333 333 |
| | | | | | | 20 | 14 | | 1.428571 429 |
| | | | | | | 19 | 11 | | 1.727272 727 |
| | | | | | mean | 25.8 | 17.3 | | 1.535110 699 |
| 07- Jun | pr | 11 | 5,3 | 1 | sc | 300 | 70 | 1710 | 4.285714 286 |
| | | | | | | 60 | 50 | | 1.2 |

| | | | | | | | | | |
|------------|--|--|--|----|------|-------|------|-----|-----------------|
| | | | | | | 74 | 61 | | 1.213114 754 |
| | | | | | | 140 | 55 | | 2.545454 545 |
| | | | | | | 125 | 70 | | 1.785714 286 |
| | | | | | | 130 | 70 | | 1.857142 857 |
| | | | | | | 80 | 80 | | 1 |
| | | | | | | 111 | 40 | | 2.775 |
| | | | | | | 100 | 80 | | 1.25 |
| | | | | | | 70 | 65 | | 1.076923 077 |
| | | | | | mean | 119 | 64.1 | | 1.898906 381 |
| 17- Jul | | | | A3 | | 130 | 50 | 400 | 2.6 |
| | | | | | | 80 | 35 | | 2.285714 286 |
| | | | | | | 135 | 40 | | 3.375 |
| | | | | | | 90 | 45 | | 2 |
| | | | | | | 100 | 50 | | 2 |
| | | | | | | 180 | 50 | | 3.6 |
| | | | | | | 135 | 75 | | 1.8 |
| | | | | | | 165 | 35 | | 4.714285 714 |
| | | | | | | 140 | 60 | | 2.333333 333 |
| | | | | | | 80 | 50 | | 1.6 |
| | | | | | mean | 123.5 | 49 | | 2.630833 333 |
| 17- Jul | | | | a2 | | 20 | 10 | 50 | 2 |
| | | | | | | 14 | 10 | | 1.4 |
| | | | | | | 18 | 10 | | 1.8 |
| | | | | | | 22 | 16 | | 1.375 |
| | | | | | | 22 | 15 | | 1.466666 667 |
| | | | | | | 24 | 20 | | 1.2 |
| | | | | | | 26 | 20 | | 1.3 |
| | | | | | | 25 | 16 | | 1.5625 |
| | | | | | | 10 | 5 | | 2 |
| | | | | | | 10 | 7 | | 1.428571 429 |
| | | | | | mean | 19.1 | 12.9 | 50 | 1.553273 81 |
| 17- Jul | | | | a3 | | 130 | 50 | | 2.6 |

| | | | | | | | | | |
|------------|--|---|------|----|------|--------------|--------------|------|-----------------|
| | | | | | | 80 | 35 | | 2.285714 286 |
| | | | | | | 135 | 40 | | 3.375 |
| | | | | | | 90 | 45 | | 2 |
| | | | | | | 100 | 50 | | 2 |
| | | | | | | 180 | 50 | | 3.6 |
| | | | | | | 135 | 75 | | 1.8 |
| | | | | | | 165 | 35 | | 4.714285 714 |
| | | | | | | 140 | 60 | | 2.333333 333 |
| | | | | | | 80 | 50 | | 1.6 |
| | | | | | mean | 123.5 | 49 | | 2.630833 333 |
| 29- Jun | | 2 | 6,31 | 17 | sc | 250 | 90 | 170 | 2.777777 778 |
| | | | | | | 150 | 70 | | 2.142857 143 |
| | | | | | | 220 | 60 | | 3.666666 667 |
| | | | | | | 260 | 80 | | 3.25 |
| | | | | | | 190 | 40 | | 4.75 |
| | | | | | | 300 | 100 | | 3 |
| | | | | | | 250 | 50 | | 5 |
| | | | | | | 260 | 80 | | 3.25 |
| | | | | | | 260 | 90 | | 2.888888 889 |
| | | | | | | | | | |
| | | | | | mean | 237.77 78 | 73.333 33 | | 3.414021 164 |
| 29- Jun | | | | 18 | sc | 200 | 60 | 2300 | 3.333333 333 |
| | | | | | | 270 | 60 | | 4.5 |
| | | | | | | 140 | 60 | | 2.333333 333 |
| | | | | | | 120 | 100 | | 1.2 |
| | | | | | | 80 | 30 | | 2.666666 667 |
| | | | | | | 40 | 25 | | 1.6 |
| | | | | | | 90 | 30 | | 3 |
| | | | | | | 70 | 25 | | 2.8 |
| | | | | | | | | | #DIV/0! |
| | | | | | | | | | #DIV/0! |
| | | | | | mean | 126.25 | 48.75 | | 2.679166 667 |
| 29- Jun | | | | 19 | sc | 200 | 50 | 300 | 4 |
| | | | | | | 290 | 100 | | 2.9 |

| | | | | | | | | | |
|------------|--|--|--|----|------|--------------|--------------|-----|-----------------|
| | | | | | | 110 | 35 | | 3.142857 143 |
| | | | | | | 100 | 50 | | 2 |
| | | | | | | 125 | 30 | | 4.166666 667 |
| | | | | | | 135 | 30 | | 4.5 |
| | | | | | | 210 | 40 | | 5.25 |
| | | | | | | 230 | 100 | | 2.3 |
| | | | | | | | | | #DIV/0! |
| | | | | | | | | | #DIV/0! |
| | | | | | mean | 175 | 54.375 | | 3.532440 476 |
| 29- Jun | | | | 20 | sc | 60 | 40 | 800 | 1.5 |
| | | | | | | 70 | 35 | | 2 |
| | | | | | | 55 | 45 | | 1.222222 222 |
| | | | | | | 125 | 50 | | 2.5 |
| | | | | | | 100 | 30 | | 3.333333 333 |
| | | | | | | 70 | 25 | | 2.8 |
| | | | | | | 100 | 25 | | 4 |
| | | | | | | | | | #DIV/0! |
| | | | | | | | | | #DIV/0! |
| | | | | | | | | | #DIV/0! |
| | | | | | mean | 82.857 14 | 35.714 29 | | 2.479365 079 |
| 29- Jun | | | | 23 | | 35 | 8 | 80 | 4.375 |
| | | | | | | 21 | 8 | | 2.625 |
| | | | | | | 24 | 4 | | 6 |
| | | | | | | 22 | 4 | | 5.5 |
| | | | | | | 23 | 5 | | 4.6 |
| | | | | | | 20 | 4 | | 5 |
| | | | | | | 82 | 30 | | 2.733333 333 |
| | | | | | | 102 | 7 | | 14.57142 857 |
| | | | | | | 70 | 10 | | 7 |
| | | | | | | | | | #DIV/0! |
| | | | | | mean | 44.333 33 | 8.8888 89 | | 5.822751 323 |
| 29- Jun | | | | 24 | sc | 140 | 80 | 700 | 1.75 |
| | | | | | | 200 | 40 | | 5 |
| | | | | | | 70 | 40 | | 1.75 |
| | | | | | | 70 | 20 | | 3.5 |
| | | | | | | 69 | 25 | | 2.76 |

| | | | | | | | | | |
|------------|--|--|--|----|------|--------------|--------------|------|-----------------|
| | | | | | | 75 | 40 | | 1.875 |
| | | | | | | 70 | 30 | | 2.333333 333 |
| | | | | | | 110 | 60 | | 1.833333 333 |
| | | | | | | | | | #DIV/0! |
| | | | | | | | | | #DIV/0! |
| | | | | | mean | 100.5 | 41.875 | | 2.600208 333 |
| 29- Jun | | | | 25 | sc | 270 | 160 | 410 | 1.6875 |
| | | | | | | 270 | 55 | | 4.909090 909 |
| | | | | | | 240 | 100 | | 2.4 |
| | | | | | | 290 | 100 | | 2.9 |
| | | | | | | 180 | 120 | | 1.5 |
| | | | | | | 220 | 40 | | 5.5 |
| | | | | | | 210 | 50 | | 4.2 |
| | | | | | | 250 | 60 | | 4.166666 667 |
| | | | | | | | | | #DIV/0! |
| | | | | | | | | | #DIV/0! |
| | | | | | mean | 241.25 | 85.625 | | 3.407907 197 |
| 29- Jun | | | | 26 | sc | 320 | 60 | 2400 | 5.333333 333 |
| | | | | | | 160 | 60 | | 2.666666 667 |
| | | | | | | 330 | 160 | | 2.0625 |
| | | | | | | 200 | 90 | | 2.222222 222 |
| | | | | | | 650 | 150 | | 4.333333 333 |
| | | | | | | 190 | 80 | | 2.375 |
| | | | | | | 220 | 80 | | 2.75 |
| | | | | | | 110 | 80 | | 1.375 |
| | | | | | | 200 | 70 | | 2.857142 857 |
| | | | | | | | | | #DIV/0! |
| | | | | | mean | 264.44 44 | 92.222 22 | | 2.886133 157 |
| 29- Jun | | | | 27 | sc | 45 | 14 | 240 | 3.214285 714 |
| | | | | | | 40 | 19 | | 2.105263 158 |
| | | | | | | 53 | 10 | | 5.3 |
| | | | | | | 70 | 16 | | 4.375 |
| | | | | | | 39 | 21 | | 1.857142 |

| | | | | | | | | | |
|------------|--|--|--|----|------|-------|------|-----|-----------------|
| | | | | | | | | | 857 |
| | | | | | | 69 | 10 | | 6.9 |
| | | | | | | 130 | 20 | | 6.5 |
| | | | | | | 64 | 15 | | 4.266666 667 |
| | | | | | | 120 | 32 | | 3.75 |
| | | | | | | 80 | 16 | | 5 |
| | | | | | mean | 71 | 17.3 | | 4.326835 84 |
| 29- Jun | | | | 28 | sc | 180 | 100 | 500 | 1.8 |
| | | | | | | 180 | 50 | | 3.6 |
| | | | | | | 300 | 100 | | 3 |
| | | | | | | 300 | 60 | | 5 |
| | | | | | | 180 | 50 | | 3.6 |
| | | | | | | 210 | 60 | | 3.5 |
| | | | | | | 330 | 45 | | 7.333333 333 |
| | | | | | | 135 | 50 | | 2.7 |
| | | | | | | 250 | 50 | | 5 |
| | | | | | | 230 | 90 | | 2.555555 556 |
| | | | | | mean | 229.5 | 65.5 | | 3.948148 148 |
| 29- Jun | | | | 29 | | 85 | 25 | 150 | 3.4 |
| | | | | | | 73 | 25 | | 2.92 |
| | | | | | | 70 | 8 | | 8.75 |
| | | | | | | 45 | 30 | | 1.5 |
| | | | | | | 43 | 20 | | 2.15 |
| | | | | | | 32 | 8 | | 4 |
| | | | | | | 74 | 18 | | 4.111111 111 |
| | | | | | | 50 | 32 | | 1.5625 |
| | | | | | | 48 | 11 | | 4.363636 364 |
| | | | | | | 70 | 15 | | 4.666666 667 |
| | | | | | mean | 59 | 19.2 | | 3.639694 164 |
| 29- Jun | | | | 30 | | 300 | 110 | 220 | 2.727272 727 |
| | | | | | | 300 | 75 | | 4 |
| | | | | | | 370 | 90 | | 4.111111 111 |
| | | | | | | 500 | 80 | | 6.25 |
| | | | | | | 510 | 70 | | 7.285714 286 |

| | | | | | | | | | |
|------------|--|--|--|----|------|--------------|--------------|-----|-----------------|
| | | | | | | 550 | 140 | | 3.928571 429 |
| | | | | | | 640 | 160 | | 4 |
| | | | | | | | | | #DIV/0! |
| | | | | | | | | | #DIV/0! |
| | | | | | | | | | #DIV/0! |
| | | | | | mean | 452.85 71 | 103.57 14 | | 4.614667 079 |
| 29- Jun | | | | 31 | | 80 | 40 | 110 | 2 |
| | | | | | | 42 | 16 | | 2.625 |
| | | | | | | 30 | 15 | | 2 |
| | | | | | | 60 | 8 | | 7.5 |
| | | | | | | 69 | 21 | | 3.285714 286 |
| | | | | | | 27 | 4 | | 6.75 |
| | | | | | | 66 | 16 | | 4.125 |
| | | | | | | 50 | 10 | | 5 |
| | | | | | | 43 | 30 | | 1.433333 333 |
| | | | | | | 50 | 17 | | 2.941176 471 |
| | | | | | mean | 51.7 | 17.7 | | 3.857671 958 |
| 29- Jun | | | | 32 | | 300 | 70 | 800 | 4.285714 286 |
| | | | | | | 200 | 100 | | 2 |
| | | | | | | 160 | 45 | | 3.555555 556 |
| | | | | | | 480 | 120 | | 4 |
| | | | | | | 260 | 60 | | 4.333333 333 |
| | | | | | | 260 | 110 | | 2.363636 364 |
| | | | | | | 160 | 40 | | 4 |
| | | | | | | 205 | 90 | | 2.277777 778 |
| | | | | | | 220 | 110 | | 2 |
| | | | | | | 300 | 60 | | 5 |
| | | | | | mean | 254.5 | 80.5 | | 3.201779 702 |

Table A1.19. Stratigraphic log measurements from 2013.

| Log | Unit | Type | Coating | X (mm) | Y (mm) | area (mm ²) | vol fraction |
|-----|------|------|---------|--------|--------|----------------------------|-----------------|
| | | 1 | n | 50 | 43 | 2150 | 8.16E-09 |
| 10 | 7 | 1 | n | 65 | 32 | 2080 | 7.39E-09 |

| | | | | | | | |
|--|---|---|---|----|----------|--------|----------|
| | | 4 | n | 55 | 33 | 1815 | 4.91E-09 |
| | | 4 | n | 60 | 30 | 1800 | 4.79E-09 |
| | | 1 | n | 40 | 30 | 1200 | 1.42E-09 |
| | | 1 | n | 20 | 22 | 440 | 7E-11 |
| | | 1 | n | 25 | 15 | 375 | 4.33E-11 |
| | | 1 | n | 30 | 11 | 330 | 2.95E-11 |
| | | 1 | n | 25 | 13 | 325 | 2.82E-11 |
| | | 1 | n | 20 | 15 | 300 | 2.22E-11 |
| | | 1 | n | 20 | 15 | 300 | 2.22E-11 |
| | | 1 | n | 25 | 11 | 275 | 1.71E-11 |
| | | 1 | n | 20 | 12 | 240 | 1.14E-11 |
| | | 1 | n | 15 | 16 | 240 | 1.14E-11 |
| | | 1 | n | 23 | 10 | 230 | 1E-11 |
| | | 1 | n | 14 | 15 | 210 | 7.61E-12 |
| | | 1 | n | 12 | 15 | 180 | 4.79E-12 |
| | | 2 | n | 17 | 10 | 170 | 4.04E-12 |
| | | 1 | n | 15 | 11 | 165 | 3.69E-12 |
| | | 4 | n | 12 | 12 | 144 | 2.45E-12 |
| | | 2 | n | 10 | 9 | 90 | 5.99E-13 |
| | | 1 | n | 15 | 5 | 75 | 3.47E-13 |
| | | 1 | n | 15 | 5 | 75 | 3.47E-13 |
| | | 1 | n | 10 | 6 | 60 | 1.77E-13 |
| | | 1 | n | 10 | 6 | 60 | 1.77E-13 |
| | | 1 | n | 6 | 5 | 30 | 2.22E-14 |
| | | 1 | n | 5 | 4 | 20 | 6.57E-15 |
| | | 1 | n | 4 | 3 | 12 | 1.42E-15 |
| | | 1 | n | 4 | 3 | 12 | 1.42E-15 |
| | | 1 | n | 4 | 2 | 8 | 4.21E-16 |
| | | | | | sum area | 13411 | 1.98E-06 |
| | | | | | area % | 1.3411 | 1.98E-18 |
| | | | | | | | 0 |
| | | 1 | n | 54 | 100 | 5400 | 1.29E-07 |
| | | 1 | n | 70 | 45 | 3150 | 2.57E-08 |
| | | 1 | n | 55 | 30 | 1650 | 3.69E-09 |
| | 8 | 1 | n | 55 | 29 | 1595 | 3.33E-09 |
| | | 1 | n | 60 | 22 | 1320 | 1.89E-09 |
| | | 4 | n | 55 | 24 | 1320 | 1.89E-09 |
| | | 1 | n | 55 | 20 | 1100 | 1.09E-09 |
| | | 1 | n | 30 | 30 | 900 | 5.99E-10 |
| | | 2 | n | 45 | 20 | 900 | 5.99E-10 |
| | | 4 | n | 24 | 35 | 840 | 4.87E-10 |
| | | 2 | n | 26 | 30 | 780 | 3.9E-10 |
| | | 1 | n | 35 | 20 | 700 | 2.82E-10 |
| | | 4 | n | 33 | 20 | 660 | 2.36E-10 |
| | | 1 | n | 30 | 20 | 600 | 1.77E-10 |

| | | | | | | | |
|----|---|---|---|-----|-------------|--------|----------|
| | | 4 | n | 30 | 20 | 600 | 1.77E-10 |
| | | 1 | n | 30 | 19 | 570 | 1.52E-10 |
| | | 4 | n | 25 | 22 | 550 | 1.37E-10 |
| | | 1 | n | 20 | 25 | 500 | 1.03E-10 |
| | | 4 | n | 25 | 20 | 500 | 1.03E-10 |
| | | 2 | n | 25 | 20 | 500 | 1.03E-10 |
| | | 1 | n | 40 | 12 | 480 | 9.09E-11 |
| | | 4 | n | 40 | 11 | 440 | 7E-11 |
| | | 1 | n | 29 | 15 | 435 | 6.76E-11 |
| | | 4 | n | 21 | 20 | 420 | 6.09E-11 |
| | | 4 | n | 25 | 15 | 375 | 4.33E-11 |
| | | 4 | n | 32 | 10 | 320 | 2.69E-11 |
| | | 4 | n | 28 | 11 | 308 | 2.4E-11 |
| | | 1 | n | 15 | 20 | 300 | 2.22E-11 |
| | | 1 | n | 25 | 12 | 300 | 2.22E-11 |
| | | 4 | n | 20 | 15 | 300 | 2.22E-11 |
| | | 1 | n | 20 | 13 | 260 | 1.44E-11 |
| | | 1 | n | 15 | 15 | 225 | 9.36E-12 |
| | | 4 | n | 20 | 10 | 200 | 6.57E-12 |
| | | 4 | n | 19 | 10 | 190 | 5.63E-12 |
| | | 1 | n | 12 | 15 | 180 | 4.79E-12 |
| | | 1 | n | 17 | 10 | 170 | 4.04E-12 |
| | | 1 | n | 15 | 10 | 150 | 2.77E-12 |
| | | 1 | n | 10 | 15 | 150 | 2.77E-12 |
| | | 4 | n | 15 | 10 | 150 | 2.77E-12 |
| | | 4 | n | 12 | 10 | 120 | 1.42E-12 |
| | | 1 | n | 17 | 7 | 119 | 1.38E-12 |
| | | 1 | n | 10 | 10 | 100 | 8.22E-13 |
| | | 4 | n | 10 | 10 | 100 | 8.22E-13 |
| | | 1 | n | 10 | 5 | 50 | 1.03E-13 |
| | | | | | area (mm^2) | 29977 | 2.21E-05 |
| | | | | | area % | 2.9977 | 2.21E-17 |
| | | | | | | | 0 |
| 12 | 3 | 2 | n | 135 | 80 | 10800 | 1.03E-06 |
| | | 2 | y | 90 | 50 | 4500 | 7.49E-08 |
| | | 1 | y | 80 | 50 | 4000 | 5.26E-08 |
| | | | | | area sum | 19300 | 5.91E-06 |
| | | | | | area % | 0.45 | 7.49E-20 |
| | 4 | 2 | y | 75 | 23 | 1725 | 4.22E-09 |
| | | | n | 80 | 80 | 6400 | 2.15E-07 |
| | | | | | area sum | 8125 | 4.41E-07 |
| | | | | | area % | 0.1725 | 4.22E-21 |
| | 2 | 1 | n | 21 | 30 | 630 | 2.05E-10 |
| | | | | | | | 0 |
| | | | | | | | 0 |

| | | | | | | | |
|----|---|---|---|-----|----------|----------------|----------|
| | | | | | area % | 0.063 | 2.05E-22 |
| | 1 | 1 | n | 11 | 12 | 132 | 1.89E-12 |
| | | 1 | n | 22 | 15 | 330 | 2.95E-11 |
| | | 1 | n | 19 | 9 | 171 | 4.11E-12 |
| | | 1 | n | 10 | 5 | 50 | 1.03E-13 |
| | | 4 | n | 22 | 25 | 550 | 1.37E-10 |
| | | | | | area sum | 1233 | 1.54E-09 |
| | | | | | area % | 0.1233 | 1.54E-21 |
| 81 | 3 | 4 | y | 8 | 12 | 96 | 7.27E-13 |
| | | 4 | n | 45 | 35 | 1575 | 3.21E-09 |
| | | | | | area sum | 1671 | 3.83E-09 |
| | | | | | area % | 0.1671 | 3.83E-21 |
| | 7 | 2 | y | 80 | 30 | 2400 | 1.14E-08 |
| | | 2 | n | 50 | 45 | 2250 | 9.36E-09 |
| | | 2 | n | 20 | 20 | 400 | 5.26E-11 |
| | | | | | area sum | 5050 | 1.06E-07 |
| | | | | | area % | 0.505 | 1.06E-19 |
| | | | | | | area (mm^2) | #VALUE! |
| 8 | 6 | 4 | n | 90 | 80 | 7200 | 3.07E-07 |
| | | 2 | n | 80 | 45 | 3600 | 3.83E-08 |
| | | 2 | n | 50 | 35 | 1750 | 4.4E-09 |
| | | | | | sum area | 12550 | 1.62E-06 |
| | | | | | area % | 1.255 | |
| | | | | | | area (mm^2) | #VALUE! |
| | | 2 | y | 130 | 90 | 11700 | 1.32E-06 |
| | | 4 | y | 120 | 90 | 10800 | 1.03E-06 |
| | 7 | 4 | n | 85 | 60 | 5100 | 1.09E-07 |
| | | | | | sum area | 27600 | 1.73E-05 |
| | | | | | area % | 2.76 | 1.73E-17 |
| | | | | | | area (mm^2) | #VALUE! |
| | 9 | 4 | n | 95 | 95 | 9025 | 6.04E-07 |
| | | 4 | n | 35 | 26 | 910 | 6.19E-10 |
| | | 4 | n | 30 | 28 | 840 | 4.87E-10 |
| | | | | | sum area | 10775 | 1.03E-06 |
| | | | | | area % | 1.0775 | 1.03E-18 |
| | | | | | | area (mm^2) | #VALUE! |
| | | 4 | y | 75 | 55 | 4125 | 5.77E-08 |
| | | 4 | n | 70 | 30 | 2100 | 7.61E-09 |
| | | 1 | n | 40 | 35 | 1400 | 2.25E-09 |
| | | 1 | n | 40 | 30 | 1200 | 1.42E-09 |
| | | 4 | n | 45 | 25 | 1125 | 1.17E-09 |
| | | 4 | n | 25 | 25 | 625 | 2.01E-10 |

| | | | | | | | |
|----|----|---|---|-----|----------|--------|----------|
| | | 4 | y | 20 | 30 | 600 | 1.77E-10 |
| | | 4 | y | 28 | 20 | 560 | 1.44E-10 |
| 10 | 5 | 4 | n | 21 | 26 | 546 | 1.34E-10 |
| | | 1 | n | 30 | 15 | 450 | 7.49E-11 |
| | | 4 | n | 20 | 19 | 380 | 4.51E-11 |
| | | 4 | n | 20 | 15 | 300 | 2.22E-11 |
| | | 4 | n | 20 | 12 | 240 | 1.14E-11 |
| | | 4 | n | 23 | 10 | 230 | 1E-11 |
| | | 4 | n | 18 | 10 | 180 | 4.79E-12 |
| | | 4 | n | 8 | 9 | 72 | 3.07E-13 |
| | | | | | sum area | 14133 | 2.32E-06 |
| | | | | | area % | 1.4133 | 2.32E-18 |
| 1 | m1 | 3 | y | 12 | 10 | 120 | 1.42E-12 |
| | | 3 | y | 12 | 12 | 144 | 2.45E-12 |
| | | 3 | n | 49 | 14 | 686 | 2.65E-10 |
| | | 4 | n | 12 | 11 | 132 | 1.89E-12 |
| | | 1 | n | 38 | 24 | 912 | 6.23E-10 |
| | | 4 | n | 14 | 9 | 126 | 1.64E-12 |
| | | 4 | n | 19 | 7 | 133 | 1.93E-12 |
| | | 4 | n | 45 | 35 | 1575 | 3.21E-09 |
| | | 4 | n | 32 | 31 | 992 | 8.02E-10 |
| | | 3 | y | 110 | 85 | 9350 | 6.72E-07 |
| | | 4 | n | 190 | 90 | 17100 | 4.11E-06 |
| | | 4 | n | 19 | 17 | 323 | 2.77E-11 |
| | | 4 | n | 45 | 25 | 1125 | 1.17E-09 |
| | | 4 | n | 30 | 25 | 750 | 3.47E-10 |
| | | 4 | n | 14 | 15 | 210 | 7.61E-12 |
| | | 4 | n | 19 | 15 | 285 | 1.9E-11 |
| | | 4 | n | 43 | 20 | 860 | 5.23E-10 |
| | | 4 | n | 19 | 16 | 304 | 2.31E-11 |
| | | 4 | n | 16 | 17 | 272 | 1.65E-11 |
| | | 4 | n | 17 | 10 | 170 | 4.04E-12 |
| | | 4 | n | 41 | 30 | 1230 | 1.53E-09 |
| | | 4 | n | 12 | 17 | 204 | 6.97E-12 |
| | | 3 | n | 22 | 18 | 396 | 5.1E-11 |
| | | 3 | n | 32 | 10 | 320 | 2.69E-11 |
| | | 3 | n | 19 | 17 | 323 | 2.77E-11 |
| | | 3 | n | 35 | 28 | 980 | 7.73E-10 |
| | | | | | | 39022 | 4.88E-05 |
| | | | | | area % | 3.9022 | 4.88E-17 |
| | m2 | 4 | n | 610 | 240 | 146400 | 0.002578 |
| | | 4 | n | 25 | 7 | 175 | 4.4E-12 |
| | | 4 | n | 72 | 25 | 1800 | 4.79E-09 |
| | | 4 | n | 60 | 25 | 1500 | 2.77E-09 |
| | | 4 | n | 50 | 32 | 1600 | 3.36E-09 |

| | | | | | | | |
|--|----|---|---|-----|--------|---------|----------|
| | | 3 | n | 17 | 13 | 221 | 8.87E-12 |
| | | 4 | n | 17 | 10 | 170 | 4.04E-12 |
| | | 4 | n | 32 | 5 | 160 | 3.36E-12 |
| | | 4 | n | 18 | 10 | 180 | 4.79E-12 |
| | | 4 | n | 24 | 18 | 432 | 6.62E-11 |
| | | 4 | n | 8 | 8 | 64 | 2.15E-13 |
| | | 2 | n | 30 | 29 | 870 | 5.41E-10 |
| | | 4 | n | 85 | 45 | 3825 | 4.6E-08 |
| | | 4 | n | 15 | 10 | 150 | 2.77E-12 |
| | | 4 | n | 8 | 4 | 32 | 2.69E-14 |
| | | 4 | n | 7 | 5 | 35 | 3.52E-14 |
| | | 4 | n | 60 | 30 | 1800 | 4.79E-09 |
| | | | | | | 159414 | 0.003328 |
| | | | | | area % | 15.9414 | 3.33E-15 |
| | m4 | 4 | n | 170 | 110 | 18700 | 5.37E-06 |
| | | 4 | n | 34 | 20 | 680 | 2.58E-10 |
| | | 4 | n | 29 | 29 | 841 | 4.89E-10 |
| | | 4 | n | 55 | 35 | 1925 | 5.86E-09 |
| | | 4 | n | 19 | 10 | 190 | 5.63E-12 |
| | | 4 | n | 10 | 10 | 100 | 8.22E-13 |
| | | 3 | n | 10 | 5 | 50 | 1.03E-13 |
| | | 4 | n | 30 | 12 | 360 | 3.83E-11 |
| | | 4 | y | 25 | 10 | 250 | 1.28E-11 |
| | | | | | | 23096 | 1.01E-05 |
| | | | | | | 2.3096 | 1.01E-17 |
| | m5 | 4 | n | 30 | 30 | 900 | 5.99E-10 |
| | | 3 | y | 115 | 80 | 9200 | 6.4E-07 |
| | | 3 | y | 16 | 15 | 240 | 1.14E-11 |
| | | 3 | y | 20 | 11 | 220 | 8.75E-12 |
| | | 3 | y | 28 | 20 | 560 | 1.44E-10 |
| | | 3 | y | 50 | 16 | 800 | 4.21E-10 |
| | | 3 | n | 11 | 5 | 55 | 1.37E-13 |
| | | 4 | n | 45 | 31 | 1395 | 2.23E-09 |
| | | 4 | n | 24 | 19 | 456 | 7.79E-11 |
| | | 1 | n | 35 | 24 | 840 | 4.87E-10 |
| | | 4 | n | 10 | 5 | 50 | 1.03E-13 |
| | | | | | | 14716 | 2.62E-06 |
| | | | | | | | 0 |
| | m6 | 4 | n | 35 | 22 | 770 | 3.75E-10 |
| | | 4 | n | 68 | 28 | 1904 | 5.67E-09 |
| | | 4 | n | 33 | 29 | 957 | 7.2E-10 |
| | | 4 | n | 20 | 21 | 420 | 6.09E-11 |
| | | 3 | n | 29 | 29 | 841 | 4.89E-10 |
| | | 3 | n | 25 | 12 | 300 | 2.22E-11 |
| | | 4 | y | 20 | 15 | 300 | 2.22E-11 |

| | | | | | | | |
|--|----|---|---|-----|-----|-------|----------|
| | | 4 | n | 19 | 14 | 266 | 1.55E-11 |
| | | 4 | n | 50 | 15 | 750 | 3.47E-10 |
| | | 4 | n | 29 | 5 | 145 | 2.5E-12 |
| | | 3 | n | 10 | 6 | 60 | 1.77E-13 |
| | | 3 | n | 11 | 9 | 99 | 7.97E-13 |
| | | 3 | n | 9 | 6 | 54 | 1.29E-13 |
| | | 4 | n | 74 | 30 | 2220 | 8.99E-09 |
| | | 4 | n | 40 | 15 | 600 | 1.77E-10 |
| | | 4 | n | 40 | 22 | 880 | 5.6E-10 |
| | | 3 | n | 55 | 40 | 2200 | 8.75E-09 |
| | | 3 | n | 90 | 50 | 4500 | 7.49E-08 |
| | | 3 | y | 54 | 25 | 1350 | 2.02E-09 |
| | | 3 | y | 13 | 9 | 117 | 1.32E-12 |
| | | 4 | y | 80 | 50 | 4000 | 5.26E-08 |
| | | | | | | 22733 | 9.65E-06 |
| | | | | | | | 0 |
| | m7 | 4 | n | 80 | 39 | 3120 | 2.5E-08 |
| | | 4 | n | 24 | 10 | 240 | 1.14E-11 |
| | | 4 | n | 20 | 7 | 140 | 2.25E-12 |
| | | 4 | n | 95 | 45 | 4275 | 6.42E-08 |
| | | 4 | n | 28 | 20 | 560 | 1.44E-10 |
| | | 4 | n | 24 | 15 | 360 | 3.83E-11 |
| | | 4 | n | 15 | 7 | 105 | 9.51E-13 |
| | | 4 | n | 35 | 30 | 1050 | 9.51E-10 |
| | | 4 | n | 40 | 30 | 1200 | 1.42E-09 |
| | | 2 | n | 35 | 10 | 350 | 3.52E-11 |
| | | 4 | n | 65 | 12 | 780 | 3.9E-10 |
| | | 4 | n | 25 | 17 | 425 | 6.31E-11 |
| | | 4 | n | 10 | 5 | 50 | 1.03E-13 |
| | | 4 | y | 12 | 6 | 72 | 3.07E-13 |
| | | 4 | n | 35 | 25 | 875 | 5.5E-10 |
| | | 4 | n | 24 | 9 | 216 | 8.28E-12 |
| | | 3 | n | 34 | 11 | 374 | 4.3E-11 |
| | | 3 | n | 32 | 15 | 480 | 9.09E-11 |
| | | | | | | 14672 | 2.59E-06 |
| | | | | | | | 0 |
| | m8 | 4 | n | 153 | 90 | 13770 | 2.14E-06 |
| | | 4 | n | 33 | 27 | 891 | 5.81E-10 |
| | | 4 | n | 20 | 5 | 100 | 8.22E-13 |
| | | 4 | n | 29 | 9 | 261 | 1.46E-11 |
| | | 4 | n | 200 | 120 | 24000 | 1.14E-05 |
| | | 4 | n | 46 | 25 | 1150 | 1.25E-09 |
| | | 4 | n | 22 | 20 | 440 | 7E-11 |
| | | 4 | n | 18 | 19 | 342 | 3.29E-11 |
| | | 3 | n | 23 | 15 | 345 | 3.37E-11 |

| | | | | | | | |
|--|--|---|---|----|----|------|----------|
| | | 3 | n | 43 | 19 | 817 | 4.48E-10 |
| | | 3 | n | 88 | 62 | 5456 | 1.33E-07 |
| | | 3 | n | 25 | 18 | 450 | 7.49E-11 |
| | | 3 | n | 22 | 19 | 418 | 6E-11 |
| | | 3 | n | 35 | 32 | 1120 | 1.15E-09 |
| | | 3 | n | 36 | 5 | 180 | 4.79E-12 |
| | | 3 | n | 53 | 24 | 1272 | 1.69E-09 |
| | | 3 | n | 54 | 34 | 1836 | 5.08E-09 |
| | | 3 | n | 74 | 50 | 3700 | 4.16E-08 |
| | | 4 | y | 19 | 12 | 228 | 9.74E-12 |
| | | 1 | n | 27 | 15 | 405 | 5.46E-11 |
| | | 4 | n | 6 | 4 | 24 | 1.14E-14 |
| | | 4 | n | 24 | 23 | 552 | 1.38E-10 |
| | | 3 | n | 14 | 14 | 196 | 6.19E-12 |
| | | 4 | n | 27 | 25 | 675 | 2.53E-10 |
| | | 3 | n | 26 | 15 | 390 | 4.87E-11 |
| | | 4 | n | 27 | 27 | 729 | 3.18E-10 |
| | | 4 | n | 20 | 5 | 100 | 8.22E-13 |
| | | 4 | n | 32 | 6 | 192 | 5.81E-12 |
| | | 4 | n | 36 | 16 | 576 | 1.57E-10 |
| | | 4 | n | 8 | 7 | 56 | 1.44E-13 |
| | | 4 | n | 21 | 5 | 105 | 9.51E-13 |
| | | 4 | n | 15 | 15 | 225 | 9.36E-12 |
| | | 4 | n | 7 | 6 | 42 | 6.09E-14 |
| | | 4 | n | 14 | 5 | 70 | 2.82E-13 |
| | | 3 | n | 14 | 6 | 84 | 4.87E-13 |
| | | 3 | n | 25 | 6 | 150 | 2.77E-12 |
| | | 3 | n | 9 | 8 | 72 | 3.07E-13 |
| | | 2 | n | 36 | 19 | 684 | 2.63E-10 |
| | | 4 | n | 9 | 5 | 45 | 7.49E-14 |
| | | 4 | n | 29 | 16 | 464 | 8.21E-11 |
| | | 4 | n | 38 | 16 | 608 | 1.85E-10 |
| | | 4 | n | 17 | 11 | 187 | 5.37E-12 |
| | | 4 | n | 27 | 23 | 621 | 1.97E-10 |
| | | 4 | n | 25 | 15 | 375 | 4.33E-11 |
| | | 4 | n | 13 | 10 | 130 | 1.8E-12 |
| | | 3 | n | 37 | 17 | 629 | 2.04E-10 |
| | | 3 | n | 15 | 5 | 75 | 3.47E-13 |
| | | 3 | n | 16 | 6 | 96 | 7.27E-13 |
| | | 3 | n | 11 | 9 | 99 | 7.97E-13 |
| | | 3 | n | 9 | 5 | 45 | 7.49E-14 |
| | | 4 | n | 15 | 20 | 300 | 2.22E-11 |
| | | 4 | n | 20 | 5 | 100 | 8.22E-13 |
| | | 4 | n | 22 | 16 | 352 | 3.58E-11 |
| | | 4 | n | 17 | 10 | 170 | 4.04E-12 |

| | | | | | | | |
|--|---|---|---|--------------------------------------|-----|--------|----------|
| | | | | | | 66399 | 0.00024 |
| | | | | | | | 0 |
| m9 | | 1 | n | 80 | 76 | 6080 | 1.85E-07 |
| | | 2 | n | 140 | 75 | 10500 | 9.51E-07 |
| | | 4 | n | 22 | 10 | 220 | 8.75E-12 |
| | | 4 | n | 26 | 19 | 494 | 9.9E-11 |
| | | 4 | n | 40 | 35 | 1400 | 2.25E-09 |
| | | 4 | n | 11 | 9 | 99 | 7.97E-13 |
| | | 4 | n | 35 | 29 | 1015 | 8.59E-10 |
| | | 4 | n | 15 | 10 | 150 | 2.77E-12 |
| | | 4 | n | 11 | 10 | 110 | 1.09E-12 |
| | | 4 | n | 15 | 11 | 165 | 3.69E-12 |
| | | 4 | n | 12 | 2 | 24 | 1.14E-14 |
| | | 4 | n | 39 | 20 | 780 | 3.9E-10 |
| | | 4 | n | 25 | 10 | 250 | 1.28E-11 |
| | | 4 | n | 7 | 6 | 42 | 6.09E-14 |
| | | 1 | n | 50 | 35 | 1750 | 4.4E-09 |
| | | 4 | n | 29 | 15 | 435 | 6.76E-11 |
| | | | | | | 23514 | 1.07E-05 |
| | | | | | | | 0 |
| 30 | 4 | 2 | n | 55 | 60 | 3300 | 2.95E-08 |
| | | | | 96 | 54 | 5184 | 1.14E-07 |
| | | | | 59 | 50 | 2950 | 2.11E-08 |
| | | | | 44 | 29 | 1276 | 1.71E-09 |
| | | | | 145 | 250 | 36250 | 3.91E-05 |
| | | | | 150 | 60 | 9000 | 5.99E-07 |
| | | | | 98 | 70 | 6860 | 2.65E-07 |
| | | | | 45 | 10 | 450 | 7.49E-11 |
| | | | | 63 | 15 | 945 | 6.93E-10 |
| | | | | | | 66215 | 0.000238 |
| | | | | | | 6.6215 | |
| | | | | lithic type | | | number |
| | | | | aphyric poorly vesic basalt | | | 1 |
| | | | | aphyric dense basaltic agglutinate | | | 2 |
| | | | | plagioclase porphyritic dense basalt | | | 3 |
| | | | | aphyric, non vesic basalt | | | 4 |
| Table A1.20. Measurements of lithic clasts. | | | | | | | |

| length on transect (m) | height on face (m) | scour dip (°) | scour lineation (°) | face strike (°) | face dip (°) |
|------------------------|--------------------|---------------|---------------------|-----------------|--------------|
| 1.6 | 0.5 | 58 | 350 | 300 | 58 |

| | | | | | |
|------|-----|----|-----|-----|----|
| 1.6 | 3 | | | 336 | 60 |
| 5.8 | 1.2 | 33 | 42 | 300 | 33 |
| 8.2 | 0.9 | | | 018 | 20 |
| 28 | 0.5 | | | 328 | 56 |
| 31 | 0.3 | 29 | 20 | 002 | 77 |
| 35.7 | 0.5 | | | 320 | 57 |
| 37 | 0.5 | 53 | 39 | 292 | 53 |
| 37 | 3.2 | | | 004 | 28 |
| 35.7 | 3.2 | 28 | 92 | 021 | 45 |
| 41 | 3.6 | | | 021 | 51 |
| 43 | 0.5 | 51 | 106 | 007 | 21 |
| 44 | 1 | | | 339 | 29 |
| 56 | 0.5 | 21 | 74 | 004 | 25 |
| 56 | 1 | | | 360 | 45 |
| 59 | 2 | 29 | 61 | 001 | 25 |
| 59 | 4 | | | 302 | 18 |
| 65 | 0.5 | | | 310 | 29 |
| 75 | 1 | | | 022 | 31 |
| 79.5 | 1 | 42 | 116 | 022 | 42 |
| 85 | 0.5 | | | 300 | 44 |

Table A1.21. Measurements of scours at location y29.

| tension gash length (mm) | distance along tension gash from its base | tension gash width (mm) | normalised width |
|-----------------------------|--|----------------------------|---------------------|
| 60 | 10 | 10 | 0.25 |
| | 20 | 12 | 0.3 |
| | 30 | 21 | 0.525 |
| | 40 | 23 | 0.575 |
| | 50 | 40 | 1 |
| | 60 | 40 | 1 |
| 80 | 10 | 4 | 0.1333333333 |
| | 20 | 13 | 0.4333333333 |
| | 30 | 15 | 0.5 |
| | 40 | 17 | 0.5666666667 |
| | 50 | 17 | 0.5666666667 |
| | 60 | 30 | 1 |
| | 70 | 20 | 0.6666666667 |
| | 80 | 8 | 0.2666666667 |
| 22 | 4 | 2 | 1 |
| | 8 | 2 | 1 |
| | 16 | 2 | 1 |
| | 22 | 2 | 1 |

Table A1.22. Measurements of tension gashes at location y26.

| length on transect (m) | height on face (m) | scour dip (°) | scour lineation (°) | face strike (°) | face dip (°) | max scour depth (mm) | tension gash width |
|---|--------------------|---------------|---------------------|-----------------|--------------|----------------------|--------------------|
| 1 | 0.5 | 42 | 236 | 130 | 42 | 5 | |
| 2 | 0.5 | 31 | 227 | 155 | 31 | 10 | |
| 3 | 0.5 | 35 | 221 | 142 | 35 | 10 | |
| 5 | 0.5 | 40 | 226 | 133 | 40 | 30 | |
| 1 | 1.5 | 16 | 248 | 142 | 16 | 10 | |
| 7.5 | 1.5 | 32 | 252 | 147 | 32 | 10 | |
| 8.5 | 1.5 | 19 | 244 | 142 | 19 | 3 | 10 |
| 9.5 | 1.5 | 32 | 226 | 159 | 32 | 5 | 8 |
| 11.5 | 1.5 | 28 | 226 | 148 | 28 | 8 | |
| 12.5 | 1.5 | 24 | 210 | 132 | 24 | 40 | |
| 14 | 1.5 | 24 | 222 | 140 | 24 | 10 | |
| 16.2 | 1.5 | 24 | 220 | 134 | 24 | 5 | |
| 17.4 | 1.5 | 24 | 228 | 128 | 22 | 10 | |
| 18.4 | 1.5 | 22 | 212 | 140 | 26 | 8 | |
| 24 | 1.5 | 26 | 240 | 160 | 31 | 0.5 | |
| 2 | 2.5 | 39 | 259 | 132 | 48 | 30 | 10 |
| 3 | 2.5 | 40 | 261 | 138 | 47 | 5 | |
| 4 | 2.5 | 37 | 245 | 132 | 37 | 30 | |
| 6.7 | 2.5 | 22 | 245 | 166 | 22 | 10 | |
| 7.7 | 2.5 | 22 | 250 | 160 | 22 | 5 | |
| 10.1 | 2.5 | 29 | 238 | 157 | 29 | 0.5 | |
| 11.2 | 2.5 | 30 | 226 | 169 | 30 | 4 | |
| 12 | 2.5 | 25 | 218 | 134 | 25 | 10 | |
| 13 | 2.5 | 36 | 215 | 146 | 36 | 10 | |
| 15 | 2.5 | 26 | 232 | 160 | 26 | 10 | |
| 18.7 | 2.5 | 28 | 225 | 160 | 28 | 3 | |
| 3.2 | 3.5 | 40 | 240 | 133 | 40 | 5 | |
| 12.9 | 3.5 | 25 | 256 | 160 | 25 | 10 | |
| 16.3 | 3.5 | 23 | 234 | 164 | 23 | 5 | |
| 17.3 | 3.5 | 20 | 236 | 150 | 20 | 50 | |
| 18.3 | 3.5 | 14 | 224 | 146 | 14 | 5 | |
| 6.3 | 4.5 | 28 | 261 | 168 | 28 | 3 | |
| 17.8 | 4.5 | 23 | 230 | 156 | 23 | | |
| 18.8 | 4.5 | 16 | 227 | 131 | 16 | | |
| Table A1.23. Measurements of scours at location Y29. | | | | | | | |

| tension gash length (mm) | tension gash width (mm) | tension gash dip (°) | total unit thickness (mm) | vertical height of tension gash from unit base (mm) |
|--------------------------|-------------------------|----------------------|---------------------------|---|
|--------------------------|-------------------------|----------------------|---------------------------|---|

| | | | | |
|---|-----|----|-----|-----|
| 4 | 0.5 | 05 | 730 | 180 |
| 4 | 0.5 | 06 | | 190 |
| 10 | 0.5 | 06 | | 205 |
| 8 | 0.5 | 12 | | 215 |
| 8 | 0.5 | 11 | | 220 |
| 3 | 0.5 | 11 | | 240 |
| 4 | 0.5 | 44 | | 340 |
| 16 | 2 | 62 | | 390 |
| | 1 | 28 | 650 | 110 |
| | 0.5 | 10 | | 160 |
| | 0.5 | 12 | | 162 |
| | 0.5 | 10 | | 165 |
| | 1 | 14 | | 172 |
| | 1 | 12 | | 176 |
| | 1 | 16 | | 178 |
| | 0.5 | 12 | | 182 |
| | 1 | 18 | | 188 |
| | 1 | 21 | | 192 |
| | 1 | 11 | | 196 |
| | 0.5 | 14 | | 200 |
| | 1 | 03 | | 208 |
| | 1 | 08 | | 240 |
| | 0.5 | 10 | | 253 |
| | 1 | 03 | | 233 |
| | 4 | 24 | | 273 |
| Table A1.24. Measurements of tension gashes at location y26. | | | | |

| length across crust (mm) | height of tension gash on crust (mm) | normalised distance across crust | tension gash length (mm) | tension gash width (mm) | tension gash strike (°) | tension gash dip (°) | crust strike (°) | crust dip (°) |
|-----------------------------|---|----------------------------------|-----------------------------|----------------------------|----------------------------|-------------------------|---------------------|------------------|
| 960 | 200 | 0.208333333 | 30 | 4 | 264 | 62 | 096 | 55 |
| | 230 | 0.239583333 | 70 | 2 | 256 | 46 | 070 | 34 |
| | 260 | 0.270833333 | 70 | 6 | 068 | 90 | 070 | 24 |
| | 300 | 0.3125 | 85 | 5 | 075 | 45 | 066 | 30 |
| | 320 | 0.333333333 | 80 | 5 | 260 | 56 | 070 | 26 |
| | 400 | 0.416666667 | 45 | 10 | 250 | 70 | 072 | 52 |
| | 450 | 0.46875 | 15 | 8 | 238 | 82 | 072 | 41 |
| | 470 | 0.489583333 | 85 | 5 | 256 | 82 | 074 | 41 |
| | 500 | 0.520833333 | 340 | 15 | 252 | 67 | 064 | 41 |
| | 530 | 0.552083333 | 70 | 10 | 238 | 64 | 073 | 41 |
| | 535 | 0.557291667 | 15 | 5 | 258 | 78 | 082 | 41 |
| | 540 | 0.5625 | 115 | 10 | 252 | 45 | 080 | 41 |
| | 550 | 0.572916667 | 135 | 9 | 250 | 80 | 060 | 41 |
| | 560 | 0.583333333 | 85 | 25 | 282 | 40 | 055 | 41 |
| | 620 | 0.645833333 | 40 | 5 | 246 | 86 | 092 | 39 |
| | 660 | 0.6875 | 150 | 10 | 242 | 44 | 078 | 48 |
| | 680 | 0.708333333 | 130 | 5 | 250 | 68 | 078 | 36 |
| | 700 | 0.729166667 | 40 | 9 | 246 | 78 | 076 | 45 |
| | 720 | 0.75 | 150 | 10 | 248 | 62 | 072 | 56 |
| | 760 | 0.791666667 | 60 | 10 | 236 | 58 | 070 | 70 |
| | 780 | 0.8125 | 75 | 8 | 262 | 56 | 067 | 68 |
| | 850 | 0.885416667 | 200 | 30 | 254 | 84 | 062 | 6 |
| | 900 | 0.9375 | 115 | 10 | 52 | 68 | 052 | 26 |
| | 955 | 0.994791667 | 120 | 20 | 200 | 42 | 038 | 6 |

Table A1.25. Measurements of tension gashes at location y28.

| tension gash length (mm) | distance along tension gash from its base | tension gash width (mm) | normalised width | normalised height along tension gash |
|---|---|-------------------------|------------------|--------------------------------------|
| 90 | 10 | 2 | 0.2 | 0.111111111 |
| | 20 | 4 | 0.4 | 0.222222222 |
| | 30 | 7 | 0.7 | 0.333333333 |
| | 40 | 9 | 0.9 | 0.444444444 |
| | 50 | 8 | 0.8 | 0.555555556 |
| | 60 | 9 | 0.9 | 0.666666667 |
| | 70 | 10 | 1 | 0.777777778 |
| | 80 | 8 | 0.8 | 0.888888889 |
| | 90 | 10 | 1 | 1 |
| 80 | 10 | 2 | 0.25 | 0.125 |
| | 20 | 1 | 0.125 | 0.25 |
| | 30 | 2 | 0.25 | 0.375 |
| | 40 | 7 | 0.875 | 0.5 |
| | 50 | 8 | 1 | 0.625 |
| | 60 | 8 | 1 | 0.75 |
| | 70 | 5 | 0.625 | 0.875 |
| | 80 | 6 | 0.75 | 1 |
| Table A1.26. Measurements of tension gashes at location y28. | | | | |

| height on tension gash on crustal transect (mm) | normalised distance across crust | tension gash width (mm) | transect length across unit crust (mm) |
|---|----------------------------------|-------------------------|--|
| 100 | 2.173913043 | 20 | 1230 |
| 170 | 3.695652174 | 30 | |
| 370 | 8.043478261 | 23 | |
| 400 | 8.695652174 | 2 | |
| 450 | 9.782608696 | 26 | |
| 530 | 11.52173913 | 20 | |
| 660 | 14.34782609 | 33 | |
| 690 | 15 | 8 | |
| 820 | 17.82608696 | 18 | |
| 750 | 16.30434783 | 3 | |
| 760 | 16.52173913 | 5 | |
| 890 | 19.34782609 | 3 | |
| 910 | 19.7826087 | 16 | |
| 920 | 20 | 7 | |
| 930 | 20.2173913 | 4 | |
| 970 | 21.08695652 | 3 | |
| 1120 | 24.34782609 | 8 | |
| 1130 | 24.56521739 | 6 | |
| 1140 | 24.7826087 | 4 | |
| 1210 | 26.30434783 | | |
| 1230 | 26.73913043 | | |

Table A1.27. Measurements of tension gashes at location y29.

| transect length across unit crust (mm) | height of tension gash on crustal transect (mm) | normalised distance across crust | tension gash length (mm) | tension gash width (mm) |
|--|---|----------------------------------|--------------------------|-------------------------|
| 675 | 20 | 0.02962963 | 25 | 4 |
| | 30 | 0.044444444 | 60 | 5 |
| | 45 | 0.066666667 | 35 | 3 |
| | 60 | 0.088888889 | 60 | 2 |
| | 70 | 0.103703704 | 30 | 1 |
| | 80 | 0.118518519 | 25 | 1 |
| | 95 | 0.140740741 | 35 | 2 |
| | 115 | 0.17037037 | 55 | 2 |
| | 130 | 0.192592593 | 5 | 1 |
| | 195 | 0.288888889 | 35 | 2 |
| | 215 | 0.318518519 | 35 | 2 |
| | 235 | 0.348148148 | 10 | 2 |
| | 240 | 0.355555556 | 10 | 1 |
| | 250 | 0.37037037 | 35 | 1 |
| | 255 | 0.377777778 | 25 | 1 |
| | 270 | 0.4 | 70 | 4 |

| | | | | |
|--|-----|-------------|----|-----|
| | 325 | 0.481481481 | 5 | 1 |
| | 350 | 0.518518519 | 10 | 0.5 |
| | 355 | 0.525925926 | 10 | 0.5 |
| | 357 | 0.528888889 | 10 | 0.5 |
| | 359 | 0.531851852 | 10 | 0.5 |
| | 461 | 0.682962963 | 10 | 0.5 |
| | 501 | 0.742222222 | 10 | 0.5 |
| | 511 | 0.757037037 | 10 | 0.5 |
| | 591 | 0.875555556 | 50 | 1 |
| | 616 | 0.912592593 | 40 | 2 |
| | 640 | 0.948148148 | 40 | 2 |
| | 665 | 0.985185185 | 40 | 2 |

Table A1.28. Measurements of tension gash distribution at Location Y29.

| tension gash length (mm) | distance along tension gash from its base | tension gash width (mm) | normalised width |
|-----------------------------|--|----------------------------|---------------------|
| 70 | 10 | 6 | 0.375 |
| | 20 | 16 | 1 |
| | 30 | 10 | 0.625 |
| | 40 | 7 | 0.4375 |
| | 50 | 11 | 0.6875 |
| | 60 | 12 | 0.75 |
| 80 | 10 | 4 | 0.4 |
| | 20 | 4 | 0.4 |
| | 30 | 8 | 0.8 |
| | 40 | 10 | 1 |
| | 50 | 8 | 0.8 |
| 50 | 10 | 8 | 0.5 |
| | 20 | 12 | 0.75 |
| | 30 | 13 | 0.8125 |
| | 40 | 15 | 0.9375 |
| | 50 | 16 | 1 |
| 13 | 4 | 3 | 0.375 |
| | 8 | 4 | 0.5 |
| | 13 | 8 | 1 |

Table A1.29. Measurements of tension gash lengths at location y29.

| transect length across unit crust (mm) | height of tension gash on crustal transect (mm) | normalised distance across crust | tension gash length (mm) | tension gash width (mm) | tension gash strike (°) | tension gash dip (°) | crust strike (°) | crust dip (°) |
|---|--|-------------------------------------|-----------------------------|----------------------------|----------------------------|-------------------------|---------------------|------------------|
| 2900 | 120 | 0.04137931 | | 80 | 328 | 28 | 134 | 72 |
| | 220 | 0.075862069 | | 6 | 348 | 32 | 340 | 05 |
| | 330 | 0.113793103 | | 50 | 340 | 16 | 125 | 38 |
| | 365 | 0.125862069 | | 30 | 310 | 43 | 144 | 47 |
| | 446 | 0.153793103 | | | 311 | 29 | 181 | 36 |
| | 740 | 0.255172414 | | 14 | 007 | 58 | 162 | 53 |
| | 910 | 0.313793103 | | 12 | 300 | 08 | 186 | 31 |
| | 960 | 0.331034483 | | 14 | 040 | 42 | 152 | 44 |
| | 1270 | 0.437931034 | | 16 | 056 | 36 | 154 | 38 |
| | 1460 | 0.503448276 | | 16 | 020 | 39 | 138 | 28 |
| | 1740 | 0.6 | | 16 | 001 | 31 | 160 | 40 |
| | 1765 | 0.60862069 | | 6 | 330 | 58 | 139 | 42 |
| | 1950 | 0.672413793 | | 8 | 348 | 44 | 152 | 33 |
| | 2460 | 0.848275862 | | 40 | 286 | 43 | 134 | 48 |
| | 2755 | 0.95 | | 8 | 296 | 44 | 118 | 31 |
| | 2900 | 1 | | 30 | 314 | 61 | 129 | 57 |
| | 550 | 0.189655172 | | 18 | 360 | 64 | 144 | 50 |
| | 655 | 0.225862069 | | 16 | 286 | 58 | 136 | 13 |
| | 830 | 0.286206897 | | 40 | 296 | 56 | 166 | 28 |
| | 870 | 0.3 | | 4 | 010 | 36 | 159 | 56 |
| | 1335 | 0.460344828 | | 24 | 346 | 08 | 146 | 32 |
| | 1365 | 0.470689655 | | 16 | 341 | 31 | 115 | 26 |
| | 1405 | 0.484482759 | | 5 | 358 | 52 | 122 | 48 |
| | 1715 | 0.59137931 | | 3 | 310 | 30 | 130 | 35 |
| | 2580 | 0.889655172 | | 5 | 340 | 29 | 180 | 33 |
| | 2675 | 0.922413793 | | 13 | 360 | 68 | 129 | 15 |
| 2200 | 230 | 0.104545455 | | 4 | 328 | 33 | 160 | 48 |
| | 340 | 0.154545455 | 110 | 3 | 032 | 30 | | |
| | 370 | 0.168181818 | 90 | 1 | | | | |
| | 390 | 0.177272727 | 50 | 4 | | | | |
| | 500 | 0.227272727 | 50 | 2 | | | | |
| | 600 | 0.272727273 | 175 | 10 | | | | |
| | 670 | 0.304545455 | 110 | 10 | | | | |
| | 750 | 0.340909091 | 115 | 5 | | | | |
| | 910 | 0.413636364 | 150 | 20 | | | | |
| | 970 | 0.440909091 | 120 | 3 | | | | |
| | 1030 | 0.468181818 | 130 | 1 | | | | |
| | 1040 | 0.472727273 | 200 | | | | | |
| | 1110 | 0.504545455 | 110 | | | | | |
| | 1200 | 0.545454545 | 140 | | | | | |
| | 1270 | 0.577272727 | 500 | | | | | |
| | 1340 | 0.609090909 | 2 | | | | 080 | |
| | 1480 | | 2 | | | | | |
| | 1530 | 0.695454545 | 160 | | | | 002 | |

| | | | | | | | | |
|--|------|-------------|-----|--|--|--|-----|--|
| | 1550 | 0.704545455 | 70 | | | | 001 | |
| | 1600 | 0.727272727 | 375 | | | | | |
| | 1640 | 0.745454545 | 100 | | | | 003 | |
| | 1700 | 0.772727273 | 130 | | | | 010 | |
| | 1760 | 0.8 | 90 | | | | 008 | |
| | 1860 | 0.845454545 | 340 | | | | 010 | |
| | 1890 | 0.859090909 | 220 | | | | | |
| | 1940 | 0.881818182 | 570 | | | | | |
| | 2000 | 0.909090909 | 800 | | | | 005 | |
| | 2100 | 0.954545455 | 800 | | | | 100 | |

Table A1.30. Measurements of tension gashes at location y29.

| transect length across crust (mm) | height on tension gash on crustal transect (mm) | normalised distance across crust | tension gash length (mm) | tension gash width (mm) | tension gash strike (°) | tension gash dip (°) | crust strike (°) | crust dip (°) |
|-----------------------------------|---|----------------------------------|--------------------------|-------------------------|-------------------------|----------------------|------------------|---------------|
| 1300 | 100 | 0.076923077 | 105 | 8 | 282 | 38 | 123 | 68 |
| | 180 | 0.138461538 | 55 | 20 | 122 | 36 | 118 | 76 |
| | 290 | 0.223076923 | 270 | 80 | 131 | 03 | 316 | 76 |
| | 340 | 0.261538462 | 30 | 5 | | | | |
| | 345 | 0.265384615 | 30 | 5 | | | | |
| | 347 | 0.266923077 | 20 | 5 | | | 104 | 86 |
| | 348 | 0.267692308 | 20 | 4 | 110 | 36 | 104 | 86 |
| | 540 | 0.415384615 | 240 | | 122 | 22 | 144 | 88 |
| | 690 | 0.530769231 | 130 | 3 | 178 | 39 | 350 | 82 |
| | 730 | 0.561538462 | 350 | 2 | 189 | 36 | 356 | 66 |
| | 800 | 0.615384615 | 400 | 40 | 193 | 36 | 016 | 62 |
| | 870 | 0.669230769 | 80 | 4 | 184 | 37 | 004 | 76 |
| | 910 | 0.7 | 200 | | 216 | 27 | 045 | 70 |
| | 1010 | 0.776923077 | 280 | 5 | 220 | 80 | 014 | 51 |
| | 1140 | 0.876923077 | 360 | 40 | 196 | 48 | 348 | 56 |
| | 1275 | 0.980769231 | 2900 | 80 | 178 | 40 | 360 | 30 |

Table A1.31. Measurements of tension gashes at location y27.

| transect length across unit crust (mm) | height on tension gash on crustal transect (mm) | normalised distance across crust | tension gash width (mm) | tension gash strike (°) | tension gash dip (°) | crust strike (°) | crust dip (°) |
|--|---|----------------------------------|-------------------------|-------------------------|----------------------|------------------|---------------|
| 3500 | 400 | 0.114285714 | 50 | 306 | 29 | 146 | 31 |
| | 410 | 0.117142857 | 12 | 288 | 39 | 138 | 28 |
| | 540 | 0.154285714 | 50 | 330 | 42 | 126 | 22 |
| | 590 | 0.168571429 | 40 | 324 | 40 | 164 | 18 |
| | 630 | 0.18 | 5 | 295 | 42 | 127 | 64 |
| | 645 | 0.184285714 | 15 | 220 | 35 | 137 | 62 |
| | 670 | 0.191428571 | 15 | 308 | 35 | 146 | 48 |
| | 705 | 0.201428571 | 25 | 340 | 42 | 146 | 19 |
| 3200 | 60 | 0.01875 | 17 | 178 | 28 | 003 | 53 |
| | 250 | 0.078125 | 12 | 333 | 64 | 150 | 58 |
| | 350 | 0.109375 | 45 | 273 | 54 | 123 | 33 |
| | 395 | 0.1234375 | 50 | 339 | 20 | 153 | 45 |
| | 585 | 0.1828125 | 10 | 346 | 44 | 340 | 108 |
| | 775 | 0.2421875 | 10 | 326 | 23 | 156 | 58 |
| | 795 | 0.2484375 | 45 | 340 | 30 | 150 | 51 |
| | 855 | 0.2671875 | 25 | 346 | 30 | 152 | 37 |
| | 1105 | 0.3453125 | 5 | 357 | 07 | 138 | 46 |
| | 1175 | 0.3671875 | 10 | 360 | 32 | 144 | 31 |
| | 1295 | 0.4046875 | 30 | 346 | 15 | 124 | 12 |
| Table A1.32. Measurements of tension gashes at location y29. | | | | | | | |

| transect length across unit crust (mm) | height on tension gash on crustal transect (mm) | normalised distance across crust | tension gash length (mm) | tension gash width (mm) | tension gash dip (°) | crust strike (°) | crust dip (°) |
|--|---|----------------------------------|--------------------------|-------------------------|----------------------|------------------|---------------|
| 340 | 200 | 0.588235294 | 5 | 0.5 | 38 | 055 | 46 |
| | 215 | 0.632352941 | 13 | 0.5 | 41 | 055 | 46 |
| | 250 | 0.735294118 | 4 | 0.5 | 36 | 055 | 46 |
| 600 | 280 | 0.466666667 | 8 | 0.5 | 19 | 088 | 38 |
| | 360 | 0.6 | 4 | 0.5 | 20 | 088 | 38 |
| | 392 | 0.653333333 | 16 | 0.5 | 23 | 088 | 38 |

Table A1.33. Measurements of tension gashes at location y35.

| tension gash length (mm) | distance along tension gash from its base | tension gash width (mm) | normalised width |
|--------------------------|---|-------------------------|------------------|
| 140 | 10 | 3 | 0.078947368 |
| | 20 | 3 | 0.078947368 |
| | 30 | 3 | 0.078947368 |
| | 40 | 5 | 0.131578947 |
| | 50 | 2 | 0.052631579 |
| | 60 | 2 | 0.052631579 |
| | 70 | 10 | 0.263157895 |
| | 80 | 10 | 0.263157895 |
| | 90 | 13 | 0.342105263 |
| | 100 | 24 | 0.631578947 |
| | 110 | 29 | 0.763157895 |
| | 120 | 30 | 0.789473684 |
| | 130 | 32 | 0.842105263 |
| | 140 | 38 | 1 |
| 60 | 10 | 4 | 0.307692308 |
| | 20 | 6 | 0.461538462 |
| | 30 | 5 | 0.384615385 |
| | 40 | 11 | 0.846153846 |
| | 50 | 13 | 1 |
| | 60 | 13 | 1 |
| 300 | 10 | 2 | 0.015384615 |
| | 20 | 2 | 0.015384615 |
| | 30 | 2 | 0.015384615 |
| | 40 | 2 | 0.015384615 |
| | 50 | 2 | 0.015384615 |

| | | | |
|-----|-----|-----|-------------|
| | 60 | 2 | 0.015384615 |
| | 70 | 4 | 0.030769231 |
| | 80 | 4 | 0.030769231 |
| | 90 | 8 | 0.061538462 |
| | 100 | 14 | 0.107692308 |
| | 110 | 130 | 1 |
| | 120 | 31 | 0.238461538 |
| | 140 | 55 | 0.423076923 |
| | 160 | 72 | 0.553846154 |
| | 180 | 114 | 0.876923077 |
| | 200 | 115 | 0.884615385 |
| | 300 | 110 | 0.846153846 |
| 100 | 10 | 0.5 | 0.015625 |
| | 20 | 1 | 0.03125 |
| | 30 | 1 | 0.03125 |
| | 40 | 16 | 0.5 |
| | 50 | 16 | 0.5 |
| | 60 | 20 | 0.625 |
| | 70 | 24 | 0.75 |
| | 80 | 32 | 1 |
| | 90 | 20 | 0.625 |
| | 100 | 20 | 0.625 |
| 50 | 10 | 4 | 0.363636364 |
| | 20 | 11 | 1 |
| | 30 | 8 | 0.727272727 |
| | 40 | 2 | 0.181818182 |
| | 50 | 1 | 0.090909091 |

Table A1.34. Measurements of tension gashes at location y37.

| tension gash length (mm) | tension gash width (mm) | tension gash dip (°) | total unit thickness (mm) | vertical height of tension gash from unit base (mm) |
|--------------------------|-------------------------|----------------------|---------------------------|---|
| 135 | 3 | 30 | 1630 | 90 |
| 310 | | 78 | | 290 |
| 150 | 8 | 84 | | 500 |
| 32 | 0.5 | 04 | | 530 |
| 34 | 2 | 11 | | 760 |
| 270 | 120 | 10 | | 870 |
| 60 | 8 | 28 | | 890 |
| 45 | 2 | 10 | | 910 |

| | | | | |
|-----|-----|----|------|------|
| 6 | 1 | 01 | | 915 |
| 4 | 1 | 01 | | 951 |
| 20 | 0.5 | 48 | | 10 |
| 40 | 2 | 22 | | 43 |
| 50 | 4 | 22 | | 80 |
| 80 | 1 | 31 | | 630 |
| 121 | 1 | 43 | | 1030 |
| 70 | 1 | 32 | | 1230 |
| 220 | 50 | 76 | | |
| | 2 | 22 | 1480 | 10 |
| | 4 | 22 | | 43 |
| | 1 | 31 | | 80 |
| | 1 | 43 | | 630 |
| | 1 | 32 | | 1030 |
| | 50 | 76 | | 1230 |

Table A1.35. Measurements of tension gashes at location y37.

| transect length along base (mm) | distance along transect | tension gash length (mm) | distance along tension gash from its base | tension gash width (mm) | normali sed width |
|---------------------------------------|-------------------------------|--------------------------------|---|-------------------------------|-------------------------|
| 675 | 80 | 82 | 10 | 7 | 0.53846 1538 |
| | | | 20 | 7 | 0.53846 1538 |
| | | | 30 | 8 | 0.61538 4615 |
| | | | 40 | 10 | 0.76923 0769 |
| | | | 50 | 13 | 1 |
| | | | 60 | 2 | 0.15384 6154 |
| | | | 80 | 8 | 0.61538 4615 |
| 675 | 230 | 80 | 10 | 2 | 0.25 |
| | | | 30 | 4 | 0.5 |
| | | | 50 | 0 | 0 |
| | | | 70 | 8 | 1 |
| | | | 80 | 4 | 0.5 |
| 675 | 260 | 64 | 10 | 16 | 0.4 |
| | | | 20 | 40 | 1 |
| | | | 40 | 13 | 0.325 |
| | | | 60 | 8 | 0.2 |
| 675 | 350 | 50 | 10 | 2 | 0.2 |
| | | | 20 | 5 | 0.5 |

| | | | | | |
|---|-----|-----|-----|----|-----------------|
| | | | 40 | 10 | 1 |
| 675 | 515 | 100 | 10 | 2 | 0.4 |
| | | | 20 | 2 | 0.4 |
| | | | 30 | 1 | 0.2 |
| | | | 40 | 1 | 0.2 |
| | | | 50 | 1 | 0.2 |
| | | | 80 | 4 | 0.8 |
| | | | 100 | 5 | 1 |
| 675 | 575 | 80 | 10 | 1 | 1 |
| | | | 80 | 1 | 1 |
| 675 | 625 | 175 | 10 | 4 | 0.26666 6667 |
| | | | 20 | 10 | 0.66666 6667 |
| | | | 40 | 10 | 0.66666 6667 |
| | | | 60 | 10 | 0.66666 6667 |
| | | | 70 | 15 | 1 |
| | | | 80 | 8 | 0.53333 3333 |
| 675 | 665 | 20 | 10 | 4 | 0.66666 6667 |
| | | | 20 | 6 | 1 |
| Table A1.36. Measurements of tension gashes at Location Y42. | | | | | |

Appendix 2: Support Material for Chapter 4

| image | area analysed (mm ²) | particle number | area (mm ²) | width (mm) | height (mm) | conduit |
|-------|----------------------------------|-----------------------------|-------------------------|------------|-------------|---------|
| 158 | 9522 | 1 | 37.69 | 117.376 | 81.358 | L6 |
| | | 2 | 26.932 | 6.904 | 5.639 | |
| | | 3 | 4.03 | 1.764 | 3.184 | |
| | | 4 | 55.439 | 12.083 | 6.713 | |
| | | 5 | 21.383 | 5.524 | 5.715 | |
| | | 6 | 12.646 | 4.143 | 5.984 | |
| | | 7 | 81.298 | 10.625 | 11.584 | |
| | | 8 | 10.352 | 4.066 | 3.567 | |
| | | 9 | 154.451 | 13.656 | 21.289 | |
| | | 10 | 36.763 | 8.861 | 6.137 | |
| | | 11 | 16.214 | 4.833 | 5.063 | |
| | | 12 | 33.201 | 6.751 | 7.135 | |
| | | 13 | 16.828 | 5.6 | 4.45 | |
| | | 14 | 75.486 | 10.779 | 11.546 | |
| | | 15 | 25.034 | 4.028 | 9.398 | |
| | | 16 | 168.373 | 13.425 | 24.127 | |
| | | 17 | 43.099 | 5.754 | 10.165 | |
| | | 18 | 11.908 | 3.567 | 4.718 | |
| | | 19 | 92.052 | 11.277 | 14.001 | |
| | | 20 | 162.392 | 13.387 | 15.267 | |
| | | 21 | 90.909 | 11.469 | 11.277 | |
| | | 22 | 31.998 | 7.71 | 7.748 | |
| | | 23 | 27.049 | 6.981 | 5.178 | |
| | | 24 | 23.152 | 6.866 | 5.677 | |
| | | 25 | 184.412 | 14.998 | 17.338 | |
| | | 26 | 32.126 | 5.984 | 8.746 | |
| | | 27 | 208.01 | 17.453 | 18.412 | |
| | | 28 | 68.386 | 11.469 | 12.198 | |
| | | 29 | 38.001 | 6.137 | 8.094 | |
| | | 30 | 6.349 | 3.644 | 2.57 | |
| | | 31 | 156.699 | 24.357 | 12.773 | |
| | | 32 | 3.687 | 2.11 | 2.992 | |
| | | 33 | 11.059 | 4.219 | 3.836 | |
| | | 34 | 55.629 | 6.981 | 11.009 | |
| | | 35 | 3.515 | 2.033 | 2.647 | |
| | | 36 | 9.798 | 5.946 | 3.299 | |
| | | sum | 2036.35 | | | |
| | | area covered by lapilli (%) | 21.38573829 | | | |
| | | | | | | |
| 160 | 8715 | 1 | 90.428 | 113.076 | 77.958 | L6 |
| | | 2 | 36.867 | 10.876 | 4.94 | |

| | | | | | | |
|-----|------|-----------------------------|-------------|---------|--------|----|
| | | 3 | 9.651 | 2.74 | 5.396 | |
| | | 4 | 36.619 | 9.589 | 7.347 | |
| | | 5 | 296.258 | 21.254 | 20.382 | |
| | | 6 | 15.047 | 5.729 | 3.861 | |
| | | 7 | 24.393 | 5.562 | 6.808 | |
| | | 8 | 41.704 | 8.759 | 5.562 | |
| | | 9 | 259.978 | 22.873 | 19.552 | |
| | | 10 | 125.327 | 17.061 | 12.993 | |
| | | 11 | 94.851 | 10.046 | 20.05 | |
| | | 12 | 96.823 | 9.755 | 13.948 | |
| | | 13 | 25.837 | 6.766 | 4.94 | |
| | | 14 | 39.512 | 7.057 | 9.714 | |
| | | 15 | 26.921 | 5.895 | 6.434 | |
| | | 16 | 64.283 | 8.136 | 10.834 | |
| | | 17 | 7.036 | 3.57 | 3.279 | |
| | | 18 | 10.244 | 3.653 | 4.151 | |
| | | 19 | 36.069 | 8.136 | 6.227 | |
| | | 20 | 41.945 | 9.838 | 7.015 | |
| | | 21 | 21.667 | 5.978 | 5.23 | |
| | | 22 | 66.874 | 8.427 | 12.121 | |
| | | 23 | 1.73 | 1.577 | 1.826 | |
| | | 24 | 22.215 | 6.102 | 5.562 | |
| | | 25 | 24.722 | 5.313 | 7.846 | |
| | | 26 | 82.638 | 8.717 | 14.944 | |
| | | 27 | 7.063 | 2.574 | 4.317 | |
| | | 28 | 43.201 | 7.597 | 8.136 | |
| | | 29 | 95.329 | 11.457 | 12.37 | |
| | | 30 | 9.093 | 4.359 | 3.113 | |
| | | 31 | 19.782 | 9.921 | 3.072 | |
| | | 32 | 2.7 | 1.785 | 2.449 | |
| | | 33 | 5.356 | 2.532 | 3.03 | |
| | | 34 | 57.124 | 7.597 | 10.253 | |
| | | 35 | 32.24 | 5.645 | 8.344 | |
| | | 36 | 9.326 | 4.566 | 2.781 | |
| | | 37 | 24.374 | 4.815 | 6.393 | |
| | | 38 | 16.615 | 6.185 | 4.815 | |
| | | 39 | 7.628 | 3.819 | 3.321 | |
| | | 40 | 25.608 | 6.6 | 5.77 | |
| | | 41 | 22.043 | 6.061 | 5.396 | |
| | | sum | 1977.121 | | | |
| | | area covered by lapilli (%) | 22.68641423 | | | |
| | | | | | | |
| 161 | 7328 | 1 | 4.005 | 103.931 | 0.039 | L6 |
| | | 2 | 56.376 | 11.638 | 8.208 | |
| | | 3 | 51.353 | 10.328 | 8.516 | |

| | | | | | | |
|-----|------|--------------------------------|-------------|---------|--------|----|
| | | 4 | 11.633 | 5.241 | 2.813 | |
| | | 5 | 18.258 | 5.511 | 4.817 | |
| | | 6 | 14.74 | 3.892 | 5.125 | |
| | | 7 | 12.602 | 5.01 | 3.776 | |
| | | 8 | 24.425 | 5.125 | 6.782 | |
| | | 9 | 6.815 | 2.967 | 3.661 | |
| | | 10 | 89.082 | 14.913 | 9.017 | |
| | | 11 | 7.094 | 2.736 | 3.854 | |
| | | 12 | 52.413 | 8.863 | 9.518 | |
| | | 13 | 41.724 | 8.17 | 7.669 | |
| | | 14 | 12.361 | 6.204 | 2.967 | |
| | | 15 | 6.167 | 2.736 | 3.198 | |
| | | 16 | 26.938 | 8.748 | 5.125 | |
| | | 17 | 25.808 | 5.395 | 6.744 | |
| | | 18 | 124.719 | 14.181 | 11.946 | |
| | | 19 | 28.311 | 5.125 | 10.25 | |
| | | 20 | 8.191 | 3.276 | 3.237 | |
| | | 21 | 27.823 | 7.283 | 5.934 | |
| | | 22 | 26.766 | 5.665 | 8.131 | |
| | | 23 | 17.128 | 5.164 | 4.701 | |
| | | 24 | 14.811 | 4.586 | 4.316 | |
| | | 25 | 28.378 | 5.934 | 6.166 | |
| | | 26 | 8.883 | 4.316 | 2.967 | |
| | | 27 | 10.607 | 5.202 | 3.699 | |
| | | 28 | 66.461 | 9.364 | 9.827 | |
| | | 29 | 158.826 | 14.258 | 16.108 | |
| | | 30 | 3.077 | 2.582 | 2.235 | |
| | | 31 | 5.783 | 2.389 | 3.738 | |
| | | 32 | 16.298 | 5.626 | 4.239 | |
| | | 33 | 26.939 | 6.281 | 5.395 | |
| | | 34 | 7.146 | 3.661 | 2.967 | |
| | | 35 | 135.975 | 17.418 | 11.291 | |
| | | 36 | 15.551 | 5.279 | 4.701 | |
| | | 37 | 19.107 | 5.164 | 5.511 | |
| | | 38 | 46.142 | 8.748 | 8.285 | |
| | | 39 | 31.525 | 6.358 | 7.514 | |
| | | 40 | 9.18 | 4.509 | 2.89 | |
| | | 41 | 17.349 | 4.855 | 4.894 | |
| | | sum | 1316.77 | | | |
| | | area covered by lapilli (%) | 17.96902293 | | | |
| 169 | 9473 | 1 | 46.517 | 116.552 | 81.281 | L6 |
| | | 2 | 349.205 | 27.931 | 18.128 | |
| | | 3 | 9.789 | 3.793 | 4.335 | |
| | | 4 | 695.94 | 33.695 | 29.261 | |

| | | | | | | |
|-----|-------|--------------------------------|-------------|--------|--------|-----|
| | | 5 | 59.725 | 10.69 | 9.458 | |
| | | 6 | 28.474 | 6.207 | 7.192 | |
| | | 7 | 30.804 | 8.374 | 6.502 | |
| | | 8 | 186.675 | 19.261 | 19.458 | |
| | | 9 | 355.854 | 17.537 | 26.502 | |
| | | 10 | 4.567 | 2.069 | 3.448 | |
| | | 11 | 27.276 | 6.453 | 6.552 | |
| | | 12 | 55.328 | 10.591 | 8.67 | |
| | | 13 | 10.961 | 3.645 | 4.68 | |
| | | 14 | 9.755 | 3.793 | 3.744 | |
| | | 15 | 139.659 | 16.207 | 13.448 | |
| | | 16 | 43.918 | 8.128 | 7.734 | |
| | | 17 | 97.986 | 9.507 | 16.305 | |
| | | 18 | 290.323 | 20.887 | 20.69 | |
| | | 19 | 92.645 | 13.744 | 13.005 | |
| | | 20 | 14.946 | 6.453 | 3.103 | |
| | | 21 | 316.819 | 20.148 | 22.167 | |
| | | 22 | 28.297 | 7.192 | 7.389 | |
| | | 23 | 37.596 | 7.143 | 7.586 | |
| | | 24 | 9.233 | 3.793 | 3.448 | |
| | | 25 | 2.245 | 1.626 | 2.217 | |
| | | sum | 2944.537 | | | |
| | | area covered by lapilli (%) | 31.08346881 | | | |
| | | | | | | |
| 227 | 11245 | 1 | 97.443 | 19.796 | 9.059 | L19 |
| | | 2 | 57.865 | 11.705 | 10.992 | |
| | | 3 | 7.301 | 2.85 | 4.427 | |
| | | 4 | 56.417 | 9.873 | 8.092 | |
| | | 5 | 14.811 | 4.478 | 4.885 | |
| | | 6 | 15.702 | 6.26 | 5.598 | |
| | | 7 | 6.467 | 2.748 | 3.359 | |
| | | 8 | 89.321 | 14.504 | 11.552 | |
| | | 9 | 26.543 | 5.751 | 7.735 | |
| | | 10 | 17.409 | 6.107 | 5.038 | |
| | | 11 | 30.563 | 6.921 | 6.463 | |
| | | 12 | 4.351 | 3.104 | 1.985 | |
| | | 13 | 24.798 | 6.616 | 5.242 | |
| | | 14 | 62.281 | 11.145 | 9.567 | |
| | | 15 | 24.606 | 6.056 | 5.649 | |
| | | 16 | 8.761 | 3.868 | 3.053 | |
| | | 17 | 10.888 | 3.308 | 4.478 | |
| | | 18 | 21.869 | 6.972 | 4.326 | |
| | | 19 | 42.01 | 7.888 | 7.837 | |
| | | 20 | 12.084 | 4.173 | 4.02 | |
| | | 21 | 57.816 | 9.517 | 8.804 | |

| | | | | | | |
|-----|------|-----------------------------|-------------|--------|--------|-----|
| | | 22 | 26.334 | 5.547 | 5.852 | |
| | | 23 | 18.52 | 5.293 | 5.089 | |
| | | 24 | 19.605 | 3.868 | 6.463 | |
| | | 25 | 22.827 | 5.7 | 5.903 | |
| | | 26 | 54.861 | 7.481 | 10.331 | |
| | | 27 | 3.527 | 1.883 | 2.799 | |
| | | 28 | 3.126 | 2.087 | 2.188 | |
| | | 29 | 5.775 | 4.02 | 2.036 | |
| | | 30 | 47.324 | 12.417 | 7.125 | |
| | | 31 | 190.111 | 24.987 | 12.57 | |
| | | 32 | 37.001 | 8.55 | 7.074 | |
| | | sum | 1118.317 | | | |
| | | area covered by lapilli (%) | 9.945015562 | | | |
| | | | | | | |
| 229 | 6182 | 1 | 3.212 | 0.084 | 76.076 | L19 |
| | | 2 | 70.721 | 10.97 | 8.565 | |
| | | 3 | 26.849 | 5.443 | 7.468 | |
| | | 4 | 10.294 | 5.148 | 2.827 | |
| | | 5 | 12.097 | 4.262 | 4.219 | |
| | | 6 | 170.537 | 16.582 | 17.848 | |
| | | 7 | 10.189 | 3.038 | 4.135 | |
| | | 8 | 20.6 | 5.57 | 5.738 | |
| | | 9 | 3.635 | 3.038 | 1.772 | |
| | | 10 | 4.278 | 3.038 | 1.941 | |
| | | 11 | 72.082 | 13.038 | 13.418 | |
| | | 12 | 8.012 | 3.713 | 2.785 | |
| | | 13 | 1.606 | 1.435 | 1.772 | |
| | | 14 | 3.536 | 2.11 | 2.363 | |
| | | 15 | 12.838 | 5.316 | 3.629 | |
| | | 16 | 58.52 | 12.278 | 10.928 | |
| | | 17 | 5.512 | 2.954 | 2.405 | |
| | | 18 | 15.799 | 5.401 | 4.262 | |
| | | 19 | 3.865 | 2.658 | 2.321 | |
| | | 20 | 7.408 | 3.586 | 2.827 | |
| | | 21 | 15.738 | 9.241 | 3.544 | |
| | | sum | 537.328 | | | |
| | | area covered by lapilli (%) | 8.691814947 | | | |
| | | | | | | |
| 231 | 9806 | 1 | 3.249 | 0.04 | 81.295 | L19 |
| | | 2 | 3.958 | 1.719 | 2.918 | |
| | | 3 | 30.976 | 7.434 | 8.074 | |
| | | 4 | 49.497 | 7.354 | 8.753 | |
| | | 5 | 2.605 | 2.198 | 1.878 | |
| | | 6 | 6.161 | 4.716 | 2.798 | |

| | | | | | | |
|--|--|----|---------|--------|--------|--|
| | | 7 | 14.104 | 4.676 | 4.836 | |
| | | 8 | 3.746 | 2.878 | 1.878 | |
| | | 9 | 4.005 | 2.198 | 2.478 | |
| | | 10 | 6.283 | 3.197 | 4.117 | |
| | | 11 | 1.31 | 1.439 | 1.439 | |
| | | 12 | 55.543 | 5.675 | 14.189 | |
| | | 13 | 4.903 | 3.197 | 2.718 | |
| | | 14 | 35.292 | 6.355 | 9.552 | |
| | | 15 | 3.708 | 2.438 | 2.198 | |
| | | 16 | 2.407 | 1.878 | 2.158 | |
| | | 17 | 12.102 | 4.396 | 4.117 | |
| | | 18 | 22.243 | 5.116 | 6.155 | |
| | | 19 | 14.059 | 4.556 | 4.756 | |
| | | 20 | 10.403 | 4.556 | 3.078 | |
| | | 21 | 4.463 | 2.238 | 3.837 | |
| | | 22 | 11.957 | 3.157 | 5.036 | |
| | | 23 | 13.425 | 4.117 | 5.516 | |
| | | 24 | 41.772 | 8.074 | 8.513 | |
| | | 25 | 15.96 | 5.116 | 4.277 | |
| | | 26 | 72.45 | 10.312 | 14.868 | |
| | | 27 | 107.704 | 12.91 | 15.588 | |
| | | 28 | 17.888 | 5.556 | 7.034 | |
| | | 29 | 20.997 | 6.555 | 5.596 | |
| | | 30 | 10.161 | 3.917 | 3.477 | |
| | | 31 | 9.495 | 3.637 | 5.316 | |
| | | 32 | 3.521 | 1.839 | 2.278 | |
| | | 33 | 3.968 | 2.118 | 2.878 | |
| | | 34 | 4.093 | 2.238 | 2.838 | |
| | | 35 | 9.406 | 3.317 | 4.077 | |
| | | 36 | 10.137 | 3.557 | 4.157 | |
| | | 37 | 44.251 | 8.713 | 9.392 | |
| | | 38 | 18.458 | 5.835 | 4.836 | |
| | | 39 | 17.567 | 4.836 | 5.476 | |
| | | 40 | 5.947 | 3.078 | 3.197 | |
| | | 41 | 53.442 | 11.271 | 8.233 | |
| | | 42 | 4.534 | 3.197 | 2.158 | |
| | | 43 | 20.733 | 7.194 | 5.875 | |
| | | 44 | 5.323 | 2.918 | 2.958 | |
| | | 45 | 2.265 | 1.559 | 2.278 | |
| | | 46 | 3.522 | 1.799 | 3.118 | |
| | | 47 | 0.85 | 0.999 | 1.159 | |
| | | 48 | 6.395 | 3.277 | 2.558 | |
| | | 49 | 12.157 | 6.875 | 2.958 | |
| | | 50 | 2.99 | 2.518 | 1.998 | |
| | | 51 | 8.056 | 4.836 | 2.958 | |

| | | | | | | |
|--|--|----|---------|--------|--------|--|
| | | 52 | 19.249 | 4.956 | 6.075 | |
| | | 53 | 24.813 | 5.036 | 9.512 | |
| | | 54 | 20.641 | 4.037 | 7.594 | |
| | | 55 | 3.859 | 2.998 | 1.799 | |
| | | 56 | 7.064 | 2.878 | 3.437 | |
| | | 57 | 3.35 | 2.318 | 2.758 | |
| | | 58 | 1.505 | 1.199 | 1.559 | |
| | | 59 | 57.725 | 7.954 | 10.791 | |
| | | 60 | 299.156 | 19.904 | 19.345 | |
| | | 61 | 44.922 | 8.793 | 8.993 | |
| | | 62 | 22.204 | 4.476 | 7.354 | |
| | | 63 | 6.882 | 2.438 | 4.037 | |
| | | 64 | 1.134 | 1.759 | 0.999 | |
| | | 65 | 9.126 | 5.516 | 2.798 | |
| | | 66 | 18.109 | 3.797 | 6.914 | |
| | | 67 | 10.466 | 5.156 | 2.918 | |
| | | 68 | 0.955 | 1.199 | 1.079 | |
| | | 69 | 5.458 | 2.798 | 2.718 | |
| | | 70 | 7.436 | 3.677 | 3.038 | |
| | | 71 | 7.46 | 3.597 | 3.477 | |
| | | 72 | 2.272 | 2.558 | 1.479 | |
| | | 73 | 50.005 | 6.155 | 10.671 | |
| | | 74 | 37.423 | 7.234 | 7.714 | |
| | | 75 | 24.765 | 6.435 | 5.755 | |
| | | 76 | 7.69 | 2.598 | 3.797 | |
| | | 77 | 4.649 | 2.558 | 2.558 | |
| | | 78 | 5.505 | 2.558 | 3.317 | |
| | | 79 | 58.821 | 10.392 | 8.673 | |
| | | 80 | 28.639 | 7.874 | 5.755 | |
| | | 81 | 7.12 | 2.958 | 3.397 | |
| | | 82 | 47.917 | 7.994 | 9.153 | |
| | | 83 | 4.553 | 2.878 | 2.478 | |
| | | 84 | 19.503 | 4.636 | 6.954 | |
| | | 85 | 16.412 | 5.316 | 4.716 | |
| | | 86 | 10.272 | 4.197 | 3.717 | |
| | | 87 | 11.811 | 4.716 | 3.877 | |
| | | 88 | 39.506 | 7.114 | 9.872 | |
| | | 89 | 63.192 | 8.753 | 8.953 | |
| | | 90 | 7.117 | 3.797 | 2.878 | |
| | | 91 | 73.273 | 10.911 | 9.992 | |
| | | 92 | 5.855 | 2.118 | 3.637 | |
| | | 93 | 3.613 | 2.118 | 2.678 | |
| | | 94 | 26.97 | 6.235 | 7.234 | |
| | | 95 | 5.719 | 2.758 | 2.958 | |
| | | 96 | 1.768 | 1.359 | 2.398 | |

| | | | | | | |
|-----|------|--------------------------------|-------------|--------|--------|-----|
| | | 97 | 3.791 | 2.158 | 2.518 | |
| | | 98 | 4.668 | 3.118 | 2.318 | |
| | | 99 | 55.979 | 11.95 | 5.875 | |
| | | 100 | 8.722 | 3.997 | 4.716 | |
| | | 101 | 7.637 | 3.477 | 2.958 | |
| | | 102 | 2.958 | 2.318 | 1.599 | |
| | | sum | 2070.08 | | | |
| | | area covered by lapilli (%) | 21.11034061 | | | |
| | | | | | | |
| 232 | 8567 | 1 | 13.292 | 5.229 | 3.913 | L19 |
| | | 2 | 12.654 | 5.342 | 4.026 | |
| | | 3 | 4.398 | 2.069 | 3.649 | |
| | | 4 | 85.147 | 11.851 | 11.099 | |
| | | 5 | 14.614 | 4.477 | 5.455 | |
| | | 6 | 23.319 | 5.869 | 5.38 | |
| | | 7 | 6.18 | 3.348 | 2.521 | |
| | | 8 | 90.058 | 10.534 | 15.162 | |
| | | 9 | 4.977 | 2.822 | 2.558 | |
| | | 10 | 3.493 | 1.693 | 3.047 | |
| | | 11 | 4.328 | 2.634 | 2.408 | |
| | | 12 | 15.019 | 5.154 | 4.138 | |
| | | 13 | 23.723 | 4.778 | 6.998 | |
| | | 14 | 50.743 | 6.659 | 10.534 | |
| | | 15 | 115.93 | 15.237 | 12.491 | |
| | | 16 | 52.002 | 9.105 | 9.067 | |
| | | 17 | 61.286 | 7.675 | 13.318 | |
| | | 18 | 6.507 | 4.101 | 2.521 | |
| | | 19 | 13.444 | 4.628 | 4.74 | |
| | | 20 | 15.196 | 5.982 | 3.875 | |
| | | 21 | 113.708 | 13.281 | 13.657 | |
| | | 22 | 26.074 | 9.105 | 5.869 | |
| | | 23 | 7.326 | 2.521 | 4.251 | |
| | | 24 | 3.718 | 2.445 | 2.144 | |
| | | 25 | 1.507 | 1.279 | 1.655 | |
| | | 26 | 4.933 | 2.333 | 2.445 | |
| | | 27 | 50.508 | 8.54 | 10.91 | |
| | | 28 | 16.351 | 4.929 | 5.004 | |
| | | 29 | 21.188 | 5.117 | 6.885 | |
| | | 30 | 7.737 | 3.01 | 3.762 | |
| | | 31 | 7.394 | 2.897 | 4.289 | |
| | | 32 | 25.607 | 6.96 | 8.728 | |
| | | 33 | 12.156 | 4.816 | 3.16 | |
| | | 34 | 28.551 | 5.192 | 7.901 | |
| | | 35 | 6.392 | 2.445 | 3.762 | |
| | | 36 | 6.62 | 3.085 | 3.047 | |

| | | | | | | |
|-----|------|--------------------------------|-------------|--------|--------|-----|
| | | sum | 956.08 | | | |
| | | area covered by lapilli (%) | 11.16003268 | | | |
| | | | | | | |
| 234 | 8591 | 1 | 41.332 | 8.917 | 7.958 | L19 |
| | | 2 | 77.788 | 10.458 | 12.333 | |
| | | 3 | 11.628 | 3.458 | 4.792 | |
| | | 4 | 23.55 | 5.458 | 6.5 | |
| | | 5 | 7.524 | 3.208 | 3.667 | |
| | | 6 | 4.076 | 2.458 | 2.792 | |
| | | 7 | 2.432 | 1.917 | 2.333 | |
| | | 8 | 11.043 | 3.5 | 4.875 | |
| | | 9 | 14.674 | 4.667 | 5.833 | |
| | | 10 | 1.729 | 1.625 | 1.625 | |
| | | 11 | 19.127 | 6.5 | 5.5 | |
| | | 12 | 8.599 | 2.542 | 4.458 | |
| | | 13 | 11.017 | 3.875 | 4.208 | |
| | | 14 | 5.583 | 3.083 | 2.75 | |
| | | 15 | 107.899 | 15 | 10.083 | |
| | | 16 | 16.41 | 4.083 | 5.875 | |
| | | 17 | 19.243 | 3.958 | 5.792 | |
| | | 18 | 3.91 | 2.833 | 2.375 | |
| | | 19 | 3.556 | 2.542 | 1.833 | |
| | | 20 | 2.078 | 1.5 | 1.708 | |
| | | 21 | 8.698 | 3.292 | 4.167 | |
| | | 22 | 6.236 | 2.625 | 2.958 | |
| | | 23 | 36.476 | 6.708 | 8.083 | |
| | | 24 | 4.149 | 3.25 | 2.125 | |
| | | 25 | 14.493 | 4.042 | 4.542 | |
| | | 26 | 1.123 | 0.958 | 1.833 | |
| | | 27 | 5.913 | 3.583 | 2.5 | |
| | | 28 | 1.498 | 1.5 | 1.792 | |
| | | 29 | 4.21 | 2.917 | 2.375 | |
| | | 30 | 6.462 | 4.875 | 2.333 | |
| | | 31 | 39.191 | 5.542 | 10.833 | |
| | | 32 | 1.457 | 1.292 | 1.917 | |
| | | 33 | 7.222 | 2.458 | 4.083 | |
| | | 34 | 3.316 | 2.083 | 2.458 | |
| | | 35 | 1.776 | 1.625 | 1.708 | |
| | | 36 | 11.128 | 3.958 | 5.125 | |
| | | 37 | 75.498 | 9.458 | 10.417 | |
| | | 38 | 2.88 | 2.208 | 1.917 | |
| | | 39 | 6.927 | 2.708 | 3.708 | |
| | | 40 | 53.632 | 11.708 | 10.708 | |
| | | 41 | 6.05 | 2.667 | 3.208 | |
| | | 42 | 4.302 | 2.292 | 2.625 | |

| | | | | | | |
|--|--|----|---------|--------|--------|--|
| | | 43 | 0.771 | 1.208 | 0.833 | |
| | | 44 | 2.965 | 2.5 | 1.833 | |
| | | 45 | 2.924 | 1.583 | 2.542 | |
| | | 46 | 34.66 | 6.792 | 8.375 | |
| | | 47 | 4.208 | 2.167 | 3.375 | |
| | | 48 | 44.175 | 8.708 | 7.458 | |
| | | 49 | 15.901 | 6.167 | 4.875 | |
| | | 50 | 11.911 | 3.5 | 4.917 | |
| | | 51 | 6.106 | 3.5 | 3.25 | |
| | | 52 | 17.962 | 5.333 | 5.833 | |
| | | 53 | 2.979 | 2.875 | 1.5 | |
| | | 54 | 2.061 | 1.583 | 2.042 | |
| | | 55 | 36.411 | 7.75 | 8.083 | |
| | | 56 | 151.983 | 13.125 | 17.958 | |
| | | 57 | 3.337 | 2.417 | 2.042 | |
| | | 58 | 19.172 | 7.125 | 4.417 | |
| | | 59 | 4.901 | 2.333 | 2.75 | |
| | | 60 | 98.17 | 13.375 | 10.333 | |
| | | 61 | 44.312 | 7.625 | 8 | |
| | | 62 | 5.382 | 2.375 | 3.167 | |
| | | 63 | 1.068 | 1.042 | 1.333 | |
| | | 64 | 1.542 | 1.208 | 1.917 | |
| | | 65 | 0.84 | 1.292 | 0.917 | |
| | | 66 | 52.316 | 14.875 | 7.125 | |
| | | 67 | 117.974 | 11.417 | 13.542 | |
| | | 68 | 1.076 | 1.208 | 1.333 | |
| | | 69 | 4.082 | 2.083 | 2.542 | |
| | | 70 | 4.198 | 2.375 | 2.667 | |
| | | 71 | 18.472 | 4.292 | 6.333 | |
| | | 72 | 154.734 | 20.792 | 13.833 | |
| | | 73 | 0.703 | 0.875 | 1.208 | |
| | | 74 | 2.99 | 2.292 | 1.542 | |
| | | 75 | 2.302 | 1.583 | 2.042 | |
| | | 76 | 3.562 | 2.583 | 1.958 | |
| | | 77 | 4.74 | 3.125 | 2 | |
| | | 78 | 2.472 | 1.833 | 2.25 | |
| | | 79 | 2.135 | 1.708 | 1.917 | |
| | | 80 | 3.736 | 1.833 | 3.292 | |
| | | 81 | 1.429 | 1.5 | 1.208 | |
| | | 82 | 13.632 | 4.708 | 5.333 | |
| | | 83 | 0.877 | 1 | 1.333 | |
| | | 84 | 10.556 | 3.792 | 3.917 | |
| | | 85 | 4.8 | 2.292 | 3.083 | |
| | | 86 | 103.72 | 10.958 | 13.042 | |
| | | 87 | 19.477 | 4.708 | 5.333 | |

| | | | | | | |
|-----|-------|--------------------------------|-------------|---------|--------|-----|
| | | 88 | 2.165 | 1.917 | 1.792 | |
| | | 89 | 11.314 | 4 | 5.125 | |
| | | 90 | 8.653 | 3.458 | 3.792 | |
| | | 91 | 4.644 | 4 | 1.667 | |
| | | 92 | 11.465 | 4.583 | 4.875 | |
| | | 93 | 17.316 | 4.792 | 5.792 | |
| | | 94 | 1.05 | 1.583 | 1.083 | |
| | | 95 | 11.745 | 3.542 | 5.583 | |
| | | 96 | 7.139 | 3 | 3.292 | |
| | | 97 | 11.898 | 3.292 | 5.667 | |
| | | 98 | 14.431 | 5.625 | 3.417 | |
| | | 99 | 8.283 | 3.875 | 3.125 | |
| | | 100 | 1.005 | 1.292 | 1.208 | |
| | | 101 | 10.095 | 4.042 | 3.125 | |
| | | 102 | 98.118 | 12.167 | 12.333 | |
| | | 103 | 4.667 | 2.25 | 2.875 | |
| | | 104 | 23.705 | 5.792 | 6 | |
| | | 105 | 2.392 | 2.5 | 1.292 | |
| | | 106 | 90.807 | 11.958 | 10.5 | |
| | | 107 | 8.589 | 4.208 | 3.25 | |
| | | 108 | 61.134 | 10.167 | 7.625 | |
| | | 109 | 1.49 | 1.375 | 1.708 | |
| | | 110 | 2.835 | 2.833 | 1.625 | |
| | | 111 | 16.745 | 4.875 | 4.375 | |
| | | sum | 2171.244 | | | |
| | | area covered by lapilli (%) | 25.27347224 | | | |
| 242 | 11189 | 1 | 24.386 | 127.023 | 88.092 | L19 |
| | | 2 | 117.167 | 11.247 | 14.911 | |
| | | 3 | 51.276 | 13.69 | 8.55 | |
| | | 4 | 68.209 | 10.331 | 9.669 | |
| | | 5 | 12.703 | 5.852 | 3.003 | |
| | | 6 | 123.204 | 13.944 | 14.148 | |
| | | 7 | 104.299 | 15.522 | 9.924 | |
| | | 8 | 18.308 | 4.326 | 6.463 | |
| | | 9 | 12.807 | 4.936 | 3.613 | |
| | | 10 | 47.047 | 8.804 | 8.092 | |
| | | 11 | 11.463 | 5.598 | 3.461 | |
| | | 12 | 36.007 | 6.819 | 7.532 | |
| | | 13 | 165.191 | 15.369 | 14.656 | |
| | | 14 | 21.687 | 5.751 | 5.242 | |
| | | 15 | 49.772 | 8.601 | 8.499 | |
| | | 16 | 56.845 | 7.888 | 12.621 | |
| | | 17 | 48.156 | 9.72 | 6.718 | |
| | | 18 | 14.48 | 5.954 | 4.02 | |

| | | | | | | |
|-----|-------|--------------------------------|-------------|---------|--------|-----|
| | | 19 | 12.872 | 4.885 | 4.122 | |
| | | 20 | 2.927 | 1.578 | 2.646 | |
| | | 21 | 141.8 | 12.417 | 15.929 | |
| | | 22 | 40.081 | 5.496 | 10.891 | |
| | | 23 | 25.075 | 6.514 | 5.954 | |
| | | 24 | 16.907 | 5.445 | 5.7 | |
| | | 25 | 11.615 | 5.344 | 3.613 | |
| | | 26 | 93.786 | 7.634 | 14.249 | |
| | | 27 | 12.411 | 5.751 | 3.003 | |
| | | 28 | 29.75 | 4.936 | 7.379 | |
| | | sum | 1370.231 | | | |
| | | area covered by lapilli (%) | 12.24623291 | | | |
| | | | | | | |
| 243 | 13812 | 1 | 271.074 | 142.209 | 97.126 | L19 |
| | | 2 | 6.579 | 3.379 | 2.723 | |
| | | 3 | 8.885 | 3.732 | 3.227 | |
| | | 4 | 116.965 | 15.179 | 11.8 | |
| | | 5 | 30.005 | 9.228 | 6.102 | |
| | | 6 | 1.879 | 1.815 | 1.715 | |
| | | 7 | 1.991 | 1.664 | 1.462 | |
| | | 8 | 20.998 | 5.951 | 5.093 | |
| | | 9 | 22.997 | 8.069 | 4.539 | |
| | | 10 | 1.33 | 1.362 | 1.362 | |
| | | 11 | 0.712 | 1.362 | 0.857 | |
| | | 12 | 2.271 | 2.824 | 1.513 | |
| | | 13 | 148.117 | 18.154 | 14.776 | |
| | | 14 | 1.574 | 1.664 | 1.261 | |
| | | 15 | 10.795 | 4.589 | 4.639 | |
| | | 16 | 59.975 | 9.128 | 9.531 | |
| | | 17 | 1.213 | 1.362 | 1.462 | |
| | | 18 | 14.559 | 4.085 | 6.051 | |
| | | 19 | 2.022 | 2.168 | 1.412 | |
| | | 20 | 23.521 | 5.345 | 6.001 | |
| | | 21 | 0.445 | 0.958 | 0.857 | |
| | | 22 | 41.716 | 7.564 | 8.018 | |
| | | 23 | 11.683 | 4.387 | 4.186 | |
| | | 24 | 1.17 | 1.412 | 1.412 | |
| | | 25 | 2.711 | 1.866 | 2.168 | |
| | | 26 | 45.526 | 9.632 | 7.615 | |
| | | 27 | 11.82 | 3.833 | 4.438 | |
| | | 28 | 111.406 | 15.482 | 11.195 | |
| | | 29 | 1.933 | 1.311 | 1.563 | |
| | | 30 | 19.508 | 5.749 | 5.648 | |
| | | 31 | 15.368 | 6.354 | 4.639 | |
| | | 32 | 20.385 | 6.354 | 5.043 | |

| | | | | | | |
|--|--|----|---------|--------|--------|--|
| | | 33 | 15.96 | 3.53 | 6.556 | |
| | | 34 | 63.716 | 12.355 | 12.758 | |
| | | 35 | 2.08 | 2.017 | 1.765 | |
| | | 36 | 1.828 | 1.462 | 2.118 | |
| | | 37 | 86.181 | 14.876 | 16.087 | |
| | | 38 | 12.199 | 3.883 | 3.984 | |
| | | 39 | 3.064 | 1.967 | 2.471 | |
| | | 40 | 32.06 | 6.001 | 7.564 | |
| | | 41 | 1.973 | 2.118 | 1.362 | |
| | | 42 | 21.303 | 6.657 | 5.043 | |
| | | 43 | 77.553 | 8.321 | 15.885 | |
| | | 44 | 5.951 | 2.421 | 3.681 | |
| | | 45 | 3.115 | 2.068 | 2.269 | |
| | | 46 | 0.778 | 1.059 | 1.059 | |
| | | 47 | 3.487 | 2.521 | 2.017 | |
| | | 48 | 6.289 | 2.37 | 3.833 | |
| | | 49 | 8.557 | 3.026 | 4.942 | |
| | | 50 | 23.605 | 8.321 | 4.589 | |
| | | 51 | 68.82 | 9.43 | 10.842 | |
| | | 52 | 480.201 | 21.836 | 38.477 | |
| | | 53 | 86.957 | 9.632 | 11.8 | |
| | | 54 | 6.264 | 3.127 | 2.572 | |
| | | 55 | 2.904 | 2.168 | 2.219 | |
| | | 56 | 75.094 | 9.027 | 15.431 | |
| | | 57 | 81.372 | 10.893 | 14.523 | |
| | | 58 | 18.447 | 6.404 | 5.144 | |
| | | 59 | 5.401 | 2.521 | 3.076 | |
| | | 60 | 4.814 | 2.572 | 3.177 | |
| | | 61 | 7.103 | 2.925 | 3.227 | |
| | | 62 | 4.501 | 2.673 | 2.168 | |
| | | 63 | 4.544 | 1.967 | 3.127 | |
| | | 64 | 2.523 | 2.521 | 1.462 | |
| | | 65 | 8.873 | 4.337 | 2.874 | |
| | | 66 | 39.702 | 8.169 | 8.926 | |
| | | 67 | 7.164 | 4.942 | 2.622 | |
| | | 68 | 12.293 | 3.833 | 5.144 | |
| | | 69 | 12.985 | 5.194 | 4.186 | |
| | | 70 | 240.783 | 16.793 | 19.213 | |
| | | 71 | 64.703 | 11.699 | 7.968 | |
| | | 72 | 47.552 | 7.363 | 9.632 | |
| | | 73 | 27.035 | 7.816 | 4.74 | |
| | | 74 | 0.926 | 1.765 | 0.958 | |
| | | 75 | 1.274 | 1.362 | 1.362 | |
| | | 76 | 2.566 | 1.462 | 2.32 | |
| | | 77 | 43.644 | 7.766 | 8.069 | |

| | | | | | | |
|--|--|-----|--------|--------|-------|--|
| | | 78 | 9.824 | 4.085 | 3.984 | |
| | | 79 | 47.255 | 7.01 | 9.178 | |
| | | 80 | 8.334 | 3.53 | 4.387 | |
| | | 81 | 12.522 | 4.186 | 4.841 | |
| | | 82 | 11.423 | 5.648 | 3.127 | |
| | | 83 | 3.624 | 2.269 | 2.32 | |
| | | 84 | 8.166 | 3.631 | 3.48 | |
| | | 85 | 2.235 | 1.916 | 1.765 | |
| | | 86 | 1.121 | 1.261 | 1.715 | |
| | | 87 | 1.292 | 1.462 | 1.311 | |
| | | 88 | 36.91 | 9.279 | 7.11 | |
| | | 89 | 30.28 | 8.825 | 5.799 | |
| | | 90 | 2.116 | 1.462 | 1.916 | |
| | | 91 | 5.47 | 3.984 | 2.32 | |
| | | 92 | 7.571 | 2.521 | 4.085 | |
| | | 93 | 18.374 | 7.11 | 4.438 | |
| | | 94 | 5.76 | 2.723 | 3.328 | |
| | | 95 | 5.198 | 3.631 | 2.572 | |
| | | 96 | 9.453 | 4.034 | 2.975 | |
| | | 97 | 79.218 | 13.868 | 8.825 | |
| | | 98 | 5.625 | 3.429 | 2.521 | |
| | | 99 | 15.551 | 5.345 | 4.387 | |
| | | 100 | 36.447 | 6.858 | 7.816 | |
| | | 101 | 13.501 | 5.093 | 3.58 | |
| | | 102 | 28.281 | 6.354 | 6.909 | |
| | | 103 | 66.775 | 10.59 | 9.329 | |
| | | 104 | 10.134 | 4.892 | 2.975 | |
| | | 105 | 39.239 | 8.119 | 7.564 | |
| | | 106 | 23.058 | 5.245 | 6.404 | |
| | | 107 | 16.41 | 4.539 | 5.598 | |
| | | 108 | 13.949 | 5.396 | 4.337 | |
| | | 109 | 16.273 | 6.203 | 3.681 | |
| | | 110 | 9.544 | 3.379 | 3.933 | |
| | | 111 | 61.794 | 10.136 | 8.169 | |
| | | 112 | 3.148 | 1.765 | 2.421 | |
| | | 113 | 57.267 | 9.884 | 9.934 | |
| | | 114 | 3.413 | 2.219 | 2.572 | |
| | | 115 | 4.527 | 2.572 | 2.572 | |
| | | 116 | 36.35 | 5.951 | 9.329 | |
| | | 117 | 33.962 | 8.119 | 6.657 | |
| | | 118 | 9.806 | 3.933 | 3.227 | |
| | | 119 | 3.011 | 2.521 | 1.614 | |
| | | 120 | 9.852 | 5.245 | 3.026 | |
| | | 121 | 4.539 | 2.421 | 2.723 | |
| | | 122 | 15.757 | 5.093 | 5.043 | |

| | | | | | | |
|--|--|-----------------------------|-------------|--------|--------|--|
| | | 123 | 97.999 | 13.162 | 10.439 | |
| | | 124 | 5.638 | 2.673 | 2.975 | |
| | | 125 | 51.169 | 8.926 | 9.38 | |
| | | 126 | 29.644 | 7.867 | 5.295 | |
| | | 127 | 30.186 | 7.514 | 8.27 | |
| | | 128 | 23.765 | 5.799 | 5.698 | |
| | | 129 | 16.563 | 6.051 | 4.438 | |
| | | 130 | 7.077 | 2.774 | 3.782 | |
| | | sum | 3865.677 | | | |
| | | area covered by lapilli (%) | 27.98781494 | | | |

Table A2.1. Measurements of the lapilli impacted into the conduit walls.

| Location | Unit | Lithofacies | Clast size (mm) | |
|----------|------|-------------|-----------------|-----|
| | | | X | Y |
| L9 | 1 | mLA | 230 | 115 |
| L9 | 1 | mLA | 108 | 50 |
| L9 | 1 | mLA | 85 | 80 |
| L9 | 1 | mLA | 330 | 160 |
| L9 | 1 | mLA | 155 | 90 |
| L9 | 1 | mLA | 100 | 30 |
| L9 | 1 | mLA | 104 | 34 |
| L9 | 1 | mLA | 75 | 54 |
| L9 | 1 | mLA | 89 | 62 |
| L9 | 1 | mLA | 131 | 110 |
| L9 | 1 | mLA | 84 | 50 |
| L9 | 1 | mLA | 95 | 70 |
| L9 | 1 | mLA | 120 | 40 |
| L9 | 1 | mLA | 130 | 75 |
| L9 | 1 | mLA | 145 | 80 |
| L9 | 1 | mLA | 120 | 109 |
| L9 | 1 | mLA | 107 | 70 |
| L9 | 1 | mLA | 140 | 60 |
| L9 | 1 | mLA | 225 | 55 |
| L9 | 1 | mLA | 108 | 55 |
| L9 | 1 | mLA | 89 | 86 |
| L9 | 1 | mLA | 69 | 26 |
| L9 | 1 | mLA | 95 | 39 |
| L9 | 1 | mLA | 84 | 44 |
| L9 | 1 | mLA | 55 | 49 |
| L9 | 1 | mLA | 126 | 70 |
| L9 | 1 | mLA | 310 | 180 |
| L9 | 1 | mLA | 110 | 85 |
| L9 | 1 | mLA | 65 | 45 |
| L9 | 1 | mLA | 310 | 180 |

| | | | | |
|-----|---|--------|------|-----|
| L9 | 2 | lensLA | 100 | 20 |
| L9 | 2 | lensLA | 70 | 30 |
| L9 | 2 | lensLA | 49 | 10 |
| L9 | 2 | lensLA | 43 | 34 |
| L9 | 2 | lensLA | 82 | 24 |
| L9 | 2 | lensLA | 42 | 40 |
| L9 | 2 | lensLA | 50 | 21 |
| L9 | 2 | lensLA | 75 | 70 |
| L9 | 2 | lensLA | 30 | 25 |
| L9 | 2 | lensLA | 35 | 11 |
| L9 | 3 | xsLA | 145 | 55 |
| L9 | 3 | xsLA | 210 | 100 |
| L9 | 3 | xsLA | 79 | 50 |
| L9 | 3 | xsLA | 42 | 33 |
| L9 | 3 | xsLA | 96 | 26 |
| L9 | 3 | xsLA | 42 | 24 |
| L9 | 3 | xsLA | 22 | 21 |
| L9 | 3 | xsLA | 21 | 20 |
| L9 | 3 | xsLA | 35 | 23 |
| L9 | 3 | xsLA | 42 | 20 |
| L9 | 4 | //bSp | 527 | 58 |
| L9 | 4 | //bSp | 1280 | 46 |
| L9 | 4 | //bSp | 1763 | 36 |
| L9 | 4 | //bSp | 2544 | 54 |
| L9 | 4 | //bSp | 3149 | 22 |
| L9 | 4 | //bSp | 668 | 53 |
| L9 | 4 | //bSp | 1352 | 40 |
| L9 | 4 | //bSp | 2424 | 25 |
| L9 | 4 | //bSp | 3516 | 22 |
| L15 | 1 | (n)LA | 110 | 85 |
| L15 | 1 | (n)LA | 220 | 70 |
| L15 | 1 | (n)LA | 135 | 50 |
| L15 | 1 | (n)LA | 80 | 30 |
| L15 | 1 | (n)LA | 90 | 50 |
| L15 | 1 | (n)LA | 65 | 58 |
| L15 | 1 | (n)LA | 100 | 85 |
| L15 | 1 | (n)LA | 60 | 40 |
| L15 | 1 | (n)LA | 80 | 70 |
| L15 | 1 | (n)LA | 160 | 50 |
| L15 | 2 | xsLA | 100 | 80 |
| L15 | 2 | xsLA | 54 | 40 |
| L15 | 2 | xsLA | 290 | 110 |
| L15 | 2 | xsLA | 180 | 70 |
| L15 | 2 | xsLA | 80 | 60 |
| L15 | 2 | xsLA | 40 | 20 |

| | | | | |
|-----|---|--------|-----|-----|
| L15 | 2 | xsLA | 60 | 55 |
| L15 | 2 | xsLA | 60 | 30 |
| L15 | 2 | xsLA | 60 | 30 |
| L15 | 2 | xsLA | 74 | 54 |
| L15 | 3 | (m)LA | 160 | 50 |
| L15 | 3 | (m)LA | 140 | 55 |
| L15 | 3 | (m)LA | 48 | 27 |
| L15 | 3 | (m)LA | 44 | 30 |
| L15 | 3 | (m)LA | 55 | 35 |
| L15 | 3 | (m)LA | 70 | 45 |
| L15 | 3 | (m)LA | 80 | 30 |
| L15 | 3 | (m)LA | 40 | 30 |
| L15 | 3 | (m)LA | 42 | 30 |
| L15 | 3 | (m)LA | 35 | 28 |
| L14 | 1 | mLA | 144 | 133 |
| L14 | 1 | mLA | 84 | 30 |
| L14 | 1 | mLA | 82 | 35 |
| L14 | 1 | mLA | 70 | 50 |
| L14 | 1 | mLA | 130 | 35 |
| L14 | 1 | mLA | 55 | 35 |
| L14 | 1 | mLA | 85 | 26 |
| L14 | 1 | mLA | 67 | 55 |
| L14 | 1 | mLA | 36 | 24 |
| L14 | 1 | mLA | 165 | 35 |
| L14 | 2 | lensLA | 14 | 11 |
| L14 | 2 | lensLA | 27 | 10 |
| L14 | 2 | lensLA | 12 | 10 |
| L14 | 2 | lensLA | 21 | 15 |
| L14 | 2 | lensLA | 54 | 41 |
| L14 | 2 | lensLA | 90 | 34 |
| L14 | 2 | lensLA | 55 | 14 |
| L14 | 2 | lensLA | 30 | 27 |
| L14 | 2 | lensLA | 79 | 30 |
| L14 | 2 | lensLA | 50 | 41 |
| L14 | 3 | (n)LA | 440 | 160 |
| L14 | 3 | (n)LA | 78 | 40 |
| L14 | 3 | (n)LA | 290 | 120 |
| L14 | 3 | (n)LA | 200 | 85 |
| L14 | 3 | (n)LA | 160 | 120 |
| L14 | 3 | (n)LA | 100 | 75 |
| L14 | 3 | (n)LA | 100 | 60 |
| L14 | 3 | (n)LA | 95 | 30 |
| L14 | 3 | (n)LA | 65 | 40 |
| L14 | 3 | (n)LA | 65 | 40 |
| L14 | 4 | xsLA | 38 | 15 |

| | | | | |
|-----|---|----------|-----|-----|
| L14 | 4 | xsLA | 33 | 20 |
| L14 | 4 | xsLA | 40 | 40 |
| L14 | 4 | xsLA | 83 | 25 |
| L14 | 4 | xsLA | 55 | 55 |
| L14 | 4 | xsLA | 32 | 19 |
| L14 | 4 | xsLA | 36 | 26 |
| L14 | 4 | xsLA | 33 | 24 |
| L14 | 4 | xsLA | 22 | 20 |
| L14 | 4 | xsLA | 43 | 25 |
| L14 | 5 | (n)LA(f) | 160 | 90 |
| L14 | 5 | (n)LA(f) | 130 | 115 |
| L14 | 5 | (n)LA(f) | 260 | 160 |
| L14 | 5 | (n)LA(f) | 300 | 80 |
| L14 | 5 | (n)LA(f) | 150 | 50 |
| L14 | 5 | (n)LA(f) | 100 | 60 |
| L14 | 5 | (n)LA(f) | 140 | 120 |
| L14 | 5 | (n)LA(f) | 105 | 70 |
| L14 | 5 | (n)LA(f) | 135 | 80 |
| L14 | 5 | (n)LA(f) | 140 | 65 |
| L10 | 1 | (m)LA(f) | 85 | 65 |
| L10 | 1 | (m)LA(f) | 60 | 55 |
| L10 | 1 | (m)LA(f) | 89 | 60 |
| L10 | 1 | (m)LA(f) | 148 | 40 |
| L10 | 1 | (m)LA(f) | 195 | 25 |
| L10 | 1 | (m)LA(f) | 100 | 60 |
| L10 | 1 | (m)LA(f) | 55 | 41 |
| L10 | 1 | (m)LA(f) | 80 | 70 |
| L10 | 1 | (m)LA(f) | 70 | 30 |
| L10 | 1 | (m)LA(f) | 80 | 60 |
| L8 | 1 | lensLA | 36 | 27 |
| L8 | 1 | lensLA | 30 | 12 |
| L8 | 1 | lensLA | 24 | 14 |
| L8 | 1 | lensLA | 29 | 6 |
| L8 | 1 | lensLA | 54 | 22 |
| L8 | 1 | lensLA | 35 | 16 |
| L8 | 1 | lensLA | 33 | 12 |
| L8 | 1 | lensLA | 100 | 36 |
| L8 | 1 | lensLA | 79 | 32 |
| L8 | 1 | lensLA | 101 | 35 |
| L8 | 2 | (n)LA | 210 | 200 |
| L8 | 2 | (n)LA | 260 | 40 |
| L8 | 2 | (n)LA | 170 | 55 |
| L8 | 2 | (n)LA | 130 | 50 |
| L8 | 2 | (n)LA | 59 | 49 |
| L8 | 2 | (n)LA | 42 | 35 |

| | | | | |
|----|---|-------|-----|-----|
| L8 | 2 | (n)LA | 85 | 29 |
| L8 | 2 | (n)LA | 34 | 31 |
| L8 | 2 | (n)LA | 175 | 75 |
| L8 | 2 | (n)LA | 130 | 60 |
| L4 | 1 | (n)LA | 480 | 130 |
| L4 | 1 | (n)LA | 185 | 95 |
| L4 | 1 | (n)LA | 165 | 55 |
| L4 | 1 | (n)LA | 200 | 130 |
| L4 | 1 | (n)LA | 295 | 180 |
| L4 | 1 | (n)LA | 187 | 130 |
| L4 | 1 | (n)LA | 230 | 120 |
| L4 | 1 | (n)LA | 195 | 97 |
| L4 | 1 | (n)LA | 170 | 60 |
| L4 | 1 | (n)LA | 170 | 110 |
| L4 | 2 | (n)LA | 130 | 36 |
| L4 | 2 | (n)LA | 80 | 34 |
| L4 | 2 | (n)LA | 48 | 28 |
| L4 | 2 | (n)LA | 280 | 170 |
| L4 | 2 | (n)LA | 54 | 11 |
| L4 | 2 | (n)LA | 39 | 25 |
| L4 | 2 | (n)LA | 33 | 20 |
| L4 | 2 | (n)LA | 105 | 30 |
| L4 | 2 | (n)LA | 54 | 19 |
| L4 | 2 | (n)LA | 50 | 21 |
| L3 | 1 | mLA | 119 | 69 |
| L3 | 1 | mLA | 100 | 70 |
| L3 | 1 | mLA | 198 | 70 |
| L3 | 1 | mLA | 81 | 60 |
| L3 | 1 | mLA | 105 | 33 |
| L3 | 1 | mLA | 86 | 79 |
| L3 | 1 | mLA | 90 | 76 |
| L3 | 1 | mLA | 85 | 53 |
| L3 | 1 | mLA | 142 | 105 |
| L3 | 1 | mLA | 89 | 40 |
| L3 | 2 | mLA | 276 | 170 |
| L3 | 2 | mLA | 215 | 100 |
| L3 | 2 | mLA | 145 | 125 |
| L3 | 2 | mLA | 120 | 97 |
| L3 | 2 | mLA | 155 | 70 |
| L3 | 2 | mLA | 170 | 140 |
| L3 | 2 | mLA | 115 | 60 |
| L3 | 2 | mLA | 100 | 95 |
| L3 | 2 | mLA | 89 | 66 |
| L3 | 2 | mLA | 66 | 39 |
| L5 | 1 | mLA | 125 | 50 |

| | | | | |
|-----|---|-------|-----|-----|
| L5 | 1 | mLA | 120 | 50 |
| L5 | 1 | mLA | 155 | 40 |
| L5 | 1 | mLA | 87 | 46 |
| L5 | 1 | mLA | 78 | 55 |
| L5 | 1 | mLA | 65 | 60 |
| L5 | 1 | mLA | 85 | 60 |
| L5 | 1 | mLA | 75 | 45 |
| L5 | 1 | mLA | 61 | 25 |
| L5 | 1 | mLA | 240 | 100 |
| L5 | 2 | mLA | 420 | 84 |
| L5 | 2 | mLA | 105 | 76 |
| L5 | 2 | mLA | 80 | 40 |
| L5 | 2 | mLA | 150 | 50 |
| L5 | 2 | mLA | 127 | 57 |
| L5 | 2 | mLA | 200 | 130 |
| L5 | 2 | mLA | 170 | 55 |
| L5 | 2 | mLA | 100 | 60 |
| L5 | 2 | mLA | 119 | 70 |
| L5 | 2 | mLA | 175 | 55 |
| L7 | 1 | //bSp | - | - |
| L11 | 1 | //bSp | - | - |
| L21 | 1 | mLA | - | - |

Table A2.2. Measurements of juvenile clast sizes and lithofacies type.

| Location | Unit | Unit thickness (m) | Av max clast size (mm) | Silicic volcanic ash abundance % |
|----------|------|--------------------|------------------------|----------------------------------|
| L9 | 1 | 1 | 140.7 | 20 |
| L9 | 1 | 1 | 127.4 | 20 |
| L9 | 1 | 1.1 | 131.3 | 20 |
| L9 | 2 | 1.2 | 57.6 | 85 |
| L9 | 3 | 1 | 73.4 | 25 |
| L9 | 4 | 3.3 | 1913 | 8 |
| L15 | 1 | 0.35 | 110 | 60 |
| L15 | 2 | 0.2 | 99.8 | 55 |
| L15 | 3 | 0.2 | 71.4 | 50 |
| L14 | 1 | 0.6 | 91.8 | 45 |
| L14 | 2 | 0.55 | 43.2 | 27 |
| L14 | 3 | 0.4 | 159.3 | 75 |
| L14 | 4 | 0.6 | 41.5 | 20 |
| L14 | 5 | 0.75 | 162 | 60 |
| L10 | 1 | 1.3 | 104 | 60 |
| L8 | 1 | 1 | 52.1 | 55 |
| L8 | 2 | 0.8 | 129.5 | 75 |
| L4 | 1 | 1 | 227 | 60 |
| L4 | 2 | 1.1 | 87.3 | 60 |

| | | | | |
|--|---|------|-------|----|
| L3 | 1 | 1 | 109.5 | 60 |
| L3 | 2 | 1.25 | 145.1 | 75 |
| L5 | 1 | 1 | 109.1 | 60 |
| L5 | 2 | 1.25 | 164.6 | 75 |
| L11 | 1 | 1.1 | 3.25 | <5 |
| L7 | 1 | 3.2 | 1.1 | 10 |
| L21 | 1 | 0.5 | 0.5 | 70 |
| Table A2.3. Summary of unit thickness, average maximum clast size and Silicic volcanic ash abundance. | | | | |

| Location | Cooling joint spacing in host lava flow (mm) | | | | | Mean |
|--|--|-----|-----|-----|-----|-------|
| L16 | 250 | 85 | 170 | 70 | 150 | 150.3 |
| | 240 | 130 | 180 | 120 | 155 | |
| | 170 | 120 | 230 | 100 | 170 | |
| | 170 | 150 | 100 | 100 | 140 | |
| | 200 | 190 | 210 | 90 | 150 | |
| | 160 | 80 | 160 | 120 | | |
| L19 | 140 | 210 | 200 | | | 189.5 |
| | 125 | 270 | | | | |
| | 250 | 190 | | | | |
| | 260 | 150 | | | | |
| | 150 | 140 | | | | |
| Table A2.4. Spacing of cooling joints in host lava flows. | | | | | | |

| Location | photo | facies | %juvenile | mean juvenile abun | location | photo | facies | %juvenile | mean juvenile abund |
|---|-------|--------|-----------|-----------------------|----------|-------|--------|-----------|---------------------|
| L3 | 367 | mLA | 59 | | L14 | 47 | lensLA | 17 | |
| | 366 | | 54 | | | 47 | | 45 | |
| | 365 | | 65 | | | 48 | | 27 | |
| | 364 | | 65 | | | 48 | | 45 | |
| | 363 | | 67 | | | 49 | | 50 | |
| | 362 | | 75 | | | 49 | | 40 | |
| | 361 | | 72 | | | 50 | | 11 | |
| | 360 | | 64 | | | 50 | | 26 | |
| | 359 | | 73 | | | 51 | | 2 | |
| | 358 | | 49 | | | 51 | | 21 | |
| | 357 | | 69 | | | 52 | | 4 | |
| | 356 | | 68 | | | 52 | | 12 | |
| | 355 | | 71 | 65 | | 53 | | 24 | |
| L5 | 398 | mLA | 58 | | | 53 | | 11 | |
| | 398 | | 58 | | | 54 | | 42 | |
| | 399 | | 79 | | | 54 | | 21 | |
| | 399 | | 78 | | | 55 | | 0 | |
| | 400 | | 82 | | | 55 | | 0 | 22 |
| | 400 | | 79 | | wp191 L3 | 285 | | 82 | |
| | 401 | | 73 | | | 285 | | 69 | |
| | 401 | | 78 | | | 286 | | 75 | |
| | 402 | | 64 | | | 286 | | 74 | |
| | 402 | | 74 | | | 287 | | 80 | |
| | 403 | | 63 | | | 287 | | 75 | |
| | 403 | | 67 | | | 288 | | 67 | |
| | 404 | | 63 | | | 288 | | 65 | |
| | 404 | | 69 | | | 289 | | 86 | |
| | 405 | | 68 | | | 289 | | 78 | |
| | 405 | | 73 | | | 290 | | 79 | |
| | 406 | | 71 | | | 290 | | 76 | |
| | 406 | | 81 | | | 291 | | 72 | |
| | 407 | | 84 | | | 291 | | 72 | |
| | 407 | | 76 | 71.9 | | 292 | | 64 | |
| | | | | | | 292 | | 63 | |
| | | | | | | 293 | | 65 | |
| | | | | | | 293 | | 68 | |
| | | | | | | 294 | | 69 | |
| | | | | | | 294 | | 71 | |
| | | | | | | 295 | | 85 | |
| | | | | | | 295 | | 80 | 73 |
| Table A2.5. Juvenile abundance calculated using IJ. | | | | | | | | | |

| Sample | Rock name | Date | Mineral | Count | % |
|---------------|---------------------|--------|----------------------|-------|------|
| WP199 PR40 | Spatter | 09-May | Tachylite | 334 | 66.8 |
| | | | Microlite | 59 | 11.8 |
| | | | Plag phenocryst | 10 | 2 |
| | | | Pyroxene phenocryst | 5 | 1 |
| | | | Palagonite | 46 | 9.2 |
| | | | Vesicle | 42 | 8.4 |
| | | | Silicic volcanic ash | 4 | 0.8 |
| Total Glass % | | | | | 83.7 |
| WP199 PR015 | Sideromelane clasts | 09-May | Sideromelane | 256 | 64.1 |
| | | | Microlite | 78 | 19.5 |
| | | | Plag phenocryst | 14 | 3.5 |
| | | | Pyroxene phenocryst | 0 | 0 |
| | | | Palagonite | 27 | 6.7 |
| | | | Vesicle | 24 | 6.0 |
| Total Glass % | | | | | 70.0 |
| WP199 PR41.2 | Ventricular bomb | 09-May | Sideromelane | 11 | 2.3 |
| | | | Microlite | 101 | 21.9 |
| | | | Plag phenocryst | 23 | 5 |
| | | | Pyroxene phenocryst | 0 | 0 |
| | | | Palagonite | 70 | 15.2 |
| | | | Vesicle | 1 | 0.2 |
| | | | Tachylite | 254 | 55.2 |
| Total Glass % | | | | | 72.8 |
| WP198 PR003.1 | spatter | 09-May | Sideromelane | 6 | 1.2 |
| | | | Microlite | 78 | 15.6 |
| | | | Plag phenocryst | 7 | 1.4 |
| | | | Pyroxene phenocryst | 4 | 0.8 |
| | | | Palagonite | 17 | 3.4 |
| | | | Vesicle | 52 | 10.4 |
| | | | Tachylite | 336 | 67.2 |
| Total Glass % | | | | | 71.8 |
| WP203 PR35 | lava | 09-May | Sideromelane | | 0 |
| | | | Microlite | 132 | 63.4 |
| | | | Plag phenocryst | 5 | 2.4 |
| | | | Pyroxene phenocryst | 11 | 5.2 |
| | | | Palagonite | 2 | 0.9 |
| | | | Vesicle | 0 | 0 |
| | | | Tachylite | 58 | 27.8 |
| Total Glass % | | | | | 28.8 |

| | | | | | |
|---------------|---------------------|--------|---------------------|-----|-------|
| WP199 PR41.1 | Ventricular bomb | 09-May | Sideromelane | 26 | 5.1 |
| | | | Microlite | 92 | 18.3 |
| | | | Plag phenocryst | 12 | 2.3 |
| | | | Pyroxene phenocryst | 7 | 1.3 |
| | | | Palagonite | 84 | 16.7 |
| | | | Vesicle | 1 | 0.1 |
| | | | Tachylite | 280 | 55.7 |
| Total Glass % | | | | | 77.6 |
| WP198 PR003.2 | Spatter | 09-May | Sideromelane | 0 | 0 |
| | | | Microlite | 116 | 23.2 |
| | | | Plag phenocryst | 18 | 3.6 |
| | | | Pyroxene phenocryst | 1 | 0.2 |
| | | | Palagonite | 14 | 2.8 |
| | | | Vesicle | 58 | 11.6 |
| | | | Tachylite | 293 | 58.6 |
| Total Glass % | | | | | 61.4 |
| WP190PR002.1 | Cored bomb | 09-May | Sideromelane | | 0 |
| | | | Microlite | 37 | 7.4 |
| | | | Plag phenocryst | 9 | 1.8 |
| | | | Pyroxene phenocryst | | 0 |
| | | | Palagonite | 30 | 6.0 |
| | | | Vesicle | 211 | 42.2 |
| | | | Tachylite | 212 | 42.4 |
| Total Glass % | | | | | 48.49 |
| WP204 PR005 | sideromelane clasts | 09-May | Sideromelane | 80 | 56.3 |
| | | | Microlite | 24 | 16.9 |
| | | | Plag phenocryst | 2 | 1.4 |
| | | | Pyroxene phenocryst | 3 | 2.1 |
| | | | Palagonite | 30 | 21.1 |
| | | | Vesicle | 3 | 2.1 |
| | | | Tachylite | 0 | 0 |
| Total Glass % | | | | | 77.4 |
| WP199 pr018 | sideromelane clasts | 09-May | Sideromelane | 228 | 59.5 |
| | | | Microlite | 76 | 19.8 |
| | | | Plag phenocryst | 19 | 4.9 |
| | | | Pyroxene phenocryst | 2 | 0.5 |
| | | | Palagonite | 30 | 7.8 |
| | | | Vesicle | 28 | 7.3 |
| | | | Tachylite | 0 | 0 |

| | | | | | |
|--|--------------|--------|---------------------|-----|------|
| Total Glass % | | | | | 67.3 |
| WP196 PR43 | Conduit wall | 09-May | Sideromelane | 0 | 0 |
| | | | Microlite | 145 | 29 |
| | | | Plag phenocryst | 17 | 3.4 |
| | | | Pyroxene phenocryst | 0 | 0 |
| | | | Palagonite | 24 | 4.8 |
| | | | Vesicle | 25 | 5 |
| | | | Tachylite | 289 | 57.8 |
| Total Glass % | | | | | 62.6 |
| WP190 PR002 | Lapilli | 09-May | Sideromelane | 0 | 0 |
| | | | Microlite | 18 | 6 |
| | | | Plag phenocryst | 6 | 2 |
| | | | Pyroxene phenocryst | 1 | 0.3 |
| | | | Palagonite | 2 | 0.6 |
| | | | Vesicle | 118 | 39.3 |
| | | | Tachylite | 155 | 51.6 |
| Total Glass % | | | | | 52.3 |
| Table A2.6. Point count measurements of pyroclasts. Glass content corrected for vesicles and Silicic volcanic ash. Point counts conducted at 20X mag. | | | | | |

| Image name | Clast size (mm) | | aspect ratio | Image name | Clast size (mm) | | aspect ratio |
|----------------------------|-----------------|-------|--------------|--------------------------|-----------------|------|--------------|
| | X | Y | | | X | Y | |
| wp 199 pr018 matrix fabric | 0.7 | 0.6 | 0.85714286 | wp204 pr 05 droplets | 0.55 | 0.23 | 0.41818182 |
| wp 199 pr018 matrix fabric | 2.3 | 1.6 | 0.69565217 | wp204 pr 05 droplets | 0.32 | 0.14 | 0.4375 |
| wp 199 pr018 matrix fabric | 1.9 | 1.3 | 0.68421053 | wp204 pr 05 pele | 0.84 | 0.07 | 0.08333333 |
| wp 199 pr018 matrix fabric | 1.5 | 1.6 | 1.06666667 | wp204 pr 05 pele1 | 1.56 | 0.21 | 0.13461538 |
| wp 199 pr018 matrix fabric | 2.2 | 0.5 | 0.22727273 | wp204 pr 05 pele1 | 0.16 | 0.08 | 0.5 |
| wp 199 pr018 matrix fabric | 0.3 | 0.1 | 0.33333333 | wp204 pr 05 quench edit | 0.38 | 0.18 | 0.47368421 |
| wp 199 pr018 matrix fabric | 0.4 | 0.3 | 0.75 | wp204 pr 05 quench edit | 0.99 | 0.47 | 0.47474747 |
| wp 199 pr018 matrix fabric | 1 | 0.4 | 0.4 | wp204 pr 05 quench edit | 2.3 | 1 | 0.43478261 |
| wp 199 pr018 matrix fabric | 0.17 | 0.1 | 0.58823529 | wp204 pr 05 quench edit | 0.9 | 0.8 | 0.88888889 |
| WP199 PR018 horiz fabric | 2.32 | 1.15 | 0.49568966 | wp204 pr 05 quench edit | 1 | 0.98 | 0.98 |
| WP199 PR018 horiz fabric | 0.95 | 0.53 | 0.55789474 | wp204 pr 05 quench edit | 0.32 | 0.2 | 0.625 |
| WP199 PR018 horiz fabric | 0.77 | 0.51 | 0.66233766 | wp204 pr 05 quench edit | 0.76 | 0.19 | 0.25 |
| WP199 PR018 horiz fabric | 0.26 | 0.06 | 0.23076923 | wp204 pr 05 quench edit | 1.34 | 0.64 | 0.47761194 |
| WP199 PR018 horiz fabric | 0.88 | 0.72 | 0.81818182 | wp204 pr 05 quench edit | 0.52 | 0.12 | 0.23076923 |
| WP199 PR018 horiz fabric | 0.38 | 0.12 | 0.31578947 | wp204 pr 05 quench edit | 0.28 | 0.09 | 0.32142857 |
| WP199 PR018 horiz fabric | 1.84 | 0.42 | 0.22826087 | wp204 pr 05 quench edit | 0.43 | 0.11 | 0.25581395 |
| WP199 PR018 horiz fabric | 1.64 | 0.86 | 0.52439024 | wp204 pr 05 quench edit | 1.13 | 0.55 | 0.48672566 |
| WP199 PR018 horiz fabric | 1.51 | 1 | 0.66225166 | wp204 pr 05 type edit | 3.52 | 1.97 | 0.55965909 |
| WP199 PR018 horiz fabric | 0.94 | 0.45 | 0.4787234 | wp204 pr 05 type edit | 2.03 | 0.73 | 0.35960591 |
| WP199 PR018 horiz fabric | 1.38 | 0.51 | 0.36956522 | wp204 pr 05 type edit | 0.34 | 0.28 | 0.82352941 |
| WP199 PR018 horiz fabric | 0.79 | 0.4 | 0.50632911 | wp204 pr 05 type edit | 0.25 | 0.17 | 0.68 |
| WP199 PR018 horiz fabric | 1.01 | 1.42 | 1.40594059 | wp204 pr 05 type edit | 0.63 | 0.16 | 0.25396825 |
| WP199 PR018 horiz fabric | 0.36 | 0.13 | 0.36111111 | wp204 pr 05 type edit | 0.72 | 0.4 | 0.55555556 |
| WP199 PR018 horiz fabric | 0.48 | 0.26 | 0.54166667 | wp204 pr005 ductile defm | 0.52 | 0.35 | 0.67307692 |
| WP199 PR018 horiz fabric | 0.38 | 0.19 | 0.5 | wp204 pr005 ductile defm | 0.13 | 0.08 | 0.61538462 |
| WP199 PR018 horiz fabric | 0.17 | 0.12 | 0.70588235 | wp204 pr005 elon | 0.86 | 0.38 | 0.44186047 |
| WP199 PR018 horiz fabric | 0.09 | 0.06 | 0.66666667 | wp204 pr005 mixed clasts | 0.49 | 0.06 | 0.12244898 |
| WP199 PR018 horiz fabric | 0.23 | 0.07 | 0.30434783 | wp204 pr005 mixed clasts | 0.48 | 0.14 | 0.29166667 |
| WP199 PR018 horiz fabric | 0.29 | 0.14 | 0.48275862 | wp204 pr005 mixed clasts | 0.39 | 0.1 | 0.25641026 |
| WP199 PR018 horiz fabric | 0.2 | 0.13 | 0.65 | wp204 pr005 mixed clasts | 0.34 | 0.44 | 1.29411765 |
| WP199 PR018 horiz fabric | 0.22 | 0.11 | 0.5 | wp204 pr005 mixed clasts | 0.31 | 0.16 | 0.51612903 |
| WP199 PR018 horiz fabric | 0.09 | 0.12 | 1.33333333 | WP190 PR02.1 | 1.39 | 0.93 | 0.66906475 |
| WP199 PR018 horiz fabric | 0.37 | 0.1 | 0.27027027 | WP190 PR02.1 | 0.36 | 0.11 | 0.30555556 |
| WP199 PR018 horiz fabric | 0.14 | 0.04 | 0.28571429 | WP190 PR02.1 | 0.43 | 0.14 | 0.3255814 |
| WP199 PR018 various shapes | 2.39 | 0.76 | 0.31799163 | WP204 005.4 | 4.37 | 1.53 | 0.35011442 |
| WP199 PR018 various shapes | 1.07 | 0.55 | 0.51401869 | WP204 005.4 | 0.067 | 0.17 | 2.53731343 |
| WP199 PR018 various shapes | 0.67 | 0.037 | 0.05522388 | WP204 005.4 | 1.74 | 0.31 | 0.17816092 |
| WP199 PR018 various shapes | 0.38 | 0.24 | 0.63157895 | WP204 005.4 | 1.61 | 0.28 | 0.17391304 |
| WP199 PR018 various shapes | 0.52 | 0.3 | 0.57692308 | WP204 005.4 | 0.46 | 0.38 | 0.82608696 |
| WP199 PR018 various shapes | 1.39 | 0.69 | 0.49640288 | WP204 005.4 | 0.37 | 0.2 | 0.54054054 |
| WP199 PR018 various shapes | 0.18 | 0.05 | 0.27777778 | WP204 005.4 | 0.067 | 0.31 | 4.62686567 |
| WP199 PR018 ves clast | 4.6 | 3.61 | 0.78478261 | WP204 005.4 | 0.43 | 0.1 | 0.23255814 |
| WP199 PR018 ves clast | 0.65 | 0.41 | 0.63076923 | WP204 005.6 | 0.27 | 0.13 | 0.48148148 |

| | | | | | | | |
|------------------------------|----------|----------|------------|-------------|------|------|------------|
| WP199 PR018 ves clast | 0.11 | 0.11 | 1 | WP204 005.6 | 1 | 0.3 | 0.3 |
| wp199 pr18 curvi edit | 3.2 | 1.35 | 0.421875 | WP204 005.6 | 3.43 | 0.36 | 0.10495627 |
| wp199 pr18 curvi edit | 0.38 | 0.3 | 0.78947368 | WP204 005.6 | 2.88 | 0.79 | 0.27430556 |
| wp199 pr18 curvi edit | 0.39 | 0.18 | 0.46153846 | | | | |
| wp199 pr18 curvi edit | 0.96 | 0.85 | 0.88541667 | | | | |
| wp199 pr18 curvi edit | 0.54 | 0.53 | 0.98148148 | | | | |
| wp199 pr18 curvi edit | 0.66 | 0.19 | 0.28787879 | | | | |
| wp199 pr18 curvi1 | 0.92 | 0.91 | 0.98913043 | | | | |
| wp199 pr18 curvi1 | 0.85 | 5 | 5.88235294 | | | | |
| wp199 pr18 curvi1 | 0.38 | 0.1 | 0.26315789 | | | | |
| wp199 pr18 curvi1 | 1.11 | 0.83 | 0.74774775 | | | | |
| wp199 pr18 curvi1 | 1.19 | 0.65 | 0.54621849 | | | | |
| wp199 pr18 curvi1 | 0.85 | 0.21 | 0.24705882 | | | | |
| wp199 pr18 curvi1 | 0.44 | 0.21 | 0.47727273 | | | | |
| wp199 pr18 curvi1 | 1.01 | 0.61 | 0.6039604 | | | | |
| wp199 pr18 curvi1 | 0.25 | 0.2 | 0.8 | | | | |
| wp199 pr18 curvi1 | 0.59 | 0.14 | 0.23728814 | | | | |
| wp199 pr18 curvi1 | 0.19 | 0.1 | 0.52631579 | | | | |
| wp199 pr18 curvi1 | 0.36 | 0.11 | 0.30555556 | | | | |
| clast type mean dimension | 0.932125 | 0.553148 | | | | | |
| | 0.80135 | 0.2095 | | | | | |
| clast type abundance (%) | 82.40741 | | | | | | |
| | 18.69159 | | | | | | |
| clast type mean aspect ratio | 0.593427 | | | | | | |
| | 0.261434 | | | | | | |

Table A2.7. Image analysis measurements of sideromelane ash.

| Location | UTM Coordinates |
|--|-----------------|
| Leitin rootless cones | 500000/7097014 |
| Búrfell rootless cones | 402187/7098548 |
| Pomeroy quarry | 544082/5094205 |
| Lava flow toward west of study area | 615513/5095129 |
| L18 | 615474/5095128 |
| L19 | 615489/5095128 |
| L20 | 577432/5094533 |
| L21 | 577432/5094533 |
| L22 | 577432/5094533 |
| L23 | 577430/5094530 |
| L17 | 639775/5126889 |
| L16 | 639845/5126787 |
| L1 | 639915/5126782 |
| L2 | 639936/5126738 |
| L12 | 640183/5126432 |
| L4 | 640008/5126657 |
| L3 | 640004/5126656 |
| L5 | 640006/5126598 |
| L7 | 639998/5126562 |
| L8 | 640059/5126568 |
| L9 | 640057/5126519 |
| L11 | 640058/5126570 |
| L6 | 640116/5126496 |
| L10 | 640138/5126486 |
| L13 | 640173/5126454 |
| L14 | 640175/5126447 |
| L15 | 640183/5126433 |
| Table A2.8. UTM coordinates of study locations. | |

| | weight (g) | size (μm) | % contribution to Silicic volcanic ash | Φ | cumulative wt % |
|---|---------------|---------------------------|---|--------------|--------------------|
| Silicic volcanic ash | 0.0004 | 500 | 0.007355916 | 1 | 0.0004 |
| | 1.6593 | 250 | 30.51417853 | 2 | 1.6597 |
| | 1.8935 | 125 | 34.82106734 | 3 | 3.5532 |
| | 1.157 | 63 | 21.27698702 | 4 | 4.7102 |
| | 0.7276 | <63 | 13.3804112 | 5.0115 88 | 5.4378 |
| whole sample weight | 6.0387 | | | | |
| juvenile weight | 0.6009 | | | | |
| Table A2.9. Sorting of Silicic volcanic ash calculated by sieving. | | | | | |

| image | clast dimension (mm) | | location | image | clast dimension (mm) | | location |
|-------|----------------------|----|----------|-------|----------------------|----|----------|
| | x | y | | | x | y | |
| 248 | 93 | 87 | L20 | 47 | 37 | 22 | L23 |
| 246 | 17 | 10 | L20 | 47 | 35 | 15 | L23 |
| 246 | 16 | 11 | L20 | 47 | 54 | 40 | L23 |
| 245 | 11 | 8 | L20 | 49 | 43 | 23 | L23 |
| 245 | 16 | 12 | L20 | 158 | 16 | 15 | L6 |
| 244 | 23 | 11 | L20 | 158 | 14 | 5 | L6 |
| 244 | 15 | 13 | L20 | 159 | 37 | 22 | L6 |
| 243 | 25 | 17 | L20 | 159 | 44 | 37 | L6 |
| 242 | 16 | 13 | L20 | 160 | 17 | 14 | L6 |
| 242 | 14 | 12 | L20 | 160 | 16 | 10 | L6 |
| 297 | 38 | 19 | L19 | 161 | 15 | 12 | L6 |
| 297 | 35 | 26 | L19 | 161 | 15 | 12 | L6 |
| 298 | 32 | 40 | L19 | 161 | 14 | 10 | L6 |
| 298 | 26 | 21 | L19 | 161 | 15 | 12 | L6 |
| 299 | 26 | 18 | L19 | 162 | 13 | 6 | L6 |
| 299 | 33 | 35 | L19 | 192 | 212 | 94 | L16 |
| 300 | 32 | 16 | L19 | 192 | 230 | 85 | L16 |
| 300 | 16 | 15 | L19 | 192 | 240 | 96 | L16 |
| 301 | 79 | 35 | L19 | 193 | 116 | 54 | L16 |
| 301 | 17 | 16 | L19 | 193 | 150 | 77 | L16 |
| 41 | 11 | 7 | L23 | 194 | 170 | 54 | L16 |
| 41 | 12 | 10 | L23 | 194 | 71 | 30 | L16 |
| 45 | 93 | 52 | L23 | 195 | 197 | 28 | L16 |
| 45 | 71 | 42 | L23 | 195 | 185 | 17 | L16 |

Table A2.10. Measurements of largest clasts in lithofacies mSp.

| Weight of clast in air | | | Weight of clast and sheet in water | | | Ws water | Wc water | SG | Density |
|------------------------|--------|-------|------------------------------------|------------------|----------|----------------------|--------------------|------|----------|
| dry uncoated | coated | wet | clast wet | sheet dry weight | sheet % | sheet wet weight (g) | clast wet no sheet | | |
| 13.2 | 13.41 | 7.71 | 7.71 | 0.21 | 1.565996 | 0.120738 | 7.589261745 | 2.35 | 2352.632 |
| 12.15 | 12.44 | 7.41 | 7.41 | 0.29 | 2.33119 | 0.172741 | 7.237258842 | 2.47 | 2473.161 |
| 15.91 | 16.2 | 8.57 | 8.57 | 0.29 | 1.790123 | 0.153414 | 8.41658642 | 2.12 | 2123.198 |
| 18.68 | 19.04 | 11.05 | 11.05 | 0.36 | 1.890756 | 0.208929 | 10.84107143 | 2.38 | 2382.979 |
| 15.24 | 15.58 | 9.34 | 9.34 | 0.34 | 2.182285 | 0.203825 | 9.136174583 | 2.5 | 2496.795 |
| 11.04 | 11.31 | 6.63 | 6.63 | 0.27 | 2.387268 | 0.158276 | 6.471724138 | 2.42 | 2416.667 |
| 8.43 | 8.66 | 4.77 | 4.77 | 0.23 | 2.655889 | 0.126686 | 4.643314088 | 2.23 | 2226.221 |
| 21.5 | 21.98 | 12.55 | 12.55 | 0.48 | 2.183803 | 0.274067 | 12.27593267 | 2.33 | 2330.859 |
| 18.5 | 18.85 | 11.03 | 11.03 | 0.35 | 1.856764 | 0.204801 | 10.82519894 | 2.41 | 2410.486 |
| 16.22 | 16.69 | 10.03 | 10.03 | 0.47 | 2.816058 | 0.282451 | 9.747549431 | 2.51 | 2506.006 |
| 22.3 | 22.62 | 13.48 | 13.48 | 0.32 | 1.414677 | 0.190698 | 13.2893015 | 2.47 | 2474.836 |
| 15.47 | 15.84 | 8.89 | 8.89 | 0.37 | 2.335859 | 0.207658 | 8.682342172 | 2.28 | 2279.137 |
| 13.16 | 13.59 | 7.93 | 7.93 | 0.43 | 3.164091 | 0.250912 | 7.679087564 | 2.4 | 2401.06 |
| 17.31 | 17.71 | 10.12 | 10.12 | 0.4 | 2.258611 | 0.228571 | 9.891428571 | 2.33 | 2333.333 |
| 9.64 | 9.7 | 5 | 5 | 0.06 | 0.618557 | 0.030928 | 4.969072165 | 2.06 | 2063.83 |
| 17.77 | 18.13 | 10.36 | 10.36 | 0.36 | 1.985659 | 0.205714 | 10.15428571 | 2.33 | 2333.333 |
| 14.07 | 14.28 | 7.91 | 7.91 | 0.21 | 1.470588 | 0.116324 | 7.793676471 | 2.24 | 2241.758 |
| 19.22 | 19.64 | 10.89 | 10.89 | 0.42 | 2.138493 | 0.232882 | 10.65711813 | 2.24 | 2244.571 |
| 14.54 | 14.92 | 8.41 | 8.41 | 0.38 | 2.546917 | 0.214196 | 8.19580429 | 2.29 | 2291.859 |
| 15.01 | 15.15 | 8.79 | 8.79 | 0.14 | 0.924092 | 0.081228 | 8.708772277 | 2.38 | 2382.075 |
| 17.24 | 17.75 | 8.83 | 8.83 | 0.51 | 2.873239 | 0.253707 | 8.576292958 | 1.99 | 1989.91 |
| 20.02 | 20.33 | 11.92 | 11.92 | 0.31 | 1.52484 | 0.181761 | 11.73823906 | 2.42 | 2417.36 |
| 5.28 | 5.51 | 3.11 | 3.11 | 0.23 | 4.174229 | 0.129819 | 2.980181488 | 2.3 | 2295.833 |
| 10.38 | 10.64 | 6.3 | 6.3 | 0.26 | 2.443609 | 0.153947 | 6.146052632 | 2.45 | 2451.613 |
| 8.97 | 9.25 | 4.62 | 4.62 | 0.28 | 3.027027 | 0.139849 | 4.480151351 | 2 | 1997.84 |
| 18.01 | 18.32 | 10.54 | 10.54 | 0.31 | 1.69214 | 0.178352 | 10.36164847 | 2.35 | 2354.756 |
| 19.56 | 19.83 | 11.42 | 11.42 | 0.27 | 1.361573 | 0.155492 | 11.26450832 | 2.36 | 2357.907 |
| 13.45 | 13.76 | 8.32 | 8.32 | 0.31 | 2.252907 | 0.187442 | 8.13255814 | 2.53 | 2529.412 |
| 18.25 | 18.37 | 9.87 | 9.87 | 0.12 | 0.653239 | 0.064475 | 9.805525313 | 2.16 | 2161.176 |
| 11.69 | 12.03 | 6.09 | 6.09 | 0.34 | 2.826268 | 0.17212 | 5.917880299 | 2.03 | 2025.253 |
| 13.23 | 13.57 | 7.61 | 7.61 | 0.34 | 2.505527 | 0.190671 | 7.419329403 | 2.28 | 2276.846 |
| 14.28 | 14.54 | 8.57 | 8.57 | 0.26 | 1.788171 | 0.153246 | 8.416753783 | 2.44 | 2435.511 |
| 20.31 | 20.72 | 11.71 | 11.71 | 0.41 | 1.978764 | 0.231713 | 11.47828668 | 2.3 | 2299.667 |
| 23.86 | 24.27 | 14.43 | 14.43 | 0.41 | 1.689328 | 0.24377 | 14.18622991 | 2.47 | 2466.463 |
| 10.63 | 10.95 | 6.43 | 6.43 | 0.32 | 2.922374 | 0.187909 | 6.242091324 | 2.42 | 2422.566 |
| 14.08 | 14.52 | 7.09 | 7.09 | 0.44 | 3.030303 | 0.214848 | 6.875151515 | 1.95 | 1954.24 |
| 15.32 | 15.66 | 9.12 | 9.12 | 0.34 | 2.171137 | 0.198008 | 8.921992337 | 2.39 | 2394.495 |
| 14.21 | 14.49 | 7.08 | 7.08 | 0.28 | 1.932367 | 0.136812 | 6.943188406 | 1.96 | 1955.466 |
| 24.05 | 24.51 | 13.72 | 13.72 | 0.46 | 1.876785 | 0.257495 | 13.4625051 | 2.27 | 2271.548 |
| 23.92 | 24.32 | 14.37 | 14.37 | 0.4 | 1.644737 | 0.236349 | 14.13365132 | 2.44 | 2444.221 |
| 13.86 | 14.27 | 7.8 | 7.8 | 0.41 | 2.87316 | 0.224107 | 7.575893483 | 2.21 | 2205.564 |
| 6.65 | 6.87 | 3.27 | 3.27 | 0.22 | 3.202329 | 0.104716 | 3.165283843 | 1.91 | 1908.333 |
| 8.4 | 8.64 | 5.15 | 5.15 | 0.24 | 2.777778 | 0.143056 | 5.006944444 | 2.48 | 2475.645 |

| | | | | | | | | | |
|-------|-------|-------|-------|------|----------|----------|-------------|------|----------|
| 15.21 | 15.51 | 8.92 | 8.92 | 0.3 | 1.934236 | 0.172534 | 8.747466151 | 2.35 | 2353.566 |
| 10.73 | 11.05 | 5.9 | 5.9 | 0.32 | 2.895928 | 0.17086 | 5.729140271 | 2.15 | 2145.631 |
| 17.28 | 17.66 | 9.84 | 9.84 | 0.38 | 2.151755 | 0.211733 | 9.628267271 | 2.26 | 2258.312 |
| 8.2 | 8.48 | 4.71 | 4.71 | 0.28 | 3.301887 | 0.155519 | 4.554481132 | 2.25 | 2249.337 |
| 13.47 | 13.75 | 6.25 | 6.25 | 0.28 | 2.036364 | 0.127273 | 6.122727273 | 1.83 | 1833.333 |
| 17.91 | 18.31 | 9.92 | 9.92 | 0.4 | 2.184599 | 0.216712 | 9.703287821 | 2.18 | 2182.36 |
| 20.06 | 20.47 | 11.94 | 11.94 | 0.41 | 2.002931 | 0.23915 | 11.70085002 | 2.4 | 2399.766 |
| 13.81 | 14.15 | 8.24 | 8.24 | 0.34 | 2.402827 | 0.197993 | 8.042007067 | 2.39 | 2394.247 |
| 13.57 | 13.91 | 7.42 | 7.42 | 0.34 | 2.444285 | 0.181366 | 7.238634076 | 2.14 | 2143.297 |
| 16.97 | 17.31 | 9.81 | 9.81 | 0.34 | 1.964183 | 0.192686 | 9.617313692 | 2.31 | 2308 |
| 10.67 | 10.97 | 6.44 | 6.44 | 0.3 | 2.734731 | 0.176117 | 6.263883318 | 2.42 | 2421.634 |
| 18.35 | 18.56 | 10.88 | 10.88 | 0.21 | 1.131466 | 0.123103 | 10.75689655 | 2.42 | 2416.667 |
| 10.74 | 10.98 | 5.62 | 5.62 | 0.24 | 2.185792 | 0.122842 | 5.49715847 | 2.05 | 2048.507 |
| 13.9 | 14.3 | 5.45 | 5.45 | 0.4 | 2.797203 | 0.152448 | 5.297552448 | 1.62 | 1615.819 |
| 6.81 | 7.22 | 4.09 | 4.09 | 0.41 | 5.67867 | 0.232258 | 3.857742382 | 2.31 | 2306.709 |
| 5.96 | 6.24 | 3.36 | 3.36 | 0.28 | 4.487179 | 0.150769 | 3.209230769 | 2.17 | 2166.667 |
| 16.69 | 17.06 | 9.48 | 9.48 | 0.37 | 2.168816 | 0.205604 | 9.274396249 | 2.25 | 2250.66 |
| 20.83 | 21.23 | 11.87 | 11.87 | 0.4 | 1.884126 | 0.223646 | 11.64635422 | 2.27 | 2268.162 |
| 11.39 | 11.65 | 4.95 | 4.95 | 0.26 | 2.23176 | 0.110472 | 4.839527897 | 1.74 | 1738.806 |
| 9.21 | 9.32 | 5.19 | 5.19 | 0.11 | 1.180258 | 0.061255 | 5.128744635 | 2.26 | 2256.659 |
| 9.41 | 9.94 | 5.35 | 5.35 | 0.53 | 5.331992 | 0.285262 | 5.064738431 | 2.17 | 2165.577 |
| 6.63 | 6.74 | 3.95 | 3.95 | 0.11 | 1.632047 | 0.064466 | 3.885534125 | 2.42 | 2415.771 |
| 13.23 | 13.52 | 7.89 | 7.89 | 0.29 | 2.14497 | 0.169238 | 7.720761834 | 2.4 | 2401.421 |
| 11.74 | 12.03 | 5.47 | 5.47 | 0.29 | 2.41064 | 0.131862 | 5.338137988 | 1.83 | 1833.841 |
| 24.62 | 24.97 | 13.58 | 13.58 | 0.35 | 1.401682 | 0.190348 | 13.38965158 | 2.19 | 2192.274 |
| 20.39 | 20.77 | 11.24 | 11.24 | 0.38 | 1.829562 | 0.205643 | 11.03435725 | 2.18 | 2179.433 |
| 11.01 | 11.34 | 6.7 | 6.7 | 0.33 | 2.910053 | 0.194974 | 6.505026455 | 2.44 | 2443.966 |
| 15.49 | 15.79 | 9.39 | 9.39 | 0.3 | 1.899937 | 0.178404 | 9.211595947 | 2.47 | 2467.188 |
| 15.58 | 15.64 | 9.32 | 9.32 | 0.06 | 0.383632 | 0.035754 | 9.284245524 | 2.47 | 2474.684 |
| 17.79 | 18.18 | 10.82 | 10.82 | 0.39 | 2.145215 | 0.232112 | 10.58788779 | 2.47 | 2470.109 |
| 11.22 | 11.48 | 5.55 | 5.55 | 0.26 | 2.264808 | 0.125697 | 5.424303136 | 1.94 | 1935.919 |
| 13.6 | 14.16 | 8.17 | 8.17 | 0.56 | 3.954802 | 0.323107 | 7.846892655 | 2.36 | 2363.94 |
| 22 | 22.32 | 12.23 | 12.23 | 0.32 | 1.433692 | 0.175341 | 12.0546595 | 2.21 | 2212.091 |
| 7.11 | 7.49 | 4.49 | 4.49 | 0.38 | 5.073431 | 0.227797 | 4.262202937 | 2.5 | 2496.667 |
| 6.71 | 6.99 | 2.34 | 2.34 | 0.28 | 4.005722 | 0.093734 | 2.246266094 | 1.5 | 1503.226 |
| 15.08 | 15.35 | 8.84 | 8.84 | 0.27 | 1.758958 | 0.155492 | 8.684508143 | 2.36 | 2357.911 |
| 15.36 | 15.7 | 8.84 | 8.84 | 0.34 | 2.165605 | 0.191439 | 8.64856051 | 2.29 | 2288.63 |
| 7.81 | 8.03 | 2.98 | 2.98 | 0.22 | 2.739726 | 0.081644 | 2.898356164 | 1.59 | 1590.099 |
| 6.41 | 6.67 | 2.68 | 2.68 | 0.26 | 3.898051 | 0.104468 | 2.575532234 | 1.67 | 1671.679 |
| 16.36 | 16.73 | 9.49 | 9.49 | 0.37 | 2.211596 | 0.20988 | 9.280119546 | 2.31 | 2310.773 |
| 6.03 | 6.27 | 3.33 | 3.33 | 0.24 | 3.827751 | 0.127464 | 3.202535885 | 2.13 | 2132.653 |
| 15.26 | 15.61 | 8.3 | 8.3 | 0.35 | 2.242152 | 0.186099 | 8.113901345 | 2.14 | 2135.431 |
| 11.43 | 11.78 | 6.64 | 6.64 | 0.35 | 2.971138 | 0.197284 | 6.442716469 | 2.29 | 2291.829 |
| 15.1 | 15.5 | 9.24 | 9.24 | 0.4 | 2.580645 | 0.238452 | 9.001548387 | 2.48 | 2476.038 |
| 9.06 | 9.34 | 5.64 | 5.64 | 0.28 | 2.997859 | 0.169079 | 5.470920771 | 2.52 | 2524.324 |

| | | | | | | | | | |
|--|--------------|--------------|------|------|----------|----------|-------------|------|----------|
| 11.57 | 11.91 | 7.19 | 7.19 | 0.34 | 2.854744 | 0.205256 | 6.984743913 | 2.52 | 2523.305 |
| 15.36 | 15.7 | 7.91 | 7.91 | 0.34 | 2.165605 | 0.171299 | 7.738700637 | 2.02 | 2015.404 |
| density range | density mean | vesicularity | | | | | | | |
| | | | | | | | | | |
| 1503 | 2249.87492 | 16.67129927 | | | | | | | |
| 2529 | | | | | | | | | |
| Table A2.11. Density measurements for the Ice Harbor lava core. Weight is in g, density in kg m ⁻³ , vesicularity in %. | | | | | | | | | |

| Weight of clast in air | | | Weight of clast and sheet in water | | | Ws water | Wc water | SG | Density |
|------------------------|--------|-------|------------------------------------|------------------|----------|----------------------|--------------------|-------------|-------------|
| dry uncoated | coated | wet | clast wet | sheet dry weight | sheet % | sheet wet weight (g) | clast wet no sheet | | |
| 17.24 | 17.72 | 9.49 | 9.49 | 0.48 | 2.708804 | 0.257065463 | 9.23 | 2.15309842 | 2153.09842 |
| 9.1 | 9.55 | 4.43 | 4.43 | 0.45 | 4.712042 | 0.208743455 | 4.22 | 1.865234375 | 1865.234375 |
| 9.79 | 10.1 | 5.55 | 5.55 | 0.31 | 3.069307 | 0.170346535 | 5.38 | 2.21978022 | 2219.78022 |
| 10.33 | 10.69 | 4.37 | 4.37 | 0.36 | 3.367633 | 0.147165575 | 4.22 | 1.691455696 | 1691.455696 |
| 9.99 | 10.31 | 4.59 | 4.59 | 0.32 | 3.103783 | 0.142463628 | 4.45 | 1.802447552 | 1802.447552 |
| 14.25 | 14.66 | 7.69 | 7.69 | 0.41 | 2.796726 | 0.215068213 | 7.47 | 2.103299857 | 2103.299857 |
| 21.84 | 22.45 | 12.76 | 12.76 | 0.61 | 2.717149 | 0.346708241 | 12.4 | 2.316821465 | 2316.821465 |
| 8.84 | 9.26 | 5.18 | 5.18 | 0.42 | 4.535637 | 0.234946004 | 4.95 | 2.269607843 | 2269.607843 |
| 17.29 | 17.8 | 9.89 | 9.89 | 0.51 | 2.865169 | 0.283365169 | 9.61 | 2.250316056 | 2250.316056 |
| 9.25 | 9.63 | 4.15 | 4.15 | 0.38 | 3.946002 | 0.163759086 | 3.99 | 1.75729927 | 1757.29927 |
| 6.78 | 7.16 | 1.95 | 1.95 | 0.38 | 5.307263 | 0.10349162 | 1.85 | 1.37428023 | 1374.28023 |
| 10.46 | 11.05 | 4.98 | 4.98 | 0.59 | 5.339367 | 0.265900452 | 4.71 | 1.820428336 | 1820.428336 |
| 9.83 | 10.31 | 5.4 | 5.4 | 0.48 | 4.655674 | 0.251406402 | 5.15 | 2.099796334 | 2099.796334 |
| 10.69 | 11.11 | 6.55 | 6.55 | 0.42 | 3.780378 | 0.247614761 | 6.3 | 2.436403509 | 2436.403509 |
| 10.32 | 10.6 | 6.24 | 6.24 | 0.28 | 2.641509 | 0.164830189 | 6.08 | 2.431192661 | 2431.192661 |
| 15.25 | 15.69 | 9.22 | 9.22 | 0.44 | 2.804334 | 0.258559592 | 8.96 | 2.42503864 | 2425.03864 |
| 14.51 | 14.97 | 6.35 | 6.35 | 0.46 | 3.072812 | 0.19512358 | 6.15 | 1.736658933 | 1736.658933 |
| 20.72 | 21.28 | 12.51 | 12.51 | 0.56 | 2.631579 | 0.329210526 | 12.2 | 2.42645382 | 2426.45382 |
| 6.26 | 6.63 | 4.18 | 4.18 | 0.37 | 5.580694 | 0.233273002 | 3.95 | 2.706122449 | 2706.122449 |
| 16.46 | 16.97 | 10.35 | 10.35 | 0.51 | 3.005303 | 0.31104891 | 10 | 2.563444109 | 2563.444109 |
| 16.56 | 17.1 | 9.05 | 9.05 | 0.54 | 3.157895 | 0.285789474 | 8.76 | 2.124223602 | 2124.223602 |
| 14.24 | 14.85 | 8.11 | 8.11 | 0.61 | 4.107744 | 0.333138047 | 7.78 | 2.203264095 | 2203.264095 |
| 8.16 | 8.53 | 4.89 | 4.89 | 0.37 | 4.337632 | 0.212110199 | 4.68 | 2.343406593 | 2343.406593 |
| 11.88 | 12.39 | 7.13 | 7.13 | 0.51 | 4.116223 | 0.293486683 | 6.84 | 2.355513308 | 2355.513308 |
| 13.36 | 13.86 | 8.5 | 8.5 | 0.5 | 3.607504 | 0.306637807 | 8.19 | 2.585820896 | 2585.820896 |
| 9.98 | 10.37 | 6.87 | 6.87 | 0.39 | 3.760849 | 0.258370299 | 6.61 | 2.962857143 | 2962.857143 |
| 12.5 | 13.04 | 5.66 | 5.66 | 0.54 | 4.141104 | 0.234386503 | 5.43 | 1.766937669 | 1766.937669 |
| 22.68 | 23.27 | 12.66 | 12.66 | 0.59 | 2.535453 | 0.320988397 | 12.3 | 2.193213949 | 2193.213949 |
| 8.55 | 8.8 | 4.01 | 4.01 | 0.25 | 2.840909 | 0.113920455 | 3.9 | 1.837160752 | 1837.160752 |
| 13.61 | 14.12 | 7.17 | 7.17 | 0.51 | 3.611898 | 0.258973088 | 6.91 | 2.031654676 | 2031.654676 |
| 20.73 | 21.15 | 10.61 | 10.61 | 0.42 | 1.985816 | 0.210695035 | 10.4 | 2.006641366 | 2006.641366 |
| 15.52 | 16.02 | 9.08 | 9.08 | 0.5 | 3.121099 | 0.283395755 | 8.8 | 2.308357349 | 2308.357349 |
| 12.08 | 12.6 | 6.81 | 6.81 | 0.52 | 4.126984 | 0.281047619 | 6.53 | 2.176165803 | 2176.165803 |
| 5.87 | 6.17 | 4.02 | 4.02 | 0.3 | 4.862237 | 0.195461912 | 3.82 | 2.869767442 | 2869.767442 |
| 8.01 | 8.6 | 4.84 | 4.84 | 0.59 | 6.860465 | 0.332046512 | 4.51 | 2.287234043 | 2287.234043 |

| | | | | | | | | | |
|-------|-------|-------|-------|-------|----------|--------------|------|-------------|-------------|
| 7.97 | 8.42 | 4.61 | 4.61 | 0.45 | 5.344418 | 0.246377672 | 4.36 | 2.209973753 | 2209.973753 |
| 5.96 | 6.44 | 4.21 | 4.21 | 0.48 | 7.453416 | 0.31378882 | 3.9 | 2.887892377 | 2887.892377 |
| 4.85 | 5.15 | 3.14 | 3.14 | 0.3 | 5.825243 | 0.182912621 | 2.96 | 2.562189055 | 2562.189055 |
| 6.66 | 7.14 | 4.56 | 4.56 | 0.48 | 6.722689 | 0.306554622 | 4.25 | 2.76744186 | 2767.44186 |
| 5.95 | 6.27 | 3.83 | 3.83 | 0.32 | 5.103668 | 0.195470494 | 3.63 | 2.569672131 | 2569.672131 |
| 10.4 | 10.8 | 6.79 | 6.79 | 0.4 | 3.703704 | 0.251481481 | 6.54 | 2.693266833 | 2693.266833 |
| 6.76 | 7.07 | 2.6 | 2.6 | 0.31 | 4.384724 | 0.114002829 | 2.49 | 1.581655481 | 1581.655481 |
| 10 | 10.5 | 5.81 | 5.81 | 0.5 | 4.761905 | 0.276666667 | 5.53 | 2.23880597 | 2238.80597 |
| 10.7 | 11.07 | 7.31 | 7.31 | 0.37 | 3.342367 | 0.24432701 | 7.07 | 2.944148936 | 2944.148936 |
| 15.75 | 16.07 | 9.73 | 9.73 | 0.32 | 1.991288 | 0.193752334 | 9.54 | 2.534700315 | 2534.700315 |
| 15.99 | 16.5 | 9.67 | 9.67 | 0.51 | 3.090909 | 0.298890909 | 9.37 | 2.415812592 | 2415.812592 |
| 13.39 | 13.73 | 8.36 | 8.36 | 0.34 | 2.476329 | 0.207021122 | 8.15 | 2.55679702 | 2556.79702 |
| 13.15 | 13.64 | 6.7 | 6.7 | 0.49 | 3.592375 | 0.24068915 | 6.46 | 1.965417867 | 1965.417867 |
| 16.48 | 16.91 | 10.39 | 10.39 | 0.43 | 2.542874 | 0.264204613 | 10.1 | 2.593558282 | 2593.558282 |
| 5.86 | 6.24 | 3.02 | 3.02 | 0.38 | 6.089744 | 0.183910256 | 2.84 | 1.937888199 | 1937.888199 |
| 6.6 | 6.89 | 4.16 | 4.16 | 0.29 | 4.208999 | 0.17509434 | 3.98 | 2.523809524 | 2523.809524 |
| 10.99 | 11.56 | 6.84 | 6.84 | 0.57 | 4.930796 | 0.337266436 | 6.5 | 2.449152542 | 2449.152542 |
| 10.86 | 11.47 | 6.85 | 6.85 | 0.61 | 5.318221 | 0.364298169 | 6.49 | 2.482683983 | 2482.683983 |
| 24.36 | 24.95 | 13.93 | 13.93 | 0.59 | 2.364729 | 0.329406814 | 13.6 | 2.264065336 | 2264.065336 |
| 9.46 | 9.92 | 5.03 | 5.03 | 0.46 | 4.637097 | 0.233245968 | 4.8 | 2.028629857 | 2028.629857 |
| 14.29 | 14.95 | 7.8 | 7.8 | 0.66 | 4.414716 | 0.344347826 | 7.46 | 2.090909091 | 2090.909091 |
| 7.44 | 7.89 | 3.6 | 3.6 | 0.45 | 5.703422 | 0.205323194 | 3.39 | 1.839160839 | 1839.160839 |
| 4.1 | 4.27 | 2.51 | 2.51 | 0.17 | 3.981265 | 0.099929742 | 2.41 | 2.426136364 | 2426.136364 |
| 6.75 | 7.12 | 3.85 | 3.85 | 0.37 | 5.196629 | 0.200070225 | 3.65 | 2.177370031 | 2177.370031 |
| 18.88 | 19.34 | 11.17 | 11.17 | 0.46 | 2.37849 | 0.265677353 | 10.9 | 2.367197062 | 2367.197062 |
| 6.78 | 7.06 | 2.63 | 2.63 | 0.28 | 3.966006 | 0.104305949 | 2.53 | 1.593679458 | 1593.679458 |
| 7.17 | 7.48 | 3.52 | 3.52 | 0.31 | 4.144385 | 0.145882353 | 3.37 | 1.888888889 | 1888.888889 |
| 7.48 | 7.81 | 2.81 | 2.81 | 0.33 | 4.225352 | 0.118732394 | 2.69 | 1.562 | 1562 |
| 11.1 | 11.54 | 5.81 | 5.81 | 0.44 | 3.812825 | 0.22152513 | 5.59 | 2.013961606 | 2013.961606 |
| 15.21 | 15.7 | 7.27 | 7.27 | 0.49 | 3.121019 | 0.226898089 | 7.04 | 1.862396204 | 1862.396204 |
| 11.87 | 12.32 | 6.27 | 6.27 | 0.45 | 3.652597 | 0.229017857 | 6.04 | 2.036363636 | 2036.363636 |
| 11.85 | 12.35 | 7.86 | 7.86 | 0.5 | 4.048583 | 0.318218623 | 7.54 | 2.750556793 | 2750.556793 |
| 8.85 | 9.23 | 3.63 | 3.63 | 0.38 | 4.11701 | 0.149447454 | 3.48 | 1.648214286 | 1648.214286 |
| 6.51 | 6.84 | 2.19 | 2.19 | 0.33 | 4.824561 | 0.105657895 | 2.08 | 1.470967742 | 1470.967742 |
| 8.28 | 8.61 | 5.54 | 5.54 | 0.33 | 3.832753 | 0.212334495 | 5.33 | 2.804560261 | 2804.560261 |
| 15 | 15.33 | 8.91 | 8.91 | 0.33 | 2.152642 | 0.191800391 | 8.72 | 2.387850467 | 2387.850467 |
| 8.4 | 8.17 | 5.1 | 5.1 | -0.23 | -2.81518 | -0.143574051 | 5.24 | 2.661237785 | 2661.237785 |
| 6.56 | 6.91 | 2.04 | 2.04 | 0.35 | 5.065123 | 0.103328509 | 1.94 | 1.41889117 | 1418.89117 |
| 11.42 | 11.67 | 5.9 | 5.9 | 0.25 | 2.142245 | 0.126392459 | 5.77 | 2.022530329 | 2022.530329 |
| 13.4 | 13.67 | 7.8 | 7.8 | 0.27 | 1.975128 | 0.154059985 | 7.65 | 2.32879046 | 2328.79046 |
| 5.51 | 5.85 | 3.25 | 3.25 | 0.34 | 5.811966 | 0.188888889 | 3.06 | 2.25 | 2250 |
| 12.21 | 12.61 | 6.89 | 6.89 | 0.4 | 3.172086 | 0.218556701 | 6.67 | 2.204545455 | 2204.545455 |
| 8.32 | 8.78 | 2.69 | 2.69 | 0.46 | 5.23918 | 0.140933941 | 2.55 | 1.441707718 | 1441.707718 |
| 6 | 6.13 | 2.68 | 2.68 | 0.13 | 2.120718 | 0.056835237 | 2.62 | 1.776811594 | 1776.811594 |
| 10.84 | 11.19 | 5.43 | 5.43 | 0.35 | 3.127793 | 0.169839142 | 5.26 | 1.942708333 | 1942.708333 |

| | | | | | | | | | |
|---------------|--------------|--------------|------|------|----------|-------------|------|-------------|-------------|
| 11.74 | 12.14 | 4.9 | 4.9 | 0.4 | 3.294893 | 0.161449753 | 4.74 | 1.67679558 | 1676.79558 |
| 4.84 | 5.22 | 2.14 | 2.14 | 0.38 | 7.279693 | 0.155785441 | 1.98 | 1.694805195 | 1694.805195 |
| 7.08 | 7.5 | 4.22 | 4.22 | 0.42 | 5.6 | 0.23632 | 3.98 | 2.286585366 | 2286.585366 |
| 6.02 | 6.31 | 3.88 | 3.88 | 0.29 | 4.59588 | 0.178320127 | 3.7 | 2.596707819 | 2596.707819 |
| 4.46 | 4.74 | 2.06 | 2.06 | 0.28 | 5.907173 | 0.121687764 | 1.94 | 1.768656716 | 1768.656716 |
| 7.96 | 8.27 | 4.71 | 4.71 | 0.31 | 3.748489 | 0.176553809 | 4.53 | 2.323033708 | 2323.033708 |
| 7.65 | 7.94 | 4.36 | 4.36 | 0.29 | 3.652393 | 0.159244332 | 4.2 | 2.217877095 | 2217.877095 |
| 5.25 | 5.48 | 2.34 | 2.34 | 0.23 | 4.19708 | 0.098211679 | 2.24 | 1.74522293 | 1745.22293 |
| 8.04 | 8.43 | 4.48 | 4.48 | 0.39 | 4.626335 | 0.207259786 | 4.27 | 2.134177215 | 2134.177215 |
| 8.84 | 9.13 | 4.71 | 4.71 | 0.29 | 3.176342 | 0.149605696 | 4.56 | 2.06561086 | 2065.61086 |
| density range | density mean | vesicularity | | | | | | | |
| | | | | | | | | | |
| 1374 | 2179.842983 | 19.26507472 | | | | | | | |
| 2962 | | | | | | | | | |
| st dev | 378.0736607 | | | | | | | | |

Table A2.12. Density measurements for the spatter bombs. Weight is in g, density in kg m⁻³, vesicularity in %.

| Weight of clast in air | | | Weight of clast and sheet in water | | | Ws water | Wc water | SG | Density |
|------------------------|--------|------|------------------------------------|------------------|----------|----------------------|--------------------|-------------|-------------|
| dry uncoated | coated | wet | clast wet | sheet dry weight | sheet % | sheet wet weight (g) | clast wet no sheet | | |
| 8.76 | 9.16 | 4.93 | 4.93 | 0.4 | 4.366812 | 0.21528384 | 4.71 | 2.165484634 | 2165.484634 |
| 8.87 | 9.3 | 4.56 | 4.56 | 0.43 | 4.623656 | 0.21083871 | 4.35 | 1.962025316 | 1962.025316 |
| 2.97 | 4.32 | 2.41 | 2.41 | 1.35 | 31.25 | 0.753125 | 1.66 | 2.261780105 | 2261.780105 |
| 14.66 | 15.01 | 7.29 | 7.29 | 0.35 | 2.331779 | 0.169986676 | 7.12 | 1.944300518 | 1944.300518 |
| 9.02 | 9.54 | 3.43 | 3.43 | 0.52 | 5.450734 | 0.186960168 | 3.24 | 1.561374795 | 1561.374795 |
| 6.15 | 6.53 | 3.39 | 3.39 | 0.38 | 5.819296 | 0.197274119 | 3.19 | 2.079617834 | 2079.617834 |
| 6.69 | 7 | 3.04 | 3.04 | 0.31 | 4.428571 | 0.134628571 | 2.91 | 1.767676768 | 1767.676768 |
| 5.67 | 6.06 | 3.3 | 3.3 | 0.39 | 6.435644 | 0.212376238 | 3.09 | 2.195652174 | 2195.652174 |
| 3.55 | 3.8 | 1.82 | 1.82 | 0.25 | 6.578947 | 0.119736842 | 1.7 | 1.919191919 | 1919.191919 |
| 4.53 | 4.77 | 2.45 | 2.45 | 0.24 | 5.031447 | 0.12327044 | 2.33 | 2.056034483 | 2056.034483 |
| 14.49 | 14.93 | 6.93 | 6.93 | 0.44 | 2.947086 | 0.204233088 | 6.73 | 1.86625 | 1866.25 |
| 9.34 | 9.72 | 5.23 | 5.23 | 0.38 | 3.909465 | 0.204465021 | 5.03 | 2.16481069 | 2164.81069 |
| 7.03 | 7.47 | 3.32 | 3.32 | 0.44 | 5.890228 | 0.195555556 | 3.12 | 1.8 | 1800 |
| 9.08 | 9.54 | 5.43 | 5.43 | 0.46 | 4.821803 | 0.261823899 | 5.17 | 2.321167883 | 2321.167883 |
| 3.08 | 3.32 | 1.39 | 1.39 | 0.24 | 7.228916 | 0.100481928 | 1.29 | 1.720207254 | 1720.207254 |
| 8.2 | 8.67 | 3.58 | 3.58 | 0.47 | 5.420992 | 0.194071511 | 3.39 | 1.703339882 | 1703.339882 |
| 6.56 | 6.92 | 3.75 | 3.75 | 0.36 | 5.202312 | 0.195086705 | 3.55 | 2.1829653 | 2182.9653 |
| 9.86 | 10.07 | 5.48 | 5.48 | 0.21 | 2.085402 | 0.11428004 | 5.37 | 2.193899782 | 2193.899782 |
| 9.31 | 9.67 | 5.21 | 5.21 | 0.36 | 3.722854 | 0.193960703 | 5.02 | 2.168161435 | 2168.161435 |
| 10.55 | 10.9 | 5.01 | 5.01 | 0.35 | 3.211009 | 0.16087156 | 4.85 | 1.850594228 | 1850.594228 |
| 4.52 | 4.96 | 0.4 | 0.4 | 0.44 | 8.870968 | 0.035483871 | 0.36 | 1.087719298 | 1087.719298 |
| 10.44 | 10.82 | 3.47 | 3.47 | 0.38 | 3.512015 | 0.121866913 | 3.35 | 1.472108844 | 1472.108844 |
| 6.43 | 7.11 | 1.98 | 1.98 | 0.68 | 9.563994 | 0.189367089 | 1.79 | 1.385964912 | 1385.964912 |
| 7.38 | 7.88 | 1.91 | 1.91 | 0.5 | 6.345178 | 0.121192893 | 1.79 | 1.319932998 | 1319.932998 |
| 8.07 | 8.45 | 3.14 | 3.14 | 0.38 | 4.497041 | 0.141207101 | 3 | 1.5913371 | 1591.3371 |
| 7.93 | 8.47 | 2.21 | 2.21 | 0.54 | 6.375443 | 0.140897285 | 2.07 | 1.353035144 | 1353.035144 |

| | | | | | | | | | |
|-------|-------|------|------|------|----------|-------------|------|-------------|-------------|
| 5.19 | 5.43 | 2.7 | 2.7 | 0.24 | 4.41989 | 0.119337017 | 2.58 | 1.989010989 | 1989.010989 |
| 7.49 | 8.06 | 2.93 | 2.93 | 0.57 | 7.07196 | 0.207208437 | 2.72 | 1.571150097 | 1571.150097 |
| 2.28 | 2.59 | 1.29 | 1.29 | 0.31 | 11.96911 | 0.154401544 | 1.14 | 1.992307692 | 1992.307692 |
| 3.03 | 3.45 | 1.06 | 1.06 | 0.42 | 12.17391 | 0.129043478 | 0.93 | 1.443514644 | 1443.514644 |
| 8.14 | 8.46 | 3.97 | 3.97 | 0.32 | 3.782506 | 0.150165485 | 3.82 | 1.884187082 | 1884.187082 |
| 3.76 | 4.09 | 1.44 | 1.44 | 0.33 | 8.06846 | 0.116185819 | 1.32 | 1.543396226 | 1543.396226 |
| 5.69 | 5.97 | 2.1 | 2.1 | 0.28 | 4.690117 | 0.098492462 | 2 | 1.542635659 | 1542.635659 |
| 6.66 | 7.07 | 2.73 | 2.73 | 0.41 | 5.799151 | 0.158316832 | 2.57 | 1.629032258 | 1629.032258 |
| 6.53 | 6.93 | 1.77 | 1.77 | 0.4 | 5.772006 | 0.102164502 | 1.67 | 1.343023256 | 1343.023256 |
| 7.23 | 7.59 | 2.08 | 2.08 | 0.36 | 4.743083 | 0.098656126 | 1.98 | 1.377495463 | 1377.495463 |
| 6.43 | 6.83 | 2.58 | 2.58 | 0.4 | 5.856515 | 0.151098097 | 2.43 | 1.607058824 | 1607.058824 |
| 5.66 | 5.95 | 1.85 | 1.85 | 0.29 | 4.87395 | 0.090168067 | 1.76 | 1.451219512 | 1451.219512 |
| 3.87 | 4.21 | 1.11 | 1.11 | 0.34 | 8.07601 | 0.089643705 | 1.02 | 1.358064516 | 1358.064516 |
| 9.92 | 10.32 | 4.24 | 4.24 | 0.4 | 3.875969 | 0.164341085 | 4.08 | 1.697368421 | 1697.368421 |
| 13.53 | 13.91 | 7.76 | 7.76 | 0.38 | 2.731848 | 0.211991373 | 7.55 | 2.261788618 | 2261.788618 |
| 2.88 | 3.16 | 0.64 | 0.64 | 0.28 | 8.860759 | 0.056708861 | 0.58 | 1.253968254 | 1253.968254 |
| 2.05 | 2.3 | 1.5 | 1.5 | 0.25 | 10.86957 | 0.163043478 | 1.34 | 2.875 | 2875 |
| 3.08 | 3.34 | 0.43 | 0.43 | 0.26 | 7.784431 | 0.033473054 | 0.4 | 1.147766323 | 1147.766323 |
| 6.29 | 6.71 | 2.31 | 2.31 | 0.42 | 6.259314 | 0.144590164 | 2.17 | 1.525 | 1525 |
| 7.68 | 8.02 | 2.82 | 2.82 | 0.34 | 4.239401 | 0.119551122 | 2.7 | 1.542307692 | 1542.307692 |
| 5.38 | 5.84 | 2.05 | 2.05 | 0.46 | 7.876712 | 0.161472603 | 1.89 | 1.540897098 | 1540.897098 |
| 5.76 | 6.11 | 2.3 | 2.3 | 0.35 | 5.728314 | 0.131751227 | 2.17 | 1.603674541 | 1603.674541 |
| 2.45 | 2.66 | 1.05 | 1.05 | 0.21 | 7.894737 | 0.082894737 | 0.97 | 1.652173913 | 1652.173913 |
| 3.49 | 3.7 | 1.63 | 1.63 | 0.21 | 5.675676 | 0.092513514 | 1.54 | 1.787439614 | 1787.439614 |
| 5.17 | 5.47 | 1.89 | 1.89 | 0.3 | 5.484461 | 0.103656307 | 1.79 | 1.527932961 | 1527.932961 |
| 3.62 | 3.92 | 1.1 | 1.1 | 0.3 | 7.653061 | 0.084183673 | 1.02 | 1.390070922 | 1390.070922 |
| 3.7 | 3.94 | 2.04 | 2.04 | 0.24 | 6.091371 | 0.124263959 | 1.92 | 2.073684211 | 2073.684211 |
| 3.68 | 3.89 | 2.02 | 2.02 | 0.21 | 5.398458 | 0.109048843 | 1.91 | 2.080213904 | 2080.213904 |
| 10.79 | 11.13 | 4.99 | 4.99 | 0.34 | 3.054807 | 0.152434861 | 4.84 | 1.812703583 | 1812.703583 |
| 4.31 | 4.4 | 1.46 | 1.46 | 0.09 | 2.045455 | 0.029863636 | 1.43 | 1.496598639 | 1496.598639 |
| 4.05 | 4.52 | 2.12 | 2.12 | 0.47 | 10.39823 | 0.220442478 | 1.9 | 1.883333333 | 1883.333333 |
| 3.41 | 3.66 | 1.94 | 1.94 | 0.25 | 6.830601 | 0.132513661 | 1.81 | 2.127906977 | 2127.906977 |
| 2.2 | 2.42 | 0.89 | 0.89 | 0.22 | 9.090909 | 0.080909091 | 0.81 | 1.581699346 | 1581.699346 |
| 3.75 | 3.96 | 2.14 | 2.14 | 0.21 | 5.30303 | 0.113484848 | 2.03 | 2.175824176 | 2175.824176 |
| 9.98 | 10.29 | 4.08 | 4.08 | 0.31 | 3.012634 | 0.122915452 | 3.96 | 1.657004831 | 1657.004831 |
| 7.71 | 8.1 | 3.74 | 3.74 | 0.39 | 4.814815 | 0.180074074 | 3.56 | 1.857798165 | 1857.798165 |
| 5.03 | 5.29 | 2.34 | 2.34 | 0.26 | 4.914934 | 0.115009452 | 2.22 | 1.793220339 | 1793.220339 |
| 7.13 | 7.37 | 3.4 | 3.4 | 0.24 | 3.256445 | 0.110719132 | 3.29 | 1.856423174 | 1856.423174 |
| 6.89 | 7.32 | 3.23 | 3.23 | 0.43 | 5.874317 | 0.189740437 | 3.04 | 1.789731051 | 1789.731051 |
| 6.05 | 6.64 | 2.46 | 2.46 | 0.59 | 8.885542 | 0.218584337 | 2.24 | 1.588516746 | 1588.516746 |
| 5.98 | 6.18 | 3.5 | 3.5 | 0.2 | 3.236246 | 0.113268608 | 3.39 | 2.305970149 | 2305.970149 |
| 5.97 | 6.32 | 3.41 | 3.41 | 0.35 | 5.537975 | 0.188844937 | 3.22 | 2.171821306 | 2171.821306 |
| 3.81 | 4.1 | 1.11 | 1.11 | 0.29 | 7.073171 | 0.078512195 | 1.03 | 1.371237458 | 1371.237458 |
| 4.96 | 5.63 | 2.45 | 2.45 | 0.67 | 11.90053 | 0.291563055 | 2.16 | 1.770440252 | 1770.440252 |
| 3.78 | 4.18 | 0.67 | 0.67 | 0.4 | 9.569378 | 0.064114833 | 0.61 | 1.190883191 | 1190.883191 |

| | | | | | | | | | |
|--|--------------|--------------|------|------|----------|-------------|------|-------------|-------------|
| 8.75 | 9.23 | 3.78 | 3.78 | 0.48 | 5.200433 | 0.196576381 | 3.58 | 1.693577982 | 1693.577982 |
| 10.67 | 11.06 | 4.7 | 4.7 | 0.39 | 3.526221 | 0.165732369 | 4.53 | 1.738993711 | 1738.993711 |
| 7.2 | 7.61 | 3.39 | 3.39 | 0.41 | 5.387648 | 0.182641261 | 3.21 | 1.803317536 | 1803.317536 |
| 5.93 | 6.35 | 1 | 1 | 0.42 | 6.614173 | 0.066141732 | 0.93 | 1.186915888 | 1186.915888 |
| 5.79 | 6.14 | 2.52 | 2.52 | 0.35 | 5.700326 | 0.143648208 | 2.38 | 1.696132597 | 1696.132597 |
| 8.87 | 9.28 | 3.24 | 3.24 | 0.41 | 4.418103 | 0.143146552 | 3.1 | 1.536423841 | 1536.423841 |
| 4.26 | 4.91 | 0.61 | 0.61 | 0.65 | 13.23829 | 0.080753564 | 0.53 | 1.141860465 | 1141.860465 |
| 6.68 | 6.85 | 2.93 | 2.93 | 0.17 | 2.481752 | 0.072715328 | 2.86 | 1.74744898 | 1747.44898 |
| 7.84 | 8.29 | 2.64 | 2.64 | 0.45 | 5.428227 | 0.143305187 | 2.5 | 1.467256637 | 1467.256637 |
| 4.01 | 4.26 | 1.47 | 1.47 | 0.25 | 5.868545 | 0.086267606 | 1.38 | 1.52688172 | 1526.88172 |
| 5.82 | 6.53 | 1.17 | 1.17 | 0.71 | 10.87289 | 0.127212864 | 1.04 | 1.218283582 | 1218.283582 |
| 9.92 | 10.47 | 5.09 | 5.09 | 0.55 | 5.253104 | 0.267382999 | 4.82 | 1.946096654 | 1946.096654 |
| 6.06 | 6.36 | 1.79 | 1.79 | 0.3 | 4.716981 | 0.084433962 | 1.71 | 1.391684902 | 1391.684902 |
| 4 | 4.3 | 1.8 | 1.8 | 0.3 | 6.976744 | 0.125581395 | 1.67 | 1.72 | 1720 |
| 5.24 | 5.58 | 2.15 | 2.15 | 0.34 | 6.09319 | 0.131003584 | 2.02 | 1.626822157 | 1626.822157 |
| 3.84 | 4.22 | 1.2 | 1.2 | 0.38 | 9.004739 | 0.108056872 | 1.09 | 1.397350993 | 1397.350993 |
| 4.9 | 5.21 | 1.58 | 1.58 | 0.31 | 5.950096 | 0.094011516 | 1.49 | 1.435261708 | 1435.261708 |
| 4.92 | 5.24 | 1.05 | 1.05 | 0.32 | 6.10687 | 0.064122137 | 0.99 | 1.250596659 | 1250.596659 |
| 3.55 | 4.16 | 1.34 | 1.34 | 0.61 | 14.66346 | 0.196490385 | 1.14 | 1.475177305 | 1475.177305 |
| density range | density mean | vesicularity | | | | | | | |
| | | | | | | | | | |
| 1087 | 1713.524578 | 36.53612674 | | | | | | | |
| 2321 | | | | | | | | | |
| st dev | 333.9175475 | | | | | | | | |
| Table A2.13. Density measurements for the armoured bombs. Weight is in g, density in kg m ⁻³ , vesicularity in %. | | | | | | | | | |

| Weight of clast in air | | | Weight of clast and sheet in water | | | Ws water | Wc water | SG | Density |
|------------------------|--------|-------|------------------------------------|------------------|----------|----------------------|--------------------|----------|-------------|
| dry uncoated | coated | wet | clast wet | sheet dry weight | sheet % | sheet wet weight (g) | clast wet no sheet | | |
| 14.94 | 15.19 | 8.6 | 8.6 | 0.25 | 1.64582 | 0.141540487 | 8.458459513 | 2.30500 | 2305.007587 |
| 15.68 | 16.13 | 9.2 | 9.2 | 0.45 | 2.789833 | 0.2566646 | 8.9433354 | 2.32756 | 2327.561328 |
| 10.55 | 10.78 | 5.45 | 5.45 | 0.23 | 2.133581 | 0.116280148 | 5.333719852 | 2.02251 | 2022.514071 |
| 14.98 | 15.18 | 8.29 | 8.29 | 0.2 | 1.317523 | 0.109222661 | 8.180777339 | 2.20319 | 2203.193033 |
| 14.55 | 14.9 | 8.28 | 8.28 | 0.35 | 2.348993 | 0.194496644 | 8.085503356 | 2.250755 | 2250.755287 |
| 10.49 | 10.83 | 6.18 | 6.18 | 0.34 | 3.139428 | 0.19401662 | 5.98598338 | 2.329032 | 2329.032258 |
| 20.21 | 20.58 | 13.15 | 13.15 | 0.37 | 1.797862 | 0.236418853 | 12.91358115 | 2.769852 | 2769.851952 |
| 13.32 | 13.75 | 8.29 | 8.29 | 0.43 | 3.127273 | 0.259250909 | 8.030749091 | 2.518315 | 2518.315018 |
| 10.79 | 10.9 | 6.91 | 6.91 | 0.11 | 1.009174 | 0.069733945 | 6.840266055 | 2.73183 | 2731.829574 |
| 8.53 | 8.88 | 5.12 | 5.12 | 0.35 | 3.941441 | 0.201801802 | 4.918198198 | 2.361702 | 2361.702128 |
| 9.83 | 10.17 | 5.46 | 5.46 | 0.34 | 3.343166 | 0.182536873 | 5.277463127 | 2.159236 | 2159.235669 |
| 15.68 | 16.02 | 9.99 | 9.99 | 0.34 | 2.122347 | 0.212022472 | 9.777977528 | 2.656716 | 2656.716418 |
| 15.09 | 15.36 | 8.53 | 8.53 | 0.27 | 1.757813 | 0.149941406 | 8.380058594 | 2.248902 | 2248.901903 |
| 9.13 | 9.39 | 5.16 | 5.16 | 0.26 | 2.768903 | 0.142875399 | 5.017124601 | 2.219858 | 2219.858156 |
| 10.89 | 11.18 | 6.72 | 6.72 | 0.29 | 2.593918 | 0.17431127 | 6.54568873 | 2.506726 | 2506.726457 |
| 11.7 | 12.05 | 7.03 | 7.03 | 0.35 | 2.904564 | 0.204190871 | 6.825809129 | 2.400398 | 2400.398406 |
| 7.48 | 7.88 | 1.92 | 1.92 | 0.4 | 5.076142 | 0.097461929 | 1.822538071 | 1.322148 | 1322.147651 |
| 10.78 | 11.03 | 6.91 | 6.91 | 0.25 | 2.266546 | 0.156618314 | 6.753381686 | 2.677184 | 2677.184466 |
| 6.65 | 6.92 | 2.96 | 2.96 | 0.27 | 3.901734 | 0.115491329 | 2.844508671 | 1.747475 | 1747.474747 |
| 10.85 | 11.13 | 5.97 | 5.97 | 0.28 | 2.515723 | 0.150188679 | 5.819811321 | 2.156977 | 2156.976744 |
| 13.35 | 13.79 | 8.49 | 8.49 | 0.44 | 3.190718 | 0.270891951 | 8.219108049 | 2.601887 | 2601.886792 |
| 13.78 | 14.11 | 7.77 | 7.77 | 0.33 | 2.338767 | 0.181722183 | 7.588277817 | 2.225552 | 2225.55205 |
| 15.96 | 16.4 | 9.33 | 9.33 | 0.44 | 2.682927 | 0.250317073 | 9.079682927 | 2.319661 | 2319.660537 |
| 4.51 | 4.81 | 2.13 | 2.13 | 0.3 | 6.237006 | 0.132848233 | 1.997151767 | 1.794776 | 1794.776119 |
| 7.93 | 8.18 | 4.28 | 4.28 | 0.25 | 3.056235 | 0.130806846 | 4.149193154 | 2.097436 | 2097.435897 |
| 13.72 | 14.07 | 7.76 | 7.76 | 0.35 | 2.487562 | 0.193034826 | 7.566965174 | 2.229794 | 2229.793978 |
| 13.86 | 14.34 | 6.99 | 6.99 | 0.48 | 3.34728 | 0.233974895 | 6.756025105 | 1.95102 | 1951.020408 |
| 9.11 | 9.3 | 5.05 | 5.05 | 0.19 | 2.043011 | 0.103172043 | 4.946827957 | 2.188235 | 2188.235294 |
| 16.79 | 17.17 | 10.32 | 10.32 | 0.38 | 2.213162 | 0.228398369 | 10.09160163 | 2.506569 | 2506.569343 |
| 12.77 | 13.18 | 6.46 | 6.46 | 0.41 | 3.110774 | 0.200955994 | 6.259044006 | 1.96131 | 1961.309524 |
| 13.42 | 13.78 | 6.83 | 6.83 | 0.36 | 2.612482 | 0.178432511 | 6.651567489 | 1.982734 | 1982.733813 |
| 14.18 | 14.35 | 8.48 | 8.48 | 0.17 | 1.184669 | 0.10045993 | 8.37954007 | 2.444634 | 2444.633731 |
| 9.18 | 9.53 | 4.34 | 4.34 | 0.35 | 3.672613 | 0.159391396 | 4.180608604 | 1.836224 | 1836.223507 |
| 13.35 | 13.66 | 8.03 | 8.03 | 0.31 | 2.2694 | 0.182232796 | 7.847767204 | 2.426288 | 2426.287744 |
| 7.7 | 7.92 | 4.41 | 4.41 | 0.22 | 2.777778 | 0.1225 | 4.2875 | 2.25641 | 2256.410256 |
| 11.27 | 11.5 | 6.52 | 6.52 | 0.23 | 2 | 0.1304 | 6.3896 | 2.309237 | 2309.236948 |
| 13.43 | 13.78 | 7.39 | 7.39 | 0.35 | 2.539913 | 0.187699565 | 7.202300435 | 2.156495 | 2156.494523 |
| 9.63 | 9.96 | 4.58 | 4.58 | 0.33 | 3.313253 | 0.151746988 | 4.428253012 | 1.851301 | 1851.301115 |
| 8.38 | 8.75 | 5.41 | 5.41 | 0.37 | 4.228571 | 0.228765714 | 5.181234286 | 2.61976 | 2619.760479 |
| 13.98 | 14.45 | 8.66 | 8.66 | 0.47 | 3.252595 | 0.28167474 | 8.37832526 | 2.495682 | 2495.682211 |
| 6.84 | 7.07 | 4.21 | 4.21 | 0.23 | 3.253182 | 0.136958982 | 4.073041018 | 2.472028 | 2472.027972 |
| 12.72 | 13.26 | 7.41 | 7.41 | 0.54 | 4.072398 | 0.301764706 | 7.108235294 | 2.266667 | 2266.666667 |
| 12.55 | 13.05 | 7.24 | 7.24 | 0.5 | 3.831418 | 0.277394636 | 6.962605364 | 2.246127 | 2246.127367 |

| | | | | | | | | | |
|-------|-------|-------|-------|------|----------|-------------|-------------|----------|-------------|
| 9.71 | 10.12 | 6.5 | 6.5 | 0.41 | 4.051383 | 0.263339921 | 6.236660079 | 2.79558 | 2795.58011 |
| 9.12 | 9.52 | 5.64 | 5.64 | 0.4 | 4.201681 | 0.23697479 | 5.40302521 | 2.453608 | 2453.608247 |
| 8.91 | 9.16 | 5.72 | 5.72 | 0.25 | 2.729258 | 0.156113537 | 5.563886463 | 2.662791 | 2662.790698 |
| 10.77 | 11.11 | 6.73 | 6.73 | 0.34 | 3.060306 | 0.205958596 | 6.524041404 | 2.53653 | 2536.52968 |
| 13.35 | 13.83 | 8.24 | 8.24 | 0.48 | 3.470716 | 0.285986985 | 7.954013015 | 2.474061 | 2474.060823 |
| 6.84 | 7.24 | 3.89 | 3.89 | 0.4 | 5.524862 | 0.214917127 | 3.675082873 | 2.161194 | 2161.19403 |
| 11.3 | 11.76 | 6.8 | 6.8 | 0.46 | 3.911565 | 0.265986395 | 6.534013605 | 2.370968 | 2370.967742 |
| 6.79 | 7.29 | 4.28 | 4.28 | 0.5 | 6.858711 | 0.293552812 | 3.986447188 | 2.421927 | 2421.92691 |
| 11.13 | 11.56 | 6.85 | 6.85 | 0.43 | 3.719723 | 0.254801038 | 6.595198962 | 2.454352 | 2454.352442 |
| 14.19 | 14.43 | 7.93 | 7.93 | 0.24 | 1.663202 | 0.131891892 | 7.798108108 | 2.22 | 2220 |
| 8.67 | 9.1 | 5.79 | 5.79 | 0.43 | 4.725275 | 0.273593407 | 5.516406593 | 2.749245 | 2749.244713 |
| 18.11 | 18.61 | 10.56 | 10.56 | 0.5 | 2.686728 | 0.283718431 | 10.27628157 | 2.311801 | 2311.801242 |
| 5.26 | 5.58 | 3.32 | 3.32 | 0.32 | 5.734767 | 0.190394265 | 3.129605735 | 2.469027 | 2469.026549 |
| 7.76 | 8.22 | 3.48 | 3.48 | 0.46 | 5.596107 | 0.194744526 | 3.285255474 | 1.734177 | 1734.177215 |
| 6.65 | 7.04 | 3.99 | 3.99 | 0.39 | 5.539773 | 0.221036932 | 3.768963068 | 2.308197 | 2308.196721 |
| 5.5 | 5.82 | 3.08 | 3.08 | 0.32 | 5.498282 | 0.169347079 | 2.910652921 | 2.124088 | 2124.087591 |
| 16.01 | 16.41 | 10.23 | 10.23 | 0.4 | 2.437538 | 0.249360146 | 9.980639854 | 2.65534 | 2655.339806 |
| 11.08 | 11.57 | 6.26 | 6.26 | 0.49 | 4.235091 | 0.265116681 | 5.994883319 | 2.178908 | 2178.907721 |
| 5.91 | 6.46 | 4.22 | 4.22 | 0.55 | 8.513932 | 0.359287926 | 3.860712074 | 2.883929 | 2883.928571 |
| 5.89 | 6.3 | 2.77 | 2.77 | 0.41 | 6.507937 | 0.180269841 | 2.589730159 | 1.784703 | 1784.70255 |
| 3.79 | 4.18 | 2.02 | 2.02 | 0.39 | 9.330144 | 0.1884689 | 1.8315311 | 1.935185 | 1935.185185 |
| 2.14 | 2.31 | 1.19 | 1.19 | 0.17 | 7.359307 | 0.087575758 | 1.102424242 | 2.0625 | 2062.5 |
| 4.58 | 4.88 | 0.07 | 0.07 | 0.3 | 6.147541 | 0.004303279 | 0.065696721 | 1.014553 | 1014.553015 |
| 9.26 | 9.7 | 5.5 | 5.5 | 0.44 | 4.536082 | 0.249484536 | 5.250515464 | 2.309524 | 2309.52381 |
| 8.33 | 8.62 | 5.42 | 5.42 | 0.29 | 3.364269 | 0.182343387 | 5.237656613 | 2.69375 | 2693.75 |
| 14.51 | 14.77 | 9.51 | 9.51 | 0.26 | 1.760325 | 0.167406906 | 9.342593094 | 2.807985 | 2807.984791 |
| 13.41 | 13.78 | 8.59 | 8.59 | 0.37 | 2.685051 | 0.230645864 | 8.359354136 | 2.655106 | 2655.105973 |
| 15.84 | 16.41 | 9.65 | 9.65 | 0.57 | 3.473492 | 0.335191956 | 9.314808044 | 2.427515 | 2427.514793 |
| 12.67 | 13.1 | 7.88 | 7.88 | 0.43 | 3.282443 | 0.258656489 | 7.621343511 | 2.509579 | 2509.578544 |
| 16.97 | 17.53 | 10.08 | 10.08 | 0.56 | 3.194524 | 0.322007986 | 9.757992014 | 2.35302 | 2353.020134 |
| 11.72 | 12.05 | 6.68 | 6.68 | 0.33 | 2.738589 | 0.182937759 | 6.497062241 | 2.243948 | 2243.947858 |
| 17.81 | 18.31 | 10.79 | 10.79 | 0.5 | 2.730748 | 0.294647733 | 10.49535227 | 2.43484 | 2434.840426 |
| 11.35 | 11.92 | 5.95 | 5.95 | 0.57 | 4.781879 | 0.284521812 | 5.665478188 | 1.99665 | 1996.649916 |
| 11.95 | 12.36 | 7.39 | 7.39 | 0.41 | 3.317152 | 0.24513754 | 7.14486246 | 2.486922 | 2486.921529 |
| 14.69 | 15.2 | 8.97 | 8.97 | 0.51 | 3.355263 | 0.300967105 | 8.669032895 | 2.439807 | 2439.807384 |
| 7.65 | 8.02 | 3.26 | 3.26 | 0.37 | 4.613466 | 0.150399002 | 3.109600998 | 1.684874 | 1684.87395 |
| 16.68 | 17.15 | 10.31 | 10.31 | 0.47 | 2.740525 | 0.282548105 | 10.0274519 | 2.50731 | 2507.309942 |
| 11.14 | 11.44 | 4.95 | 4.95 | 0.3 | 2.622378 | 0.129807692 | 4.820192308 | 1.762712 | 1762.711864 |
| 9.14 | 9.51 | 5.18 | 5.18 | 0.37 | 3.890641 | 0.201535226 | 4.978464774 | 2.196305 | 2196.30485 |
| 16.73 | 17.23 | 9.69 | 9.69 | 0.5 | 2.901915 | 0.281195589 | 9.408804411 | 2.285146 | 2285.145889 |
| 13.36 | 13.73 | 5.89 | 5.89 | 0.37 | 2.694829 | 0.158725419 | 5.731274581 | 1.751276 | 1751.27551 |
| 12.22 | 12.52 | 6.37 | 6.37 | 0.3 | 2.396166 | 0.152635783 | 6.217364217 | 2.035772 | 2035.772358 |
| 7.07 | 7.44 | 4.25 | 4.25 | 0.37 | 4.973118 | 0.211357527 | 4.038642473 | 2.332288 | 2332.288401 |
| 9.17 | 9.52 | 5.98 | 5.98 | 0.35 | 3.676471 | 0.219852941 | 5.760147059 | 2.689266 | 2689.265537 |
| 7.8 | 8.32 | 4.48 | 4.48 | 0.52 | 6.25 | 0.28 | 4.2 | 2.166667 | 2166.666667 |

| | | | | | | | | | |
|---|--------------------|--------------|------|------|----------|-------------|-------------|----------|-------------|
| 8.16 | 8.7 | 5.2 | 5.2 | 0.54 | 6.206897 | 0.322758621 | 4.877241379 | 2.485714 | 2485.714286 |
| 9.12 | 9.54 | 4.58 | 4.58 | 0.42 | 4.402516 | 0.20163522 | 4.37836478 | 1.923387 | 1923.387097 |
| density range | density mean of 90 | vesicularity | | | | | | | |
| 1014 | 2278.858136 | 15.59784683 | | | | | | | |
| 2883 | | | | | | | | | |
| St dev | | | | | | | | | |
| Table A2.14. Density measurements for the hypocrystalline lapilli. Weight is in g, density in kg m ⁻³ , vesicularity in %. | | | | | | | | | |

| photo | wp | facies | orange fragment dimension (mm) | axis | fragment area (mm ²) | area analysed (mm ²) | orange fragment % |
|--------------|-----|--------|--------------------------------|------|----------------------------------|----------------------------------|-------------------|
| 1010619edit1 | 199 | mLA | 27.03 | x | 617.06787 | 10000 | 24.14903692 |
| 1010619edit1 | 199 | mLA | 22.829 | y | | | |
| 1010619edit1 | 199 | mLA | 18.664 | x | 294.23796 | | |
| 1010619edit1 | 199 | mLA | 15.765 | y | | | |
| 1010619edit1 | 199 | mLA | 44.65 | x | 1259.9337 | | |
| 1010619edit1 | 199 | mLA | 28.218 | y | | | |
| 1010619edit1 | 199 | mLA | 19.159 | x | 243.664162 | | |
| 1010619edit1 | 199 | mLA | 12.718 | y | | | |
| 1010621edit1 | 199 | mBr | 0 | x | 0 | 10000 | 0 |
| 1010621crop3 | 199 | mBr | 0 | y | 0 | 10000 | 0 |
| 1010621edit2 | 199 | mBr | 14.292 | x | 240.8202 | 10000 | 4.048967 |
| 1010621edit2 | 199 | mBr | 16.85 | y | | | |
| 1010621edit2 | 199 | mBr | 17.738 | x | 164.0765 | | |
| 1010621edit2 | 199 | mBr | 9.25 | y | | | |
| 1010621crop2 | 199 | mBr | 0 | x | 0 | 10000 | 0 |
| 1010624edit1 | 199 | mBr | | y | | 10000 | 0 |
| 1010629edit1 | 199 | mBr | 78.354 | x | 3448.35954 | 10000 | 51.4288006 |
| 1010629edit1 | 199 | mBr | 44.01 | y | | | |
| 1010629edit1 | 199 | mBr | 22.738 | x | 621.65692 | | |
| 1010629edit1 | 199 | mBr | 27.34 | y | | | |
| 1010629edit1 | 199 | mBr | 27.78 | x | 1072.8636 | | |
| 1010629edit1 | 199 | mBr | 38.62 | y | | | |
| 1010629edit2 | 199 | mBr | 96.636 | x | 6542.643744 | 10000 | 77.23632644 |
| 1010629edit2 | 199 | mBr | 67.704 | y | | | |
| 1010629edit2 | 199 | mBr | 28.458 | x | 699.21306 | | |
| 1010629edit2 | 199 | mBr | 24.57 | y | | | |
| 1010629edit2 | 199 | mBr | 18.256 | x | 481.77584 | | |
| 1010629edit2 | 199 | mBr | 26.39 | y | | | |
| 1010629edit3 | 199 | mBr | 43.171 | x | 1025.570276 | 10000 | 23.39864486 |
| 1010629edit3 | 199 | mBr | 23.756 | y | | | |
| 1010629edit3 | 199 | mBr | 36.091 | x | 643.791258 | | |
| 1010629edit3 | 199 | mBr | 17.838 | y | | | |
| 1010629edit3 | 199 | mBr | 36.484 | x | 670.502952 | | |
| 1010629edit3 | 199 | mBr | 18.378 | y | | | |
| 1010629edit4 | 199 | mBr | 25.828 | x | 809.96608 | 10000 | 8.0996608 |
| 1010629edit4 | 199 | mBr | 31.36 | y | | | |

| | | | | | | | |
|--------------|-----|--------|--------|---|------------|-------|-------------|
| 1060629edit5 | 199 | mBr | 106.43 | x | 7604.4235 | 10000 | 76.044235 |
| 1060629edit5 | 199 | mBr | 71.45 | y | | | |
| 1010629edit6 | 199 | mBr | 70.65 | x | 7872.5295 | 10000 | 78.725295 |
| 1010629edit6 | 199 | mBr | 111.43 | y | | | |
| 1010630edit1 | 199 | mLA | 35.439 | x | 856.950459 | 10000 | 27.85823798 |
| 1010630edit1 | 199 | mLA | 24.181 | y | | | |
| 1010630edit1 | 199 | mLA | 24.365 | x | 295.815465 | | |
| 1010630edit1 | 199 | mLA | 12.141 | y | | | |
| 1010630edit1 | 199 | mLA | 27.931 | x | 365.309549 | | |
| 1010630edit1 | 199 | mLA | 13.079 | y | | | |
| 1010630edit1 | 199 | mLA | 12.278 | x | 157.195234 | | |
| 1010630edit1 | 199 | mLA | 12.803 | y | | | |
| 1010630edit1 | 199 | mLA | 13.294 | x | 120.682932 | | |
| 1010630edit1 | 199 | mLA | 9.078 | y | | | |
| 1010630edit1 | 199 | mLA | 37.895 | x | 747.2894 | | |
| 1010630edit1 | 199 | mLA | 19.72 | y | | | |
| 1010630edit1 | 199 | mLA | 18.257 | x | 242.580759 | | |
| 1010630edit1 | 199 | mLA | 13.287 | y | | | |
| 1010639edit | 199 | mLA | 0 | x | 0 | 10000 | 0 |
| 1010639edit2 | 199 | mLA | 16.05 | y | 177.834 | 10000 | 1.77834 |
| 1010639edit2 | 199 | mLA | 11.08 | x | | | |
| 1010639edit4 | 199 | mLA | | y | 0 | 10000 | 0 |
| 1010641edit1 | 199 | mLA | 21.1 | x | 280.841 | 10000 | 2.80841 |
| 1010641edit1 | 199 | mLA | 13.31 | y | | | |
| 1010641edit2 | 199 | mLA | 40.641 | x | 547.231065 | 10000 | 14.45516226 |
| 1010641edit2 | 199 | mLA | 13.465 | y | | | |
| 1010641edit2 | 199 | mLA | 12.958 | x | 138.171154 | | |
| 1010641edit2 | 199 | mLA | 10.663 | y | | | |
| 1010641edit2 | 199 | mLA | 9.366 | x | 102.201792 | | |
| 1010641edit2 | 199 | mLA | 10.912 | y | | | |
| 1010641edit2 | 199 | mLA | 16.015 | x | 657.912215 | | |
| 1010641edit2 | 199 | mLA | 41.081 | y | | | |
| 1010641edit2 | 199 | mLA | 0 | x | 0 | 10000 | 0 |
| 1010641edit4 | 199 | mLA | 6.76 | y | 64.22 | 10000 | 0.6422 |
| 1010641edit4 | 199 | mLA | 9.5 | x | | | |
| 1010642edit1 | 199 | mLA | 15.81 | y | 255.9639 | 10000 | 2.559639 |
| 1010642edit1 | 199 | mLA | 16.19 | x | | | |
| 1010642edit2 | 199 | mLA | 17.75 | y | 253.2925 | 10000 | 2.532925 |
| 1010642edit2 | 199 | mLA | 14.27 | x | | | |
| 1010642edit3 | 199 | mLA | 0 | y | | 10000 | 0 |
| 1010642edit4 | 199 | mLA | 0 | x | | 10000 | 0 |
| 1010652edit2 | 199 | lensLA | 22.72 | y | 433.2704 | 10000 | 4.332704 |
| 1010652edit2 | 199 | lensLA | 19.07 | x | | | |
| 1010652edit1 | 199 | lensLA | | y | | | 0 |
| 1010652edit3 | 199 | lensLA | 10.12 | x | 36.1284 | 10000 | 0.361284 |

| | | | | | | | |
|--|-----|--------|-------|---|----------|-------|----------|
| 1010652edit3 | 199 | lensLA | 3.57 | y | | | |
| 1010653edit1 | 199 | lensLA | | x | | | 0 |
| 1010655edit1 | 199 | lensLA | 20.01 | y | 222.7113 | 10000 | 2.227113 |
| 1010655edit1 | 199 | lensLA | 11.13 | x | | | |
| 1010655edit2 | 199 | lensLA | | y | 0 | 10000 | 0 |
| 1010655edit3 | 199 | lensLA | | x | | | |
| 1010658edit1 | 199 | lensLA | | y | 0 | 10000 | 0 |
| 1010658edit2 | 199 | lensLA | | x | 0 | 10000 | 0 |
| 1010662edit1 | 199 | lensLA | | y | 0 | 10000 | 0 |
| 1010648edit1 | 199 | lensLA | | x | 0 | 10000 | 0 |
| Table A2.15. Measurements of ventricular and globular bomb fragments in lithofacies lensLA, mSp and mLA. | | | | | | | |

Appendix 3: Support Material for Chapter 5

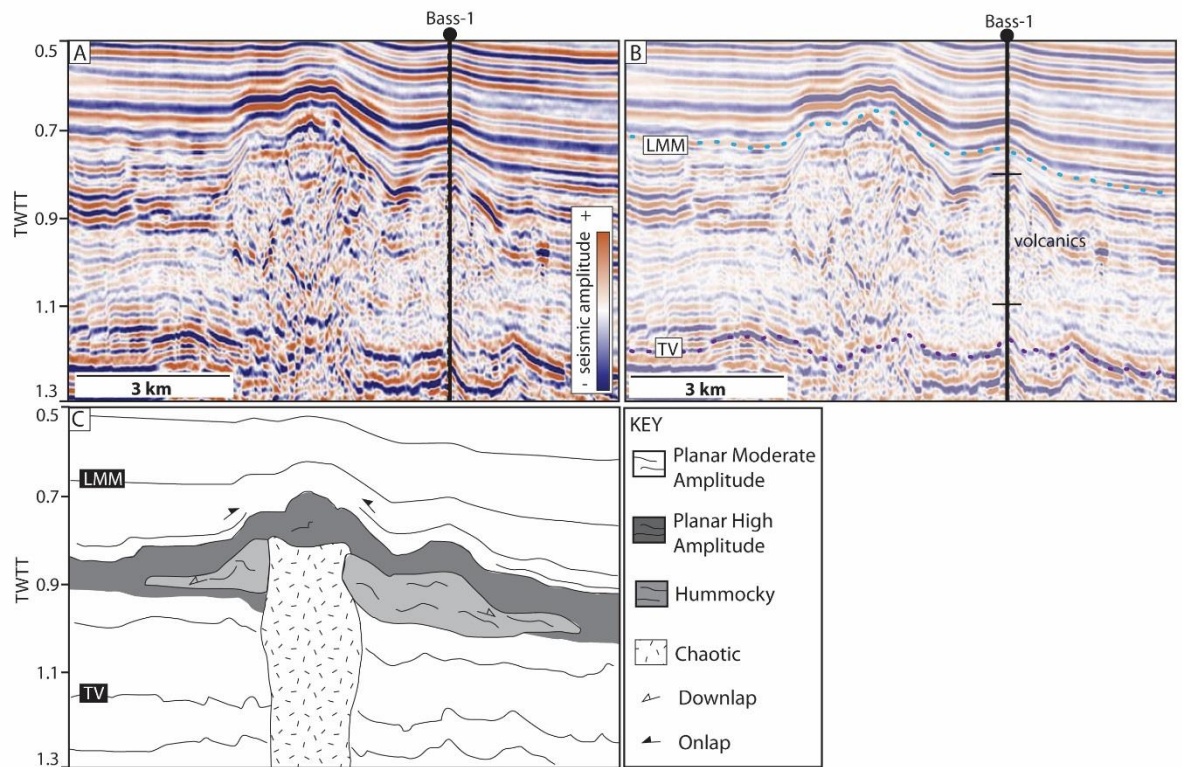


Figure A.1. Seismic section (A) and interpretations (B and C) of the cone-shaped edifice observed on the 2D seismic line between the Yolla and Labatt surveys. The edifice has identical internal facies to the edifices observed in the Labatt and Yolla surveys, although its morphology is somewhat different. Well data from King-1 indicates that the edifice is composed of volcanic rock. LMM=Lower Mid Miocene, TV= Top Volcanic.

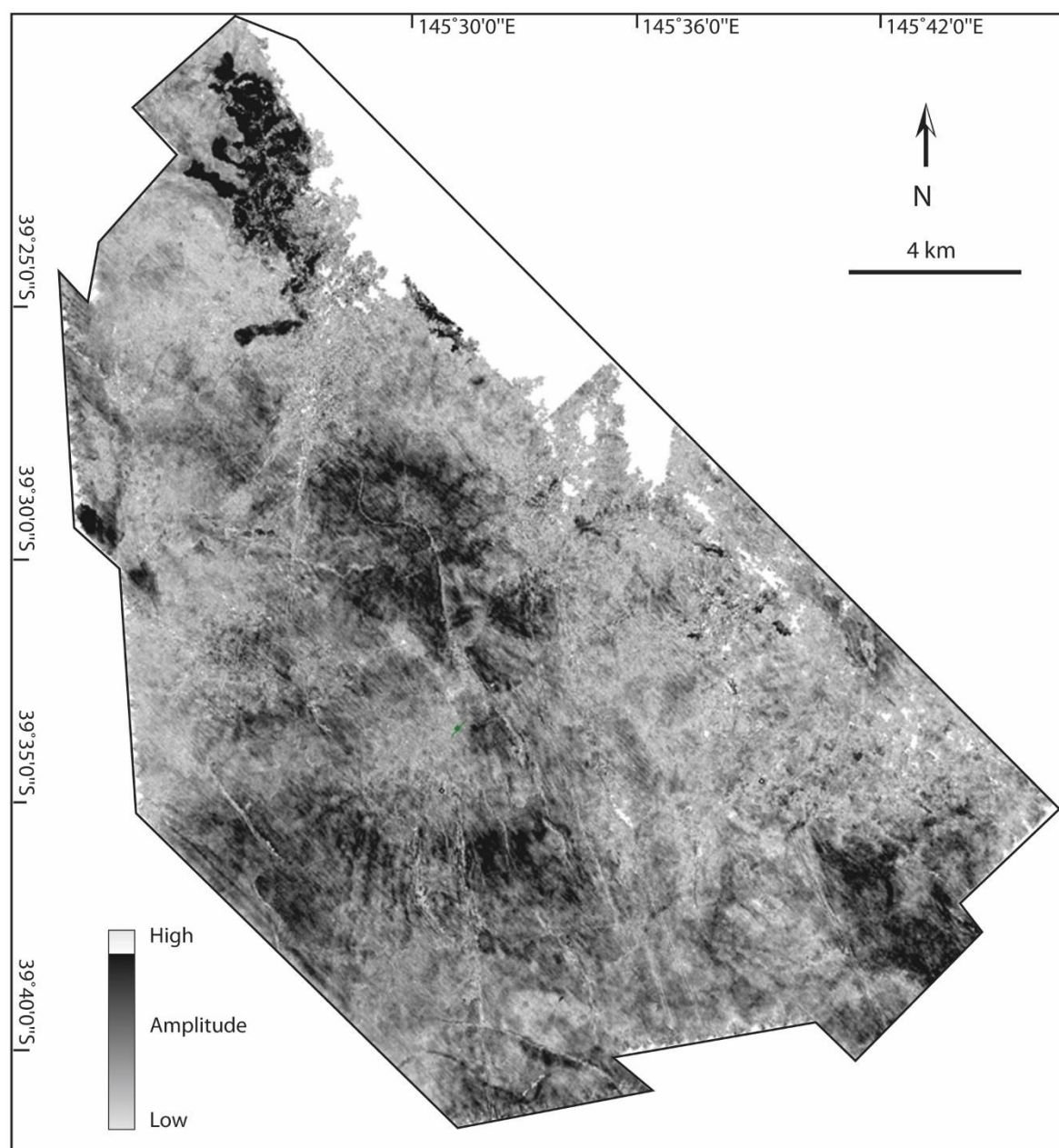


Figure A2. Amplitude map of the Lower Volcanic Horizon in the Labatt survey.

| Vent number | Basal Diameter (m) | Crater Diameter (m) | Height/Depth (m) | Volume (km ³) | Height/diameter ratio | Vent type | Distribution | Flank dip (°) | Spacing to nearest neighbour (km) | Depth to underlying sill (m) |
|-------------|--------------------|---------------------|------------------|---------------------------|-----------------------|------------|--------------|---------------|-----------------------------------|------------------------------|
| 1 | 3743 | 955 | 319 | 1.15 | 0.085 | Cratered | Chain 1 | 9 | 2863 | - |
| 2 | 3988 | - | 247 | 1.00 | 0.061 | Flat | Chain 1 | 7 | 2863 | - |
| 3 | 3033 | - | 136 | 0.69 | 0.045 | Pointed | Isolated | 5 | - | 835 |
| 4 | 4851 | 382 | 382 | 1.36 | 0.078 | Cratered | Chain 2 | 8 | 1817 | 1034 |
| 5 | 3177 | - | 523 | 1.11 | 0.164 | Flat | Isolated | 18 | - | - |
| 6 | 4276 | 408 | 203 | 1.02 | 0.047 | Cratered | Chain 2 | 5 | 2208 | - |
| 7 | 3415 | 444 | 337 | 1.05 | 0.098 | Cratered | Chain 2 | 11 | 2208 | - |
| 8 | 1673 | - | 167 | 0.49 | 0.100 | Pointed | Isolated | 11 | - | - |
| 9 | 2106 | - | 194 | 0.64 | 0.092 | Flat | Clustered | 10 | - | - |
| 10 | 1722 | - | 143 | 0.48 | 0.083 | Flat | Clustered | 9 | - | 546 |
| 11 | 1978 | - | 147 | 0.53 | 0.074 | Flat | Clustered | 8 | - | 495 |
| 12 | 1085 | - | 169 | 0.37 | 0.156 | Flat | Clustered | 17 | - | 494 |
| 13 | 1174 | - | 127 | 0.35 | 0.108 | Flat | Clustered | 12 | - | 660 |
| 14 | - | 1166 | 118 | 0.34 | - | Pit crater | Clustered | - | - | - |
| 15 | - | 900 | 81 | 0.25 | - | Pit crater | Clustered | - | - | 1172 |
| 16 | - | 1296 | 70 | 0.31 | - | Pit crater | Clustered | - | - | 1207 |
| 17 | - | 450 | 107 | 0.17 | - | Pit crater | Clustered | - | - | - |
| 18 | - | 341 | 98 | 0.14 | - | Pit crater | Clustered | - | - | - |
| 19 | - | 374 | 93 | 0.15 | - | Pit crater | Clustered | - | - | 1155 |
| 20 | - | 433 | 101 | 0.17 | - | Pit crater | Clustered | - | - | - |
| 21 | - | 382 | 122 | 0.16 | - | Pit crater | Clustered | - | - | - |
| 22 | - | 1027 | 75 | 0.27 | - | Pit crater | Clustered | - | - | - |
| 23 | - | 458 | 99 | 0.17 | - | Pit crater | Clustered | - | - | - |
| 24 | - | 549 | 118 | 0.21 | - | Pit crater | Clustered | - | - | - |
| 25 | - | 823 | 112 | 0.27 | - | Pit crater | Clustered | - | - | - |
| 26 | - | 350 | 101 | 0.14 | - | Pit crater | Clustered | - | - | - |
| 27 | - | 670 | 51 | 0.18 | - | Pit crater | Clustered | - | - | - |
| 28 | - | 499 | 103 | 0.18 | - | Pit crater | Clustered | - | - | - |
| 29 | 4500 | 1107 | 351 | 1.34 | 0.07 | Cratered | Clustered? | 8 | - | - |
| 30 | 1663 | - | 183 | 0.51 | 0.11 | Pointed | Chain 3 | 12 | 843 | - |
| 31 | 1986 | - | 192 | 0.58 | 0.09 | Pointed | Chain 3 | 10 | 1373 | - |
| 32 | 3246 | - | 280 | 0.91 | 0.08 | Pointed | Chain 3 | 9 | 1843 | - |
| 33 | 1743 | 517 | 151 | 0.55 | 0.08 | Pointed | Chain 3 | 9 | 843 | - |
| 34 | 2484 | - | 382 | 0.85 | 0.15 | Pointed | Clustered | 17 | - | - |

Table A3.1 Summary of measurements for vents described in this study. Vents 1–28 are found within the Labatt survey, 29 – 34 are within the Yolla survey.

Appendix 4: Material Published in Support of the Thesis*

*This manuscript was officially accepted into the Bulletin of Volcanology on the 21/07/15

DOI 10.1007/s00445-015-0958-3

Rootless cone eruption processes informed by dissected tephra deposits and conduits

P. Reynolds^{1*}, R. J. Brown¹, T. Thordarson², E.W. Llewellyn¹, K. Fielding³

¹Department of Earth Sciences, Durham University, Science Labs, Durham, DH1 3LE, UK

²Faculty of Earth Sciences and Nordvulk, University of Iceland, Sturlugata 7, 101 Reykjavík, Iceland

³Formerly at: Hess Corporation, Level 9, The Adelphi Building, 1-1 John Adam Street, London, WC2N 6AG, UK

*Corresponding author: peter.reynolds@durham.ac.uk, +447887863550

Abstract

Rootless cones result from the explosive interaction between lava flows and underlying water-saturated sediment or volcanoclastic deposits. Rootless explosions can represent a significant far-field hazard during basaltic eruptions, but there are few detailed studies of their deposits. A rootless cone field in the 8.5 Ma Ice Harbor flow field of the Columbia River Basalt Province, NW USA, is revealed by sections through rootless conduit and cone structures. The Ice Harbor lava flow hosting the rootless cones was emplaced across a floodplain or lacustrine environment that had recently been mantled by a layer of silicic volcanic ash from a major explosive eruption. Our observations indicate a two-stage growth model for the rootless cones: (1) initial explosions generated sediment-rich tephra emplaced by fallout and pyroclastic density currents; and (2) later weaker explosions that generated spatter-rich fountains. Variable explosive activity resulted in a wide range of pyroclast morphologies and vesicularities. Cross-sections through funnel-shaped conduits also show how the conduits were constructed and stabilised. The growth model is consistent with decreasing water availability with time, as inferred for rootless cones described in Iceland.

The Ice Harbor rootless cones provide further lithological data to help distinguish between rootless cone-derived tephra and tephra generated above an erupting dyke.

Keywords: rootless cones; basalt lava; pāhoehoe; Columbia River Basalt Province; lava-water interaction.

1. Introduction

Explosive interaction between water-logged sediments (or volcanoclastic deposits) and molten lava can result in the formation of rootless cones, also known as ‘pseudocraters’ (Fig. 1; Thorarinsson 1953). Rootless cones are present within flow fields where the lava advanced over lacustrine, marsh and fluvial environments (Fagents and Thordarson 2007; Hamilton et al. 2010a, 2010b). Explosions are driven by the interaction of molten lava with a water-saturated, unconsolidated substrate. Explosions initiated by interaction of molten lava with substrate pore water eject clasts composed of lava crust, disrupted liquid lava and substrate-derived sediment onto a stationary surface of an active lava flow, thereby building a cone. Similar rootless edifices, known as littoral cones, form when lava flows interact with seawater in a littoral environment (Moore and Ault 1965; Fisher 1968; Jurado-Chichay et al. 1996; Mattox and Mangan 1997; Jaeger et al. 2007). Rootless cone-like structures have also been observed on the surface of Mars near the Martian equator (Lanagan et al. 2001; Bruno et al. 2004; Fagents and Thordarson 2007; Hamilton et al. 2010a) and have been used to infer the former presence of fluids in the Martian substrate.

Two models for rootless eruptions have been proposed; one assuming static heat transfer and the other inferring dynamic heat transfer. The static heat transfer model infers rapid emplacement of lava above a water-logged substrate. Water trapped beneath the lava flow is converted to steam producing eruptions that are analogous to phreatic explosions (Thorarinsson 1951, 1953).

In contrast, the dynamic heat transfer model of Fagents and Thordarson (2007) argues that the explosive interactions are driven by physical (dynamic) mixing of the lava and the water-logged substrate. The model is based on observations that sediment from the substrate is physically mixed into the rootless cone deposits and found between the core and the rim in armoured bombs. Furthermore, the cones feature multiple layers of tephra, which increase upwards in grain size from coarse ash/fine lapilli to bomb-size clasts

(Fagents and Thordarson 2007; Hamilton et al. 2010). The presence of layering implies sustained eruptions (estimated to have lasted for hours to days; Thordarson and Höskuldsson 2008), maintained by quasi-steady input of molten lava to the explosion site.

During rootless cone activity on pāhoehoe lavas, initial sedimentation occurs from explosions that produce pyroclastic density currents (PDCs) that deposit broad, sheet-like platform deposits around the vent (Hamilton et al. 2010a). Later tephra jets and lava fountains deposit lapilli- to bomb-sized scoria and spatter that build a cone (Thordarson et al. 1998; Fagents and Thordarson 2007; Hamilton et al. 2010a). The deposits of rootless activity are usually unconsolidated, except in proximal regions (Hamilton et al. 2010a). Rootless cones vary from 1–40 m in height and 2–450 m in basal diameter. The cones are crudely bedded, inversely graded, and may contain layers of rheomorphic spatter. The degree of explosivity is thought to be controlled by the explosion site geometry, the rate of lava influx, and the amount and availability of external water. Tephra deposits within rootless cone fields can cover areas of up to 150 km² and may exhibit complex stratigraphic relationships (Fagents and Thordarson 2007; Hamilton et al. 2010a and references therein).

Despite the abundance of rootless cones (e.g. Greeley and Fagents 2001; Lanagan et al. 2001; Fagents et al. 2002; Bruno et al. 2004; Fagents and Thordarson 2007; Hamilton et al. 2010a, 2010b, 2010c, 2011; Keszthelyi and Jaeger 2014), there is little documentation of their constituent pyroclasts and the characteristics of their host lava flows (e.g. Melchior Larsen et al. 2006; Hamilton et al. 2010a; 2010 b). Furthermore, rootless cones are superficially similar to small scoria cones and spatter cones, both in size and componentry (e.g. Fagents and Thordarson 2007). They may also have a linear spatial arrangement, similar to that of edifices along a dyke (e.g. Hamilton et al. 2010a). The limited knowledge of the internal stratigraphy of rootless cones coupled with their similarity to other volcanic edifices means that it can be difficult to distinguish rootless tephra from tephra generated during dyke-fed eruptions. This is particularly the case in flood basalt provinces, where pyroclastic successions are usually poorly preserved and poorly exposed (e.g. Swanson et al. 1975; Reidel and Tolan 1992; Brown et al. 2014).

In this paper, we document a newly discovered rootless cone field within the 8.5 Ma Ice Harbor pāhoehoe lava flow field in the Columbia River Basalt Province (CRBP), USA. Erosional dissection allows us to examine the tephra deposits and conduits of the rootless cones. We use these features to inform on the nature of the explosions that created the

rootless cones and to help define criteria that distinguish the deposits of rootless cones from those of dyke-fed eruptions.

2. Geological setting of the Columbia River Basalt Province

Flood basalt volcanism in the NW USA initiated c. 17 m.y. ago in the Steens Mountain region, Oregon. Over the following ~11 m.y. the volume of erupted mafic magma exceeded $>210\,000\text{ km}^3$ across Oregon and Washington (now considered part of the CRBP; Camp et al. 2003; Reidel et al. 2013). Eruptions were fed by ~300 km-long dyke swarms from crustal magma chambers under east-central Oregon/west-central Idaho (Wolff et al. 2008; Ramos et al. 2013). Volcaniclastic rocks in the CRBP are generally scarce, although exceptionally preserved examples of proximal tephra deposits (Swanson et al. 1975; Reidel and Tolan 1992; Brown et al. 2014), hyaloclastite deposits (Tolan et al. 2002), inferred rootless deposits (Thordarson and Self 1998) and drowned rootless cones (Keszthelyi and Jaeger 2014) are known.

The rootless cone deposits in this study occur in the 8.5 Ma Ice Harbor Member (Fig. 2), which is composed of three pāhoehoe lava flow fields that are the youngest products ascribed to the CRBP (McKee et al. 1977; Swanson et al. 1979). The lavas have been divided into three chemically distinct types that were fed from a dyke system that was up to 90 km in length and on average $<15\text{ km}$ in width (Swanson et al. 1975). The lava flow field has a minimum volume of 1.2 km^3 (Swanson et al. 1975) and individual lava flows are typically $<15\text{ m}$ thick. The pāhoehoe lavas are interbedded with the Ellensburg Formation sediments – diatomaceous muds, lacustrine sands and silts, volcaniclastic silt, conglomerates, and silicic volcanic ash probably sourced from eruptions of volcanoes in the NW USA. These sediments record deposition both within extensive lava-dammed lakes and by ephemeral and established rivers (Schminke 1967; Smith 1988; Tolan et al. 2002).

3. Method

Field studies involved detailed sedimentary logging of tephra successions, lithofacies analysis, geological mapping and sampling. Locations were recorded using a handheld GPS unit with an accuracy of $\pm 5\text{ m}$. Petrographic characterisation was undertaken by optical microscopy on representative thin sections. Vesicle and clast dimensions and abundances were calculated using the image analysis software ImageJ (<http://imagej.nih.gov/ij/>) with

representative samples and outcrop photographs. The crystal content of the cone deposits was calculated by point-counting representative samples. Clast densities were calculated on clasts >16 mm across using the method of Houghton and Wilson (1989). Grain size was determined by sieving.

4. Ice Harbor rootless cone field

The Ice Harbor rootless cone field is composed of: 1) the substrate over which the lava flows were emplaced (silicic volcanic ash); 2) the host pāhoehoe lava flows; 3) rootless cone conduits within the lava flows; 4) rootless cone- and platform-forming tephra deposits. The cone field is inferred to have occupied an area of ≥ 1 km², based on the distribution of the conduits and associated tephra. The cone field is overlain by later Ice Harbor lava flows.

4.1 Volcanic ash substrate

The pre-eruption substrate beneath the Ice Harbor flow field does not crop out in the study area, and the nature of the substrate has been inferred from analysis of material incorporated into the rootless cone tephra deposits. This material is composed of white, silicic, volcanic ash and forms 10–85 vol. % of all rootless cone tephra deposits. The volcanic ash is well-sorted ($1.2 \sigma\Phi$) and individual particles are platy, angular or cusped in shape and occasionally preserve vesicles. The volcanic ash has a median diameter of <0.25 mm. Smaller particles are blade shaped, whilst coarser particles have complex morphologies and exhibit bubble junctures.

Interpretation

The silicic volcanic ash is interpreted as a pyroclastic fall deposit within the Ellensburg Formation (e.g. Schminke 1967). The monolithologic character of the volcanic ash and the absence of organic matter or detrital sediment indicate that the volcanic ash had not been substantially reworked and that burial by the Ice Harbor lava may have occurred shortly after fallout. We infer that the volcanic ash fell out onto a flood plain or shallow lake; common features across the plateau-like CRBP during the Miocene (e.g. Schminke 1967; Smith 1988; Tolan et al. 2002). These environments are conducive to the formation of

rootless cones (e.g. Thorarinsson 1951, 1953; Fagents and Thordarson 2007; Hamilton et al. 2010a, 2010b).

4.2 Ice Harbor lava flows

The rootless cone field crops out along the banks of the Snake River (Fig. 2). The flow field is composed of pāhoehoe sheet lobes that reach 8 m thick and exhibit the tripartite structure typical of pāhoehoe sheet lobes in the CRBP (e.g. Self et al. 1998; Thordarson and Self 1998). They have lower crusts that contain distorted pipe vesicles, massive, dense cores with columnar joints and vesicular upper crusts. The groundmass of the flows is composed of interstitial glass, and plagioclase and pyroxene microlites. Pyroxene and rare swallow-tail plagioclase phenocrysts and glomerocrysts 0.1–3 mm in diameter constitute 1–4 vol. % of the rock. Vesicles are partially filled with zeolite minerals. The Ice Harbor sheet lobes that contain the rootless cones have poorly vesicular cores and incipiently vesicular crusts (as defined by Houghton and Wilson 1989) that exhibit hackly, entablature-style joints spaced 11–21 cm apart.

Interpretation

We infer that inflation of the flows took several weeks, based on a lava upper crust thickness of ≥ 2 m and the relationship: $t = 164.8C^2$; where t = time in hours and C = crustal thickness in metres (see Hon et al. 1994). The presence of entablature-style jointing in the lava indicates that the flows were subjected to water enhanced cooling, implying emplacement in an environment where surface water was abundant (e.g. Long and Wood 1986). The swallow tail plagioclase microlites indicate that the lava cooled rapidly; this texture is also found in pillow lavas (e.g. Bryan 1972; Jafri and Charan 1992).

4.3 Rootless cone conduits

Cliffs along the Snake River reveal funnel-shaped, upward-flaring features in the Ice Harbor sheet lobes (Fig. 3). These features range from 1–4 m in diameter, are up to 4 m deep and have cross-sectional areas of 8–12 m². Their walls dip inwards $\sim 60^\circ$. All the funnels appear to terminate ≥ 0.5 m above the bases of the sheet lobes and sometimes form irregular, isolated cavities; these are likely 2D section effects (Fig. 3). Hackly cooling joints

spaced ~16 cm apart radiate away from the funnel walls and extend up to ~4 m into the surrounding lava core (Fig. 3).

The inner surfaces of the funnels are coated with ropey-textured and bread-crust spatter that is ≤ 6 cm thick. The spatter has a hypohyaline groundmass texture, contains sheared vesicles and has multiple chilled rinds. The surface of the spatter has angular, hypocrySTALLINE and hypohyaline clasts of upper lava crust embedded in it. These clasts cover 10–30% of each funnel wall. There is a patchy, heterogeneous distribution of silicic volcanic ash across the surfaces; typically $< 5\%$. These funnels are often partially filled with tephra with a similar composition to the overlying cone deposits (massive spatter bombs, mSp; see below).

Twelve of these features have been recognised along a 450 m transect (Fig. 2); five on the north bank of the river and seven on the south. The features are spaced 3–206 m apart with tephra deposits exposed above them. Exposures spaced less than 5 m apart may represent irregular sections through the same feature.

Interpretation

We interpret these funnel-shaped features as remnants of rootless conduits because they have spatter, angular lapilli and patches of silicic ash plastered onto their inner wall which can only have occurred via explosive interactions. They are also filled with lapilli- to bomb-sized tephra. These features distinguish them from features described within rubbly pāhoehoe flows (e.g. Duraiswami et al. 2008; Keszthelyi et al. 2009). Sheared vesicles and rope-like textures on the conduit wall result from rheomorphic flow of spatter. The funnel shape of the conduits and their radiating cooling joints are similar to features seen in rootless cones in Iceland (e.g. Hamilton et al. 2010a).

Based on the abundance of conduits and the possibility that some locations represent irregular cross sections through the same conduit (e.g. L16/17; L1/2/6; L12/13) we suggest that the flow field hosted at least eight rootless cones. Since the size of the conduits is proportional to the size of the overlying cone (e.g. Hamilton et al. 2010a), the cones were likely to have been ≥ 5 m in basal diameter.

4.4 Rootless cone tephra deposits

Proximal rootless platform and cone-forming deposits are widely exposed over a 450 m-long transect along the south bank of the Snake River, and are intermittently exposed along the north bank of the river (Fig. 2). The tephra deposits are composed of juvenile pyroclasts (described below), silicic volcanic ash and fragmented lava crust.

4.4.1 Juvenile pyroclast types

The tephra deposits contain four different pyroclast types derived from the fragmentation and modification of the host lava flow (Fig. 4; Table 1). These juvenile clasts are (1) sideromelane ash and lapilli of both blocky and fluidal morphologies; (2) hypocrySTALLINE bombs (with both ventricular and globular morphologies) and angular lapilli; (3) armoured scoria bombs and lapilli; and (4) spatter bombs. All clasts have hypohyaline to hypocrySTALLINE groundmasses and are mineralogically similar to the host lava. The pyroclasts are incipiently to poorly vesicular, ranging between 15–36% vesicles, and are non to incipiently welded. The density of pyroclasts ranges from 1700–2300 kg m⁻³. The pyroclast types and their occurrence is summarised in Table 1.

Interpretation

The density of the Ice Harbor rootless tephra is significantly higher than that of non-welded basaltic pyroclasts produced during dyke-fed eruptions (typically 240–1440 kg m⁻³; Houghton and Wilson 1989; Parcheta et al. 2013). This suggests that the pyroclasts were sourced from lava that had already degassed at the source fissure and during transport to the rootless cone site. The ventricular and globular bombs are atypical of the deposits of fissure eruptions (e.g. Valentine and Gregg 2008); they are interpreted as water-quenched globules of lava ejected from beneath the lava flow during explosive activity. These bombs were subsequently mechanically fragmented into angular lapilli upon eruption and deposition, enhanced by cooling contraction fractures. The spatter bombs are interpreted as proximal deposits from rootless lava fountains (e.g. as observed during the 1783–1785 Laki eruptions, see Thordarson et al. 1998). Recycling by intermittent fountains appears necessary to form the armoured bombs. The blocky sideromelane clasts indicate cooling-contraction granulation and/or mechanical fragmentation. The fluidal, elongate sideromelane clasts indicate ductile disruption of molten lava and are common components of deposits from magmatic volatile driven eruptions (e.g. Walker and Croasdale 1971),

phreatomagmatism (e.g. Zimanowski et al. 1997; Morrissey et al. 2000; Büttner et al. 2002) and peperite (see section 4.4.3; Skilling et al. 2002).

4.4.2 Pyroclastic lithofacies

The tephra deposits can be sub-divided into four lithofacies according to their componentry, grain size and depositional structures (Fig. 5; Table 2). In general the pyroclastic lithofacies appear moderately to very poorly sorted and are composed of juvenile clasts with <10–85 vol. % silicic volcanic ash. Lithofacies with the largest juvenile clasts tend to have the least silicic volcanic ash (Fig. 6). The lithofacies form proximal platform, cone or conduit-filling deposits. Sheet deposits are not found; these are commonly unconsolidated (Hamilton et al. 2010a). Contacts between the tephra deposits and underlying lavas are not exposed (Fig. 6).

Platform deposits include massive or normally graded lapilli-ash (m/nLAf), lenses of lapilli-ash (lensLA) and cross-stratified lapilli-ash (xsLA; Table 2; Fig. 5). These deposits are 1–5.5 m in thickness (Fig. 7) and are present beneath the parallel-bedded spatter (//bSp; Figs. 6 and 7). Pyroclasts within the deposits are dominantly of lapilli size. They are exposed over a ~600 m long transect. Bedding dips vary from 10–20°.

Cone deposits are composed of parallel-bedded spatter (//bSp; Table 2) that is 1–3 m thick (Fig. 6) and contains predominantly bomb-sized clasts. Deposits are exposed over a ~200 m long transect. The spatter varies from horizontally bedded to dipping up to 20°; whether this is towards or away from a conduit is unclear (Figs. 6 and 7).

The conduits are partially filled with massive spatter (mSp; Table 2) and are not observed in contact with overlying cone and/or platform deposits.

Interpretation

The Ice Harbor platform deposits are inferred to have been deposited from both PDCs and by fallout (e.g. Hamilton et al. 2010a). The occurrence of massive/normally graded lapilli-ash (m/nLAf), lenses of lapilli-ash (lensLA) and cross-stratified lapilli-ash (xsLA) beneath the spatter-rich deposits (e.g. //bSp) suggests that the platform was constructed prior to cone formation. Intermittent deposits of normally-graded lapilli ash (nLA) and cross-stratified lapilli-ash (xsLA; Fig. 6) overlying the spatter layers suggests that the cone field is composed of numerous overlapping cones formed in a sequence of rootless

eruptions (e.g. Fagents and Thordarson 2007). The thickness and spatial distribution of the exposures suggest that the tephra platforms were ~5 m thick and were likely to be laterally extensive over 100's of metres. Cone-forming and conduit-filling deposits of rootless cones commonly contain spatter-rich lithofacies (Hamilton et al. 2010a), as observed in this study. These coarse-grained deposits are produced as the explosivity of the eruptions decreases (Fagents and Thordarson 2007).

4.4.3 Lava-silicic volcanic ash interaction textures in tephra deposits

A variety of peperite-like textures are observed in the tephra deposits (Fig. 8). Fluidal textures include spatter bombs that inter-finger with the silicic volcanic ash and associated globular and elongate spatter lapilli and ash found intimately mixed with the silicic volcanic ash. Within 2 cm of the spatter, the silicic volcanic ash is often thermally altered, becoming dark in colour and fused (e.g. Schminke 1967). Where fused, the silicic volcanic ash contains vesicles ≤ 2 mm in diameter. Vesicles in the spatter also contain silicic ash. Blocky textures include jigsaw-fit bombs; these clasts have hairline fractures filled with silicic volcanic ash. Other bombs have rinds that are partially separated from their core, encapsulating a 2 mm-thick domain of silicic volcanic ash between rind and core. These domains contain mm-scale globules of lava.

Interpretation

Peperite-like textures indicate interaction between hot juvenile clasts and unconsolidated sediment (e.g. Skilling et al. 2002). Vesicles in the fused silicic volcanic ash indicate that gas was generated during interaction (e.g. Kokelaar 1982; Skilling 2002; Squire and McPhie 2002). Silicic ash-filled vesicles in the spatter indicate that the sediment was mobilised during interaction (e.g. Goto and McPhie 1996; Skilling 2002 and references there-in). The fluidal and blocky textures indicate variations in mechanical stress, movement of lava, lava-silicic ash density contrasts and variations in lava viscosity and clast size (e.g. Skilling et al. 2002; Squire and McPhie 2002). These textures may represent a failed phreatomagmatic fragmentation process formed beneath the lava flow (e.g. Busby-Spera and White 1987; Hooten and Ort 2002). The bombs with encapsulated silicic volcanic ash are interpreted as intrusions of lava into the underlying substrate. Lava

globules in the silicic volcanic ash domain indicate that the cores of these bombs were molten during intrusion.

5. Emplacement of the Ice Harbor rootless cones

We infer that the Ice Harbor lava flows traversed a lacustrine or floodplain environment (Fig. 9). The ground was mantled by a layer of silicic volcanic ash fall derived from a major explosive eruption. As the lava flows inflated they developed brittle basal crusts (Hon et al. 1994). These crusts were weakened by the development of cooling fractures (Thordarson and Self 1998) which created a zone of weakness along the base of the flows. Cracking and subsequent failure of the crust would have been facilitated by heterogeneous subsidence of the flows during inflation (e.g. Fagents and Thordarson 2007; Hamilton et al. 2010a). Failure of the basal crust allowed extrusion of lava, analogous to the axial cleft of a tumulus (e.g. Walker 1991; Rossi and Gudmundsson 1996; Hamilton et al. 2010a).

Extrusion of lava through the basal crust resulted in the intimate mixing of molten lava with the water-saturated silicic volcanic ash. This mixing of the lava and sediment is evidenced by the peperite-like textures and abundance of silicic volcanic ash (i.e. substrate) in the tephra deposits. Lava-substrate mixing was followed by explosions. These fragmented the lower lava crust and burst through the molten lava core creating transient conduits. The preservation of conduits requires the cooling and solidification of the conduit walls over time to prevent pressure-driven collapse of the walls between explosions. The presence of spatter lining the walls of the conduits indicates that they were stabilised from both material ejected during the explosions, as well as from the chilling of the molten lava core. Explosive activity deposited the massive/normally graded lapilli-ash (lithofacies m/nLA (f)) on top of the lava flow. Some of the pyroclastic material formed PDCs (depositing lithofacies lensLA and xsLA; Table 2). These processes constructed the tephra platforms.

Spatter-rich lithofacies (e.g. //bSp and mSp; Table 2) were produced during rootless lava fountaining and cap the rootless cone successions and fill some conduits. The coarse clast size of these lithofacies indicates decreasing explosivity as water availability declined. Explosions also embedded juvenile clasts and lava crust lithics into the hot and ductile conduit walls.

The presence of the cones on top of sheet lobes suggests that the cones developed repelled, non-aligned spatial distributions (e.g. Hamilton et al. 2010a, 2010b). The cones were likely to have formed in topographic lows where lava and water were most abundant, and in regions of enhanced substrate compressibility (Hamilton et al. 2010a, 2010b). Exposures do not allow determination of the symmetry of the cones (e.g. radial or elongate). Growth of the cones was terminated by the decreasing availability of ground water, or by water being prevented from gaining access to the explosion site. Continued cooling stabilised the conduit walls and over time cooling joints radiated out into the core (e.g. Fig. 9).

6. Comparison with other rootless cones

The deposits in this study are comparable with the platform and cone-building deposits of rootless cones in Iceland (e.g. Table 3; Fig. 10), which show a similar pattern of sediment-rich PDC deposits overlain by coarse-grained fall deposits. These PDC and fall deposits are composed of scoria lapilli and bombs, spatter bombs and clastogenic lava, all intimately mixed with silt- to cobble-sized sediment. The coarse grainsize of the platform deposits in this study relative to others described in Iceland (Hamilton et al. 2010a) may result from the proximity of the Ice Harbor tephra platforms to the explosion source, or from less efficient magma-water interaction. The substrate properties (e.g. grainsize distribution and thermal conductivity) may also have affected explosivity (e.g. Sohn 1996; White 1996). Furthermore, the properties of the substrate would have evolved during the eruptions, due to mixing of pyroclasts and silicic volcanic ash beneath the lava flow. However, the role of sediment properties in governing the explosivity of rootless eruptions is as-yet unknown.

7. Conclusions

The Ice Harbor tephra deposits provide insights into the construction and componentry of a rootless cone field. Cross sections of conduits suggest that ≥ 8 cones were present in a cone field ≥ 1 km² in area. Cone- and platform-forming deposits are composed of admixed juvenile clasts, clasts from the host lava flow and silicic volcanic ash from an earlier, major explosive eruption in NW USA. Construction of the cone field occurred through a combination of deposition from PDCs and lava fountaining. Explosivity decreased with

time as a result of decreasing water availability in the underlying silicic volcanic ash. This study demonstrates that the abundance of sediment (in this case, silicic volcanic ash) in the tephra, juvenile clast morphology and clast density are useful criteria for distinguishing between rootless tephra and tephra produced above an erupting dyke.

Acknowledgements

PR acknowledges a studentship funded by Hess Corporation as part of the Volcanic Margins Research Consortium. Reviewers Bernd Zimanowski and Laszlo Keszthelyi are thanked for their thoughtful input, as is associate editor Pierre-Simon Ross.

References

- Brown RJ, Blake S, Thordarson T, Self S (2014) Pyroclastic edifices record vigorous lava fountains during the emplacement of a flood basalt flow field, Roza Member, Columbia River Basalt Province, USA. *Geol Soc Am Bull* 126:875-891
- Bruno BC, Fagents S, Thordarson T, Baloga SM, Pilger E (2004) Clustering within rootless cone groups on Iceland and Mars: Effect of nonrandom processes. *J Geophys Res* 109:1991-2012
- Bryan WB (1972) Morphology of quench crystals in submarine basalts. *J Geophys. Res.* 77:5812-5819
- Busby-Spera CJ, White, JD (1987) Variation in peperite textures associated with differing host-sediment properties. *B Volcanol* 49:765-776
- Büttner R, Dellino P, La Volpe L, Lorenz V, Zimanowski B (2002) Thermohydraulic explosions in phreatomagmatic eruptions as evidenced by the comparison between pyroclasts and products from Molten Fuel Coolant Interaction experiments. *J. Geophys. Res.* 107:2277
- Camp VE, Ross ME, Hanson WE (2003) Genesis of flood basalts and Basin and Range volcanic rocks from Steens Mountain to the Malheur River Gorge, Oregon. *Geol Soc Am Bull* 115:105-128
- Duraiswami RA, Bondre NR, Managave S (2008) Morphology of rubbly pahoehoe (simple) flows from the Deccan Volcanic Province: Implications for style of emplacement. *J Volcanol Geotherm Res* 177:822-836
- Fagents SA, Thordarson T (2007) Rootless cones in Iceland and on Mars. In: Chapman M, Skilling IP (eds) *The Geology of Mars: Evidence from Earth-Based Analogues*. Cambridge University Press, pp 151–177
- Fagents SA, Lanagan P, Greeley R (2002) Rootless cones on Mars: a consequence of lava-ground ice interaction. *Geological Society, London, Special Publications* 202:295-317
- Fisher RV (1968) Puu Hou littoral cones, Hawaii. *Geologische Rundschau* 57:837-864
- Goto Y, McPhie J (1996) A Miocene basanite peperitic dyke at Stanley, northwestern Tasmania, Australia. *J Volcanol Geoth Res* 74:111-120
- Greeley R, Fagents SA (2001) Icelandic pseudocraters as analogs to some volcanic cones on Mars. *J. Geophys. Res.* 106:20527-20546

- Hamilton CW, Thordarson T, Fagents SA (2010a) Explosive lava–water interactions I: architecture and emplacement chronology of volcanic rootless cone groups in the 1783–1784 Laki lava flow, Iceland. *B Volcanol* 72:449-467
- Hamilton CW, Fagents SA, Thordarson T (2010b) Explosive lava–water interactions II: self-organization processes among volcanic rootless eruption sites in the 1783–1784 Laki lava flow, Iceland. *B Volcanol* 72:469-485
- Hamilton CW, Fagents SA, Wilson L (2010c), Explosive lava-water interactions in Elysium Planitia, Mars: Geologic and thermodynamic constraints on the formation of the Tartarus Colles cone groups, *J. Geophys. Res.* 115:1991-2012
- Hamilton CW, Fagents SA, Thordarson T (2011) Lava–ground ice interactions in Elysium Planitia, Mars: Geomorphological and geospatial analysis of the Tartarus Colles cone groups, *J. Geophys. Res.* 116:1991-2012
- Hon K, Kauahikaua J, Delinger R, Mackay K (1994) Emplacement and inflation of pahoehoe sheet flows: Observations and measurements of active lava flows on Kilauea Volcano, Hawaii. *Geol Soc Am Bull* 106:351-370
- Hooten JA, Ort MH (2002) Peperite as a record of early-stage phreatomagmatic fragmentation processes: an example from the Hopi Buttes volcanic field, Navajo Nation, Arizona, USA. *J Volcanol Geoth Res* 114:95-106
- Houghton BF, Wilson CJN (1989) A vesicularity index for pyroclastic deposits. *B Volcanol* 51:451-462
- Jaeger WL, Keszthelyi LP, McEwen AS, Dundas CM, Russell PS (2007) Athabasca Valles, Mars: A Lava-Draped Channel System. *Science* 317:1709-1711
- Jafri SH, Charan SN (1992) Quench textures in pillow basalt from the Andaman-Nicobar Islands, Bay of Bengal, India. *Proc. Indian Acad. Sci. (Earth Planet Sci)* 101:99-107
- Jurado-Chichay Z, Rowland S, Walker GL (1996) The formation of circular littoral cones from tube-fed pāhoehoe: Mauna Loa, Hawai'i. *B Volcanol* 57:471-482
- Keszthelyi LP, Jaeger WL (2014) A field investigation of the basaltic ring structures of the Channeled Scabland and the relevance to Mars. *Geomorph.* doi:10.1016/j.geomorph.2014.06.027
- Keszthelyi LP, Baker VR, Jaeger WL, Gaylord DR, Bjornstad BN, Greenbaum N, Self S, Thordarson T, Porat N, Zreda MG (2009) Floods of water and lava in the Columbia River Basin: Analogs for Mars. *Geol Soc Am Field Guides* 15:845-874.
- Kokelaar BP (1982) Fluidization of wet sediments during the emplacement and cooling of various igneous bodies. *J Geol Soc* 139:21-33
- Lanagan PD, McEwen AS, Keszthelyi LP, Thordarson T (2001) Rootless cones on Mars indicating the presence of shallow equatorial ground ice in recent times. *Geophys Res Lett* 28:2365-2367
- Long PE, Wood BJ (1986) Structures, textures, and cooling histories of Columbia River basalt flows. *Geol Soc Am Bull.* 9:1144-1155.
- Mattox TN, Mangan MT (1997) Littoral hydrovolcanic explosions: a case study of lava–seawater interaction at Kilauea Volcano. *J Volcanol Geoth Res* 75:1-17
- McKee E, Swanson D, Wright T (1977) Duration and volume of Columbia River basalt volcanism, Washington, Oregon and Idaho. In: *Geol. Soc. Am. Abstr. Programs.* pp 463-464
- Melchior Larsen L, Ken Pedersen A, Krarup Pedersen G (2006) A subaqueous rootless cone field at Niuluut, Disko, Paleocene of West Greenland. *Lithos* 92:20-32
- Moore JG, Ault WU (1965) Historic littoral cones in Hawaii. *Pacific science* XIX(3-11)

- Morrissey M, Zimanowski B, Wohletz KH, Buettner R (2000) Phreatomagmatic fragmentation. In: Sigurdsson H (ed) *Encyclopedia of volcanoes*, pp 431-445.
- Parcheta CE, Houghton BF, Swanson DA (2013) Contrasting patterns of vesiculation in low, intermediate, and high Hawaiian fountains: A case study of the 1969 Mauna Ulu eruption. *J Volcanol Geoth Res* 255:79-89
- Ramos FC, Wolff JA, Starkel W, Eckberg A, Tollstrup DL, Scott S (2013) The changing nature of sources associated with Columbia River flood basalts: Evidence from strontium isotope ratio variations in plagioclase phenocrysts. *Geol Soc Am Spec Pap* 497:231-257
- Reidel SP, Tolan TL (1992) Eruption and emplacement of flood basalt: An example from the large-volume Teepee Butte Member, Columbia River Basalt Group. *Geol Soc Am Bull* 104:1650-1671
- Reidel SP, Camp VE, Tolan TL, Martin BS (2013) The Columbia River flood basalt province: stratigraphy, areal extent, volume, and physical volcanology. *Geol Soc Am Spec Pap* 497:1-43
- Rossi MJ, Gudmundsson A (1996) The morphology and formation of flow-lobe tumuli on Icelandic shield volcanoes. *J Volcanol Geotherm Res* 72:291-308
- Schminke H-U (1967) Fused Tuff and P  perites in South-Central Washington. *Geol Soc Am Bull* 78:319-330
- Self S, Keszthelyi L, Thordarson T (1998) The importance of pahoehoe. *Annu. Rev. Earth Planet. Sci.* 26:81-110
- Simpson K, McPhie J (2001) Fluidal-clast breccia generated by submarine fire fountaining, Trooper Creek Formation, Queensland, Australia. *J Volcanol Geoth Res* 109:339-355
- Skilling IP, White JDL, McPhie J (2002) Peperite: a review of magma-sediment mingling. *J Volcanol Geoth Res* 114:1-17
- Smith GA (1988) Neogene synvolcanic and syntectonic sedimentation in central Washington. *Geol Soc Am Bull* 100:1479-1492
- Sohn YK (1996) Hydrovolcanic processes forming basaltic tuff rings and cones on Cheju Island, Korea. *Geol Soc Am Bull* 108:1199-1211
- Sumner JM, Blake S, Matela RJ, Wolff JA (2005) Spatter. *J Volcanol Geoth Res* 142(1-2):49-65
- Swanson DA, Wright TL, Helz RT (1975) Linear vent systems and estimated rates of magma production and eruption for the Yakima Basalt on the Columbia Plateau. *Am J Sci* 275:877-905
- Swanson D, Wright TL, Hooper PR, Bentley RD (1979) Revisions in stratigraphic nomenclature of the Columbia River Basalt Group. *U.S Geol Surv Bull* 1457 G1-G59
- Thorarinsson S (1951) Laxargljufur and Laxarhraun: a tephrochronological study. *Geograf Annal* 2:1-89
- Thorarinsson S (1953) The crater groups in Iceland. *B Volcanol* 14:3-44
- Thordarson T, Self S (1998) The Roza Member, Columbia River Basalt Group: A gigantic pahoehoe lava flow field formed by endogenous processes? *J. Geophys. Res.* 103:27411-27445
- Thordarson T, H  skuldsson    (2008) Postglacial volcanism in Iceland. *J  kull* 58:197-228.
- Thordarson T, Miller D, Larsen G (1998) New data on the Leidolfsfell cone group in South Iceland. *J  kull* 46: 3-15

- Tolan TL, Beeson MH, Lindsey KA (2002) The effects of volcanism and tectonism on the evolution of the Columbia River system. In: *A Field Guide to Selected Localities in the South-western Columbia River Plateau and Columbia River Gorge of Washington and Oregon State*. Northwest Geological Society
- Valentine GA, Gregg TKP (2008) Continental basaltic volcanoes – Processes and problems. *J Volcanol Geoth Res* 177:857-873
- Walker GPL (1991) Structure, and origin by injection of lava under surface crust, of tumuli, 'lava rises', 'lava-rise pits', and 'lava inflation clefts' in Hawaii. *B Volcanol* 53:546–558
- Walker GPL, Croasdale R (1971) Characteristics of some basaltic pyroclastics. *Bulletin Volcanologique*, 35:303-317
- White JDL (1996) Impure coolants and interaction dynamics of phreatomagmatic eruptions. *J Volcanol Geoth Res* 74:155-170
- Wolff J, Ramos F, Hart G, Patterson J, Brandon A (2008) Columbia River flood basalts from a centralized crustal magmatic system. *Nat Geo* 1:177-180
- Zimanowski B, Büttner R, Lorenz V, Häfele HG (1997) Fragmentation of basaltic melt in the course of explosive volcanism. *J Geophys Res* 102:803-814

Figure Captions

Fig. 1 Generalised structure of a rootless cone. The cones form on active lava flows. The conduits in the host lava flow are irregular funnels that widen upwards. The upper parts of the conduits are filled with tephra. Cooling joints in the host lava flow radiate from the conduit. Cone forming deposits are composed of lapilli- to bomb-sized material that is often reversely graded and formed by fallout. Platform and sheet deposits are formed by fallout and deposition from pyroclastic density currents. Adapted from Hamilton et al. (2010a)

Fig. 2 Location of the study area. **a** The CRBP in the NW USA, adapted from Brown et al. (2014). **b** Map of the area showing the Ice Harbor fissure as described by Swanson et al. (1975) and our field area on the banks of the Snake River. **c** Sites of the tephra and conduit deposits described in this study

Fig. 3 Field photographs and schematic diagrams showing the varying geometries of rootless conduits. **a** Field sketch showing the upper part of a funnel-shaped conduit at location 6 (UTM Nad83 zone 11T, 359 987 E/5 126 647 N). View to the southwest. **b** Field photograph of massive spatter (mSp) within the conduit in **a**, composed of spatter bombs,

silicic volcanic ash and hypocrySTALLINE lapilli. **c** Irregular lower part of a conduit in the lava flow at location 22 (UTM Nad83 zone 11T, 359 724 E/5 128 162 N) with cooling joints (white) radiating from the conduit/lava core contact (outlined). The ruler is 1 m. Inset **d** shows a close up of the conduit inner wall with embedded juvenile and lava crust lithic clasts. The ruler is 25 cm. Image **e** shows a cross section through the conduit wall, with hypohyaline lapilli embedded into the surface. **f** Interpretive sketch of e. **g** Plan view of a section of conduit wall, approximately 100 mm across, showing clasts that are inferred to have become embedded in the conduit wall during explosions (dashed outlines)

Fig. 4 Clast types recognised in this study. **a** Folded spatter bomb with embedded lapilli (dashed outline). Graticules on the scale card are 1 cm (UTM Nad83 zone 11T, 359 942 E/5 126 519 N). **b** Ventricular clast (outlined). The clast has an amoeboid shape with a hypohyaline rind approx. 10 mm thick that grades inwards into the core. Vesicles up to 8 cm in diameter (dashed outline) have angular shapes and give clasts their characteristic ventricular morphology (UTM Nad83 zone 11T, 359 942 E/5 126 519 N). **c** Globular bomb (outlined). The bombs have a sub-spherical shape and a black hypohyaline rind ~1 cm thick that becomes more orange in colour toward the core. Sub angular, dull black coloured basaltic lapilli (arrowed) are contained within the cores of the bombs. Cooling joints (dashed lines) penetrate from the clast margin up to 10 mm towards the core (UTM Nad83 zone 11T, 359 942 E/5 126 519 N). **d** Armoured bomb (solid outline) with 1 cm thick dense rind and vesicular core (dashed outline) (UTM Nad83 zone 11T, 360 015 E/5 126 664 N). **e** Sideromelane clast (arrowed) formed by fragmentation in a brittle state (arrowed). **f** Sideromelane clast (arrowed) formed by ductile disruption of molten lava

Fig. 5 Lithofacies found in the study area. **a** mLA with ventricular bomb (outlined) enclosing laminated silicic volcanic ash. Graticules on the scale card are 1 cm (UTM Nad83 zone 11T, 359 881 E/5 126 506 N) **b** lensLA with hypocrySTALLINE lapilli-rich lenses. Dashed white outlines indicate lenses (UTM Nad83 zone 11T, 359 868 E/5 126 485 N) **c** lensLA with silicic ash-rich lenses. White outlines indicate lenses (UTM Nad83 zone 11T, 359 868 E/5 126 485 N) **d** xsLA, white outlines indicate beds. The ruler is 25 cm long (UTM Nad83 zone 11T, 359 868 E/5 126 485 N) **e** //bSp, showing bedded spatter bombs. The ruler is 50 cm (UTM Nad 83 zone 11T, 359 942 E/5 126 519 N)

Fig. 6 Lithofacies logs of tephra deposits south of the river. Clast size is shown on the top axis with divisions at 32, 64, 128 and 256 mm (Location 9 uses 32, 64, 128, 256 and >1000 mm divisions). Silicic volcanic ash abundance (black squares; %) is shown across the bottom axis in 25% graticules. Logs are shown at relative altitudes. For locations of the sections see Fig. 2

Fig. 7 Photographs and interpretive pictures of Location 9 (UTM Nad 83 zone 11T, 359 942 E/5 126 519 N). **a, b** Outcrop of platform-forming admixed tephra and silicic volcanic ash. **c,d** Outcrop of cone-forming tephra composed of lithofacies //bSp

Fig. 8 Peperite-like textures produced by the interaction of juvenile clasts and silicic volcanic ash. **a** Fluidal peperite with elongate and globular clasts in lithofacies //bSp (UTM Nad 83 zone 11T, 359 942 E/5 126 519 N). **b** Blocky peperite with jigsaw-fit fractures (circled). Graticules are 1 cm (UTM Nad 83 zone 11T, 360 014 E/5 126 649 N). Thin section **c** and interpretive sketch **d** shows section of mingled spatter and silicic volcanic ash. The spatter clasts exhibit elongate and globular morphologies. The silicic ash is thermally altered and contains vesicles. Vesicles within the spatter clasts enclose silicic volcanic ash. Section of a ventricular bomb **e** and interpretive sketch **f** are also shown. The hypohyaline rind is spalling from the core and has encapsulated a domain of silicic volcanic ash. Fluidal basalt clasts are found within the silicic ash domain (arrowed) indicating that the core of the bomb was molten when the sediment was encapsulated

Fig. 9 Inferred eruption chronology for the cones. **a** Lava flow traverses wet ground and subsides heterogeneously into the underlying silicic volcanic ash. **b** Initial mingling of lava with the silicic ash results in the formation of globular and ventricular juveniles and peperite-like textures. **c** Interaction between molten lava and water saturated silicic volcanic ash results in explosive brecciation of the host lava flow and fragmentation of the globular and ventricular juveniles into lapilli and ash sized clasts. Episodic eruptions and dilute PDC's deposit poorly sorted juveniles and clasts sourced from the host lava flow, forming sheet and platform deposits (lithofacies m/nLA(f), lensLA, xsLA). Minor clast recycling may occur, producing armoured bombs. Substrate pore water is gradually depleted beneath

the lava flow. **d** Decreasing water availability results in less efficient fragmentation and lava fountains are generated. These fountains produce lithofacies that builds a cone. Lapilli are also impacted into the cooling conduit walls. **e** With time water availability decreases and eruptions cease. The lava flow may continue to inflate and deform the conduit. Post-eruption cooling of the lava promotes the formation of cooling joints that radiate from the conduit

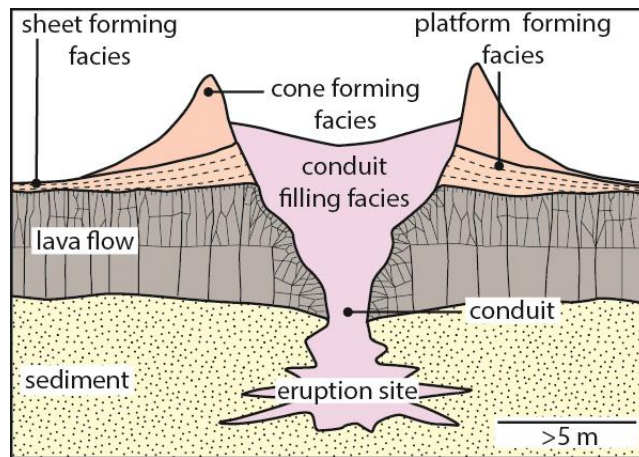
Fig. 10 Photographs of Leitin and Búrfell rootless cones in southern Iceland (UTM Nad 83, zone 27, 500 000 E/7 097 014 N; 402 187 E/7 098 548 N respectively). **a** Overlapping cone stratigraphies composed of crudely bedded spatter and scoria bombs and lapilli and clastogenic lava. The sequence is ~6 m thick. **b** Bomb-sized clast of sediment (outlined) within a sequence of scoria and spatter. The ruler is 40 cm long. **c** Sediment-rich pyroclastic density current deposit at the base of the cone forming stratigraphy. The reddish colour is given by the agglutinated sediment (inferred to be a lacustrine siltstone), not oxidation of the pyroclasts. The scale card is 120 mm long. **d** Bomb-sized, ventricular-type pyroclast (outlined) within the bedded spatter and scoria. The ruler is ~25 cm long. **e** Initial cone-forming fall deposit, composed of scoria lapilli. Beds often form inversely-graded couplets. The bed indicated is ~6 cm thick. Beds thickness and clast size increases up-section. **f** Cross section of the conduit wall, with lapilli sized pyroclasts agglutinated to the outer wall. Cooling joints (dashed lines) radiate from the contact and are perpendicular to the conduit contact. The arrow points towards the core of the lava flow. The ruler is 30 cm long. **g** A lava flow affected by rootless cone formation. The lava flow can be divided into a colonnade (CN) and an entablature (EN), and has an irregular upper contact that forms the rootless conduit. The lava is ~10 m thick

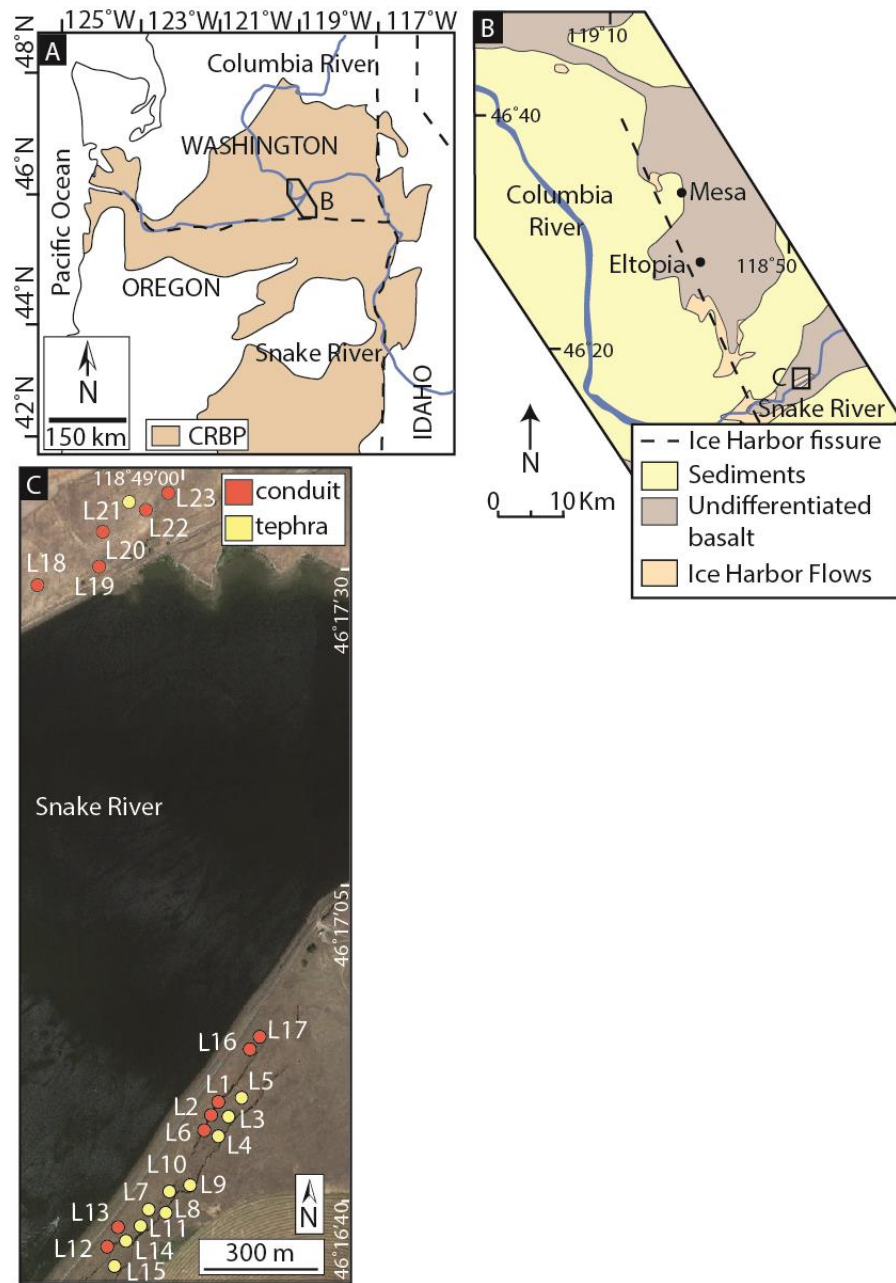
Table 1 Summary descriptions of pyroclast types

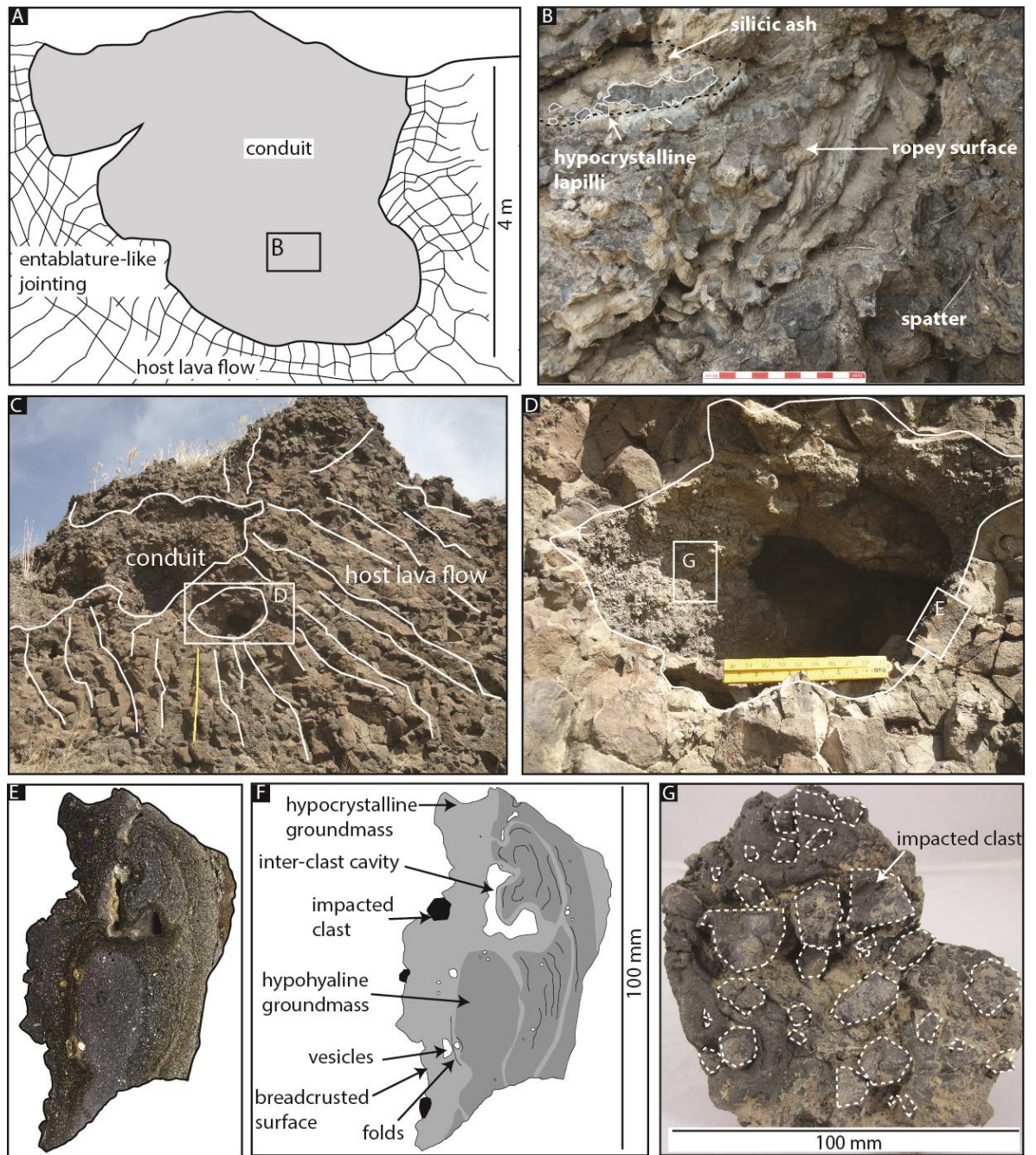
Table 2 Summary descriptions of cone-forming and conduit deposits

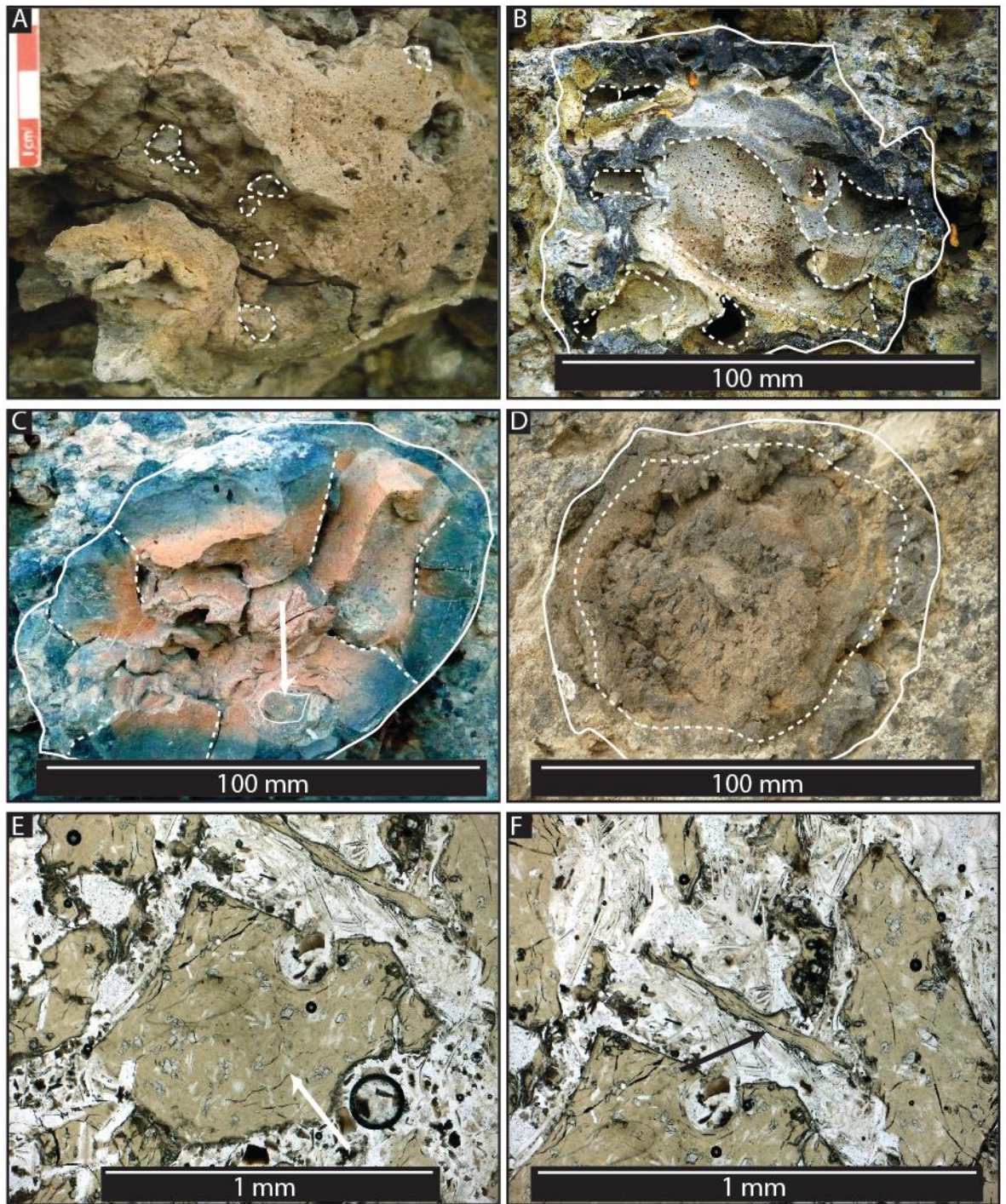
Table 3 Comparison of rootless and littoral cone structures using data from Simpson and McPhie (2001); Mattox and Mangan (1997); Moore and Ault (1965); Fisher (1968);

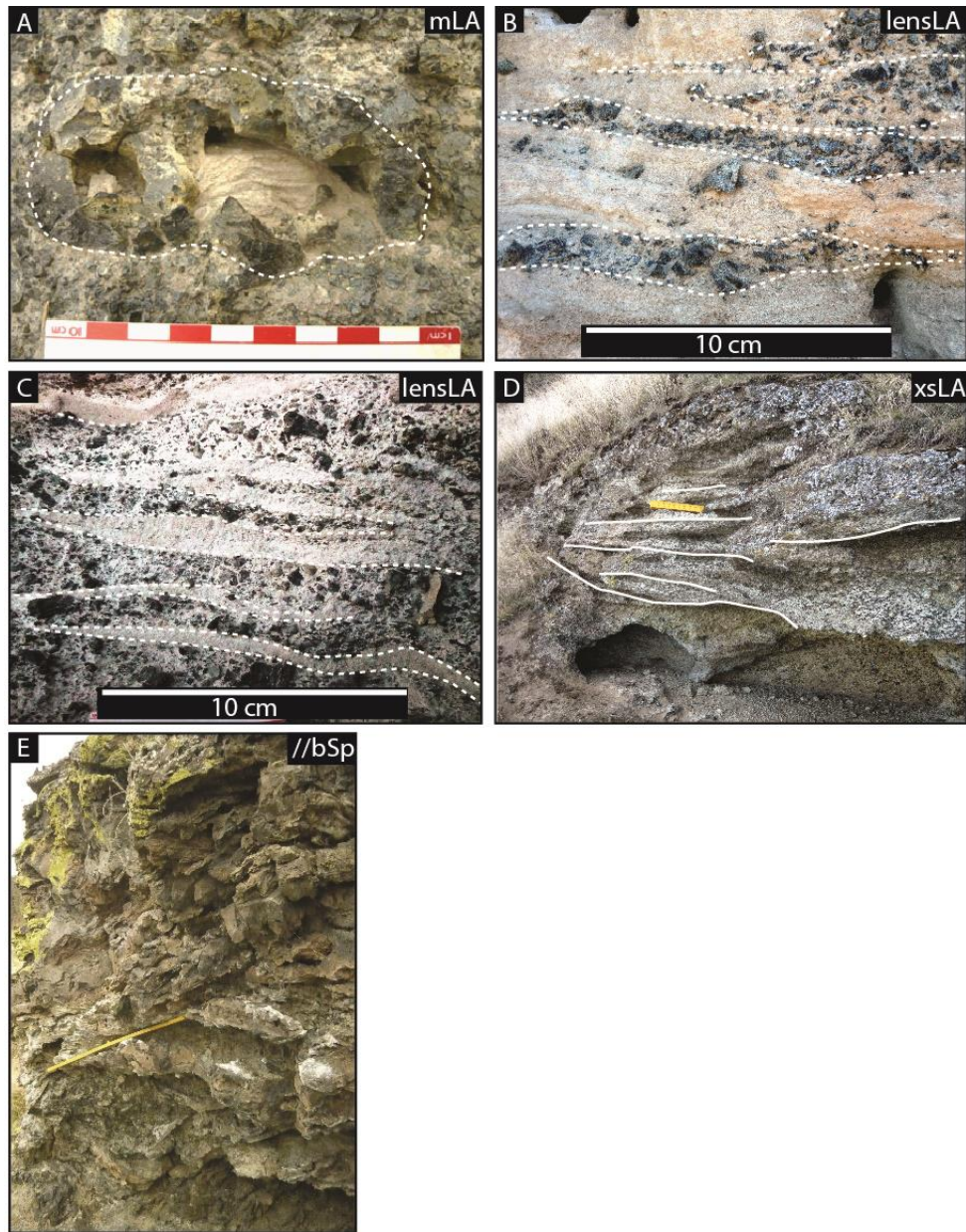
Hamilton et al. (2010a); Melchior Larsen et al. (2006); Jurado-Chichay et al. (1996); and this study



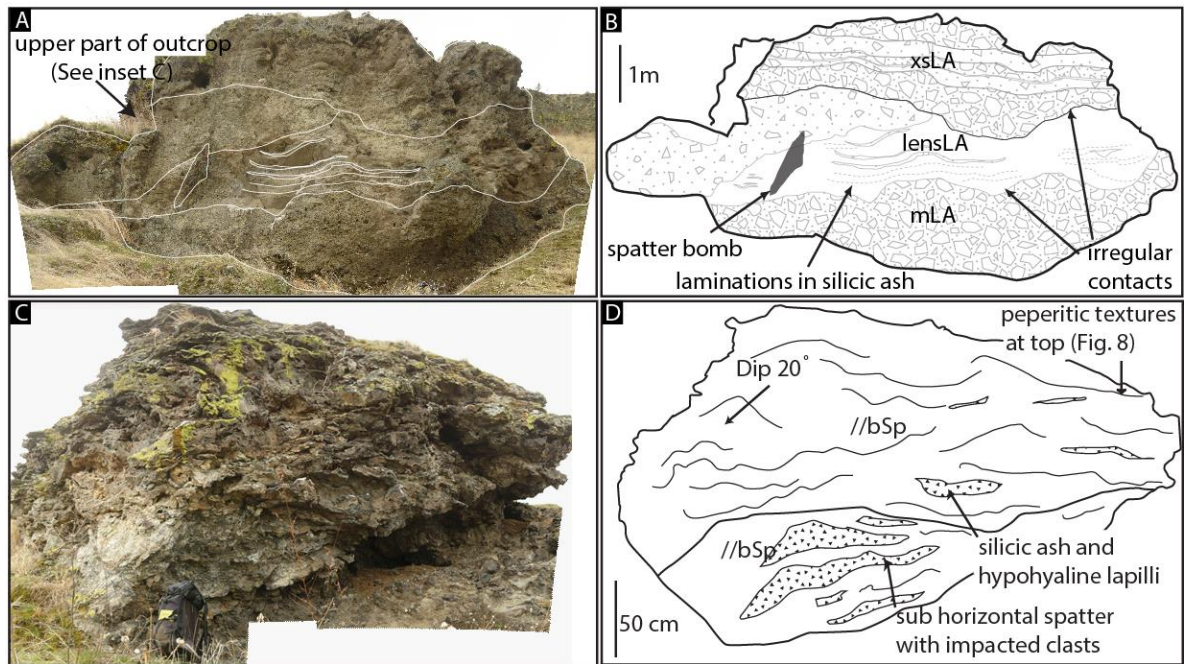


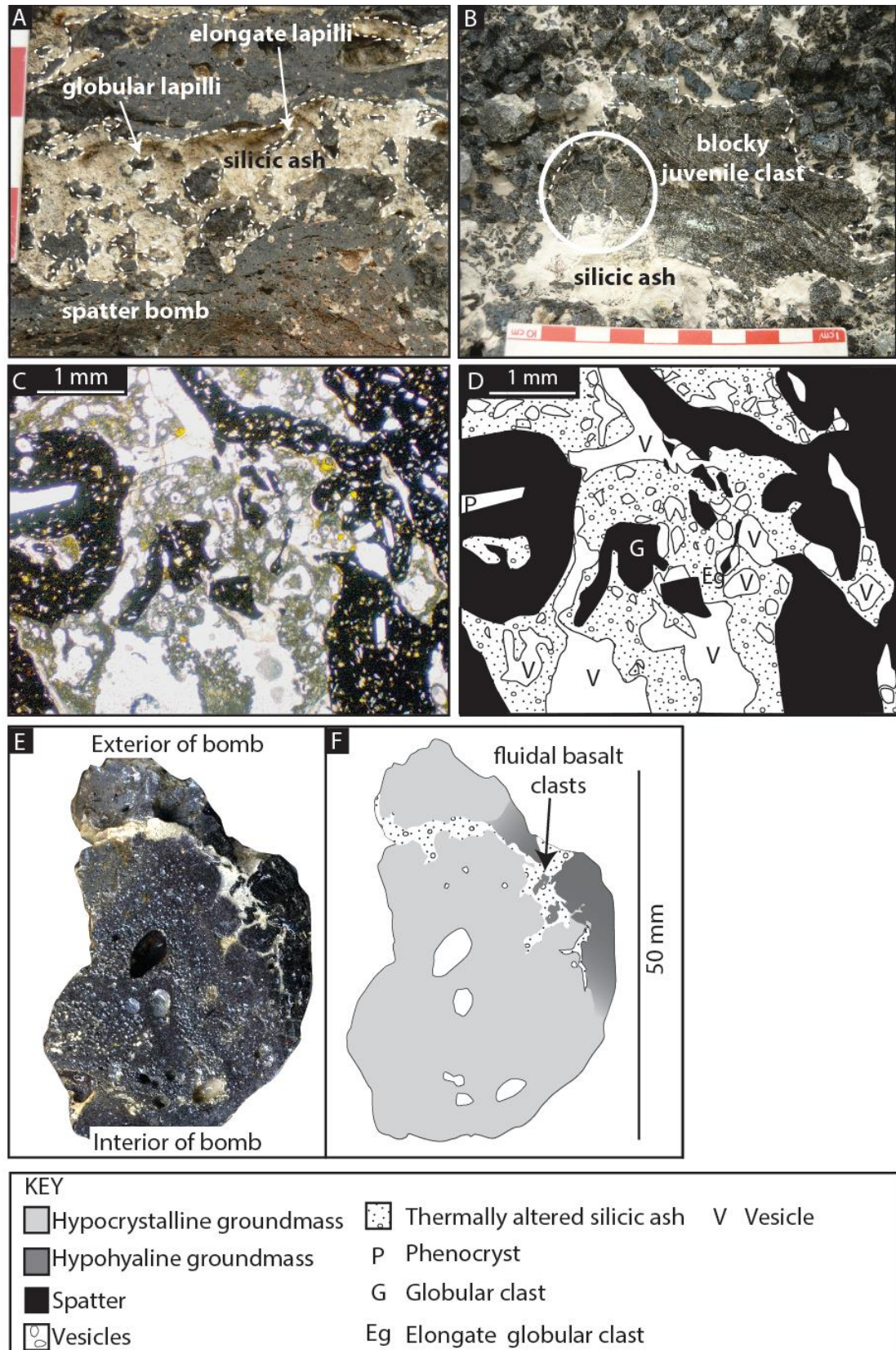


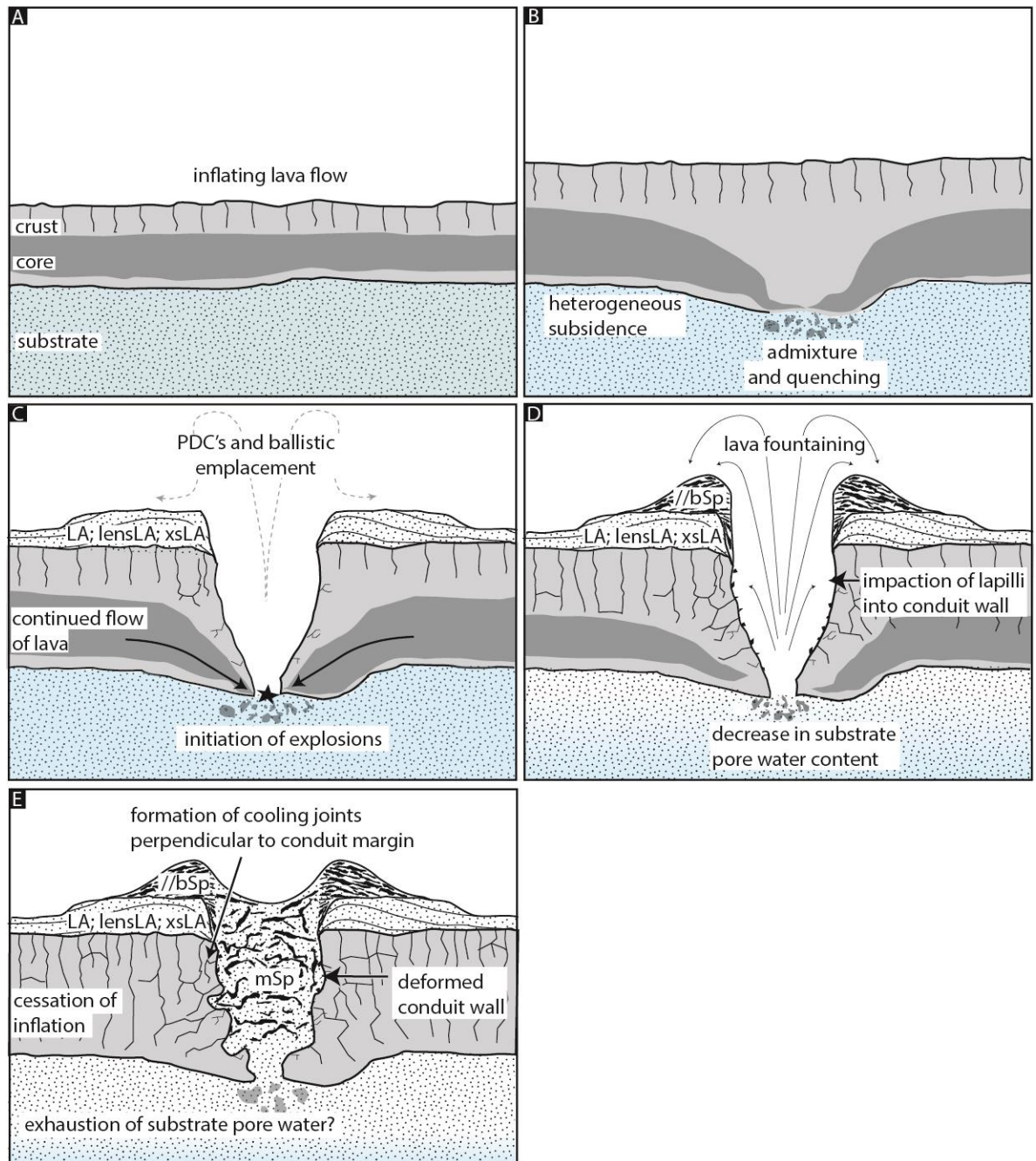


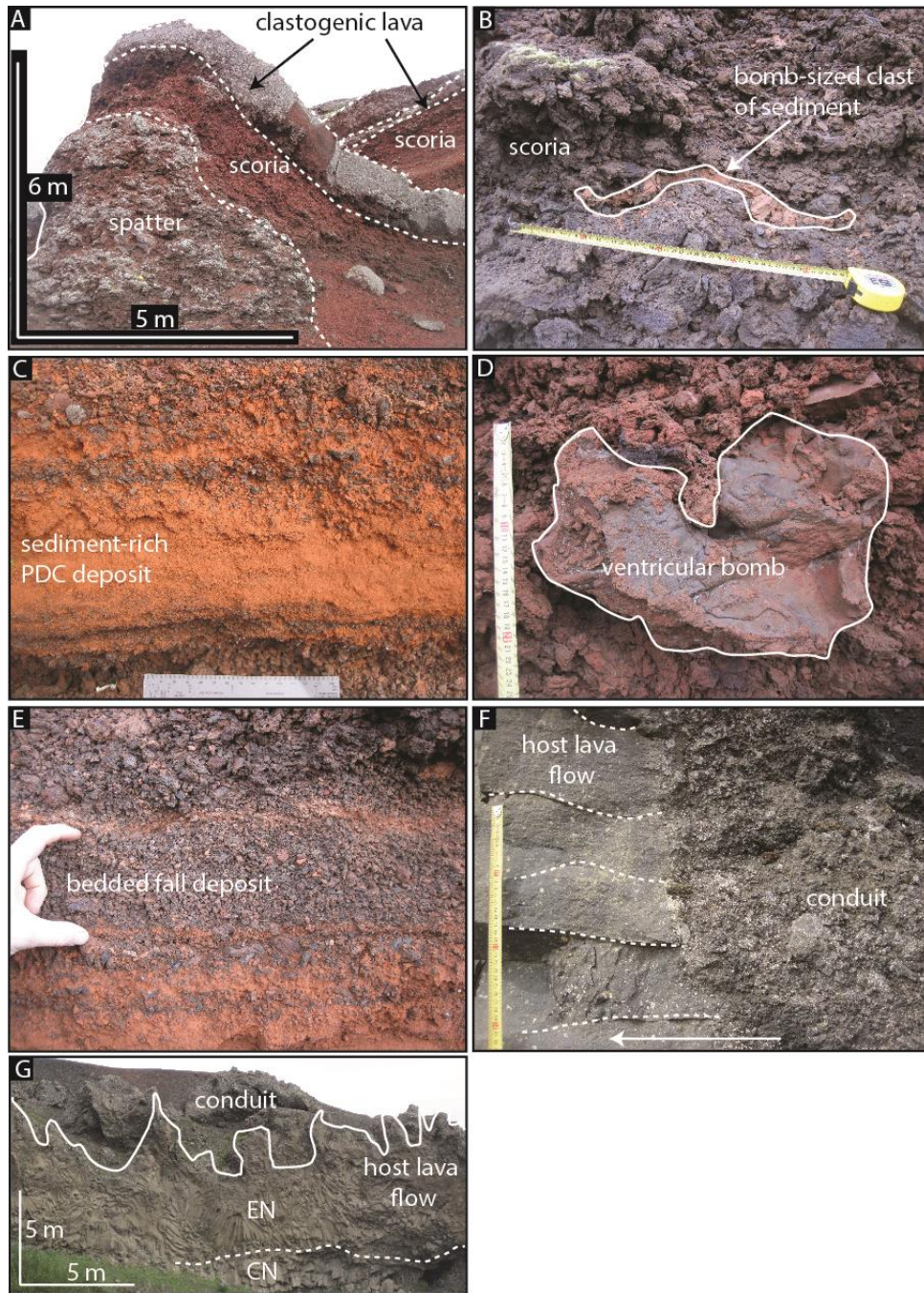












| Juvenile clast type | Description | Mean density (kg m^{-3}) | Mean vesicularity (%) | Mean crystallinity (%) | Interpretation |
|---|--|-------------------------------------|-----------------------|------------------------|---|
| Spatter bombs | Lithology: Forms irregular bombs with fluidal and ropey exteriors Structure: Clast supported (/bSp); beds are parallel and dip 20°. Massive in lithofacies mSp. Occurrence: Tephra deposits; extending a maximum distance of ~70 m from source vent. | 2200 | 19 | 31 | Bombs indicate proximal fall deposition from a roofless lava fountain. |
| Hypocrystalline lapilli and ventricular or globular bombs | Lithology: Forming ventricular and globular shaped bombs frequently fragmented into blocky and equant clasts that occasionally preserve ropey textures on relict exterior surfaces; dominantly lapilli to bomb size; occasionally with radial fractures. Structure: Generally clast supported, occasionally matrix supported; forms cross stratified, massive and graded units (xsLA and m/nLA); also lenses and channels (lensLA). | 2300 | 15 | 44 | Clasts represent quenched globules of lava, ejected from beneath/within the host lava flow during tephra jetting. Bombs were mechanically fragmented into angular shapes upon eruption and deposition, and due to cooling contraction granulation. |
| Cored scoria bombs and lapilli | Occurrence: All tephra and conduit facies. Lithology: Black resinous rinds up to 10 mm thick and black scoriaceous cores; forming rounded bombs frequently fragmented into blocky and equant clasts; dominantly lapilli to bomb size. Structure: Clast-matrix supported; massive | 1700 | 36 | 52 | Produced by recycling of clasts in the conduit during intermittent and/or dry tephra jetting. |
| Blocky or fluidal sideromelane ash and lapilli | Occurrence: All tephra deposits. Lithology: Clast shapes vary from blocky and equant to fluidal and elongate. Structure: Varying from matrix to clast supported; massive (/bSp, mSp and xsLA), graded (m/nLA) and lenses and channels (lensLA). | - | - | 28 | Blocky and equant clasts indicate cooling contraction granulation and/or mechanical fragmentation; fluidal, elongate shapes indicate ductile disruption of magma. Bedding structures are interpreted to record deposition during the passage of density currents. |

Table 1.

| Lithofacies | Components | Description | Av. max clast size (mm) | % silicic ash | Interpretation |
|---|---|---|-------------------------|---------------|---|
| LA Sub facies: n (normal graded), m (massive) f (fabric) | Hypocrystalline lapilli and bombs, sideromelane ash, silicic volcanic ash, clasts of lava crust | Very poorly sorted, hypocrystalline lapilli with rare ash sized fragments; clast supported in silicic ash. | 128 | 20–75 | Platform forming deposit. The general lack of evidence for traction sedimentation in the juvenile clasts suggest proximal fall deposition, localised fabrics suggest a minor amount of lateral transport. The coarse nature of some deposits results from the ballistic emplacement of bombs. |
| lensLA | Hypocrystalline lapilli, sideromelane ash, silicic volcanic ash, clasts of lava crust | Lenses and channels of moderately well sorted, sideromelane and hypocrystalline lapilli; clast supported in silicic volcanic ash, and lenses and channels of substrate within sideromelane and hypocrystalline lapilli dominated rock. Irregular lower contact. | 60 | 25–85 | Platform forming deposit. Indicates deposition from dilute PDC. Erosion and transportation of material occurred in locally confined channels. Irregular lower contacts may suggest local erosion of underlying units. |
| xsLA | Hypocrystalline lapilli and bombs, sideromelane ash, silicic volcanic ash, clasts of lava crust | Cross stratified, moderately sorted sideromelane and hypocrystalline lapilli; clast supported in silicic volcanic ash; beds approximately 5 cm thick. | 70 | 20–55 | Platform forming deposit. Crude cross-bedding formed during deposition from PDC's, currents were locally erosive. |
| //bSp Sub facies: m (massive) | Spatter bombs, hypocrystalline lapilli, silicic volcanic ash, clasts of lava crust | Parallel-bedded spatter bombs with embedded angular hypocrystalline lapilli and silicic volcanic ash. Sub facies is massive. | >1000 | <10 | Cone forming deposit, sub facies (mSp) conduit fill deposit. Bomb beds indicate proximal fall deposition from rootless lava fountains. Large grain size indicates decreasing explosivity when water availability was decreasing towards the end of the eruptions. |

Table 2.

| Field area | Cone height (m) | Cone basal diameter (m) | Structure | Juvenile clast types | Environmental setting | Grading | Bedding | Deposition method | Substrate inclusions |
|--------------------------------------|-----------------|-------------------------|--|---|-----------------------------|--------------------|--|--|--|
| Greenland | 25 | 100–200 | Fines upwards into ash layers rich in shale, largest clasts proximal, central sediment filled chimney | Pillows and pillow fragments up to 0.5 m size and glass-rich fluidal clasts at the base, yellow/brown sand-sized volcanic clasts at the top | Subaqueous lacustrine | Normal | Bedding seen as clast alignment, flanks dip 20° | (No data) | Partly consolidated shale; 10–20 vol. % |
| Iceland | 1–35 | 2–450 | Capped by spatter 1–2 m thick, inverse grading is common, occasionally with rheomorphic layers, form steep hornitos or broad cinder/tuff cones | Scoria and spatter, ash, lapilli and bombs | Lakes, marshes etc. | Inverse | <0.2 m thick beds of mud and ash, decimetre to metre thick beds of juveniles | PDC and fall | Common in lower sequences as beds, inclusions and coatings; no amounts given |
| Columbia River Ice Harbor lava flows | ≥ 3 | ≥ 5 | Substrate-rich tephra platforms at base, capped by spatter | Hypocrystalline ash and lapilli, spatter, cored, ventricular and globular bombs | Flood plain or shallow lake | Inverse | Decimetre to metre thick beds | PDC and fall | Common in all except uppermost beds, admixed with juvenile clasts; <10–85 vol. % |
| Hawaii | 10–90 | 20–100's | Monomictic, variably welded and agglutinated, often form crescent shaped ridges at the shoreline | Scoria and spatter, ash, lapilli and cored bombs, Limu-o-Pele, lava crust lithics | Entry of lava into ocean | Normal and inverse | Massive to crudely bedded in proximal facies; poorly to moderately bedded in distal facies | Tephra jets, littoral lava fountains, lithic blasts, lava squeeze up and flow from cone, bubble bursts | (No data) |

Table 3.